CHARACTERIZING WASTE ROCK USING AUTOMATED QUANTITATIVE ELECTRON MICROSCOPY

by

Randy J Blaskovich

A THESIS SUBMITTED IN PARTIAL FULFILLMENT OF THE REQUIREMENTS FOR THE DEGREE OF

MASTER OF APPLIED SCIENCE

in

The Faculty of Graduate Studies

(Mining Engineering)

THE UNIVERSITY OF BRITISH COLUMBIA

(Vancouver)

May 2013

Abstract

The leaching of metals from waste rock is directly related to the mineralogical composition of the rock. The overall study objective was to evaluate the application of automated quantitative electron microscopy to weathering waste rock. The value of mineral liberation analysis in optimizing mineral processing operations has been well documented. Application of automated mineralogical techniques, such as the Mineral Liberation Analyzer, to environmental studies is less common with no waste rock characterization studies found that specifically use the Mineral Liberation Analyzer.

Mineral Liberation Analyzer methodology limitations and advantages were explored in the context of detection and quantification of primary and secondary metal-associated mineral phases. Mineral Liberation Analyzer application to waste rock weathering studies was assessed using laboratory, field cell, and experimental pile samples which were separated into particle-size fractions. Mineral Liberation Analyzer characterization included bulk modal and metal-associated mineralogy, size distribution, and mineral liberation, association, and exposure or availability (to weathering processes) and mineralogical features useful to an environmental modeller. The Mineral Liberation Analyzer consisted of a FEI Quanta 600 scanning electron microscope equipped with dual Bruker-AXS silicon drift detectors, tungsten filament and proprietary software.

The Mineral Liberation Analyzer demonstrated characterization of Antamina mine waste rock which would aid the understanding of weathering processes at this and other sites, such as tailings and heap leach activity. Important mineralogical and elemental features determined were: availability / exposure, particle / grain size and shape, association (such as locking and potential mineral-mineral interactions), quantity and type (such as crystal structure reactivity), fractures and porosity. The scope of this study does not extend to linking lithology to secondary mineralogy. The Mineral Liberation Analyzer, in conjunction with geochemistry, particle surface analysis tools, chemical speciation

modeling and diagnostic sequential leach can advance waste rock characterization, to improve mitigation strategies for waste rock drainage.

Preface

The results of this study were published in abbreviated form in the proceedings of the 9th International Conference on Acid Rock Drainage (ICARD) 2012 conference: Blaskovich, R., Brienne, S., Klein, B., Beckie, R.D., Mayer, K.U., Aranda, C.A., Haupt, C. (2012), “Quantitative Mineralogy to Assess Waste Rock Weathering at the Antamina Mine”.

I was responsible for developing the test approach, conducting test work, interpreting test work data and documenting the results.
I consulted with my supervising committee and colleagues who provided feedback.

Table of Contents

List of Tables

List of Figures

List of Acronyms and Symbols

Symbol	Description
120x	refers to a microscope magnification of 120 times
n-D	such as 2-D or 3-D – two or three dimensional, respectively
Å	Angstrom
AAS	Atomic Absorption Spectroscopy
AAN	Average Atomic Number
ABA	Acid-Base Accounting
AG	Acid Generating
AP	Acid Producing
ARD	Acid Rock Drainage
AR&T	Applied Research & Technology
asl	above sea level
BET	Brunauer-Emmet-Teller
BSE	Back-Scatter Electron
cm	centimeter
C*n*	such as C5 or C6 – Warman cyclosizer 5^{th} or 6^{th} size fraction, respectively
cps	counts per second
CPU	Computer Processing Unit
CSIRO	Commonwealth Scientific and Industrial Research Organisation
CT	(3-D X-ray) Computed Tomography
^{0}C	degree Celsius
dk	dark
EDS	Energy Dispersive Spectrometer
e.g.	for example; Latin *exempli gratia,* for the sake of an example
EMPA	Electron MicroProbe Analysis
EPA	Environmental Protection Agency
eV	electron Volt
EXAFS	Extended X-ray Absorption Fine Structure

FEG-SEM	Field Emission Gun - Scanning Electron Microscope
FWHM	Full Width Half Maximum (peak height)
g	gram
GXMAP	Grain X-ray Map
h	Planck's constant
HPD	Halocentric Peak Determination
hr	hour
HRXMT	High Resolution X-ray MicroTomography
ICP	Inductively Coupled (Argon) Plasma
ICP-AES	Inductively Coupled (Argon) Plasma – Atomic Emission Spectrometry
ICP/MS	Inductively Coupled (Argon) Plasma / Mass Spectrometer
i.e.	that is, such as; Latin *id est*, that is
JKMRC	Julius Kruttschnitt Mineral Research Centre
kcps	kilo-counts per second
kg	kilogram
kV	kilovolt
LA-ICP/MS	Laser Ablation - Inductively Coupled (Argon) Plasma / Mass Spectrometer
λ	wavelength
lt	light
Ltd	Limited
m	mass
m.	meter
MEND	Mine Environment Neutral Drainage
mg	milligram
ML	Metal Leach
MLA	Mineral Liberation Analyzer
mm	millimeter
Mn Kα	Manganese (primary) X-ray excitation line Kα
MOI	Mineral Of Interest
msec	millisecond

Mt	Million tonnes
nm	nanometer
NP	Neutralizing Potential
NRD	Neutral Rock Drainage
OH^-	hydroxyl cation
PAG	Potential Acid Generating
Pb(II)	lead in oxidation state 2, Pb^{+2}
Pb(IV)	lead in oxidation state 4, $Pb+^{4}$
pH	potential for Hydrogen; scale range 0-14, zero being the highest acidity
PSSA	Phase Specific Surface Area
PIXE	Proton Induced X-ray Emission
PTS	polished thin section
QEMSCAN	Quantitative Evaluation of Minerals by Scanning Electron Microscope
QEM-SEM	Quantitative Evaluation of Materials by Scanning Electron Microscope
S	South
SDD	Silicon Drift Detector
S.A.	South America
SEM	Scanning Electron Microscope
SHE	Standard Hydrogen Electrode
SI/MS	Secondary Ion / Mass Spectrometer
SL	Sequential Leach
SPL	Sparse Phase Liberation
SPLP	synthetic precipitation leaching procedure
SLR	Sequential Leach Residue
STEM	Scanning Transmission Electron Microscopy
SXBSE	Select Extended Back-Scatter Electron
S-XRD	Synchrotron XRD
S-XRF	Synchrotron XRF
T	tonne
ToF-SI/MS	Time of Flight – Secondary Ion Mass / Spectrometry

UBC	University of British Columbia
µm	micron or micrometer
µsec	micro-second
υ	velocity
v.	very
V.	Volt
VMS	volcanic massive sulphide
W	West
WDS	Wavelength Dispersive Spectrometer
wt%	weight-percent
XANES	X-ray Absorption Near-Edge Structure
XBSE	Extended Back-Scatter Electron
XBSE_STD	Extended Back-Scatter Electron _ Standard
XMOD	X-ray Modal (mineralogy)
XRD	X-Ray Diffractometer
XRF	X-Ray Fluorescence
XSPL	Extended Sparse Phase Liberation

Acknowledgments

I acknowledge with much gratitude the following:

- God for His patience and provision for my curiosity, ability, patience, and perseverance to complete this project.
- My wife Ann and children, my extended family, my friends and my colleagues for their encouragement, patience and prayers as I drifted in and out of seclusion to complete course requirements and generate this document.
- Teck Metals Ltd for access to the Mineral Liberation Analyzer for analytical method development and waste rock evaluation, for encouragement, funding and patience; *Compania Minera Antamina S.A*. and University of British Columbia for encouragement and funding.
- The comments provided by Bern Klein, Stephane Brienne, and Nichola McKay, which helped to improve the manuscript.
- *Compania Minera Antamina S.A*., University of British Columbia and Teck Metals Ltd for permission to publish this work.

CHAPTER 1 Introduction

1.1 Introduction

The purpose of this study was to assess and advance the application of quantitative mineralogy for its application to waste rock weathering studies. The Mineral Liberation Analyzer (MLA) is a well-known and effective tool to determine mineralogical information to support the development and improvement of mineral processes. However, there are no published studies demonstrating its application to waste rock weathering. The MLA was assessed by applying it to analysis of waste rock from the Antamina copper-zinc mine in Peru to determine mineralogical factors important to weathering processes. Through the application to this study, conclusions are drawn about the benefits and limitations of the MLA technology as an aid to understanding weathering mechanisms.

1.2 Acid rock and neutral rock drainage

In order to predict and model weathering, waste rock needs to be characterized. Methods included determination of metal concentrations and mineralogical composition which were then correlated to environmental outcomes. Minerals can be classified according to their acid generating and neutralizing potential.

The reactivity of the minerals with neutralizing potential (NP) are presented in Table 1.1 [Jambor and Blowes, 1998; Kwong, 1993; Lawrence and Scheske, 1997; Sverdrup, 1990]. However, the sum of the NP of individual minerals is not necessarily the total NP of a waste rock (or tailing) because there are many mineralogical factors that can interfere with the access of neutralizing minerals to acid generating constituents. These factors include mineral liberation (i.e. availability or exposure) and associations, crystal structure (e.g. calcite is more reactive than aragonite), fractures and porosity, texture, size and shape of the mineral grains, mineral composition, and weathering state

(alteration products can coat / armour mineral surfaces and / or be reactive themselves).

Table 1.1. Rock reactivities of non-sulphide minerals at pH 5 (relative to calcite).

Group	Rock-Mineral Type	Relative Reactivity @ pH5
Dissolving	calcite, aragonite, dolomite, magnesite, brucite	1
Fast weathering	anorthite, olivine, nepheline, garnet, leucite, diopside, wollastonite	0.4
Intermediate weathering	epidote, pyroxenes (enstatite, hypersthene, augite), amphiboles, (hornblende, tremolite, actinolite), biotite, chlorite, talc, titanite, serpentine	0.2
Slow weathering	plagioclase feldspars (albite, oligoclase, labradorite), clays (vermiculite, montmorillonite)	0.01
Very slow weathering	K-Feldspar (microcline, orthoclase, sanidine), muscovite	0.01
Inert	quartz, rutile, zircon	0.004

Sources (Jambor and Blowes, 1998; Kwong, 1993; Lawrence and Scheske, 1997; Sverdrup, 1990)

Overall, all Antamina mine waste rock samples of this study are classified as non-acid generating according to a screening criteria suggested by Price [1997]. Visual classification can be used, sometimes with relatively satisfactory result – though not always, as evidenced by the Antamina mine waste rock releasing metals to the drainage [Aranda *et al.,* 2009]. This suggested that classification methods such as Acid Base Accounting (ABA) may not be sufficient for predicting metal leach (ML) behaviour. In mine studies other than Antamina, mineralogical and chemical analyses were performed using optical microscopy and Inductively Coupled Plasma – Atomic Emission Spectroscopy (ICP-AES), respectively [for example: Ulusoy and Kursun, 2011]; however, these analyses were reported to be relatively time-consuming, labour intensive and missed the finer detail associated with secondary mineral phases.

On a broad scale, waste rock could be evaluated for reactivity. Antamina mine's Class C waste rock was noted to be coarse-textured with high permeability (porosity) with potential harbours for formation of secondary mineralization. The reactive Class A waste rock was described as highly friable and finer-grained, and could easily produce metal-containing drainage. It is not clear how to evaluate drainage from the variably reactive Class B waste rock as it is not visually obvious and could be designated as Class A or Class C waste rock based on elemental chemical analysis. This variability, specifically at the micro-level of secondary phases, potentially reactive phases, exposed primary sulphide phases, and everything between, shows the difficulty of classifying waste rock material in the field – without considering such macro-physical attributes as water flow pathways. This is partly the reason for the University of British Columbia (UBC) study. While there have been many studies of environmental impact from neutral drainage, a controlled study at field scale levels could not be found.

1.3 Mine location, geology and task

In 2005, a research program was initiated to study and improve the understanding of the weathering of Antamina waste rock (i.e. hydrological, biological, geochemical, mineralogical, physical) with technical expertise provided by *Compania Minera Antamina S.A.*, UBC [Corazao Galegos *et al.,* 2007; Bay *et al.,* 2009] and Teck Metals Ltd's Applied Research & Technology group. One aspect of this research program was to study the reactivity of the waste rock. Several graduate student projects, developed by UBC (in conjunction with Antamina mine staff) focused on characterization of the main types of waste rock and evaluation of their geochemical reactivity in the laboratory and at the waste rock dump through:

(1) field cell experiments - 200 litre plastic drums filled with specific rock types [Aranda *et al.,* 2009; Aranda, 2009; Hirsche, 2012];

(2) experimental waste dumps - five instrumented 36m x 36m x 10m waste rock piles were constructed [Corazao Galegos *et al.,* 2007]; and,

(3) cover study experiments - five test plots were constructed from waste rock using different cover types [Urrutia Varese, 2012].

The results of the quantitative mineralogical study presented in this thesis were used to support the interpretation of the experimental program.

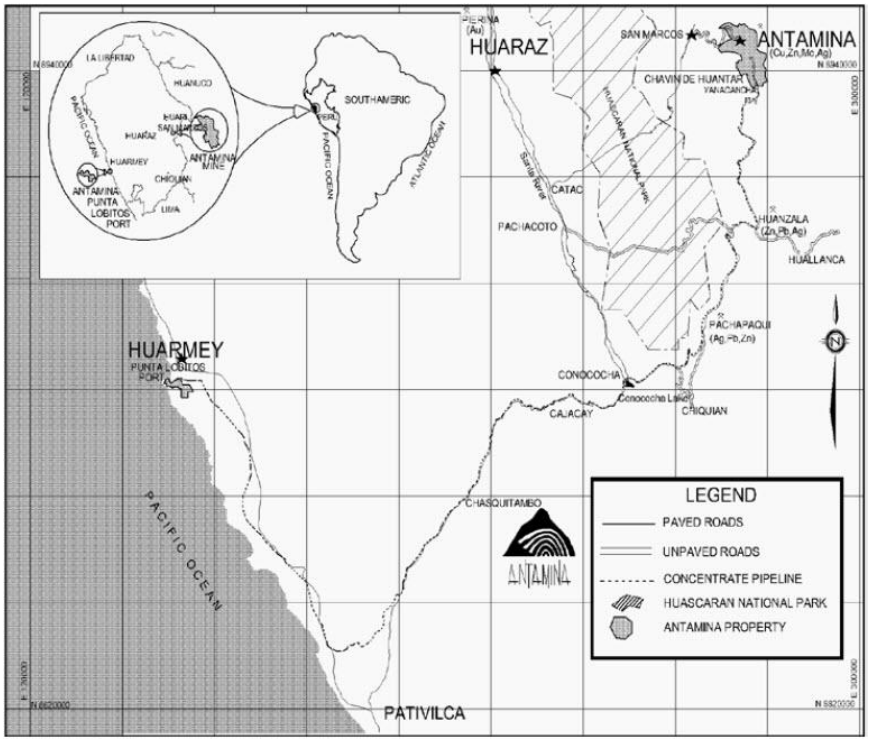

Figure 1.1. Location of the Antamina mine.

The South American Antamina Mine (latitude 9° 32’ S, longitude 77° 03’ W) is located in the Peruvian Andes range, 270 km north of Lima and 200 km west of Huarez, at 4100-4700 m asl (Figure1.1). The climate can be characterized by an average annual temperature of 8°C (ranging from -8 to +23°C) and annual precipitation of 1200 mm (ranging 1100 – 1300 mm) with a distinct ‘wet’ (November through April) and ‘dry’ period (May through October). The Antamina polymetallic skarn deposit was formed when quartz monzonite intruded into Cretaceous limestone [Lipten and Smith, 2005; Golder, 2004]. The metals of economic interest are copper (Cu), zinc (Zn), silver (Ag) and

molybdenum (Mo). The ore deposit has an indicated resource of 745 Mt with 1.06 wt% Cu, 0.67 wt% Zn, 11.7 g/T Ag, 0.026 wt% Mo, on the basis of an average 0.3 wt% Cu cut-off grade. Mine production began October 2001 and mine life is estimated to last until 2029 [Brown, 2006; Strand *et al.*, 2010]. Approximately 300 Mt/day of waste rock are generated. Over the 28-year planned mine life, 1.5 billion tons of waste rock will be deposited by end-dumping on steep mountain faces into piles that are 200-300 meters deep. The high-carbonate waste rock surrounding the polymetallic ore emits near-neutral pH effluents. The waste rock is classified as reactive, moderately reactive or less reactive according to the criteria summarized in Table 1.2.

Table 1.2. Antamina mine waste rock classification criteria[1].

Class	Reactivity	Rock Type	Zn (%)	As (%)	Visual Sulphide[1] (%)	Location
A	Reactive	Mineralized / Oxidized rock [including Skarn (endo / exo), Hornfels, Marble, Limestone (some Intrusive)]; high Zn, As, S	> 0.15	> 0.04	> 3	within pit limits; East dump
B	Moderately reactive	Hornfels, Marble and Limestone; moderate Zn	0.07 - 0.15	< 0/04	2 - 3	stockpile pads; construction material; Tucush or East dump
C	Less reactive	Hornfels, Marble and Limestone; low Zn, As, S	< 0.07	< 0.04	< 2	wherever needed (e.g. East dump, Tucush dump, tailings dam, water reservoir dam, access roads)

[1] Antamina 2010, Ore Control Procedure Manual.

Five distinct waste rock types were specified by Golder (2004): hornfels, marble, skarn, intrusives and limestone, although hornfels and marble comprise the majority of the waste rock. These lithotypes were further grouped into three reactivity groupings for on-site classification of the waste rock for specific dump sites based upon sulphide content and expected metal loading (i.e. zinc and arsenic) of the leachate. It was estimated that the distribution of waste rock types according to the classification scheme would be

44% reactive, 42% less reactive, with the balance being moderately reactive [Golder, 2006; Watermark Consulting Inc, 2000].

To reduce the environmental impact of mining activity as a consequence of metal release, a better understanding of waste rock weathering is required. Some key metal-bearing mineral of interest (MOI) may be present in trace amounts, which would challenge understanding and predictive modeling without adequate particle statistics and increased knowledge of their chemical behaviour during waste rock weathering. Quantitative mineralogy on specific lithologic rock types will support the establishment of an effective waste rock classification scheme. It is proposed that quantitative mineralogy will support the interpretation of results from weathering experiments resulting in improved waste rock management practices and reduced environmental impact of mining.

1.4 Objectives and study

The objective of this study is to demonstrate and advance the application of quantitative mineralogy to waste rock weathering studies. Quantitative mineralogy was conducted using scanning electron microscopy and MLA technology. Waste rock samples came from the Antamina mine. At the Antamina mine, waste rock is classified into three broad reactivity types, Class A (reactive), Class B (moderate) and Class C (non-reactive) [see Table 1.2]. To better understand the weathering processes, field cell tests, experimental waste rock piles and large cover studies were conducted at the Antamina mine site by UBC.

The study presented in this thesis will develop MLA methodology applicable to waste rock characterization and demonstrate MLA output that could benefit the interpretation of waste rock weathering processes. The main metals of interest focused on in this study were arsenic (As), antimony (Sb), copper (Cu), lead (Pb), molybdenum (Mo) and zinc (Zn).

Chapter 2 summarizes the relevant literature on waste rock weathering, the role of mineralogy and characterization methodologies and techniques used to identify and quantify minerals. In chapter 3 the experimental program is presented. In chapter 4, the MLA methodology parameters were explored in the context of automated quantification of waste rock features. Chapter 5 presents the MLA output in the context of waste rock characterization. Section 5.1 presents the bulk mineralogy of the Antamina mine waste rock. Section 5.2 and 5.3 present specific mineralogical information generated by the MLA with a focus on aspects of interest to weathering and metal leaching. Section 5.4 summarizes the application of automated quantitative mineralogy to waste rock weathering. Specific association of lithology to mineralogy is beyond the scope of this study. Finally, chapter 6 presents the conclusions and recommendations resulting from this study.

CHAPTER 2 Literature review: characterization of mined material

2.1 Introduction

The mining industry requires effective mineral classification and quantification. Mineral information rather than elemental information is often preferred because different minerals in both metal-bearing ore and gangue can have different impact on plant performance [Lorenzen and van Deventer, 1994; White, 1998].

Traditional ore and rock characterization was based on the mineralogist's observations from hand specimens and thin sections using optical microscopes. The tools available limited the extent of quantitative data, objective reporting and statistical validity. Automated mineralogical identification techniques provide objective quantification of sample mineralogy, as compared to mineralogical inference from chemical analysis or traditional methods. Automated mineralogy refers to technologies which collect and/or analyse mineral data with some degree of automation. The technologies combine the scanning electron microscope (SEM), electron beam measurement technology and imaging software to produce detailed analysis of mineral samples [Gottlieb *et al.,* 2000; Petruk, 2000; Gu, 2003].

The automated mineralogical procedure analyzes a number of polished sample mounts in order to identify the mineralogical phases, their availability and associations. Three-dimensional (3-D) results are extrapolated from a two-dimensional (2-D) sample mount through stereological correction [King and Schneider, 1998; Spencer and Sutherland, 2000]. The application of a stereological correction eliminates the potential analysis of multiple samples to offset 2-D effects.

In recent years, image processing techniques have applied an X-ray source in conjunction with backscatter electron (BSE) imaging to identify the elements associated with each mineral phase [Gottlieb *et al.,* 2000; Petruk, 2000; Gu, 2003]. There have

been great advances in automation of numerous mineral identification and quantification technologies, including optical, X-ray beam, laser beam, electron beam (SEM, electron microprobe analysis [EMPA]), and proton beam techniques [AMIRA, 2002].

2.2 Metal leaching from mine waste material

In many parts of the world the highest grade mineral deposits are being depleted. The significant deposits of today are usually complex mixed sulphide-oxide ores. These ores represent a challenge in mineral processing and often parts of the deposit are untreated for metallurgical and / or economic reasons. The mine site's rock material undergoes mineral weathering reactions which result in acid production, acid neutralization and trace metal release. The geochemistry has been reviewed by others [e.g.: Nordstrom, 1999; Nordstrom and Alpers, 1999; Smith, 1999; Smith and Huyuk, 1999].

Oxidation weathering of sulphides results in sulphate generation. Sulphide oxidation is dependent upon the sulphide composition and its reactivity, the availability of oxygen, water and the appropriate bacteria. Sulphide oxidation increases with increasing surface area and lower pH [Nordstrom and Alpers, 1999].

The weathering leach of sulphide minerals has been described elsewhere [White, 1998]. The majority of acid rock drainage (ARD) results from the oxidation of iron sulphides, such as in Equation 1 and 2 for pyrite and pyrrhotite, respectively [Stumm and Morgan, 1981].

$$FeS_{2(s)} + (15/4)O_{2(aq)} + (7/2)H_2O \rightarrow Fe(OH)_{3(s)} + 2SO_4^{-2}{}_{(aq)} + 4H^+_{(aq)} \quad (1)$$

$$Fe_{1-x}S_{(s)} + [(9-3x)/4]O_{2(aq)} + [(5-3x)/2]H_2O \rightarrow (1-x)Fe(OH)_{3(s)} + SO_4^{-2}{}_{(aq)} + 2H^+_{(aq)} \quad (2)$$

Oxidation of sulphides by ferric iron is shown in Equation 3 and 4. Equation 5 shows that dissolved ferric ion can precipitate and generate acid. Equation 6 shows the bacterial oxidation of ferrous to ferric iron which consumes acid [White, 1998]. Note that

pyrite / pyrrhotite oxidation could also generate ferrous iron, and in the presence of more oxygen could be converted to ferric iron (see Equation 6).

$$FeS_{2(s)} + 14Fe^{+3}_{(aq)} + (19/2)H_2O + 15/4O_{2(aq)} \rightarrow 15Fe(OH)_{3(s)} + 2SO_4^{-2}{}_{(aq)} + 46H^{+}_{(aq)} \quad (3)$$

$$Fe_{1-x}S_{(s)} + (8-2x)Fe^{+3}_{(aq)} + [(9-3x)/4]O_{2(aq)} + [(53-15x)/2]H_2O \rightarrow (9-3x)Fe(OH)_{3(s)} + SO_4^{-2}{}_{(aq)} + (26-6x)H^{+}_{(aq)} \quad (4)$$

$$Fe^{+3}_{(aq)} + 3H_2O \rightarrow Fe(OH)_{3(s)} + 3H^{+}_{(aq)} \quad (5)$$

$$4Fe^{+2}_{(aq)} + O_2 + 4H^{+} \rightarrow 4Fe^{+3}_{(aq)} + 2H_2O \quad (6)$$

In the context of particle mineralogy, ARD occurs when: (1) sulphide mineral is present and at high enough concentration to impact the environment; (2) sulphide mineral is reactive; and, (3) environmental conditions are favourable for oxidation (i.e. presence of oxygen / oxidizer and water) [White, 1998]. Acid generated can be neutralized in various acid consuming reactions such as contact with carbonates and silicates. When the drainage becomes less acidic / more neutral pH it is termed Neutral Rock Drainage (NRD).

Characterizing waste rock is challenging due to secondary mineral formation reactions [Petrunic *et al.,* 2005; Jambor and Blowes, 1998]. The reaction products of weathering can react with other sulphides, precipitate as sulphates (possibly hydrated), and / or react with host rock minerals to neutralize acid. Any acid that is not neutralized will result in ARD. Sulphates that precipitate have the potential to store acid and / or metals released from the mine waste during such events as snow melts or rain events, and may release them at a later time [Jerz and Rimstidt, 2003]. Common weathering sulphate minerals found in mineralized rock drainages include melanterite ($FeSO_4 \cdot 7H_2O$), rozenite ($FeSO_4 \cdot 4H_2O$), szomolikite ($FeSO_4 \cdot H_2O$), romerite ($Fe^{+2}(Fe^{+3})_2(SO_4)_4 \cdot 14H_2O$) and copiapite ($Fe^{+2}(Fe^{+3})_4(SO_4)_6(OH)_2 \cdot 20H_2O$) [Alpers *et al.*, 1994]. Iron sulphates can experience dehydration reactions in which they transform into goethite (FeO(OH)) and jarosite ($KFe_3^{+3}(SO_4)_2(OH)_6$) [White, 1998].

2.3 Neutralization of mined rock drainage

Neutralization of ARD can occur with acid-buffering gangue minerals in the host rock. Gangue includes both non-sulphide and low-grade sulphide-bearing minerals. There are several MOIs which can affect ARD neutralization. Sherlock et al. [1995] stated that minerals which can potentially neutralize ARD (in order of reactivity) are: (1) calcium and magnesium bearing carbonates; (2) oxides and hydroxides of calcium, magnesium and aluminum; (3) soluble, non-resistant silicates; and, (4) phosphates (mainly apatite). Each different mineral phase can affect the overall chemical reactivity of the waste rock dump, and each MOI can itself be affected by the physical attributes of the particles in which they reside.

The distinction between ARD and NRD is leachable water of approximately pH 6.4 [Drever, 1988; Alpers *et al.*, 1994]. The neutralization reaction for the dominant carbonate is shown in Equations 7 and 8. Equation 7 represents the dominant calcite-mediated neutralization below pH 6.4 and Equation 8 shows the dominant calcite-mediated neutralizing reaction above pH 6.4:

$$CaCO_{3(s)} + 2H^{+}_{(aq)} = H_2CO_{3(aq)} + Ca^{+2}_{(aq)} \quad (7)$$

$$CaCO_{3(s)} + H^{+}_{(aq)} = HCO_{3\,(aq)}^{-} + Ca^{+2}_{(aq)} \quad (8)$$

The rate of acid neutralization by carbonates is high [Sherlocke *et al.*, 1995]. Carbonates may include calcite ($CaCO_3$), magnesite ($MgCO_3$), siderite ($FeCO_3$), dolomite ($CaMg(CO_3)_2$) and ankerite ($CaFe(CO_3)_2$). Three separate weathering processes, each at a different pH range, may occur: circum-neutral carbonate dissolution; acidic hydroxide dissolution; and, very acidic silicate dissolution [Blowes and Ptacek, 1994].

Weathering of silicates can also neutralize acid; however, their dissolution rates and consequent acid neutralization are slow relative to the carbonate minerals [Nesbitt and Jambor 1998]. Silicate neutralization of acid will increase as particle size decreases.

Although mine drainage acidity commonly receives the most attention, the source of poor drainage quality is related to the leached metals. ARD water discharge does not meet environmental guidelines such as those provided by the Environmental Protection Agency [USEPA, 1994a].

The degree of availability of the waste rock particle mineral phase for oxidation reactions affects the mine drainage composition. The particle texture's mineral availability can be qualified as either fully liberated, fully locked in a host particle, partially liberated at the surface or exposed through a crack or pore in the particle [Ghorbani *et al.*, 2011]. Once metals are released to the environment their fate is influenced by many factors. Metal mobility, in a broad sense, can be estimated; however, at the microscopic level it is much more difficult [Smith and Huyuk 1999]. Metals can be present as dissolved in the leachate or removed as secondary mineral phases which may be present on their own or as coatings on other particles. The oxidation of sulphide minerals and weathering (dissolution) of carbonate minerals is surface-controlled. These reactions can be controlled by the presence of secondary coatings. Mineral surface oxidation is therefore controlled by availability, particle size and texture.

2.4 Evaluation of analysis techniques for mine waste rock mineralogy

Mineralogical studies are traditionally performed manually using point-counting techniques which require the skill and knowledge of a mineralogist [Neilson and Brockman, 1977]. Automation techniques offer the advantages of increased number of particles examined, improved sampling statistics and objective particle accounting.

Sample characterization begins with the collection of representative samples. The sample integrity must be preserved during collection, storage and sample preparation.

Sampling theory specifically related to waste rock has been discussed in the Canadian Mine Environment Neutral Drainage (MEND) Program literature [MEND, 2001].

A widely used method to indicate the properties of rock material to future oxidation processes is the static test. Static tests are short in duration (hours to days) and low cost. Static tests predict the waste rock's ability to produce and neutralize acid based on elemental, not mineralogical, composition. Details of these tests are discussed elsewhere [White *et al.*, 1999]. The most used static test is ABA [Sobek *et al.*, 1978]. This test uses the total sulphur or sulphide-sulphur content to calculate the quantity of acid producing (AP) minerals in the sample [White *et al.*, 1999]. The total sulphur calculation may over estimate acid production due to the presence of non-acid generating sulphate minerals (e.g. barite, $BaSO_4$). The sulphide-sulphur calculation may underestimate acid production due to the production of other sulphate-containing mineral phases (e.g. melanterite). The neutralization potential (NP) of the waste rock is dependent upon the mineralogy which incorporates major rock-forming elements and carbon (see Table 1.1).

Paste pH is a common field test that estimates the presence of soluble acid salts on the rock [MEND, 1990]. The United States Environmental Protection Agency (EPA) synthetic precipitation leaching procedure (SPLP) is used to indicate the presence of more soluble acid salts in rock drainage [USEPA, 1994b].

Kinetic tests, such as humidity cells and columns, estimate the potential quality of drainage from the weather-leached waste rock. This type of test will often not simulate actual rock weathering but can deliver helpful information when there is no other information available. The kinetic test accelerates weathering processes through application of abundant oxygen and water (to transport reaction products) [Sapsford *et al.*, 2009].

In environmental studies, metal releases require knowledge of the interaction between different mineral phases. Assigning trace metals to specific minerals will require mineralogical information. A sequential chemical leach may be used to assign these metals to general mineral phases. The sequential leach (SL) process fractionates specific metal-bearing MOIs with a combination of reagents. The MOIs are extracted into the leach solution as a function of the mineral phase dissolution [Lorenzen, 1995].

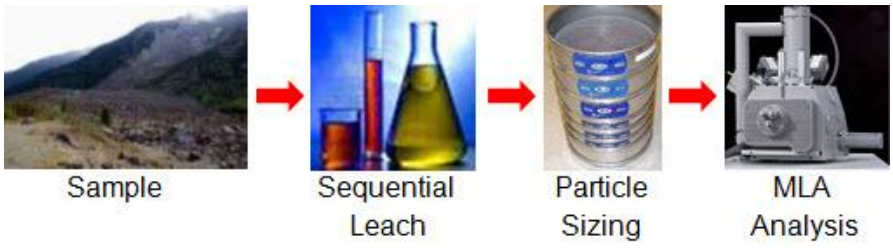

Figure 2.4.1. Pictorial representation of sequential leach work flow.

The general stages of a SL study are shown in Figure 2.4.1. In this study, some of the samples (see Table 3.2.4) were exposed to the SL steps shown in Table 2.4.1 [Klein *et al.*, 2011].

Table 2.4.1. Sequential leach extraction procedure.

Step	Action	Analysis
1	Sample: dry 500-1500 g.	Use in Step 2
2	Water soluble and weakly exchangeable: mix sample with 95g/kg $MgCl_2$, adjust to pH7, and agitate 1 hr.	Leach 1 for chemical elemental analysis; Residue 1 used in Step 3
3	Exchangeable cations and anions, and elements bound to carbonates: mix sample with 82g/kg Na acetate, adjust to pH5 (use HNO_3), agitate 0.5 hr.	Leach 2 for chemical elemental analysis; Residue 2 used in Step 4
4	Elements bound to Fe and Mn oxides: mix sample with 8.3g/kg NH_2OH / 9.1g/kg HCl, digest in 60^{O}C water bath 3 hrs.	Leach 3 for chemical elemental analysis; Residue 3 used in Step 5
5	Elements bound to organic matter and sulphides: first mix sample with 63g/kg HNO_3 leach, then 0.7g/kg H_2O_2, adjust to pH2, agitate 4 hrs.	Leach 4 for chemical elemental analysis; Residue 4 used in Step 6
6	Elements bound to oxides, sulphides, some silicates: mix sample with aqua regia (5.4g/kg HCl: 3.1g/kg HNO3), digest in 85^{O}C water bath 3 hrs.	Leach 5 for chemical elemental analysis; Residue 5 used in Step 7
7	Residue: dry, sieve into size fractions	Mineralogical analysis

A diagnostic SL can improve the understanding of weathering behaviour associated with specific mineral phases. Quantitative results for trace mineral phases and associated metals are complicated by the following factors: (1) analytes redistribute during the extraction (e.g. readsorption of analytes, incomplete dissolution, organic-bound metal liberated by organic matter destruction or exchange processes, or samples have the ability to alter – such as raise pH and therefore decrease extracted analyte solubility); (2) extraction is incomplete; (3) “new” mineral precipitation (e.g. insoluble pyromorphite, $Pb_5(PO_4)_3Cl$); and, (4) poor reagent selectivity [personal communication].

Chemical analysis of waste rock can be used to estimate the presence of minerals with acidic and neutralizing abilities, quantify the trace metals, and determine whole rock

composition. The chemical analysis can be destructive, such as using acid digestion or fusion followed by Atomic Absorption Spectroscopy (AAS) or Inductively Coupled (Argon) Plasma spectrometry (ICP), or non-destructive, such as using X-ray Fluorescence (XRF) or EMPA.

Optical microscopy (reflected or polarized light), X-ray diffraction (XRD) and / or SEM in conjunction with an energy or wavelength dispersive spectrometer (EDS and WDS, respectively) can be used to determine the mineralogy. XRD cannot be used to identify amorphous minerals, which often include the secondary phases generated during the weathering processes of waste rock (e.g. iron oxyhydroxides and aluminosilicates). The application of the Rietveld method can establish the quantity of amorphous content [PANalytical, 2009]. Analyses can be augmented by SEM which has a higher magnification capability than optical microscopy. WDS (and improved EDS) can be used to quantify the lower atomic number elements (i.e. ≤ 6). The mineralogical analysis determinations are improved if the samples are analyzed as polished thin sections, which are about 30 µm thick slices of whole rock. The combination of SEM and X-ray analysis vastly improves the ability to obtain compositional information for the smaller particle grains and fine features such as particle rim coatings [Sutherland *et al.*, 1988].

2.5 Applied mineralogy definitions

To quantify weathering mineralogy a measurement is required. The measurement of mineralogical information includes: “Characteristics like chemical composition, relative proportions, distribution, texture, types of intergrowths, size distribution, liberation degree and crystal structure of different ore minerals and their products are very important to understanding the different stages of weathering” [Márquez *et al.,* (2006)].

Mineralogical texture is the random structure in which different minerals occur together in the rock [Jones, 1987]. This definition separates it from the use of many image processing techniques that treat texture as known and repetitive.

Microtexture (defined as texture that is identifiable using a microscope) is usually measured on three types of sample: (i) polished thin section (PTS), a sample of unbroken rock, typically 1-2 cm in length and width, polished to about 30 μm thickness for examination with a microscope – optical polarizing microscope or SEM / MLA; (ii) polished rock surfaces, several centimeters in length and width and thickness (~3 mm), examined with an optical microscope or a SEM; and, (iii) polished particle samples, are rock fragments that have been broken into small particles (usually less than 1 mm), mounted in resin and polished, with advantage of good sampling statistics.

The simplest and smallest form of textural feature is a grain. A grain is a single crystal consisting mostly of a single mineral in which a lattice of atoms of the constituent elements is aligned geometrically in a particular orientation [Jones, 1987]. Individual grains are often difficult to distinguish and so should more aptly be referred to as phase-regions. A phase-region is a connected region consisting mainly of a single mineral. The border between phase regions having different orientations or consisting of different minerals constitutes a grain boundary. An inclusion of a different mineral refers to partial replacement of the original mineral by another mineral during geological evolution [Jones, 1987].

A feature is a particular region of rock that has different characteristics from adjacent parts of the rock, most notably edges or boundaries between dissimilar regions [Jones, 1987].

The image analysis presented in this thesis is based chiefly on mineral maps, which are images in which a particular mineral or mineral group has been assigned to each pixel. These maps have been derived from MLA (SEM-based) images where the minerals were identified by their X-ray emission spectra. The image pixel size for this study was about 2 μm.

2.6 Automated mineralogy developments

2.6.1 Introduction

A mineral deposit can only be exploited economically and efficiently if there is detailed knowledge of the nature and distribution of the minerals in the deposit. Deposit information would include identity, composition, amount and size of each mineral phase because mineral interaction during processing depends upon the mineral and the particle properties. The mineral processing definition of liberation was refined to indicate the amount of unassociated gangue [Lorenzen and van Deventer, 1994; White, 1998].

The advantages of complementary approaches by mineralogists and metallurgists have been highlighted [Henley, 1983]. Chemical analysis, physical separations and XRD analysis reported bulk mineralogy though lacked information on mineral size and texture. Chemical analysis results, sometimes accompanied by EMPA, were applied to normative methods to back-calculate mineral quantity. Physical separations provided size distributions (and density information) which were supplemented with XRD and optical analysis. The XRD provided mineral identity and quantity to as low as a few percent. Optical microscopists provided the supporting information to complete the mineralogy report. The labour intensive and time consuming approach provided the motivation for automation.

2.6.2 History

Gaudin was the first to use the term ‘locking’ in reference to the amount of target mineral available to the concentration process [Gaudin, 1939]. The required liberation in the process necessitated the development of image analysis (including preparation of polished sample mounts), geometrical treatment of the particle images and quantification of the mineral phases [Henley, 1983]. The final step would be forming a relationship between the measured parameters and the actual mineral processing, such

as grinding, concentration or heap leach. Automated mineralogy techniques were needed to statistically manage the thousands of grains present in the samples.

The first automated scanning instruments were either optical or X-ray based instrumentation, such as optical reflectance or BSE and fluorescence, respectively. Initially stereological transformation of the measured data was dealt with by assuming particles were spherical in shape and had perfect random cuts through the spheres (due to polishing). However, it was noted that non-spherical geometries (more reasonable for rock particle shapes) reported very different size distributions, which lead to more sophisticated particle measuring methods [Petruk, 1976]. Smaller size fractions generated better volume-percent results after the stereological transformation of the raw image data.

King proposed linking image analysis and stereological transformation into a predictive liberation model [King, 1979]. The fundamental problem was using an unrealistic geometry to assess the mineral process when in reality rock fragments do not form spheres. Microscopy techniques were used to obtain the particle images. The difficulties of quantification and determining the liberation of mineral phases in complex particles from an image was acknowledged. The microscopic examination of polished sample mounts was complicated by stereological bias and poor mineral phase discrimination of the optical images [Henley, 1983]. Barbery introduced an improved stereological transformation method for raw image data which provided more accurate results [Barbery *et al.,* 1984]. To achieve statistical accuracy for the reported data a large number of particles were needed to be observed. Automated scanning instruments were used to achieve these objectives.

An example of automated image analysis involved simple binary particles (iron oxide and silica) in a narrow size range (-595/+417 µm) which were mounted into polished sections and analyzed by the QEM-SEM (Quantitative Evaluation of Minerals by Scanning Electron Microscopy) [Sutherland *et al.,* 1988]. The QEM-SEM, developed by

CSIRO in Australia, was based upon a SEM equipped with a BSE detector and an EDS [Miller *et al.*, 1982; Reid *et al.*, 1984]. The JKMRC MLA was presented as an automated mineral measurement tool in 1997 [Gu and Napier-Munn, 1997]. The QEM-SEM (and MLA) was linked to a computer that controlled stage and electron beam movement, to collect and analyze the particle images and associated X-ray spectra from polished sample mounts. This instrument used a stereological correction algorithm based on a method developed by Hill *et al.* [Hill *et al.*, 1987] in which the stereological error was diminished by assessing the particle area rather than chords with no assumption of particle shape. Good agreement between QEM-SEM measurements and calculated composition (from density fractionation) confirmed the method for estimating unknown distributions of particle compositions. The low noise, high resolution BSE image enabled accurate discrimination of the mineral phases in a particle.

In the early 1980s, the use of computers were linked to developments to improve instrumentation (fast, reliable, memory for image data storage), software (complex programs easier to use, advanced particle feature recognition), SEMs (easier to use and more reliable), BSE detector (atomic number resolution improved) and EDSs and WDSs (higher spectral resolution). Disadvantages of using SEMs included: more expensive instrumentation; relatively more measurement time compared to optical methods; difficulties in discrimination of phase boundaries; non-recognition of minerals with similar BSE intensity and very different chemical composition; no differentiation between polymorphs (minerals with same composition and different crystal structure); and, reduced definition of particle features (since the electron beam often penetrated below the particle surface) [Shouwstra and Smit, 2011].

In the 1980s, statistical reliability required the analysis of at least 1000 particles (or features) and included several point analyses per particle. The most efficient EDS and WDS delivered a single point spectrum in excess of 1 second resulting in long sample analysis times. Three innovative approaches were put forward to resolve this challenge:

i) A microprobe equipped with four WDS's used a line-scan approach [Jones: 1982; 1984]. The system also deployed an automated stage scan (removed analysis subjectivity) [Reid and Zuiderwyk, 1975]. Each WDS was set up for a specific wavelength / element, basing sample mineralogy upon four elements. Sample X-ray acquisition was decreased to ten milliseconds per analysis point.

ii) An analysis based on the BSE gray-level image was used [Petruk, 1988]. When minerals were encountered with similar BSE intensity a microprobe (with EDS) automatically returned to the area to discriminate the mineral phases based upon X-ray information. Sample measurement time was improved by: only using X-ray analysis when needed; and, collection of a single X-ray spectrum from the centroid of each BSE gray scale range.

iii) The QEM-SEM, developed by CSIRO [Frost *et al.*, 1977] could automatically analyze samples once the SEM operating conditions were set. The BSE detector provided an image of the particles which were subsequently mapped point-by-point using an EDS. To speed the analysis, four EDSs were placed close to the sample mount surface (~25 mm) and operated at ten times their normal count rate with only the desired particle features measured (to decrease analysis time). Most of the common minerals were identified in about 25 milliseconds, enabling a 1-2 hour sample analysis for 1000 count spectra on each mineral phase detected. The system could perform the analysis in point, line or area mode with an X-ray collected at each point and the mineral identified / classified during the scan through comparison with a reference library based upon BSE intensity and X-ray spectra. The limitation to this method was reduced energy resolution.

Petruk's method [Petruk, 1988] used the most up to date image analyzer at the time, to reject touching particles and manage particle 'edge effects' (i.e. BSE gray level 'thinned' into resin at particle image edges). The method did not make stereological corrections. Jones' method [Jones, 1982] did not display a full 2-D image (due to line-scan analysis) yet could calculate mineral composition, liberation and particle size distribution. The method addressed the stereological correction by calculating transformations for

defined geometrical shapes (i.e. sphere, ellipsoid). The QEM-SEM method off-line analysis of the image data provided modal abundance, mineral phase surface areas, mineral associations, and particle grain size distributions. Line-scans provided the additional information of particle / grain size distribution, mineral association and liberation. The Petruk area scan while slower, delivered less biased liberation data and particle images than the Jones line-scan approach [Latti and Adair, 2001; Pascoe *et al*., 2007; King and Schneider, 1998; Fandrich *et al*., 1998; Lastra, 2007].

2.7 Automated mineralogy on-going issues

2.7.1 Sample collection and sampling statistics

Mineralogical investigations are performed on small amounts of sample material. As a consequence, the mode of sample collection and sampling statistics are important. For example, the number of 25 mm polished sample mounts (with equal amounts of pyrite and quartz) required to reliably report 1 mg/kg of 10 µm gold grains would be 200 for 50% accuracy [Jones and Cheung, 1988]. The task of sampling must be representative of the bulk chemistry as well as the particle size and textural characteristics.

Sampling methodology to account for representativeness and randomness was developed by Gy [Gy, 1979]. Gy's methodology was linked to mathematical approaches that took into consideration image analysis and stereology [King, 1983 & 1984; Barbery *et al.*, 1983; Gay, 2004].

Sampling waste rock dumps for characterization studies is complicated because the particle size ranges from the coarsest material produced by blasting to the finest material retained after precipitation run-through. Studies recommended that sub-2 mm rock fragments are representative of more than 75% of the waste rock surface area [Price and Kwong, 1997].

The representative samples from the ore deposit or plant must be sub-sampled representatively, and then mounted for SEM (or optical) particle analysis. The blended sample can be sub-sampled by a spinning riffler to produce replicate subsamples with minimal variance. Sample preparation requires a contrast between the mounting medium and the sample particles. For electron beam systems, a chlorinated epoxy resin has proved to be a good mounting medium as the resin BSE intensity was below that of most minerals. The modal abundance of minerals estimated from measurements of the polished sample mounts was unbiased provided the particles were distributed randomly within the sample mount [Latti and Adair, 2001; Pascoe *et al*., 2007; King and Schneider, 1998; Fandrich *et al*., 1998; Lastra, 2007]. Random particle orientation within a sample mount and preventative particle agglomeration were achieved by mixing the sample particles with crushed graphite and epoxy resin [Jackson *et al.*, 1984]. Mineral density differences that affect particle settling rates in the sample mount before the epoxy cured could be addressed through use of a transverse mounting technique (see Appendix 4). Having the analyzed sample particles close to the same size simplified sample preparation and data interpretation [Jones, 1982; Petruk, 1988; Frost *et al*., 1977].

2.7.2 Stereology

Rock texture can be imaged from a carefully prepared and polished sample mount. The texture imaged from automated imaging analysis plays an important role in the 2-D particle image mineral distribution from the conversion of 3-D particle distributions. The major difficulties in interpretation of the particle / phase measurements are: (1) size estimates are biased because the polishing ensures the particle will be equal to or smaller than the true size; (2) the imaged particle shape depends on the particle's orientation within the sample mount; and, (3) poor discrimination between adjacent particles or phases which artificially enlarges the particle.

A stereological model was applied which assumed spherical or ellipsoidal particle shape [Russ, 1986]. The performance of the model to correct stereology was confirmed by comparing the simulated particle size distributions and the mean mineral grade by size class with the corresponding values obtained from measurements of the polished sample mounts of the ground sample [Latti and Adair, 2001]. The stereological model was also confirmed by chemical analysis (such as XRF or AAS), X-ray methods, modal and image analysis.

For a narrow size fraction such as -105/+90 µm, more than 60% of the measured particles are predicted to come from the correct size range [Pascoe *et al.*, 2007]. Area size distributions of the polished sample mounts were used to validate the stereological model [Pascoe *et al.*, 2007]. Previous mineral liberation studies, measured by the line scan approach were found to have higher stereological error than liberation by area measurement [King and Schneider, 1998; Fandrich *et al.,* 1998; Lastra, 2007].

2.7.3 Particle statistics

The automated SEM (MLA) analysis employs fast data acquisition (about 80 analyses per second) and facilitates analysis of large sample populations. The MLA software stage automation steps the electron beam across the sample mount surface at a user-defined pixel resolution, to as low as one pixel, with the pixel size defined by the user-defined horizontal field width or magnification (e.g. sub-micron resolution). At each pixel, the instrument collects a BSE signal and EDS spectrum and correlates them with predetermined mineral definitions developed from the sample material and stored in an X-ray spectra mineral database [Fandrich *et al.*, 2007; Gu, 2003].

There is trade-off between the number of polished sample mounts to get improved particle statistics and the cost / time to obtain the results. Consequently, some automated mineralogy users choose to examine the same number of particles (e.g. 5000) in each of the sample's size fractions. Another approach to analyze ore

concentrates is to only analyze 90% passing 106 microns sample particles, imaging 60,000 particles for the modal abundance mineralogy [personal communications].

More rigorous acceptance criteria for particle statistics are required when studying minor and trace minerals. One approach was to accept 8 grains of metal-associated phases per product-fraction (no consideration of total grain population), whereas another facility required a minimum of 40 detected grains for each phase [personal communications].

The simplest approach to report statistically credible data would be to report the numbers of grains and / or particles and the size of the phase of interest for pertinent mineral phase liberation data as well as the associated pixel statistics from the modal data. Using this information, accompanied by repeat analyses of sample mounts (duplicate and / or triplicate) an error estimate can be achieved.

In automated mineralogy laboratories, particle statistics are not easily forthcoming. Proposed basic statistics are presented below in Table 2.7.3.1. The variation in particle number depends upon the particle size, the quantity of the target phase and the grain size of the target phase. Note that target phase grain size may not be known *before* the analysis.

Table 2.7.3.1. Suggested MLA analysis scheme for particle statistics (VMS ore*).

Size Fraction (microns)	Minimum Number of Particles to Measure	Adjustment to Trace Phase (if *minimum* number *not* reached)
+300	2500	7500
-300/+150	5000	10,000
-150/+75	10,000	20,000
-75/+38	15,000	30,000
-38/+20	10,000	20,000
-20/+11	10,000	20,000
-11/+6	5000	10,000

* Volcanic Massive Sulphide

If the quantity of the phase of interest is high and the ore is simple, the time for the image analysis could be decreased by using half of the suggested minimum number of particles. Table 2.7.3.1 cannot be used as a generic rule-of-thumb when studying porphyry deposits due to the fine grain size of copper minerals, the complexity of copper mineral speciation, and secondary copper mineral formation in hypogene/supergene zones [personal communication]. Furthermore, the table entries could be improved by weighting on the number of phase-specific particles. For example, although elemental data reconciles to the head (i.e. recombination of all size fractions), if the MLA detected 100 pixels of chalcocite which represented 4 grains, repeatability between polished sample mounts makes standard deviation calculations meaningless [personal communication].

2.7.4 Operator and instrument errors

To expose errors made during sample preparation, duplicate or triplicate samples can be analyzed. Precision of the analytical instrument can be tested by repeated analysis of one selected sample.

2.8 Technique options for automated mineralogy

The trend over the last two decades has been to apply semi or fully automated mineral data collection, because of increased speed and characterization efficiency. Several systems have been discussed in the literature, including optical analysis, spectrographic analysis and microscopic approaches [Lane *et al*., 2008; Evans *et al.*, 2011; Fandrich *et al.*, 2007; Pascoe *et al.*, 2007; Hoal *et al.*, 2009].

2.8.1 Digital optical imaging

Optical systems were based upon light reflectance from a polished sample mount. Optical systems are cheap, image collection is fast, and they somewhat automate the task of the mineralogist. However, the optical properties of some minerals are poorly defined due to the phase boundary region, the light source wavelength limited spatial resolution to 0.5 µm [Ofori *et al.*, 2006], and reflectivity is sensitive to the polished mount surface. Both reflected and transmitted light can be applied to the sample with the aid of crossed polarizers for identification of minerals (e.g. quartz from calcite). Optical microscopy data is limited in that often 500-1000 grains represent the total grain population. A review of optical methods emphasized the limitations for complex sulphide ores [Barbery, 1984].

In the last decade optical microscopy has advanced to include photometric, polarizing and micro-chemical techniques [Stanley, 1998; Criddle, 1998; Jones, 1987]. In 1962, reflectance tables were published to add to the mineral identification criteria [International, 1962].

Correct detection of mineral phases in polished sample mounts are hampered by touching particles, non-opaque gangue mineral discrimination from resin (i.e. low reflectance) and mineral reflectance overlap. Digital cameras have improved mineral phase discrimination. The stereological effect is reduced because a large number of particles can be analyzed. The complexity of the mineral content, non-opaque mineral resolution and physical limits to spatial resolution limit the optical approach. Automated optical imaging analysis was successfully demonstrated with gold particles [Oosthuyzen, 1985]. Colour filter wheels have enabled phase segmentation of some previously unresolved similar-spectrum minerals [Lane, 2008].

2.8.2 EMPA

The most mature microbeam analysis, combining the analytical capabilities of the SEM and XRF, is the EMPA [Reed, 1990]. EMPA mapping was developed to characterize samples that were difficult to analyze using traditional SEM techniques. The electron microprobe was first applied in the field of solid state physics in 1950 by Raymond Castaing. The first scanning EMPA, equipped with EDS having spatial resolution of 0.5 µm, analyzed 20 μm^2 in about 14 hours [Jones and Gavrilovic, 1968]. By applying a WDS [Jones and Cheung, 1988] with resolution ~2 µm, 1 cm^2 was analyzed in 56 hours. Data acquisition speed was increased by using BSE scanning to detect specific BSE gray levels and only then applying EDS analysis, delivering a 1 cm^2 scan in 1 hour. CSIRO [Pounceby *et al.*, 2001] used EMPA mapping with image processing on a system equipped with one EDS and 5 WDSs to analyze a 6 mm x 9 mm sample in 13 hours. An advantage of the EMPA is that it can be used to accurately characterize mineral surface elemental composition of solid solutions and fine inclusions. The generally accepted detection limit using WDS is 100 mg/kg [Newbury *et al.*, 1986] though can be reduced by using a longer acquisition (counting) time, such as greater than 100 seconds. Spectral overlaps can be overcome by applying higher or lower accelerating voltages. EMPA with WDS is the most commonly used electron beam technique for quantitative elemental analysis.

2.8.3 XRD

The XRD can identify bulk (crystalline) mineral phases. Every mineral has a unique XRD pattern that is dependent upon the crystal structure [Warren, 1969]. XRD quantification of the mineralogy is most accurate when using the refinement technique created by Rietveld [1969]. Most clay minerals are altered species (substitutions, dislocations, interstratifications) and do not usually produce accurate quantification [Omotoso *et al*., 2006]. Amorphous species are not identified using the XRD [Warren, 1969]]. The Rietveld quantification method requires knowledge in

crystallography and mineralogy. The XRD analysis does not provide mineral size, mineral association or particle images.

Synchrotron XRD (S-XRD) adds to XRD capabilities by enabling the identification of minerals in aqueous systems. This is due to the higher energy beam used to excite the atoms [De Marco *et al.*, 2006]. S-XRD measurements can be performed with high spatial and time resolution because the radiation is at least 10^4 times brighter and counting statistics are 10^6 times faster than the standard XRD [Parise, 2000]. Surface analysis becomes possible because the typical penetration depth of the traditional XRD and S-XRD are 0.1-10 mm and 1-5 nm, respectively [Klug and Alexander, 1974; Zaera, 2012]. There is no particle imaging.

2.8.4 SEM

The electron microscope was first used in biological applications in 1931 by Ernst Ruska [Bogner *et al.*, 2007], before it was applied to mineralogy. Automated mineralogy and its application to liberation analysis has been described by: Andrews and Mika (1975); Steiner (1975); King (1979); Meloy (1984); King (1990); Barbery (1991); King and Schneider (1998); Fandrich *et al.* (2007); and, Michelic *et al.* (2011).

SEM mineralogical techniques are most commonly applied to particulate samples (i.e. less than 1 mm in length). SEM has been used to analyze large particles with fine mineral inclusions and phases with BSE intensity below that of the resin. Typically spatial resolution is affected by the electron beam interaction volume which can penetrate 1-5 µm below the polished mount surface. The generation of mineral maps from an SEM image currently require substantial human, generally up to about an hour per sample.

New sample preparation, mounting and measurement methods to address the imaging, particle statistics and analysis time have been developed [Hoal *et al*., 2009; Lastra,

2007; van der Waal and Kruesemann, 2011]. Mineral BSE intensity discrimination improved and the more complex particles were identified by X-ray analysis. BSE detector improvements enabled discrimination of mineral phases (in an epoxy mount) corresponding to an average atomic number of about 0.5 (i.e. about five BSE gray scale units) [King and Schneider, 1998]. Stereological correction techniques for both linear and area-based analysis were developed [King and Schneider, 1998]. Typical SEM filament lifetime was extended from days to months in order to address additional time requirements for multiple sample analyses. Successive measurement of large sample batches lead to the development of large automated stages with multiple sample holders.

Automated systems in current use include JKMRC's MLA (Mineral Liberation Analyzer) [Gu: 2003, 2004] and Intellection's QEMSCAN (Quantitative Evaluation of Mineralogy by SCANning electron microscopy) [Gottlieb *et al.*, 2000]. Improvements in the systems have been described [van der Waal and Kruesemann, 2011].

Currently, the main users of automated mineralogy are mining company laboratories, mineral processing research institutes and service providers. There is a recent advance into plant-based technology, such as the FEI bench top MLA EXpress, to provide real-time data to plant operations [FEI, 2012].

2.8.5 Time of Flight – Secondary Ion / Mass Spectrometer (ToF-SI/MS)

Secondary ion mass spectrometry (SI/MS) is a well-established technique that was originally designed for the analysis of organic materials. The technique was extended to geological materials [MacRae, 1995]. SI/MS analyzes the composition of solid surfaces and thin films using an ion beam to excite atoms on the surface which then eject secondary ions from a depth of 1-2 nm [MacRae, 1995].

Quantitative data with a calibration standard series composed of a matrix similar to the sample can provide detection limit 0.2-0.3 mg/kg; however, it cannot be used for the major element or non-sulphide minerals [Adriaens *et al*., 1999; VanVaeck *et al*., 1999]. Disadvantages of ToF-SI/MS include: matrix effects (surface artifacts); only ejected ions are measured (not the higher presence neutral species); excessive charging of insulating materials, which includes gangue minerals (e.g. silicates, carbonates); and, optical limitations which make it a challenge to locate particle-grains. ToF-SI/MS records the sub-micron full mass spectrum mapping within every pixel. Elemental detection limits range to as low as 0.001 mg/kg [Vickerman and Briggs, 2001].

2.8.6 Synchrotron X-ray Fluorescence (S-XRF), Extended X-ray Absorption Fine Structure (EXAFS) and X-ray Absorption Near-Edge Structure (XANES)

Synchrotron spectrometric methods use high energy to characterize minerals. Methods include X-ray fluorescence (S-XRF) and extended X-ray absorption fine structure (EXAFS) and X-ray absorption near-edge structure (XANES) analysis [Majuste *et al.*, 2013]. X-ray fluorescence (XRF) is well established for quantitative elemental analysis though has high detection limits of 10-100 mg/kg. With the use of the higher energy synchrotron, the spatial resolution is about 2 μm and the detection limit is greatly improved to 0.01-0.1 mg/kg. While elemental composition can be determined to low concentration levels, there is no accompanying particle image. X-ray absorption analysis looks at three energy regions of a particle: the edge; the near edge XANES (provides information on the geometry of the local structure), and the extended edge EXAFS (provides local structure information). Synchrotron technology is extremely expensive and requires a large footprint, limiting its commercial viability.

2.8.7 Laser Ablation – Inductively Coupled Plasma / Mass Spectrometer (LA-ICP/MS)

Accompanied by laser ablation, the inductively coupled plasma mass spectrometer (ICP/MS) is in general use [Becker and Dietze, 1999]. LA-ICP/MS can report bulk sample analysis with a beam / spot size of greater than 100 µm and can perform microprobe analysis if the spot size is less than 100 µm. The detection limit is dependent upon the ablation volume and elemental counting time [Gunther *et al.*, 1999]. Bulk analysis will deliver a lower detection limit as it does not require higher spatial resolution for the microprobe analysis approach. This technique can have spatial resolution of 0.5~50 µm and has detection limits of low to sub mg/kg values. Minimal sample preparation (no wet chemistry) and quick turnaround time make it attractive. The method cannot provide elemental maps of a particle due to single-point analysis [Becker and Dietze, 1999].

2.8.8 Proton Induced X-ray Emission (PIXE)

PIXE is a well-established non-destructive technique that can perform simultaneous trace multi-element analysis [Remond et al., 1987]. PIXE can be used as an imaging technique with poor detection limits. Alternatively it can be used to detect low elemental concentrations. PIXE (with proton beam 5-20 µm) can provide 3-30x better detection limit than the EMPA (with beam size 1-10 µm) providing 100-400 mg/kg detection limit. X-ray spectral overlap interferences impede detection mainly because electrons are much more intense than the protons. PIXE can be used for elemental mapping [Remond *et al.*, 1987].

2.8.9 X-ray Photoelectron Spectroscopy (XPS)

XPS can deliver elemental composition of a solid surface within the top 4-10 nm [Van der Heide, 2011] for particle sizes too small for XRD analysis. This feature is beneficial

to elemental composition determination of amorphous materials. There is no imaging available with this technique.

2.8.10 High Resolution X-ray MicroTomography (HRXMT)

The application of X-ray microtomography to mineralogy is new. HRXMT enables 3-D reconstruction of the sample [Garcia *et al.*, 2009]. The computerized reconstruction is based on summation of *voxels* (volume elements) to form a spatial description of the sample with a resolution of ~1 µm. The identification of trace MOIs in the range of mg/kg will require examination of a large number of samples to provide accurate and reliable data [Garcia *et al.*, 2009].

The advancement of 3-D geometric imaging with HRXMT produces 3-D images of the internal structure of a particle sample with ~1 μm^3 voxel resolution for a mineral structure of 10 μm^3 size [Miller and Lin, 2004, 2009]. HRXMT is a non-destructive non-invasive technique capable of generating 3-D particle images from 1000 million voxel sample size. A full HRXMT analysis takes a few hours for 5 µm spatial resolution to half day for 1 µm resolution.

2.9 Automated quantitative electron microscopy

There are advantages and disadvantages with the many techniques described above to the application of automated quantitative mineralogy. The approach can make use of many techniques and methodologies.

The diagnostic SL is an excellent technique to separate the various reactive components of the sample. The SL technique cannot deliver a quantitative result for trace mineral phases because analytes may redistribute during each step of the SL. The SEM can perform high-resolution imaging of rock and particle surfaces. The advantages of SEM over light microscopy include higher magnification (more than 100,000 times)

and greater depth of field (more than 100 times). The automated SEM data does not rely on operator input, such as: (1) user does not hunt-and-peck for MOI to include in the study; and, (2) delivers the same mineral information for economic (i.e. valued) and gangue mineralogy. Optical, XRD and SEM methods can be time consuming and labour-intensive, and usually generate semi-quantitative results from data sets that are too small to be statistically useful. Commercial automated SEM systems, such as JKMRC's MLA and Intellection's QEMSCAN, increase the speed and accuracy of particle liberation analysis, and deliver better particle statistics.

The current technique of choice in process mineralogy studies is either the MLA or QEMSCAN [van der Wal and Kruesemann, 2011]. A process mineralogy program should include geology, sampling, hardness, mineralogy, and mineral processing [Lotter *et al.,* 2011] as well as mineralogy. The quality and usefulness of the mineralogical data being produced by the MLA and QEMSCAN has been demonstrated in the field of ore characterization [van der Wal and Kruesemann, 2011]. The application of these techniques into the environmental realm is new.

In this study, waste rock was characterized using the automated quantitative MLA system [see Appendices 2 and 4]. The MLA rapidly scanned the sample, collected particle images, and then analyzed them to obtain elemental information with relative detection limits of less than half a mass-percent. The MLA can deliver up to sixteen sample analyses overnight without an operator. This approach, while applied to waste rock, could equally be applied to heap leaching and tailings dumps. Outcomes of this study will indicate the usefulness of the MLA for waste rock characterization.

2.10 Summary

Automated quantitative electron microscopy brings together a range of technologies. Energy dispersive X-ray spectrometers (on the market for 40 years) can detect elements down to low atomic number boron simultaneously. Scanning electron

microscopes (known to be stable analysis platforms) have significantly improved in their ease of use. The MLA and QEMSCAN methods can accurately conduct about 10,000 pixel analyses per minute with low detection limits, such 1 mg/kg, with the ability to analyze 50,000 or more particles for tailings or low-grade materials in about an hour. These systems can analyze up to 16 different samples overnight without the need of an operator, and rapidly identify and quantify minerals in polished sample mounts with such mineral features as abundance, grain size and liberation distributions [Gotlieb *et al.*, 2000; Gu, 2003; Fandrich *et al.*, 2007; van der Waal and Kruesemann, 2011].

Automated mineralogy supplements classical analysis techniques, such as optical microscopy, semi-automated or computer-controlled SEM, XRD, XRF and EMPA. Comparison of the MLA to the classical techniques shows:

- Particle by particle analysis, not just bulk analysis.
- Objective image capture, rather than subjective operator image capture.
- Quantitative and qualitative data, not just qualitative data.
- Data and particle images recorded in digital format, rather than just data.
- Result formats include tabulated, graphical and pixel images, not just tabulated.

The MLA technology provides a micro level view, though the software can provide a macro view to show the complete sample mount surface scanned. The key attribute to automated mineralogy data are the graphical images. Data quality relies on the image quality, which in turn relies on high quality sample preparation and modern analytical and imaging software.

Some attractive reasons why current automated mineralogical techniques will continue to improve while new ones are being developed:

- Operator independent analysis.
- Objective data and analysis output (i.e. without human operator bias).
- Computers enable fast image processing.

- Large numbers of statistically reliable measurements on large numbers of particles.

In summary, automatic quantitative mineralogical techniques allow more analyses with higher accuracy while minimizing human resources. In the near future, it will be possible to routinely generate large numbers of three-dimensional images by HRXMT. Mineral identification through tomography may not be as precise as that available from optical microscopy or SEM, but the 3-D nature of the images will advance automated mineralogy.

In the end, the analyst must stay informed of the latest application developments of each technique. A fundamental understanding of what is being measured in the sample and how the technique performs the measurement are essential to putting the mineralogical data into its proper context for successful interpretation. Finding a concise balance between the large amounts of data collected and the right amount of data to highlight is not a simple task. Without a thorough understanding of the project issue(s), irrelevant information could easily be provided or conversely, relevant information might be unknowingly withheld. Decisions must be made on sampling technique, sample preparation technique, analytical approach, data processing and data reporting. Quality reporting can only occur if quality assurance / quality control was planned for each stage of the project.

CHAPTER 3 Experimental program

3.1 Sampling

The samples for this thesis work were collected after considerable discussion and review of sampling practices (see section 2.7.1). In an overall mineralogical sense, rock fragments can range from tiny to very large (e.g. greater than 10 cm). If the fragment has an enclosed reactive metal-bearing mineral phase and is fractured, degradation could occur inside the particle. With this in mind it should be acceptable to crush the larger rock fragments in order to expose the results of weathering chemistry.

Price and Kwong (1997) examined -100 mm rock fragments taken from the top 1 meter of the mine site dump. The rock fragments were sorted into size fractions, -100 / +19 mm, -19 / +11 mm, -11 / +2 mm, -2 mm / +50 µm and -50 µm, then each fraction subjected to paste pH, carbonate NP, Sobek NP and sulphide-sulphur determinations. Although the results showed variations with particle size, the authors concluded "…the data provided illustrated: differences in the composition of different particle size fractions, the inadequacy of a whole sample assay as a means of characterizing weathering, and the importance of separately analyzing a fine particle size fraction (less than 2 mm) when evaluating weathering effects". The investigators noted that the sub-2 mm fraction of their samples represented 10 to 30% of the sample mass. In another study, Price [1997] noted that most laboratory (i.e. static) analyses do not distinguish between liberated and unliberated mineral species. Price recommended that in the absence of site-specific data that specified liberation size, the sub-2 mm fraction of waste rock should be considered the reactive fraction in ARD prediction studies. In western Canada a widely used approximation for the reactive portion of waste rock dumps is 10 to 20% of the entire dump site, based on observations from the sub-2 mm material [Price, 1997]. In another report Murray [1997] gave an average of 15 to 25% for reactive waste rock with a range of 0 to 35% based on Canadian precious and base metal mines. Based upon elemental assay data it may be possible to justify elimination

of coarse fractions (e.g. greater than 2 mm) and only examine the sub-2 mm material because it contains more than 75% of the exposed surface area. Greater surface area equates to more mineral surface available for chemical and biological weathering.

Some sampling weaknesses to consider:

- Sampling technique may not provide representative samples of the bulk stockpiles due to the massive expanse and variability of the waste rock piles, even after consideration has been given to all precautionary measures.
- Field cells may not mimic the waste rock dump due to unnaturally high rock contact and / or the reaction products may / may not be flushed away.
- Inadequate post-sampling stabilization and storage may allow samples to become weathered (i.e. compromised) prior to analysis.

Because quality / credible data is subject to sampling and analyses' methods and procedures, good practices must be followed for representative sampling The rock fragment samples collected for this study were stage-crushed to sub-1.19 mm (if too large for SEM examination) and then the crushed material sized and blended to produce a representative homogeneous sample. The sample was subsampled by rotary riffler to produce replicate samples for mineralogical and elemental assessment. Particle sizing the sample refines the mineralogical assessment by creating subdivision within the particles to further amplify mineralogical differences (e.g. texture, alteration). The elemental assessment would enable metal content correlation to the different waste rock behaviours.

3.2 Sample description

The Antamina mine waste rock materials submitted for MLA mineral characterization were used to determine the applicability of the MLA to both unweathered and weathered waste rock studies. The applicability was evaluated through the measurement of mineralogical features important to waste rock weathering. It should be noted that the

samples, excluding those of Table 3.2.2, were unweathered waste rock. Table 3.2.4 samples were split and a portion of each sample subjected to a sequential leach [Klein *et al.*, 2011].

Table 3.2.1. Pile segment description.

Field cell[1]	Wasterock Type	Phase of Pile Creation	Alteration	Mineralization
FC-0	Class B; black marble	Protective layer (Pile#1)	1% surface oxidation; <1% calcite vein	0.5% v.fine disseminated pyrite
FC-1	Class B; diopside marble	1st tipping phase (Pile#1)	1% surface oxidation; <1% secondary Cu mineral (malachite)	<1% fine disseminated pyrite
FC-2	Class B; diopside marble	2nd tipping phase (Pile#1)	2% surface oxidation; <1% secondary Cu mineral (chrysocolla); <1% calcite vein with pyrite	2-3% coarse disseminated cubic pyrite with trace chalcopyrite, sphalerite, galena
FC-3	Class B; diopside marble	3rd tipping phase (Pile#1)	<1% surface oxidation; <1% calcite vein with pyrite	<1% fine disseminated pyrite with trace chalcopyrite, sphalerite
FC-4	Class B; gray hornfels	3rd & 4th tipping phase (Pile#1)	<1% surface oxidation; <1% calcite vein	1% v. fine disseminated pyrite

[1] Material from different locations in the open pit was provided in size fractions: -1190 µm / +600 µm, -600 µm / +300 µm, -300 µm / +150 µm, -150 µm / +106 µm, -106 µm / +75 µm, -75 µm / +53 µm; particles greater than 1.2 mm and less than ~15 µm were not analyzed by MLA.

Samples submitted for this study included blasted rock and drill core. One set of blasted rock samples (see Table 3.2.1) was collected by hand from different locations in the open pit, all rock fragments no larger than 10 cm and all rock material representative of that used in both experimental Pile#1 and field cell construction. One set of blasted rock samples (see Table 3.2.2) was hand collected from the base of weathered (~2 year-old)

field cells. Drill core samples (see Table 3.2.3) were taken from particular depths / elevations in the waste rock dumps, with half of the core (lengthwise) used in this study. One set of blasted waste rock samples (see Table 3.2.4) was collected using a shovel with all rock fragments generally less than 10 cm.

Table 3.2.1 describes blasted waste rock from the Antamina field cell experiments which were sized into 12 size fractions ranging from 10 cm to 53 µm (270 mesh), though only 9 size fractions (i.e. sub-1190 µm to 53µm) were used in the MLA analysis. These rock samples were to be considered as fresh unweathered rock surface.

Table 3.2.2. Field cell "sand" description.

Field Cell	Wasterock Type	"Sand" Particle Size[1]	Mineralization
Cell 5	Class A (high range); Intrusive	34% less than 1119 µm	Pure monzonite; feldspar (quartz veins with minor biotite), silicates
Cell 6	Marginal-grade Cu Ore	43% less than 1119 µm	Pink endoskarn, some Intrusive; fine calcite in matrix
Cell 7	Class A (average range); Endoskarn	46% less than 1119 µm	Pink endoskarn, some Intrusive; calcite in matrix; leachate: ~50mg/L
Cell 8	Class A; Hornfels	24% less than 1119 µm	Typical gray hornfels; scattered pyrite-pyrrhotite, oxidation in fractures
Cell 14	Class B; Marble	25% less than 1119 µm	Combination of marble, marble-diopside, gray marble, white marble; scattered pyrite-pyrrhotite, calcite veins, Mg Oxides rare

[1] Material was sized: -2000 µm / +850 µm, -850 µm / +297 µm, -297 µm / +147 µm, -147 µm / +53 µm, -53 µm / +44 µm, -44 µm.

Table 3.2.2 lists "sand" samples which were collected from drain-holes in the bottom of five separate field cells that contained blasted waste rock. The samples were studied to determine the immobilization of metals such as Mo. UBC laboratory tests were conducted using a riffled portion of this "sand" to study Mo attenuation mechanisms (e.g. precipitation, adsorption). The lab tests used fine marble particles (e.g. less than

125 µm) mixed with aqueous solutions containing Mo^{+2}, Cu^{+2}, Zn^{+2}, Pb^{+2} and sulphate (SO_4^{-2}) salts [Conlan *et al.,* 2012].

Table 3.2.3. Drill core description.

Drill Core	Wasterock Type	Particle Size (µm)[1]	Mineralization
A1018 (17.25m)	Class C; marble	-1190/+53	Light-gray lime-marble; white, light-green and dark-gray mineralization; red-brown oxidation phases
A951 (176.00m)	Class B; marble	-1190/+53	Light-gray banded lime-marble; white and brown mineralization
A431 (306.00m)	Class A; marble	-1190/+53	Gray banded lime-marble; dark-gray, white and brown mineralization; reddish-brown oxidation phases
A355 (70.50m)	Class B; hornfels	-1190/+53	Whitish-gray hornfels; mineralized veining contains dark-gray, brown, gray and grayish-white phases
A355 (160.50m)	Class C; hornfels	-1190/+53	Whitish-gray hornfels
A162A (97.50m)	Class A; hornfels	-1190/+53	Whitish-gray hornfels; banded layers containing grayish-black and greenish-gold mineralization

[1] Material was provided in size fractions: -1190 µm / +600 µm, -600 µm / +300 µm, -300 µm / +150 µm, -150 µm / +106 µm, -106 µm / +75 µm, -75 µm / +53 µm.

Drill core samples from Table 3.2.3 were used to study waste rock zones thought to be the more reactive marble and hornfels units in an effort to form a link between mineralogy (e.g. grain size, texture, primary and secondary mineralization) and results of a new diagnostic SL that could indicate potential weathering behaviour (see Table 2.4.1). In Table 3.2.3 are shown the supplied six 47.25 mm diameter drill core intervals for study. They were sized and proportioned for chemical assay and MLA analysis (i.e. 9 size fractions, with a top size of 600 µm).

Table 3.2.4 samples were used to test a new diagnostic SL procedure which would help to improve waste rock classification at the mine site in real time. Samples submitted for analysis were unweathered waste rock (head) and diagnostic sequential leach residue (SLR).

Table 3.2.4. Pile and field cell description.

Field Cell[1]	Wasterock Type	Acid Potential*	Description[3]	Leachate Metal Content
Tucush 01	Class B; marble/hornfels	-	Coarse pieces	High Zn, Cu
Tucush 03	Class A; marble/hornfels	Non-AG	Coarse sand	Low Zn (13 g Zn/kg)
Tucush 04[2]	Class C; marble/ hornfels	Non-AG	Fine-coarse sand	Low Zn (0.035 g Zn/kg)
Cell 6	Marginal-grade Cu ore	Non-AG; finite source of acidity (NP)	Fine-coarse sand	High Mo (2.8 g Mo/kg); sulphates
UBC3-2A	Class A; exoskarn	PAG	Coarse sand	High Zn, Cu (24 g Zn/kg, 12 g Cu/kg)
UBC2-3A	Class A; intrusive	PAG	Coarse sand	High Cu (8 g Cu/kg)
Cell 21	Class C; marble	-	Coarse pieces; enough NP buffer capacity	High As (0.092 g As/kg)
Cell 24	Class B; marble	-	Coarse (14 pieces)	High As (0.026 g As/kg)

* AG = acid generating; PAG = potentially acid generating; NP = neutralization potential

[1] Head sample and Sequential Leach Residue (SLR) sample

[2] Head sample, no SLR sample

[3] Material was provided in size fractions: -25400 µm / +4800 µm, -4800 µm / +1200 µm, -1200 µm / +600 µm, -600 µm / +297 µm, -297 µm / +105 µm, -105 µm / +53 µm, -53 µm.

3.3 Sample preparation for analysis

An unbiased laboratory classification was required to ensure the design of the various experimental piles and field cells used material consistent with the plan. Overall, the Antamina Geology classification was found to be acceptable [Golder, 2010; Antamina, 2001] with few exceptions. For example, a report [Golder, 2010] of the field cell material [Table 3.2.4] showed: Cell 21 was visually designated Class C waste rock by Antamina Geology classification, but was considered Class A after performing a subsample chemical assay; Cell 24 was visually designated Class B waste rock by Antamina Geology classification, but considered Class C after performing a subsample chemical assay; Cell 6 was visually designated Class B marginal-grade Cu by Antamina Geology classification (classified as non-AG meaning little sulphide leaching, little NP and

contained the lowest Zn content) yet might be better classified as Class A. The Antamina mine geologists generally do an excellent job when classifying waste rock.

Random sampling of the screened fraction material was achieved using a micro-rotary riffler. A riffled portion from each screen fraction was submitted for various chemical elemental assays. Generally, elemental concentrations were determined by ICP-AES (atomic emission spectroscopy) analysis for 33 trace metals, total sulphur by Leco furnace, and sulphide sulphur by four acid digest. In the case of Table 3.2.4, if minimal SLR sample was available, no MLA analysis was performed (i.e. chemical analysis only) and if minimal Head sample was available, no chemical analysis was performed (i.e. MLA analysis only).

For all samples a riffled representative portion of the -1.19 mm material was dry-screened into several size fractions. The sieve-screens were reported to have been inspected carefully before use to avoid sample cross-contamination. The particle size fractions used in this study are listed in Tables 3.2.1 through 3.2.4. Note that the majority of the material in each sample was coarse and often represented more than 98% of the entire sample mass (e.g. greater than 2 mm).

Considerations during sample preparation:

- Submitted samples were wet when collected at the mine site. The material was reported to have been dried at ambient low temperatures (~20-22°C) in a ‘dust-free’ location. This was to reduce the potential alteration of MOIs and prevent agglomeration formation (i.e. ‘cementing’ particles together). It was important not to alter the condition of the mineral phases - especially those which could be fragile.
- Samples may contain water-soluble minerals. Although wet-screening provides a more accurate separation of the particle sizes, it may cause the loss of some water-soluble mineral species. For this reason, samples were dry screened / sieved into size fractions. All samples were dry-screened into + / -2 mm fractions based upon the method of Goldberg et al [Goldberg *et al.,* 1996].

- The samples were prepared for MLA analysis ‘as received’ meaning the samples were already dry-screened and separated into size fractions. Some samples required stage-crushing to 100%-passing 1190 µm if rock fragments were too large for MLA analysis. For example, the drill core (Table 3.2.3) was stage-crushed before screening to 100% passing 2.54 mm. The stage-crushed samples were accompanied by the conditional understanding that modal abundance data would be quantitative, while liberation, association and MOI-metal locking (i.e. exposure, availability) would be semi-quantitative.

MLA liberation analysis involves particle mounting, polishing and carbon-coating of a cylindrical epoxy resin molded shape (see details in Appendix 4). MLA analysis sample considerations:

- Typically it is preferable for particle sizes in each mount to be in a narrow size range because the MLA is not very effective at simultaneously resolving both fine and coarse particles due to complexities of magnification (i.e. horizontal field width) and accelerating voltage, which was also discussed in Section 2.7.
- Packing density of the epoxy mount was not explored in this study though it is generally considered that a particle packing density of 40-60% in epoxy resin is acceptable to achieve optimal analysis conditions.
- Grains less than ~1 µm were not measured directly and the minimum particle area captured was ~4 μm^2. The beam excitation volume was considered to be an encumbrance to acquiring good images of the smaller grains using the magnifications adopted for this study.

CHAPTER 4 Mineral Liberation Analyzer analysis parameters applicable to waste rock characterization

4.1 Introduction

Quality management of MLA technology is important because incorrect data most often results in incorrect decisions for mine site management. Overall internal risks to the validity of the data produced by automated mineralogical instruments are related to changes in hardware, software, techniques, operators, and key user files (i.e. data manipulation). The hardware, software and operators are not changeable, which leaves techniques and user files that could be changed. The user files will be examined in view of elemental reconciliation. MLA techniques comprise many facets - some will be discussed here.

In this MLA study, the sample size fractions were examined without further manipulation of sample, with the exception that if sample material was greater than 1.19 mm it was stage-crushed to 100% passing 1.19 mm (see Section 3.3). Any samples subjected to stage-crushing could still report semi-quantitative mineral association data along with modal mineralogy and grain size distribution.

This chapter will discuss mineralogical features important to weathering, extracted from MLA analysis of Antamina mine waste rock samples. This chapter will also discuss potential MLA operating parameters for waste rock characterization and propose suitable parameters.

4.2 Relevant mineralogical features of weathering waste rock particles

Waste rock piles are a complex blend of reactions such as sulphide oxidation which produces a variety of secondary mineral phase features. Knowledge of the distribution

of the features within the waste rock pile will assist in understanding and predicting metal release mechanisms.

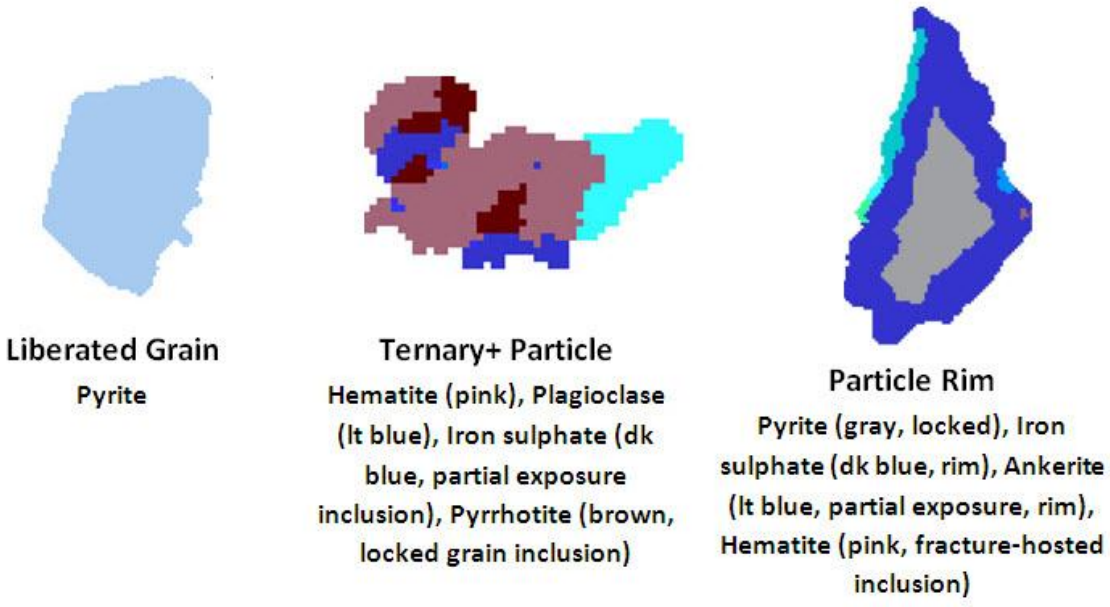

Figure 4.2.1. Examples of weathering particle terminology: MLA digitized particles.

A brief explanation of particle weathering features and oxidation terminology follows with examples of MLA digitized particle images in Figure 4.2.1:

- Grain – feature composed of a single MOI.
- Liberated grain – MOI grain not attached to any other MOI grain (i.e. free).
- Particle – fragment of rock containing at least one MOI.
- Inclusion – MOI grain partially or wholly encompassed within a larger MOI particle. *Partially encompassed*, such that grain has some surface exposure or availability. *Wholly encompassed or locked*, such that there is no exposure to the particle surface. *Grain boundary inclusion*, such that the grain lies on the boundary between two different MOIs. *Fracture-hosted grain inclusion*, such that the grain lies in contact with fractures that lead to the particle surface.
- Rimming – MOI is altered along part or whole of particle perimeter / surface.

- Middling – intergrowth or blend of at least two different MOIs. The inclusion can be numerous and complex.
- Binary particle – two different MOIs in contact with each other.
- Ternary+ particle – at least three different MOIs in contact with each other.

Through the course of this study, many particles and their mineral phases and textures were observed. The following mineralogical features are considered important to metal-bearing particle weathering processes at most waste rock dump sites:

- The presence of sulphide minerals and / or metal-bearing mineral phases.
- Leachability of sulphides in sulphuric acid and / or ferric iron environment.
- Mineralogy in terms of the importance of sulphide-sulphide systems that exhibit strong galvanic interactions under leaching conditions.

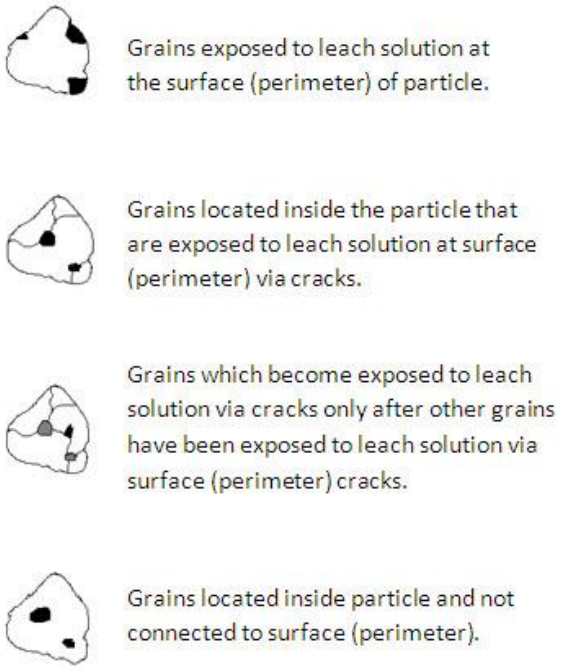

Figure 4.2.2. Description of leachability in terms of locking.

- Quantification of secondary metal-bearing mineral phases:
    - Modal mineralogy (type and abundance of mineral phases present within each particle).
    - Grain (size and shape distribution; surface area and potential reactivity; particle textural (can supply localized areas on, or in, the particle for reaction to environmental conditions)).
    - Association (grains classified according to accessibility to adjacent minerals with which they may co-react (e.g. galvanic interaction, such as ferric sulphate and arsenopyrite or chalcopyrite and covellite)).
    - Locking (grains classified according to availability / exposure to leach solution (see Figure 4.2.2)).
    - Cracks and pores (not quantified in this study, though clearly important as a route for initial leach solution contact and leach solution transport).
    - Coatings (secondary mineralization can passivate the particle surface (e.g. calcium oxide precipitation on calcite) or act as a porous bridge between mineral phases to promote galvanic interaction (e.g. ferric ion precipitation on sphalerite)).

4.3 Mineral Liberation Analyzer imaging and image analysis

The Mineral Liberation Analyzer (MLA) is an automated system that integrates image analysis with SEM and EDS. The following describes the operation of the system.

4.3.1 Image acquisition and analysis

Imaging and image analysis, fundamental to mineral liberation analysis, is commonly used to evaluate mineral phases [ASM International, 2000; Russ, 2002]. The low noise, high resolution image (stable BSE signal) and 0.5 µm spatial resolution enable the MLA, advanced image analysis techniques to accurately discriminate mineral phases within a particle.

The principal MLA image analysis functions used during data collection are: background removal; particle de-agglomeration; and, phase segmentation. An important image analysis consideration is stereology [Spencer and Sutherland, 2000; see Section 2.7.2]. Stereology in the context of image analysis is extracting quantitative information about 3-D properties from 2-D planar sections. Stereology is a completely different approach from computed tomography (HRXMT) which reconstructs the complete internal 3-D object (see Section 2.8.10). The MLA algorithm's typical approach is to assume that all particles are spherical. The MLA image analysis software records the 2-D image of the 3-D particle. Subsequently the particle shape algorithm computes a circle and rectangle ratio based upon standard industry algorithms which 'fit a circle' and / or 'fit a rectangle' over the particle. These 'fit' ratios are applied to the image to automate a deagglomeration routine to digitally break up designated agglomerates (according to user defined criteria).

The MLA analysis proceeds through the software components shown in Figure 4.3.1.1. The basis for all quantitative operations is the measurement. The Measure software controls SEM operation and EDS X-ray spectrum collection. X-ray spectra and mineral phases are managed through ParticleX, XSTD and MineralDatabaseMaker. ImageProcessTool manipulates the digitized particle images. Each pixel of the particle image is assigned an array of MOI properties, such as X-ray spectrum, density, size, association and availability. Dataview collates the digitized image information, with the ability to present the information in both numerical and graphical formats.

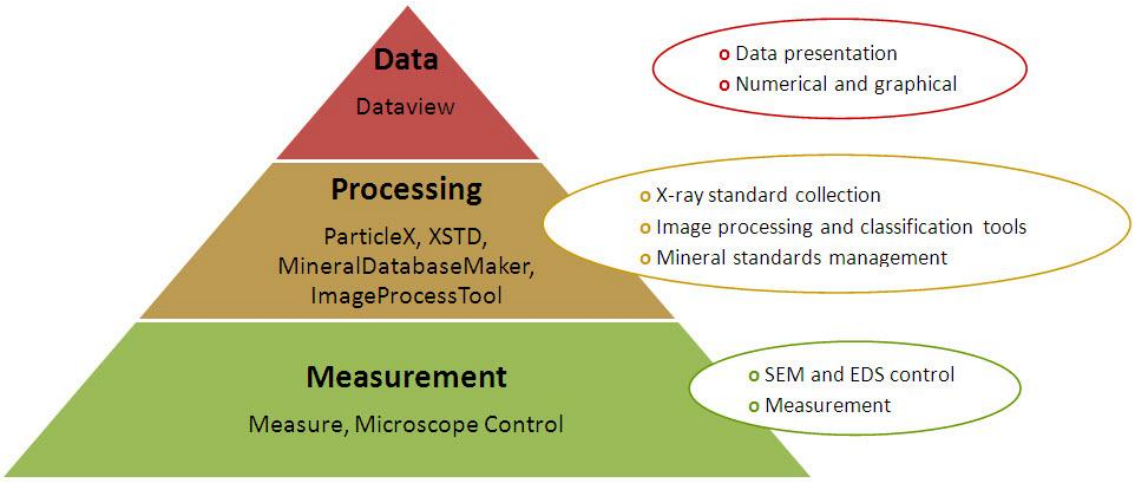

Figure 4.3.1.1. Mineral Liberation Analyzer data flow.

In Figure 4.3.1.2 is shown the graphic output from MLA software during a sample analysis.

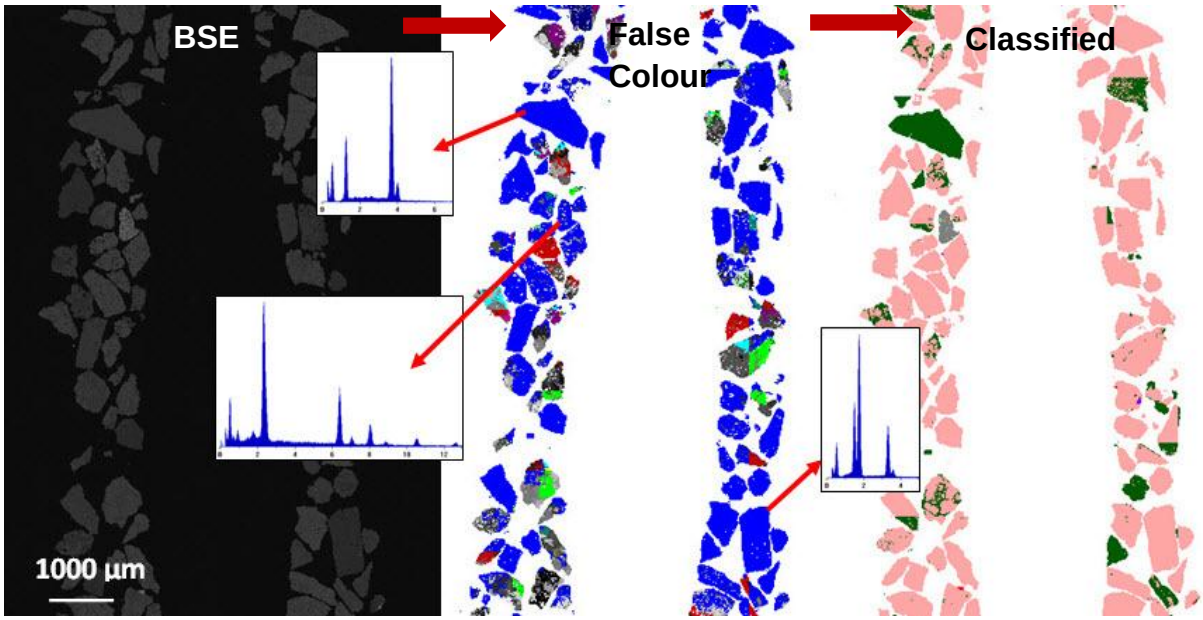

Figure 4.3.1.2. Typical (twin) transverse mount (with the highest density (e.g. brightest and / or heaviest) particles mounted nearest the center of the mount (FC-2, -1190 / +600 µm, mosaic frame-merge). ParticleX separates particles, delineates each detected phase to which is attached an X-ray spectrum. ImageProcessTool collates the particle data [colour: red = pyrite; blue = copper phases; green = carbonates; gray = oxides; pink = silicates].

The BSE image undergoes background extraction, then particle segmentation and EDS X-ray analysis of each particle segment to produce a false-colour image. Each segmented area of the particle which would represent at least one pixel will have associated with it a false-colour and X-ray spectrum (see Figure 4.3.1.3).

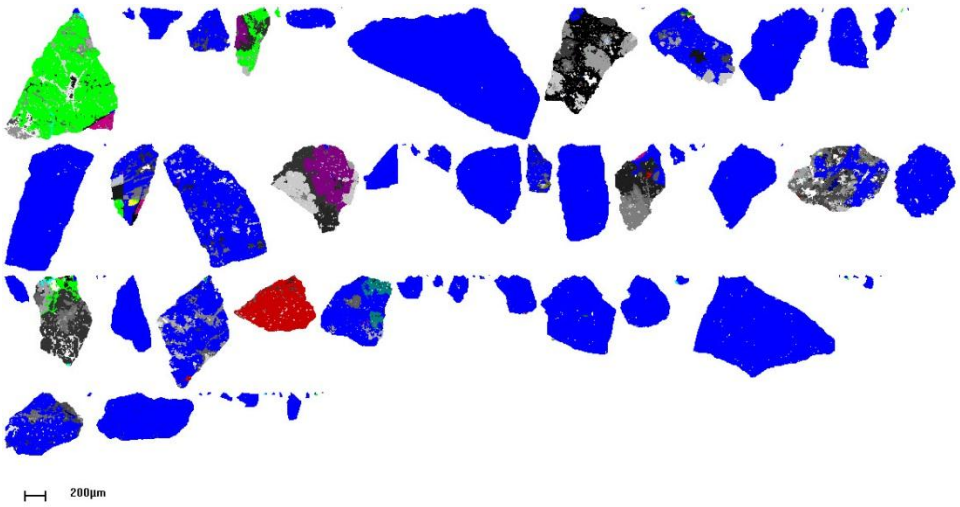

Figure 4.3.1.3. Typical particle line-up of false-colour segmented particles (FC-2, -1190/+600 µm, mosaic frame-merge).

At each (user-defined) pixel, the EDS spectrum is correlated with a user-developed library of mineral definitions which are specific to the samples. Each pixel is then assigned (classified) a mineral name based on the elemental spectral data from the database. Mineral identification by X-ray analysis requires a library of high quality EDS spectra**.** Creating the local mineral library database directly from the sample is not mandatory (i.e. could use a generic mineral database) though: (1) ensures MLA measurement conditions are consistent with the MOI database; (2) elemental composition reflects sample rock chemistry.

The MLA software does provide tools to correct misclassified phases, however this aspect was not explored in this study because multiple inspections (i.e. thousands)

indicated more than 97% correct phase assignment. Most incorrect classifications belonged to tiny grains of non-sulphide mineral.

The classified particle mage (Figure 4.3.1.4) and its associated MOI data are the basis for all further quantitative analysis through the DataView software. The BSE digitized image data and its associated MOI data, such as grain size, shape factors, association and liberation can be displayed by the DataView software numerically and graphically. DataView is the data presentation software that enables the user to store, examine, process and present qualitative and quantitative mineralogical data generated from MLA measurement analysis. Presentation data include (not exhaustive list): modal mineralogy, calculated assay, elemental distributions, particle and mineral grain size distributions, particle density distributions, mineral associations and locking (i.e. availability), phase specific surface area (PSSA) and mineral liberation by particle composition and free surface.

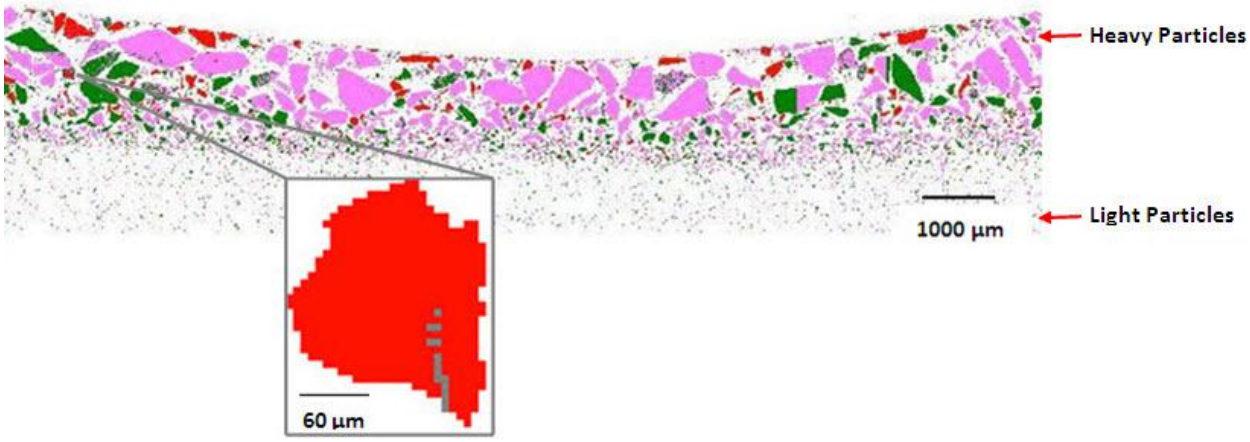

Figure 4.3.1.4. Image of MLA phase-classified particle map [Tucush-01, -1190/+600 µm size fraction): mosaic frame-merge – after classified, grouped, and re-coloured [colour: red = pyrite; blue = copper phases; green = carbonates; gray = oxides; pink = silicates].

Details of the spectrum identification process can be found in Appendix 4.

4.3.2 Analysis Modes

The MLA offers a number of measurement modes that implement the fundamental BSE image and corresponding X-ray analysis to meet different mineralogical information requirements. The five modes of MLA analysis considered for this study were:

1. Extended BSE mode (XBSE) implements area or point X-ray analysis to efficiently and effectively analyze mineralogical samples containing MOIs with sufficient BSE contrast to generate effective segmentation. The high resolution BSE imaging of grain boundaries and speed of X-ray mineral identification make this method ideal for most mineralogical samples. A specific (i.e. local) mineral classification standard was developed for the waste rock using SEM and EDS. The digitized, segmented BSE image triggered the collection of a single point (or area) EDS spectrum from the geometric centre of each segmented phase. BSE image, X-ray information and particle features are saved with the data.
2. X-ray Modal analysis (XMOD) is a fast method, though strictly collects bulk modal mineralogy. XMOD is similar to the classical point counting method used with an optical microscope; however, the MLA (or automated SEM) is used in place of a microscopist and optical microscope. The mineral identification is determined by X-ray analysis at each counting point on a user-defined grid. This mode uses BSE imaging to discriminate particle matter from background and then collects X-ray spectra from each particle-grid intersection. The X-ray spectra (and x-y coordinates on sample surface) are saved with the data. This method does not provide particle image data, such as association, locking and grain size. XMOD can be used in a relatively fast line scan measurement mode where X-ray spectra are collected at a step size of one pixel in the x- direction and a user-determined y- displacement spacing to provide a quasi-mineral association.
3. The Grain X-ray Mapping mode (GXMAP) is usually applied to X-ray mapping of phases that are similar in BSE brightness (i.e. average atomic number (AAN), density) which are not discriminated and segmented into individual mineral phases.

The user selects the mineral phases to map through either a BSE trigger (e.g. chalcopyrite and pentlandite, both with AAN 23.5) or a specific mineral phase X-ray spectrum trigger (e.g. high and low iron sphalerite). A series of MLA-generated mixed spectra, interpolated at 10% intervals between the nominated pure pair of X-ray spectra, is compared with the actual sample phase (mixed) spectra. GXMAP is a flexible mapping technique that collects MOI X-ray data on a user prescribed x-y grid. In the case of only metal-bearing MOI phases, GXMap was an inefficient approach (e.g. only two X-ray points on the segmented phase making method of little use and adding costly analysis time). Same data as the XBSE mode though higher detail on user-defined MOIs.

4. The sparse phase liberation with XBSE mode (SPL_XBSE) searches BSE images for particles, based upon a MOI BSE gray scale trigger range, with subsequent XBSE analysis of phases that match the trigger. Post-MLA processing is identical to the XBSE method and generates similar data – though only for SPL triggered particles. It cannot provide modal mineralogy information because only selected (triggered) particles are analyzed. The selectivity of the SPL measurement is designed to efficiently measure low concentration mineral phases (e.g. ore in tailings, sulphides in waste rock) where the mineral associations are important. A specialised version of SPL analysis called SPL_XMAP maps the MOI internal mineral associations once detected (i.e. GXMAP applied to a SPL analysis). The metal-bearing MOI phases may be too small or very thin coatings and the beam excitation volume would “gray” any discrimination (segmentation) of phases.
5. Extended SPL analysis (XSPL) employs a two-tiered analysis trigger based upon BSE gray level, followed by a mineral X-ray spectral trigger, before finally recording the mineral phase data. However, this mode was only useable for high density phases (i.e. high AAN, bright BSE image) and most secondary mineralization, due to “gray” discrimination was difficult to detect.

4.3.3 Evaluation of the Mineral Liberation Analyzer

4.3.3.1 Considerations

The MLA applies image analysis to segment contrasting BSE gray level intensity into digitized false-coloured particles separated (extracted) from the background (resin). The BSE gray level intensities are regulated by the mean AAN or density of each mineral phase (i.e. higher density display as brighter and whiter). An X-ray spectrum is acquired for each segmented false-colour region of the particle, which is then compared (through a chi-squared algorithm) with a mineral phase X-ray classification library (database). For this study, measurement used the MLA XBSE analysis mode. For this study the MLA was operated at accelerating voltage 25 kV to improve detection of fine phases often associated with metals, such as secondary MOIs. Further information on MLA analysis can be found elsewhere [Gu, 2003; Fandrich *et al*., 2007; Appendices 2 and 4].

To perform the MLA analysis:

- First consideration must be the sample and its preparation for analysis. The resin used to mount the sample must have particular specifications. The resin must: (1) be stable and cure hard; (2) have little to zero out-gassing under vacuum; and (3) display a low BSE coefficient. No contamination should be introduced prior to image analysis, including weighing, mixing with resin, and polishing.
- During polishing the resin must be relatively resilient to the process (e.g. little to zero particle ‘pull-outs’ / plucking from the resin).
- The chosen transverse mounting method (see Section 4.3.5.5 and Appendix 4) segregates particles based upon mass (related to density) and can be noted in the BSE image shown in Figures 4.3.1.2 and 4.3.1.4. When the MLA analyzes the sample mount it rasters the electron beam in a North-South direction (relative to Figure 4.3.1.4) to ensure that it collects data for each data point along the density continuum.

- The polished sample face must be coated with a thin (~200 Å) conductive material (e.g. graphite) to ensure release of electron beam energy from the sample mount.
- The MLA analysis requirements are important, such as: SEM electron beam stability which is affected by vacuum pressure and filament saturation; MLA analysis parameters that match client needs, which would involve particle image detail, background extraction, segmentation of digitized particle images, X-ray spectra collection, and MOI classification criteria.
- The MLA mineral database library contains (primary and secondary) mineral phases detected in the sample waste rock. It is used to classify and assign segmented particle phases with mineral names and associated textural information (see Chapter 5). Details can be found in Appendix 4.

4.3.3.2 Strengths

Below is a partial list of positive assets regarding use of the MLA for mineralogical assessment of waste rock:

- Automation infers objective mineralogy.
- Superior particle texture discrimination enables high resolution phase segmentation.
- EDS is used instead of Wavelength Dispersive Spectrometer (WDS). WDS differs from EDS in that it is qualifying mineral elemental components based upon wavelength, whereas EDS quantifies those components based upon x-ray energy. Compared to EDS, the WDS poorly handles edge effects such as particles poorly held by resin that exhibit a rough perimeter / surface texture after polishing. In the past, WDS (relative to EDS) could better separate similar X-ray energy peaks (e.g. S, Mo, Pb) however this is no longer a limitation of EDS.
- Detailed mineralogical / mineral chemistry.
- Minerals can be studied in their “as received” natural state.
- Particle shape, inclusions and porosity can be studied (e.g. leaching residue).

- Mineral phase coating, liberation and locking can be studied.
- Often poorly crystalline secondary mineralization, unsuitable for XRD mineral phase determination, can be determined with the MLA.
- Often small (size, concentration) secondary mineralization, beyond the resolution of optical microscopy, can be detected by MLA.
- Mineral phases with similar BSE gray levels (i.e. similar AAN) can be determined using GXMap mode to discriminate phases.
- Bruker Esprit third-party software provides an excellent halocentric peak determination (HPD) application to correctly identify elemental components. This is especially useful for a non-mineralogist.
- The MLA software default simplified first approximation assumption is that all particles are spherical. If this is unsuitable (e.g. molybdenite grains are long and narrow) the user can alter the phase shape assumption for separate or all mineral phases (i.e. user-defined sub-routine scripting).

4.3.3.3 Limitations

Below is a list of limitations to be considered when using the MLA for mineralogical assessment of waste rock:

- Polymorph minerals will not be distinguished (e.g. rutile, anatase, brookite) because the EDS cannot discriminate crystallinity.
- EDS spectral resolution may be challenged (e.g. magnetite and hematite). It may be possible to resolve phases using MLA mode SXBSE (Select XBSE) or Advanced Classification subroutine.
- Possible challenges with hydroxide and carbonate mineral phases (e.g. Fe – OH? or -CO_3?) due to the conductive coating applied to the sample mount surface (e.g. graphite). The coating can absorb X-ray energy which causes inaccurate EDS detection of spectral energy lines (e.g. O, H, C).

- Alteration products of primary MOIs may not be in the local (user-defined) X-ray mineral classification database.
- In coarse size fractions (e.g. greater than 1 cm) mineral liberation and grain size cannot adequately be represented using the MLA due to insufficient particle statistics unless multiple sample mounts are analyzed (see Section 2.7.3).
- Lack of operator knowledge of mineral chemistry and EDS limitations.
- Minerals must be mounted and polished. Poor edge retention of mounted particles during polishing will skew MOI data.
- Secondary minerals occurring in trace amounts or in thin rims may not be identified by MLA due to electron beam excitation volume exceeding the phase size. MLA analysis was not designed for nanometer depth surface analysis, but instead for modal abundance and liberation in mineral processing plants.
- Minerals occurring in trace amounts (less than 200 mg/kg / 0.02 wt%) in solid solution within a host mineral will not be identified by MLA (e.g. As in pyrite). EMPA or LA-ICP/MS could provide the information to amend the MLA X-ray mineral classification database.

4.3.4 Summary

The automated quantitative electron microscopic technique of MLA reveals previously undisclosed mineral species and their relationships. The MLA performs rapid waste rock characterization by combining software directives with SEM and EDS [Fandrich *et al*., 2007]. MLA techniques direct the SEM to discriminate (segment) mineral phases based upon image analysis of BSE signal intensity and EDS acquisition of characteristic X-ray spectra from particles and their component grains. The X-ray spectra are compared with a database library of mineral spectra to identify and then quantify the component minerals.

The automated MLA is based on: (1) television (TV) rate image scanning (i.e. rapid raster); (2) X-ray resolution tied directly to the integrated EDS X-ray system; and, (3) a

conventional SEM tungsten filament electron source. The MLA delivers spatial and spectral resolution with the capability of locating and positively identifying micron-sized MOIs. The different measurement mode options, such as simple point-counting or advanced X-ray and particle mapping, provide orders of magnitude measurements (from thousands to millions) of point- and / or particle-counts in an automated, unattended operation.

The key benefit of the MLA is the spatially resolved mineralogical data and associated elemental spectra, which provide improved information for (trace) MOIs, particle size and shape distributions, and quantitative data, including mineral abundance, association and exposure. Although the MLA technique is usually perceived as being operator independent, a trained operator is required to ensure quality representative sampling and sample preparation, make decisions on MLA operating conditions, and provide quality control on the results. Relative to the historic, manual (subjective) point counting methods, objective and high confidence results are acquired by the MLA which provide accurate mineralogical data to accompany geochemical, particle surface and elemental information.

The reasons for choosing the MLA technology are:

- Automated image analysis is a fast method that eliminates operator bias and fatigue.
- Automated image analysis brings reliability, accuracy and reproducibility regardless who is performing the analysis.
- Automated image analysis allows statistically significant sampling of thousands of particles in one measurement.

4.4 Mineral Liberation Analyzer analysis parameters

Choosing the analysis technique is an important decision for waste rock characterization. Subsequent to this decision, suitable operating parameters must be determined for using the technology.

4.4.1 Automated electron microscopy instrument specifics

The Teck MLA system consists of: an off-the-shelf FEI Quanta 600 SEM with tungsten source electron beam and by-design working distance of 10 mm; dual Bruker-Nano XFlash 4010 SDDs (10 mm2 crystal, electronic Peltier cooling technology) for spectral interpretation and data processing. The tungsten-source electron beam, operating at accelerating voltage 15kV or 25kV (in this study) has a typical diameter of 0.25–0.5 nm. The SEM was coupled to an EDS system and FEI MLA software (version 2.9). The electron beam delivered both spatial resolution and penetration depth of ~1-5 µm (high vacuum, 25kV accelerating voltage) and spectral resolution of ~150eV (Mn Kα at FWHM, 20-25kV accelerating voltage, 275 kcps signal processing board).

Particle size fraction material greater than Warman cyclosizer C6 (~6 µm) was analyzed using an accelerating voltage of 25kV. Particle size fraction material equivalent to Warman cyclosizer C6 or smaller was analyzed using accelerating voltage 15 and 25 kV. For samples with unsized material the higher accelerating voltage was used.

The MLA measurement module controls the hardware settings of the SEM, including electron beam accelerating voltage, SEM magnification, BSE brightness and contrast, spot size, and working distance. The two parallel EDS-detectors allow for fast acquisition of data (generally 100-200 X-ray analyses per second), enabling the automated analysis of large sample particle populations to deliver statistically reliable data sets. Normally, measurements are carried out on a sequence of closely sized particle fractions (although not necessarily sequential) of a sample.

Operational set-up was adjusted for the finest particles measured being ~2 μm and the finest mineral inclusions ~0.5 μm (both limited by the electron beam excitation volume due to mineral phase density). The image and EDS resolution limitation that affects analysis can be improved by decreasing accelerating voltage. Low-density phases, especially finer grains, can be problematic.

4.4.2 Comparison of two Mineral Liberation Analyzers

In an effort to analyze the hundreds samples generated in this study, the use of two MLAs was considered. For the most expedient use of time, it was considered simplest if both MLAs operated with the same MLA analysis parameters. However, it was not known whether there were significant performance differences between the two MLAs. Performance was checked through a study suggested by FEI Company Inc. (the manufacturer of the SEM and MLA system). In this study, each MLA was operated with exactly the same parameter settings and the X-ray photon impulses received by the detector were measured based on several target materials. The tests were performed at two different accelerating voltages, 15 and 25 kV, as these voltages were considered best options for the overall study sample analysis.

The target materials chosen for analysis were: (1) *quartz*, least dense mineral phase to be analyzed; (2) *copper,* with mid-range BSE gray level and density; and (3) *gold*, highest density and BSE gray level that might be found in the sample particles. The two MLAs operated with identical SEM parameters delivered absolute signal responses within 7-10% of each other over a wide range of spot sizes (see Table 4.4.2.1; more detail in Appendix 3a). The difference in SDD response was not significant enough to impact particle image data collection.

Table 4.4.2.1. Comparison of MLA X-ray acquisition: ability to use same parameters.

Ratio of MLA X-ray Counts (MLA#1/MLA#2)						
Spot Size	**25kV accelerating voltage**			**15kV accelerating voltage**		
	Quartz	**Copper**	**Gold**	**Quartz**	**Copper**	**Gold**
3	1.20	1.10	1.13	1.00	1.05	1.04
3.5	1.06	1.21	1.11	1.04	1.00	1.09
4	1.09	1.08	1.11	1.06	1.03	1.08
4.5	1.10	1.09	1.11	1.04	1.04	1.11
5	1.15	1.09	1.11	1.07	1.07	1.12
5.5	1.05	1.10	1.13	1.07	1.07	1.16
6	1.14	1.12	1.14	1.05	1.05	1.15
6.5	1.13	1.10	1.13	1.03	1.06	1.16
7	1.16	1.10	1.14	1.13	1.11	1.16
Average	1.12	1.11	1.12	1.05	1.05	1.12
Std Dev	0.05	0.04	0.01	0.03	0.03	0.04

4.4.3 Mode of analysis

Initial testing was performed using MLA measurement modes XBSE, XMOD, SPL-XBSE and GXMap (see section 4.3.2). The latter three analysis modes proved to not be as useful as the XBSE measurement. XMOD delivered a modal analysis, but did not supply any BSE gray-level particle images or associated particle data. The SPL-XBSE measurement mode, designed to specifically collect particle image data for particular BSE gray-levels, was adequate for high density larger mineral phases but was challenged to detect BSE gray-level ranges of the lower density mineral phases, such as iron oxides and sulphates, and their often very small size. GXMap was able to collect BSE gray-level images of the particles but added extra analysis time with insignificant enhancement of the particle data collected. It was also difficult to establish the GXMap trigger X-ray file for oxide MOIs due to grain size and spectra mixed with host particle phases.

The MLA XBSE mode of analysis was chosen for this study.

4.4.4 Elemental reconciliation

The reconciliation of chemical assay data to MLA-calculated assay data is an important aspect for assurance of credible MLA data. Figure 4.4.4.1 shows the total sample geochemistry by ICP or AAS analysis and the calculated elemental results from the MLA analysis. The individual size fraction elemental assay data is in Appendix 5. The comparison indicates that the MLA X-ray classification standard used for post-analysis processing of MLA digitized image data was generally in good agreement with the geochemical data. This indicates the MLA mineral database created had acceptable defining properties for the metal mineral phases and major phases.

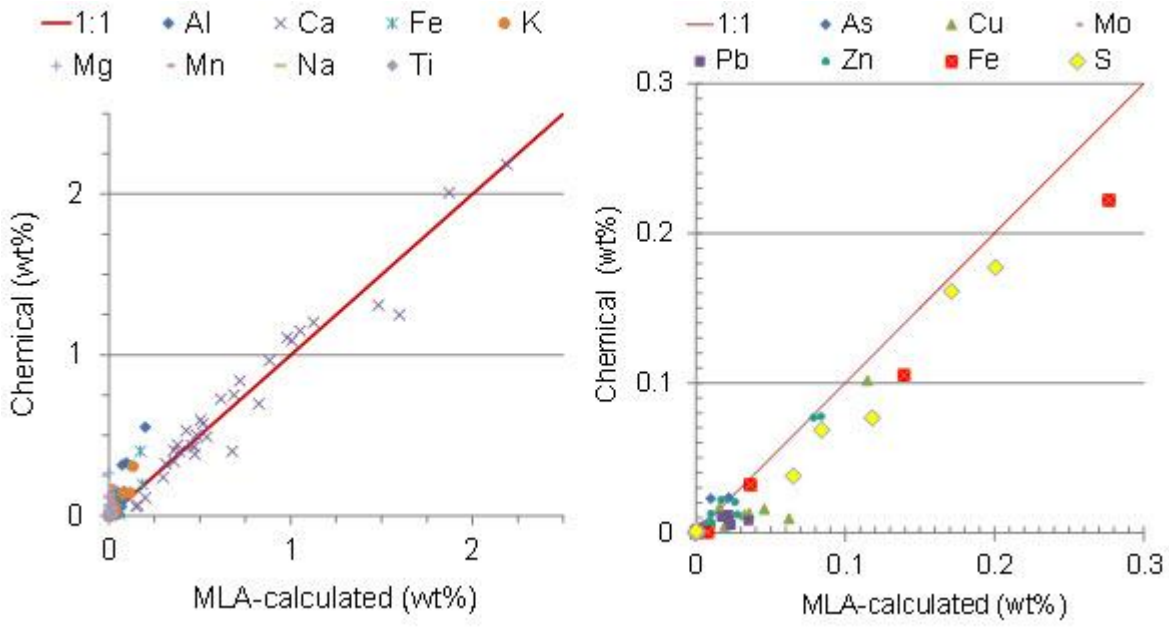

Figure 4.4.4.1. Elemental reconciliation: chemical assay vs. MLA-calculated assay.

The majority of the metals involved secondary mineral phases where either the metal was adsorbed on or incorporated into the phase's lattice. Using a well-defined (i.e. detailed) MLA X-ray classification standard in conjunction with well-chosen MLA data collection parameters, it is possible to follow trace elemental concentration trends to levels below detection limits of the chemical (digestion) analysis and SEM (see Figure

4.4.4.1). This could be verified by using elemental analysis methods with lower detection limits such as EMPA, to improve assignment of optimal densities in the MLA X-ray classification standard. Uncertain density assignment can cause MOIs to be over- or under-reported.

In Figure 4.4.4.1 many MLA-calculated assay results were found to be higher than those from the chemical assay technique – especially at the very low concentrations. This is likely directly related to a physical limitation of the SEM itself. The excitation volume of the electron beam marginally exaggerates the area of the trace metal's MOI. In Figure 4.4.4.1, the trace (secondary) metal MOIs were in many instances smaller in size than the electron beam excitation volume (e.g. particle coating). The calculated amount, while far below the detection limit of the SEM and EDS, could still indicate MOI trends. If required, over-reporting due to electron beam excitation volume could be compensated by incorporating EMPA MOI data into the X-ray classification mineral data base. Acknowledging the trace metal content, this data is considered acceptable.

4.4.5 Sample mounting technique

As discussed in Appendix 4, a decision was required with respect to the mounting method for the samples to be analyzed by the MLA. The two mounting approaches evaluated were "single" and "transverse". The single-mount is attractive because the sample preparation can be completed an entire day sooner than the transverse mount preparation. A brief study was performed using a larger and smaller size fraction (e.g. -106 / +75 µm and sub-38 µm). The larger sized particles were chosen to determine if a "nugget effect" would occur which would significantly skew reported results – especially for trace MOIs. The smaller sized particles were chosen because the vast majority of secondary mineral phases are small and more reactive (i.e. high surface area), hence any skewing of the data could dramatically change weathering interpretations.

This study (see Appendix 6) generated the following observations:

- The procedure for single-mount resulted in the denser particles (e.g. higher density / mass due to either large particle volume or higher density minerals) settling in the sample mount face that was to be polished. The polishing process can remove hundreds of microns of material from the mount face if not careful. If the particle sizes are sub-one hundred microns, clearly they would be at least partially removed from the analysis.
- Rare occurrence ("nugget") particles, such as oxides, secondary carbonates, sulphates, phosphates, sulphides, and silicates, were removed from the single-mount during the polishing process because they had settled in the polishing zone of the sample mount. In the waste rock, the rare occurrence phases were expected to be small in size and concentration. Take note that particles can be composed of grains and a single particle can represent one grain. Particle count and grain count of the smaller particles was approximately identical indicating little association between different MOI phases (i.e. liberated). The polished single-mount would skew reported results due to loss of some MOIs during polishing. In test samples the sulphide particle count was lower than the grain count indicating that sulphide phases were in binary or ternary+ association with other mineral phases. These mixed-phase particles would have higher density and hence settle near the surface of the single-mount face and be polished out during sample mount preparation. Metal element Zn showed the most significant content change comparing transverse and single mount.
- The MLA applies a stereology algorithm to calculate mass based on a 3-D spherical particle shape with the volume calculated from 2-D radius of area for each mineral phase. The single-mount (30 mm diameter) has a face area of ~700 mm^2 and transverse-mount (~5 mm x ~25 mm x 2 pieces) has a face area of ~250 mm^2 from twin pieces. The mass of sample mixed into the resin for each sample mount was ~1.5 g (average). The packing density of the single-mount was ~50% while that of the transverse-mount was ~60%, which generates a potential analyzable particle surface area of ~350 and ~150 mm^2, respectively. Taking into account the difference

in the actual particle analysis surface area, it was clear that there was a significant difference between the two mount methods. This would suggest potentially more particles for analysis in the single-mount; however, the transverse-mount would provide a true evaluation of the particle phase density continuum compared to the single-mount. The MLA software normalizes the digitized particle image data to 100%.

- Table 4.4.5.1 provides an example to show the effect of mounting method. If the single-mount decreased from 1000 to 250 sulphide grains due to polishing, and the total particle count was 50,000, then the single-mount would report 0.7% sulphides instead of 2%. This represents a significant change in critical phase content (results reported as normalized) meanwhile the carbonates would show a less significant effect. Clearly the reported data would artificially skew MOI presence. While the single-mount data appeared to report higher levels of metal MOIs, the particle count was actually significantly reduced for those MOIs, with the end result of skewing the data due to normalization.

Table 4.4.5.1. Effect of the mounting method.

	Single-mount				Transverse-mount			
	Before grind-polish		After grind-polish		Before grind-polish		After grind-polish	
	Number particles	Fraction of total (%)	Number particles	Fraction of total (%)	Number particles	Fraction of total (%)	Number particles	Fraction of total (%)
Total	50000	na	35000	na	50000	na	50000	na
Sulphides	1000	2.0	250	0.7	1000	2.0	1100	2.2
Carbonates	42000	84	30000	86	42000	84	41000	82

The decision was made to use transverse-mount for all subsequent sample analysis.

4.4.6 Electron beam spot size

The SEM images a sample by scanning it with a high-energy beam of electrons in a raster scan pattern. The electrons interact with the atoms that make up the sample, producing X-ray photon pulses that contain feature information, such as a surface topography, composition, grain size and association. The primary electron beam interacts with the sample within a teardrop-shaped volume known as the interaction or excitation volume, which can penetrate as much as ~5 µm into the sample surface. The size of the interaction volume depends on the electron's landing energy, the atomic number of the specimen and the specimen's density. The size of the interaction volume affects the minimum spatial resolution of the image. The SEM “spot size” is an arbitrary relative value placed upon the diameter of the electron beam. The FEI company defines spot size to be proportional to $\log_2$(probe current). As spot size increases, more electrons are directed at the sample surface. The result is a larger interaction volume and higher photon signal returned to the BSE detector - though poorer spatial resolution. The SEM electron beam column final aperture which also plays a role in resolution (note: same for both MLAs) was not investigated in this study.

A comparison method can be used when adjusting the spot size whereby the electron beam is applied to an object and the X-ray photon counts-per-second (cps) returning from the object are measured. In this study, the beam was directed at a piece of pure quartz. Quartz, chosen because it would be the lowest density MOI in the samples, would return to the detector the corresponding lowest expected X-ray photon counts-per-second. By using quartz as the reference material to adjust the spot size, ample counts (impulses) were assured for all MOIs with densities at or above MOI quartz.

Two spot sizes were chosen for comparison, analyzing the same samples with identical MLA analysis routine at 60,000 cps and 100,000 cps with respect to quartz (Appendix 7). In the MLA software, the user can enter a value for the acquisition (count) time per X-ray collection sampling point (e.g. 25 msec). The grain sampling point is determined

through the MLA particle segmentation routine (based upon differing BSE AAN gray levels). The expected result of increasing spot size was an increase in spectral resolution, decrease in spatial resolution and decrease in analysis time.

A comparison showed that increasing the spot size decreased the analysis run time ~5%. The larger spot size, due to increased electron beam interaction volume could negatively affect the MLA software's particle segmentation routine (based on density). The increased spot size would have the largest affect upon the trace (small) mineral phases. Larger spot size resulted in improved MOI X-ray spectral resolution which improved confidence in the classification.

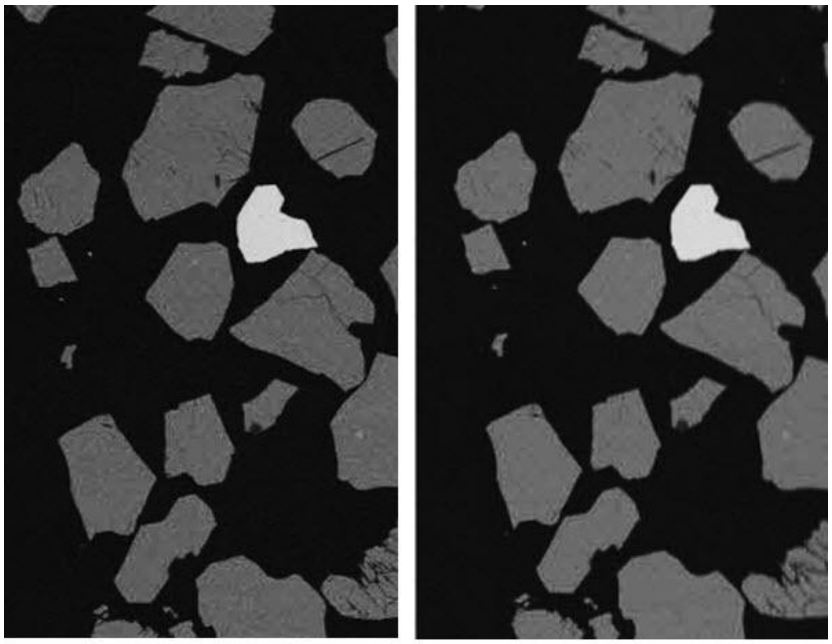

Figure 4.4.6.1. BSE particle image comparing spatial resolution with respect to spot size.

The visual examination did not expose significant improvement in the MLA BSE imaging and segmentation due to increased spot size (see Figure 4.4.6.1) though it did marginally reduce analysis time. The decision was to use the spot size that delivered

60,000 cps when the electron beam was targeting MOI quartz to ensure more mineralogical detail collected per pixel.

4.4.7 Electron beam dwell time

As the SEM electron beam scans over the particle image in a raster pattern, the particle surface is recorded digitally. At each pixel the detector collects BSE image information with the beam dwelling on each pixel for a time period. Typically, with MLA operation the dwell time is set at 16 µsec / pixel. In this study, dwell times of 8, 16 and 32 were investigated to determine if better resolution could be obtained while maintaining a reasonable analysis time (see Appendix 8).

It was found that the relatively smaller dwell time (i.e. 8 µsec / pixel) was often too short to acquire satisfactory image data for the MLA segmentation algorithm, and the relatively larger dwell time (i.e. 32 µsec / pixel) was found to often lead to better resolved X-ray spectral data.

Using dwell time 8 µsec / pixel, the overall MLA analysis time decreased a modest ~2.5%. With dwell time 32 µsec / pixel, the overall MLA analysis time increased significantly by ~39%. The higher dwell time did not significantly change the X-ray classification of mineral phases nor the consequent modal abundance of the mineral phases. The decision was made to use dwell time 16 µsec / pixel for all further MLA analyses.

4.4.8 Particle count

Using optical microscopy, the modal abundance of mineral phases can be determined through the use of a technique called point-counting. In point-counting the sample

surface is overlaid with a grid and at every grid line intersection (i.e. crosshair) if there is a mineral phase, the particle information is recorded. This method is usually objective, very labour intensive and time-consuming. Typically 300 points (minimum) on the sample surface are tabulated and the final result reported as a normalized percentage for each phase. However, there are limitations to the use of optical microscopy in that the wavelength of the light source limits the size of the smallest grain that can be identified (according to the deBroglie inverse relationship between wavelength and electron velocity) [see Section 4.4.9; Ofori *et al*., 2006]. With the use of the SEM (and electron beam as the light source) the magnification and depth of field increase greatly, and the MLA capitalizes on this aspect to improve particle/MOI statistics. A comparison study was performed of MLA analysis applied to the same samples with the MLA particle collection parameter for the minimum number of particles collected being set at 2000, 12,000, and 20,000 (see Appendix 9).

Overall MLA analysis time decreased 66% (average) when collecting a minimum of 2000 particles, compared to an increase of 38% analysis time (average) when collecting minimum 20,000 particles, relative to benchmark collection of minimum 12,000 particles. The greatly decreased analysis time was attractive. However, this study showed that lower particle count would skew modal abundance data, especially for low number metal MOI occurrences. Higher particle number collection de-emphasized the “nugget effect”. With increased particle count, the trace metal MOI content was sometimes significantly affected. It should be noted that the minimum particle count for the MLA analysis reported a particle count more than fourty times that used in a typical optical point-count technique. The duration of the MLA analysis time could also be affected by the sample mount particle packing density.

The minimum number of particles used as the threshold to halt analysis was set at 12,000.

For this study the average sample displayed 600 +/- 340 particles per frame-of-view. The MLA analyzed 400 +/- 100 particles per minute. The duration of each sample analysis time period was 220 +/- 30 minutes.

4.4.9 Accelerating voltage

The accelerating voltage is used to increase the velocity of the electrons in the beam. The electron velocity impacts the wavelength according to the relationship $\lambda = h / m\upsilon$, with λ being the deBroglie wavelength, h being Planck's constant, m and v being the electron's mass and velocity, respectively. Spatial resolution is a measure of the amount of textural detail that can be discerned on an image. One of the factors controlling image detail and spatial resolution is the wavelength of the electron beam that produces the image.

However, the ability to focus the electrons to a small point (via spot size) and the beam excitation (interaction) volume within the sample material itself must reach a balance. Low-voltage SEM can show fine (nanometre-scale) surface features, while high-voltage SEM can probe deeper into the material and retrieve more elemental X-ray information. The operator's judgment of image quality depends on the information required from the sample. Either may be better for different applications. In this study the accelerating voltages 15kV and 25kV were compared (see Appendix 10).

MLA reports detected phases normalized to 100 percent. Relative to 25kV accelerating voltage, the results generally showed that lower accelerating voltage caused the often greater in quantity lower density gangue phases to be reported in higher proportions, while the higher density mineral phases (e.g. sulphides) were generally reported with decreased proportion. Checking X-ray spectral data revealed that the gangue was generally reported correctly. However, the lower voltage decreased the ability to detect some mineral phases, specifically the critical-to-know fine metal MOIs. Poor detection plus MLA normalization of data, artificially exaggerated the gangue content.

Knowing the majority of the waste rock was composed of carbonates and silicates, while any metal MOIs would be present in much smaller relative proportions, a higher accelerating voltage was chosen to enable detection of the trace and minor secondary mineral phases.

4.4.10 Magnification (or horizontal field width)

All SEMs have an optimal working distance for imaging. The working distance is the distance from the bottom of the SEM column (i.e. final aperture) to the sample surface and affects spatial resolution and depth of field. In general, a shorter working distance should be used for higher spatial resolution imaging, at the sacrifice of depth of field. The FEI Quanta 600 SEM working distance of 10 mm was better suited for this study's application (see section 4.3.3 and Appendix 2). Generally, to improve spatial resolution a smaller spot size can be used in conjunction with a shorter working distance (see section 4.4.7). Ideally a higher energy beam confined to a very small spot size would be most useful for examining the fine-detail of waste rock secondary mineral phases in a time-efficient manner (e.g. FEG SEM).

Another aspect of the SEM that can be employed to improve MLA image analysis is magnification. Spatial resolution refers to the ability to distinguish between, or identify, very closely spaced points. Sample textural features can impose spatial resolution limitations. The magnification at which a sample is investigated affects the interpretation of the acquired data. Particle features that are evident at one magnification may be absent at other magnifications. Thus, there is a magnification impact on MLA imaging, segmentation and consequent quantification of waste rock mineralogy and features. In this study, a progressive magnification was applied to evaluate a possible improvement of MOI quantification. Note that frame size (i.e. pixel resolution) remained constant at 1000 x 1000 pixels throughout all aspects of the study.

The study results showed that analysis time will increase with increasing magnification (Appendix 11) if targeting the same minimum number of analyzed particles (Table 4.4.10.1). In the table, the particle size value represents the top-size for the size fraction. Due to the regimented action of the SEM raster, the MLA analysis does not end until the line raster has been completed - even though the minimum particle count may have been achieved. For this reason and the higher magnification, there were ~33% more particles (and frames) collected – which increased analysis time. The results also showed that better spatial resolution (via higher magnification) of the phases lead to better X-ray spectra collection (i.e. fewer mixed spectra) which improved MLA mineral phase identification. For example, watanabeite ($Cu_4As_{1.4}Sb_{0.6}S_5$) and enargite (Cu_3AsS_4) classification was refined using the higher magnification. Using the initial (benchmark) magnifications shown, the average time for an MLA analysis was 220 minutes.

Table 4.4.10.1. Change in MLA analysis time with magnification.

Mesh Size (US)	Particle Size (µm)	Initial Analysis Time (hr)	Magnification Change (from → to)	Change in MLA Analysis Time (%)
16	1190	2.0 – 2.5	120 → 200	~290
30	600	2.0 – 2.5	120 → 200	~300
50	300	2.5	120 → 225	~360
100	150	1.5 – 2.5	150 → 250	~260
140	106	1.5 – 2.5	175 → 275	~260
200	75	2.0 – 2.5	200 → 275	~230
270	53	1.0 – 2.0	200 → 275	~150
-270	-53	0.5 – 0.75	200 → 275	~150

When the magnification was increased, more minor inclusions and grains were detected, which consequently increased the analysis time. Closer inspection revealed that the smallest particles and grains, most often composed of a single phase, did not add significant analysis time. The larger increase in analysis time was associated with large multiphase particles.

For this study, the lower magnifications (see Table 4.4.10.1) were used in the interest of analysis time and associated costs.

4.4.11 Random sampling

The sample particles, more specifically the MOIs that compose the particles, are supposed to be randomly presented in the sample mount. If this is true, then the orientation of the sample mount in the MLA sample holder should not alter mineralogical determination. A brief study was performed to test this hypothesis (Appendix 12). The MLA analysis was performed such that sample mounts were re-analyzed in a different orientation in the sample holder (e.g. rotated ninety degrees). This change in orientation was expected to emphasize the nugget effect if present. To further determine the randomness of sample preparation, a duplicate sample (i.e. completely separate portion) was prepared and analyzed.

The overall change in number of frames analyzed (for the same user-defined analysis parameters) was ~10%, while the particle count changed ~23% (comparing Original analysis vs. Reposition analysis). The change in frame and particle number was definitive evidence of changed sample mount positioning and indicative of sample mounts which displayed variable particle density. Although there was a change in particle count, the overall normalized modal abundance of mineral phases and the MLA calculated elemental assay data did not change significantly. The metal distribution associated with a mineral did show some change, though was noted to be mainly

associated with Sb, As and Zn. The change was investigated and found to be mainly caused by the “nugget effect”.

Additionally, the sampling techniques can be assessed by reviewing the analyses of sample duplicates and replicates (see Appendix 13). Duplicate refers to a second sample aliquot riffled from the same sample portion which was then taken through all sample preparation steps in parallel with the original sample portion. A replicate refers to a completely separate sample analysis which was performed on a different day on a different MLA.

The effects of the “nugget” could be reduced by analyzing a larger number of particles through analysis of multiple sample mounts. Particle statistics were improved and “nugget effect” reduced by appending the digitized particle data files of duplicate sample mounts (i.e. particularly important for larger particle sizes). For each MOI, the average modal weight-percent difference between duplicate sample mounts compared to the appended sample data was 1.6 wt% +/- 1.4 wt%; for replicate the average modal weight-percent difference was 16.8 wt% +/- 4.9 wt%. The replicate analysis showed greater variation: 86% of time due to extremely trace quantities of MOIs (e.g. 0.00001 wt% compared to 0.00002 wt%); and, 14% of time due to the nugget effect (e.g. 0.0007 wt% compared to 0.01 wt%). Result variation was further exacerbated by electron beam size differences of the two MLAs used in this study (i.e. interaction volume; see section 4.4.4 and 4.4.6). These causes for variation were observed in the particle image data and should be taken into consideration when reporting mineralogical data. At the same time, the extremely low reported concentrations can be ignored. Higher MOI content in the sample (e.g. greater than 1 wt%) plus increased total particle counts significantly reduced variation between duplicate sample MOI concentrations. Appending the data files was especially helpful when reviewing trace metal MOIs particle statistics.

This study showed that better representation of the sample size fraction MOIs would be achieved using appended data files (i.e. improved particle statistics) especially with

respect to trace MOIs. This translated to a minimum of two sample mounts being analyzed, if sufficient material was available.

4.4.12 Summary of Mineral Liberation Analyzer operating parameters

MLA technology can be used to identify MOI primary and secondary phases which can then be used in predictive weathering models. A suitable method of analysis would include an XBSE analysis of at least two transverse-mounts, using an electron beam spot size and magnification (horizontal field width) based more on spatial rather than spectral resolution, with an accelerating voltage capable of reasonable MOI detection in the shortest analysis time. Suitable conditions from this study are summarized in Table 4.4.12.1.

Table 4.4.12.1. Summary of suitable MLA operating parameters.

Parameter	Suitable value
comparison of two MLAs	use same operating parameters
MLA analysis mode	XBSE
elemental reconciliation	acceptable
sample mounting technique	transverse
spot size	60 kcps on pure quartz
dwell time	16 µsec / pixel
particle / grain count	minimum 12000 particles
accelerating voltage	25 kV
magnification (or horizontal field width)	lower if possible
random sampling	acceptable, use duplicates when possible

CHAPTER 5 Demonstration of Mineral Liberation Analyzer application to waste rock characterization

Waste rock pile weathering of particles generates secondary amorphous MOIs and elemental ions which can impact the environment. The secondary MOIs are difficult to identify without such instrumentation as SEM and EDS. Mounted samples from the Antamina mine were subjected to MLA analysis to explore applicability to waste rock characterization. The scope of this study was to demonstrate the usefulness of MLA technology to characterize waste rock, not specifically to quantify and determine weathering mechanisms. This chapter will demonstrate the ability to detect (and quantify) some of the determined waste rock characteristics (see Chapter 4) through example waste rock particles.

5.1 Waste rock bulk modal mineralogy

Modal abundance using MLA technology is very dependent upon several factors, which include sample mount integrity, SEM, and the MLA image analysis and X-ray classification database. Using the MLA classification algorithm (chi-squared probability) mineral phase names from the database library (verified, see Section 4.4.4) were assigned to discriminated segments of each particle. The data summary shown in Table 5.1.1 is a compilation of Appendix 14, which comprises unweathered waste rock samples from field cells and drill core, both representing the same experimental pile (i.e. see Tables 3.2.1 and 3.2.3, respectively).

Generally, hornfels could potentially produce more ARD than marble due to association with more sulphides. Class A waste rock showed most sulphides in the coarser hornfels; Class C showed most sulphides in the finer hornfels. Class B waste rock was variable. This further confirmed the difficulty in classifying Class B waste rock reactivity. Hornfels form when minerals in igneous or sedimentary rocks recrystallize during metamorphism to form larger crystal structures accompanied by micro-spaces (pores)

between grains. The presence of pores in the hornfels could provide protected environments where sulphides are able to be leached (see chapter 2) even in a largely carbonaceous environment. The variability of Class B waste rock reactivity was reflected in the potential internal and external particle weathering possibilities.

Table 5.1.1. Observations from MLA analysis: modal abundance.

Class	Mineral Group	Observation
A	Sulphide	Hornfels contain 3 times more than Marble. In the finest size fraction: Hornfels contain least, and Marble contain most.
	Carbonate	Hornfels and Marble contain largest presence in mid-size particles (-300/+75µm).
	Silicate	Hornfels and Marble contain largest presence in smallest particles. Hornfels contain considerably more than Marble (i.e. 4 times more).
	Phosphate	Hornfels contain most in the coarse particles, opposite to the silicate trend. Marble contain most in the smallest particles, similar to the silicate trend and opposite to the carbonate trend.
	Oxide	Hornfels and Marble have same oxide content in all size fractions. Based on particle size, there was no preferential oxide precipitation/formation.
	Sulphate, Etc (incl. Molybdate, Tungstate)	Hornfels contain 3 times more than Marble. In the finest size fraction: Hornfels contain least and Marble contain most.
B	Sulphide	Variable (can be highest or lowest content in fines, most often seen as lowest in mid-size particles).
	Carbonate	Not often contain largest content in finest size fraction, more often contain largest content in mid-size fraction.
	Silicate	Variable (usually have largest content in finest size fraction, though sometimes least content in finest size fraction).
	Phosphate	Diopside Marble can contain largest content in fines. The least phosphate content was often seen in mid-size particles.
	Oxide	Usually largest content in fines. Often least content in mid-size particles.
	Sulphate, Etc (incl. Molybdate, Tungstate)	Can contain largest content in fines. Often least content in mid-size particles.
C	Sulphide	Hornfels have much larger sulphide content than Marble; Hornfels contain largest presence in finest particles. Marble contain similar content throughout all particle sizes.
	Carbonate	The Hornfels and Marble trend showed highest presence of carbonate in the finest size fraction (mainly calcite).
	Silicate	The Hornfels and Marble trend indicated the finest particles contain least content.
	Phosphate	Hornfels contain about the same phosphate content in all size fractions. Marble contain the least phosphate content in the finest sized particles.
	Oxide	The Hornfels and Marble trend show oxide content was largest in mid-size particles.
	Sulphate, Etc (incl. Molybdate, Tungstate)	Hornfels contain largest content in mid-size particles. Marble contain largest content in the finest sized particles.

Generally the more reactive Class A and B waste rock displayed a larger carbonate presence in mid-sized particles (i.e. -300 / +75 µm). It was assumed that any fine carbonate particles would be readily dissolved. Unreactive Class C waste rock displayed a larger carbonate presence in the fines (i.e. -53 µm) which suggested either high pH environment or low potential ARD production. The noted lack of carbonate in the larger particle size fractions (greater than 300 µm) may be due to leaching and dissolution before field sampling began. The fine, higher surface area, Class C carbonate particles was assumed to have a higher reactivity, yet the carbonates were not found associated with other phases as armouring precipitates. Some larger Class C particles displayed coatings (armour) of oxide.

Class A and B waste rock showed most silicates in the fine particle size range. Class C showed least silicates in the fine particle size range. Hornfels contained ~4 times more silicates than marble. Considering the waste rock classification scheme currently in use, waste rock may be less reactive when there are larger particles of silicates which lock reactive phases making them unavailable for ARD development (see section 5.2).

The coarser sized particles in Class A waste rock had the largest phosphate content while the finest sized particles in (diopside) marble showed the most phosphate. In Class C material, hornfels' phosphate content was about the same in all particles sizes while marble showed the lowest content of phosphate in the finest sized particles. Class B waste rock showed lowest phosphate content in the mid-sized particles.

The smallest particles were expected to have the highest oxide concentrations because smaller particles (i.e. higher surface area) were considered more reactive and could readily generate (or would be) oxides, while larger particles would provide surface area to coat. Class A waste rock did not show any preferential precipitation of oxides to a particular particle size even though it was considered the most reactive. Class C showed the highest oxide presence in mid-sized particles.

Iron is associated with common minerals such as hematite (Fe2O3), limonite / goethite (FeO(OH)), and pyrite (FeS_2), as well as many others (see section 2.2). These MOIs, MLA-detected in the Antamina mine waste rock sample, revealed exposed thin layers of elemental sulphur and jarosite on SLR sulphide MOI surfaces as observed by particle rims containing As, S, O, Fe, K, and low-level Ag. The low-level Ag, assumed to be temporarily part of the thin jarosite rim phase, was also noted by Cordoba et al. [2009]. The observation suggested that the Fe oxide coating or rim acted as an attenuator of As and Ag and may also partially passivate the MOI reactive surface.

Detection of poorly crystallized fine-grained iron mineral phases such as ferrihydrite ($Fe_2O_{3-0.5y}(OH)_y \cdot nH_2O$, where $0 \leq y \leq 2$ and $0.8 \leq n \leq 1.1$) and schwertmannite ($Fe_2O_{3-x}(SO_4)_x \cdot nH_2O$, where $0.4 \leq x \leq 0.5$ and $1.5 \leq n \leq 2.8$) were found through manual searching while developing the X-ray classification database; however, due to the phase's nano-size, SEM spatial resolution limitation, and MLA analysis parameters chosen to perform analysis in reasonable time, they remained undetected. Similar to previous studies of the Antamina Mine waste rock, hydrous iron sulphates such as melanterite ($FeSO_4 \cdot 7H_2O$) and rozenite ($FeSO_4 \cdot 4H_2O$) and hydrous phosphate vivianite ($Fe_3(PO_4)_2 \cdot 8H_2O$) were not detected [Antamina, 2001]. The main secondary iron minerals detected in the waste rock were iron sulphate and iron oxyhydroxides (e.g. goethite and hematite) which occurred as coatings on both larger and finer rock fragments.

The dominating sulphate oxyanion mineral was associated with iron, and in near vicinity to sulphides (i.e. if ARD was possible, sulphate generation was possible). Hornfels, which had the highest oxide presence in the mid-sized particles, also had the highest sulphate content. Marble showed highest sulphate content in the finest sized particles, which was also where higher carbonate presence was determined.

MLA scoping analysis provided large amounts of mineralogical information for interpretation, which should be used in conjunction with other analytical results such as geochemistry and surface analysis.

5.2 Waste rock metal-bearing phase mineralogy

5.2.1 Metal-bearing mineral association

Information on availability of a (reactive) mineral phase will benefit the development of a waste rock weathering model. The available mineral phase may involve direct contact with the ARD / NRD fluids or may react through direct contact with an adjacent associated mineral phase such as galvanic interaction (see explanation in Section 5.3.1.2). To demonstrate the usefulness of the MLA to characterize waste rock, the image data can be focused on a specific metal.

MLA Dataview software was used to group the mineral modal abundance data into MOIs associated with a specific metal (either as part of the mineral composition locked in the crystal lattice or adsorbed to surface). Sample analysis data representing samples taken from the experimental piles and field cells (see Table 3.2.4) were used for this focus. These samples were subjected to a sequential leach (see Section 2.4). The grouping of the MOIs with respect to specific metals is shown in Appendix 16.

A rearrangement of the bulk modal mineralogy (see section 5.1) with the perspective of MOI and associated metals provided a new perspective to waste rock degradation. MLA mineral association reported liberated minerals, and minerals sharing a boundary with resin (i.e. free surface) or another mineral. This demonstration of data focus did not incorporate particle size though it is possible. It was noted that after the SL, typically the amount of sub-53 µm particles was greatly decreased (with no MOI bias). Note that the SLR represents a weathering surrogate example for secondary MOIs in the natural

waste rock environment. Table 5.2.1.1 shows notable mineral phases for select metal associations. The following observations were made:

Table 5.2.1.1. Prevalent select metal-bearing mineral phases: before and after SL.

Metal	Head	SLR
As	FeOxyhydroxide, FeSulphate, Siderite, Watanabeite	FeOxyhydroxide, FeSulphate
Sb	Watanabeite	Watanabeite
Cu	Apatite, Chalcopyrite, FeCuSilicate, FeOxyhydroxide, FeSulphate, Grunerite (UBC2-3A), Mica, Pyrite, Siderite (UBC2-3A), Sphalerite, Tennantite (Tucush 03, UBC2-3A), Titanite, Watanabeite	Apatite, Chalcopyrite, FeCuSilicate, FeOxyhydroxide, FeSulphate, Mica, Sphalerite, Titanite
Mo	FeSulphate, Molybdenite, Stibnite, Watanabeite	FeSulphate, Molybdenite, Watanabeite (Tucush 03)
Pb	Apatite, Chalcopyrite, FeOxyhydroxide, Galena, Grunerite (UBC2-3A), Titanite	Apatite, Chalcopyrite, FeOxyhydroxide, Titanite
Zn	Apatite, Chalcopyrite, FeOxyhydroxide, FeSulphate, Grunerite, Mica, Siderite, Sphalerite, Tennantite, Watanabeite	Apatite, Chalcopyrite, FeOxyhydroxide, FeSulphate, Mica, Sphalerite

(i) Antimony, Sb

Of the two significant Sb-associated MOIs, stibnite [$Sb_2S_{3]}$] and watanabeite [$Cu_4(As,Sb)S_5$], the latter was slightly more prevalent. In the SLR, stibnite content decreased and watanabeite content increased, suggesting that stibnite may be an As attenuator. The MLA classification algorithm reported watanabeite though it may be As adsorbed to stibnite surface (often found closely associated to Cu-bearing particles). In the SLR, when watanabeite content decreased (relative to Head) it appeared that As leached first, followed by Cu, resulting in the secondary MOI stibnite (see section 5.3).

(ii) Arsenic, As

In this study, millions of MLA-analyzed particles showed few primary As species. The Antamina mine geologists reported primary sulphides such as arsenopyrite in the waste rock [Antamina, 2001]; however, these were not observed in the samples analyzed. This suggested that As-bearing MOIs (such as arsenopyrite) visually seen

by the geologists, were easily dissolved or aggressively leached. Possible explanations include catalysis and galvanic activity. For example, the unobserved primary As-bearing sulphides may be due to dissolution processes with similarities to the Ag catalysis in chalcopyrite dissolution as suggested by others, such as Nazari *et al.* [2011], Price *et al*., [1986] and Ballester *et al*. [1990].

Arsenic was associated with numerous mineral phases including oxyhydroxides, carbonates, sulphates, suggesting that As was quite mobile in ARD and / or NRD. The SLR showed As-associated oxide content decreased the most (relative to other phases) suggesting weak attenuation by other phases. During the SL, the MOIs siderite [$FeCO_3$], molybdofornacite [$Pb_2Cu[(As,P)O_4][(Mo,Cr)O_4](OH)$], tennantite [$(CuFe)_{12}As_4S_{13}$], and watanabeite decreased in concentration while iron sulphate remained relatively unchanged. Secondary As-associated MOI enargite [Cu_3AsS_4] not detected in the Head, appeared after the SL; however, due to electron beam penetration this MOI may actually have been iron-leached chalcopyrite [$CuFeS_2$] with adsorbed As. EMPA surface analysis would be helpful in determining the MOI present.

(iii) Copper, Cu

The concentration of Cu-associated carbonate siderite and phosphate apatite [$Ca_5(PO_4)_3(OH)$] showed least resistance to SL conditions (i.e. content significantly decreased). Copper-associated MOIs that decreased in content during the SL were tennantite, pyrite [FeS_2], grunerite [$Fe_7(Si_8O_{22})(OH)$] and iron-copper oxide [$Fe_2(Cu_{0.4})O_4$]. Chalcopyrite appeared to resist SL conditions as the amount did not change during the SL. After the SL there was increased presence of Cu-associated MOIs (altered) mica [$(K,Na)(Fe,Al,Mg)_2(Si,Al)_4O_{10}(OH)_2$], titanite [$CaTiSiO_5$], iron sulphate and iron oxyhydroxides. It appeared that As, then Cu, was leached from the MOIs. The pyrite and chalcopyrite content increased perhaps representing degradation products of arsenopyrite [$FeAsS_2$] and tennantite, respectively.

(iv) Molybdenum, Mo

Molybdenite [MoS_2], wulfenite [$PbMoO_4$] and MoSulphatePowelliteClay [$4MoSO_4 \bullet CaMoO_4 \bullet AlSi_2O_5(OH)_4$] showed decreased content in the SLR. Other secondary MOIs detected in the SLR, were iron sulphate, molybdofornacite and stibnite. The latter MOI may be a degradation product of watanabeite (suggested for Sb-bearing phases) or unlocked from a larger particle during the SL.

(v) Lead, Pb

Galena [PbS], apatite, wulfenite and grunerite were leached during the SL as indicated by reduced presence. In the SLR, MOIs with increased concentration detected by the MLA were chalcopyrite and titanite. Pb-associated titanite was detected in the SLR; however, Pb-free titanite was not detected before or after the SL which made any conclusion difficult. Titanite may be a good Pb sequestration MOI.

(vi) Zinc, Zn

Zinc was associated with MOIs both before and after the SL. The decreased concentration of Zn-associated carbonate siderite and phosphate apatite [$Ca_5(PO_4)_3(OH)$] suggested poor resistance to SL conditions. In the SLR other Zn-associated MOIs that showed decreased content were chalcopyrite and grunerite. Increased MOI content in SLR was noted for Zn-associated iron sulphate, iron oxyhydroxides, (altered) mica and watanabeite. It was interesting that the concentration of enargite associated with Zn did not change significantly as a result of the SL which suggested Zn association with the MOI may have protected it from dissolution.

In summary, the MLA analysis of specific metal associated MOIs in the waste rock after the SL, revealed that some MOIs could either resist dissolution / leaching or were formed. A more in-depth analysis of the MOIs with other techniques such as EMPA or FEG-SEM would be very helpful due to inadequate MLA (SEM) resolution.

Primary As MOIs, such as arsenopyrite, were present in very trace amounts (evidence being no detection by MLA). The higher presence of secondary MOI wulfenite ($PbMoO_4$) suggested it precipitated Mo more readily than powellite ($CaMoO_4$) after the SL [Conlan *et al.,* 2012]. The Mo-bearing MOIs contained traces of As suggesting that Mo and As could be attenuated with Pb in the waste rock dump [Petrunic *et al.*, 2006]. Other elements that hydrolyze weakly (e.g. Zn, Co, Cd, Ni) existed as cations and appeared to have mainly formed low-solubility hydroxide or carbonate phases. Earlier studies [Golder, 2010; Golder, 2004] confirmed that the Antamina waste rock pile contained these oxyanions and cations which were attenuated as secondary minerals [Blowes *et al.,* 1995] or with other MLA-detected MOI phases, such as clays (e.g. altered mica) and titanite.

Cell UBC2-3A (unweathered) Head waste rock blend of Cu-bearing grunerite and siderite content decreased after SL exposure.

Cations Cu and Zn, appeared more susceptible to association with MOIs watanabeite and mica-type clays in both Head and SLR samples which suggested SL (weathering surrogate) conditions are not the only attenuation factor involved. Watanabeite appeared to be a stronger attenuator of Mo.

Cu and Pb more strongly favoured the MOI titanite surface than Zn and potential metal oxyanions As, Sb, and Mo.

Zn, mobilized during the SL, was trapped with iron oxyhydroxides, iron sulphate and apatite. Zinc minerals, such as zincosite [$ZnSO_4$], wulfingite [$Zn(OH)_2$], and smithsonite [$(Zn,Cd)_{10}(CO_3)_{10}$] were the most probable source of freed Zn (evidence being these trace phases were not detected after the SL).

5.2.2 Metal-bearing mineral availability (or locking)

MLA Dataview software was used to group the modal abundance data into a single mineral phase or a group of phases. The grouping used the following arbitrary availability or exposure definitions: (1) “locked” refers to the MOI perimeter with less than 30% exposed; (2) “partially exposed” (also termed middlings) refers to the MOI perimeter with 30-90% exposure; and, (3) “liberated” refers to 90-100% of the MOI perimeter exposed. With this capability, the MOIs involved in the SL (weathering surrogate) processes could be highlighted in terms of availability (exposure). Samples of Table 3.2.4, which represent samples submitted to the SL of Section 2.4 (i.e. Head and SLR) were used for this focus. The grouping of mineral phases found in Appendix 15 display the bulk and metal-associated MOI’s degree of exposure or availability (also termed liberation) to the SL (weathering surrogate) process. It was outside the scope of this study to quantify and / or coordinate lithology to secondary mineralization.

It was not possible to analyze “large” particles using the SEM due to practicality. For example, magnification 120x provided MLA (SEM) horizontal field (frame) width just large enough to avoid seeing shadow from the SEM electron beam column. In this case one 3 mm^2 particle engulfed the entire frame of view. In this study, to facilitate better particle statistics, a maximum particle size limitation of 1190 µm was imposed, and a duplicate mount was analyzed – if material was available (see Chapter 3; Sections 2.71 and 2.73). Any waste rock fragment of size greater than 1190 µm was stage-crushed to 100% passing 1190 µm. The 1190 µm particle size was chosen as the largest possible particle size to analyze in order to measure as representative a texture and MOI association as possible (i.e. to better assess the natural rock) plus dictate a reasonable number of particles per sample mount.

To ensure credible MLA image analysis data, a large number of occurrences of each MOI must be measured, being cognizant of the amount of time and cost for MLA engagement. For the samples analyzed in this study there was an average of

680 +/- 340 particles/frame at analysis rate 400 +/- 100 particles/minute using an MLA time of 220 +/- 20 minutes/analysis. The following bulk modal mineralogy with respect to availability was observed:

(i) Sulphides

Results for Cell 06 sulphide MOIs, grouped and normalized to 100%, are shown in Figure 5.2.2.1. “Head” refers to fresh (i.e. unweathered) waste rock and “SLR” refers to waste rock sequential leach residue. The horizontal (x-) axis displays the various size fractions of the waste rock sample (measured in microns). The vertical (y-) axis references the normalized weight-percent presence of a MOI.

The highest sulphide liberation was in the finer size fractions and increased noticeably after the SL. Partially exposed sulphide content decreased greatly after the SL - especially in the -600/+297 µm size fraction. Cell 06 was described to be non-AG (see Table 3.2.4) so it could be assumed that it included a large carbonate content. It was found that the SL significantly decreased the concentration of host carbonate particles, while liberated locked sulphides and secondary MOIs such as iron oxyhydroxides were formed. The remaining sulphide residue may either be unleachable or the SL was incomplete (i.e. insufficient reagent).

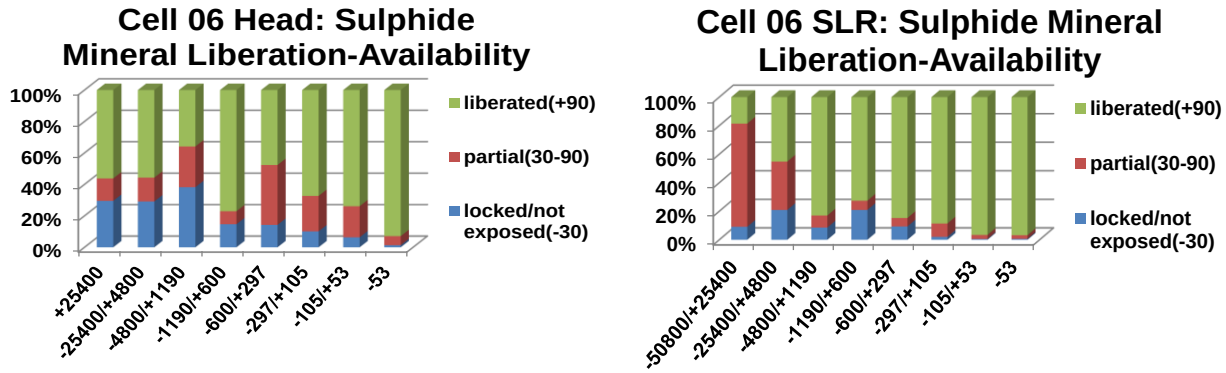

Figure 5.2.2.1. Example of Cell 06 grouped sulphide MOIs: (a) before SL (head); and, (b) after SL (SLR). The horizontal axis refers to the various size fractions of the waste rock sample (microns). The vertical axis refers to weight-percent (normalized).

(ii) Carbonates

Results for Tucush 03 carbonate MOIs, grouped and normalized to 100%, are shown in Figure 5.2.2.2. Tucush 03 was described as a Class A blend of marble and hornfels (see Table 3.2.4). The MLA analysis showed carbonates were prevalently liberated in all size fractions. The SLR results indicated increased locked material especially in the -600/+297 µm size fraction. SEM EDS examination of particles suggested the SL caused rapid carbonate dissolution followed by rapid MOI phase precipitation which prevented further carbonate dissolution. This armouring and / or precipitation was not observed in the finest size fraction material which suggested that these high surface area particles were in a constant state of flux and provided no firm surface to precipitate on. The finding of SLR carbonate remaining could suggest that the SL was incomplete (i.e. insufficient reagent).

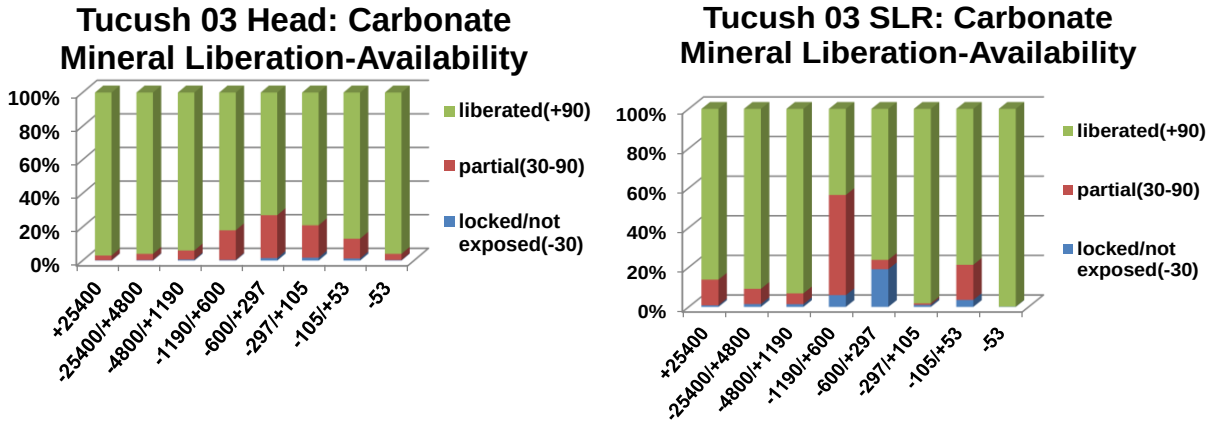

Figure 5.2.2.2. Example of Tucush 03 grouped carbonate MOIs: (a) before SL (head); and, (b) after SL (SLR). The horizontal axis refers to the various size fractions of the waste rock sample (microns). The vertical axis refers to weight-percent (normalized).

(iii) Silicates

Silicate MOIs, as mentioned in chapters 1 and 2, have a higher acid neutralizing capacity than carbonates though slower dissolution rates. The more reactive waste rock carbonates would out-compete silicates in neutralization processes. Nonetheless silicates can still affect the long term ARD of a waste rock pile after carbonate depletion. For example, at low drainage pH <1, clay silicates begin to

neutralize acid [Blight and Ralph, 2004; Shiers *et al.*, 2005]. MLA analysis highlighted silicate neutralization around some particle perimeters which suggested carbonate was unavailable at times.

MLA detection suggested when some silicates dissolve ARD neutralization caused metal attenuation. Examination of MLA-detected MOIs revealed local textural concavities which represented acid-consuming (neutralizing) silicate minerals, such as Antamina mine's pyroxene, amphibole, titanite and clay (e.g. Table 1.1). In the basic pH drainage of the Antamina mine waste rock, (altered) mica was often found associated with Cu and Zn. Examination of the (altered) mica particles with SEM and EDS sometimes showed a jarosite-like phase on the surface which suggested either low pH local environment or particles with textural features that protected jarosite from expected dissolution.

Results for Class A PAG UBC3-2A (see Table 4.2.4) silicate MOIs, grouped and normalized to 100%, are shown in Figure 5.2.2.3. The SL simply increased silicate liberation suggesting silicate surfaces were not preferred for secondary oxide precipitation (assuming secondary oxide precipitation was an active process).

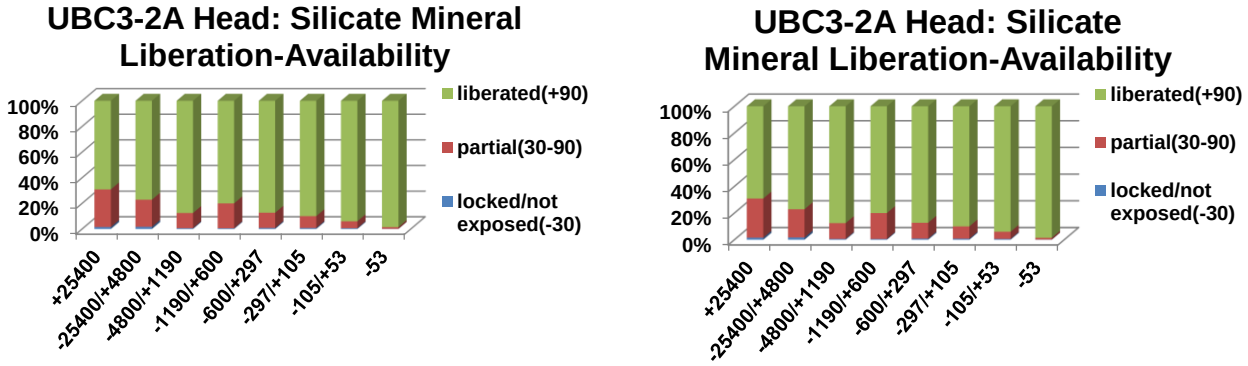

Figure 5.2.2.3. Example of UBC3-2A grouped silicate MOIs: (a) before (head); and, (b) after (SLR). The horizontal axis refers to the various size fractions of the waste rock sample (microns). The vertical axis refers to weight-percent (normalized).

The following metal-associated modal mineralogy was observed:

(i) Antimony (Sb)

MOI phases associated with antimony were not numerous (3-8 particles per size fraction) compared to the other metals in this study. Particle statistics per sample mount for the other metal-associated MOIs studied were: *arsenic*, 200-700; *copper*, 900-4000; *molybdenum*, 100-500; *lead*, 300-2000; and *zinc*, 600-3000. The few metal Sb occurrences discouraged conclusions. The low number of occurrences suggest the waste rock either does not attenuate Sb well or that there was little Sb in the waste rock initially. More samples of the waste rock would need to be analyzed to make stronger statements. Sb-bearing MOIs in Class A Tucush 04, UBC3-2A and UBC2-3A were more than 95% liberated in all size fractions. The high liberation is indicative of potentially high ARD activity.

(ii) Arsenic (As), copper (Cu) and zinc (Zn)

MOI phases that were associated with arsenic, copper or zinc were more liberated after the SL, especially in the sub-297 µm particles.

(iii) Molybdenum (Mo)

Results for UBC2-3A waste rock material with Mo-bearing MOIs, grouped and normalized to 100%, are shown in Figure 5.2.2.4. The MOIs were generally more liberated, though the finer size fractions only contained non-liberated material. From this could be suggested: (1) Mo-bearing MOIs do not leach readily in the SL; (2) formation of secondary Mo-attenuated phases; and / or (3) more complex Mo-bearing phases underwent partial dissolution. The major Mo-bearing MOIs, especially after the SL, were iron sulphate and molybdenite. UBC2-3A waste rock was described as Class A PAG particles – yet Mo-bearing species locking did not change after the SL conditions.

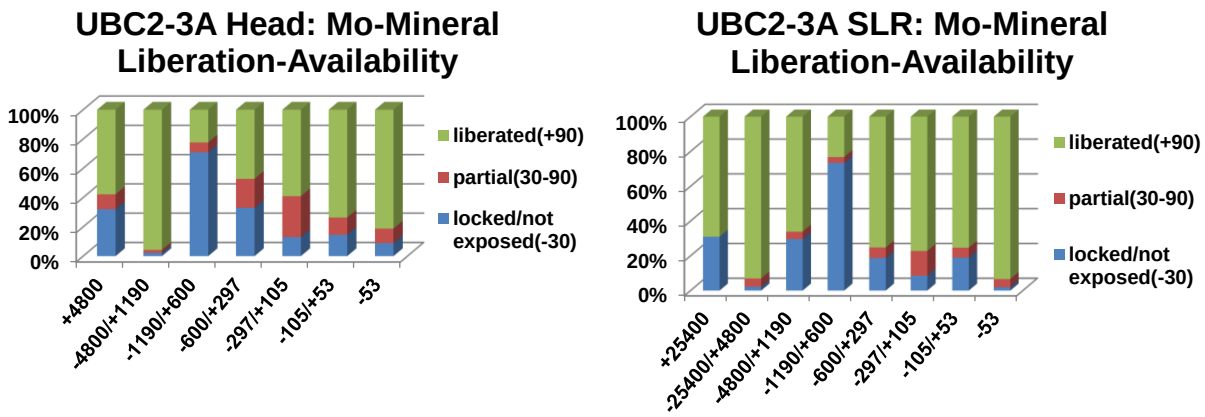

Figure 5.2.2.4. Example of UBC2-3A grouped Mo-bearing MOIs: (a) before (head); and, (b) after (SLR). The x-axis refers to the various size fractions of the waste rock sample in units of microns. The y-axis refers to weight-percent (normalized).

(iv) Lead (Pb)

After the SL, lead-bearing MOIs showed increased exposure as the Pb-bearing particle size decreased, especially sizes below 105 µm, suggesting that larger particles were better suited as Pb attenuators.

5.2.3 Mineral phase type of association

In developing a weathering model it is useful to know such parameters as mineralogy, degree of exposure and mineral phase(s) associated with the MOI. In this section (see Appendix 18 for detail) MLA Dataview was used to examine the type of association between the MOI and adjacent phases. It is not within the scope of this study to assess and / or coordinate lithology to secondary mineralization. The exposure or availability of the MOI grain was defined by the type of MOI association and degree of contact to other mineral phases. Particles were classified into the following groups based on MOI area percent (normalized): “liberated”, meaning no contact with other mineral phases; and non-liberated phases. Non-liberated phases would be mineral grains associated in either “binary” (refers to the MOI being associated with one other mineral phase) or “ternary+” (refers to the MOI being associated with two or more mineral phases). In this context non-liberated phases would have part of their perimeter / surface exposed and

available for leaching (see Figure 4.2.1). In the following discussion, all MOIs will be assumed to have a binary association unless specifically stated to be ternary association or liberated. In the figures, all phases refer to binary association, if not labeled Liberated% or Ternary+%,

Type of association data examples are shown in Figure 5.2.3.1 for sulphide and carbonate MOIs.

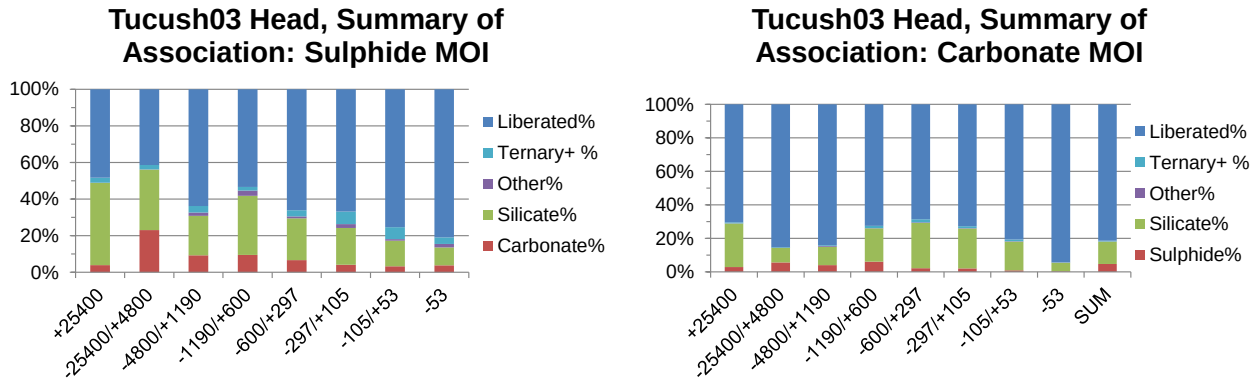

Figure 5.2.3.1. Example of MLA application: MOI association based on contact.

Bulk modal mineralogy showed:

(i) Sulphides

Binary associations with sulphides were rare, with less than 3% (overall) in the Head samples and less than 10% in the SLR samples. The higher presence in the SLR suggested dissolution and liberation of previously locked sulphides. No ternary associations with sulphides were found. Samples from UBC3-2A, described as Class A coarse sand (see Table 3.2.4) showed a trend of binary sulphide associations from more than 25% in the coarse -1190/+600 µm size fraction to less than 10% in -105/+53 µm size fraction to full liberation in the -53 µm size fraction. Binary association of sulphides was generally with silicates, and significantly less with carbonates. After the SL, sulphides were highly liberated. Carbonates in binary association with sulphides appeared to be coatings on sulphide grains. Silicates in binary association with sulphides appeared to lock carbonate grains. The -53 µm size

fraction had the highest sulphide liberation (i.e. greater than 90%); lowest sulphide liberation was in the coarser size fractions (e.g. 5-70% in -1190/+600 µm size fraction). In all SLR samples there was a trace amount of sulphide ternary association (e.g. less than 2%).

(ii) Carbonates

Before the SL, carbonates with grain size less than 297 µm generally showed high (75%) liberation. After the SL, the SLR contained decreased carbonate liberation, especially in the coarser size fractions (i.e. greater than 297 µm), though increased binary association to silicates. This was likely the exposure of silicates which did not dissolve as easily as the carbonates, yet remained attached to the carbonates (i.e. incomplete SL). The lowest carbonate liberation was observed in the largest grain size. The SLR carbonates were mainly in binary association with silicates (i.e. up to 60%) and to a much lesser degree with other phases (i.e. less than 5%), while ternary associations insignificant (i.e. less than 5%) suggesting the SL released any MOIs that were locked in the carbonate particles.

(iii) Silicates

Generally, Head silicate grains (not shown) had minimal (<3%) binary association and grains smaller than 297 µm were mostly liberated (i.e. >90%). After the SL, more than 95% of all silicate grains were liberated. Before the SL, silicates associated with another mineral phase were rarely (i.e. <3%) in binary association with carbonates. However, after the SL the silicate binary association to carbonates increased, especially in the coarser size fractions (e.g. greater than 105 µm). This observation suggested both incomplete SL and secondary precipitation on silicate grains, as was evidenced by SEM-EDS examination that showed phases of oxide and sulphate (see section 5.1). Any secondary carbonate, such as siderite, dissolved during the SL (see section 5.1).

The groupings of select metal-bearing MOIs are shown in Appendix 1. The following observations were made:

(i) Sb-bearing phases

After the SL, there were no Ternary+ associations. The Head samples showed high liberation in the -53 µm size fraction and after the SL the Sb-bearing phases were found to be liberated from larger -105/+53 µm grains (e.g. 90-95%) with only 5-10% binary association to silicates. The SL significantly reduced Sb-bearing phase associations. For example, in -105 µm particles, the Tucush 01 Head had 50% Sb-bearing MOI binary association with silicates, 40% Ternary+ and 10% liberated grains, yet after the SL ~100% liberation was detected. Sb-bearing phases were usually quite small in the waste rock, hence when an Sb-phase was found in a large size fraction it suggested that the Sb was either present as partially exposed MOI or adsorbed to a secondary precipitation (e.g. silicate). An example of Sb-bearing MOI comparison between Head and SLR can be seen in Figure 5.2.3.2.

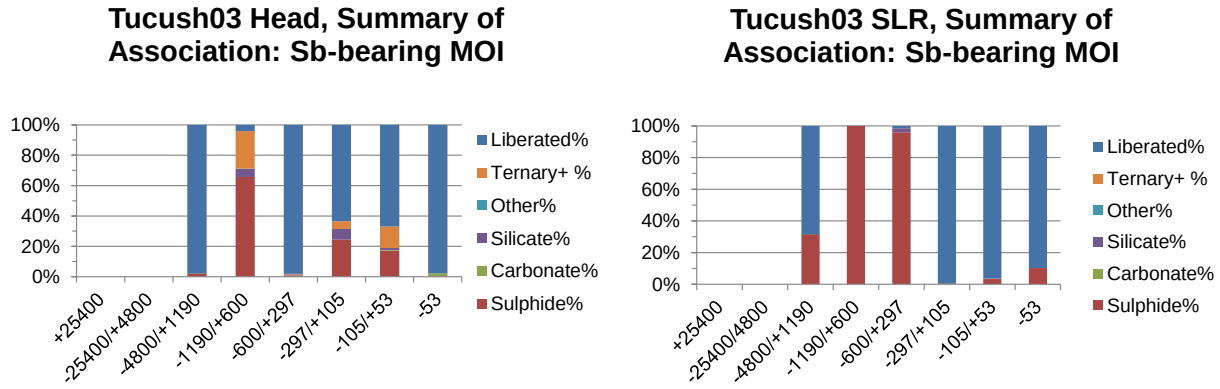

Figure 5.2.3.2. Example of Sb-bearing phase contact association.

(ii) As-bearing phases

After the SL it was noted that As-associated MOIs were more than 80% liberated with zero carbonate association in the remaining 20% that was unliberated. Generally binary association with sulphide increased 5-10% after the SL, with one exception - Cell 06 had similar sulphide association before and after the SL. The

SLR showed As-bearing silicates significantly decreased. Ternary associations were more prevalent before the SL. However, the SL could cause complex Ternary+ associations in all size fractions as seen in Figure 5.2.3.3. The SLR increase in binary sulphide association with As-bearing MOI (relative to Head) suggested the SL decreased the amount of primary As-bearing phases, followed by As association with sulphide, oxide and sulphate phases (see section 5.2).

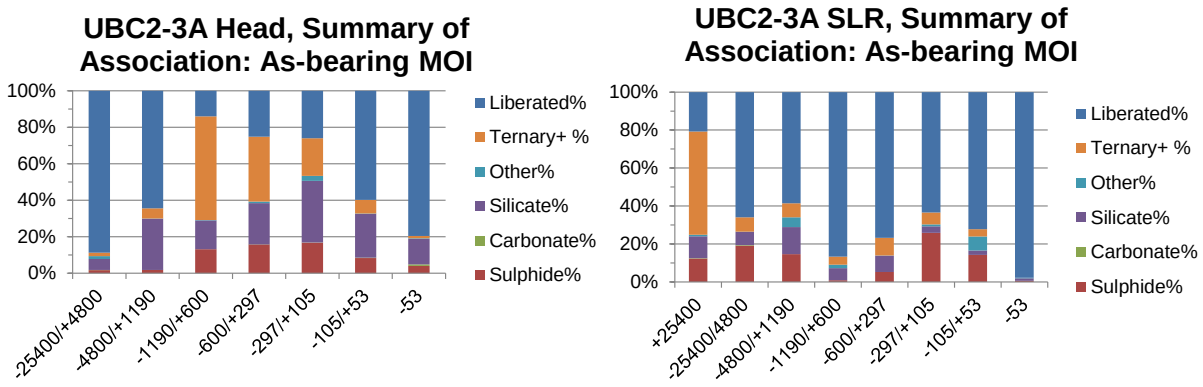

Figure 5.2.3.3. Example of As-bearing phase contact association.

(iii) Cu-bearing phases

Generally more than 80% liberation was observed in the Head -53 µm size fraction and SLR -297 µm size fractions. Binary silicate associations with Cu-bearing MOIs decreased after the SL (i.e. 10-20% present after SL, and up to 60% before SL). No carbonate associations were noted below 1190 µm grain size. After the SL, there was less than 5% sulphide association with Cu-bearing phases. Ternary+ associations were relatively more prevalent in the Head samples, with less than 5% in the SLR.

(iv) Pb-bearing phases

Liberation was greater than 85% in both the Head and SLR -53 µm material. Generally after the SL, liberation was greater than 80% in the -297 µm material with one exception - Cell 06 liberation of Pb-bearing MOIs did not significantly change. After the SL, sulphide association to Pb-bearing MOIs increased in some samples

(e.g. UBC3-2A and UBC2-3A, especially in - 297/+53 µm grain size; see Figure 5.2.3.4). After the SL there was zero carbonate association with Pb-bearing phases.

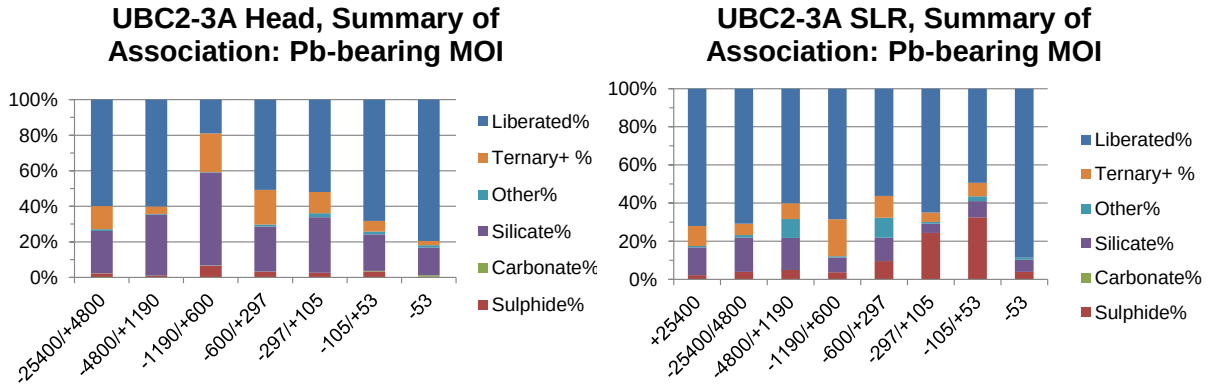

Figure 5.2.3.4. Example of Pb-bearing phase contact association.

(v) Mo-bearing phases

More than 85% liberation was noted in Head -53 µm and SLR -297 µm size fractions, with the exceptions of UBC3-2A and UBC2-3A where after the SL there were binary silicate and sulphide associations, as well as ternary+ associations. This was considered unusual because ternary+ associations were generally few or not detected after the SL. After the SL there were no carbonate associations detected in -297 µm sized particles. After the SL, Cell 06 was noted to have the largest content of liberated Mo-bearing phases, especially in -297 µm size fractions (see Figure 5.2.3.5). Silicate association with Mo-bearing MOIs was seen in the -1190/+600 µm size fraction after the SL suggesting the SL either altered silicate surfaces to sequester Mo atoms or silicate associated with Mo-bearing MOI were unlocked from a host particle.

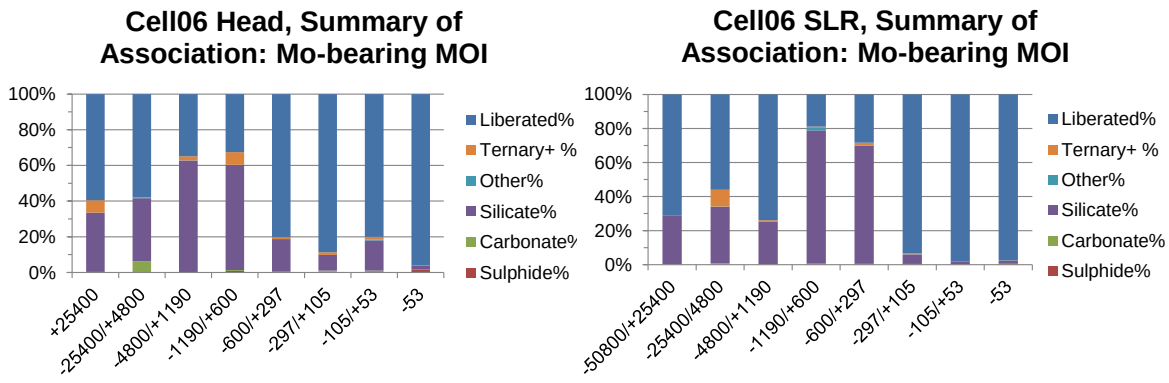

Figure 5.2.3.5. Example of Mo-bearing phase contact association.

(vi) Zn-bearing phases

The -53 µm SLR samples showed more than 90% liberation. After the SL no carbonate associations were seen in -1190 µm size fractions. After the SL, Zn-bearing phases included silicates and sulphides (in that preference order). After the SL, Zn-bearing phase association to sulphides significantly increased (i.e. doubled) which suggested zinc adsorption to particle surfaces (see section 5.1). Ternary+ association decreased after the SL.

5.3 Secondary minerals of interest

Weathering rates of metal-bearing MOIs in the laboratory, field cell or experimental pile and actual releases in the field are very different. Natural field sites have many uncontrollable (and unknown) features. Precipitated secondary minerals associated with host material released and / or leached during a leaching test will complicate reaction interpretation.

The scope of this study was not to develop weathering mechanisms, but to demonstrate the usefulness of the MLA for waste rock characterization. The selected metals, specifically Sb, As, Cu, Pb, Mo, and Zn, associated with both primary and secondary phases were studied. On-site mine weathering studies have shown that Class B waste

rock sometimes had unexpected higher effluent metal content than Class A waste rock [Antamina, 2001]. Many studies have shown pH increases cause metal concentration in waste water drainage to decrease [e.g. Plumlee *et al.,* 1999]. Recent observations at the Antamina mine site have shown that similar metal attenuation does occur [Golder, 2004]. In this study example of MLA analysis, it was to demonstrate detection and identification of MOIs which may help understand waste rock weathering processes. The mandate was to identify, rather than to quantify, the secondary metal-bearing MOIs (though the MLA could perform the quantification).

The MLA analysis provided interesting information for waste rock characterization based on the type of association, MOI association and MOI availability. The MLA analysis does produce massive quantities of MOI mineralogical feature data, which includes recorded x-y coordinates for all phases (i.e. particle segments). Any recorded phase can be easily relocated by directing MLA software to move the stage to place the electron beam and EDS exactly on those coordinates of the sample mount surface to manually investigate the MOI.

For this demonstration of MLA software application, the samples described in Table 3.2.2 (i.e. “sand” collected from bottom of field cells) represented weathered waste rock particles from the field cells described in Table 3.2.1. UBC laboratory tests were conducted using these “sand” samples to investigate the sequestration / attenuation of Mo and the results are recorded elsewhere [Conlan, 2009; Conlan *et al.,* 2012].

The MLA analysis mode XBSE_STD located the mineral phases and collected an X-ray spectrum. High resolution BSE imaging of grain boundary definition and speed of single X-ray mineral identification make this method ideal for most mineralogical samples.

A review of the MLA data was made to determine the association of waste rock secondary mineralization (e.g. altered sulphides) with other mineral phases (e.g.

primary or secondary). In Table 5.3.1 is a summary of prevalent select metal-associated mineral phases located in samples during the MLA analysis.

Table 5.3.1. Prevalent select metal-associated mineral phases in "sands" (see Table 3.2.2).

Waste rock type	Sb	As	Cu	Pb	Mo	Zn
Hornfels	-	FeSulphate, Hematite, Schwertmannite, Siderite	Apatite, FeCuSilicate, FeSulphate, Grunerite, Hematite, K-Feldspar, Mica-Altered, Titanite	Chalcopyrite, Grunerite, Magnesite, Titanite	FeSulphate	FeSulphate, Grunerite, Mica-Altered, Siderite, Magnesite
Intrusive	Stibnite, Watanabeite	FeSulphate, Hematite, Tennantite	Apatite, Chalcopyrite, Enargite, FeCuSilicate, FeSulphate, Hematite, K-Feldspar, Mica-Altered, Sphalerite	Chalcopyrite, Grunerite, Magnesite, Titanite	FeSulphate, Molybdenite, PbMoOxide	Chalcopyrite, FeSulphate, Mica-Altered, Sphalerite, Grunerite, Magneiste
Marginal Cu	-	FeSulphate	Apatite, Chalcopyrite, K-Feldspar, Mica-Altered, Titanite	Chalcopyrite, Galena, Grunerite, Titanite	FeSulphate, Molybdenite	Chalcopyrite, Mica-Altetred, Sphalerite, Grunerite, FeSulphate
Endoskarn	-	FeSulphate	Apatite, Chalcopyrtie, Grunerite, K-Feldspar, Mica-Altered, Sphalerite	Chalcopyrite, Galena, Grunerite, Titanite, Magnesite	FeSulphate, Molybdenite	Chalcopyrite, Mica-Altetred, Sphalerite, Grunerite, FeSulphate, Siderite
Marble	Stibnite	FeSulphate, Siderite	Apatite, Chalcopyrite, FeCuSilicate, Grunerite, Hematite, K-Feldspar, Mica-Altered, Titanite	Chalcopyrite, Galena, Grunerite, Titanite, Magnesite, Molybdofornacite	FeSulphate, Molybdofornacite	Mica-Altered, Grunerite, Sphalerite, FeSulphate

5.3.1 Arsenic-bearing phases

Arsenic sulphides exist primarily as arsenopyrite (FeAsS), realgar (As_2S_2), orpiment (As_2S_3) and enargite (Cu_3AsS_4) in most deposits [Dave *et al.*, 2008]. There were three principal arsenic bearing minerals identified at the Antamina mine site: arsenopyrite, tennantite and enargite. These MOIs could have variable As (and Sb) concentrations as a result of solid solution chemistry or leaching. Arsenic has also been associated with a number of copper sulphide species which perhaps indicated the high mobility of this element [Gasparini, 1983; Olsen *et al.*, 2003]. From Table 5.3.1, the As-associated mineral phases are mainly iron-bearing sulphate, carbonate and oxide. There were no prevalent As-associated silicate phases recorded, compared to the other selected metals studied (i.e. Sb, Cu, Mo, Pb, Zn). After exposure to the SL procedure only the former two MOIs were prevalent (see Table 6.2.1.1).

Possible explanations for low detection of primary As-bearing MOIs include:

- Arsenic can be extracted from particle surfaces of sulphide minerals such as pyrite, chalcopyrite, arsenopyrite and enargite. In the waste rock samples analyzed by MLA, trace quantities of enargite (Cu_3AsS_4) were detected. Guo *et al*. [2011] found As leaching may not occur easily in an acidic environment in the absence of silver catalysts, and suggested ferric ion was not an effective leaching agent in the absence of silver catalysis. Lattanzi *et al.,* [2008] reported enargite oxidation was slow in acid though the rate increased at higher pH. Observation in this study and previous study suggested that the low abundance of primary As-bearing MOIs, such as arsenopyrite and enargite in the waste rock samples may be a reflection of observed higher pH drainage (i.e. NRD) and / or presence of silver ions.
- Bacterial leaching (sulphur and / or iron oxidizing) and weathering can release minor metals associated with primary arsenic sulphide minerals (such as iron) into the environment. The sulphates formed [Rohwerder *et al.*, 2003] during oxidation could inhibit further leaching by coating the As-bearing phases [Sand *et al.*, 2001]. MLA analysis detected iron sulphate associated with several metals though it was not possible to determine if the metal was present as a sulphate species or adsorbed to iron sulphate.
- In some samples, the MLA analysis detected trace Ag both before (head) and after the SL (SLR) as a sulphosalt. A theoretical As leach mechanism might be: Arsenic on the particle surface (either adsorbed or transferred from the sulphide lattice) exchanges with silver ions with consequent release of As to the environment and a Ag_2S phase forms on the surface [(see section 5.1; Cordoba *et al*., 2009]. The Ag_2S phase is attacked by oxygen and acid to regenerate the silver ions. This cycle progressively liberates As on the particle surface. Using SEM-EDS, some particle surface residue was determined to contain K, Fe, S and O which appeared to be jarosite without elemental sulphur. Assuming the Fe is present as ferric ion, the ferric ion could precipitate as a hydroxide in the circumneutral pH of the carbonate-rich waste rock. This would remove ferric iron

from the ferrous-ferric cycle. In the samples analyzed iron hydroxide was difficult to classify using EDS due to an inability to detect low atomic number hydrogen (i.e. could not confirm this aspect of theory). Nonetheless, ferric ion could be constantly generated from many other iron sources, hence should not be a reaction limiting factor. If trace silver was present, sulphide mineral leaching (e.g. pyrite, chalcopyrite, arsenopyrite, enargite) would increase as the ferric ion concentration increased [Cordoba *et al.,* 2009]. This could explain the few primary As MOIs detected. It was also noted in the SLR BSE images that particle surface layers appeared porous. The rare findings of both silver and arsenopyrite species, plus apparent porous surface layers support arsenopyrite leaching through a catalytic mechanism.

It was possible to direct the MLA stage to detected As-associated MOIs using MLA digitized image data. The following observations were made from EDS study of select particles representing Table 3.2.2:

- Arsenic, associated with a Pb molybdate phase, was identified in Intrusive sample, size fraction -44 µm. The core of the particle contained molybdenite which altered at its rim to form either (Ca,Pb)molybdate or Ca oxide blended with Pb molybdate. The molybdate phase's rim appeared to integrate arsenic into its matrix to form molybdofornacite [$Pb_2Cu(AsO_4)(MoO_4)(OH)$]. It is proposed that the molybdofornacite's rim released arsenic as it altered to a blended layer of Mo oxide wulfenite ($PbMoO_4$) and powellite ($CaMoO_4$).

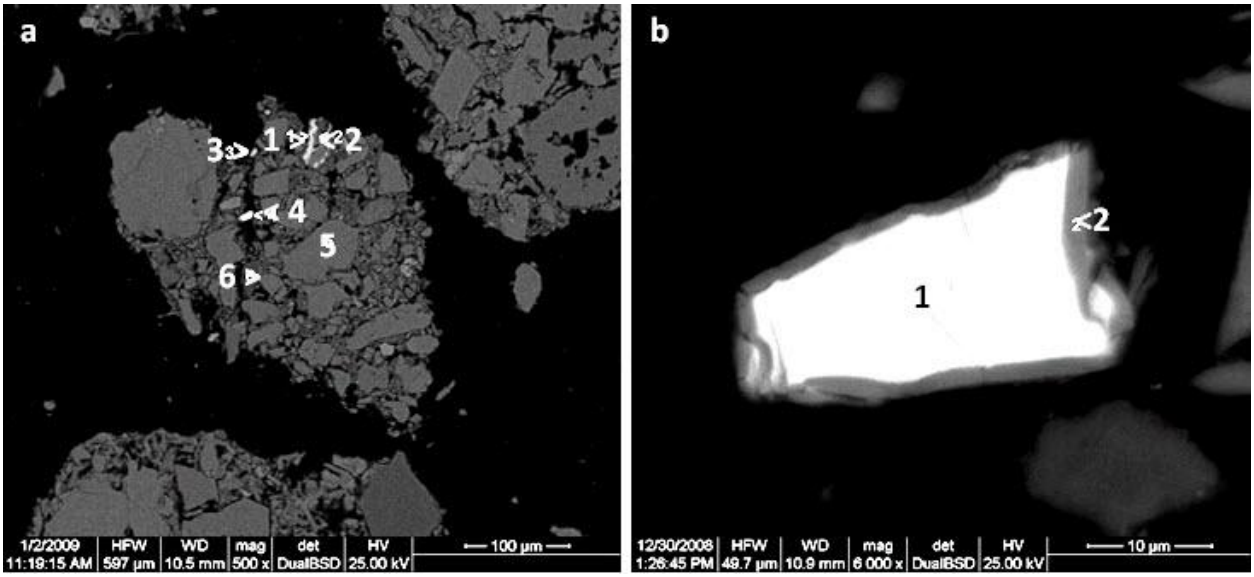

Figure 5.3.1.1. Photomicrographs showing example particles of As-bearing waste rock: (a) Marble: rim of Mn oxide with minor Pb, As, Cu, Zn [1], partially exposed Diopside [2], FeCa silicate blended with Fe oxide containing trace Pb, Cu and Zn [3], fracture-hosted grain inclusion of conichalcite blended with Pb carbonate containing trace Zn [4], host mineral phases calcite and Ca oxide [5], garnet [6]; (b) Endoskarn: chalcopyrite [1], rim phase of calci-aluminosilicate blended with Fe oxide containing trace Zn and As [2]. Either the As was present in the chalcopyrite as solid solution and leached out, or As was adsorbed (integrated) to the rim phase.

- Calcite and Ca oxide sequestered Pb in the form of carbonate (cerrusite, $PbCO_3$). Molybdofornacite's content of Pb and Mo decreased to form Cu arsenate mineral [conichalcite: $CaCu(AsO_4)(OH)$]. The presence of calcite suggested a basic environment which could promote As oxyanion stability. In the presence of calcite and Ca oxide host, a diopside ($CaMgSi_2O_6$) particle's rim became associated with oxides of Mn, Pb and Cu. It was not clear if diopside partially dissolved and attenuated the cations or was simply a site for oxide precipitation (see Figure 5.3.1.1(a)). Fe oxide or hydroxide was noted to be associated with arsenic.
- Chalcopyrite particle weathering developed an iron oxide rim containing Si and traces of Zn and As (see Figure 5.3.1.1 (b)). This may suggest silicate buffering.

5.3.2 Copper-bearing phases

From Table 5.3.1, the Cu-bearing mineral phases are mainly the phosphate apatite, oxides hematite and FeOxideCu ($Fe_2Cu_{0.04}O_4$), and the silicates mica (altered), titanite, K-feldspar, and grunerite. Cu-bearing iron sulphate, while not as significant as those mentioned, was only noted in the hornfels and intrusive waste rock.

At the Antamina mine, chalcopyrite was detected in the waste rock. While some copper minerals such as MOI chalcopyrite may not readily undergo oxidation and dissolution [Sandstrom *et al.*, 2005; Mehta and Murr, 1982a; Hackl *et al.*, 1995; Dreisinger, 2006; Córdoba *et al.*, 2008a, 2008b; Klauber, 2008], copper can still be detected in the NRD. This shows the importance of understanding oxidation pathways.

From a chemical viewpoint, galvanic interaction could play an important role in aqueous mineral dissolution. Sulphides in direct contact with minerals of different rest potential can experience this galvanic effect which could increase dissolution of one or both minerals. For example, the presence of pyrite increases chalcopyrite dissolution 2-15 times [Córdoba *et al.*, 2008a, 2008b; Nazari *et al.*, 2011].

Table 5.3.2.1. Rest potentials for select mineral phases.

Mineral	Chemical formula	Rest potential (V vs. SHE)
Pyrite	FeS_2	0.66
Chalcopyrite	$CuFeS_2$	0.56
Sphalerite	ZnS	0.46
Chalcocite	Cu_2S	0.44
Covellite	CuS	0.42
Bornite	Cu_5FeS_4	0.36
Pentlandite	NiFeS	0.35
Copper	Cu	0.34
Pyrrhotite	$Fe_{(1-x)}S$	0.31
Galena	PbS	0.28
Argentite	Ag_2S	0.21
Stibnite	Sb_2S_3	0.09
Molybdenite	MoS_2	0.08

In an aqueous environment most sulphide minerals function like an electrode (i.e. can conduct electrons). MOI rest potentials will indicate tendency to react when in contact with another mineral. Table 5.3.2.1 shows rest potentials for select MOIs [Kocabag, 1985; Hayes and Ralston, 1988]. In a complex particle the region with the higher rest potential (cathode) would be protected from degradation, which has been reported elsewhere [for example: Nichol, 1975; Mehta and Murr, 1982b, 1983; Natarajan and Iswasaki, 1983; Liu and Zhao, 2007; Tshilombo, 2004; Dixon and Mayne, 2007]. Pyrite generally has the highest rest potential of the common sulphides and therefore most often represents the cathode. Using Table 5.3.2.1 a galvanic interaction between MOI argentite and pyrite would explain why silver ions could be found in the ARD / NRD solution environment. To increase electron flow between adjacent MOIs would require either larger rest potential difference or increased cathode surface area (e.g. smaller particles).

However, most detected chalcopyrite grains were not large. As mentioned, it was suggested that chalcopyrite was leached through a galvanic interaction with pyrite (FeS_2). The dissolution reaction for ferric oxidation of chalcopyrite ($CuFeS_2$) is shown in Equation 9.

$$CuFeS_2 + 4Fe^{+3} \rightarrow Cu^{+2} + 5Fe^{+2} + 2S^0 \qquad \text{Eq. 9}$$

Direct acid dissolution of chalcopyrite (see Equation 10) was reported to be negligible when compared to Equation 9 [Liu and Zhao, 2007].

$$CuFeS_2 + O_2 + 4H^+ \rightarrow Cu^{+2} + Fe^{+2} + 2S^0 + 2H_2O \qquad \text{Eq. 10}$$

During the leach process ferric ions would be consumed. This might imply chalcopyrite dissolution would slow over time; however, ferric ions can be regenerated through ferrous oxidation, according to Equation 6 [Holmes and Crundwell, 2000].

$$4Fe^{+2} + O_2 + 4H^+ \rightarrow 4Fe^{+3} + 2H_2O \quad \text{Eq. 6}$$

The overall chalcopyrite oxidation reaction in Equation 10 (sum of Equations 9 and 6) emphasizes the strong influence of galvanic ion interaction [Hiroyoshi *et al.*, 2000, 2001, 2004, 2008].

SEM-EDS examination of chalcopyrite particles with observed rim phases suggested iron ions were released first from the surface to form iron deficient chalcocite (Cu_2S). The chalcocite rim appeared to degrade to form covellite (CuS) and / or copper sulphate according to Equation 11 or 12.

$$2Cu_2S + 2H_2SO_4 + O_2 \rightarrow 2CuS + 2CuSO_4 + 2H_2O \quad \text{Eq. 11}$$

$$Cu_2S + 2Fe_2(SO_4)_3 \rightarrow 2CuSO_4 + 2FeSO_4 + S^0 \quad \text{Eq. 12}$$

Covellite particles may also oxidize to form a simple sulphate (see Equation 13). In the samples studied by MLA, copper sulphate phases were detected which suggested both chalcocite and covellite were involved in chalcopyrite degradation. These detected intermediate chalcopyrite degradation products were associated with chalcopyrite particle rims.

$$CuS + Fe_2(SO_4)_3 \rightarrow CuSO_4 + 2FeSO_4 \quad \text{Eq. 13}$$

Modal mineralogy of the samples in this study suggested “pure” chalcopyrite did not degrade significantly during the SL (i.e. similar content in SLR). Based upon chemistries mentioned, this may suggest that either chalcocite and / or covellite hinder chalcopyrite dissolution or elevated pH affected ferric ion chemistry. Van Aswegen *et al.* [2007] found that ferric iron could precipitate at pH values above 2 as jarosite (see Equation 14) where X could be monovalent cations K^+, NH_4^+, Na^+, Ag^+, etc. [Deveci *et al.*, 2004].

However, only trace amounts of jarosite were detected in the samples which suggested that the higher pH NRD environment affected the chalcopyrite dissolution.

$$X^{+} + 3Fe^{+3} + 2SO_4^{-2} + 6H_2O \rightarrow XFe_3(SO_4)_2(OH)_6 + 6H^{+} \qquad \text{Eq. 14}$$

Another possible route for Cu ions in NRD will be proposed. In the MLA analysis of the Head and SLR, the amount of chalcopyrite ($CuFeS_2$) associated with Pb decreased in the SLR relative to the Head; however, the amount of Pb-free ("pure") chalcopyrite was unchanged (see section 5.1). Nava and Gonzalez [2006] and Nazari *et al.* [2011] among others, reported that trace silver associated with pyrite improved chalcopyrite leaching. The MLA detected both Pb associated with chalcopyrite and traces of silver in sulphosalts (and also suspected to be in pyrite lattices). Galvanic interactions between galena and chalcopyrite could exist because galena has a lower rest potential than chalcopyrite (see Table 5.3.2.1) causing release of Pb ions which could be attracted and adsorbed to the chalcopyrite particle surface.

MLA analysis revealed that some silicates, such as grunerite, did not associate with oxides (e.g. oxyhydroxides, sulphates or phosphates). Modal mineralogy determined by MLA analysis showed Pb- and Cu-bearing grunerite dissolved in the SL. This could either reflect the breakdown of the silicate or the removal of surface adsorbed Pb and Cu ions.

Using MLA digitized image data it was possible to direct the MLA stage to detected Cu-associated MOIs. The following observations were made from EDS study of select particles representing Table 3.2.2:

- Chalcopyrite dissolution is expected to start at the particle perimeter exposed to the environment. A chalcopyrite particle rim was identified that was composed of Cu silicate [dioptase $CuSiO_2(OH)_2$], Cu sulphate [dolerophanite Cu_2SO_4], and minor amounts of Ca sulphate [anhydrite $CaSO_4$], and trace Zn and As (see

Figure 5.3.2.1(a)). It is proposed that chalcopyrite was initially coated with Ca sulphate where the sulphur leached from chalcopyrite formed into the sulphate. The Ca sulphate partially converted to Cu sulphate where Cu ions were supplied from the chalcopyrite. Copper sulphate was then replaced by Cu silicate and the sulphate perhaps bonded with Ca in the calcite-rich environment. This result suggested silicate buffering or neutralization. Iron was not detected in the rim, which either indicated that iron sulphate in the rim preceded secondary Ca sulphate or Fe was not attenuated in the particle rim.

- When chalcopyrite weathering began, Fe content decreased in the perimeter to form a new Fe-poor Cu sulphide phase (see Figure 5.3.2.1(b)). It was noted that the phase with decreased sulphur [3] did not contain sulphur as sulphate, perhaps due to the presence of silicate. Also (leached) Cu did not appear in the Fe oxide phase, suggesting Cu has a pH dependency for attenuation.
- Chalcopyrite can be leached through interior particle cracks (see Figure 5.3.2.2(a)) to release sulphur to the environment. The fractures in a chalcopyrite host particle appeared to aid particle degradation from inside to perimeter, forming a secondary phase of FeCu oxide (delafossite, $CuFeO_2$). The particle rim was composed of a blend of Fe oxide (magnetite, $FeO{\cdot}Fe_2O_3$) and Cu silicate (dioptase). It is proposed that once oxide began to form, it enabled (“bridged”) reagent and product exchange. Particle observation suggested that Cu attenuation by a silicate was more stable than oxide.

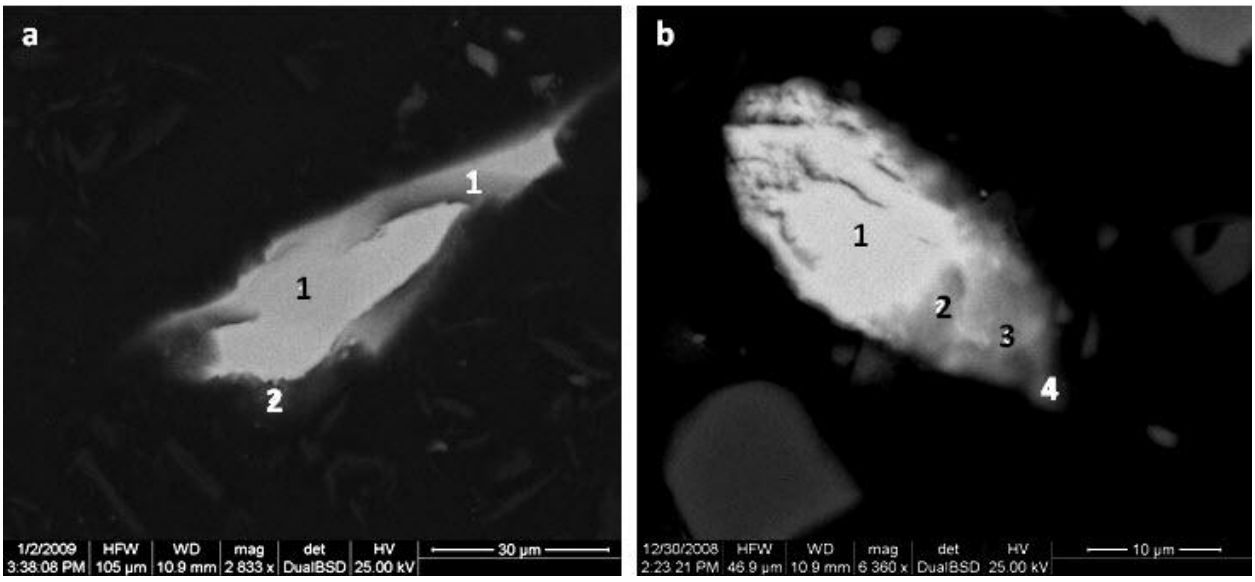

Figure 5.3.2.1. Photomicrographs showing example particles of Cu-bearing waste rock: (a) Intrusive: Chalcopyrite grain [1] showing rim degradation to blend of Cu silicate, Cu sulphate and Ca sulphate containing Zn and As [2]; (b) Endoskarn: Chalcopyrite host grain [1] blended with an Fe silicate containing trace Al and Ca (fayalite, $Fe_2(SiO_4)(OH)_4$) [2], chalcopyrite released Fe and resembled a Cu-rich sulphide phase [bornite, Cu_5FeS_4], which transitioned to Cu silicate [dioptase] blended with Fe oxides containing trace Ca (magnetite, $FeO.Fe_2O_3$ and hercynite, $FeAl_2O_4$) [3], which then transitioned to a chlorite (clinochlore, $(MgFe)_5Al_{0.5}(Si_3Al)O_{10}(OH)_8$]) and Fe oxide containing trace Ca (wustite FeO) [4].

- Oxide association appeared to facilitate degradation of the chalcopyrite host particle (see Figure 5.3.2.2(b)) exposed through fractures / cracks. The particle surface rim was oxidized to a Zn-rich Fe sulphate phase mixed with FeCu oxide and Fe oxide (zincian melanterite, $(Fe,Cu)SO_4$ mixed with delafossite and limonite, $FeO(OH)\cdot 2H_2O$, respectively).

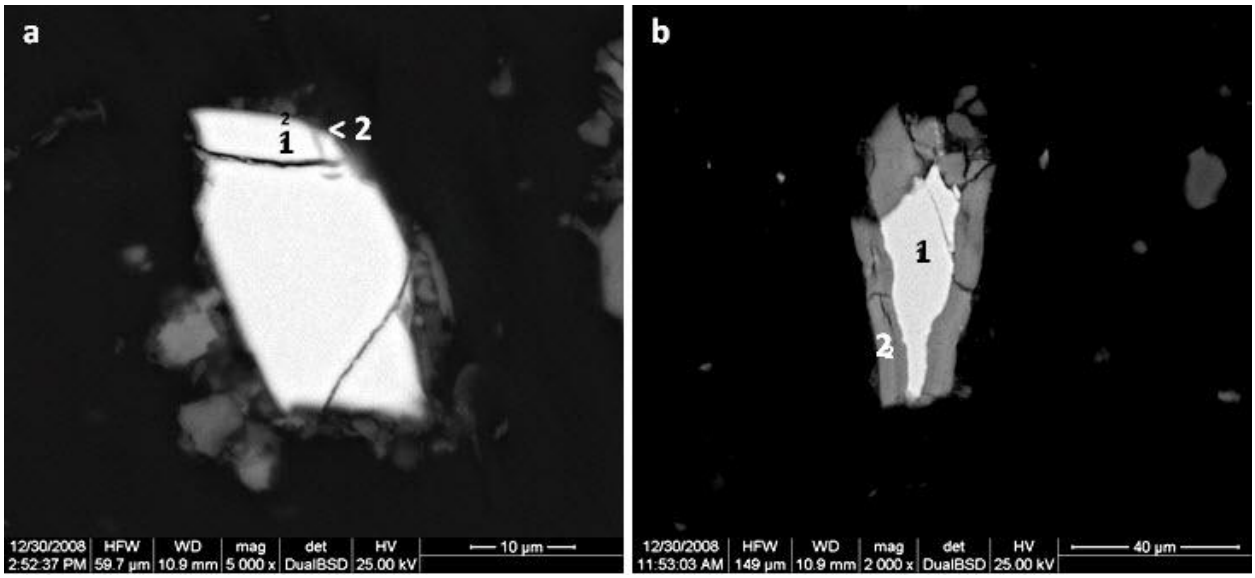

Figure 5.3.2.2. Photomicrographs showing example particles of Cu-bearing waste rock: (a) Hornfels: copper iron oxide secondary phase [1] showing further weathering on the rim to iron oxide and copper silicate [2]; (b) Endoskarn: chalcopyrite host [1] showing thick rim of secondary phases copper iron oxide (with minor Zn), iron oxide (limonite) and calcium silicate [2].

- A close-up examination of the rim of a chalcopyrite particle revealed that there were multiple layers from oxide (innermost) to sulphide-sulphate (mid-layers) to oxide (outermost) (see Figure 5.3.2.3). The host chalcopyrite [1] initially became relatively iron deficient (i.e. bornite, Cu_5FeS_4) and blended with a formed iron oxide (bernalite, $Fe(OH)_3$) [2]. The porous oxide phase acted as a catalyst / conduit to transfer sulphur ions from the host particle to form a Cu-rich ferrous sulphate (cuprian melanterite, $(Fe,Cu)SO_4$) mixed with iron oxide (limonite, $FeO(OH)\cdot 2H_2O$) [3]. The outer perimeter / surface of the particle [4], exposed to the weathering environment was composed of a mix of Cu-rich ferrous sulphate (cuprian melanterite), Cu-rich ferric oxide (cuprian hematite, Fe_2O_3) and copper oxide.

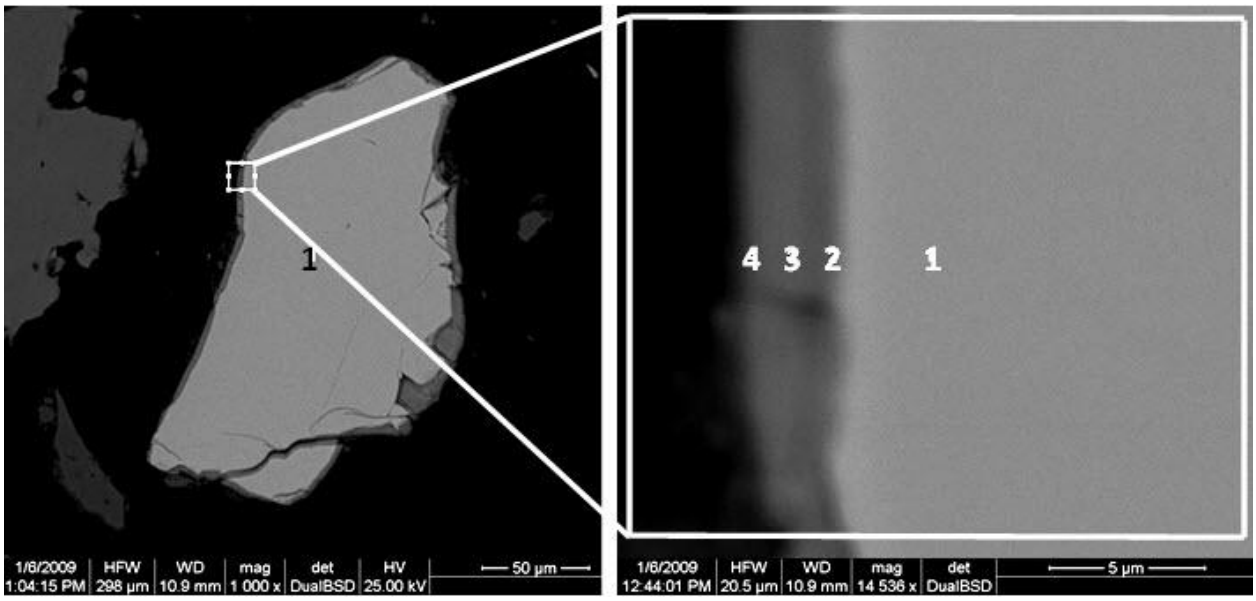

Figure 5.3.2.3. Photomicrographs showing example particle of Cu-bearing waste rock: Endoskarn: chalcopyrite host [1], Bornite blended with Fe oxide [2], Cu-rich Fe sulphate-oxide [3], and Cu-rich Fe sulphate-oxide mixed with Cu oxide [4].

- Chalcopyrite can be protected from weathering, not by a physical barrier but by galvanic interaction. Sphalerite containing partially exposed chalcopyrite appeared to slow chalcopyrite degradation (Figure 5.3.2.4(a)). The area where chalcopyrite would be exposed to the environment displayed phases of Zn-Cu carbonate [rosasite, $(ZnCu)_2(CO_3)(OH)_2$], FeMg silicate [ferrosaponite, $Ca_{0.3}(Fe_2Mg)(Si_3Al)_4O_{10}(OH)_2$)] and Ca oxide. Copper and zinc sulphate were not detected anywhere along the chalcopyrite rim exposed to the drainage which suggested Zn acted to slow oxidation / degradation. In Figure 5.3.2.4(b) this theory was supported by molybdenite [1] altering to powellite ($CaMoO_4$) [2]. The outer layer of the particle [3] was composed of powellite, Mn oxide containing trace Cu and Zn (pyrolusite, MnO_2 and crednerite, $CuMnO_2$) and a Zn oxide (wulfingite, $Zn(OH)_2$), though no sulphate phases. The expected mineral phase in this outer layer, as per many other observances, should be sulphate yet no sulphur species were located. This suggested sulphate will not be found in the presence of Zn and / or Mo.

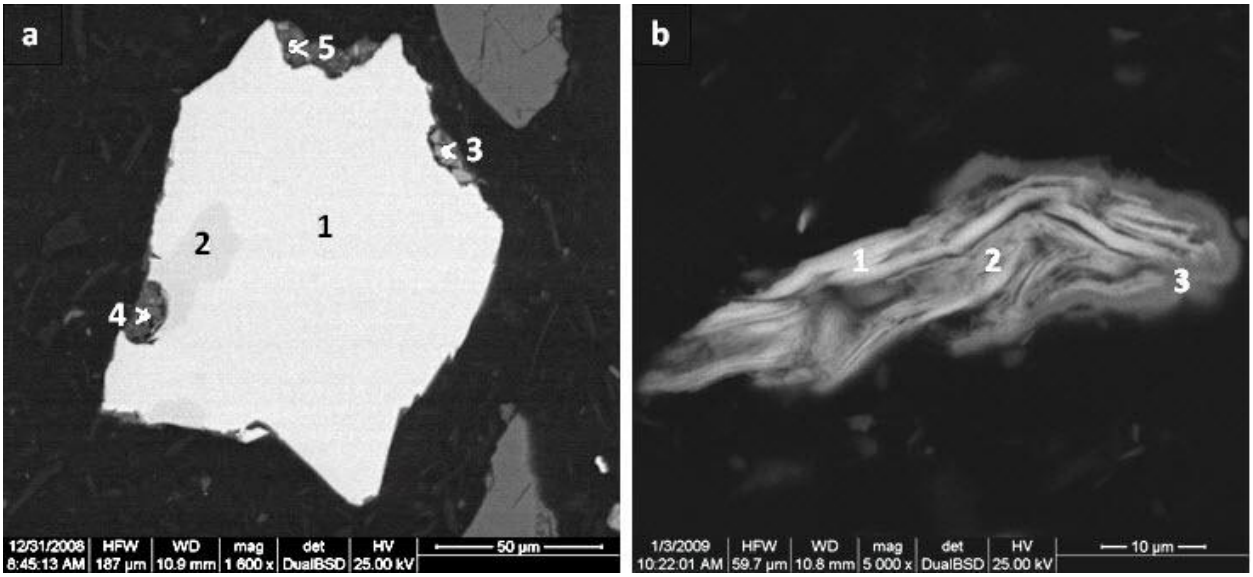

Figure 5.3.2.4. Photomicrographs showing example particles of Cu-bearing waste rock: (a) Marble: sphalerite host [1], partially exposed chalcopyrite through crack [2], Fe-rich blend of silicate, sulphate and oxide mingled with ZnCu carbonate (claraite) with trace Pb [3], ZnCu carbonate mixed with FeMg silicate and Ca oxide([4], and ZnCu carbonate (claraite) mixed with MgAlFe silicate (sudoite) and Ca oxide [5]; (b) Intrusive: molybdenite [1].

5.3.3 Lead-bearing phases

As shown in Table 5.3.1, the main Pb-associated mineral phases were the silicates grunerite and titanite, the carbonate magnesite, as well as the sulphide chalcopyrite. In the presence of dissolving carbonates molybdenite appeared to associate with Pb though not elsewhere. Pb-associated chalcopyrite was present in all waste rock samples and often in higher amounts than Pb-free (“pure”) chalcopyrite suggesting chalcopyrite surfaces attracted Pb ions.

Geological and environmental conditions affect which metal will be associated with a mineral phase. In nature, Pb can be found in its principal sulphide galena (PbS) and secondary minerals including cerussite ($PbCO_3$), anglesite ($PbSO_4$), Pb(II) oxide (i.e. PbO, litharge / massicot), Pb(IV) oxide (i.e. PbO_2, plattnerite) and a mixed valence state

oxide (i.e. minium, $PbO{\cdot}Pb_2O_3$). All of these secondary MOIs were detected in trace amounts in the Antamina waste rock mineralogy. The rarity is likely due to trace presence in the waste rock of primary Pb-sulphide minerals (see section 5.2.1).

Leached Pb may also form other secondary Pb-bearing minerals (briefly, dependent upon pH) such as a blended Pb and Fe sulphate [plumbojarosite, $PbFe_3(SO_4)_4(OH)_{12}$] or if Mo were present, wulfenite ($PbMoO_4$). As previously mentioned, Pb sequestered by sulphates, such as Pb-jarosite, was one of the first phases to leach in ARD conditions. The dissolution of jarosite would release Pb ion and in the presence of liberated Mo ions, a Pb-Mo sink such as wulfenite could form. While these phases were not found directly by the MLA analysis, they were located and examined by SEM-EDS to support this theory.

Erdem and Ozverdi [2011] suggested that Pb-bearing anglesite could be transformed to susannite ($Pb_4SO_4(CO_3)_2(OH)_2$) and cerrusite ($PbCO_3$) minerals in a more basic pH drainage. The high NP capacity of the Antamina mine waste rock, due to marbles, could mobilize Pb and Zn ions in solution due to their amphoteric behaviour [Erdem and Ozverdi, 2011; Geysen *et al*., 2004a, 2004b]. Mobilized Pb ions would then be available to form wulfenite Pb-Mo sink. Of the four Pb-bearing mineral species mentioned here, susannite was not detected in the waste rock samples, adding support to observation that sulphate-bearing phases are less stable.

To immobilize low-level Pb in waste rock and tailings [Ozverdi and Ergun, 2010], studies have been done using phosphate [Melamed *et al.*, 2003; Liu and Zhao, 2007; Song *et al.*, 2009] and hydroxyapatite [Xu and Schwartz, 1994; Mavropouloos *et al.*, 2004; Cao *et al.*, 2009] to form insoluble chloropyromorphite $Pb_5(PO_4)_3Cl$ [Cao *et al.*, 2008]. No chlorine-associated phosphate compounds were found in this study.

Using the MLA digitized image data it was possible to direct the MLA stage to detected Pb-associated MOIs. The following observations were made from EDS study of select particles representing Table 3.2.2:

- Decreased Pb-bearing mineral content in sample size fractions provided direct evidence that galena underwent partial dissolution during the weathering process, (see section 5.1). Dependent upon the particle's local environment, Pb ions could be sequestered as wulfenite ($PbMoO_4$) and / or Pb oxide (plattnerite, PbO_2) (see Figure 5.3.3.1(a)). The MLA analysis detected a rare metal alloy of lead and bismuth in the waste rock (size fraction -297/+147 µm) (see Figure 5.3.3.1(b)) which suggested an unusual local particle environment.

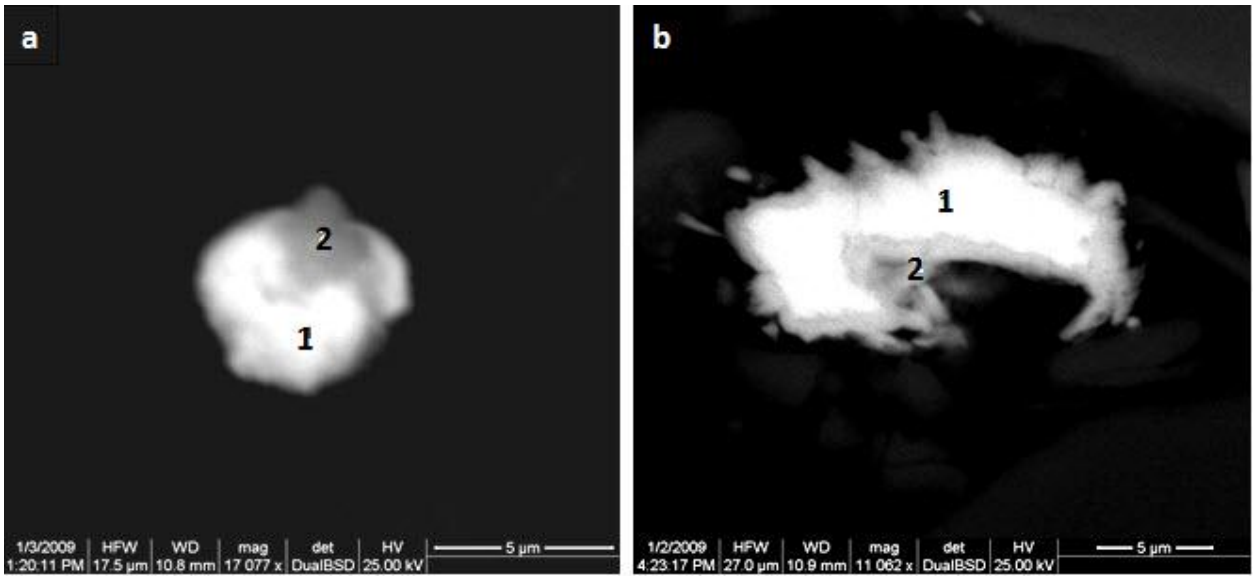

Figure 5.3.3.1. Photomicrographs showing example particles of Pb-bearing waste rock: (a) MarginalCu: fully liberated galena particle [1] converting to Pb molybdate and oxide [2]; (b) Intrusive: a somewhat liberated Pb-Bi alloy ($Pb_3Bi[Cu_{0.09}Fe_{0.1}Ca_{0.09}]$) [1] with rim altered to Pb molybdate and oxide [2].

- The waste rock samples contained minor concentrations of Pb-bearing galena, relative to lesser Mo-associated phases. There appeared to be an overall higher

tendency to form Pb molybdate (wulfenite) rather than Ca molybdate (powellite) which suggested a phase formation competition.

- In Figure 5.3.3.2(a) native lead was found as a middling with calcite. It is proposed that the weathering process generated Pb oxide associated both with and without powellite. Powellite was not detected in the presence of Ca oxide which suggested either Ca oxide formation out-competes Ca molybdate formation or unacceptable environmental conditions.
- In Figure 5.3.3.2(b) the tip of a calcite particle was converted to Ca oxide. The Ca oxide appeared to sequester the Pb ions as Pb oxide and wulfenite. The wulfenite showed minor alteration to powellite, presumably due to a local basic pH particle environment from calcite dissolution.
- In Figure 5.3.3.2(c) molybdenite was exposed to the external environment by a pore which enabled the tip of the sulphide phase to convert to a blend of wulfenite, powellite and a rare Mo oxide phase (MoO_3). The noted absence of sulphate suggested sulphur was released / leached from the Mo sulphide and oxyanion molybdate formed. Other molybdenite was completely locked in a local environment showing no degradation. The feldspar surface (rim) appeared to dissolve and reprecipitate with Pb and Ca oxides associated with molybdates.
- In Figure 5.3.3.2(d) the molybdenite grain in the centre of the feldspar particle underwent oxidation to form powellite, Cu molybdate with minor Zn [vergasovaite, $(Cu_3)O(MoO_4)(SO_4)$] and Zn oxide. This observation suggested an intermediate transition state was formed that involved both sulphate and molybdate. Next to this core particle was Mn carbonate [rhodochrosite, $MnCO_3$], and a silicate blend [calderite, $(MnCa)_3(AlFe)_2(SiO_4)_3$ with rhodonite, $(MnCa)SiO_3$] intermingled with minor oxides of Cu, Zn, Co and Pb. In this instance wulfenite was not formed, even though Pb ions were present, which suggested the Mn presence either inhibited Pb molybdate formation or Mn phase presence indicated an unacceptable pH range (i.e. wulfenite forms at low pH).

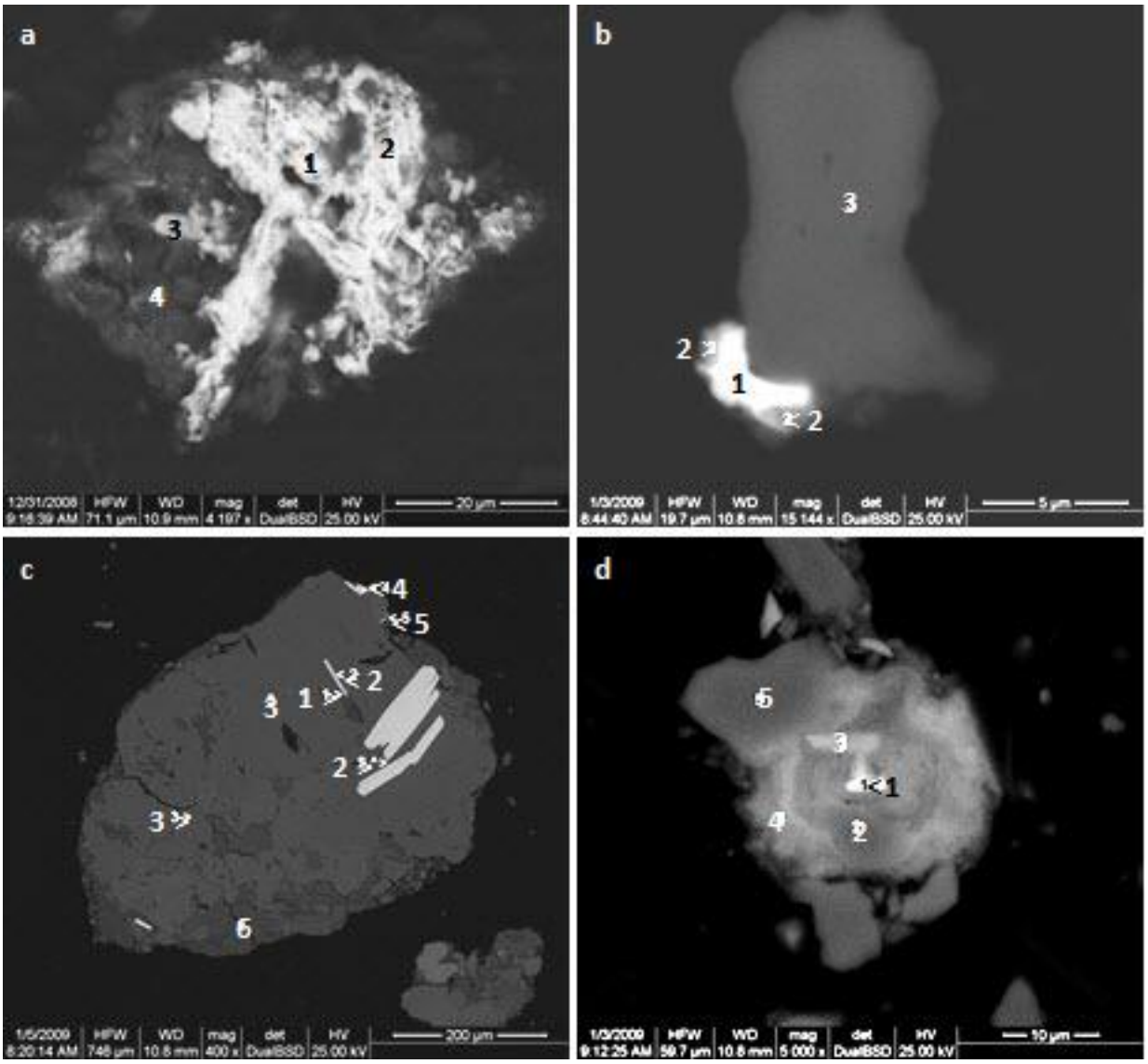

Figure 5.3.3.2. Photomicrographs showing example particles of Pb-bearing waste rock: (a) Marble: lead metal [1], Pb oxide (with trace Ag and Zn) mixed with minor content of wulfenite and powellite [2], Pb oxide mixed with wulfenite and Ca oxide [3], calcite [4]; (b) Intrusive: core of Ca oxide mixed with Pb oxide and molybdate [1], Pb oxide mixed with Ca oxide and molybdate [2], calcite [3]; (c) Endoskarn: wulfenite, powellite and Mo oxide [1], molybdenite [2], K-feldspar host particle [3]; wulfenite and Pb oxide [4], Ca oxide and Pb and Ca molybdate [5], Mg and Al silicate (enstatite, $Mg_2Si_2O_6$ and kyanite, Al_2SiO_5) [6]; (d) Intrusive: molybdenite, Cu molybdate and Zn oxide [1] are surrounded by Mn carbonate [3] and silicate [4] containing minor presence of oxides (Cu, Zn, Pb, Co), K-feldspar [5].

- During secondary phase formation, sulphide galena and carbonate calcite reacted to form lead oxide (see Figure 5.3.3.3(a)).
- A possible weathering mechanism for Pb-bearing galena may be:
  Galena (in the presence of dissolving $CaCO_3$) → Pb Oxide → Ca Oxide [see Figure 5.3.3.2(b)] or Pb molybdate [see Figure 5.3.3.2(c)], dependent mostly upon local particle environment. Note that these suggested mechanisms may not be observed in the SL (surrogate weathering).

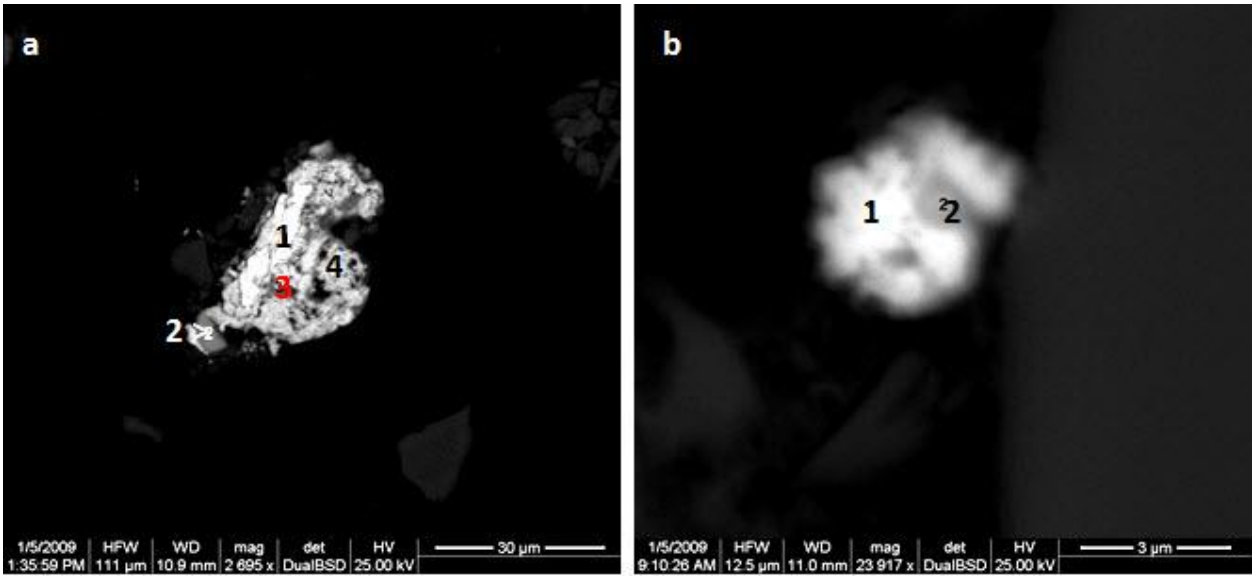

Figure 5.3.3.3. Photomicrographs showing example particles of Pb-bearing waste rock: (a) Marble: galena with calcite (underneath) [1], Pb oxide [3], Pb and Ca oxide [4], Mn carbonate with minor Zn (rhodochrosite, $MnCO_3$) and Mn oxide (quenselite, $PbMnO_2(OH)$, crednerite, $CuMnO_2$) [2]; (b) Endoskarn: adjacent to a large calcite particle is a blended particle composed of wulfenite, Ca oxide, Pb oxide [1] and powellite [2].

- In Figure 5.3.3.4, sulphur leached from galena was not attenuated in the adjacent layer, though Pb was sequestered with molybdate (wulfenite). The leached sulphur was attenuated in the subsequent layer as Ca sulphate associated with Pb oxide

and Pb molybdate. The Pb molybdate appeared to alter to Ca molybdate (powellite) in the presence of clay (kaolinite-smectite, Al-SiO-OH-$H_2O{\cdot}6H_2O$).

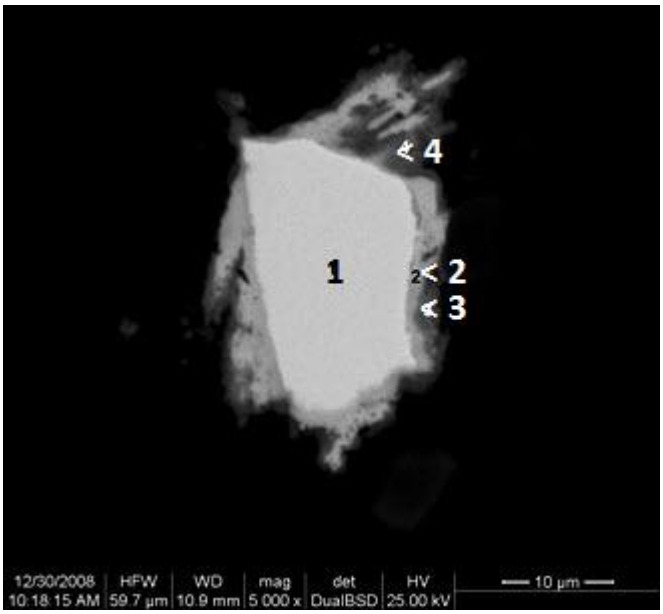

Figure 5.3.3.4. Photomicrograph showing example particle of Pb-bearing waste rock: Endoskarn: galena [1], wulfenite with minor Ca oxide [2], Ca sulphate, powellite, Pb oxide and clay [3], powellite and Pb oxide [4].

- A re-occurring theme throughout many examined particles suggested leached sulphur does not form stable sulphate in the layer adjacent to the sulphide phase, though is found in the subsequent layer. The presence of Pb oxide in the outer layer would suggest that Pb sulphate has a lower stability than Pb oxide in the exposed environment. The presence of clay may provide buffering capacity to Ca sulphate precipitation in the presence of Pb oxide.

5.3.4 Zinc-bearing phases

From Table 5.3.1, the main Zn-associated mineral phases were the silicates mica (altered) and grunerite, iron sulphate, and the sulphides sphalerite and chalcopyrite. Zn-associated chalcopyrite was not detected in marble and hornfels waste rock samples

though was present in the other waste rock types (see Table 3.2.2, 3.2.3, 3.2.4). Perhaps leaching conditions associated with the rock types are too basic and too acidic (respectively) to accommodate Zn attenuation. Under weathering conditions, the MOI Zn sulphide in association with other phase(s) did not appear to be altered while associated phase(s) were altered.

Using the MLA digitized image data it was possible to direct the MLA stage to detected Zn-associated MOIs. The following observations were made from EDS study of select particles representing Table 3.2.2:

- In Figure 5.3.4.1(a) when sulphide sphalerite undergoes oxidation, it briefly formed (assumed as there was only trace presence detected) a Zn sulphate (zinkosite, $ZnSO_4$), which quickly altered to Zn oxide (wulfingite, $Zn(OH)_2$)).
- Fully liberated sulphide sphalerite particles developed rims containing “pure” Zn and / or Pb oxides (see Figure 5.3.4.1(b)). Contrary to a study by Vinals *et al.* [2004], the Zn sulphide particle here did not appear to be a common metal carrier. If other metals were present in the lattice, phase dissolution should have released the metals to be detected as attenuated in the secondary mineral phase’s rim - which none were noted.
- When Zn sulphide underwent dissolution / degradation, iron as an impurity in sphalerite, or sulphur were the first elements to leach as evidenced by detection at the particle rim (see Figure 5.3.4.1(c)). Zn silicate formed in the presence of feldspar (see Figure 5.3.4.1(d)), suggesting silicate dissolution and reprecipitation.

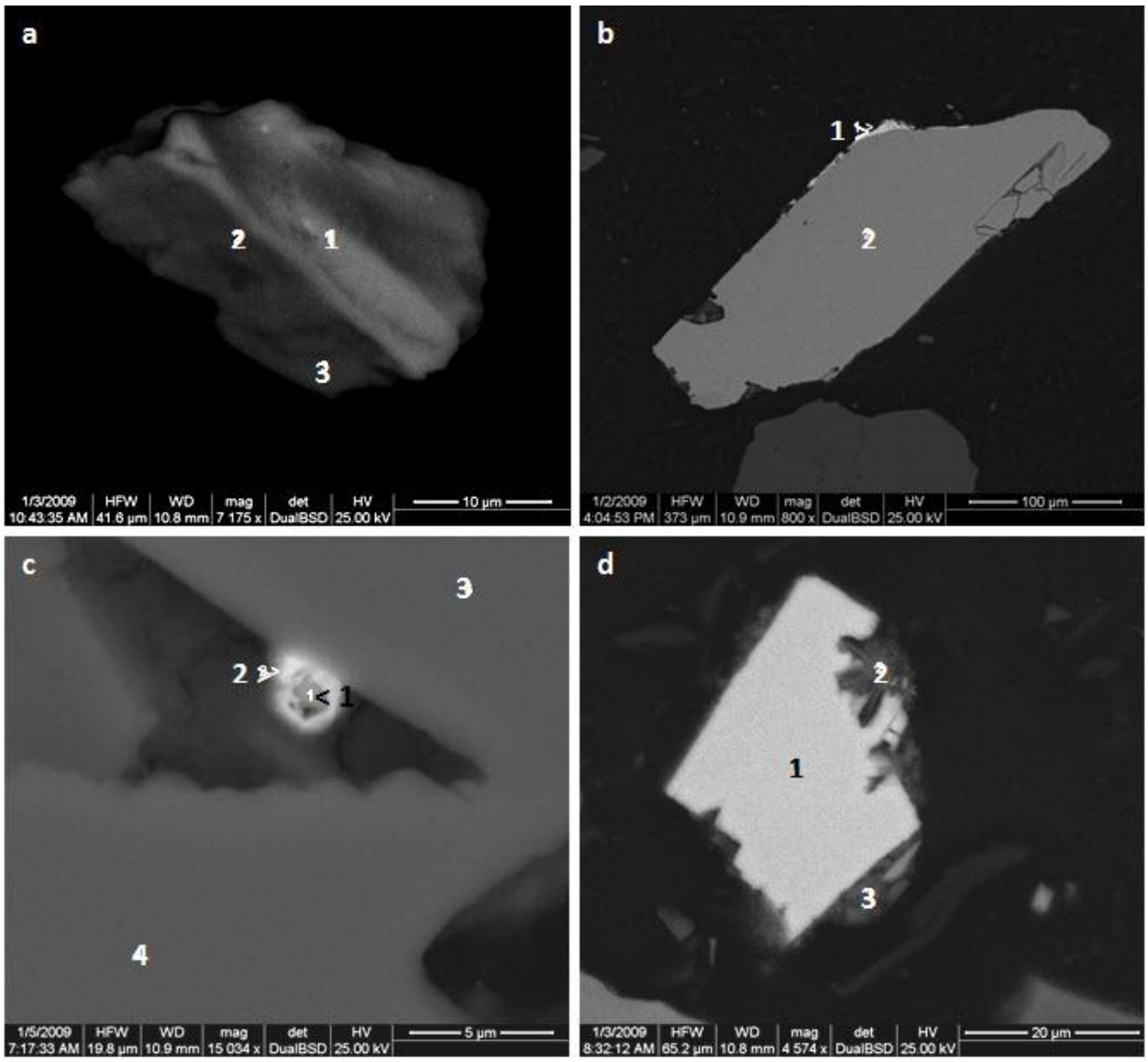

Figure 5.3.4.1. Photomicrograph showing example particles of Zn-bearing waste rock: (a) Intrusive: Zn sulphide [1], Zn sulphide with minor Zn sulphate [2], Zn sulphide with minor Zn oxide [3]; (b) Intrusive: Zn sulphide [2], Pb and Zn oxide [1]; (c) Endoskarn: calci-aluminosilicate (anorthite, $Ca_2Al_2Si_2O_8$, pigeonite, $(CaFe)(Mg)Si_2O_6$) and Ca oxide) [3 & 4], Zn sulphide [1], wulfenite, Zn sulphide and Ca silicate (wollastonite, $Ca_2Si_2O_6$) [2]; (d) Intrusive: Zn sulphide [1], Zn sulphide, silicates (anorthite, $CaAl_2Si_2O_6$, quartz, SiO_2) [2], silicate (willemite, Zn_2SiO_4, K-feldspar, $KAlSi_3O_8$, quartz, SiO_2) [3].

5.3.5 Molybdenum-bearing phases

From Table 5.3.1, the main Mo-associated mineral phases identified were molybdenite and Fe sulphate. In potentially high pH marble waste rock, molybdenum was often associated with molybdofornacite (see section 5.2.1). Note that molybdenite's molecular formula, determined by EDS analysis was most often represented by Mo_2S_3 (i.e. a shared crystal structure) instead of the accepted formula MoS_2.

Dissolved metal loadings in the ground water at waste rock dump sites are significantly different when comparing ARD and NRD primarily because metal mobility is pH dependent. At near-neutral pH, metal ions chemically remain positively charged and either attach to hydroxyl groups (OH^-) at available sorption sites or form insoluble precipitates [Johanessan *et al.*, 1992]; however, formed oxyanions such as As and Mo remain relatively mobile. The overall dissolution reaction for molybdenite oxidation is shown in Equation 15.

$$2MoS_2 + 9O_2 + 6H_2O \rightarrow 2MoO_4^{-2} + 4SO_4^{-2} + 12H^+ \qquad \text{Eq. 15}$$

MLA analysis of waste rock samples revealed intermediate / transitional mineral phases with compositions near Mo-bearing powellite and wulfenite. The modal analysis indicated there were more occurrences of powellite than wulfenite in the waste rock samples. This was likely because there was low availability of Pb ions and secondly due to pH effects in local particle environments.

Laboratory batch and column experiments showed that molybdenum could be attenuated through powellite ($CaMoO_4$) and wulfenite ($PbMoO_4$) precipitation, with insignificant surface adsorption [Conlan, 2009]. MLA examination of field samples from barrel-cells in place for five years at Antamina mine site provided direct evidence that molybdenum, as an oxyanion, was attenuated as powellite and wulfenite [Conlan, 2009]. Observations suggested that wulfenite more effectively removed Pb and Mo ions

from the drainage leachate than powellite. From SEM BSE images examined using EDS, it is proposed that wulfenite formation was favoured when the pH was less than circumneutral and Pb ions were available. Few other molybdate precipitates (e.g. Fe, Cu, Zn) were observed in the waste rock samples analyzed, possibly due to poor stability or undetectable due to small size. Besides wulfenite and powellite, molybdenum ions (at sub-circumneutral pH) were also found associated with ferric oxides and other MOIs.

Using the MLA digitized image data it was possible to direct the MLA stage to detected Mo-associated MOIs. The following observations were made from EDS study of select particles representing Table 3.2.2:

- There are two main processes that occur in the formation of molybdate: (1) oxidation of molybdenite, which releases sulphur (to form the oxyanion sulphate) and Mo cation; and, (2) oxidation of marble ($CaCO_3$) to form Ca oxide. Figure 5.3.5.1(a) shows a calcite particle with minor amounts of Ca oxide degrading to a partial rim composed of secondary mineral precipitation products Ca oxide, powellite ($CaMoO_4$) and minor silicates [magnesiochloritoid, $MgAl_2SiO_5(OH)_2$ and kaolinite-smectite, $Al{\cdot}Si{\cdot}O{\cdot}OH{\cdot}H_2O$]. The detection of minor amounts of clay silicate in the rim suggested that aluminosilicates might aid sequestration of Mo through a buffering action.
- Molybdenite, in the presence of Mn and Ca carbonate [rhodochrosite ($MnCO_3$) and calcite ($CaCO_3$), respectively] dissolved to form Ca molybdate. The prevalence of calcium oxide where molybdates were precipitated suggested a preferred surface for molybdate formation. Blended with the molybdate was dioptase [$CuSiO_2(OH)_2$], which degraded to either form a non-Ca silicate [K-feldspar] or perhaps K-feldspar, was a silicate degradation product that buffered molybdate formation (see Figure 5.3.5.1(b)).

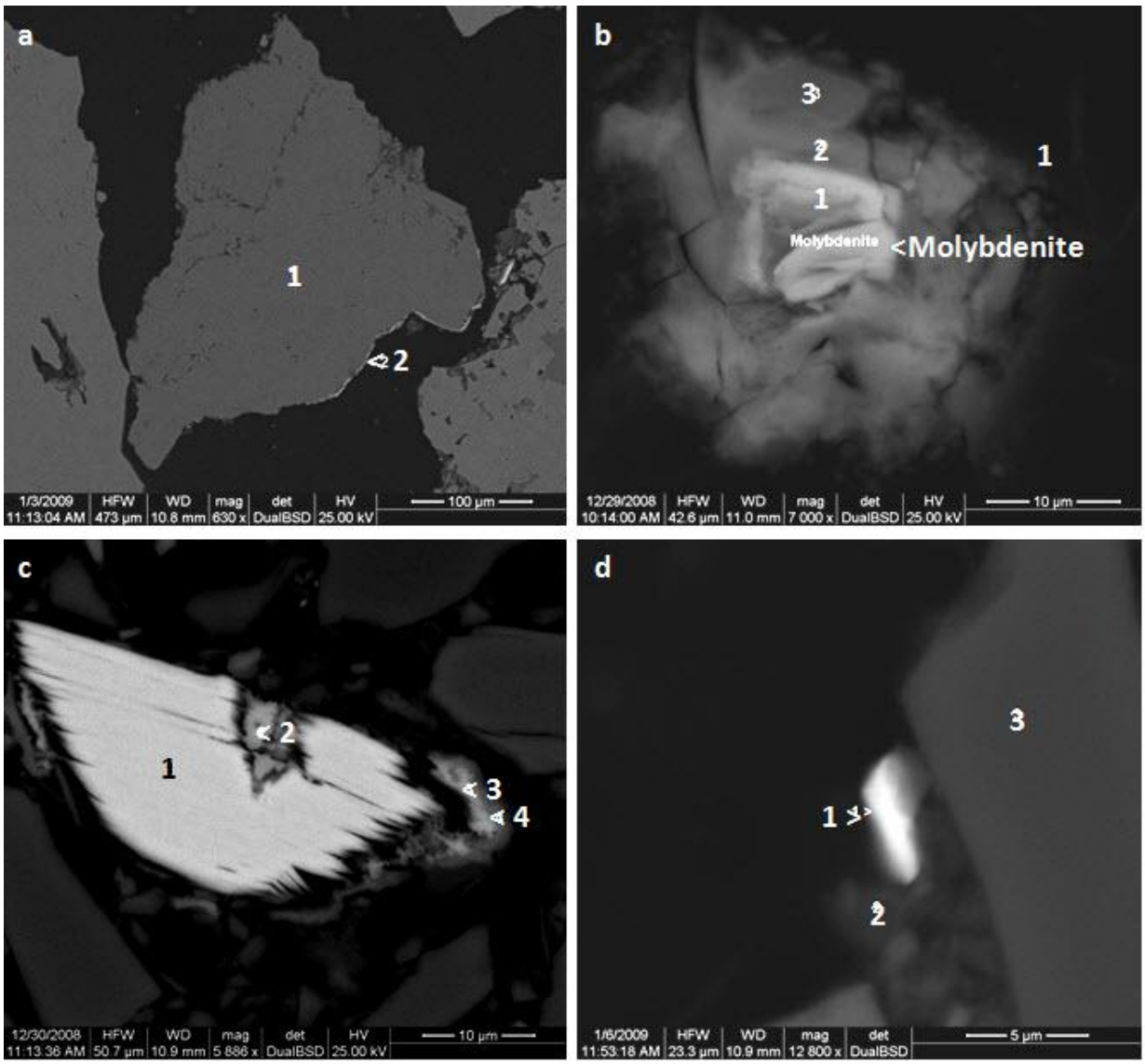

Figure 5.3.5.1. Photomicrograph showing example particles of Mo-bearing waste rock: (a) Marginal Cu: calcite and Ca oxide [1], rim of powellite, Ca oxide and aluminosilicates [2]; (b) Intrusive: molybdenite on MnCa carbonate (with trace Cu and Zn) [1], powellite and Cu silicate (and trace Zn) [2], potassic feldspar (with trace Cu and Zn) [3]; (c) Endoskarn: molybdenite [1], powellite [2], powellite, CaMn oxide [marokite, $CaMn_2O_4$], Ca, Cu and Zn oxide, Ca sulphate, and trace clay [kaolinite, $KAl_2Si_2O_5(OH)_4$] [3], CaMn silicate [kittatinnyite, $Ca_2Mn_3Si_2O_8(OH)_4 \cdot 9(H_2O)$] [4]; (d) Endoskarn: attached to quartz particle [3] was blended particle of wulfenite, Pb oxide and calci-aluminosilicate [hydrogrossular, $Ca_2Al(SiO_4)_2(OH)_7$] [1] from which was formed a phase blend of powellite and aluminosilicate [muscovite, $KAl_2(Si_3Al)O_{10}(OH,F)_2$ and pyrophyllite, $Al_2Si_4O_{10}(OH)_2$] [2].

- Molybdenite grains after assumed physical stress (suggested by observed bent or impacted phase structure) formed molybdenum oxide (powellite) which was often observed as a porous (spongy-looking) phase. The porous-looking phase was especially evident in the presence of stressed molybdenite that was unprotected from external influences (see Figure 5.3.5.1(c)). The sponge-like appearance suggested it was crystalline; however, the SEM could not focus adequately on the very fine structure due to electron beam interaction volume exceeding grain dimensions. The porous phase appeared to be the result of off-grade wulfenite subjected to physical stress in the presence of lead oxide (Figure 5.3.5.1(d)). If molybdenite was locked, or protected, a more amorphous powellite phase formed.

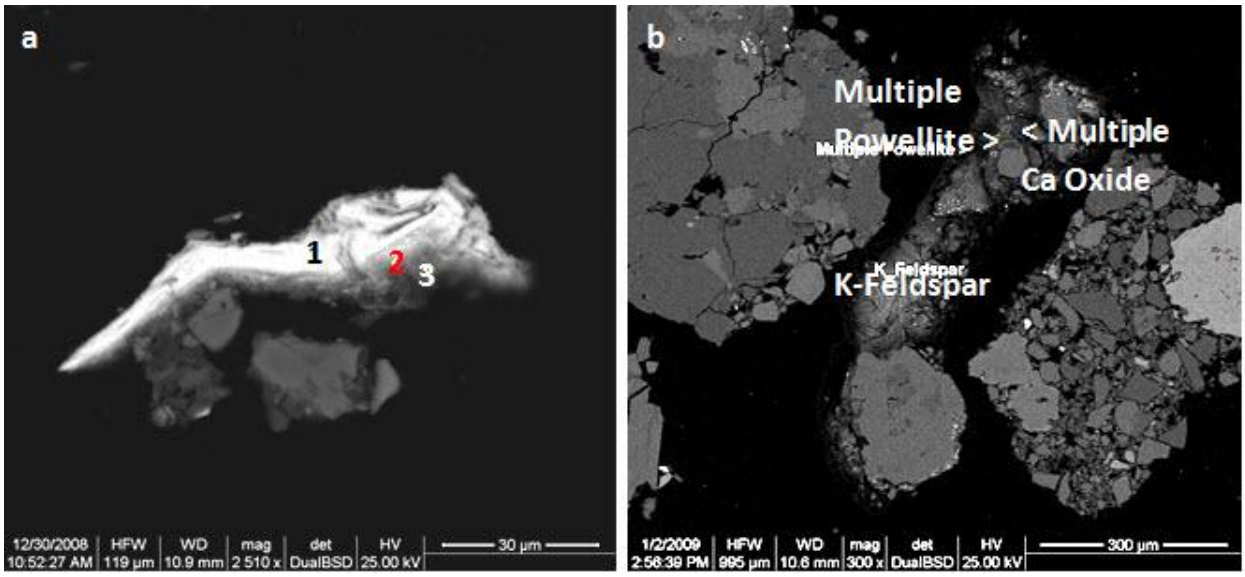

Figure 5.3.5.2. Photomicrographs showing example particles of Mo-bearing waste rock: (a) Endoskarn: molybdenite [1], molybdenite, powellite, minor clay [2], powellite, clay, minor Ca sulphate [3]; (b) Intrusive: K-feldspar host particle with multiple micro-sites of powellite and Ca oxide blended with Ca silicate.

- Molybdenite in the presence of silicates [mullite ($Al_8(Si_4)O_{16}(OH)_4$) and sillimanite (Al_2SiO_5)] and calcite, altered to adjacent layer powellite and calcium oxide, with no detectable sulphate. In the next sequential layer the leached sulphur was trapped as

Ca sulphate (see Figure 5.3.5.2(a)). The formation of both Mo oxide and Ca molybdate phases suggested there was an influence from the particle's local environment. Ca molybdate associated with mica (e.g. K-feldspar) appeared to convert to Ca oxide and Ca silicate [wollastonite, $Ca_2Si_2O_6$] and release Mo ions (see Figure 5.3.5.2(b)).

- The outer layer of Mo-associated particles was partially to fully composed of Ca sulphate. The Ca sulphate phase may have formed from a reformation of Ca oxide phase with addition of leached sulphur from the host sulphide phase (e.g. molybdenite).

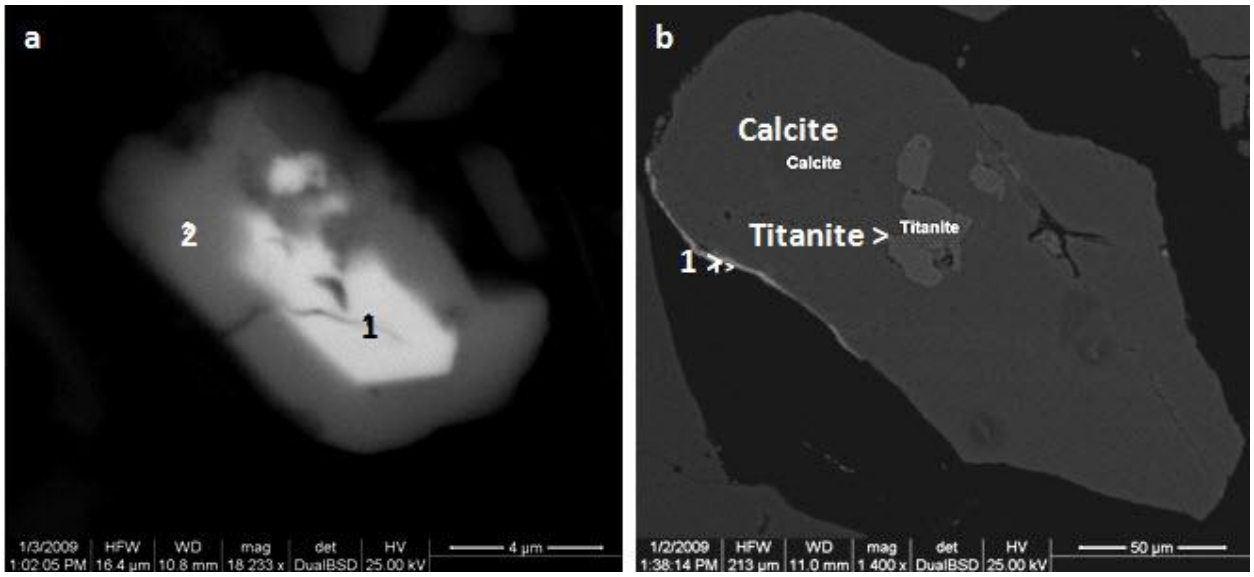

Figure 5.3.5.3. Photomicrographs showing example particles of Mo-bearing waste rock: (a) MarginalCu: galena [1], powellite and Ca oxide [2]; (b) Marble: particle rim [1] composed of Mn carbonate [rhodochrosite, $MnCO_3$], calcite, Pb oxide, and Zn-Cu carbonate [zincrosasite, $ZnCu(CO_3)(OH)_2$].

- Wulfenite appeared to form in the presence of Pb ions and Ca oxide, and then altered to powellite (see Figure 5.3.5.3(a)). Conlan [2009] noted there was a stronger tendency to form wulfenite than powellite in the presence of Pb ions. Particle observations suggested that the pH of the local particle environment affected its formation and stability. Pb molybdate (wulfenite) may preferably

precipitate on non-calcium bearing surfaces, such as silicates [see Figure 5.3.4.1(c)]. The majority of MLA-detected galena particles were associated with Mo, especially when in near association to calcite and Pb / Ca oxide phases - with only a few exceptions observed (see Figure 5.3.5.3(b)). The consistent observation in these rare instances was the presence of Mn, suggesting either Mn inhibited Pb molybdate precipitation or it was an indicator of unacceptable pH conditions for molybdate precipitation.

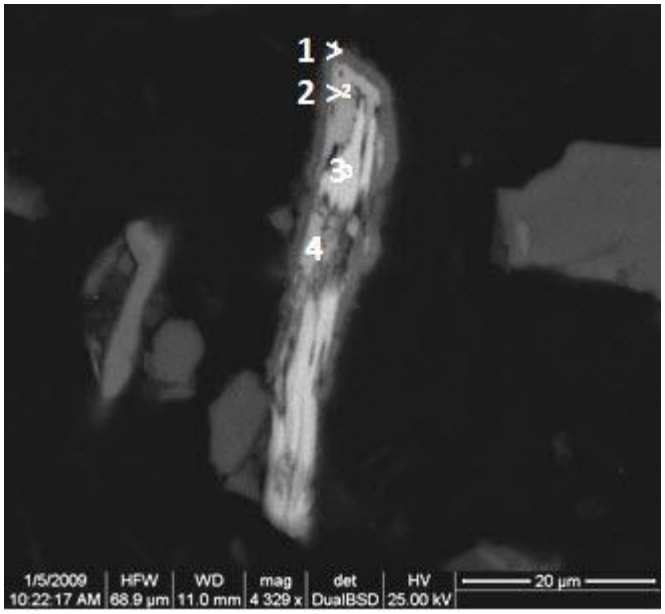

Figure 5.3.5.4. Photomicrograph showing example particle of Mo-bearing waste rock: Endoskarn: molybdenite [3] was stressed and formed powellite and Mo Oxide [molybdate, MoO_3 with minor Mn and Ca] [2] or powellite (with trace Mn and Cu) [4], to then develope a rim [1] of Mn oxide [hausmannite, Mn_2O_4] mixed with Pb oxide, Ca sulphate, and minor oxides of Cu and Zn.

- A transition phase was detected that formed between parent molybdenite and its oxide (see Figure 5.3.5.2(a), Figure 5.3.5.4). A proposed weathering mechanism for Mo-bearing molybdenite may be:

  Molybdenite (in the presence of Ca oxide or degrading $CaCO_3$) → $MoSO_4$ (very brief) → Mo Oxide (brief) → powellite ($CaMoO_4$) and Ca sulphate (dependent

upon more basic pH, temperature, exposure) or wulfenite ($PbMoO_4$) and Ca sulphate (dependent upon lower pH) (see Figure 5.3.3.2(b) and Figure 5.3.5.1(d)). Ca oxide appeared to be required to precipitate on molybdenite in order to initiate oxidation (i.e. leach of sulphur and / or Mo). This suggested that the oxide acted as a quasi-catalyst.

Table 5.3.5.1 shows an example of another aspect of the power of MLA data. In this example the compiled image data (see Table 3.2.2) was used to examine the selected relationship between Pb-bearing galena, Mo-bearing molybdenite and the number of particles located in each size fraction. The MLA data suggested the following:

(i) Hornfels and marble had the lowest content of galena and molybdenite. The host hornfels may have low mineral presence due to high porosity providing acid access to grain inclusions; the host marble may have low mineral presence due to ARD dissolving carbonate and releasing mineral inclusion(s).

Table 5.3.5.1. Modal MOI comparison between waste rock types (normalized weight percent and number of particles): galena and molybdenite.

Waste rock Type	Marginal Cu		Endoskarn		Intrusive	
Size fraction (µm)	Galena(wt%)/ #Particles	Molybdenite(wt%)/ #Particles	Galena(wt%)/ #Particles	Molybdenite(wt%)/ #Particles	Galena(wt%)/ #Particles	Molybdenite(wt%)/ #Particles
-2000 µm/+850	0.0006 / 1	0.9 / 45	0.01 / 1	0.2 / 36	0 / 0	0.1 / 7
-850 µm/+297	0.04 / 4	0.5 / 73	0.002 / 1	0.2 / 31	0.0001 / 1	0.00006 / 1
-297 µm/+147	0.2 / 6	0.6 / 91	0 / 0	0.8 / 74	0.002 / 3	0.02 / 14
-147 µm/+53	0.00009 / 1	1.1 / 116	0.08 / 5	0.6 / 102	0.0001 / 1	0.1 / 28
-53 µm/+44	0.0004 / 1	0.9 / 138	0.02 / 1	0.3 / 73	0.003 / 2	0.1 / 18
-44	0.004 / 1	0.8 / 93	0.01 / 2	0.4 / 61	0.01 / 2	0.1 / 18

Waste rock Type	Marble		Hornfels	
Size fraction (µm)	Galena(wt%)/ #Particles	Molybdenite(wt%)/ #Particles	Galena(wt%)/ #Particles	Molybdenite(wt%)/ #Particles
-2000 µm/+850	0.005 / 1	0.0004 / 1	0.0002 / 1	0 / 0
-850 µm/+297	0 / 0	0.00003 / 1	0 / 0	0 / 0
-297 µm/+147	0.01 / 2	0 / 0	0.00004 / 1	0.07 / 1
-147 µm/+53	0.01 / 2	0 / 0	0 / 0	0 / 0
-53 µm/+44	0.05 / 4	0.0002 / 1	0 / 0	0 / 0
-44	0.004 / 1	0.003 / 1	0 / 0	0.002 / 1

(ii) In size fractions greater than 147 µm, galena and molybdenite were mainly locked. In size fractions smaller than 147 µm, undissolved galena particles were more exposed, as noted by locking data (see section 5.2.2).

(iii) Overall there were few galena particles, hence few available Pb atoms to form secondary precipitates such as molybdate wulfenite. Generally, it appeared that the -147/+44 µm particle size range had the lowest content of both galena and molybdenite. This could be because it is the optimal particle size range for mineral phase liberation and dissolution. Both the larger and finer particle size fractions than -147/+44 µm had higher galena content due to MOI locking and / or no Mo associated phases, respectively. Galena was more liberated and showed slightly higher content in the high surface area fines (i.e. -44 µm) which indicated galena did not dissolve during weathering and may require association with other phases or catalysts, or the leach did not reach completion (which infers some resistance to the leach conditions).

(iv) All size fractions for each sample had similar Molybdenite content which suggested its mode of dissolution was not dependent upon association with other mineral phases (such as, galvanic interaction) because some molybdenite particles were liberated. Molybdenite appeared to be “formed” through degradation of other Mo-bearing sulphides (e.g. molybdofornacite). The MLA classification algorithm matched the EDS-collected phase (based upon threshold criteria) to molybdenite because the large Mo and S spectrum peaks met the classification threshold criteria (i.e. possible trace Pb, Cu, As peaks were not accounted).

(v) During the MLA scoping analysis, the potential Pb and Mo attenuators wulfenite and powellite were not detected, though molybdofornacite was detected. The MLA results showed highest molybdofornacite content in sub-147 µm size fractions. The MLA-identified molybdofornacite may actually be a Pb oxide phase that attenuated Cu, As and Mo, but due to SEM electron beam physics satisfactory resolution between the phases was inhibited.

5.4 Summary

The metal-bearing MOI phases detected using the MLA BSE analysis, often with complicated, blended spectra, were in most cases successfully classified using the MLA X-ray classification software algorithms. Sometimes manual scrutiny at a higher spatial and spectral resolution was used and selective mineral interpretation was applied. Some caution must be exercised because SEM spatial and spectral limitations were challenged by the finer secondary mineral phases during MLA particle phase segmentation.

Visual inspection of particles (especially those associated with a metal) can provide valuable insights to waste rock dump management. The MLA was able to detect and record particle images along with associated mineralogical information. In Figure 5.4.1 are shown MLA digitized particles from Antamina mine waste rock. Particles can contain grains of more reactive phases locked within them, have reactive phases partially exposed (on the surface or through a crack), be totally exposed (i.e. liberated) or have coatings of secondary mineral phase(s) that may be reactive (e.g. galvanic interaction).

A waste rock model based upon ABA analysis alone might report little reactive sulphide, while chemical analysis might report high availability of sulphide. This would clearly not be accurate, as shown in MOI pyrrhotite in the top left particle of Figure 5.4.1. If the environmental modeller were curious as to why a sulphide was not weathered / leached or why it was present (see molybdofornacite in lower right particle, Figure 5.4.1), visual examination of particles would be beneficial. Seeing the particle, knowing the associations between mineral phases, knowing each mineral phases' degree of exposure to the environment (or internal galvanic interaction), knowing each mineral phases' grain size (i.e. often smaller size reflected higher surface area and therefore higher potential reactivity), and then combining this information with the macro-properties of the waste rock pile (e.g. temperature, water channelling, etc) and nature's weather patterns should improve the weathering (oxidation) model.

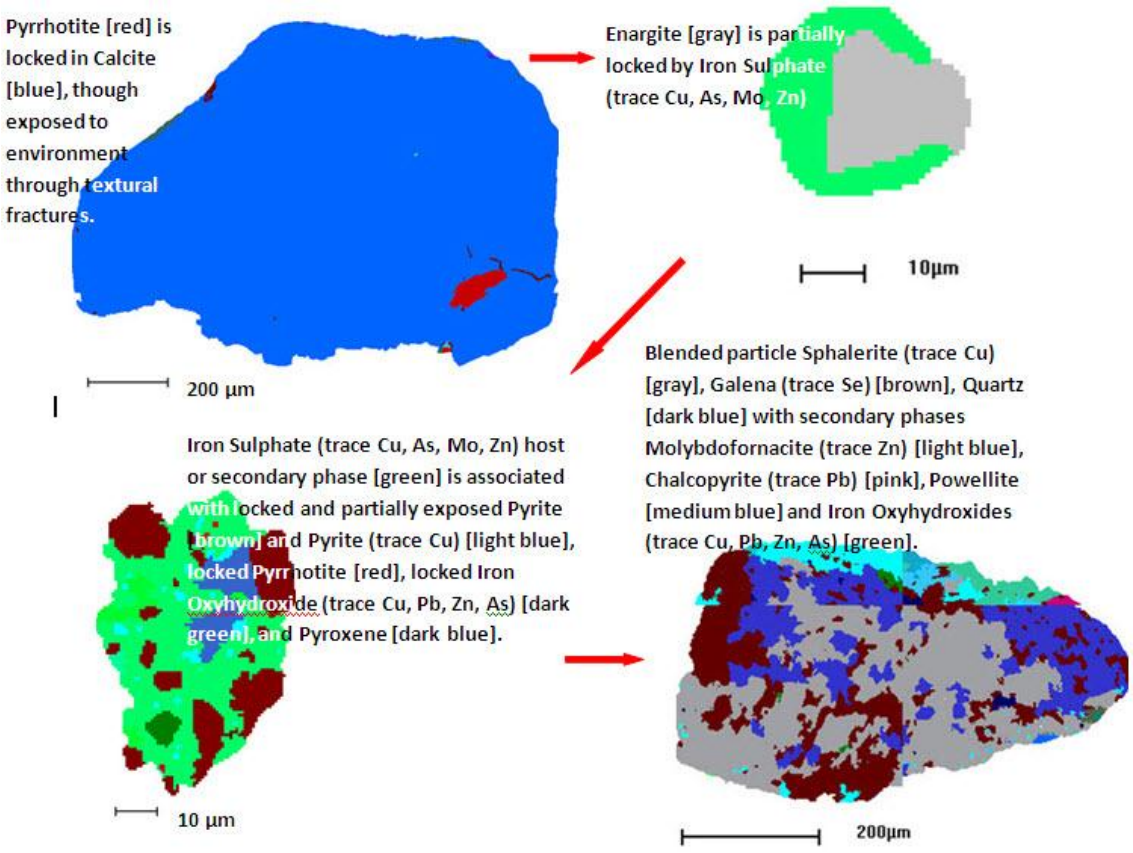

Figure 5.4.1. Examples of particle complexity in waste rock weathering.

Metals detected in the Antamina mine waste rock drainage are those which remain mobile under neutral or alkaline conditions. Some elements are more mobile in NRD, such as the stable oxyanions of As, Mo, Se, Cr, Sb, and V. Other elements were attenuated with such phases as clays (altered mica) and titanite.

Sulphides detected by MLA in the waste rock pile samples comprised minor amounts of: copper minerals, as bornite, chalcopyrite, tennantite and enargite; the iron sulphide minerals pyrite and pyrrhotite; and, trace amounts of galena, molybdenite, sphalerite, watanabeite and stibnite.

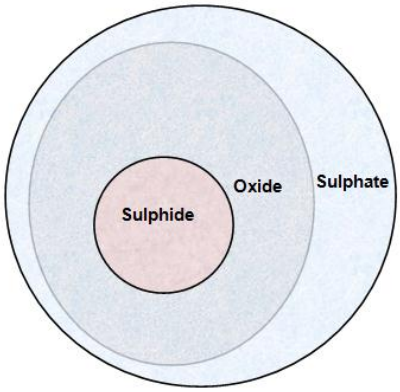

Figure 5.4.2. Observed sulphide dissolution phase layers.

Typically, the layer next to the MOI core sulphide was not composed of sulphate but oxide. The next sequential layer contained sulphate phases (see Figure 5.4.2).

Pyrrhotite, reported to be present in the Antamina ore body, was found in much lesser abundance than pyrite in the waste rock likely due to its higher reactivity (see Table 5.3.2.1). The low content and small grain size of sulphide phases added challenge to MLA image analysis. SEM electron beam physical limitations may mistakenly cause reporting mineral phases which are in fact secondary MOIs with attenuated metals.

The Antamina mine waste rock test pile samples exhibited ARD neutralization post-SL, through carbonates (calcite, siderite) and silicates (pyroxenes, chlorite, epidote, plagioclase, feldspar, FeOxideCu and muscovite). The most prevalent silicates detected in the waste rock dump samples were pyroxenes, plagioclase, feldspar and an FeOxideCu phase. Other silicates to note were mica, quartz, titanite, and grunerite.

Apatite, the main phosphate mineral phase detected, appeared to sequester metals though functioned in this capacity under pH control (i.e. attenuation decreased as pH increased). It was also noted that apatite did not associate with As, Sb and Mo.

Hydrous iron sulphates and hydrous phosphates were not detected using the MLA analysis conditions, which may have been partially due to their small size, SEM spatial resolution limitations, MLA analysis parameters used to perform the analysis and MOI

pH dependence. Iron oxyhydroxides (goethite and hematite) and iron sulphate were the most prevalent phases detected both before and after the SL.

CHAPTER 6 Conclusions and recommendations

6.1 Conclusions

The ready availability of particle composition data from automated mineral analysis systems, such as the MLA, makes the approach practical.

The MLA acquires mineralogical information in primarily metallurgical processing applications. In time it will become better recognized as a tool for environmental studies.

In this study, the MLA has demonstrated its ability to detect MOIs in major-to-trace quantities and show overall metal / MOI mineralogy trends in the waste rock pile. The ability of the MLA to detect and quantify metal-associated MOIs, coupled with the ability to remotely move the MLA stage to place specific particles under the electron beam for intensive EDS examination, have enabled improved particle characterization. The study scope did not specifically include theorizing waste rock weathering mechanisms, although the identified MOI mineralogy, proportions and particle images (especially those with metal association) provided insights to waste rock weathering mechanisms. The MLA can provide quantitative information with respect to waste rock MOI / metal availability and association. This has not been found in the literature.

The MLA analysis records the SEM stage position of the detected MOIs making it simple to move the SEM stage to each MOI for visual and / or EDS inspection. Seeing the particle and quantifying the mineral phase associations, the mineral phase availability to environment or adjacent MOI, the mineral phase grain size, can provide helpful information to improve waste rock weathering (oxidation) models. MLA analysis used in conjunction with other analytical results, such as surface analysis, geochemistry, chemical speciation modeling, and diagnostic sequential leach will provide useful data for environmental modellers.

The waste rock MLA XBSE analysis method requires (at least) duplicate transverse mounted particle samples using 25kV accelerating voltage and a carefully chosen magnification to maximize information on metals while minimizing analysis time. It is best to use an accelerating voltage of 25kV for the MLA analysis of waste rock as a lower voltage is less effective at detecting the often finer metal-associated particles.

Automated mineralogy, one of the fastest growing developments in mineralogical assessment in the last two decades, generates massive quantities of data in relatively short time. To interpret the data, the mineralogist must understand how the data was collected in addition to the software processing abilities. MLA limitations to studying secondary MOIs are the electron beam interaction volume (i.e. SEM spatial resolution), EDS spectral resolution (e.g. Mo and S energy lines), choice of MLA analysis parameters (i.e. affects degree of detail) and depth of mineral knowledge.

Based upon the results of this study, small silicate particles with high surface area appeared to dissolve and then participate in layered coatings to protect sulphide from oxidation. The dissolution of the silicate muscovite generated clay MOIs which were often found associated with secondary metal-bearing precipitation products. The aluminosilicate clays may act as pH buffers during metal sequestration and precipitation, particularly for oxyanions (e.g. As and Mo). Silicates in association with high carbonate content did not acquire secondary precipitation coatings / armour.

The majority of MLA-detected carbonates were calcite which contained trace amounts of iron, magnesium and / or manganese (Mn). Under the SL conditions, carbonates (calcite and siderite) and phosphates (apatite) appeared to dissolve easily (i.e. less detected in SLR) hence could be considered poor metal attenuators in an acidic environment. Apatite was not associated with As, Sb and Mo, perhaps because P can form an oxyanion. Oxides appeared slightly more resistant to SL conditions than carbonates and phosphates and do not appear to precipitate at lower acidic pH. Oxides, such as the iron oxyhydroxides, were found associated with larger particles as

armouring, though not on smaller particles of the same phase. Hydroxides and oxides were detected more often than sulphates. Metal-associated sulphate MOI content, affected by pH, decreased during SL conditions.

Some general comments can be made for waste rock particles of As-bearing MOIs: arsenic sulphide does not dissolve easily in an acidic environment unless a catalyst such as Ag^+ ion is present. This suggests ferric ion is an ineffective leaching agent by itself with respect to degradation of As-bearing sulphides. Arsenic adsorbed or substituted in a MOI lattice could be replaced by Ag^+ ions. The precipitated Ag_2S would then return Ag^+ ions to the environment through the ferric-ferrous couple electron transfer. The catalysis would progressively release As from the MOI. Data and observations suggest that this may also apply to minerals other than As-bearing sulphides.

Under SL (acidic) conditions, the primary MOI stibnite appeared to perform as an As attenuator, with MLA analysis of the SLR reporting increased presence of what was qualified as watanabeite, as well as decreased stibnite. The SLR watanabeite may be stibnite with As adsorbed to its surface. Watanabeite was often found associated with Cu, Zn and Mo.

Galena appeared to resist SL dissolution, which may be linked to its relative rest potential.

The majority of galena particles located by MLA were associated with Mo and altered to secondary MOI lead-molybdate. Galena particles in the presence of Mn-bearing phases did not associate with Mo, suggesting Mn may inhibit Pb-molybdate mineral formation or its presence may indicate unacceptable environmental conditions for Pb-Mo co-attenuation. Formation of the lead molybdate wulfenite appeared to prefer a lower pH environment, while calcium molybdate powellite formed at higher pH, usually in the vicinity of dissolving carbonate. This study suggested that Cu may be a catalyst in

molybdate formation. Arsenic-bearing wulfenite and molybdofornacite could be Mo-As-Pb attenuators in the waste rock dump.

A possible weathering mechanism for Pb-bearing MOIs based on journal refereed studies and this MLA study of many waste rock particles is as follows: Pb associated with chalcopyrite appeared to enhance chalcopyrite leaching. Trace silver sulphosalts and Ag associated with pyrite and jarosite were detected in the waste rock samples. Silver has a strong affinity to Pb-bearing MOIs. In the Antamina mine circumneutral waste rock environment, Pb-bearing chalcopyrite may have dissolved due to a silver-catalyzed dissolution.

Certain elements appeared more mobile or liberated in the Antamina mine waste rock, specifically oxyanions of As and Mo. In this study liberated metals As, Sb, Cu, Mo, Pb, and Zn were attenuated / sequestered by clays (e.g. altered mica) and titanite, dependent upon SL conditions (weathering surrogate). Copper and zinc preferred association with mica-type clays both before and after the SL, suggesting no influence from specific leaching and weathering conditions. Copper and lead preferred association with titanite. Liberated Zn was relatively more attenuated in iron oxyhydroxides, iron sulphate and apatite.

6.2 Recommendations

Antamina waste rock characterization using MLA technology enabled better understanding of metal attenuation and mobilization mechanisms under NRD conditions. Using MLA mineralogical information, particle surface analysis, geochemistry, and diagnostic sequential leach, modeling and prediction of metal mobilization would benefit.

Waste rock classification should consider lithology, particle size distribution, mineralogy, metal leach characteristics, mineral availability / exposure, and mineral association (i.e.

liberated, binary, and ternary+). At the operational level it is not practical to wait for MLA analysis results; therefore, a less time-consuming diagnostic SL is attractive. Nonetheless, MLA mineralogical characterization of the SLR will be required first to develop the SL.

Care should be taken with sample selection to ensure representation from all waste rock variations present in the dump. During sampling, care should be taken to not crush / disturb material so that secondary mineralization can be analyzed in its natural placement (i.e. association / availability).

The particle size in this study was limited to sub-1.19 mm. This was to decrease breakage of rock fragments and increase knowledge of MOI associations. However, the largest particle size fraction lacked good particle statistics for some MOI phases. This could be remedied by analyzing several sample mounts, though this would increase the cost of instrument analysis time and sample preparation. Using the largest particle size fraction of 850 µm (maximum) in two sample mounts would deliver improved particle statistics in a cost-effective manner. A characterization comparison study of rock fragments should be done to verify the ability to assess waste rock dumps based on sub-2 mm particle size. Sub-10 µm particles are potentially the most reactive and should be considered in the characterization of waste rock as a separate size fraction.

The optimal size for the final aperture in the SEM electron beam column should be investigated with respect to metal-bearing particles studied (accounting for spot size, accelerating voltage and vacuum pressure).

The rapid MLA XSPL method, still under development, could be used to better detect and characterize small rare phases. The under-development metal search uses the SPL mode with a metal X-ray spectral trigger to find the MOI.

The suggested sequence of analysis for a SEM mounted waste rock sample: (1) use WDS (wavelength dispersive spectrometry) to define whether carbon (or other low atomic number element) is present (i.e. definitive qualification of low-energy spectral data); and then, (2) EDS analysis to determine the 'whole rock' elemental composition (within technique detection limits).

Due to the challenges of determining fine secondary precipitation coatings and thin films with EDS, it would be beneficial to use EMPA to improve compositional data of such mineral phases. The EMPA data, with a detection limit of 100-300 mg/kg, could be inserted into the user-created MLA X-ray classification database**.**

To improve SEM imaging resolution and data acquisition time, the use of the FEG-SEM with MLA software should be considered. The FEG-SEM has 30-50% faster acquisition of X-ray impulses, improved excitation source [10 times smaller beam size than regular tungsten filament, stable beam current, and higher input count rates] and higher brightness for better image resolution.

The MLA analyzes particle cross-sections, not particle surface. The electron beam usually penetrates / interacts more than 1-2 µm below the analysis surface. Analysis of 3-D particle images by HRXMT should be considered to provide information on "in situ" particle mineral phase associations and availability. A current option available for 3-D particle analysis might be Focused Ion Beam (FIB) technology; however, it is a time consuming destructive technique that can only be done one particle at a time. The utilization of X-ray HRXMT, SEM and MLA can significantly improve the analysis of the particle surface and distribution of particle surface cracks and interior cracks. The MLA and similar systems cannot perform analysis during leaching or particle breaking processes, while HRXMT can.

To further expand the "holy grail" of waste rock management, the concepts and applications from the rapidly developing field of geometallurgy could be used. Although

geometallurgy is not new, it has become increasingly recognized as an activity that leads to efficient project evaluation and mine optimization. Waste rock management efforts would benefit from initial characterization of the ores for the mine plan.

The waste rock examined in this study was primarily considered ‘unweathered’. In the years ahead it would be useful to perform MLA analysis on representative samples of the same materials to comparatively observe mineral phase content shifts. This would enhance weathering mechanism models.

References

Chapter 1

Aranda, C.A., 2009. “Assessment of waste rock weathering characteristics at the Antamina mine based on field cell experiment”, M.A.Sc. thesis, University of British Columbia (Mining Engineering), May 2012, Vancouver, Canada.

Aranda, C.A., Klein, B., Beckie, R.D., Mayer, K.U., 2009. ”Assessment of waste rock weathering characteristics at the Antamina mine based on field experiments”, In: Securing the Future and 8th ICARD; Proceedings of the workshop, Skelleftea, Sweden, June 23-26, 2009.

Bay, D.S., Peterson, H.E., Singurindy, O., Aranda, C., Dockrey, J.W., Sifuentes Vargas, F., Mayer, K.U., Smith, L., Klein, B., Beckie, R.D., 2009. “Assessment of neutral pH drainage from three experimental waste-rock Piles at the Antamina mine, Peru”, 12 pages in the proceedings of Securing the Future and 8th International Conference on Acid Rock Drainage, June 23-26, 2009, Skellefteå, Sweden.

Brown, D., Verburg, R., Letient, H., Aranda, C., 2006. ”Geochemical characterization and water quality prediction at the Antamina mine”, 7th International Conference on Acid Rock Drainage (ICARD), March 26-30, 2006, St. Louis MO. R.I. Barnhisel (ed.) Published by the American Society of Mining and Reclamation (ASMR), p.291-305.

Corazao Galegos, J.C., Bay, D.S., Beckie, R.D., Klein, B., Mayer, K.U., Smith, L., Wilson, G.W., Brienne, S., Letient, H., 2007. ”Design and construction of field-scale waste rock piles at the Antamina mine, Peru”, Geotechnical News, v.25(1), p49-53.

Golder Associates Limited, 2004. “Waste rock geochemistry – Phase 2, Antamina mine Peru”, Final Version 4.0, December 2004, Golder Associates Ltd, Mississauga, Canada.

Golder Associates Limited, 2006. ”Waste dump and stockpile water quality estimates – Phase 3 – Antamina mine, Peru”, Final version 4, February 2006, Golder Associates Ltd, Peru, S.A.

Hirsche, D.T., 2012. “A field cell and humidity cell study of metal attenuation in neutral rock drainage from the Antamina Mine, Peru”, M.Sc. thesis, University of British Columbia, Vancouver, Canada (Geological Science), May 2012.

Jambor, J.L. & Blowes, D.W., 1998. “Theory and applications of mineralogy in environmental studies of sulfide-bearing mine wastes”, In: Modern Approaches to Ore and Environmental Mineralogy, Ed. Cabri, L. & Vaughan, D., Short Course Series, v.27, ch.12, p.367-401. Mineralogical Association of Canada, Ottawa.

Kwong, Y.T.J., 1993. “Prediction and prevention of acid rock drainage from a geological and mineralogical perspective”, MEND (Mine Environment Neutral Drainage), report 1.32.1., 47 p.

Lawrence, R.W. and Scheske, M., 1997. “A method to calculate the neutralization potential of mining wastes”, Environmental Geology, v.32(2), p.100-106.

Lipten, E.J., Smith, S.W., 2005. ”The geology of the Antamina copper-zinc deposit, Peru, South America”, In: Porter, T.M. (Ed.), Super porphyry copper and gold deposits: a global perspective, v.1, p.189-204, PGC Publishing, Adelaide.

Price, W.A., 1997. “Guidelines and recommended methods for the prediction of metal leaching and acid rock drainage at mine sites in British Columbia”**,** British Columbia Ministry of Employment and Investment, Energy and Minerals Division, Smithers, BC, (April), 143p.

Strand, R., Usher, B., Stracotta, C., Jackson, J., 2010. “Integrated water balance and water quality modelling for mine closure planning at Antamina”, Proceedings on the first international seminar on the reduction of risk in the management of tailings and mine waste, Mine Closure 2010 - A. Fourie, M. Tibbett and J. Wiertz (eds), Perth, Australia, p.63-74.

Sverdrup, H.U., 1990. “Kinetics of base cation release due to chemical weathering”, Lund University Press, Lund Sweden; In Treatise on Geochemistry: Environmental geochemistry, Volume 9 of Treatise on Geochemistry, Karl K. Turekian (Eds. H.D. Holland, K.K. Turekian), Elsevier Pergammon, 2004, 246 p.

Ulusoy, U., Kursun, I., 2011. “Comparison of different 2D image analysis measurements techniques for the shape of talc particles produced by different media milling”, Minerals Engineering, v.24(2), p.91-97.

Urrutia Varese P.L., 2012. “Assessment of cover systems for waste rock in the Antamina Mine, Peru”, M.A.Sc. thesis, University of British Columbia, Vancouver, Canada.”, University of British Columbia M.A.Sc. thesis (Mining Engineering), November 2012.

Watermark Consulting Inc., 2000. “Antamina Peak Rock Program, Geochemical Testing as of Jan 2000, Final Report” (February 2000) for *Compañía Minera Antamina S.A.*

Chapter 2

Adriaens, A., VanVaeck, L., and Adams, F., 1999. “Static secondary ion mass spectrometry (S-SIMS) Part 2: material science applications”, Mass Spectrometry Reviews, v.18, p.48-81.

Alpers, C. N., Blowes, D. W., Nordstrom, D. K., Jambor, J. L. 1994. “Secondary minerals and acid-mine water chemistry”, In: Short Course Handbook on Environmental Geochemistry of Sulfide Mine Wastes, Waterloo, Ontario, Mineralogical Association of Canada, p.247-270.

AMIRA P387A, 2002. “Prediction and kinetic control of acid mine drainage”, ARD Test Handbook.

Andrews, J.R.G., Mika, T., 1975. “Comminution of heterogeneous material: development of a model for liberation phenomena”, Proceedings of 11th International Mineral Processing Congress, Cagliari, p.59-88.

Barbery, G., Bloise, C., Gateau, C., Reinhart, C., 1983. “Mineral liberation measurements and their interpretation”, Special Publication of the Geological Society of South Africa, v.7, p.469-473.

Barbery, G., 1984. “Mineral liberation analysis using stereological methods: A review of concepts and problems”, Applied Mineralogy II, Park, W.C., Hausen, D.M. and Hagni, R.D. (eds), AIME, p.171-190.

Barbery, G., 1991. “Mineral liberation: measurement, simulation and practical use in mineral processing”, Les Editions GB, Quebec, 351p.

Becker, J.S., Dietze, H.-J., 1999. “Determination of trace elements in geological samples by laser ablation inductively coupled plasma mass spectrometry”, Journal of Analytical Chemistry, v.365, p.429-434.

Blowes, D., Ptacek, C., 1994. ”Acid-neutralization mechanisms in inactive mine tailings”, In: Environmental Geochemistry of Sulphide Mine-Wastes, Mineral Association of Canada (short course), Jambor, J., Blowes, D. (eds), v.22, p.271-292.

Bogner, A., Joneau, P.-H., Thollet, G., Basset, D., Gauthier, C., 2007. “A history of scanning electron microscopy developments: towards “wet-STEM” imaging”, Micron, v.38, p.390-401.

Criddle, A.J., 1998. “Ore microscopy and photometry (1890-1998)”, In: Modern Approaches to Ore and Environmental Mineralogy, Cabri, L.J. and Vaughan, D.J. (eds.), Mineral Association of Canada, Short Course, v.27, p.1-74.

De Marco, R., Bailey, S., Jiang, Z-T., Morton, J., Chester, R., 2006. “An in situ chronoamperometry/synchrotron radiation grazing incidence X-ray diffraction study of the electrochemical oxidation of pyrite in chloride media”, Electrochemistry Communications, v.8, p.1661-1664.

Drever, J.I., 1988. “The Geochemistry of Natural Waters”, Prentice Hall, Inc., Englewood Cliffs, New Jersey, 437p.

Evans, C.L., Wightman, E.M., Manlapig, E.V., Coulter, B.L., 2011. “Application of process mineralogy as a tool in sustainable processing”, Minerals Engineering, v.24, p.1242-1248.

Fandrich, R., Schneider, C.L., Gay, S.L., 1998. “Two stereological correction models: allocation method and kernel transformation method”, Minerals Engineering, v.11(8), p.707-715.

Fandrich, R., Gu, Y., Burrows, D., Moeller, K., 2007. “Modern SEM based mineral liberation analysis”, International Journal of Mineral Processing, v.84(1-4), p.310-320.

FEI, 2012. Personal conversations with José Ayala, Business Development Manager, FEI Natural Resources - North America, FEI Company, Hillsboro, Oregon, January & October 2012.

Frost, M. T., O'Hara, K., Suddaby, P., Grant, G., Reid, A.F., Wilson, A.F., Zuiderwyk, M., 1977. “A description of two automated control systems for the electron microprobe”, X-ray Spectrometry, v.5(4), p.180-187.

Garcia, D., Lin, C.L., Miller, J.D., 2009. “Quantitative analysis of grain boundary fracture in the breakage of single multiphase particles using X-ray microtomography procedures”, Minerals Engineering, v.22(3), p.236-243.

Gaudin, A.M., 1939. “Principles of mineral dressing”, McGraw-Hill, New York, p.70-91.

Gay, S.L., 2004. “A liberation model for comminution based on probability theory”, Minerals Engineering, v.17(4), p.525-534.

Gay, S., 2004. Simple texture-based liberation modelling of ores. Minerals Engineering v.17, p.1209-1216.

Ghorbani, Y., Becker, M., Mainza, A., Franzidis, J-P., and Petersen, J., 2011. "Large particle effects in chemical/biochemical heap leach processes – A review," Minerals Engineering, v.24(11), p. 1172-1184.

Gottlieb, P., Wilkie, G., Sutherland, D., Ho-Tun, E., Suthers, S., Perera, K. Jenkins, B., Spencer, S., Butcher, A., Rayner, J., 2000. “Using quantitative electron microscopy for process mineralogy applications”, JOM Journal of Metals, v.52, p.24-25.

Gu, Y., 2003. “Automated scanning electron microscope based mineral liberation analysis”, JOM Journal of Minerals & Materials Characterization & Engineering, v.2, p.33-41.

Gu., Y., 2004. “Rapid mineral liberation analysis with X-ray and BSE processing”, In: 8th International Congress on Applied Mineralogy, ICAM 2004, Sao Paulo, Brazil, p.119-122.

Gu, Y., Napier-Munn, T., 1997. “JK / Philips mineral liberation analyzer – an introduction”, Minerals Processing ’97 Conference, Capetown, SA, p.2.

Gunther, D., Jackson, S.E., Longerich, H.P., 1999. “Laser ablation and arc / spark solid sample introduction into inductively coupled plasma mass spectrometers”, Spectrochimica Acta Part B, v.54(3-4), p.381-409.

Gy, P., 1979. “Sampling of particulate materials: theory and practice”, Developments in Geomathematics 4, Elsevier Scientific Publishing Company, 430p.

Henley, K.J., 1983. “Ore dressing mineralogy –a review of techniques, applications and recent developments”, Special Publication of the Geological Society of South Africa, v.7, p.175-200.

Hill, G. S., Rowlands, N., Finch, J.A., 1987. “Data correction in two-dimensional liberation studies”, In: Process Mineralogy VII, Vassiliou, A.H., Hausen, D.M., and Carson, D.J.T. (eds), Warrendale, PA, The Metallurgical Society, p. 617-632.

Hoal, K.O., Stammer, J.G., Appleby, S.K., Botha, J., Ross, J.K., Botha, P.W., 2009. “Research in quantitative mineralogy: examples from diverse applications”, Minerals Engineering, v.22, p.402-408.

International Mineralogical Association, Commission on Ore Microscopy, 1962. “The quantitative data file for ore minerals of the commission on ore microscopy of the International Mineralogical Association”, Quantitative Data.

Jackson, B.R., Reid, A.F., Zuiderwyk, M.A., 1984. “Rapid production of high quality polished sections for automated image analysis of minerals”, Proceedings of the Australasian Institute of Mining and Metallurgy, v.289, p.93-97.

Jambor, J.L. & Blowes, D.W., 1998. “Theory and applications of mineralogy in environmental studies of sulfide-bearing mine wastes”, In: Modern Approaches to Ore and Environmental Mineralogy, Ed. Cabri, L. & Vaughan, D., Short Course Series, v.27, ch.12, p.367-401. Mineralogical Association of Canada, Ottawa.

Jerz, J.K., Rimstidt, J.D., 2003. “Efflorescent iron sulfate minerals: Paragenesis, relative stability, and environmental impact”, American Mineralogist, v. 88(11-12), p. 1919-1932.

Jones, M.P., 1982. “Designing an X-ray image analyzer for measuring mineralogical data”, In: XIV International Mineral Processing Congress, CIM, Toronto, v.3(4.1-4.7).

Jones, M.P., 1984. “Recent developments in the rapid collection of quantitative mineral data”, Proceedings of the Second International Congress on Applied Mineralogy, Los Angeles, p.141-145.

Jones, M.P., 1987. “Applied mineralogy, a quantitative approach”, Graham and Trotman (eds), London, UK, 259p.

Jones, M.P., Cheung, T.S., 1988. “Automatic method for finding gold grains in ores and mill products”, Asian Mining, p.73-81.

Jones, M.P., Gavrilovic, J., 1968. “Automated searching unit for the quantitative location of rare phases by electron-probe X-ray microanalysis”, Transactions of the Institute of Mining and Metallurgy, Section B, v.77, p.B137-B143.

King, R.P., 1979. “A model for the quantitative estimation of mineral liberation of grinding”, International Journal of Mineral Processing, v.6, p.207-220.

King, R.P., 1983. “Stereological methods for the prediction and measurement of mineral liberation”, Special Publication of the Geological Society of South Africa, v.7, p.449-464.

King, R.P., 1984. “Measurement of particle size distribution by image analyzer”, Powder Technology, v.39(2), p. 279–289.

King, R.P., 1990. “Calculation of the liberation spectrum in products produced in continuous milling circuits”, In: Proceedings 7th European Symposium on Comminution, Ljubljana, v.2., p.429-444.

King R.P., Schneider, C.L., 1998. “Stereological correction of linear grade distributions for mineral liberation”, Powder Technology, v.98(1), p.21-37.

Klein, B., Blaskovich, R., Haupt, C., Mayer, U., Beckie, R., 2011. “Assessing weathering in field cells experiments using quantitative mineralogy and sequential leaching”, Tailings and Mine Waste Conference, Vancouver, BC, Canada, November 6-9, 2011.

Klug, H.P., Alexander, L.E., 1974. “X-ray diffraction procedures: for crystalline and amorphous materials”, 2nd edition, John Wiley and Sons Inc, New York USA, 966p.

Lane, G.R., Martin, C., Pirard, E., 2008. “Techniques and applications for predictive metallurgy and ore characterization using optical image analysis”, Mineral Engineering, v.21, p.568-577.

Lastra, R., 2007. “Seven practical application cases of liberation analysis”, International Journal of Mineral Processing, v.84, p.337-347.

Latti, D., Adair, B.J.I., 2001. “An assessment of stereological correction procedures”, Minerals Engineering, v.14(12), p.1579-1587.

Lorenzen, L., 1995. “Some guidelines to the design of a diagnostic leaching experiment”, Minerals Engineering, v.8(3), p.247-256.

Lorenzen, J.S.J., van Deventer, L., 1994. “The interrelationship between mineral liberation and leaching behaviour”, International Journal of Mineral Processing, v.41, p. 1-15.

Lotter, N.O., Kormos, L.J., Oliveira, J., Fragomeni, D., Whiteman, E., 2011. “Modern process mineralogy: two case studies”, Minerals Engineering, v.24(7), p.638-650.

MacRae, N.D., 1995. “Secondary-ion mass spectrometry and geology”, The Canadian Mineralogist, v.33, p.219-236.

Majuste, D., Ciminelli, V.S.T., Eng, P.J., Osseo-Asare, K., 2013. “Applications of *in situ* synchrotron XRD in hydrometallurgy: literature review and investigation of chalcopyrite dissolution”, Hydrometallurgy, v.131-132, p.54-66.

Márquez, M., Gaspar, J., Bessler, K.E., Magela. G, 2006. “Process mineralogy of bacterial oxidized gold ore in São Bento Mine (Brasil)”, Hydrometallurgy; v.83, p.114–23.

Meloy, P.T., 1984. “Liberation theory – eight, modern usable theorems”, International Journal of Mineral Processing, v.13, p.313-324.

MEND Manual, Volume 2 - Sampling and Analysis, January, 2001, Natural Resources Canada.

MEND. 1990. “Acid rock drainage prediction manual- A manual of chemical evaluation procedures for the prediction of acid generation from mine wastes”, MEND Project 1.16.1b. A report prepared for CANMET-MSL Division, Department of Energy, Mines, and Resources, Canada by Coastech Research, Inc., Vancouver, B.C.

Michelic, S.K., Wieser, G., Bernhard, C., 2011. “On the representativeness of automated SEM / EDS analyses for inclusion characterization with special regard to the measured sample area”, Iron and Steel Institute of Japan International, v.51(5), p.769-775.

Miller, P.R., Reid, A.F., Zuiderwyk M., 1982. “QEM-SEM image analysis in the determination of modal assays, mineral associations and mineral liberation”, In: Proceedings of XIV International Mineral Processing Congress, CIM, Toronto.

Miller, J.D., Lin, C.L., 2004. “Three-dimensional analysis of particulates in mineral processing systems by cone-beam X-ray microtomography”, Minerals and Metallurgical Processing, v.21, p.113-124.

Miller, J.D., Lin, C.L., 2009. “High resolution X-ray micro CT (HRXMT) – advances in 3D particle characterization for mineral processing operations”, In: Recent Advances in Mineral Processing Plant Design, SME, Melhotra, D., Taylor, P.R., Spiller, R., Levrier, M. (eds.), p.48-59.

Neilson, M.J., Brockman, G.F., 1977. “The error associated with point-counting”, American Mineralogist, v.62, p.1238-1244.

Nesbitt, H.W., Jambor, J.L. 1998. “Role of mafic minerals in neutralizing ARD, demonstrated using a chemical weathering methodology”, In: Modern Approaches to Ore and Environmental Mineralogy. Mineralogical Association of Canada Short Course Series, Cabri, L.J. and Vaughan, D.J. (eds.), v.27, p.403-421.

Newbury, D.E., Joy, D.C., Echlin, C.E., Fiori, C.E., Goldstein, J.I., 1986. “Advanced scanning electron microscopy and X-ray microanalysis”, Plenum Press, New York (ASEMXM), 181p.

Nordstrom, D.K. 1999. “Some fundamentals of aqueous geochemistry”. In: The Environmental Geochemistry of Mineral Deposits. Part A: Processes, Techniques, and Health Issues. Vol. 6A, Chapter 4. Reviews in Economic Geology. Society of Economic Geologists, Inc., Chelsea, MI. p.117-123.

Nordstrom, D.K., Alpers, C.N. 1999. “Geochemistry of acid mine waters”. In: The Environmental Geochemistry of Mineral Deposits. Part A: Processes, Techniques, and Health Issues. Vol. 6A, Chapter 4. Reviews in Economic Geology. Society of Economic Geologists, Inc., Chelsea, MI. p.133-160.

Ofori, P., O’Brien, G., Firth, B., Jenkins, B., 2006. “ Flotation process diagnostics and modeling by coal grain analysis”, Minerals Engineering, v.19(6-8), p.633-640.

Omotoso, O., McCarty, D.K., Hillier, S., Kleeberg, R., 2006. “Some successful approaches to quantitative mineral analysis as revealed by the 3rd Reynolds Cup contest”, Clays and Clay Mineralogy, v.54(6), p.748-760.

Oosthuyzen, E.J., 1985. “Image analysis of gold-bearing ores and products”, Mintek 50 – International Conference on Mineral Science and Technology, The Council of Mineral Technology.

PANalytical, 2009. Personal conversations with Allan Ball – PANalytical Sales Representative.

Parise, J.B., 2000. “Synchrotron studies of phase transformations”, Transformation Processes in Minerals (Reviews in Mineralogy and Geochemistry, v.39, p.285-318.

Pascoe, R.D., Power, M.R., Simpson, B., 2007. “QEMSCAN analysis as a tool for improved understanding of gravity separator performance”, Minerals Engineering, v.20, p.487-495.

Petruk, W., 1976. “Application of quantitative mineralogical analysis of ores to ore dressing”, CIM Bulletin, v.69, p.146-153.

Petruk, W., 1988. “The capabilities of the microprobe Kontron image analysis system: application to mineral analysis”, Scanning Microscopy, v.2, p.1247-1256.

Petruk, W., 2000. “Applied mineralogy in the mining industry”, First Edition, Elsevier Science, Amsterdam.

Petrunic, B., Al, T., Weaver, L., 2005. ”A transmission electron microscopy analysis of secondary minerals formed in tungsten mine tailings with an emphasis on arsenopyrite oxidation”, Applied Geochemistry, v.21, p.1259-1273.

Pounceby, M., Macrae, C.M., Wilson, N., 2001. “Electron microprobe mapping – a diagnostic tool for ilmenite characterization”, In: International Heavy Minerals Conference, AusIMM, Freemantle, p.69-74.

Price, W.A., Kwong, Y.T.J., 1997. “Waste rock weathering, sampling and analysis: Observations from the British Columbia Ministry of Employment and Investment database”, Proceedings 4th International Conference on Acid Rock Drainage, Vancouver, p.31-45.

Reed, S.J.B., 1990. “Recent developments in geochemical analysis”, Chemical Geology, v.83(1-2), p.1-9.

Reid, A.F., Zuiderwyk, M.A., 1975. “QEM-SEM: An interface system for minicomputer control of instruments and devices”, CSIRO Division of Mineral Chemistry, Investigation report, August.

Reid, A.F., Gottlieb, P., MacDonald, K.J., Miller, P.R., 1984. “QEM-SEM image analysis of ore minerals: volume fraction, liberation and observational variances”, Applied Mineralogy, The Metallurgical Society of AIME, p.191-204.

Remond, G., Cesbron, F., Traxel, K., Campbell, J.L., Cabri, L.J. (1987). “Electron microprobe analysis and proton induced X-ray spectrometry applied to trace element analysis in sulfides: problems and prospects”, Scanning Microscopy, v.1, p.l0l7-1037.

Rietveld, H.M., 1969. “A profile refinement method for nuclear and magnetic structures”, Journal of Applied Crystallography, v.2(2), p.65-71.

Russ, J.C., 1986. “Practical stereology (Edition 1)”, Springer-Verlag, New York, 185p.

Sapsford, D.J., Bowell, R.J., Dey, M., Williams, K.P., 2009. “Humidity cell tests for the prediction of acid rock drainage”, Minerals Engineering, v.22, p.25–36.

Sherlock, E.J., Lawrence, R.W., Poulin, R., 1995. "On the neutralization of acid rock drainage by carbonate and silicate minerals", Environmental Geology, v.25(1), p.43-54.

Shouwstra, R.P., Smit, A.J., 2011. “Developments in mineralogical techniques – what about the mineralogists?”, Minerals Engineering, v.24, p.1224-1228.

Smith, K.S. 1999. “Metal sorption on mineral surfaces: An overview with examples relating to mineral deposits”, In: The Environmental Geochemistry of Mineral Deposits. Part B: Case Studies and Research Topics. Vol. 6B, Chapter 7, Filipek, L., Plumlee, G. (eds). Reviews in Economic Geology. Society of Economic Geologists, Inc., Chelsea, MI. p.161-182.

Smith, K.S., Huyuk, H.L.O. 1999. “An overview of the abundance, relative mobility, bioavailability, and human toxicity of metals”, In: The Environmental Geochemistry of Mineral Deposits. Part A:Vol. 6A, Chapter 2. Plumlee, G., Logsdon, M. (eds.). Reviews in Economic Geology, Society of Economic Geologists, Inc., Chelsea, MI. p.29-70.

Sobek, A.A., Schuller, W.A., Freeman, J.R., Smith, R.M. 1978. “Field and laboratory methods applicable to overburden and minesoils”, EPA 600/2-78-054, 203 p.

Spencer, S., Sutherland, D., 2000. “Stereological correction of mineral liberation grade distributions estimated by the single sectioning of particles”, Image Analysis and Stereology, v. 19, p. 175-182.

Stanley, C.J., 1998. “Optical microscopy in studying ores and process products”, In: Modern Approaches to Ore and Environmental Mineralogy, Cabri, L.J. and Vaughan, D.J. (eds.), Mineralogical Association of Canada, Short Course, v.27, p.123-137.

Steiner, H.J., 1975. “Liberation kinetics in grinding operations”, In: Proceedings of 11th International Mineral Processing Congress, Cagliari, p.33-58.

Stumm, W., Morgan, J.J. 1981. "Aquatic chemistry - An introduction emphasizing chemical equilibria in natural waters", John Wiley & Sons, Inc., 470 p.

Sutherland, D., Gottlieb, P., Jackson, R., Wilkie, G., Stewart, P., 1988. "Measurement in section of particles of known composition", Minerals Engineering, v.1(4), p.317-326.

U.S. Environmental Protection Agency, 1994a. "Acid mine drainage – Technical report", U.S. Environmental Protection Agency (USEPA), Washington, USA.

U.S. Environmental Protection Agency, 1994b. "Test methods for evaluating solid waste, physical / chemical methods (SW0846)", 3rd edition, update 2B: Environmental Protection Agency, National Center for Environmental Publications, Cincinnati, OH 45268, EPASW-846.3.2B. URL http://www.epa.gov/epaoswer/hazwaste/test/sw846.htm

Van der Heide, P., 2011. "X-ray photoelectron spectroscopy: An introduction to principles and practices", John Wiley and Sons Inc., Hoboken, NJ, USA.

van der Wal, D. and Kruesemann, H., 2011. "Examples of automated petrography systems (MLA / QEMSCAN) used in the minerals industry", VIII Congress of CIS Dressers (Ore Mining & Dressing Plants), Moscow, February 28 to March 2, Congress Centre of the World Trade.

VanVaeck, L., Adriaens, A., and Gijbels, R., 1999. "Static secondary ion mass spectrometry: (S-SIMS) Part 1. methodology and structural interpretation", Mass Spectrometry Reviews, v.18, p.1-47.

Vickerman, J.C., Briggs, D., 2001. "ToF-SIMS: surface analysis by mass spectrometry", IM Publications and Surface Spectra Limited, Manchester, UK.

Warren, B.E., 1969. "X-ray diffraction", Addison-Wesley Publishing Company, Inc., Reading, Massachusetts, Dover Publications, Inc., 381p.

White, W.M., 1998. "Weathering, soils and biogeochemical cycling", Geochemistry (Cornell University), chapter 13, p.563-587.

White, W.W. III, Lapakko, K.A., Cox, R.L. 1999. "Static-test methods most commonly used to predict acid-mine drainage: Practical guidelines for use and interpretation", In: Reviews in Economic Geology, V. 6A, The Environmental Geochemistry of Mineral Deposits, Part A: Processes, Techniques, and Health Issues. Plumlee, G.S. and Logsdon, M.J. (eds.), Society of Economic Geologists Inc., Littleton, CO. p.325-338.

Zaera, F., 2012. "Probing liquid/solid interfaces at the molecular level", Chemical Reviews, v.112, p.2920-2986.

Chapter 3

Antamina, 2001. "*Geologia de Antamina*", *Compania Minera Antamina S.A.*, Geology Department, Yanacancha, Peru.

Conlan, M.J.W., Mayer, K.U., Blaskovich, R.J., Beckie, R.D., 2012. "Solubility controls for molybdenum in neutral rock drainage", Geochemistry: Exploration, Environment, Analysis; 2012 Geological Society of London, v.12, p.21-32.

Goldberg, S., Forster, H., Godfrey, C., 1996. "Molybdenum adsorption on oxides, clay minerals and soils", Soil Science Society of America Journal, v.60(2), p.425-432.

Golder Associates, 2010. "Waste tailings and geochemistry – field cell monitoring December 2002 to May 2009", Final version 4, revision 1, January 2010, Golder Associates, Peru, S.A.

Klein, B., Blaskovich, R., Haupt, C., Mayer, U., Beckie, R., 2011. “Assessing weathering in field cells experiments using quantitative mineralogy and sequential leaching”, Tailings and Mine Waste Conference, Vancouver, BC, Canada, November 6-9, 2011.

Murray, D.R., 1977. “Pit Slope Manual Supplement 10-1”, CANMET Report 77-31, Department of Energy, Mines and Resources Canada, Ottawa, Ontario.
Natarajan, K.A., Iwasaki, I., 1983. “Role of galvanic interactions in the bioleaching of Duluth gabbro copper-nickel sulphides”, Separation Science & Technology, v.18, p.1095-1111.

Price, W.A., 1997. “Guidelines and recommended methods for the prediction of metal leaching and acid rock drainage at mine sites in British Columbia**”,** British Columbia Ministry of Employment and Investment, Energy and Minerals Division, Smithers, BC, (April), 143p.

Price, W.A., Kwong, Y.T.J., 1997. “Waste rock weathering, sampling and analysis: Observations from the British Columbia Ministry of Employment and Investment database”, Proceedings 4th International Conference on Acid Rock Drainage, Vancouver, p.31-45.

Chapter 4

ASM International, 2000. “Practical guide to image analysis”, Materials Park, OH, American Society for Metals (ASM) International, v.20, p.75-99.

Fandrich, R., Gu, Y., Burrows, D., Moeller, K., 2007. ”Modern SEM-based mineral liberation analysis”, International Journal of Mineral Processing, v.84, p.310-320.

Gu, Y., 2003. “Automated scanning electron microscope based mineral liberation analysis: an introduction to JKMRC / FEI Mineral Liberation Analyzer”, Journal of Minerals and Materials Characterization and Engineering, v.2(1), p.33-41.

Ofori, P., O’Brien, G., Firth, B., Jenkins, B., 2006. “ Flotation process diagnostics and modeling by coal grain analysis”, Minerals Engineering, v.19(6-8), p.633-640.

Russ, J.C., 2002. “The image processing handbook”,4th edition, New York, CRC Press, p.444-462.

Spencer, S., Sutherland, D., 2000. “ Stereological correction of mineral liberation grade distributions estimated by single sectioning of particles”, Image Analysis Stereology, v.19, p.175-182.

Chapter 5

Antamina, 2001. “*Geologia de Antamina*”, *Compania Minera Antamina S.A.*, Geology Department, Yanacancha, Peru.

Ballester, A., Gonzalez, F., Blazquez, M.L., Mier, J.L., 1990. ”The influence of various ions in the bioleaching of metal sulphides”, Hydrometallurgy, v.23, p.221-235.

Blight, K.R., Ralph, D.E., 2004. “Effect of ionic strength on iron oxidation with batch cultures of chemo-lithotrophic bacteria”, Hydrometallurgy, v.73, p.325-334.

Blowes, D.W., Al, T.A., Lortie, L., Gould, W.D., Jambor, J.L., 1995. “Microbiological, chemical and mineralogical characterization of the Kidd Creek mine tailings impoundment, Timmons area, Ontario”, Geomicrobiology Journal. v.13, p.13-31.

Cao, X., Ma, L.Q., Singh, S.P., Zhou, Q., 2008. ”Phosphate induced lead immobilization from different lead minerals in soils under varying pH conditions”, Environmental Pollution, v.1(152), p.184-192.

Cao, X., Wahbi, A., Ma, L., Li, B., Yang, Y., 2009. ”Immobilization of Zn, Cu and Pb in contaminated soils using phosphate rock and phosphoric acid”, Journal of Hazardous Materials, v.2-3(164), p.555-564.

Conlan, M.J.W., 2009. ”Attenuation mechanisms for molybdenum in neutral rock drainage”, MASc thesis, University of British Columbia.

Conlan, M.J.W., Mayer, K.U., Blaskovich, R.J., Beckie, R.D., 2012. ”Solubility controls for molybdenum in neutral rock drainage”, Geochemistry: Exploration, Environment, Analysis; 2012 Geological Society of London, v.12, p.21-32.

Córdoba E.M., Muñoz J.A., Blázquez M.L., González F., Ballester, A., 2008a. “Leaching of chalcopyrite with ferric ion. Part I: general aspects”, Hydrometallurgy, v.93(3-4), p.81-87.

Córdoba E.M., Muñoz J.A., Blázquez M.L., González F., Ballester, A., 2008b. “Leaching of chalcopyrite with ferric ion. Part II: effect of redox potential”, Hydrometallurgy, v.93(3-4), p.88-96.

Córdoba E.M., Muñoz J.A., Blázquez M.L., González F., Ballester, A., 2009. “Comparative kinetic study of the silver-catalyzed chalcopyrite leaching at 35 and 68 deg-C”, International Journal of Mineral Processing, v.92, p.137-143.

Dave, S.R., Gupta, K.H., Tipre, D.R., 2008. “Characterization of arsenic resistant and arsenopyrite oxidizing Acidiothiobacillus ferrooxidans from Hutti gold leachate and effluents”, Bioresource Technology, v.99, p.7514-7520.

Deveci, H., Akcil, A., Alp, I., 2004. ”Bioleaching of complex zinc sulphides using mesophilic and thermophilic bacteria: comparative importance of pH and iron”, Hydrometallurgy, v.73, p.293-303.

Dixon, D.G., Mayne, D.D., 2007. “Galvanox – a novel galvanically assisted atmospheric leaching technology for copper concentrates”, Proceedings of Copper / Cobre 2007 Conference, Toronto (Canada), Riveros P. *et al.*(eds.), CIM Montreal, Canada, v.IV(1), p.191.

Dreisinger, D., 2006. “Copper leaching from primary sulfides: options for biological and chemical extraction of copper”, Hydrometallurgy, v.83, p.10-20.

Erdem, M., Ozverdi, A., 2011. ”Environmental risk assessment and stabilization / solidification of zinc extraction residue: II Stabilization / solidification”, Hydrometallurgy, v.105, p.270-276.

Gasparini, C., 1983. “The mineralogy of gold and its significance in metal extraction”, Canadian Mining and Metallurgical Bulletin, v.76, p.144-153.

Geysen, D., Imbrechts, K., Vandercasteele, C., Jaspers, M., Wauters, G., 2004a. ”Immobilization of lead and zinc in scrubber residues from MSW combustion using soluble phosphates”, Waste Management, v.24(5), p.471-481.

Geysen, D., Vandercasteele, C., Jaspers, M., Wauters, G., 2004b. ”Comparison of immobilization of air pollution control residues with cement and silica”, Journal of Hazardous Materials, v.B107, p.131-143.

Golder Associates Limited, 2004. “Waste rock geochemistry – Phase 2, Antamina mine Peru”, Final Version 4.0, December 2004, Golder Associates Ltd, Mississauga, Canada.

Golder Associates, 2010. ”Waste tailings and geochemistry – field cell monitoring December 2002 to May 2009”, Final version 4, revision 1, January 2010, Golder Associates, Peru, S.A.

Guo, P., Guangji, Z., Junya, C., Yuanyuan, L., Zhaoheng, F., Chao, Y., 2011. “Catalytic effect of Ag^{+} and Cu^{+2} on leaching realgar (As_2S_2)”, Hydrometallurgy, v.106, p.99-103.

Hackl, R.P., Dreisinger, D.B., Peters, E., King, J.A., 1995. ”Passivation of chalcopyrite during oxidative leaching in sulphate media”, Hydrometallurgy, v.39, p.25-48.

Hayes, R.A., Ralston, J., 1988. “The collectorless flotation and separation of sulphide minerals by E_h control”, International Journal of Mineral Processing, v.23, p.55-84.

Hiroyoshi, N., Miki, H., Hirajima, T., Tsunekawa, M., 2000. “A model for ferrous chalcopyrite leaching”, Hydrometallurgy, v.57, p.31-38.

Hiroyoshi, N., Miki, H., Hirajima, T., Tsunekawa, M., 2001. “Enhancement of chalcopyrite leaching by ferrous ions in acidic ferric sulphate solutions”, Hydrometallurgy, v.60, p.185-197.

Hiroyoshi, N., Kuroiwa, S., Miki, H., Tsunekawa, M., Hirajima, T., 2004. “Synergistic effect of cupric and ferrous ions on active-passive behaviour in anodic dissolution of chalcopyrite in sulphuric acid solutions”, Hydrometalllurgy, v.74, p.103-116.

Hiroyoshi, N., Kitagawa, H., Tsunekawa, M., 2008. “Effect of solution composition on the optimum redox potential for chalcopyrite leaching in sulphuric acid solutions”, Hydrometallurgy, v.91, p.144-149.

Holmes, P.R., Crundwell, F.K., 2000. “The kinetics of the oxidation of pyrite by ferric ions and dissolved oxygen: an electrochemical study”, Geochimica et Cosmochimica Acta, v.64(2), p.263-274.

Johanessan, K.H., Maest, A.S., Lyons, W.B., 1992. “Oxyanion mechanisms in Eastern Sierra Nevada surface waters”, In: History of water: Eastern Sierra Nevada, Owens Valley, White Inyo-Mountains, White Mountain Research station Symposium, v.4(7.4), p.348-366.

Klauber, C.A, 2008. “Critical review of the surface chemistry of acidic ferric sulphate dissolution of chalcopyrite with regards to hindered dissolution”, International Journal of Mineral Processing, v.86(1-4), p.1-17.

Kocabag, D., 1985. “The effect of grinding media and galvanic interactions upon the flotation of sulphide minerals”, Complex Sulfides, Process Symposium, v.5, p.81.

Lattanzi, P., Da Pelo,S., Musu, E., Atzei, D., Elsener, B., Fantauzzi, M., Rossi, A., 2008. ”Enargite oxidation: a review”, Earth-Science Reviews, v.86, p62-88.

Liu, R., Zhao, D., 2007. ”Reducing leachability and bioaccessibility of lead in soils using a new class of stabilized iron phosphate nanoparticles”, Water Research, v.12(41), p.2491-2502.

Mavropoulos, E., Rocha, N.C.C., Morreira, J.C., Rossi, A.M., Soares, G.A., 2004. ”Characterization of phase evolution during lead immobilization by synthetic hydroxyapatite”, Materials Characterization, v.1(53), p.71-78.

Mehta, A.P., Murr, L.E., 1982a. ”Kinetic study of sulphide leaching between chalcopyrite, pyrite and sphalerite in the presence of *T. ferroxidans* (30 degC) and a thermophilic microorganism (55 degC)”, Biotechnology and Bioengineering, v.24(4), p.919-940.

Mehta, A.P., Murr, L.E., 1982b. “Kinetic study of sulphide leaching by galvanic interaction between chalcopyrite, pyrite and sphalerite in the presence of *T. ferroxidans* and thermophilic micro-organism”, Biotechnology and Bioengineering, v.24(4), p.919-940.

Melamed, R., Cao, X., Chen, M., Ma, L.Q., 2003. ”Field assessment of lead immobilization in a contaminated soil after phosphate application”, Science of The Total Environment, v.1-3(305), p.117-127.

Natarajan, K.A., Iwasaki, I., 1983. “Role of galvanic interactions in the bioleaching of Duluth gabbro copper-nickel sulphides”, Separation Science & Technology, v.18, p.1095-1111.

Nava, D., Gonzalez, I., 2006. “Electrochemical characterization of chemical species formed during the electrochemical treatment of chalcopyrite in sulfuric acid”, Electrochimica Acta, v.51, p.5295-5303.

Nazari, G., Dixon, D.G., Dreisinger, D.B., 2011. “Enhancing the kinetics of chalcopyrite leaching in the Galvanox™ process”, Hydrometallurgy, v.105(3,4), p.251-258.

Nichol, M.J., 1975. “Mechanism of aqueous reduction of chalcopyrite by copper, iron, and lead”, Transactions of the Institution of Mining and Metallurgy, v.84, p.206.

Olsen, G.J., Brierley, J.A., Brierley, C.L., 2003. “Bioleaching review Part B: progress in bioleaching: applications of microbial processes by the minerals industries”, Applied Microbiology and Biotechnology, v.63, p.249-257.

Ozverdi, A., Ergun, M., 2010. ”Environmental risk assessment and stabilization / solidification of the zinc extraction residue: I Environmental risk assessment”, Hydrometallurgy, v.100, p.103-109.

Petrunic, W.M., Al, T.A., Weaver, L., 2006. “A transmission electron microscopy analysis of secondary minerals formed in tungsten-mine tailings with an emphasis on arsenopyrite oxidation.” Applied Geochemistry, v.21(8), p.1259-1273.

Plumlee, G.S., Smith, K., Montour, M., Ficklin, W., Mosier, M., 1999. “Geologic controls on the composition of natural waters and mine waters draining diverse mineral deposit types”, In: Filipek, L.H., Plumlee, G.S. (Eds.), Environmental Geochemistry of Mineral Deposits: Part B. Case Studies and Research Topics, Reviews in Economic Geology, v.6B, p.373– 432.

Price, D.W., Warren, G.W., Drouven, B., 1986. ”The electrochemical behaviour of silver sulphide in sulphuric acid solutions”, Journal of Applied Electrochemistry, v.16, p.719-731.

Rohwerder, T., Gehrke, T., Kinzler, K., Sand, W., 2003. “Bioleaching review Part A” progress in bioleaching: fundamentals and mechanisms of bacterial metal sulphide oxidation”, Applied Microbiology and Biotechnology, v.63, p.239-248.

Sand, W., Gehrke, T., Jozsa, P., Schippers, A., 2001. “(Bio)chemistry of bacterial leaching – direct vs. indirect bioleaching”, Hydrometallurgy, v.59, p.159-175.

Sandstrom, A., Shchukarev, A., Jan, P.J., 2005. “XPS characterization of chalcopyrite chemically and bioleached at high and low redox potential”, Minerals Engineering, v.18, p.505-515.

Shiers, D.W., Blight, K.R., Ralph, D.R., 2005. “Sodium sulphate and sodium chloride effects on batch culture of iron oxidizing bacteria”, Hydrometallurgy, v.80, p.75-82.

Song, Y.C., Sivakumar, S., Nguyen, T.T., Kim, S.H., Kim, B.G., 2009. “The immobilization of heavy metals in biosolids using phosphate amendments – comparison of EPA (6010 and 3051) and selective sequential extraction methods”, Journal of Hazardous Materials, v.1-3(167), p.1033-1037.

Tshilombo, A.F., 2004. “Mechanism and kinetics of chalcopyrite passivation and depassivation during ferric and microbial leaching”, PhD Thesis, University of British Columbia.

Van Aswegen, P.C., van Niekerk, J., Olivier, W., 2007. “The BIOX process for the treatment of refractory gold concentrates”, in: Rawlings, D.D.,Jonson, D.B., (Eds), Biomining. Springer, Berlin, p.2-33.

Vinals, J., Fuentes, G., Hernandez, M.C., Herreros O., 2004. “Transformation of sphalerite particles into copper sulfide particles by hydrothermal treatment with Cu(II) ions”, Hydrometallurgy, v.75, p.177–187.

Xu, Y., Schwartz, F.W., 1994. ”Lead immobilization by hydroxyapatite in aqueous solutions”, Journal of Contaminant Hydrology, v.3(15), p.187-206.

Appendices

Andersen, J.C.O., Rollinson, G., Snook, B., Herrington, R., Fairhurst, R., 2009. ”Use of QEMScan for the characterization of Ni-rich and Ni-poor goethite in laterite ores”, Minerals Engineering, v.22, p.1119-1129.

Gu, Y., 2003. “Automated scanning electron microscope based mineral liberation analysis: an introduction to JKMRC / FEI Mineral Liberation Analyzer”, Journal of Minerals and Materials Characterization and Engineering, v.2(1), p.33-41.

Fandrich, R., Gu, Y., Burrows, D., Moeller, K., 2007. ”Modern SEM-based mineral liberation analysis”, International Journal of Mineral Processing, v.84, p.310-320.

JKMRC, 2004. “MLA System User Operating Manual Module 1 (2004)”: Julius Kruttschnitt Mineral Research Centre.

Jones, M.P., 1987. “Applied mineralogy: a quantitative approach”, Applied Mineralogy, A Quantitative Approach, Graham and Trotman, London, UK, 259 p.

Webmineral, 2010. “http: / / www.webmineral.com”, accessed 2010-2011.

APPENDICES

APPENDIX 1 Mineral phases

A detailed MOI X-ray classification standard was developed which encompassed many MOIs expected to be present in weathered rock mass (e.g. oxidized metals which adsorbed or absorbed other elements into their matrices). Elements in brackets represent elements which were detected in minor and trace association with the major mineral phase.

1) General grouping

Note: DANA type separation (trace Sulphide presence grouped into Other)

Sulphide

Bornite, Chalcopyrite, Chalcopyrite(Zn), Chalcopyrite(Pb), Enargite, Enargite(Zn), Galena(Se), Molybdenite, Pyrite, Pyrite(Cu), Pyrrhotite, RealgarOrpiment, Sphalerite, Sphalerite(Cu), Stibnite, Watanabeite(Zn), Other [Ag sulphosalt, Arsenopyrite, Bismuthinite, Chalcocite, Galenobismutite, Siegenite(Cu,Fe), Siegenite(Cu,Zn), Tennantite(Zn,Fe)]

Carbonate

Calcite, Dolomite, Otavite(Zn,Cu), SideriteMnAsZnCrCu, Other [Ankerite, Malachite, Rhodochrosite, Smithsonite]

Silicate

Biotite, Chlorite, Kaolinite, K-Feldspar, Mica, MicaAltered (Cu,Zn), Muscovite, Plagioclase, Pyroxene, Quartz, Talc(Fe), Titanite(Cu,Pb), Other

[AmphiboleAnthophyllite, Andalusite, Apophyllite, Carpholite, Epidote, Fayalite, FeOxideCu, Grossular, GruneritePbCuZn, Melilite, MoCaSilicateOxide, MoSulphatePowelliteClay, Phlogopite, Sericite, Willemite, Wollastonite, Zircon]

Phosphates

Apatite, Apatite (Cu,Pb,Zn), Fornacite•Conichalcite, Goyazite, Monazite(Ce), Tyrolite(Pb)

Oxides

FeOxyhydroxides [FeOxideSulphate(Cu,Pb,Zn,As), FeOxyhydroxide], OtherOxides [Bismutostibiconite, Cassiterite, Cuprite, FeTiOxide, ParamelaconiteZn, PbCaOxideMoZnW, PbMoOxide, Portlandite, Spinel, Srebrodolskite, Wulfingite]

Sulphates

FeSulphate[FeSulphate, FeSulphateLimonite(CuAsMoZn)], Barite, Gypsum, OtherSulphates [Alunite, Celestine, Goslarite, MoCaSulphateMnCuFeZn]

Other

ChloroOrganic, Fluorite, Jarosite(Cu), MolybdofornaciteZnCu, Powellite, Scheelite, TrampMetal, Wulfenite

2) **Simple grouping**

Note: mineralogy was divided into DANA classification at its simplest level

Sulphide

AgSulphosalt, Arsenopyrite, Bismuthinite, Bornite, Chalcocite, Chalcopyrite, Chalcopyrite(Pb), Chalocpyrite(Zn), Enargite, Enargite(Zn), Galena(Se), Galenobismutite, Siegenite(Cu,Zn), Molybdenite, Pyrite, Pyrite(Cu), Pyrrhotite,

RealgarOrpiment, Sieginite(Cu,Fe), Sphalerite, Sphalerite(Cu), Stibnite, Tennantite(Zn,Fe), Watanabeite(Zn)

Carbonate

Ankerite, Calcite, Dolomite, Malachite, Otavite(Zn,Cu), Rhodochrosite, SideriteMnAsZnCrCu, Smithsonite

Silicate

AmphiboleAnthophyllite, Andalusite, Apophyllite, Carpholite, Biotite, MoCaSilicateOxide, Chlorite, Epidote, Fayalite, FeOxideCu, Grossular, Grunerite(Pb,Cu,Zn), K-Feldspar, Kaolinite, Melilite, Mica, MicaAltered(Cu,Zn), MoSulphatePowelliteClay, Muscovite, Phlogopite, Plagioclase, Pyroxene, Quartz, Sericite, Talc(Fe), Titanite(Pb,Cu), Willemite, Wollastonite, Zircon

Phosphate

Apatite, Apatite(Cu,Pb,Zn), Fornacite•Conichalcite, Goyazite, Monazite(Ce), Tyrolite(Pb)

Oxide

Bismutostibiconite, Cassiterite, Cuprite, FeOxideSulphate(Cu,Pb,Zn,As), FeOxyhydroxide, FeTiOxide, ParamelaconiteZn, PbMoOxide, PbCaOxideMoZnW, Portlandite, Spinel, Srebrodolskite, Wulfingite

Sulphate

Alunite, Barite, Celestine, FeSulphate, FeSulphateLimonite(CuAsMoZn), Goslarite, Gypsum, MoCaSulphateMnCuFeZn

Other

ChloroOrganic, Fluorite, Jarosite(Cu), MolybdofornaciteZnCu, Powellite, Scheelite, TrampMetal, Wulfenite

3) **Metal-MOI grouping**

Note: mineralogy was separated into grouped phases based upon what Antamina considered to be “problem” elements (i.e. metal). The metal MOIs are represented in the list below. Element in bracket was detected by EDS and could be substituted in lattice, adsorbed on surface or solid solution in lattice.

Antimony MOI

Bismutostibiconite, Stibnite, Watanabeite(Zn)

Arsenic MOI

Arsenopyrite, Enargite, Enargite(Zn), FeOxideSulphate(Cu,Pb,Zn,As), FeSulphateLimonite(CuAsMoZn), Fornacite•Conichalcite, RealgarOrpiment, SideriteMnAsZnCrCu, Tennantite(Zn,Fe), Tyrolite(Pb), Watanabeite(Zn), MolybdofornaciteZnCu

Copper MOI

Apatite(Cu,Pb,Zn), Bornite, Chalcocite, Chalcopyrite, Chalcopyrite(Pb), Chalcopyrite(Zn), Cuprite, Enargite, Enargite(Zn), FeOxideCu, FeOxideSulphate(Cu,Pb,Zn,As), FeSulphateLimonite(CuAsMoZn), Fornacite•Conichalcite, Grunerite(Pb,Cu,Zn), Jarosite(Cu), Siegenite(Cu,Zn), Malachite, MicaAltered(Cu,Zn), MoCaSilicateOxide, MoCaSulphateMnCuFeZn, MolybdofornaciteZnCu, MoSulphatePowelliteClay, Otavite(Zn,Cu), ParamelaconiteZn, PbMoOxide, Powellite, Pyrite(Cu), SideriteMnAsZnCrCu, Sieginite(Cu,Fe), Smithsonite, Sphalerite(Cu), Tennantite(Zn,Fe), TitaniteMix(Pb,Cu), TrampMetal, Tyrolite(Pb), Watanabeite(Zn), Wulfenite

Lead MOI

Apatite(Cu,Pb,Zn), Chalcopyrite(Pb), FeOxideSulphate(Cu,Pb,Zn,As), Fornacite•Conichalcite, Galena(Se), Galenobismutite, Grunerite(Pb,Cu,Zn), Molybdofornacite(Zn)= Molybdofornacite(Zn,Cu), MoSulphatePowelliteClay, MoCaSilicateOxide, PbMoOxide, PbCaOxideMoZnW, Powellite, TitaniteMix(Pb,Cu), Tyrolite(Pb), Wulfenite

Molybdenum MOI

FeSulphateLimonite(CuAsMoZn), MoSilicateOxide, MoCaSilicateOxide, MoCaSulphateMnCuFeZn, Molybdenite, Molybdofornacite(Zn,Cu), MoSulphatePowelliteClay, PbMoOxide, PbOxide(Zn), Powellite, Wulfenite

Zinc MOI

AgSulphosalt, Apatite(Cu,Pb,Zn), Chalcopyrite(Zn), Enargite(Zn), FeOxideSulphate(Cu,Pb,Zn,As),, FeSulphateLimonite(CuAsMoZn), Goslarite, Grunerite(Pb,Cu,Zn), Siegenite(Cu,Zn), MicaAltered(Cu,Zn), MoCaSulphateMnCuFeZn, Molybdfornacite(Zn,Cu), Otavite(Zn,Cu), ParamelaconiteZn, PbCaOxideMoZnW, Powellite, SideriteMnAsZnCrCu, Smithsonite, Sphalerite, Sphalerite(Cu), Tennantite(Zn,Fe), TrampMetal, Tyrolite(Pb), Watanabeite(Zn), Willemite, Wulfenite, Wulfingite

It was noted that Cu, As and Zn were present in many of the mineral phases. Antimony presence in phases was challenging to detect for several possible reasons: (1) small phase difficult to detect; (2) the primary source of Sb was minimal; and, (3) the element was free to be flushed out with the drainage water)

4) Mineral of Interest Elemental Composition

Elements detected within MOI have been normalized to 100 percent.
Displayed are: MOI name – Element1, nn; Element2, nn, etc ; where nn = normalized percent for Element.

MOI Name	Possible Stoichiometric Formula	Elemental Composition (normalized weight-%)
Pyrite1	FeS_2	S, 53.45; Fe, 46.55
Pyrite2	$FeS_{2.1}$	S, 36.5; Fe, 63.5
PyriteCu	$Fe(Cu)S_2$	S, 53.4; Fe, 37.5; Cu, 9.1
Arsenopyrite	FeAsS	S, 19.69; Fe, 34.3; As, 46.01
RealgarOrpiment	As_5S_6	S, 34.5; As, 65.5
Stibnite	Sb_2S_3	S, 28.32; Sb, 71.68
AgSulphosalt	$Ag_2(ZnSe_{0.2})S$	S, 10.3; Zn, 17.5; Se, 5.5; Ag, 66.7
Chalcocite	Cu_2S	S, 20.15; Cu, 79.85
Bornite	Cu_5FeS_4	S, 25.56; Fe, 11.13; Cu, 63.31
Chalcopyrite	$CuFeS_2$	S, 34.94; Fe, 30.43; Cu, 34.63
ChalcopyritePb	$Cu_{0.8}(Pb_{0.1})FeS_{2.2}$	S, 34.94; Fe, 30.43; Cu, 25.13; Pb, 9.5
ChalcopyriteZn	$Cu(Zn_{0.02})FeS_{2.2}$	S, 34.94; Fe, 30.43; Cu, 33.73; Zn, 0.9
Enargite	Cu_3AsS_4	S, 32.57; Cu, 48.41; As, 19.03
EnargiteZn	$Cu_{2.8}As_{1.2}(Zn_{0.4}Fe_{0.1}Cd_{0.02})S_{3.2}$	S, 26.7; Fe, 1.85; Cu, 42.2; Zn, 8.05; As, 20.6; Cd, 0.6
TennantiteZnFe	$Cu_{11.2}As_{4.8}(Zn_{1.4}Fe_{1.4})S_{12.8}$	S, 26; Fe, 5; Cu, 42.6; Zn, 6; As, 20.4
WatanabeiteZn	$Cu_{4.2}(As_{1.2}Sb_{0.6})(Zn_{0.4})S_{4.8}$	S, 27.1; Cu, 42.9; Zn, 3.8; As, 13.6; Sb, 12.6
Sphalerite	ZnS	S, 32.91; Zn, 67.09
SphaleriteCu	$Zn_{0.98}(Cu_{0.05}Fe_{0.04})S_{0.96}$	S, 30.8; Fe, 2.1; Cu, 3.1; Zn, 64
GalenaSe	$Pb_{1.3}(Fe_{0.3}Se_{0.2})S$	S, 9.5; Fe, 6.2; Se, 3.7; Pb, 80.6
Galenobismutite	$PbBi_2S_4$	S, 17; Pb, 27.5; Bi, 55.5
Bismuthinite	Bi_2S_3	S, 18.7; Bi, 81.3

MOI Name	Possible Stoichiometric Formula	Elemental Composition (normalized weight-%)
Molybdenite	MoS_2	S, 40.06; S, Mo, 59.94
SiegeniteCuFe	$(Ni_{0.9}Co_{1.9})(Cu_{0.2}Fe_{0.09})S_4$	S, 40.5; Fe, 1.8; Co, 34.9; Ni, 18.2; Cu, 4.6;
SiegeniteCuZn	$Co_3(Ni_{1.8}Cu_{0.4}Zn_{0.04})S_{5.2}$	S, 42.2; Co, 31.1; Ni, 21.1; Cu, 4.8; Zn, 0.8
FeOxyHydroxides	$Fe_{1.2}O_{1.9}$	O, 30.06; Fe, 69.94
FeOxideSulphateCuPbZnAs	$Fe_{0.9}O_{1.4}$•0.1$FeS0_4(Al_{0.04}Si_{0.03}Mg_{0.04}Cu_{0.03}Pb_{0.02})(Zn_{0.003}As_{0.005}Ca_{0.002})$	O, 31.2; Mg, 1; Al, 1; Si, 0.9; S, 3.9; Ca, 0.1; Fe, 54.8; Cu, 2.2; Zn, 0.2; As, 0.4; Pb, 4.1
FeTiOxide	$FeTi_{0.6}(Al_{0.005}Si_{0.005}Ca_{0.002})O_{2.4}$	O, 31; Al, 0.1; Si, 0.1; Ca, 0.1; Ti, 25.7; Fe, 43
Srebrodolskite	$Ca_{0.8}Fe_2(Ti_{0.6}Al_{0.2}Si_{0.3}Mg_{0.2})O_5$	O, 29.4; Mg, 2; Al, 2.4; Si, 2.7; Ca, 11.5; Ti, 10.9; Fe, 41.1
Cuprite	Cu_2O	O, 11.18; Cu, 88.82
ParamelaconiteZn	$Cu_2^{+1}Cu_2^{+2}$ $(Zn_{0.1})O_3$	O, 48.1; Cu, 42.3; Zn, 9.6;
Wulfingite	Zn(OH)2	O, 32.2; Zn, 65.8
PbMoOxide	$CaMoO_4$•2PbO($K_{0.1}Al_{0.2}Mg_{0.2}Si_{0.8}Fe_{0.06}Cu_{0.05}$)	O, 41.6; Mg, 0.4; Al, 0.7; Si, 2.2; K, 0.4; Ca, 6.35; Fe, 0.35; Cu, 0.3; Mo, 13.7; Pb, 34
PbCaOxide(MoZnW)Srebrodolskite	$Pb_{5.3}Ca_{2.7}Mo_{1.5}Fe_{1.3}Zn_{0.7}O_{11\ 3}$PbO•$Ca(Zn_{0.2}W_{0.05})MoO_4$•0.5$Ca_2Fe_2O_5$	O, 52.14; Ca, 3.9; Fe, 3.2; Zn, 1.4; Mo, 3.5; W, 0.3; Pb, 35.56
Cassiterite	SnO_2	O, 21.24; Sn, 78.77
Portlandite	$CaSi_{0.02}(OH)_{2.2}$	O, 45.6; Si, 0.5; Ca, 53.9
Spinel	$MgAl_2O_4$	O, 45; Mg, 17.1; Al, 37.90
Calcite	$CaCO_3$	C, 12; O, 48, Ca, 40
Dolomite	$CaMg(C_{0.3}O_{3.2})_2$	C, 13; O, 52.1; Mg, 13.2; Ca, 21.7
Ankerite	$CaFe(C_{0.3}O_{2.8})_2$	C, 11.1; O, 44.45; Ca, 18.56; Fe, 25.86
SideriteMnAsZnCrCu	$Fe(Mg_{0.1}Mn_{0.07}As_{0.06}Zn_{0.03}Cr_{0.01}Cu_{0.008})C_{1.3}O_{3.5}$	C, 104; O, 40.6; Mg, 3.4; Cr, 0.6; Mn, 2.7; Fe, 37.4;
Smithsonite_trans	5(ZnCd)(CO_3)•$CuSO_4$	C, 13.2; O, 33; Mg, 0.5; Al; 0.6; Si, 0.3; S..K, 0.5; Ca, 0.2; Cu, 5.6; Zn, 13.9; Cd, 30.4

MOI Name	Possible Stoichiometric Formula	Elemental Composition (normalized weight-%)
Rhodochrosite	$MnCO_{2.9}$	C, 10.45; O, 41.8; Mn, 47.8
GruneriteCuPbZn	$Fe_7Si_{8.2}O_{18}(Cu_{1.4}PbAlZn_{0.5}Ca_{0.5})$	O, 23.6; Mg, 6.6, Al, 1.1; Si, 21.2; Ca, 0.9; Fe, 33.4; Cu, 3.5; Zn, 1.2; Pb. 8.5
Malachite	$Cu_2C_{0.9}O_3(OH)_{1.8}$	C, 5.4; O, 36.3; Cu, 57.5
OtaviteZnCu	$(CdZn)_{1.7}C_{1.3}O_3•0.3CuSO_4•Al_{1.3}Si_{0.03}(OH)_2$	C, 5.2; O, 35; Al, 0.8; Si, 0.4; S, 2.1; Cu, 6.3; Zn, 15.6; Cd, 34.6
Fluorite	CaF_2	F, 48.7; Ca, 51.3
Alunite	$KAl_3(SO_4)_2(OH)_6$	O, 54.1; Al, 19.5; S, 15.5; K, 9.4
Gypsum	$CaSO_4•2H_2O$	O, 55.8; S, 18.6; Ca, 23.3
Barite	$BaSO_4$	O, 27.4; S, 13.7; Ba, 58.8
Celestine	$SrSO_4$	O, 34.8; S, 17.5; Sr, 47.7
FeSulphate	$FeSO_4$	O, 23.1; S, 4.2; Fe, 72.7
FeSulphateLimonite(CuAsMoZn)	$0.5FeSO_4•0.5Fe(OH)_3(Cu_{0.2}As_{0.2}Mo_{0.03}Al_{0.02}Zn_{0.01})$	O, 33.4; Al, 0.4; S, 10.3; Fe, 36.3; Cu, 8.1; Zn, 0.4; As, 8.5; Mo, 1.8
JarositeCu	$(K_{0.5}Cu_{0.2})Fe_3(SO_4)_2(OH)_6$	O, 44.7; S, 12.8; K, 5.3; Fe, 33.4; Cu, 2.5
MoCaSulphateMnCuFeZn	$CaMo(SO_4)_2•MoS(OH)[Mn_{0.1}Al_{0.05}Si_{0.05}Fe_{0.01}Cu_{0.01}K_{0.01}Zn_{0.005}]$	O, 29.1; Al, 0.3; Si, 0.3; S, 18.7; K, 0.1; Ca, 8; Mn, 0.9; Fe, 0.1; Cu, 0.2; Zn, 0.1; Mo, 42.1
MolybdofornaciteZnCu	$Pb_2Cu[(As_{0.9})O_4]_{0.6}[(Mo)O_4](OH)[Zn_{0.2}]•CuO$	O, 23.7; Cu, 10.3; Zn, 1.1; As, 7; Mo, 5.6; Pb, 52.3
Powellite_trans	$4.8CaMoO_4•CaSO_4(H_2O)•Ca(OH)_2•0.3(SiO_2)•0.2(Mn,Pb)O_2$	O, 35.5; Al, 0.4; Si, 0.7; S, 2.5; Ca, 22.4; Mn, 1.1; Fe, 0.1; Cu, o.2; Zn, 0.3; Mo, 35.3; Pb, 1.5
Scheelite	$CaWO_4$	O, 22.2; Ca, 13.9; W, 63.8
Wulfenite_trans	$PbMoO_4•MoSO_4(Zn_{0.2}Cu_{0.1})•0.6Ca(OH)_2$	O, 41.1; S, 3.8; Ca, 2.6; Cu, 0.9; Zn, 1.1; Mo, 18.1; Pb, 32.4
Apatite	$Ca_5(PO_4)_3F$	O, 38.1; F, 3.8; P, 18.4; Ca, 39.7;

MOI Name	Possible Stoichiometric Formula	Elemental Composition (normalized weight-%)
ApatiteCuPbZn	$Ca_{5.5}(PO_4)_3F(Cu_{0.1}Pb_{0.05}Zn_{0.05})$	O,38.1; F, 3.7; P, 18.4; Ca, 35.4; Cu, 1.4; Zn, 0.9; Pb, 2.1
Goyazite	$SrAl_3(PO_4)_2(OH)_5•(H_2O)$	O, 48.5; Al, 17.5; P, 13.4; Sr, 19
MonaziteCe	$(Ce_{0.2}La_{0.1}Nd_{0.08}Th_{0.02})PO_4$	O, 26.6; P, 12.9; La, 14.5; Ce, 29.2; Nd, 12; Th, 4.8
ChloroOrganic	$C(S_{0.09}Fe_{0.09}Ti_{0.05}Na_{0.03}Si_{0.03})Cl_{2.4}$	C, 10.6; Na, 0.7; Si, 0.9; S, 2.6; Cl, 78.4; Ti, 2.4; Fe, 4.4
Fornacite•Conichalcite	$PbCu(AsO_4)(OH)•CaCu(AsO_4)(OH)$	O, 28.9; Ca, 4.3; Cu, 16; As, 18.4; Pb, 32.4
TyrolitePb	$CaCu(AsO_4)_{1.1}(PbO)_{0.4}(CO_3)_{1.5}(OH)_4•6H_2O$	C, 4.1; O, 35.2; Ca, 8; Cu, 16.4; Zn, 1.6; As, 17.3; Pb, 17.4
Quartz	$SiO_{1.8}$	O, 53.3; Si, 46.7
Plagioclase	$(Na_{0.6}Ca_{0.6})(Al_2Si_2)O_{8.6}$	O, 47.5; Na, 4.3, Al, 20; Si, 20.8, Ca, 7.4
K_Feldspar	$KAlSi_{3.6}O_{9.6}$	O, 46; Al, 9.7; Si, 30.3; K, 14
AmphibolAnthophylit	$Mg_7(Si_8O_{22})(OH)_2•Fe_{1.7}AlSiO_{7.7}$	O, 46.2; Mg, 4.3; Al, 8.2; Si, 13.5; Fe, 27.7
Grossular	$Ca_3Al_2Si_3O_{12}$	O, 42.6; Al, 12; Si, 18.7; Ca, 26.7
CarpholiteMn	$MnAl_2(Si_{2.4}O_6)(OH)_{3.8}Mn_{1.4}$	O, 38.8; Al, 10.9; Si, 17; Mn, 33.3
Pyroxene	$Ca_{1.1}Mg_{1.1}Si_2O_{6.1}$	O, 44.3; Mg, 11.2; Si, 25.9; Ca, 18.5
Fayalite	Fe_2SiO_4	O, 31.4; Si, 13.8; Fe, 54.8
Biotite	$K(MgFe)(AlSi_{3.5}O_{10})(OH)_2$	O, 45.2; Mg, 5.7; Al, 6.4; Si, 19.8; K, 9.2; Fe, 13.2
Mica	$(KNa_{0.01})(Fe_{0.3}Al_{0.3}Mg_{0.2})(Si_{0.9})O_{8.2}(OH)_{1.2}$	O, 44.4; Na, 0.3; Mg, 4.7; Al, 9.2; Si, 24.7; K, 11; Ti, 1; Fe, 4.4
Muscovite	$KAl_2(Al_{1.5}Si_{3.5}O_{10})(OH)_2$	O, 48.2; Al, 20.3; Si, 21.1; K, 9.8
Sericite	$Na_{0.1}KAlSi_2O_{4.8}$	O, 38.8; Na, 1.2; Al, 12.7; Si, 28.3; K, 19
Phlogopite	$KMg_3(Si_3Al)O_{10}(OH)_2$	O, 44.4; Mg, 17.4; Al, 6.4; Si, 20.1; K, 9.3
MicaAlteredCuZn	$(K_{0.1})(FeAl_{0.7}Mg_{1.6})(Cu_{0.3}Zn_{0.07})(Si_{2.3})O_{7.3}(OH)_{0.3}$	O, 37; Mg, 12.1; Al, 5.8; Si, 19.1; K, 1.3; Ca, 1.2; Fe, 16.5; Cu, 5.6; Zn, 1.3
Chlorite	$(Mg_3Fe_{1.8})Al(Al_{0.8}Si_3)O_{10}(OH)_{7.4}$	O, 46.5; Mg, 11.8; Al, 8.7; Si, 13.6; Fe, 18

MOI Name	Possible Stoichiometric Formula	Elemental Composition (normalized weight-%)
Epidote	$Ca_2(Al_2Fe)Si_3O_{12}(OH)$	O, 43; Al, 11.2; Si, 17.4; Ca, 16.6; Fe, 11.6
Kaolinite	$Al_2Si_2O_5(OH)_4$	O, 55.8; Al, 20.9; Si, 21.8
Apophyllite	$KCa_4(Si_4O_{10})_2F•8H_2O$	O, 50.2; F, 2.1; Si, 25.2; K, 4.4; Ca, 18
MoSulphatePowelliteClay	$4MoSO_4(Mg_{0.05})$ •$CaMoO_4$•$AlSi_{2.5}O_{8.5}$	O, 37.2; Mg, 0.1; Al, 4.2; Si, 4.7; S, 9.1; Ca, 3.8; Mo, 40.9
FeOxideCu	$Fe_2(Cu_{0.4}Si_{0.2}Ca_{0.09})O_4$	O, 29.6; Si, 4.2; Ca, 1.6; Fe, 51; Cu, 13.5
MoSulphateAlteredGrossular	$MoSO_4$•$CaAl_{0.7}(Mn_{0.07}K_{0.03}Pb_{0.02}Cu_{0.01}Na_{0.01})Si_{0.7}O_{2.9}$	O, 33; Na, 0.1; Al, 5; Si, 6.3; S, 9.4; K, 0.5; Ca, 11.2; Mn, 1; Cu, 0.2; Mo, 32; Pb, 1.3
TalcFe	$Mg_3(Fe_{1.8})Si_4O_{10}(OH)_2$•$Si_2O_3$	O, 40.6; Mg, 12.2; Si, 27.6; Fe, 19.6
Andalusite	Al_2SiO_5	O, 49.4; Al, 33.3; Si, 17.3
TitaniteMixCuPb	$Ca_{1.2}Ti(Fe_{0.2}Cu_{0.1}Pb_{0.07})SiO_{5.5}$	O, 35.7; Si, 11.3; Ca, 19.6; Ti, 20.1; Fe, 5.1; Cu, 2.3; Pb, 6
Willemite	Zn_2SiO_4	O, 28.7; Si, 12.6; Zn, 58.7
Zircon	$ZrSiO_{4.4}$	O, 34.9; Si, 15.3; Zr, 49.8
Bismutostibiconite	$Bi(Sb_{1.5}Fe_{0.4})O_{5.5}$	O, 18.1; Fe, 4.5; Sb, 33.5; Bi, 43.9
Goslarite	$ZnSO_4•7H_2O$	O, 61.2; S, 11.2; Zn, 22.7
Melilite	$(CaNa)_2(AlMgFe)(SiAl)_2O_7$	O, 41.7; Na, 4.3; Mg, 2.7; Al, 11.1; Si, 15.7; Ca, 2 2.4; Fe, 2.1
Wollastonite	$CaSiO_3$	O, 41.3; Si, 24.2; Ca, 34.5;

APPENDIX 2 Comparison: Mineral Liberation Analyzer vs. QEMSCAN

The QEMSCAN, collects X-ray for the spectra limited to 1000 counts / impulses. To improve spectral resolution would require a complete readjustment of all mineral spectra total counts in the global reference mineral library. In the MLA, the most important aspect is to collect all mineral phase X-ray spectra at the same accelerating voltage. While QEMSCAN provides global database X-ray files, they must be refined for the specific rock being analyzed. MLA enables the user to develop the X-ray classification file using the actual fragment particles to ensure a good match. The global level refers to a generic mineral phase database with spectra collated from many different instruments and rock sources. The local level refers to a mineral phase database developed from the actual rock sample (i.e. local) MOIs.

The MLA and QEMSCAN were not designed for discriminating sub-microscopic features (e.g. solid solution Au / Ag carriers), leaving such tasks to techniques such as EMPA and ToF-SI/MS (see Section 2.8).

QEMSCAN technology was developed for high throughput X-ray analysis and does this well; however, BSE imaging was considered less important. QEMSCAN uses a large 25-mm working distance (WD) due to crowded space in the vacuum chamber from four detectors. The large WD is great for collecting X-ray spectra though sacrifices image quality. A limitation of the QEMSCAN system is that there can be little uncertainty in the ore (i.e. needs to be relatively simple) or it will take a long time to discriminate the particle phases. For this reason QEMSCAN uses four Silicon Drift Detectors (SDD). To improve imaging, the WD could be decreased; however, the instrument would lose X-ray data critical to mineral identification because the take-off angle (from sample surface to detector) would be incorrect.

MLA technology was primarily developed for high quality BSE imaging. The smaller 10-mm WD enables closer examination of the sample, to improve BSE imaging and deliver superior BSE gray level discrimination (relative to QEMSCAN).

MLA technology provides the user the option of focusing on the BSE image or X-ray spectra or both. MLA imaging relies on BSE gray level (with the exception of MLA XMAP routine which is triggered by X-ray spectrum). The “lock out” specification that MLA has “head and shoulders” above the QEMSCAN is superior BSE imaging. (Aside: a “lock out” specification refers to the belief that one system can do something another system cannot do. This is a strong statement when made in the industry). The improved BSE imaging capability provides higher success searches for *bright* (i.e. high AAN) particle phases than QEMSCAN (e.g. search for Platinum Group Metals , Au, U – not a problem for MLA). MLA uses two SDDs to acquire the X-ray spectra more quickly, closing the gap in analysis time with QEMSCAN.

The MLA is a more “all round” instrument (i.e. versatile). For example, creation of MLA X-ray files is very flexible. The QEMSCAN X-ray collection routine identifies minerals through the number of X-ray counts for each element in a mineral. However, as already mentioned QEMSCAN collects only 1000 count spectra and because of this it is not easy to identify small grains of, for example Pt and Pd, without concerted off-line manual work to separate out overlapped element peaks. For this reason complex (and this does not mean “crazy” ore!) mineralogy may not be accurately analyzed by QEMSCAN. QEMSCAN uses a global mineral list to compare known mineral phase X-ray spectra to the unknown spectrum. For example, QEMSCAN determines quartz and then is more challenged to tease out other silicates (e.g. amphibole, pyroxene) relative to MLA. On the MLA it is not difficult to distinguish MOIs. *Id est*: the User can decide how to apply the tool for mineral analysis. The QEMSCAN does not give authority to the user to do this (in 2011).

Bottom line: QEMSCAN, relative to MLA, is less capable to discriminate BSE gray levels (such as pyrrhotite and hematite) due to the larger working distance. MLA uses smaller WD and BSE imaging to distinguish gray levels.

Snapshot:

QEMSCAN

- Centered on X-rays (i.e. high X-ray throughput analysis, not higher quality BSE imaging).
- Large WD of 25 mm (i.e. larger take-off angle) is positioned for high X-ray count though poor for BSE imaging.
- Uses a Global mineral list supplied by QEMSCAN to assign the mineral phase name to the spectrum. Recently, QEMSCAN provided the ability to adjust X-ray spectra.
- Not easy to compare MOI spectra without manual work to distinguish the elements (i.e. complex mineralogy cannot be analyzed easily).
- Can decrease WD to improve imaging, though will lose X-ray impulse collection.

MLA

- Centered on BSE imaging (i.e. phase distinction by AAN, not high X-ray counts).
- Low WD (10 mm) enables superior BSE gray level distinction and imaging.
- Uses a Local mineral list (i.e. user-defined spectra and mineral names = control of the tool).
- Gives the user control of how the analysis will be performed. Flexible X-ray spectra file set-up.
- Level of data confidence is assigned by user determined criteria.
- Both imaging and X-ray collection are optimized to approximately the same WD.

APPENDIX 3 Instrument

Appendix 3a: Mineral Liberation Analyzer comparison

Prior to the use of both MLAs owned by Teck AR&T (2012), consideration had to be given regarding data comparability if the same MLA data capture parameters were to be used. Applying the same parameters would increase productivity (i.e. analysis set up time, etc). To evaluate if combining data would be 'seamless', the energy measured in 1000's counts per second (kcps) was compared. Separate conversations with two SEM service engineers (FEI Company) confirmed that this comparison was a simple, yet effective approach. The results can be seen in Table A3.1 and A3.2.

Table A3.1. X-ray signal impulse comparison: MLA#1.

MLA#1 (D7706)						
SpotSize	kcps (at 25kV accelerating voltage)			kcps (at 15kV accelerating voltage)		
	Quartz	**Copper**	**Gold**	**Quartz**	**Copper**	**Gold**
3	3	4.6	6	1.4	2	2.4
3.5	5.4	9.9	11.5	2.8	3.8	4.9
4	10.5	17	22	5.5	7.5	9.6
4.5	20	32	41.6	10.6	14.4	18.6
5	37	58	78	19.9	27.1	35.3
5.5	64	102	145	36.3	49.1	66
6	119	183	263	65	86	121
6.5	217	315	461	109	144	216
7	390	515	785	188	245	375

Table A3.2. X-ray signal impulse comparison: MLA#2.

MLA#2 (D8516)						
SpotSize	kcps (at 25kV accelerating voltage)			kcps (at 15kV accelerating voltage)		
	Quartz	Copper	Gold	Quartz	Copper	Gold
3	2.5	4.2	5.3	1.4	1.9	2.3
3.5	5.1	8.2	10.4	2.7	3.8	4.5
4	9.6	15.7	19.8	5.2	7.3	8.9
4.5	18.1	29.3	37.5	10.2	13.8	16.8
5	32.3	53	70	18.6	25.4	31.4
5.5	61	93	128	34	46	57
6	104	164	231	62	82	105
6.5	192	286	408	106	136	186
7	337	469	686	167	220	323

In Table A3.3 is the ratio of MLA#1 signals to MLA#2 signals relative to spot size and accelerating voltage. The two accelerating voltages used here were also used in the study (see section 4.4.7).

The photon impulse energy observed, as SEM spot size was changed, was based upon three materials: (1) gold – highest BSE gray level, density (i.e. AAN) and count rate; (2) quartz – lowest BSE gray level, density (i.e. AAN) and count rate; (3) copper – midway density and count rate (relative to gold and quartz). The observations show the MLAs have comparable photon impulse energy detection. MLA#1 has slightly more sensitive detectors and could match MLA#2 by reducing MLA#1 spot size ~10% (relative to MLA#2). The strong similarity between MLA#1 and 2 helped decide that data from both MLAs could be blended together. Using the same MLA analysis parameters greatly improved throughput time for the several hundred sample mounts that were to be analyzed.

Table A3.3. Comparison of MLA data compatibility.

Ratio of Counts (MLA#1 / MLA#2)						
Spot Size	**25kV accelerating voltage**			**15kV accelerating voltage**		
	Quartz	**Copper**	**Gold**	**Quartz**	**Copper**	**Gold**
3	1.20	1.10	1.13	1.00	1.05	1.04
3.5	1.06	1.21	1.11	1.04	1.00	1.09
4	1.09	1.08	1.11	1.06	1.03	1.08
4.5	1.10	1.09	1.11	1.04	1.04	1.11
5	1.15	1.09	1.11	1.07	1.07	1.12
5.5	1.05	1.10	1.13	1.07	1.07	1.16
6	1.14	1.12	1.14	1.05	1.05	1.15
6.5	1.13	1.10	1.13	1.03	1.06	1.16
7	1.16	1.10	1.14	1.13	1.11	1.16
Average	1.12	1.11	1.12	1.05	1.05	1.12
Std Dev	0.05	0.04	0.01	0.03	0.03	0.04

Appendix 3b: Comparison of traditional analytical instruments

The primary techniques used to visually determine the nature of geological samples involve the human eye, the optical microscope and the SEM. The naked unaided eye has physical resolution ~0.1 mm, the light microscope (limited by light source wavelength) has physical resolution ~0.2 µm and the SEM (limited by electron source wavelength) has physical resolution ~1 nm. Visual MOI determinations should be augmented by other methods, such as the preferred X-ray instrumentation used in the geological field of XRF, XRD and SEM (see Section 2.8).

Below is a brief list of strengths and limitations of these methods. In Table A3.4 is a comparison of the basics of each method.

XRF strength:

- Suited for bulk (major) element analysis.
- Multi-element analysis generally complete in ~20 minutes.

XRF limitation:

- Poor EDS detection for elements with atomic number Z < 11 (i.e. Na).
- Require matrix matched calibration standards.
- No mineralogy, including texture, association, availability and grain size.

XRD strength:

- can quickly analyze mineralogy (e.g. 5 minutes for a particular MOI peak; 20 minutes for a particular MOI).
- Sample preparation is quick ~15 minutes(i.e. micronize / mill / grind and press into a disk).
- Minimal sample required (e.g. 0.1 g).
- Millions of grains represented and homogenized during milling.
- More accurate for large crystalline structures than small ones (e.g. sub-2 µm).
- Data interpretation relatively straight-forward.

XRD limitation:

- Homogeneous and single phase material easier to evaluate than mixed phase material.
- Can only include 10-15 phases in quantification of mineral phases using Rietveld refinement.
- Must have access to a standard inorganic compounds crystallographic reference library (e.g. d-spacing, Miller indices *hkl*) such as globally available ICDD (International Center for Diffraction Data).
- Mineralogical determination is not accurate unless referenced with another method. The method will be found listed with the MOI identified with ICDD.
- No textural information reported (e.g. MOI associations, inclusions, liberation).

- Sensitive to sample preparation (e.g. pressing can lead to preferred orientation; over-milling can lead to low intensity or broad peaks).
- Cannot analyze amorphous phases.
- Operator knowledge of crystallography and mineralogy required.
- No direct elemental information.

SEM strength:

- Solid material characterization, from large to small grain size (e.g. 0.5 µm).
- Easy to use.
- Detailed 3-D and topographical imaging (exceptional relative resolution).
- Significantly more mineralogical information (e.g. texture, association, availability, grain size).
- Can determine amorphous and crystalline mineralogy.
- Detailed surface (generally 1-5 µm sub-surface) elemental analysis.
- Minimal sample preparation (includes polished resin mount).
- Electron beam microscopy is more forgiving than optical microscopy with respect to polishing artefacts.
- Rapid digitized image elemental mapping; often completed in less than five minutes.

SEM limitation:

- Sample must be: dry solid (i.e. no out-gassing); fit inside the vacuum chamber; have a conductive coating for low vacuum; and, be stable at less than 10^{-5} torr vacuum pressure.
- Not always accurate EDS detection for elements with atomic number $Z < 11$ (i.e. Na).

Table A3.4. X-ray method comparison.

Instrument	XRF	XRD	MLA/QEMSCAN
Spectrometer	d-spacing of Analyzing Crystal	X-ray wavelength of Source	characteristic energy of MOI X-rays
Measures	peak position θ and intensity of secondary X-rays from whole sample	peak position θ and intensity of diffracted X-rays from each mineral	peak energy and intensity of X-rays from each particle's mineral(s); BSE images
Comparison method	peak intensity of like-matrix Standards	peak position of Standard (ICDD[1]) library and peak height of Rietveld[2] refinement	peak energy and intensity to specific mineral phase; Standardless
Results	element-% in sample	MOI-% in sample	element-% in MOI; MOI-% in sample; % associations for element and/or MOI; % liberation for element and/or MOI; % grain size for element and/or MOI; particle images
Samples	powder pellet fusion, polished metal, liquid; "destructive"	powder pellet (micronize gives 1-5 µm particles, but optimal is 0.5-1.0 µm particles); MOI not to be amorphous; "non-destructive"	polished resin mount of particles; "non-destructive" (i.e. electrons do not change the sample)
Detection Limit	0.001-0.015 wt%	1-5 wt% element and MOI (mixed phase systems); example, down to 3 wt% kaolinite/chlorite, 1 wt% siderite/hematite/goethite, 0.5 wt% calcite	element and MOI: EDS[3] 0.1-0.5wt%; WDS[4] 0.01 -0.05 wt%

[1]ICDD - International Centre for Diffraction Data

[2]Rietveld Refinement - method of analysing powder diffraction data in which the crystal structure is refined by fitting the entire profile of the diffraction pattern to a calculated profile using a least-squares approach.

[3]EDS - Energy Dispersive Spectrometer; electron energy, E (eV) = 1240.7/λ (nm)

[4]WDS - Wavelength Dispersive Spectrometer

APPENDIX 4 Mineral Liberation Analyzer sample preparation and analysis details

Appendix 4a: Sample preparation and analysis overview

Micro-riffling removes potential subjectivity from the sampling process. A sample proportion was selected by micro-riffling the whole sample mass (often screened into size fractions) for subsequent epoxy resin mounting. To improve particle statistics, if sufficient sample was available, two sample portions were put aside for duplicate mounts, especially for larger sized particles (e.g. greater than 105 µm). A general rule of thumb is to mount approximately 10% of the samples in duplicate to provide assurance of sample particle randomness.

Sample preparation generally followed the standard MLA protocol [Gu, 2003; Fandrich *et al.,* 2007]. In Figure A4.1 is shown the progression of sample particles from collection in the field to readiness for SEM or MLA analysis.

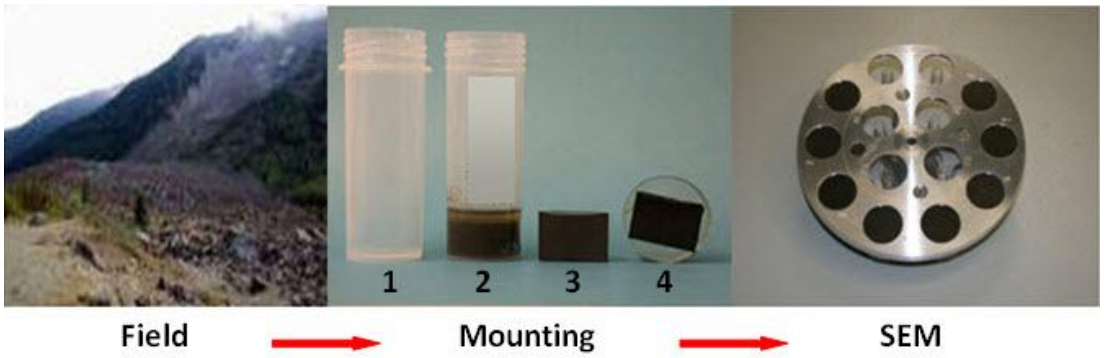

Figure A4.1. Sample is collected in the field and brought to the lapidary laboratory. After representative sample aliquot has been collected, it is mixed with epoxy resin in a cylindrical vial [1], allowed to cure in the vial [2], vial is bisected to expose cross-section of particles [3] and then re-mounted in epoxy resin with cut face being polished [4]. The polished sample, once carbon-coated, is placed in the SEM sample holder in readiness for MLA analysis.

The 30 mm diameter cylindrical mount contains sample particles mixed with epoxy resin and hardener. Graphite is mixed with the particles in order to decrease artificial agglomeration imaging by the MLA software – a result of particle density and electron beam excitation volume (i.e. particles in close proximity to each other). The initial resin cure occurs in a pressure vessel for at least three hours at ~30 psig. The pressure vessel operates under the same conditions as a pressure canner – though without heat / steam. The resin impregnated mount is then allowed to finish curing overnight, either in the pressure vessel or at ambient temperature and pressure. The grinding and polishing generally follows the MLA protocol [JKMRC, 2004]. A conductive coating of carbon is applied to prevent charging – a result of application of the SEM's electron beam to the sample surface. A secondary benefit of carbon coating the planed surface would be a "seal" which would impede further MOI oxidation. The final representative 2D cross section of the sample is presented for MLA analysis.

Considerations:

During sample mounting randomness of particle distribution is imperative. Application of pressure could change the randomness of particle orientation (e.g. phyllosilicates). To diminish preferred particle orientation (such as phlogopite phyllosilicate): (1) mix the particles with partially cured epoxy; (2) do not apply pressure; and, (3) use graphite addition.

The Single mount can be seen in Figure A4.1 in the SEM sample holder and also in Figure A4.2. The particles are mixed with resin and graphite in the sample mold, resin allowed to cure, and then the mold is backfilled with more resin. The Transverse mount can be seen in Figure A4.1 in the Mounting mold [4] and its preparation has been described above.

In this way the un-skewed particle density spectrum is analyzed along the transverse-cut face. There is a need for caution with a single mount because if the

polishing is not performed carefully, there is a higher probability that some or all of the higher density phase material will be polished away [more detail in section 4.4.5].

In the study of waste rock, the determination of secondary mineral phases would improve understanding of weathering processes. Specifically, water exposure and / or heat exposure might alter or dissolve mineral during polishing of the epoxy-particle sample mount. To decrease such possibilities all sample were polished with oil-based diamond abrasives using non-aqueous cooling lubricant to keep the temperature low (due to friction) at the sample mount face-abrasive contact zone.

Appendix 4b: Analysis detail

In Figure A4.2 is shown the procedure from particle-mounted sample to MLA classified particle. Note that the following discourse refers to the software used in this study – MLA version 2.9.

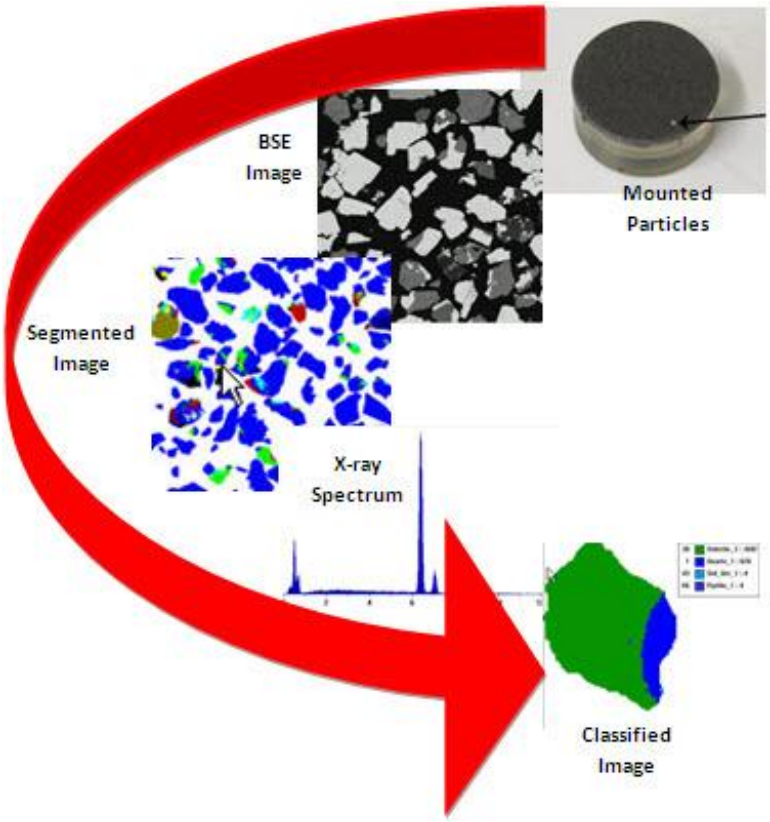

Figure A4.2. MLA analysis of Sample mount: the electron beam scans in a raster pattern over the polished sample face to generate a BSE image of the embedded particles in the resin. The MLA software extracts the resin background and digitizes the particles. Each differing BSE gray level within each particle is segmented and assigned a false-colour. Each false-coloured segment is assigned an X-ray spectrum. Each segment of the particle is then compared (i.e. X-ray spectrum) with the user-created MLA library of X-ray classification spectra and after rigorous chi-square testing is assigned a mineral phase name.

Agglomeration

The MLA system has automated background extraction and de-agglomeration functionality. On-line de-agglomeration expedites post-MLA processing of the image files. The deagglomeration functionality detects agglomerates and separates particles according to user-specified parameters. Despite precautions to prevent agglomeration, such as applying low density packing of particles in sample mount, some particles will be close together or touch each other. The MLA software, due to beam excitation volume affecting imaging, may be challenged to delineate particle boundaries (e.g. at a point or along a face). If not recognized by the MLA software and treated appropriately, agglomerated particles can lead to inaccurate liberation results (e.g. a number of smaller particles agglomerated together and appear to the particle recognition software as one large particle with multiple inclusions). While the majority of de-agglomeration is "automated" on-line, often there is some "manual" particle deagglomeration required during off-line image processing. As a general rule-of-thumb, smaller particle size fractions have a higher probability of requiring more off-line de-agglomeration (depending on particle packing density and mounting procedure).

Segmentation

Once the individual particles have been separated (extracted) from the background (i.e. epoxy), the liberation analysis defines the distinct mineral phases of each particle. This process, called phase segmentation [Jones, 1987], overlays a false-colour to each different mineral phase (e.g. Figures 4.3.1.2 and 4.3.1.3) according to the determined regions of homogeneous or average BSE gray level within the particle's BSE image corresponding to minerals of unique AAN [Gu, 2003].

For this reason it is very important that the BSE gray level scale not drift significantly during an MLA analysis. Variation in the BSE brightness caused by mineral impurities, sample mount defects and particle boundaries within the resin, result in blended BSE ranges. This blended BSE gray level overlap is often not fully resolved, resulting in slight overestimations of some mineral phases. Visual inspection of the image data

often shows the classification of unresolved mineral phases can be affected, though without significantly impacting the overall results due to the statistically large number of particles collected during the measurement. It is important to be aware that if the client is interested in trace MOIs, that overall results will be impacted. While the MLA imaging software provides tools to correct misclassified phases, this was not explored in this study. Multiple inspections (i.e. thousands) indicated overall correct phase classification. Most incorrect classifications belonged to tiny grains of non-sulphide mineral phases.

The MLA phase segmentation routine also recognizes and eliminates particle image features that are polishing artefacts, such as cracks, shading, tiny voids or the dark perimeter (halo) around many particles (i.e. edge effects).

Each segmented area (single centroid) of the particle is also associated with an X-ray spectrum corresponding to each AAN mineral phase (Figure 4.3.1.3). The "cleanest" spectrum is collected at the centre of each segmented phase to avoid contamination from bordering phases. This spectrum is linked (tagged) to its corresponding segment in the particle image with frame number and x-y coordinates, and stored with the X-ray particle image.

Classification

The MLA spectrum identification process involves an error-based modified chi-squared matching search of the user-defined mineral standard library to find the most probable fit for the measured spectra. Quality of match can be reviewed to evaluate the classification for specific minerals. Automated mineralogical systems require mineral composition input to the database. Reference books can be used as a basis for calculation, though do not account for natural mineral composition variation. Through the use of “real time” EDS, accurate elemental compositions of sample mineral phases can be collected from the sample – unlike the remote collection from a variety of sources used with XRD and QEMSCAN. Specific considerations of X-ray classification standard development would include:

(a) The chemistry and density information in the global mineral classification list contains average elemental composition for each mineral, from such sources as web-based Webmineral [Webmineral, 2010]. The local (sample) mineral classification list will contain different information because the EDS is used to provide compositional data from the sample. The local (sample) mineral phase library will contain more applicable MOI spectra and density from the sample rock fragments.

(b) Low X-ray photon counts for a MOI spectrum restrict the lower limit of detection of minor constituents within the mineral and limit the differentiation of minerals with closely matching spectra. Each phase has a set number of X-ray counts per spectrum. The typical QEMSCAN minimum 1000 X-ray counts per spectrum does facilitate rapid spatial analysis though limits the precision of trace elemental concentration measurements. The MLA uses a 'user'-defined threshold (e.g. 10000 counts) which would improve peak energy resolution. The user must consider whether the imposed minimum photon count threshold for the X-ray spectrum is sufficient to discriminate mineral phases. Based on the intensity of individual X-ray energies, as discussed by Andersen [2009], the typical 3% lower limit of detection for X-ray photon counts must be taken into account. This is important to optimization of the electron beam dwell time on each pixel and cost of analysis. For best analysis the X-ray standard library must match the sample analysis conditions, particularly for qualifying trace elements distributed within MOIs. To improve detection, a slightly increased EDS point acquisition time can be imposed by decreasing spot size (which also improves detection of fine mineral phases because beam excitation volume is decreased or alternatively increase the collection threshold for X-ray photon counts per spectrum (though would add time to the analysis).

(c) X-ray interferences are a function of the average spectral resolution of the EDS (reported to be 150 eV FWHM, Mn Kα; see section 4.3.3) combined with a limitation of the MLA version 2.9 software (see Appendix 3 and section 4.3.3) in that it could only differentiate mineral phases based upon mineral spectra stored in the database.

If no spectral match is made, the phase is assigned as Unknown or Invalid. An Invalid refers to spectra with photon counts that do not meet user-defined minimum count threshold criteria, even though the spectrum matched MOI spectrum in the database. For some elements, such as Mo, the operator must have a general awareness of EDS interferences and software limitations, in order to validate spectrum matches.

(d) The electron beam excitation volume (a function of the accelerating voltage, final column aperture, spot size and MOI density) can alter mineral content and association. The spatial resolution of the beam excitation volume was particularly significant for the characterization of low density clay (e.g. kaolinite) and fine-grained mineral phases (e.g. secondary mineral precipitation). Mineral grains of smaller size than the electron beam diameter will result in mixed spectra with wide compositional variability. As a consequence, multiple mixed spectra are required for MOI classification which is time-consuming and challenging. In this study, the match criteria for classification was fixed at 87% accuracy to ensure that MOI species were classified with confidence – which required extended computer processing unit (CPU) time and analysis cost.

(e) Phases may be present in very small content. For example, ettringite ($Ca_6Al_2(SO_4)_3(OH)_{12}•26H_2O$) might be in Antamina mine waste rock; however, due to (expected) thin film presence was not detected using analysis conditions in this study. A change in the MLA analysis parameter conditions could theoretically collect data for such MOIs. Due to time constraints this aspect was not explored.

(f) Examples of minerals with similar elemental composition that challenge MLA detection due to electron beam behaviour and EDS performance are:

i) Realgar and orpiment phases were merged in database and the mineral phase named RealgarOrpiment because a definitive spectrum could not be found in the samples (partly due to solid solution chemistry [realgar As_4S_4; orpiment As_2S_3] and partly due to the small size of the MOI);

ii) Spectral X-ray energy interferences (overlap) challenged resolution. For example, energy lines for Pb-Mα and Mo-Mα; and for molybdenite (MoS_2) and

elemental sulphur, variation depended upon polish quality. Observation using EDS showed the elemental peak was most often correctly assigned (i.e. 97% accurate);

Iii) Minerals may differ primarily by light element concentration - which are not directly detected (e.g. H, B) or have variable detection (e.g. C, O). Examples would be carbonates, which are assigned based upon display of a large EDS carbon peak in conjunction with other MOI element abundances, as well as study of MOI texture in the BSE gray level image.

iv) Minerals with very similar x-ray spectra, having compositional variation within themselves, such as clays, plagioclase series, precipitated oxide coatings. The list of minerals identified for an MLA analysis can be extensive. Several spectra may represent the same MOI due to slight elemental variation. These must be accounted for in the mineral classification standard library. In these instances, a grouping function enables collation of these individual mineral phase spectra under a single MOI name and composition.

v) Modal abundance results, especially for secondary mineral phase precipitates, may be under reported due to sample preparation artefacts which confused MLA image analysis algorithm, caused the artefact to be reported instead. Many trace MOI mineral phase compositions were reviewed by EDS and by visual inspection before assigning a name and composition to these phases.

vi) During MLA analysis, if particle cracks are not completely resolved spatially, the crack will not be included as part of the particle perimeter. The consequence is that any grain inclusion while truly exposed to the outer perimeter of the particle would be classified as being locked. This can be somewhat overcome in the latest MLA software release (version 3.1) through the application of Void inclusion with analysis. Note that cracks and pores were not quantified in this study.

APPENDIX 5 Elemental reconciliation

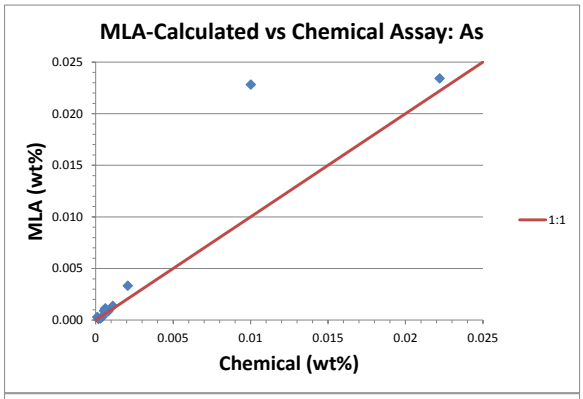

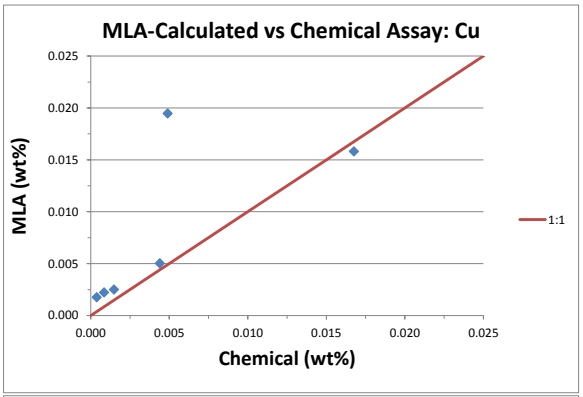

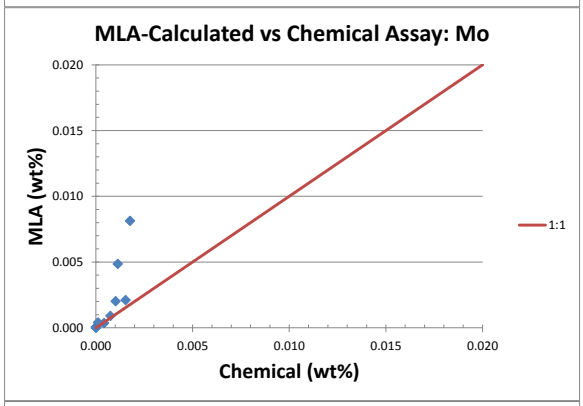

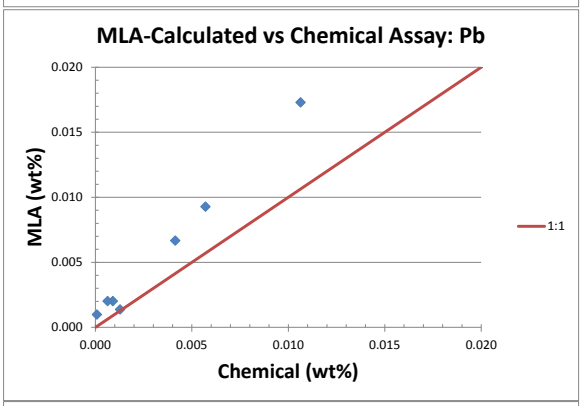

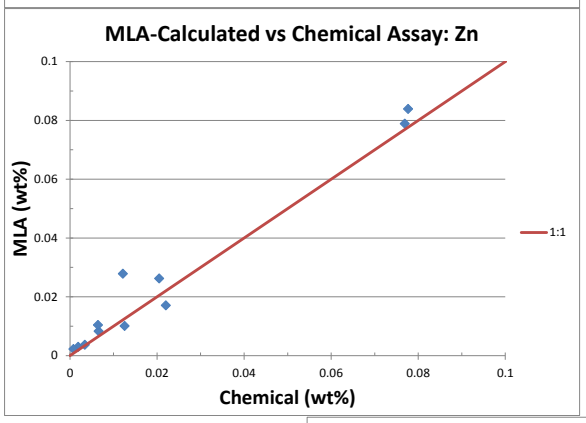

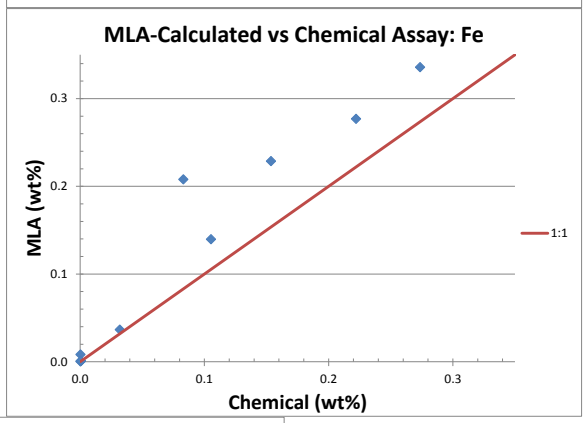

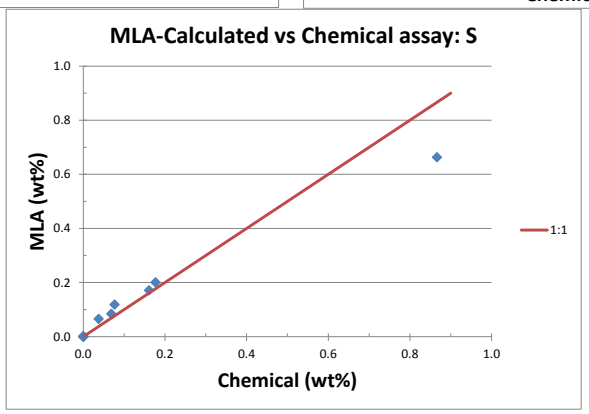

APPENDIX 6 Transverse vs. Single mount

Number of particles analyzed

Particle Size (µm)	Sample Name	Number of particles	
		Transverse Mount	Single Mount
75	FC-0	7302	10839
	FC-2	9841	12097
	FC-4	12305	11398
C1C2	FC-0	12112	11089
	FC-2	13019	11954
	FC-4	11905	11765
C3C4	FC-0	12369	8886
	FC-2	12007	11906
	FC-4	13728	11255
C5C6	FC-0	10811	2328
	FC-2	11220	5396
	FC-4	7731	4229

Grouping: Dana – modal mineralogy

Mineral Phase	Weight-%		Area (%)		Area (um^2)		Particle Count		Grain Count	
	Transverse	Single	Transverse	Single	Transverse	Single	Transverse	Single	Transverse	Single
	FieldCell-0 +75µm									
Tramp Metal	0.00	0.00	0.00	0.00	257	0	1	0	1	0
Sulphide	0.35	0.57	0.19	0.32	49358	142355	29	70	29	80
Oxide Hydroxide	0.29	0.35	0.17	0.21	44065	90927	25	48	27	50
Carbonate Halide	82.70	81.76	84.63	84.04	21470889	37060705	5941	8825	5975	8877
Sulphate Molybdate Chromate	0.12	0.07	0.08	0.05	20045	19958	22	28	25	33
Phosphate Arsenate	0.06	0.28	0.04	0.22	10970	97864	67	123	68	126
Silicate	16.49	16.97	14.88	15.16	3775092	6685387	1603	2362	2008	3017
Total	100.00	100.00	100.00	100.00	25370675	44097195	7688	11456	8133	12183
	FieldCell-2 +75µm									
Tramp Metal	0.00	0.00	0.00	0.00	0	634	0	5	0	5
Sulphide	5.06	7.51	3.24	4.88	1038267	2591243	399	726	443	856
Oxide Hydroxide	1.21	1.30	0.82	0.91	263738	481735	138	208	139	216
Carbonate Halide	11.67	12.32	13.64	14.63	4369531	7768414	1646	2272	1650	2295
Sulphate Molybdate Chromate	0.07	0.10	0.05	0.07	15815	34544	57	98	63	110
Phosphate Arsenate	0.30	0.20	0.27	0.18	85429	96535	148	291	150	299
Silicate	81.69	78.56	81.98	79.33	26267322	42123108	8277	10070	12063	16799
Total	100.00	100.00	100.00	100.00	32040101	53096213	10665	13670	14508	20580
	FieldCell-4 +75µm									
Tramp Metal	0.00	0.00	0.00	0.00	72	0	4	0	4	0
Sulphide	0.39	0.75	0.21	0.40	55293	126696	82	75	91	82
Oxide Hydroxide	0.15	0.21	0.09	0.12	23136	38521	22	24	22	24
Carbonate Halide	97.13	95.98	97.55	96.68	25379425	30328780	11777	10904	11797	10913
Sulphate Molybdate Chromate	0.02	0.08	0.01	0.09	3247	28036	27	34	28	34
Phosphate Arsenate	0.04	0.08	0.03	0.06	7324	18804	105	63	107	64
Silicate	2.27	2.90	2.11	2.64	548126	828631	828	542	967	575
Total	100.00	100.00	100.00	100.00	26016623	31369468	12845	11642	13016	11692

Mineral Phase	Weight-%		Area (%)		Area (um^2)		Particle Count		Grain Count	
	Transverse	Single	Transverse	Single	Transverse	Single	Transverse	Single	Transverse	Single
	FieldCell-0 C1C2									
Tramp Metal	0.00	0.00	0.00	0.00	0	22	0	2	0	2
Sulphide	0.74	0.72	0.42	0.41	43786	44884	75	84	87	97
Oxide Hydroxide	0.41	0.98	0.25	0.52	26034	56970	63	118	66	119
Carbonate Halide	76.97	75.87	79.84	78.96	8316535	8622721	8831	8256	8908	8329
Sulphate Molybdate Chromate	0.12	0.15	0.08	0.09	7859	9962	49	47	60	58
Phosphate Arsenate	0.20	0.15	0.16	0.12	16656	12685	84	118	86	121
Silicate	21.55	22.13	19.25	19.90	2005031	2173747	3969	3440	5129	4568
Total	100.00	100.00	100.00	100.00	10415901	10920992	13071	12065	14336	13294
	FieldCell-2 C1C2									
Tramp Metal	0.03	0.04	0.02	0.03	1616	2598	5	8	5	8
Sulphide	7.29	10.06	4.85	6.82	460766	637366	888	985	993	1140
Oxide Hydroxide	1.68	1.47	1.19	1.06	112862	98606	228	234	232	250
Carbonate Halide	13.15	10.33	15.91	12.81	1510676	1196928	2040	1590	2050	1600
Sulphate Molybdate Chromate	0.30	0.21	0.21	0.14	20143	13132	126	96	155	110
Phosphate Arsenate	0.26	0.18	0.24	0.17	22853	15464	175	118	177	118
Silicate	77.30	77.71	77.58	78.98	7368277	7379198	10453	9867	14400	14573
Total	100.00	100.00	100.00	100.00	9497193	9343293	13915	12898	18012	17799
	FieldCell-4 C1C2									
Tramp Metal	0.00	0.00	0.00	0.00	109	0	2	0	2	0
Sulphide	0.85	0.80	0.47	0.44	48725	49350	102	110	115	118
Oxide Hydroxide	0.21	0.61	0.12	0.36	12603	40609	27	56	27	58
Carbonate Halide	96.50	95.67	97.15	96.48	10153542	10936885	11321	11214	11337	11232
Sulphate Molybdate Chromate	0.01	0.09	0.01	0.05	953	6120	35	41	36	43
Phosphate Arsenate	0.02	0.02	0.02	0.02	1744	1752	85	70	87	70
Silicate	2.41	2.81	2.24	2.66	233682	301683	964	693	1095	790
Total	100.00	100.00	100.00	100.00	10451358	11336398	12536	12184	12699	12311

Note: C1C2 refers to the combined C1 & C2 size fractions from a Warman cyclosizer particle sizer.

Mineral Phase	Weight%		Area (%)		Area (um)		Particle Count		Grain Count	
	Transverse	Single	Transverse	Single	Transverse	Single	Transverse	Single	Transverse	Single
	FieldCell-0 C3C4									
Tramp Metal	0.00	0.00	0.00	0.00	65	0	5	0	5	0
Sulphide	0.13	0.32	0.08	0.18	2405	5383	25	37	31	44
Oxide Hydroxide	0.36	0.43	0.21	0.26	6513	7630	63	56	72	61
Carbonate Halide	72.56	71.37	74.84	73.92	2269316	2171688	8605	6586	8667	6646
Sulphate Molybdate Chromate	0.16	0.09	0.10	0.06	2906	1668	45	38	59	47
Phosphate Arsenate	0.35	0.30	0.28	0.24	8389	6952	54	58	60	58
Silicate	26.44	27.49	24.49	25.35	742660	744654	4727	3275	6124	4686
Total	100.00	100.00	100.00	100.00	3032253	2937975	13524	10050	15018	11542
	FieldCell-2 C3C4									
Tramp Metal	0.03	0.05	0.02	0.03	493	726	7	9	7	9
Sulphide	3.21	3.54	2.03	2.28	49806	55447	414	446	505	543
Oxide Hydroxide	1.08	1.33	0.73	0.91	17894	22137	149	207	159	214
Carbonate Halide	18.61	16.21	21.34	18.86	524272	458341	2362	2063	2375	2088
Sulphate Molybdate Chromate	0.22	0.23	0.15	0.16	3679	3890	73	58	86	70
Phosphate Arsenate	0.22	0.25	0.19	0.21	4694	5208	81	85	81	87
Silicate	76.63	78.40	75.54	77.55	1855370	1885061	9596	9846	12367	13613
Total	100.00	100.00	100.00	100.00	2456209	2430810	12682	12714	15580	16624
	FieldCell-4 C3C4									
Tramp Metal	0.01	0.00	0.01	0.00	304	0	4	0	4	0
Sulphide	0.35	0.21	0.19	0.11	7693	4036	66	48	79	53
Oxide Hydroxide	0.12	0.08	0.07	0.05	2729	1769	26	18	28	19
Carbonate Halide	92.99	94.00	93.79	94.62	3711482	3391735	12411	10333	12432	10343
Sulphate Molybdate Chromate	0.03	0.05	0.02	0.03	837	1103	30	37	36	38
Phosphate Arsenate	0.06	0.04	0.05	0.03	1893	1084	47	37	53	37
Silicate	6.43	5.62	5.87	5.16	232160	184793	2087	1344	2404	1498
Total	100.00	100.00	100.00	100.00	3957098	3584521	14671	11817	15036	11988

Note: C3C4 refers to the combined C3 & C4 size fractions from a Warman cyclosizer particle sizer.

Mineral Phase	Weight%		Area (%)		Area (um)		Particle Count		Grain Count	
	Transverse	Single	Transverse	Single	Transverse	Single	Transverse	Single	Transverse	Single
	FieldCell-0 C5C6									
Tramp Metal	1.04	0.35	0.58	0.20	597	52	70	6	70	6
Sulphide	0.48	3.57	0.28	2.26	283	595	26	11	29	11
Oxide Hydroxide	2.36	0.91	1.49	0.57	1521	151	109	23	109	23
Carbonate Halide	15.52	16.80	16.40	17.85	16756	4713	2771	692	2799	699
Sulphate Molybdate Chromate	0.83	0.35	0.53	0.22	537	59	58	10	59	10
Phosphate Arsenate	2.64	4.97	2.06	3.03	2107	799	175	33	175	33
Silicate	77.14	73.05	78.66	75.88	80361	20037	7860	1626	8410	1751
Total	100.00	100.00	100.00	100.00	102162	26406	11069	2401	11651	2533
	FieldCell-2 C5C6									
Tramp Metal	0.33	0.64	0.19	0.37	369	265	56	36	56	36
Sulphide	4.27	3.56	2.60	2.11	4910	1510	566	232	597	242
Oxide Hydroxide	2.31	2.04	1.52	1.29	2867	924	241	125	243	125
Carbonate Halide	6.64	11.94	7.02	12.77	13263	9127	1093	716	1113	719
Sulphate Molybdate Chromate	1.36	1.71	0.87	1.09	1653	781	84	58	85	60
Phosphate Arsenate	1.33	1.36	1.10	1.10	2082	784	144	75	145	75
Silicate	83.76	78.76	86.70	81.26	163905	58068	9364	4324	10212	4592
Total	100.00	100.00	100.00	100.00	189049	71459	11548	5566	12451	5849
	FieldCell-4 C5C6									
Tramp Metal	0.53	0.32	0.29	0.17	265	94	104	36	104	36
Sulphide	0.70	0.34	0.39	0.20	356	106	43	14	46	14
Oxide Hydroxide	1.36	0.52	0.82	0.31	744	168	89	39	91	39
Carbonate Halide	72.87	68.55	75.58	70.77	68901	38260	5600	2905	5623	2922
Sulphate Molybdate Chromate	0.28	0.15	0.18	0.09	160	50	37	18	38	18
Phosphate Arsenate	0.27	0.30	0.21	0.21	190	111	20	10	20	10
Silicate	23.98	29.82	22.54	28.26	20544	15277	1963	1286	2003	1320
Total	100.00	100.00	100.00	100.00	91159	54066	7856	4308	7925	4359

Note: C5C6 refers to the combined C5 & C6 size fractions from a Warman cyclosizer particle sizer.

MLA Calculated Assay

Sample	FC-0 +75um		FC-2 +75um		FC-4 +75um		FC-0 C1C2		FC-2 C1C2		FC-4 C1C2		FC-0 C3C4		FC-2 C3C4		FC-4 C3C4		FC-0 C5C6		FC-2 C5C6		FC-4 C5C6	
Mount type	Transverse	Single	Transverse	Single	Transverse	Single	Transverse	Single	Transverse	Single	Transverse	Single	Transverse	Single	Transverse	Single	Transverse	Single	Transverse	Single	Transverse	Single	Transverse	Single
Ag	0	0	0	0	0	0	0	0	0	0	0	0	0	0	0	0	0	0	0	0	0	0	0.01	0
Al	1.47	1.48	6.77	6.83	0.19	0.2	1.75	1.84	6.91	6.67	0.23	0.25	2.31	2.28	6.42	6.14	0.37	0.33	5.73	5.37	8.21	7.5	1.57	2.03
As	0.01	0	0.02	0.01	0	0.01	0.01	0.01	0.02	0.02	0	0	0	0	0.01	0.01	0.01	0	0.03	0.01	0.01	0.03	0.01	0.02
Ba	0	0	0	0	0	0	0	0	0	0	0	0	0	0	0	0	0	0	0	0	0	0	0	0
Bi	0	0	0	0	0	0	0	0	0	0	0	0	0	0	0.01	0	0	0	0	0	0.01	0	0	0
C	9.92	9.81	1.39	1.47	11.66	11.52	9.23	9.1	1.56	1.23	11.58	11.48	8.69	8.56	2.2	1.92	11.16	11.28	1.83	2	0.71	1.37	8.73	8.21
Ca	34.14	33.92	6.99	7.28	39.09	38.72	32.49	32.18	8.52	7.29	38.85	38.54	30.8	30.38	11.12	10.09	37.86	38.13	10.58	10.22	8.42	9.74	30.29	28.95
Cd	0	0	0	0	0	0	0	0	0	0	0	0	0	0	0	0	0	0	0	0	0	0	0.07	0
Ce	0	0	0	0	0	0	0	0	0	0	0	0	0	0	0	0	0	0	0	1.17	0.01	0	0	0
Cl	0	0	0	0	0	0	0	0	0	0	0	0	0	0	0	0	0	0	0	0	0	0	0	0
Co	0	0	0	0	0	0	0	0	0	0	0	0	0	0	0	0	0	0	0	0	0	0	0	0
Cr	0	0	0	0	0	0	0	0	0	0	0	0	0	0	0	0	0	0	0	0	0	0	0	0
Cu	0.07	0.08	0.43	0.51	0.02	0.06	0.16	0.16	0.56	0.62	0.05	0.05	0.14	0.14	0.36	0.37	0.07	0.03	0.52	0.55	0.71	0.56	0.32	0.2
F	0	0.01	0.02	0.01	0	0	0.01	0.01	0.01	0.01	0	0	0.02	0.02	0.02	0.02	0	0	0.17	0.12	0.09	0.08	0.02	0.03
Fe	0.63	**0.84**	3.56	**4.76**	0.26	**0.44**	1.04	1.07	5.01	5.75	0.5	0.77	1.22	1.35	3.32	3.44	0.38	0.3	4.32	**3.35**	5.22	4.98	3.03	2.52
H	0.01	0.01	0.04	0.04	0	0	0.01	0.01	0.04	0.03	0	0	0.02	0.02	0.04	0.03	0.01	0	0.1	0.08	0.04	0.04	0.06	0.07
K	0.52	0.51	2.37	2.23	0.03	0.03	0.5	0.5	2.23	2.18	0.04	0.03	0.85	0.83	2.85	2.77	0.16	0.15	3.37	3.31	4.13	4.34	1.13	1.54
La	0	0	0	0	0	0	0	0	0	0	0	0	0	0	0	0	0	0	0	0.58	0.01	0	0	0
Mg	0.55	0.61	1.42	1.41	0.08	0.11	0.86	0.91	1.92	1.79	0.08	0.1	0.95	1.03	2.36	2.29	0.39	0.31	2.8	2.36	3.07	2.61	1.3	1.58
Mn	0.73	0.81	8.57	8.46	0.05	0.08	1.04	1.02	8.92	**10.26**	0.04	0.04	0.83	0.94	6.64	7.84	0.03	0.02	0	0	0.02	0.17	0	0
Mo	0	0	0.04	0.03	0	0	0	0	0.07	0.04	0	0	0	0	0.02	0.02	0	0	0	0	0.16	0.16	0.02	0
Na	0.09	0.09	0.14	0.15	0.03	0.03	0.12	0.13	0.11	0.1	0.04	0.04	0.22	0.19	0.16	0.12	0.05	0.04	0.43	0.47	0.18	0.19	0.11	0.14
Nd	0	0	0	0	0	0	0	0	0	0	0	0	0	0	0	0	0	0	0	0.48	0.01	0	0	0
Ni	0	0	0	0	0	0	0	0	0	0	0	0	0	0	0	0	0	0	0	0	0	0	0	0
O	47.29	47.06	42.92	41.64	47.7	47.5	46.77	46.64	40.91	39.31	47.45	47.42	47	46.9	43.21	42.81	47.61	47.72	45.81	44.61	43.23	43.59	46.47	46.83
P	0.01	0.05	0.06	0.04	0.01	0.01	0.04	0.03	0.05	0.03	0	0	0.07	0.06	0.04	0.05	0.01	0.01	0.46	**0.69**	0.24	0.24	0.05	0.04
Pb	0.05	0.05	0.21	0.29	0.03	0.07	0.07	0.09	0.24	0.34	0.02	0.04	0.06	0.05	0.21	0.22	0.02	0.01	0.22	0.12	0.43	0.37	0.09	0.1
S	0.17	**0.27**	2.43	**3.68**	0.19	**0.35**	0.33	0.32	3.63	**4.92**	0.41	0.41	0.07	0.14	1.59	1.75	0.14	0.1	0.32	**1.82**	2.1	1.79	0.37	**0.18**
Sb	0	0	0	0	0	0	0	0.01	0	0	0	0	0	0	0	0	0	0	0	0.02	0	0	0.01	0.01
Se	0	0	0	0.01	0	0	0	0	0	0.01	0	0	0	0	0	0	0	0	0	0	0	0	0	0
Si	4.24	4.22	22.25	20.82	0.61	0.8	5.31	5.42	18.9	18.82	0.6	0.77	6.6	6.91	19.06	19.73	1.7	1.53	22.57	22.08	22.14	21.3	5.77	**7.26**
Sn	0	0	0	0	0	0	0	0.29	0.02	0.02	0	0	0	0	0	0.01	0	0	0	0	0	0	0	0
Sr	0	0	0	0	0	0	0	0	0	0	0	0	0	0	0	0	0	0	0.02	0.01	0	0	0	0
Th	0	0	0	0	0	0	0	0	0	0	0	0	0	0	0	0	0	0	0	0.19	0	0	0	0
Ti	0.09	0.09	0.2	0.19	0.01	0.02	0.15	0.16	0.21	0.19	0.01	0	0.13	0.13	0.28	0.25	0.02	0.01	0.57	**0.25**	0.55	0.57	0.25	0.22
W	0	0	0	0	0	0	0	0	0.02	0.01	0	0.01	0	0.01	0	0.01	0	0.01	0	0	0.03	0	0	0
Zn	0	0.07	0.16	0.14	0.04	0.03	0.09	0.08	0.14	**0.37**	0.1	0.03	0.02	0.07	0.07	0.1	0.02	0.02	0.14	0.12	0.27	0.35	0.14	0.07
Zr	0	0	0.03	0	0	0	0	0.02	0.01	0	0	0	0.02	0	0	0.01	0	0	0	0.02	0.02	0.02	0.19	0
Total	100	100	100	100	100	100	100	100	100	100	100	100	100	100	100	100	100	100	100	100	100	100	100	100

Mineral Liberation & Association: relative to sulphide

FC-0	+75um				CIC2				C3C4				C5C6			
	Binary		Ternary		Binary		Ternary		Binary		Ternary		Binary		Ternary	
Sulphide Weight % locked in...	**Transverse**	**Single**	**Transverse**	**Single**	**Transverse**	**Single**	**Transverse**	**Single**	**Transverse**	**Single**	**Transverse**	**Single**	**Transverse**	**Single**	**Transverse**	**Single**
Tramp Metal	0	0	0	0	0	0	0	0	0	0	0	0	0	0	0	0
Oxide Hydroxide	4.04	5.07	0.36	1.77	2.7	0.5	0.91	1.95	0	0.21	8.88	3.02	0.29	0	0.12	0
Carbonate Halide	1.12	0.12	0	0.11	0.16	0.97	1.68	2.37	3.46	11.74	0.71	6.53	0	0	0.05	0
Sulphate Molybdate Chromate	0	2.59	0.03	0.01	3.63	5.25	2.3	0.86	33.47	8.08	8.85	6.72	0	0	0	0
Phosphate Arsenate	0	0	0	0	0	0	0	0	0	0	0	0	0	0	0	0
Silicate	0.26	4.82	0	0.5	2.26	12.99	7.5	2.57	6.5	6.13	6	10.91	28.57	0.51	0.12	0

Sulphide Distribution Summary	**Transverse**	**Single**	**Transverse**	**Single**	**Transverse**	**Single**	**Transverse**	**Single**
Liberated (%)	94.19	85.01	78.86	72.55	32.12	46.67	70.86	99.49
Total Binary (%)	5.42	12.6	8.74	19.71	43.43	26.15	28.86	0.51
Total Ternary (%)	0.39	2.39	12.39	7.74	24.45	27.18	0.29	0
Total Lib+Bin (%)	99.61	97.61	87.61	92.26	75.55	72.82	99.71	100
Total Lib+Bin+Tern (%)	100	100	100	100	100	100	100	100

Mineral Liberation & Association: relative to sulphide

FC-2	+75um				CIC2				C3C4				C5C6			
	Binary		Ternary		Binary		Ternary		Binary		Ternary		Binary		Ternary	
Sulphide Weight % locked in...	**Transverse**	**Single**	**Transverse**	**Single**	**Transverse**	**Single**	**Transverse**	**Single**	**Transverse**	**Single**	**Transverse**	**Single**	**Transverse**	**Single**	**Transverse**	**Single**
Tramp Metal	0	0	0	0	0	0	0	0	0	0	0	0	0	0	0	0
Oxide Hydroxide	0.41	0.47	0.44	0.15	0.55	0.38	0.28	0.1	1.98	0.84	0.14	0.29	3.19	0.11	0.27	2.03
Carbonate Halide	0.88	1.06	0	0.19	0.52	0.25	0.04	0.03	1.55	2.24	0.03	0.01	0.53	0.71	0.02	1.82
Sulphate Molybdate Chromate	0.15	0.71	0	0.01	2.5	2.61	0.6	0.28	4.04	1.44	0.15	0.54	1	0.39	0.1	2.97
Phosphate Arsenate	0.31	0.5	0.49	0	0.1	0.24	0	0	0	0	0	0	0	0	0	0
Silicate	11.65	11.53	0.92	0.52	5.18	7.12	0.76	0.13	4.09	7.58	0.26	1.11	6.93	9.42	0.22	0.18

Sulphide Distribution Summary	**Transverse**	**Single**	**Transverse**	**Single**	**Transverse**	**Single**	**Transverse**	**Single**
Liberated (%)	84.74	84.86	89.47	88.87	87.76	85.94	87.74	82.36
Total Binary (%)	13.4	14.27	8.85	10.59	11.65	12.11	11.65	10.64
Total Ternary (%)	1.86	0.87	1.69	0.53	0.59	1.95	0.61	7
Total Lib+Bin (%)	98.14	99.13	98.31	99.47	99.41	98.05	99.39	93
Total Lib+Bin+Tern (%)	100	100	100	100	100	100	100	100

Mineral Liberation & Association: relative to sulphide

FC-4	+75um				CIC2				C3C4				C5C6			
	Binary		Ternary		Binary		Ternary		Binary		Ternary		Binary		Ternary	
Sulphide Weight % locked in...	**Transverse**	**Single**	**Transverse**	**Single**	**Transverse**	**Single**	**Transverse**	**Single**	**Transverse**	**Single**	**Transverse**	**Single**	**Transverse**	**Single**	**Transverse**	**Single**
Tramp Metal	0	0	0	0	0	0	0	0	0	0	0	0	0.31	0	0	0
Oxide Hydroxide	0	0	0	0	0	0	0.12	1.51	2.03	5.53	0.83	1.23	0	1.15	0	0
Carbonate Halide	11.72	11.15	1.03	4.87	14.73	11.04	1.54	0.17	11.77	17.89	0.72	0.09	2.04	13.14	0	0
Sulphate Molybdate Chromate	3.75	1.22	0	0	1.13	2.36	0.33	0.23	3.97	6.05	0.75	2.36	4.44	0	0	0
Phosphate Arsenate	0	0	0	0	0	0	0	0	0	0	0.01	0	0	0	0	0
Silicate	2.41	2.17	0.79	1.1	3.51	1.23	0.21	0.02	17.24	1.36	1.32	0.87	0	0.86	0	0

Sulphide Distribution Summary	**Transverse**	**Single**	**Transverse**	**Single**	**Transverse**	**Single**	**Transverse**	**Single**
Liberated (%)	80.3	79.49	78.44	83.43	61.36	64.62	93.21	84.84
Total Binary (%)	17.88	14.54	19.36	14.63	35	30.83	6.79	15.16
Total Ternary (%)	1.82	5.97	2.2	1.94	3.63	4.55	0	0
Total Lib+Bin (%)	98.18	94.03	97.8	98.06	96.37	95.45	100	100
Total Lib+Bin+Tern (%)	100	100	100	100	100	100	100	100

APPENDIX 7 Effect of spot size

Modal Mineralogy & Analysis Particulars (weight-%, normalized)

Mineral Group	Sample	A951 176m, Class B		A431 306m, Class A		A431 306m, Class A		A355 160.5m, Class C		A355 160.5m, Class C		A355 70.5m, Class B		A355 70.5m, Class B		A355 70.5m, Class B		A162 97.5m, Class A		A162 97.5m, Class A		A162 97.5m, Class A	
	Size Fraction	-300/+150 µm		-1190/+600 µm		-75/+53 µm		-1190/+600 µm		-150/+106 µm		-600/+300 µm		-600/+300 µm		-150/+106 µm		-1190/+600 µm		-600/+300 µm		-106/+75 µm	
	Spot Size*	60 kcps	100 kcps	60 kcps	100 kcps	60 kcps	100 kcps	60 kcps	100 kcps	60 kcps	100 kcps	60 kcps	100 kcps	60 kcps	100 kcps	60 kcps	100 kcps	60 kcps	100 kcps	60 kcps	100 kcps	60 kcps	100 kcps
Sulphide	Bornite	0.000	0.000	0.020	0.016	0.051	0.071	0.000	0.000	0.000	0.000	0.000	0.000	0.000	0.000	0.000	0.000	0.500	0.652	0.360	0.599	0.916	0.861
	Galena	0.100	0.125	0.060	0.062	0.174	0.218	0.000	0.000	0.000	0.004	0.030	0.026	0.030	0.827	0.058	0.169	1.030	1.038	0.100	0.097	0.039	0.030
	Sphalerite	0.060	0.009	0.450	1.261	1.909	1.864	0.310	1.170	0.130	0.197	0.340	0.270	0.420	1.678	1.646	1.475	1.420	1.854	2.040	2.112	2.511	2.263
	Chalcopyrite	0.050	0.015	0.260	1.102	0.576	0.611	0.160	0.578	0.200	0.120	0.090	0.100	0.370	0.901	0.452	0.407	1.880	2.154	1.480	1.413	1.361	1.419
	Pyrrhotite	0.000	0.001	0.030	0.024	0.053	0.058	0.980	4.012	2.750	2.528	0.310	2.186	0.400	0.978	1.190	1.351	0.370	0.343	0.010	0.554	0.182	0.194
	Realgar-Orpiment	0.000	0.000	0.000	0.000	0.000	0.000	0.000	0.000	0.000	0.000	0.000	0.000	0.000	0.000	0.000	0.000	0.000	0.000	0.000	0.000	0.000	0.000
	Stibnite	0.000	0.000	0.000	0.000	0.000	0.000	0.000	0.000	0.000	0.000	0.000	0.000	0.000	0.000	0.000	0.000	0.020	0.004	0.000	0.001	0.001	0.005
	Watanabeite	0.000	0.000	0.000	0.000	0.000	0.000	0.000	0.000	0.000	0.000	0.000	0.000	0.000	0.000	0.000	0.000	3.730	2.562	2.930	3.210	2.041	1.881
	Pyrite	0.070	0.091	0.020	0.023	0.000	0.002	1.490	3.916	1.440	1.887	3.680	6.489	5.680	7.301	12.993	12.585	0.470	0.445	0.150	0.191	0.227	0.311
	Molybdenite	0.000	0.003	0.190	0.225	0.041	0.047	0.000	0.000	0.000	0.000	0.000	0.000	0.000	0.000	0.001	0.000	0.020	0.018	0.010	0.006	0.000	0.000
	Enargite	0.000	0.000	0.020	0.036	0.032	0.030	0.000	0.000	0.000	0.000	0.000	0.000	0.000	0.000	0.000	0.000	1.000	1.625	1.870	2.614	0.626	0.522
	Others	0.000	0.000	0.000	0.001	0.002	0.023	0.000	0.001	0.000	0.000	0.000	0.000	0.000	0.000	0.001	0.001	0.020	0.113	0.010	0.020	0.072	0.022
	Subtotal	**0.280**	**0.244**	**1.050**	**2.751**	**2.840**	**2.923**	**2.940**	**9.678**	**4.520**	**4.736**	**4.450**	**9.071**	**6.900**	**11.684**	**16.340**	**15.989**	**10.460**	**10.809**	**8.960**	**10.817**	**7.974**	**7.508**
Carbonate	Calcite	88.580	88.205	63.790	63.900	84.601	87.158	57.920	53.898	67.570	68.601	45.550	42.747	46.790	39.857	44.527	44.654	47.740	46.945	44.830	44.597	59.433	60.409
	Otavite	0.000	0.000	0.000	0.000	0.000	0.000	0.000	0.000	0.000	0.000	0.000	0.000	0.000	0.000	0.000	0.000	0.000	0.000	0.000	0.000	0.000	0.000
	Siderite	0.000	0.000	0.000	0.000	0.000	0.000	0.000	0.000	0.000	0.000	0.000	0.000	0.000	0.000	0.000	0.000	0.000	0.000	0.000	0.000	0.000	0.000
	Dolomite	0.000	0.000	0.190	0.089	0.312	0.133	0.000	0.000	0.000	0.000	0.000	0.001	0.000	0.000	0.018	0.019	0.010	0.001	0.000	0.000	0.000	0.000
	Others	0.000	0.000	0.000	0.001	0.004	0.016	0.000	0.000	0.000	0.027	0.000	0.000	0.000	0.000	0.005	0.003	0.000	0.000	0.000	0.000	0.000	0.000
	Subtotal	**88.580**	**88.205**	**63.980**	**63.989**	**84.918**	**87.307**	**57.920**	**53.898**	**67.570**	**68.629**	**45.550**	**42.748**	**46.790**	**39.857**	**44.551**	**44.676**	**47.750**	**46.947**	**44.830**	**44.598**	**59.434**	**60.409**
Silicate	Biotite	0.000	0.000	0.020	0.005	0.108	0.066	0.740	0.102	0.340	0.364	0.350	0.822	0.440	0.192	0.250	0.442	0.880	0.214	0.530	0.236	0.154	0.161
	Chlorite	0.000	0.000	0.030	0.027	0.009	0.025	0.010	0.006	0.130	0.022	0.360	0.112	0.100	0.373	0.109	0.260	0.030	0.005	0.070	0.219	0.049	0.050
	K_Feldspar	0.100	0.053	0.120	0.188	0.061	0.057	4.390	2.208	3.100	2.428	5.470	3.950	4.950	3.534	3.988	3.671	0.450	0.558	0.440	0.715	0.215	0.198
	Kaolinite	0.000	0.000	0.000	0.000	0.000	0.000	0.000	0.000	0.000	0.001	0.000	0.108	0.410	0.509	0.002	0.444	0.000	0.000	0.000	0.000	0.000	0.000
	Muscovite	0.000	0.000	0.000	0.001	0.000	0.000	0.000	0.001	0.040	0.008	0.020	0.026	0.000	0.000	0.054	0.085	0.000	0.000	0.170	0.000	0.000	0.000
	Plagioclase	0.560	0.494	0.860	1.573	0.299	0.427	8.050	9.932	6.260	6.104	15.240	14.882	14.610	17.865	11.157	12.028	2.520	1.948	2.430	1.228	0.479	0.471
	Pyroxene	3.320	3.746	13.680	10.321	5.153	4.040	10.300	7.089	5.850	4.944	7.860	6.926	8.200	7.265	7.422	6.835	7.110	7.188	9.370	10.362	14.415	13.767
	Quartz	0.590	0.707	0.000	0.000	0.044	0.044	0.400	0.632	0.920	0.948	1.000	1.259	0.790	0.954	1.127	1.725	1.660	1.380	0.990	2.106	1.237	1.166
	Talc	0.060	0.000	0.000	0.000	0.000	0.000	0.000	0.000	0.000	0.000	0.000	0.000	0.000	0.000	0.000	0.000	0.000	0.000	0.000	0.000	0.000	0.000
	Mica	0.050	0.139	0.690	0.106	0.159	0.164	4.370	6.642	3.560	4.451	3.830	2.406	2.980	1.881	3.140	3.112	0.500	0.378	0.530	0.324	0.256	0.189
	Titanite	0.100	0.138	0.060	0.020	0.092	0.058	1.180	0.178	0.470	1.931	0.680	1.602	0.400	2.207	0.555	1.115	0.110	0.063	0.140	0.239	0.072	0.068
	Others	6.340	6.248	18.870	19.956	6.077	4.468	9.540	6.337	6.500	4.259	15.070	14.755	11.880	11.568	10.888	8.779	28.320	30.173	31.060	28.868	15.485	15.839
	Subtotal	**11.120**	**11.523**	**34.330**	**32.196**	**12.003**	**9.349**	**38.980**	**33.128**	**27.170**	**25.459**	**49.880**	**46.850**	**44.760**	**46.348**	**38.692**	**38.496**	**41.580**	**41.906**	**45.730**	**44.295**	**32.363**	**31.909**
Phosphate	**Total**	0.020	0.026	0.040	0.032	0.024	0.046	0.110	1.261	0.250	0.872	0.020	1.301	1.460	0.816	0.132	0.437	0.100	0.161	0.430	0.171	0.131	0.084
Oxide	FeOxyhydroxides	0.000	0.000	0.000	0.001	0.035	0.054	0.000	0.029	0.200	0.059	0.020	0.004	0.000	0.001	0.214	0.172	0.020	0.014	0.000	0.000	0.048	0.068
	Others	0.000	0.000	0.000	0.000	0.001	0.000	0.000	0.000	0.000	0.000	0.000	0.000	0.000	0.000	0.003	0.000	0.000	0.133	0.000	0.001	0.003	0.002
	Subtotal	**0.000**	**0.000**	**0.000**	**0.001**	**0.036**	**0.054**	**0.000**	**0.029**	**0.200**	**0.059**	**0.020**	**0.004**	**0.000**	**0.001**	**0.216**	**0.172**	**0.020**	**0.147**	**0.000**	**0.001**	**0.051**	**0.070**
Sulphate	FeSulphate	0.000	0.001	0.000	0.000	0.000	0.000	0.050	2.006	0.280	0.246	0.040	0.025	0.040	1.276	0.065	0.228	0.010	0.010	0.000	0.004	0.043	0.008
	Barite	0.000	0.000	0.000	0.000	0.000	0.000	0.000	0.000	0.000	0.000	0.000	0.000	0.000	0.000	0.000	0.000	0.000	0.000	0.000	0.000	0.000	0.000
	Gypsum	0.000	0.000	0.000	0.002	0.001	0.000	0.000	0.000	0.000	0.000	0.020	0.000	0.000	0.000	0.001	0.001	0.070	0.002	0.010	0.001	0.002	0.000
	Others	0.000	0.000	0.000	0.000	0.000	0.000	0.000	0.000	0.000	0.000	0.000	0.000	0.000	0.000	0.000	0.000	0.000	0.000	0.000	0.000	0.000	0.000
	Subtotal	**0.000**	**0.001**	**0.000**	**0.002**	**0.001**	**0.000**	**0.050**	**2.006**	**0.280**	**0.246**	**0.060**	**0.025**	**0.040**	**1.276**	**0.066**	**0.229**	**0.080**	**0.012**	**0.010**	**0.006**	**0.045**	**0.008**
Other	**Total**	0.000	0.000	0.610	1.028	0.178	0.321	0.000	0.000	0.010	0.001	0.000	0.003	0.020	0.018	0.003	0.002	0.020	0.019	0.040	0.113	0.004	0.011
Total Mineralogy		**100.0**	**100.0**	**100.0**	**100.0**	**100.0**	**100.0**	**100.0**	**100.0**	**100.0**	**100.0**	**100.0**	**100.0**	**100.0**	**100.0**	**100.0**	**100.0**	**100.0**	**100.0**	**100.0**	**100.0**	**100.0**	**100.0**
	# Particles Analyzed	2564	1965	513	377	12579	12525	295	309	4860	5214	1110	870	819	922	7634	7467	601	552	1222	1288	7838	12564
	# Grains Analyzed	4299	3035	8569	5826	15110	13857	5891	2407	9565	8865	6206	4119	7087	4573	17267	15151	14754	12278	8982	10727	11463	17424
	# Frames Analyzed	72	54	60	63	112	120	64	64	96	96	72	72	63	72	108	108	70	70	63	72	105	140
	Analysis Time (min)	32	22	43	35	49	45	36	30	41	42	36	31	31	31	54	49	54	50	34	38	46	60

* = spot size measured on pure quartz in number of thousands of X-ray counts per second (kcps).

MLA-calculated Assay (weight-%, normalized)

Sample	A951 176m, Class B		A431 306m, Class A		A431 306m, Class A		A355 160.5m, Class C		A355 160.5m, Class C		A355 70.5m, Class B		A355 70.5m, Class B		A355 70.5m, Class B		A162 97.5m, Class A		A162 97.5m, Class A		A162 97.5m, Class A	
Size Fraction	-300/+150 µm		-1190/+600 µm		-75/+53 µm		-1190/+600 µm		-150/+106 µm		-600/+300 µm		-600/+300 µm		-150/+106 µm		-1190/+600 µm		-600/+300 µm		-106/+75 µm	
Spot Size*	60 kcps	100 kcps	60 kcps	100 kcps	60 kcps	100 kcps	60 kcps	100 kcps	60 kcps	100 kcps	60 kcps	100 kcps	60 kcps	100 kcps	60 kcps	100 kcps	60 kcps	100 kcps	60 kcps	100 kcps	60 kcps	100 kcps
Ag	0.0000	0.0000	0.0000	0.0000	0.0011	0.0034	0.0000	0.0000	0.0000	0.0000	0.0000	0.0000	0.0001	0.0000	0.0000	0.0000	0.0000	0.0000	0.0000	0.0000	0.0002	0.0000
Al	1.1	1.1	2.7	3.2	0.9	0.7	4.4	4.0	3.0	2.7	6.1	5.8	5.9	5.9	3.0	4.5	4.6	4.5	4.6	4.2	2.3	2.4
As	0.0001	0.0001	0.0045	0.0075	0.0067		0.0043	0.1706	0.0237	0.0212	0.0036	0.0021	0.0031	0.1085	0.0047	0.0186	0.6421	0.7013	0.7690	0.9617	0.4069	0.3624
Ba	0	0	0	0	0	0	0	0	0	0	0	0	0	0	0	0	0	0	0	0	0	0
Bi	0.0000	0.0000	0.0000	0.0000	0.0000	0.0000	0.0016	0.0011	0.0000	0.0002	0.0004	0.0002	0.0005	0.0000	0.0000	0.0006	0.0010	0.0010	0.0008	0.0009	0.0000	0.0000
C	10.6	10.6	7.7	7.7	10.2	10.5	7.0	6.5	8.1	8.2	5.5	5.1	5.6	4.8	7.4	5.4	5.3	5.6	5.4	5.4	7.1	7.2
Ca	36	36	28	28	35	36	27	24	29.3	30	22	21	23	20	28	21	22	23	23	23	28	28
Cd	0.0000	0.0000	0.0001	0.0002	0.0002	0.0002	0.0000	0.0000	0.0000	0.0000	0.0000	0.0000	0.0000	0.0000	0.0000	0.0000	0.0022	0.0080	0.0056	0.0098	0.0006	0.0007
Ce	0	0	0	0	0	0	0	0	0	0	0	0	0	0	0	0	0	0	0	0	0	0
Cl	0	0	0	0	0	0	0	0	0	0	0	0	0	0	0	0	0	0	0	0	0	0
Co	0	0	0	0	0	0	0	0	0	0	0	0	0	0	0	0	0	0.000	0.002	0	0	0
Cr	0	0	0	0	0	0	0	0	0	0	0	0	0	0	0	0	0	0	0	0	0	0
Cu	0.02	0.01	0.14	0.42	0.27	0.30	0.10	0.38	0.13	0.14	0.09	0.16	0.22	0.59	0.41	0.28	3.04	3.00	2.86	3.43	2.31	2.11
F	0.001	0.001	0.098	0.304	0.078	0.139	0.004	0.067	0.013	0.035	0.020	0.059	0.065	0.039	0.410	0.024	0.019	0.034	0.031	0.059	0.006	0.008
Fe	0.10	0.11	0.32	0.53	0.37	0.40	1.84	5.67	3.03	3.06	2.44	4.90	3.39	5.16	0.63	7.48	3.01	3.09	2.80	3.10	1.60	1.62
H	0.000	0.001	0.003	0.003	0.002	0.002	0.017	0.038	0.016	0.017	0.019	0.014	0.018	0.029	0.006	0.023	0.034	0.033	0.043	0.040	0.015	0.014
K	0.01	0.02	0.03	0.03	0.02	0.02	1.16	1.09	0.85	0.85	1.23	0.85	1.03	0.71	0.11	0.86	0.16	0.15	0.17	0.14	0.06	0.05
La	0	0	0	0	0	0	0	0	0	0	0	0	0	0	0	0	0	0	0	0	0	0
Mg	0.4	0.4	1.6	1.2	0.6	0.5	1.5	1.2	1.0	0.9	1.4	1.1	1.3	1.1	1.5	1.1	1.0	1.0	1.1	1.2	1.7	1.6
Mn	1.6	1.5	5.5	5.2	1.7	1.2	0.6	0.7	0.8	0.4	2.3	3.0	1.7	2.1	5.6	1.5	4.6	3.8	3.3	2.9	2.4	2.5
Mo	0.000	0.002	0.115	0.135	0.025	0.028	0.001	0.036	0.005	0.004	0.001	0.000	0.001	0.023	0.105	0.004	0.015	0.011	0.004	0.004	0.000	0.000
Na	0.02	0.02	0.04	0.07	0.01	0.02	0.53	0.51	0.38	0.34	0.89	0.76	0.75	0.91	0.08	0.62	0.11	0.11	0.15	0.06	0.03	0.02
Nd	0	0	0	0	0	0	0	0	0	0	0	0	0	0	0	0	0	0	0	0	0	0
Ni	0	0	0	0	0	0	0	0	0	0	0	0	0	0	0	0	0	0.00001	0.0008	0	0	0
O	47.3	47.3	45.1	44.4	45.8	45.9	45.4	42.0	44.9	44.7	44.2	41.8	43.3	40.6	44.3	39.1	40.3	40.7	41.4	40.7	42.7	42.9
P	0.004	0.005	0.007	0.006	0.004	0.008	0.020	0.232	0.046	0.160	0.004	0.239	0.269	0.150	0.003	0.080	0.020	0.030	0.080	0.032	0.024	0.015
Pb	0.09	0.11	0.07	0.06	0.16	0.19	0.08	0.09	0.04	0.14	0.07	0.15	0.08	0.83	0.43	0.23	0.88	0.90	0.13	0.14	0.06	0.06
S	0.1	0.1	0.3	0.9	0.9	0.9	1.3	4.3	1.9	2.1	2.2	4.4	3.5	5.3	0.7	7.9	3.2	3.2	2.7	3.3	2.5	2.4
Sb	0.0000	0.0000	0.0002	0.0003	0.0002	0.0000	0	0	0	0	0.00003	0.00000	0.00009	0.00000	0.00003	0.00000	0.44	0.33	0.37	0.41	0.26	0.24
Se	0.0036	0.0046	0.0022	0.0023	0.0066	0.0083	0.0000	0.0000	0.0000	0.0001	0.0011	0.0010	0.0011	0.0306	0.0195	0.0063	0.0393	0.0384	0.0037	0.0036	0.0014	0.0011
Si	2.4	2.5	7.1	6.5	2.5	2.0	8.8	7.6	6.3	5.8	11.0	10.1	10.0	10.0	7.1	8.8	8.8	8.4	9.2	9.3	7.2	7.1
Sn	0	0	0	0	0	0	0	0	0.00011	0	0	0	0	0	0	0	0	0	0	0	0	0
Sr	0	0	0	0	0	0	0	0	0	0	0	0	0	0	0	0	0	0	0	0	0	0
Th	0	0	0	0	0	0	0	0	0	0	0	0	0	0	0	0	0	0	0	0	0	0
Ti	0.02	0.03	0.01	0.00	0.02	0.01	0.28	0.10	0.13	0.43	0.17	0.34	0.10	0.46	0.00	0.25	0.03	0.05	0.04	0.05	0.02	0.01
W	0.00	0.00	0.26	0.26	0.01	0.02	0.00	0.00	0.00	0.00	0.00	0.00	0.01	0.01	0.27	0.00	0.00	0.00	0.00	0.00	0.00	0.00
Zn	0.04	0.01	0.30	0.84	1.26	1.24	0.20	0.77	0.09	0.14	0.22	0.19	0.29	1.10	0.31	0.96	1.55	1.44	1.53	1.66	1.73	1.58
Zr	0.0004	0.0002	0.0008	0.0004	0.0025	0.0020	0.0011	0.0009	0.0003	0.0002	0.0013	0.0007	0.0008	0.0005	0.0004	0.0005	0.0001	0.0000	0.0002	0.0002	0.0000	0.0001
Total	100.00	100.00	100.00	100.00	100.00	99.99	100.00	100.00	100.00	100.00	100.00	100.00	100.00	100.00	100.00	100.00	100.00	100.00	100.00	100.00	100.00	100.00

* = spot size measured on pure quartz in number of thousands of X-ray counts per second (kcps).

Metal Distribution by Mineral (weight-%, normalized)

Element of Concern ANTIMONY, Sb

Sample	A951 176m, Class B		A431 306m, Class A		A431 306m, Class A		A355 160.5m, Class C		A355 160.5m, Class C		A355 70.5m, Class B		A355 70.5m, Class B		A355 70.5m, Class B		A162 97.5m, Class A		A162 97.5m, Class A		A162 97.5m, Class A	
Size Fraction	-300/+150 µm		-1190/+600 µm		-75/+53 µm		-1190/+600 µm		-150/+106 µm		-600/+300 µm		-600/+300 µm		-150/+106 µm		-1190/+600 µm		-600/+300 µm		-106/+75 µm	
Spot Size*	60 kcps	100 kcps	60 kcps	100 kcps	60 kcps	100 kcps	60 kcps	100 kcps	60 kcps	100 kcps	60 kcps	100 kcps	60 kcps	100 kcps	60 kcps	100 kcps	60 kcps	100 kcps	60 kcps	100 kcps	60 kcps	100 kcps
Stibnite	0.0000	0.0000	0.0001	0.0003	0.0002	0.0000	0.0000	0.0000	0.0000	0.0000	0.0000	0.0000	0.0000	0.0000	0.0000	0.0000	0.0061	0.0043	0.0019	0.0010	0.0010	0.0054
WatanabeiteZn	0.0000	0.0000	0.0017	0.0004	0.0001	0.0000	0.0000	0.0000	0.0000	0.0000	0.0000	0.0000	0.0000	0.0000	0.0000	0.0000	1.8574	2.5621	2.9251	3.2101	2.0406	1.8813
Bismutostibiconite	0.0001	0.0000	0.0002	0.0000	0.0000	0.0000	0.0000	0.0000	0.0000	0.0000	0.0001	0.0000	0.0003	0.0000	0.0002	0.0000	0.0000	0.0000	0.0000	0.0000	0.0000	0.0000
Subtotal	**0.0001**	**0.0000**	**0.0021**	**0.0007**	**0.0003**	**0.0000**	**0.0000**	**0.0000**	**0.0000**	**0.0000**	**0.0001**	**0.0000**	**0.0003**	**0.0000**	**0.0002**	**0.0000**	**1.8635**	**2.5665**	**2.9270**	**3.2111**	**2.0417**	**1.8867**
Sulphide	0.28	0.24	1.71	2.75	2.84	2.92	2.35	9.68	4.52	4.74	4.46	9.07	6.91	11.68	16.34	15.99	7.14	8.24	6.03	7.61	5.93	5.62
Carbonate	88.58	88.20	64.52	63.99	84.92	87.31	55.43	53.90	67.57	68.63	45.55	42.75	46.80	39.86	44.55	44.68	48.33	46.95	44.83	44.60	59.43	60.41
Silicate	11.12	11.52	33.01	32.20	12.00	9.35	41.97	33.13	27.16	25.46	49.88	46.85	44.77	46.35	38.69	38.50	42.51	41.91	45.72	44.30	32.36	31.91
Phosphate	0.019	0.026	0.059	0.032	0.024	0.046	0.135	1.261	0.251	0.872	0.023	1.301	1.460	0.816	0.132	0.437	0.111	0.161	0.435	0.171	0.131	0.084
Oxide	0.000	0.000	0.004	0.001	0.036	0.054	0.001	0.029	0.206	0.059	0.023	0.004	0.005	0.001	0.216	0.172	0.004	0.147	0.009	0.001	0.051	0.070
Sulphate	0.002	0.001	0.012	0.002	0.002	0.000	0.109	2.006	0.283	0.246	0.067	0.025	0.040	1.276	0.066	0.229	0.029	0.012	0.008	0.006	0.045	0.008
Other	0.00	0.00	0.68	1.03	0.18	0.32	0.00	0.00	0.01	0.00	0.00	0.00	0.02	0.02	0.00	0.00	0.02	0.02	0.04	0.11	0.00	0.01
Subtotal	**100.000**	**100.000**	**99.998**	**99.999**	**100.000**	**100.000**	**100.000**	**100.000**	**100.000**	**100.00**	**100.000**	**100.000**	**100.000**	**100.000**	**100.000**	**100.000**	**98.137**	**97.434**	**97.073**	**96.789**	**97.958**	**98.113**
Total	100.0	100.0	100.0	100.0	100.0	100.0	100.0	100.0	100.0	100.0	100.0	100.0	100.0	100.0	100.0	100.0	100.0	100.0	100.0	100.0	100.0	100.0

* = spot size measured on pure quartz in number of thousands of X-ray counts per second (kcps).

Element of Concern ARSENIC, As

Sample	A951 176m, Class B		A431 306m, Class A		A431 306m, Class A		A355 160.5m, Class C		A355 160.5m, Class C		A355 70.5m, Class B		A355 70.5m, Class B		A355 70.5m, Class B		A162 97.5m, Class A		A162 97.5m, Class A		A162 97.5m, Class A	
Size Fraction	-300/+150 µm		-1190/+600 µm		-75/+53 µm		-1190/+600 µm		-150/+106 µm		-600/+300 µm		-600/+300 µm		-150/+106 µm		-1190/+600 µm		-600/+300 µm		-106/+75 µm	
Spot Size*	60 kcps	100 kcps	60 kcps	100 kcps	60 kcps	100 kcps	60 kcps	100 kcps	60 kcps	100 kcps	60 kcps	100 kcps	60 kcps	100 kcps	60 kcps	100 kcps	60 kcps	100 kcps	60 kcps	100 kcps	60 kcps	100 kcps
Arsenopyrite	0.0000	0.0000	0.0000	0.0000	0.0000	0.0000	0.0000	0.0000	0.0000	0.0000	0.0000	0.0000	0.0000	0.0000	0.0000	0.0000	0.0000	0.0000	0.0000	0.0000	0.0000	0.0000
RealgarOrpiment	0.0000	0.0000	0.0000	0.0000	0.0000	0.0000	0.0000	0.0000	0.0000	0.0000	0.0000	0.0000	0.0000	0.0000	0.0000	0.0000	0.0000	0.0000	0.0000	0.0000	0.0000	0.0000
Enargite	0.0000	0.0000	0.0075	0.0069	0.0026	0.0011	0.0000	0.0000	0.0000	0.0000	0.0000	0.0000	0.0000	0.0000	0.0000	0.0000	0.4820	0.2856	0.9288	0.9782	0.5283	0.4002
EnargiteZn	0.0000	0.0000	0.0135	0.0291	0.0292	0.0285	0.0000	0.0000	0.0006	0.0004	0.0000	0.0000	0.0000	0.0000	0.0000	0.0000	0.3660	1.3396	0.9392	1.6355	0.0975	0.1216
TennantiteZnFe	0.0000	0.0000	0.0011	0.0007	0.0001	0.0178	0.0000	0.0000	0.0000	0.0000	0.0000	0.0000	0.0000	0.0000	0.0000	0.0000	0.0139	0.1065	0.0042	0.0085	0.0414	0.0223
WatanabeiteZn	0.0000	0.0000	0.0004	0.0004	0.0001	0.0000	0.0000	0.0000	0.0000	0.0000	0.0000	0.0000	0.0000	0.0000	0.0000	0.0000	3.4656	2.5621	2.9251	3.2101	2.0406	1.8813
FeOxideSulphateCuPbZnAs	0.0000	0.0001	0.0031	0.0013	0.0348	0.0534	0.0010	0.0290	0.1328	0.0590	0.0190	0.0014	0.0046	0.0006	0.2137	0.1328	0.0008	0.0110	0.0044	0.0002	0.0472	0.0573
SideriteMnAsZnCrCu	0.0000	0.0000	0.0000	0.0000	0.0000	0.0000	0.0000	0.0000	0.0000	0.0000	0.0000	0.0000	0.0000	0.0000	0.0003	0.0001	0.0000	0.0000	0.0000	0.0000	0.0000	0.0000
FeSulphateLimoniteCuAsMoZn	0.0008	0.0010	0.0001	0.0000	0.0000	0.0001	0.0503	2.0057	0.2707	0.2456	0.0416	0.0248	0.0363	1.2759	0.0633	0.2126	0.0103	0.0097	0.0017	0.0041	0.0022	0.0064
FornaciteConichalcite	0.0000	0.0000	0.0000	0.0000	0.0000	0.0000	0.0000	0.0000	0.0000	0.0000	0.0000	0.0000	0.0000	0.0000	0.0000	0.0000	0.0000	0.0000	0.0000	0.0000	0.0000	0.0000
TyrolitePb	0.0000	0.0000	0.0000	0.0000	0.0000	0.0000	0.0000	0.0000	0.0000	0.0000	0.0000	0.0000	0.0000	0.0000	0.0000	0.0000	0.0000	0.0000	0.0000	0.0000	0.0000	0.0000
Subtotal	**0.0008**	**0.0010**	**0.0257**	**0.0383**	**0.0668**	**0.1009**	**0.0512**	**2.0347**	**0.4041**	**0.3049**	**0.0606**	**0.0262**	**0.0409**	**1.2765**	**0.2773**	**0.3454**	**4.3386**	**4.3145**	**4.8034**	**5.8364**	**2.7573**	**2.4890**
Sulphides	0.28	0.24	1.03	2.71	2.81	2.88	2.93	9.68	4.52	4.74	4.46	9.07	6.91	11.68	16.34	15.99	6.70	6.52	4.16	4.98	5.27	5.08
Carbonates	88.58	88.20	63.97	63.99	84.92	87.31	57.92	53.90	67.57	68.63	45.55	42.75	46.80	39.86	44.55	44.68	44.46	46.95	44.83	44.60	59.43	60.41
Silicates	11.12	11.52	34.32	32.20	12.00	9.35	38.98	33.13	27.16	25.46	49.88	46.85	44.77	46.35	38.69	38.50	44.36	41.91	45.72	44.30	32.36	31.91
Phosphates	0.019	0.026	0.037	0.032	0.024	0.046	0.111	1.261	0.251	0.872	0.023	1.301	1.460	0.816	0.132	0.437	0.107	0.161	0.435	0.171	0.131	0.084
Oxides	0.000	0.000	0.000	0.000	0.002	0.001	0.000	0.000	0.073	0.000	0.004	0.002	0.000	0.000	0.003	0.039	0.004	0.136	0.005	0.001	0.004	0.013
Sulphates	0.001	0.000	0.005	0.002	0.001	0.000	0.000	0.000	0.013	0.000	0.025	0.000	0.004	0.000	0.003	0.016	0.015	0.002	0.006	0.001	0.042	0.002
Other	0.00	0.00	0.61	1.03	0.18	0.32	0.00	0.00	0.01	0.00	0.00	0.00	0.02	0.02	0.00	0.00	0.01	0.02	0.04	0.11	0.00	0.01
Subtotal	**99.999**	**99.999**	**99.974**	**99.962**	**99.933**	**99.899**	**99.949**	**97.965**	**99.596**	**99.695**	**99.939**	**99.974**	**99.959**	**98.724**	**99.723**	**99.655**	**95.661**	**95.686**	**95.197**	**94.164**	**97.243**	**97.511**
Total	100.0	100.0	100.0	100.0	100.0	100.0	100.0	100.0	100.0	100.0	100.0	100.0	100.0	100.0	100.0	100.0	95.7	95.7	95.2	94.2	97.3	97.6

Element of Concern COPPER, Cu

Sample	A951 176m, Class B		A431 306m, Class A		A431 306m, Class A		A355 160.5m, Class C		A355 160.5m, Class C		A355 70.5m, Class B		A355 70.5m, Class B		A355 70.5m, Class B		A162 97.5m, Class A		A162 97.5m, Class A		A162 97.5m, Class A	
Size Fraction	-300/+150 µm		-1190/+600 µm		-75/+53 µm		-1190/+600 µm		-150/+106 µm		-600/+300 µm		-600/+300 µm		-150/+106 µm		-1190/+600 µm		-600/+300 µm		-106/+75 µm	
Spot Size*	60 kcps	100 kcps	60 kcps	100 kcps	60 kcps	100 kcps	60 kcps	100 kcps	60 kcps	100 kcps	60 kcps	100 kcps	60 kcps	100 kcps	60 kcps	100 kcps	60 kcps	100 kcps	60 kcps	100 kcps	60 kcps	100 kcps
TrampMetal	0.0000	0.0000	0.0002	0.0000	0.0027	0.0026	0.0006	0.0000	0.0079	0.0001	0.0011	0.0011	0.0013	0.0001	0.0011	0.0011	0.0004	0.0000	0.0048	0.0067	0.0010	0.0001
PyriteCu	0.0003	0.0001	0.0000	0.0001	0.0000	0.0001	0.0005	0.0185	0.0333	0.0035	0.0774	0.2105	0.1906	0.7891	0.2044	0.2121	0.0193	0.0235	0.0211	0.0085	0.0170	0.0162
Chalcocite	0.0000	0.0000	0.0013	0.0000	0.0000	0.0000	0.0000	0.0000	0.0000	0.0000	0.0000	0.0000	0.0000	0.0000	0.0000	0.0000	0.0094	0.0053	0.0017	0.0102	0.0302	0.0000
Bornite	0.0000	0.0000	0.0212	0.0157	0.0514	0.0707	0.0000	0.0000	0.0000	0.0000	0.0000	0.0000	0.0000	0.0000	0.0001	0.0001	0.7221	0.6524	0.3591	0.5988	0.9158	0.8609
Chalcopyrite	0.0453	0.0050	0.0349	1.0159	0.3665	0.4101	0.1181	0.0546	0.1830	0.0964	0.0590	0.0628	0.3076	0.5171	0.3159	0.2496	1.7339	1.4612	0.9783	0.9405	1.0027	0.9855
ChalcopyritePb	0.0024	0.0000	0.2089	0.0805	0.1055	0.1193	0.0300	0.5211	0.0126	0.0232	0.0255	0.0355	0.0628	0.1345	0.1051	0.1221	0.1372	0.5637	0.3391	0.4173	0.1992	0.2643
ChalcopyriteZn	0.0000	0.0101	0.0134	0.0055	0.1041	0.0821	0.0074	0.0019	0.0044	0.0004	0.0018	0.0014	0.0017	0.2496	0.0310	0.0355	0.0939	0.1289	0.1660	0.0553	0.1588	0.1690
Enargite	0.0000	0.0000	0.0075	0.0069	0.0026	0.0011	0.0000	0.0000	0.0000	0.0000	0.0000	0.0000	0.0000	0.0000	0.0000	0.0000	0.4820	0.2856	0.9288	0.9782	0.5283	0.4002
EnargiteZn	0.0000	0.0000	0.0135	0.0291	0.0292	0.0285	0.0000	0.0000	0.0006	0.0004	0.0000	0.0000	0.0000	0.0000	0.0000	0.0000	0.3660	1.3396	0.9392	1.6355	0.0975	0.1216
TennantiteZnFe	0.0000	0.0000	0.0011	0.0007	0.0001	0.0178	0.0000	0.0000	0.0000	0.0000	0.0000	0.0000	0.0000	0.0000	0.0000	0.0000	0.0139	0.1065	0.0042	0.0085	0.0414	0.0223
WatanabeiteZn	0.0000	0.0000	0.0004	0.0004	0.0001	0.0000	0.0000	0.0000	0.0000	0.0000	0.0000	0.0000	0.0000	0.0000	0.0000	0.0000	3.4656	2.5621	2.9251	3.2101	2.0406	1.8813
SphaleriteCu	0.0582	0.0070	0.3301	0.3089	0.9172	0.6519	0.3007	1.1654	0.1281	0.1968	0.3252	0.2689	0.3717	1.3155	1.5631	1.3879	0.4316	0.6044	0.8745	0.6928	1.4360	0.8153
SiegeniteCuFe	0.0000	0.0000	0.0000	0.0000	0.0000	0.0000	0.0000	0.0000	0.0000	0.0000	0.0000	0.0000	0.0000	0.0000	0.0000	0.0000	0.0000	0.0000	0.0044	0.0000	0.0000	0.0000
SiegeniteCuZn	0.0000	0.0000	0.0000	0.0000	0.0000	0.0000	0.0000	0.0000	0.0000	0.0000	0.0000	0.0000	0.0000	0.0000	0.0000	0.0000	0.0000	0.0000	0.0000	0.0000	0.0000	0.0000
FeOxideSulphateCuPbZnAs	0.0000	0.0001	0.0031	0.0013	0.0348	0.0534	0.0010	0.0290	0.1328	0.0590	0.0190	0.0014	0.0046	0.0006	0.2137	0.1328	0.0008	0.0110	0.0044	0.0002	0.0472	0.0573
Cuprite	0.0000	0.0000	0.0000	0.0000	0.0000	0.0000	0.0000	0.0000	0.0016	0.0000	0.0000	0.0000	0.0000	0.0000	0.0011	0.0000	0.0002	0.0000	0.0000	0.0000	0.0032	0.0017
ParamelaconiteZn	0.0000	0.0000	0.0000	0.0000	0.0000	0.0000	0.0000	0.0000	0.0000	0.0000	0.0000	0.0000	0.0000	0.0000	0.0000	0.0000	0.0000	0.0000	0.0000	0.0000	0.0000	0.0000
PbMoOxide	0.0000	0.0000	0.0000	0.0001	0.0014	0.0000	0.0000	0.0000	0.0000	0.0000	0.0001	0.0000	0.0000	0.0001	0.0000	0.0000	0.0001	0.0000	0.0000	0.0000	0.0000	0.0000
SideriteMnAsZnCrCu	0.0000	0.0000	0.0000	0.0000	0.0000	0.0000	0.0000	0.0000	0.0000	0.0000	0.0000	0.0000	0.0000	0.0000	0.0003	0.0001	0.0000	0.0000	0.0000	0.0000	0.0000	0.0000
Smithsonite_trans	0.0000	0.0000	0.0000	0.0000	0.0000	0.0000	0.0000	0.0000	0.0000	0.0000	0.0000	0.0000	0.0000	0.0000	0.0000	0.0000	0.0000	0.0000	0.0000	0.0000	0.0000	0.0000
GruneritePbCuZn	0.0054	0.0000	0.0001	0.0000	0.0001	0.0002	0.0002	0.0000	0.0000	0.0001	0.0000	0.0000	0.0000	0.0000	0.0000	0.0000	0.0014	0.0013	0.0000	0.0000	0.0000	0.0000
Malachite	0.0000	0.0000	0.0000	0.0000	0.0000	0.0000	0.0000	0.0000	0.0000	0.0000	0.0000	0.0000	0.0000	0.0000	0.0000	0.0000	0.0000	0.0000	0.0000	0.0000	0.0000	0.0000
OtaviteZnCu	0.0000	0.0000	0.0000	0.0000	0.0000	0.0000	0.0000	0.0000	0.0000	0.0000	0.0000	0.0000	0.0000	0.0000	0.0000	0.0000	0.0000	0.0000	0.0000	0.0000	0.0000	0.0000
FeSulphateLimoniteCuAsMoZn	0.0008	0.0010	0.0001	0.0000	0.0000	0.0001	0.0503	2.0057	0.2707	0.2456	0.0416	0.0248	0.0363	1.2759	0.0633	0.2126	0.0103	0.0097	0.0017	0.0041	0.0022	0.0064
JarositeCu	0.0000	0.0000	0.0000	0.0000	0.0000	0.0000	0.0000	0.0000	0.0001	0.0001	0.0000	0.0000	0.0002	0.0000	0.0001	0.0000	0.0000	0.0000	0.0000	0.0000	0.0000	0.0000
MoCaSulphatemnCuFeZn	0.0000	0.0000	0.0000	0.0000	0.0000	0.0000	0.0000	0.0000	0.0000	0.0000	0.0002	0.0000	0.0001	0.0000	0.0000	0.0000	0.0030	0.0000	0.0000	0.0000	0.0000	0.0000
MolybdofornaciteZnCu	0.0000	0.0000	0.0002	0.0000	0.0001	0.0000	0.0000	0.0000	0.0000	0.0000	0.0002	0.0005	0.0005	0.0000	0.0011	0.0000	0.0020	0.0047	0.0014	0.0003	0.0010	0.0007
Powellite_trans	0.0000	0.0000	0.0000	0.0000	0.0000	0.0000	0.0000	0.0000	0.0000	0.0000	0.0000	0.0000	0.0000	0.0000	0.0000	0.0000	0.0000	0.0000	0.0000	0.0000	0.0000	0.0000
Wulfenite_trans	0.0000	0.0000	0.0000	0.0000	0.0001	0.0000	0.0000	0.0000	0.0000	0.0000	0.0001	0.0000	0.0002	0.0000	0.0004	0.0000	0.0001	0.0000	0.0000	0.0000	0.0000	0.0000
ApatiteCuPbZn	0.0189	0.0235	0.0374	0.0306	0.0201	0.0452	0.1106	1.2612	0.2512	0.8716	0.0231	1.3007	1.4603	0.8158	0.1304	0.4374	0.1060	0.1613	0.4341	0.1703	0.1306	0.0828
FornaciteConichalcite	0.0000	0.0000	0.0000	0.0000	0.0000	0.0000	0.0000	0.0000	0.0000	0.0000	0.0000	0.0000	0.0000	0.0000	0.0000	0.0000	0.0000	0.0000	0.0000	0.0000	0.0000	0.0000
TyrolitePb	0.0000	0.0000	0.0000	0.0000	0.0000	0.0000	0.0000	0.0000	0.0000	0.0000	0.0000	0.0000	0.0000	0.0000	0.0000	0.0000	0.0000	0.0000	0.0000	0.0000	0.0000	0.0000
MicaAlteredCuZn	0.0473	0.0796	0.6831	0.1018	0.1397	0.1633	0.0925	0.0470	0.1918	0.2101	0.3653	0.7217	0.6163	0.3341	0.2332	0.6456	0.0645	0.3569	0.1113	0.2612	0.1821	0.1075
FeOxideCu	0.0000	0.0000	0.0004	0.0001	0.0008	0.0001	0.0000	0.0000	0.0003	0.0011	0.0011	0.0000	0.0000	0.0000	0.0013	0.0032	0.0000	0.0000	0.0000	0.0000	0.0000	0.0000
MoSulphatePowelliteClay	0.0000	0.0000	0.0000	0.0000	0.0000	0.0000	0.0000	0.0000	0.0000	0.0000	0.0000	0.0000	0.0000	0.0000	0.0003	0.0000	0.0000	0.0000	0.0000	0.0000	0.0000	0.0000
TitaniteMixPbCu	0.1048	0.1379	0.0552	0.0200	0.0916	0.0580	1.1764	0.1785	0.4652	1.9313	0.6770	1.6022	0.3969	2.2074	0.5551	1.1146	0.1557	0.0629	0.1449	0.2385	0.0721	0.0681
Subtotal	**0.2835**	**0.2643**	**1.4121**	**1.6175**	**1.8681**	**1.7044**	**1.8882**	**5.2829**	**1.6835**	**3.6395**	**1.6176**	**4.2314**	**3.4510**	**7.6395**	**3.4209**	**4.5545**	**7.8193**	**8.3412**	**8.2440**	**9.2367**	**6.9068**	**5.8611**
Sulphides	0.17	0.22	0.42	1.29	1.26	1.54	2.48	7.92	4.16	4.42	3.97	8.49	5.97	8.68	14.12	13.98	3.55	3.08	1.41	2.26	1.51	1.97
Carbonates	88.58	88.20	63.97	63.99	84.92	87.31	57.92	53.90	67.57	68.63	45.55	42.75	46.80	39.86	44.55	44.68	44.46	46.95	44.83	44.60	59.43	60.41
Silicates	10.96	11.31	33.58	32.07	11.77	9.13	37.71	32.90	26.50	23.32	48.83	44.53	43.76	43.81	37.90	36.73	44.14	41.48	45.47	43.80	32.11	31.73
Phosphates	0.000	0.003	0.000	0.001	0.004	0.001	0.000	0.000	0.000	0.000	0.000	0.000	0.000	0.000	0.001	0.000	0.001	0.000	0.001	0.001	0.000	0.001
Oxides	0.000	0.000	0.000	0.000	0.000	0.001	0.000	0.000	0.071	0.000	0.004	0.002	0.000	0.000	0.002	0.039	0.004	0.136	0.005	0.001	0.001	0.011
Sulphates	0.001	0.000	0.005	0.002	0.001	0.000	0.000	0.000	0.013	0.000	0.025	0.000	0.004	0.000	0.003	0.016	0.012	0.002	0.006	0.001	0.042	0.002
Other	0.00	0.00	0.61	1.03	0.17	0.32	0.00	0.00	0.00	0.00	0.00	0.00	0.02	0.02	0.00	0.00	0.01	0.01	0.03	0.11	0.00	0.01
Subtotal	**99.717**	**99.736**	**98.588**	**98.383**	**98.132**	**98.296**	**98.112**	**94.717**	**98.317**	**96.361**	**98.382**	**95.769**	**96.549**	**92.360**	**96.579**	**95.445**	**92.181**	**91.659**	**91.756**	**90.763**	**93.093**	**94.139**
Total	100.0	100.0	100.0	100.0	100.0	100.0	100.0	100.0	100.0	100.0	100.0	100.0	100.0	100.0	100.0	100.0	100.0	100.0	100.0	100.0	100.0	100.0

* = spot size measured on pure quartz in number of thousands of X-ray counts per second (kcps).

Element of Concern MOLYBDENUM, Mo

Sample	A951 176m, Class B		A431 306m, Class A		A431 306m, Class A		A355 160.5m, Class C		A355 160.5m, Class C		A355 70.5m, Class B		A355 70.5m, Class B		A355 70.5m, Class B		A162 97.5m, Class A		A162 97.5m, Class A		A162 97.5m, Class A	
Size Fraction	-300/+150 µm		-1190/+600 µm		-75/+53 µm		-1190/+600 µm		-150/+106 µm		-600/+300 µm		-600/+300 µm		-150/+106 µm		-1190/+600 µm		-600/+300 µm		-106/+75 µm	
Spot Size*	60 kcps	100 kcps	60 kcps	100 kcps	60 kcps	100 kcps	60 kcps	100 kcps	60 kcps	100 kcps	60 kcps	100 kcps	60 kcps	100 kcps	60 kcps	100 kcps	60 kcps	100 kcps	60 kcps	100 kcps	60 kcps	100 kcps
Molybdenite	0.0004	0.0027	0.1919	0.2254	0.0412	0.0470	0.0000	0.0000	0.0000	0.0000	0.0002	0.0000	0.0003	0.0000	0.0006	0.0000	0.0221	0.0178	0.0061	0.0060	0.0000	0.0000
PbMoOxide	0.0000	0.0000	0.0000	0.0001	0.0014	0.0000	0.0000	0.0000	0.0000	0.0000	0.0001	0.0000	0.0000	0.0001	0.0000	0.0000	0.0001	0.0000	0.0000	0.0000	0.0000	0.0000
PbCaOxideMoZnW	0.0000	0.0000	0.0000	0.0000	0.0000	0.0000	0.0000	0.0000	0.0000	0.0000	0.0000	0.0000	0.0000	0.0000	0.0000	0.0000	0.0000	0.0000	0.0000	0.0000	0.0000	0.0000
FeSulphateLimoniteCuAsMoZn	0.0008	0.0010	0.0001	0.0000	0.0000	0.0001	0.0503	2.0057	0.2707	0.2456	0.0416	0.0248	0.0363	1.2759	0.0633	0.2126	0.0103	0.0097	0.0017	0.0041	0.0022	0.0064
MoCaSulphateMnCuFeZn	0.0000	0.0000	0.0000	0.0000	0.0000	0.0000	0.0000	0.0000	0.0000	0.0000	0.0002	0.0000	0.0001	0.0000	0.0000	0.0000	0.0030	0.0000	0.0000	0.0000	0.0000	0.0000
MolybdofornaciteZnCu	0.0000	0.0000	0.0002	0.0000	0.0001	0.0000	0.0000	0.0000	0.0000	0.0000	0.0002	0.0005	0.0005	0.0000	0.0011	0.0000	0.0020	0.0047	0.0014	0.0003	0.0010	0.0007
Powellite_trans	0.0000	0.0000	0.0000	0.0000	0.0000	0.0000	0.0000	0.0000	0.0000	0.0000	0.0000	0.0000	0.0000	0.0000	0.0000	0.0000	0.0000	0.0000	0.0000	0.0000	0.0000	0.0000
Wulfenite_trans	0.0000	0.0000	0.0000	0.0000	0.0001	0.0000	0.0000	0.0000	0.0000	0.0000	0.0001	0.0000	0.0002	0.0000	0.0004	0.0000	0.0001	0.0000	0.0000	0.0000	0.0000	0.0000
CaMoSilicate	0.0000	0.0000	0.0000	0.0000	0.0000	0.0000	0.0000	0.0000	0.0000	0.0000	0.0000	0.0000	0.0000	0.0000	0.0000	0.0000	0.0000	0.0000	0.0000	0.0000	0.0000	0.0000
MoSulphatePowelliteClay	0.0000	0.0000	0.0000	0.0000	0.0000	0.0000	0.0000	0.0000	0.0000	0.0000	0.0000	0.0000	0.0000	0.0000	0.0003	0.0000	0.0000	0.0000	0.0000	0.0000	0.0000	0.0000
Subtotal	**0.0011**	**0.0037**	**0.1922**	**0.2255**	**0.0428**	**0.0471**	**0.0503**	**2.0057**	**0.2708**	**0.2456**	**0.0424**	**0.0253**	**0.0375**	**1.2759**	**0.0657**	**0.2126**	**0.0376**	**0.0322**	**0.0092**	**0.0104**	**0.0033**	**0.0071**
Sulphides	0.28	0.24	0.86	2.53	2.80	2.88	2.93	9.68	4.52	4.74	4.46	9.07	6.91	11.68	16.34	15.99	11.00	10.79	8.95	10.81	7.97	7.51
Carbonates	88.58	88.20	63.97	63.99	84.92	87.31	57.92	53.90	67.57	68.63	45.55	42.75	46.80	39.86	44.55	44.68	44.46	46.95	44.83	44.60	59.43	60.41
Silicates	11.12	11.52	34.32	32.20	12.00	9.35	38.98	33.13	27.16	25.46	49.88	46.85	44.77	46.35	38.69	38.50	44.36	41.91	45.72	44.30	32.36	31.91
Phosphates	0.019	0.026	0.037	0.032	0.024	0.046	0.111	1.261	0.251	0.872	0.023	1.301	1.460	0.816	0.132	0.437	0.107	0.161	0.435	0.171	0.131	0.084
Oxides	0.000	0.000	0.003	0.001	0.035	0.054	0.001	0.029	0.206	0.059	0.023	0.004	0.005	0.001	0.216	0.172	0.005	0.147	0.009	0.001	0.051	0.070
Sulphates	0.001	0.000	0.005	0.002	0.001	0.000	0.000	0.000	0.013	0.000	0.025	0.000	0.004	0.000	0.003	0.016	0.012	0.002	0.006	0.001	0.042	0.002
Other	0.00	0.00	0.61	1.03	0.18	0.32	0.00	0.00	0.01	0.00	0.00	0.00	0.02	0.02	0.00	0.00	0.01	0.01	0.04	0.11	0.00	0.01
Subtotal	**99.999**	**99.996**	**99.808**	**99.775**	**99.957**	**99.953**	**99.950**	**97.994**	**99.729**	**99.754**	**99.958**	**99.975**	**99.963**	**98.724**	**99.934**	**99.787**	**99.962**	**99.968**	**99.991**	**99.990**	**99.997**	**99.993**
Total	100.0	100.0	100.0	100.0	100.0	100.0	100.0	100.0	100.0	100.0	100.0	100.0	100.0	100.0	100.0	100.0	100.0	100.0	100.0	100.0	100.0	100.0

* = spot size measured on pure quartz in number of thousands of X-ray counts per second (kcps).

Element of Concern LEAD, Pb

Sample	A951 176m, Class B		A431 306m, Class A		A431 306m, Class A		A355 160.5m, Class C		A355 160.5m, Class C		A355 70.5m, Class B		A355 70.5m, Class B		A355 70.5m, Class B		A162 97.5m, Class A		A162 97.5m, Class A		A162 97.5m, Class A	
Size Fraction	-300/+150 µm		-1190/+600 µm		-75/+53 µm		-1190/+600 µm		-150/+106 µm		-600/+300 µm		-600/+300 µm		-150/+106 µm		-1190/+600 µm		-600/+300 µm		-106/+75 µm	
Spot Size*	60 kcps	100 kcps	60 kcps	100 kcps	60 kcps	100 kcps	60 kcps	100 kcps	60 kcps	100 kcps	60 kcps	100 kcps	60 kcps	100 kcps	60 kcps	100 kcps	60 kcps	100 kcps	60 kcps	100 kcps	60 kcps	100 kcps
ChalcopyritePb	0.0024	0.0000	0.1485	0.0805	0.1055	0.1193	0.0300	0.5211	0.0126	0.0232	0.0255	0.0355	0.0628	0.1345	0.1051	0.1221	0.1372	0.5637	0.3391	0.4173	0.1992	0.2643
GalenaSe	0.0972	0.1248	0.1548	0.0622	0.1745	0.2175	0.0002	0.0002	0.0007	0.0036	0.0304	0.0259	0.0288	0.8265	0.0576	0.1690	1.0617	1.0380	0.0991	0.0974	0.0385	0.0304
Galenobismutite	0.0000	0.0000	0.0000	0.0000	0.0000	0.0000	0.0000	0.0000	0.0000	0.0002	0.0000	0.0000	0.0000	0.0000	0.0000	0.0000	0.0000	0.0000	0.0000	0.0000	0.0000	0.0000
FeOxide SulphateCuPbZnAs	0.0000	0.0001	0.0035	0.0013	0.0348	0.0534	0.0010	0.0290	0.1328	0.0590	0.0190	0.0014	0.0046	0.0006	0.2137	0.1328	0.0008	0.0110	0.0044	0.0002	0.0472	0.0573
PbMoOxide	0.0000	0.0000	0.0001	0.0001	0.0014	0.0000	0.0000	0.0000	0.0000	0.0000	0.0001	0.0000	0.0000	0.0001	0.0000	0.0000	0.0001	0.0000	0.0000	0.0000	0.0000	0.0000
PbCaOxideMoZnW	0.0000	0.0000	0.0000	0.0000	0.0000	0.0000	0.0000	0.0000	0.0000	0.0000	0.0000	0.0000	0.0000	0.0000	0.0000	0.0000	0.0000	0.0000	0.0000	0.0000	0.0000	0.0000
GruneritePbCuZn	0.0054	0.0000	0.0011	0.0000	0.0001	0.0002	0.0002	0.0000	0.0000	0.0001	0.0000	0.0000	0.0000	0.0000	0.0000	0.0000	0.0014	0.0013	0.0000	0.0000	0.0000	0.0000
MolybdofornaciteZnCu	0.0000	0.0000	0.0007	0.0000	0.0001	0.0000	0.0000	0.0000	0.0000	0.0000	0.0002	0.0005	0.0005	0.0000	0.0011	0.0000	0.0020	0.0047	0.0014	0.0003	0.0010	0.0007
Powellite_trans	0.0000	0.0000	0.0000	0.0000	0.0000	0.0000	0.0000	0.0000	0.0000	0.0000	0.0000	0.0000	0.0000	0.0000	0.0000	0.0000	0.0000	0.0000	0.0000	0.0000	0.0000	0.0000
Wulfenite_trans	0.0000	0.0000	0.0008	0.0000	0.0001	0.0000	0.0000	0.0000	0.0000	0.0000	0.0001	0.0000	0.0002	0.0000	0.0004	0.0000	0.0001	0.0000	0.0000	0.0000	0.0000	0.0000
ApatiteCuPbZn	0.0189	0.0235	0.0589	0.0306	0.0201	0.0452	0.1106	1.2612	0.2512	0.8716	0.0231	1.3007	1.4603	0.8158	0.1304	0.4374	0.1060	0.1613	0.4341	0.1703	0.1306	0.0828
FornaciteConichalcite	0.0000	0.0000	0.0000	0.0000	0.0000	0.0000	0.0000	0.0000	0.0000	0.0000	0.0000	0.0000	0.0000	0.0000	0.0000	0.0000	0.0000	0.0000	0.0000	0.0000	0.0000	0.0000
TyrolitePb	0.0000	0.0000	0.0000	0.0000	0.0000	0.0000	0.0000	0.0000	0.0000	0.0000	0.0000	0.0000	0.0000	0.0000	0.0000	0.0000	0.0000	0.0000	0.0000	0.0000	0.0000	0.0000
MoSulphatePowelliteClay	0.0000	0.0000	0.0000	0.0000	0.0000	0.0000	0.0000	0.0000	0.0000	0.0000	0.0000	0.0000	0.0000	0.0000	0.0003	0.0000	0.0000	0.0000	0.0000	0.0000	0.0000	0.0000
TitaniteMixPbCu	0.1048	0.1379	0.0705	0.0200	0.0916	0.0580	1.1764	0.1785	0.4652	1.9313	0.6770	1.6022	0.3969	2.2074	0.5551	1.1146	0.1557	0.0629	0.1449	0.2385	0.0721	0.0681
Subtotal	**0.2287**	**0.2863**	**0.4387**	**0.1946**	**0.4281**	**0.4936**	**1.3184**	**1.9900**	**0.8625**	**2.8890**	**0.7752**	**2.9662**	**1.9540**	**3.9848**	**1.0637**	**1.9757**	**1.4650**	**1.8429**	**1.0230**	**0.9239**	**0.4887**	**0.5036**
Sulphides	0.18	0.12	1.41	2.61	2.56	2.59	2.90	9.16	4.51	4.71	4.40	9.01	6.81	10.72	16.18	15.70	9.82	9.21	8.52	10.30	7.74	7.21
Carbonates	88.58	88.20	64.52	63.99	84.92	87.31	57.92	53.90	67.57	68.63	45.55	42.75	46.80	39.86	44.55	44.68	44.46	46.95	44.83	44.60	59.43	60.41
Silicates	11.01	11.39	32.93	32.18	11.91	9.29	37.81	32.95	26.69	23.53	49.20	45.25	44.37	44.14	38.14	37.38	44.21	41.84	45.58	44.06	32.29	31.84
Phosphates	0.000	0.003	0.000	0.001	0.004	0.001	0.000	0.000	0.000	0.000	0.000	0.000	0.000	0.000	0.001	0.000	0.001	0.000	0.001	0.001	0.000	0.001
Oxides	0.000	0.000	0.001	0.000	0.000	0.001	0.000	0.000	0.073	0.000	0.004	0.002	0.000	0.000	0.003	0.039	0.004	0.136	0.005	0.001	0.004	0.013
Sulphates	0.002	0.001	0.012	0.002	0.002	0.000	0.051	2.006	0.283	0.246	0.067	0.025	0.040	1.276	0.066	0.229	0.025	0.012	0.008	0.006	0.045	0.008
Other	0.00	0.00	0.68	1.03	0.18	0.32	0.00	0.00	0.01	0.00	0.00	0.00	0.02	0.02	0.00	0.00	0.01	0.01	0.04	0.11	0.00	0.01
Subtotal	**99.771**	**99.714**	**99.561**	**99.805**	**99.572**	**99.506**	**98.682**	**98.010**	**99.138**	**97.111**	**99.225**	**97.034**	**98.046**	**96.015**	**98.936**	**98.024**	**98.535**	**98.157**	**98.977**	**99.076**	**99.511**	**99.496**
Total	100.0	100.0	100.0	100.0	100.0	100.0	100.0	100.0	100.0	100.0	100.0	100.0	100.0	100.0	100.0	100.0	100.0	100.0	100.0	100.0	100.0	100.0

Element of Concern ZINC,Zn

Sample	A951 176m, Class B		A431 306m, Class A		A431 306m, Class A		A355 160.5m, Class C		A355 160.5m, Class C		A355 70.5m, Class B		A355 70.5m, Class B		A355 70.5m, Class B		A162 97.5m, Class A		A162 97.5m, Class A		A162 97.5m, Class A	
Size Fraction	-300/+150 µm		-1190/+600 µm		-75/+53 µm		-1190/+600 µm		-150/+106 µm		-600/+300 µm		-600/+300 µm		-150/+106 µm		-1190/+600 µm		-600/+300 µm		-106/+75 µm	
Spot Size*	60 kcps	100 kcps	60 kcps	100 kcps	60 kcps	100 kcps	60 kcps	100 kcps	60 kcps	100 kcps	60 kcps	100 kcps	60 kcps	100 kcps	60 kcps	100 kcps	60 kcps	100 kcps	60 kcps	100 kcps	60 kcps	100 kcps
TrampMetal	0.0000	0.0000	0.0002	0.0000	0.0027	0.0026	0.0006	0.0000	0.0079	0.0001	0.0011	0.0011	0.0013	0.0001	0.0011	0.0011	0.0004	0.0000	0.0048	0.0067	0.0010	0.0001
AgSulphosalt	0.0000	0.0000	0.0000	0.0000	0.0017	0.0051	0.0000	0.0000	0.0000	0.0000	0.0000	0.0000	0.0002	0.0000	0.0000	0.0000	0.0000	0.0000	0.0000	0.0000	0.0003	0.0000
ChalcopyriteZn	0.0000	0.0101	0.0134	0.0055	0.1041	0.0821	0.0074	0.0019	0.0044	0.0004	0.0018	0.0014	0.0017	0.2496	0.0310	0.0355	0.0939	0.1289	0.1660	0.0553	0.1588	0.1690
EnargiteZn	0.0000	0.0000	0.0135	0.0291	0.0292	0.0285	0.0000	0.0000	0.0006	0.0004	0.0000	0.0000	0.0000	0.0000	0.0000	0.0000	0.3660	1.3396	0.9392	1.6355	0.0975	0.1216
TennantiteZnFe	0.0000	0.0000	0.0011	0.0007	0.0001	0.0178	0.0000	0.0000	0.0000	0.0000	0.0000	0.0000	0.0000	0.0000	0.0000	0.0000	0.0139	0.1065	0.0042	0.0085	0.0414	0.0223
WatanabeiteZn	0.0000	0.0000	0.0004	0.0004	0.0001	0.0000	0.0000	0.0000	0.0000	0.0000	0.0000	0.0000	0.0000	0.0000	0.0000	0.0000	3.4656	2.5621	2.9251	3.2101	2.0406	1.8813
Sphalerite	0.0009	0.0019	0.1191	0.9525	0.9920	1.2119	0.0068	0.0048	0.0057	0.0000	0.0156	0.0012	0.0468	0.3623	0.0828	0.0870	1.6521	1.2499	1.1637	1.4192	1.0749	1.4472
SphaleriteCu	0.0582	0.0070	0.3301	0.3089	0.9172	0.6519	0.3007	1.1654	0.1281	0.1968	0.3252	0.2689	0.3717	1.3155	1.5631	1.3879	0.4316	0.6044	0.8745	0.6928	1.4360	0.8153
SiegeniteCuZn	0.0000	0.0000	0.0000	0.0000	0.0000	0.0000	0.0000	0.0000	0.0000	0.0000	0.0000	0.0000	0.0000	0.0000	0.0000	0.0000	0.0000	0.0000	0.0000	0.0000	0.0000	0.0000
FeOxideSulphateCuPbZnAs	0.0000	0.0001	0.0031	0.0013	0.0348	0.0534	0.0010	0.0290	0.1328	0.0590	0.0190	0.0014	0.0046	0.0006	0.2137	0.1328	0.0008	0.0110	0.0044	0.0002	0.0472	0.0573
ParamelaconiteZn	0.0000	0.0000	0.0000	0.0000	0.0000	0.0000	0.0000	0.0000	0.0000	0.0000	0.0000	0.0000	0.0000	0.0000	0.0000	0.0000	0.0000	0.0000	0.0000	0.0000	0.0000	0.0000
Wulfingite	0.0000	0.0000	0.0000	0.0000	0.0000	0.0000	0.0000	0.0000	0.0000	0.0000	0.0000	0.0000	0.0000	0.0000	0.0000	0.0000	0.0000	0.0000	0.0000	0.0000	0.0000	0.0000
PbCaOxideMoZnW	0.0000	0.0000	0.0000	0.0000	0.0000	0.0000	0.0000	0.0000	0.0000	0.0000	0.0000	0.0000	0.0000	0.0000	0.0000	0.0000	0.0000	0.0000	0.0000	0.0000	0.0000	0.0000
SideriteMnAsZnCrCu	0.0000	0.0000	0.0000	0.0000	0.0000	0.0000	0.0000	0.0000	0.0000	0.0000	0.0000	0.0000	0.0000	0.0000	0.0003	0.0001	0.0000	0.0000	0.0000	0.0000	0.0000	0.0000
Smithsonite_trans	0.0000	0.0000	0.0000	0.0000	0.0000	0.0000	0.0000	0.0000	0.0000	0.0000	0.0000	0.0000	0.0000	0.0000	0.0000	0.0000	0.0000	0.0000	0.0000	0.0000	0.0000	0.0000
GruneritePbCuZn	0.0054	0.0000	0.0001	0.0000	0.0001	0.0002	0.0002	0.0000	0.0000	0.0001	0.0000	0.0000	0.0000	0.0000	0.0000	0.0000	0.0014	0.0013	0.0000	0.0000	0.0000	0.0000
OtaviteZnCu	0.0000	0.0000	0.0000	0.0000	0.0000	0.0000	0.0000	0.0000	0.0000	0.0000	0.0000	0.0000	0.0000	0.0000	0.0000	0.0000	0.0000	0.0000	0.0000	0.0000	0.0000	0.0000
Goslarite	0.0000	0.0000	0.0003	0.0000	0.0001	0.0000	0.0001	0.0000	0.0000	0.0000	0.0002	0.0000	0.0000	0.0000	0.0001	0.0000	0.0010	0.0001	0.0001	0.0001	0.0000	0.0000
FeSulphateLimoniteCuAsMoZn	0.0008	0.0010	0.0001	0.0000	0.0000	0.0001	0.0503	2.0057	0.2707	0.2456	0.0416	0.0248	0.0363	1.2759	0.0633	0.2126	0.0103	0.0097	0.0017	0.0041	0.0022	0.0064
MoCaSulphateMnCuFeZn	0.0000	0.0000	0.0000	0.0000	0.0000	0.0000	0.0000	0.0000	0.0000	0.0000	0.0002	0.0000	0.0001	0.0000	0.0000	0.0000	0.0030	0.0000	0.0000	0.0000	0.0000	0.0000
MolybdofornaciteZnCu	0.0000	0.0000	0.0002	0.0000	0.0001	0.0000	0.0000	0.0000	0.0000	0.0000	0.0002	0.0005	0.0005	0.0000	0.0011	0.0000	0.0020	0.0047	0.0014	0.0003	0.0010	0.0007
Powellite_trans	0.0000	0.0000	0.0000	0.0000	0.0000	0.0000	0.0000	0.0000	0.0000	0.0000	0.0000	0.0000	0.0000	0.0000	0.0000	0.0000	0.0000	0.0000	0.0000	0.0000	0.0000	0.0000
Wulfenite_trans	0.0000	0.0000	0.0000	0.0000	0.0001	0.0000	0.0000	0.0000	0.0000	0.0000	0.0001	0.0000	0.0002	0.0000	0.0004	0.0000	0.0001	0.0000	0.0000	0.0000	0.0000	0.0000
ApatiteCuPbZn	0.0189	0.0235	0.0374	0.0306	0.0201	0.0452	0.1106	1.2612	0.2512	0.8716	0.0231	1.3007	1.4603	0.8158	0.1304	0.4374	0.1060	0.1613	0.4341	0.1703	0.1306	0.0828
TyrolitePb	0.0000	0.0000	0.0000	0.0000	0.0000	0.0000	0.0000	0.0000	0.0000	0.0000	0.0000	0.0000	0.0000	0.0000	0.0000	0.0000	0.0000	0.0000	0.0000	0.0000	0.0000	0.0000
MicaAlteredCuZn	0.0473	0.0796	0.6831	0.1018	0.1397	0.1633	0.0925	0.0470	0.1918	0.2101	0.3653	0.7217	0.6163	0.3341	0.2332	0.6456	0.0645	0.3569	0.1113	0.2612	0.1821	0.1075
Willemite	0.0000	0.0000	0.0000	0.0000	0.0000	0.0000	0.0000	0.0000	0.0000	0.0000	0.0000	0.0000	0.0000	0.0000	0.0000	0.0000	0.0000	0.0000	0.0000	0.0000	0.0000	0.0000
Subtotal	**0.1315**	**0.1232**	**1.2021**	**1.4308**	**2.2421**	**2.2620**	**0.5701**	**4.5151**	**0.9932**	**1.5839**	**0.7933**	**2.3216**	**2.5399**	**4.3537**	**2.3205**	**2.9399**	**6.2125**	**6.5365**	**6.6304**	**7.4641**	**5.2136**	**4.7114**
Sulphides	0.22	0.22	0.57	1.45	0.80	0.93	2.62	8.51	4.38	4.54	4.11	8.80	6.49	9.76	14.66	14.48	5.00	4.82	2.88	3.80	3.12	3.05
Carbonates	88.58	88.20	63.97	63.99	84.92	87.31	57.92	53.90	67.57	68.63	45.55	42.75	46.80	39.86	44.55	44.68	44.46	46.95	44.83	44.60	59.43	60.41
Silicates	11.07	11.44	33.63	32.09	11.86	9.19	38.89	33.08	26.96	25.25	49.51	46.13	44.15	46.01	38.46	37.85	44.30	41.55	45.61	44.03	32.18	31.80
Phosphates	0.000	0.003	0.000	0.001	0.004	0.001	0.000	0.000	0.000	0.000	0.000	0.000	0.000	0.000	0.001	0.000	0.001	0.000	0.001	0.001	0.000	0.001
Oxides	0.000	0.000	0.000	0.000	0.002	0.001	0.000	0.000	0.073	0.000	0.004	0.002	0.000	0.000	0.003	0.039	0.004	0.136	0.005	0.001	0.004	0.013
Sulphates	0.001	0.000	0.004	0.002	0.001	0.000	0.000	0.000	0.013	0.000	0.025	0.000	0.004	0.000	0.003	0.016	0.011	0.002	0.006	0.001	0.042	0.002
Other	0.00	0.00	0.61	1.03	0.17	0.32	0.00	0.00	0.00	0.00	0.00	0.00	0.02	0.02	0.00	0.00	0.01	0.01	0.03	0.11	0.00	0.01
Subtotal	**99.868**	**99.877**	**98.798**	**98.569**	**97.758**	**97.738**	**99.430**	**95.485**	**99.007**	**98.416**	**99.207**	**97.678**	**97.460**	**95.646**	**97.680**	**97.060**	**93.787**	**93.464**	**93.370**	**92.536**	**94.786**	**95.289**
Total	100.0	100.0	100.0	100.0	100.0	100.0	100.0	100.0	100.0	100.0	100.0	100.0	100.0	100.0	100.0	100.0	100.0	100.0	100.0	100.0	100.0	100.0

* = spot size measured on pure quartz in number of thousands of X-ray counts per second (kcps).

APPENDIX 8 Effect of dwell time

Modal Mineralogy (weight-%, normalized)

Mineral Group	Sample	A951 176m, Class B			A431 306m, Class A			A431 306m, Class A			A355 160.5m, Class C			A355 160.5m, Class C			A355 70.5m, Class B			A355 70.5m, Class B			A355 70.5m, Class B			A162 97.5m, Class A			A162 97.5m, Class A			A162 97.5m, Class A		
	Size Fraction	-300/+150 µm			-1190/+600 µm			-75/+53 µm			-1190/+600 µm			-150/+106 µm			-600/+300 µm			-600/+300 µm			-150/+106 µm			-1190/+600 µm			-600/+300 µm			-106/+75 µm		
	Dwell Time	16	8	32	16	8	32	16	8	32	16	8	32	16	8	32	16	8	32	16	8	32	16	8	32	16	8	32	16	8	32	16	8	32
Sulphide	Bornite	0.000	0.000	0.000	0.020	0.007	0.022	0.051	0.069	0.065	0.000	0.000	0.000	0.000	0.000	0.000	0.000	0.000	0.000	0.000	0.000	0.000	0.000	0.000	0.000	0.500	0.691	0.476	0.360	0.335	0.389	0.916	0.840	0.797
	Galena	0.100	0.111	0.111	0.060	0.061	0.053	0.174	0.183	0.199	0.000	0.000	0.000	0.000	0.003	0.004	0.030	0.378	0.385	0.030	0.384	0.405	0.058	0.291	0.214	1.030	1.060	0.925	0.100	0.093	0.094	0.039	0.037	0.037
	Sphalerite	0.060	0.052	0.052	0.450	0.683	0.378	1.909	2.133	1.855	0.310	0.373	0.197	0.130	0.118	0.156	0.340	0.264	0.267	0.420	0.805	0.831	1.646	1.590	1.596	1.420	1.949	1.758	2.040	2.359	2.252	2.511	2.537	2.402
	Chalcopyrite	0.050	0.033	0.042	0.260	0.271	0.270	0.576	0.575	0.628	0.160	0.038	0.854	0.200	0.145	0.151	0.090	0.088	0.092	0.370	0.507	0.386	0.452	0.472	0.447	1.880	1.580	1.903	1.480	1.470	1.391	1.361	1.526	1.386
	Pyrrhotite	0.000	0.005	0.003	0.030	0.024	0.025	0.053	0.052	0.052	0.980	3.088	3.959	2.750	2.973	3.419	0.310	1.843	1.768	0.400	1.385	1.962	1.190	1.475	1.596	0.370	0.196	0.362	0.010	0.135	0.123	0.182	0.153	0.185
	Realgar-Orpiment	0.000	0.000	0.000	0.000	0.000	0.000	0.000	0.000	0.000	0.000	0.000	0.000	0.000	0.000	0.000	0.000	0.000	0.000	0.000	0.000	0.000	0.000	0.000	0.000	0.000	0.000	0.000	0.000	0.000	0.000	0.000	0.000	0.000
	Stibnite	0.000	0.000	0.000	0.000	0.000	0.000	0.000	0.000	0.000	0.000	0.000	0.000	0.000	0.000	0.000	0.000	0.000	0.000	0.000	0.000	0.000	0.000	0.000	0.000	0.020	0.005	0.005	0.000	0.001	0.001	0.001	0.000	0.000
	Watanabeite	0.000	0.000	0.000	0.000	0.000	0.000	0.000	0.000	0.000	0.000	0.000	0.000	0.000	0.000	0.000	0.000	0.000	0.000	0.000	0.000	0.000	0.000	0.000	0.000	3.730	1.787	2.553	2.930	2.405	2.505	2.041	1.867	1.853
	Pyrite	0.070	0.077	0.077	0.020	0.021	0.021	0.000	0.001	0.000	1.490	2.482	2.433	1.440	1.622	1.732	3.680	5.895	6.063	5.680	6.245	6.709	12.993	12.426	12.749	0.470	0.409	0.442	0.150	0.156	0.158	0.227	0.274	0.258
	Molybdenite	0.000	0.000	0.000	0.190	0.177	0.190	0.041	0.055	0.050	0.000	0.000	0.000	0.000	0.000	0.000	0.000	0.000	0.000	0.000	0.000	0.000	0.001	0.000	0.000	0.020	0.021	0.022	0.010	0.005	0.007	0.000	0.000	0.000
	Enargite	0.000	0.000	0.000	0.020	0.014	0.018	0.032	0.034	0.035	0.000	0.000	0.000	0.000	0.000	0.000	0.000	0.000	0.000	0.000	0.000	0.000	0.000	0.000	0.000	1.000	2.168	1.898	1.870	2.362	2.818	0.626	0.603	0.639
	Others	0.000	0.000	0.000	0.000	0.001	0.002	0.002	0.002	0.015	0.000	0.002	0.002	0.000	0.000	0.000	0.000	0.000	0.000	0.000	0.000	0.000	0.001	0.000	0.001	0.020	0.010	0.013	0.010	0.009	0.013	0.072	0.022	0.034
	Subtotal	**0.28**	**0.28**	**0.28**	**1.05**	**1.26**	**0.98**	**2.84**	**3.11**	**2.90**	**2.94**	**5.98**	**7.44**	**4.52**	**4.86**	**5.46**	**4.45**	**8.47**	**8.58**	**6.90**	**9.33**	**10.29**	**16.34**	**16.25**	**16.60**	**10.46**	**9.87**	**10.36**	**8.96**	**9.33**	**9.75**	**7.97**	**7.86**	**7.59**
Carbonate	Calcite	88.580	87.962	87.244	63.790	61.279	63.095	84.601	84.680	85.349	57.920	53.066	51.292	67.570	67.400	68.307	45.550	44.227	44.212	46.790	44.375	46.353	44.527	44.870	44.701	47.740	43.489	47.920	44.830	43.750	46.278	59.433	59.400	59.762
	Otavite	0.000	0.000	0.000	0.000	0.000	0.000	0.000	0.000	0.000	0.000	0.000	0.000	0.000	0.000	0.000	0.000	0.000	0.000	0.000	0.000	0.000	0.000	0.000	0.000	0.000	0.000	0.000	0.000	0.000	0.000	0.000	0.000	0.000
	Siderite	0.000	0.000	0.000	0.000	0.000	0.000	0.000	0.000	0.000	0.000	0.000	0.000	0.000	0.000	0.000	0.000	0.000	0.000	0.000	0.000	0.000	0.000	0.002	0.000	0.000	0.000	0.000	0.000	0.000	0.000	0.000	0.000	0.000
	Dolomite	0.000	0.000	0.000	0.190	0.125	0.128	0.312	0.292	0.183	0.000	0.000	0.000	0.000	0.003	0.000	0.000	0.000	0.000	0.000	0.000	0.066	0.018	0.022	0.044	0.010	0.001	0.000	0.000	0.001	0.001	0.000	0.006	0.000
	Others	0.000	0.000	0.000	0.000	0.000	0.001	0.004	0.003	0.014	0.000	0.000	0.000	0.000	0.000	0.003	0.000	0.000	0.000	0.000	0.000	0.000	0.005	0.004	0.013	0.000	0.001	0.000	0.000	0.001	0.000	0.000	0.000	0.000
	Subtotal	**88.58**	**87.96**	**87.24**	**63.98**	**61.40**	**63.22**	**84.92**	**84.97**	**85.55**	**57.92**	**53.07**	**51.29**	**67.57**	**67.40**	**68.31**	**45.55**	**44.23**	**44.21**	**46.79**	**44.38**	**46.42**	**44.55**	**44.90**	**44.76**	**47.75**	**43.49**	**47.92**	**44.83**	**43.75**	**46.28**	**59.43**	**59.41**	**59.76**
Silicate	Biotite	0.000	0.124	0.124	0.020	1.320	0.003	0.108	0.052	0.093	0.740	0.593	0.582	0.340	0.308	0.375	0.350	0.616	0.743	0.440	0.396	0.265	0.250	0.419	0.326	0.880	0.806	1.111	0.530	0.744	0.291	0.154	0.124	0.109
	Chlorite	0.000	0.000	0.000	0.030	0.026	0.030	0.009	0.020	0.007	0.010	0.003	0.007	0.130	0.052	0.049	0.360	0.198	0.374	0.100	0.267	0.559	0.109	0.510	0.221	0.030	0.036	0.015	0.070	0.016	0.083	0.049	0.029	0.028
	K_Feldspar	0.100	0.144	0.118	0.120	0.000	0.002	0.061	0.049	0.052	4.390	3.925	1.144	3.100	2.454	2.344	5.470	3.268	2.282	4.950	3.833	3.263	3.988	3.422	3.715	0.450	0.165	0.462	0.440	0.335	0.235	0.215	0.170	0.249
	Kaolinite	0.000	0.000	0.000	0.000	0.000	0.000	0.000	0.000	0.000	0.000	0.000	0.000	0.000	0.000	0.001	0.000	0.082	0.129	0.410	0.286	0.399	0.002	0.257	0.462	0.000	0.000	0.000	0.000	0.000	0.000	0.000	0.000	0.000
	Muscovite	0.000	0.000	0.000	0.000	0.000	0.000	0.000	0.000	0.000	0.000	0.000	0.000	0.040	0.001	0.024	0.020	0.137	0.196	0.000	0.007	0.008	0.054	0.103	0.087	0.000	0.000	0.000	0.170	0.046	0.002	0.000	0.000	0.002
	Plagioclase	0.560	0.557	0.418	0.860	1.631	0.692	0.299	0.533	0.353	8.050	11.326	11.142	6.260	7.279	6.258	15.240	15.739	15.164	14.610	15.891	15.207	11.157	11.435	10.383	2.520	2.862	1.442	2.430	1.361	1.192	0.479	0.662	0.497
	Pyroxene	3.320	3.928	4.485	13.680	13.655	13.297	5.153	4.262	4.186	10.300	9.146	5.818	5.850	5.837	5.848	7.860	10.007	8.106	8.200	6.787	5.909	7.422	7.249	7.293	7.110	10.000	8.666	9.370	11.156	9.836	14.415	14.204	14.104
	Quartz	0.590	0.641	0.649	0.000	0.000	1.172	0.044	0.073	0.058	0.400	0.234	0.447	0.920	0.939	0.980	1.000	0.927	1.376	0.790	0.994	1.124	1.127	1.585	1.639	1.660	1.318	1.558	0.990	2.027	1.955	1.237	1.125	1.107
	Talc	0.060	0.000	0.000	0.000	0.000	0.000	0.000	0.000	0.000	0.000	0.000	0.000	0.000	0.000	0.000	0.000	0.000	0.000	0.000	0.000	0.000	0.000	0.000	0.000	0.000	0.000	0.000	0.000	0.000	0.000	0.000	0.000	0.000
	Mica	0.050	0.000	0.121	0.690	0.151	0.477	0.159	0.170	0.281	4.370	7.231	6.425	3.560	4.515	3.852	3.830	3.050	3.501	2.980	3.292	3.045	3.140	3.986	3.217	0.500	0.668	0.562	0.530	0.355	0.440	0.256	0.241	0.167
	Titanite	0.100	0.178	0.062	0.060	0.005	0.024	0.092	0.058	0.071	1.180	0.587	1.371	0.470	0.707	1.489	0.680	0.418	1.293	0.400	1.090	1.238	0.555	0.756	2.136	0.110	0.050	0.077	0.140	0.192	0.042	0.072	0.016	0.054
	Others	6.340	6.173	6.431	18.870	19.673	19.377	6.077	6.431	6.066	9.540	5.890	13.881	6.500	4.544	4.295	15.070	12.357	13.155	11.880	12.909	11.149	10.888	8.103	8.318	28.320	30.458	27.087	31.060	30.389	29.453	15.485	16.035	16.190
	Subtotal	**11.12**	**11.74**	**12.41**	**34.33**	**36.46**	**35.07**	**12.00**	**11.65**	**11.17**	**38.98**	**38.93**	**40.82**	**27.17**	**26.64**	**25.52**	**49.88**	**46.80**	**46.32**	**44.76**	**45.75**	**42.17**	**38.69**	**37.82**	**37.80**	**41.58**	**46.36**	**40.98**	**45.73**	**46.62**	**43.53**	**32.36**	**32.61**	**32.51**
Phosphate	**Subtotal**	0.020	0.013	0.038	0.040	0.015	0.034	0.024	0.017	0.029	0.110	0.985	0.179	0.250	0.464	0.358	0.020	0.437	0.838	1.460	0.329	1.065	0.132	0.407	0.676	0.100	0.032	0.707	0.430	0.272	0.220	0.131	0.046	0.084
Oxide	FeOxyhydroxides	0.000	0.000	0.000	0.000	0.001	0.002	0.035	0.039	0.058	0.000	0.000	0.000	0.200	0.213	0.103	0.020	0.031	0.016	0.000	0.161	0.004	0.214	0.415	0.095	0.020	0.008	0.007	0.000	0.002	0.188	0.048	0.044	0.044
	Others	0.000	0.000	0.000	0.000	0.000	0.000	0.001	0.000	0.000	0.000	0.000	0.000	0.000	0.000	0.045	0.000	0.000	0.000	0.000	0.000	0.000	0.003	0.000	0.001	0.000	0.000	0.000	0.000	0.000	0.000	0.003	0.000	0.002
	Subtotal	**0.000**	**0.000**	**0.000**	**0.000**	**0.001**	**0.002**	**0.036**	**0.039**	**0.058**	**0.000**	**0.000**	**0.000**	**0.200**	**0.213**	**0.148**	**0.020**	**0.031**	**0.016**	**0.000**	**0.161**	**0.004**	**0.216**	**0.415**	**0.096**	**0.020**	**0.008**	**0.008**	**0.000**	**0.002**	**0.188**	**0.051**	**0.044**	**0.046**
Sulphate	FeSulphate	0.000	0.000	0.026	0.000	0.000	0.000	0.000	0.000	0.000	0.050	1.032	0.102	0.280	0.419	0.204	0.040	0.036	0.037	0.040	0.038	0.033	0.065	0.202	0.071	0.010	0.222	0.008	0.000	0.003	0.006	0.043	0.035	0.005
	Barite	0.000	0.000	0.000	0.000	0.000	0.000	0.000	0.000	0.000	0.000	0.000	0.000	0.000	0.000	0.000	0.000	0.000	0.000	0.000	0.000	0.000	0.000	0.000	0.000	0.000	0.000	0.000	0.000	0.000	0.000	0.000	0.000	0.000
	Gypsum	0.000	0.000	0.000	0.000	0.001	0.002	0.001	0.001	0.000	0.000	0.000	0.000	0.000	0.000	0.000	0.020	0.000	0.000	0.000	0.001	0.000	0.001	0.001	0.000	0.070	0.006	0.001	0.010	0.001	0.001	0.002	0.000	0.000
	Others	0.000	0.000	0.000	0.000	0.000	0.000	0.000	0.000	0.000	0.000	0.000	0.000	0.000	0.000	0.000	0.000	0.000	0.000	0.000	0.000	0.000	0.000	0.000	0.000	0.000	0.000	0.000	0.000	0.000	0.000	0.000	0.000	0.000
	Subtotal	**0.000**	**0.001**	**0.026**	**0.000**	**0.001**	**0.002**	**0.001**	**0.001**	**0.000**	**0.050**	**1.032**	**0.102**	**0.280**	**0.419**	**0.204**	**0.060**	**0.036**	**0.037**	**0.040**	**0.039**	**0.033**	**0.066**	**0.203**	**0.071**	**0.080**	**0.228**	**0.009**	**0.010**	**0.004**	**0.008**	**0.045**	**0.035**	**0.006**
Other	**Subtotal**	0.000	0.000	0.000	0.610	0.861	0.685	0.178	0.215	0.303	0.000	0.000	0.164	0.010	0.005	0.000	0.000	0.001	0.004	0.020	0.018	0.019	0.003	0.000	0.001	0.020	0.005	0.019	0.040	0.022	0.026	0.004	0.003	0.004
Total Mineralogy		**100.0**	**100.0**	**100.0**	**100.0**	**100.0**	**100.0**	**100.0**	**100.0**	**100.0**	**100.0**	**100.0**	**100.0**	**100.0**	**100.0**	**100.0**	**100.0**	**100.0**	**100.0**	**100.0**	**100.0**	**100.0**	**100.0**	**100.0**	**100.0**	**100.0**	**100.0**	**100.0**	**100.0**	**100.0**	**100.0**	**100.0**	**100.0**	**100.0**
# Particles Analyzed		2564	2336	2332	513	419	442	12579	12501	12500	295	299	307	4860	5196	5193	1110	950	934	819	1048	1011	7634	6563	6550	601	508	569	1222	1305	1311	7838	11073	10997
# Grains Analyzed		4299	3696	4006	8569	8355	8315	15110	15098	14405	5891	1625	2954	9565	10377	8555	6206	4795	4675	7087	5642	6373	17267	16919	14896	14754	10502	12743	8982	9307	10299	11463	16094	15150
# Frames Analyzed		72	63	63	60	63	63	112	120	120	64	64	64	96	88	88	72	64	64	63	64	64	108	96	96	70	63	63	63	64	64	105	117	117
Analysis Time (min)		32	25	39	43	42	58	49	49	74	36	37	50	41	27	56	36	31	45	31	31	47	54	49	66	54	53	65	34	35	50	46	57	76

APPENDIX 9 Effect of particle / grain count per analysis

Modal Mineralogy (weight-%, normalized)

Mineral Group	Sample	A951 176m, Class B			A431 306m, Class A			A431 306m, Class A			A355 160.5m, Class C			A355 160.5m, Class C			A355 70.5m, Class B			A355 70.5m, Class B			A355 70.5m, Class B			A162 97.5m, Class A			A162 97.5m, Class A			A162 97.5m, Class A		
	Size Fraction	-300/+150 µm			-1190/+600 µm			-75/+53 µm			-1190/+600 µm			-150/+106 µm			-600/+300 µm			-600/+300 µm			-150/+106 µm			-1190/+600 µm			-600/+300 µm			-106/+75 µm		
	#Particles to Collect	12000	2000	20000	12000	2000	20000	12000	2000	20000	12000	2000	20000	12000	2000	20000	12000	2000	20000	12000	2000	20000	12000	2000	20000	12000	2000	20000	12000	2000	20000	12000	2000	20000
Sulphide	Bornite	0.000	0.000	0.000	0.020	0.015	0.017	0.051	0.098	0.060	0.000	0.000	0.000	0.000	0.000	0.000	0.000	0.000	0.000	0.000	0.000	0.000	0.000	0.000	0.000	0.500	0.708	0.665	0.360	0.491	0.533	0.916	0.890	0.806
	Galena	0.100	0.126	0.125	0.060	1.256	0.526	0.174	0.029	0.178	0.000	0.000	0.000	0.000	0.000	0.026	0.030	0.241	0.200	0.030	0.658	0.022	0.058	0.036	0.137	1.030	1.057	1.061	0.100	0.096	0.098	0.039	0.000	0.029
	Sphalerite	0.060	0.008	0.009	0.450	0.635	0.458	1.909	1.742	1.858	0.310	0.203	0.222	0.130	0.037	0.126	0.340	0.200	0.328	0.420	0.880	0.957	1.646	1.070	1.466	1.420	1.318	1.883	2.040	2.412	2.255	2.511	2.410	2.337
	Chalcopyrite	0.050	0.014	0.015	0.260	0.281	1.070	0.576	0.584	0.569	0.160	0.509	0.467	0.200	0.006	0.116	0.090	0.167	0.108	0.370	0.570	0.583	0.452	0.325	0.388	1.880	2.812	2.269	1.480	1.316	1.415	1.361	1.551	1.480
	Pyrrhotite	0.000	0.001	0.002	0.030	0.024	0.024	0.053	0.000	0.040	0.980	3.013	4.933	2.750	2.462	2.511	0.310	0.683	1.816	0.400	1.308	1.425	1.190	1.329	1.317	0.370	0.345	0.353	0.010	0.567	0.574	0.182	0.333	0.190
	Realgar-Orpiment	0.000	0.000	0.000	0.000	0.000	0.000	0.000	0.000	0.000	0.000	0.000	0.000	0.000	0.000	0.000	0.000	0.000	0.000	0.000	0.000	0.000	0.000	0.000	0.000	0.000	0.000	0.000	0.000	0.000	0.000	0.000	0.000	0.000
	Stibnite	0.000	0.000	0.000	0.000	0.000	0.000	0.000	0.000	0.000	0.000	0.000	0.000	0.000	0.000	0.000	0.000	0.000	0.000	0.000	0.000	0.000	0.000	0.000	0.000	0.020	0.002	0.005	0.000	0.001	0.001	0.001	0.000	0.002
	Watanabeite	0.000	0.000	0.000	0.000	0.000	0.000	0.000	0.000	0.000	0.000	0.000	0.000	0.000	0.000	0.000	0.000	0.000	0.000	0.000	0.000	0.000	0.000	0.000	0.000	3.730	3.210	2.534	2.930	3.130	2.491	2.041	1.442	1.774
	Pyrite	0.070	0.090	0.091	0.020	0.022	0.022	0.000	0.001	0.023	1.490	3.833	3.237	1.440	1.368	1.884	3.680	6.772	6.381	5.680	6.220	6.025	12.993	9.159	12.186	0.470	0.441	0.447	0.150	0.856	0.173	0.227	0.475	0.336
	Molybdenite	0.000	0.003	0.003	0.190	0.176	0.176	0.041	0.062	0.038	0.000	0.000	0.000	0.000	0.000	0.000	0.000	0.000	0.000	0.000	0.000	0.000	0.001	0.000	0.000	0.020	0.016	0.016	0.010	0.004	0.002	0.000	0.000	0.000
	Enargite	0.000	0.000	0.000	0.020	0.019	0.024	0.032	0.002	0.027	0.000	0.000	0.000	0.000	0.000	0.000	0.000	0.000	0.000	0.000	0.000	0.000	0.000	0.000	0.000	1.000	0.943	1.400	1.870	2.188	2.825	0.626	0.531	0.615
	Others	0.000	0.000	0.000	0.000	0.000	0.000	0.002	0.000	0.004	0.000	0.002	0.002	0.000	0.000	0.000	0.000	0.000	0.000	0.000	0.000	0.000	0.001	0.000	0.001	0.020	0.016	0.019	0.010	0.010	0.007	0.072	0.006	0.048
	Subtotal	**0.280**	**0.242**	**0.246**	**1.050**	**2.430**	**2.316**	**2.840**	**2.517**	**2.799**	**2.940**	**7.560**	**8.860**	**4.520**	**3.873**	**4.662**	**4.450**	**8.063**	**8.833**	**6.900**	**9.637**	**9.013**	**16.340**	**11.920**	**15.496**	**10.460**	**10.869**	**10.651**	**8.960**	**11.071**	**10.374**	**7.974**	**7.637**	**7.616**
Carbonate	Calcite	88.580	87.733	87.640	63.790	65.033	61.538	84.601	85.216	85.110	57.920	51.491	58.015	67.570	68.312	67.620	45.550	41.594	43.211	46.790	39.439	45.118	44.527	46.725	45.093	47.740	45.399	43.261	44.830	43.145	44.514	59.433	60.752	60.261
	Otavite	0.000	0.000	0.000	0.000	0.000	0.000	0.000	0.000	0.000	0.000	0.000	0.000	0.000	0.000	0.000	0.000	0.000	0.000	0.000	0.000	0.000	0.000	0.000	0.000	0.000	0.000	0.000	0.000	0.000	0.000	0.000	0.000	0.000
	Siderite	0.000	0.000	0.000	0.000	0.000	0.000	0.000	0.000	0.001	0.000	0.000	0.000	0.000	0.001	0.000	0.000	0.000	0.000	0.000	0.000	0.000	0.000	0.000	0.000	0.000	0.000	0.000	0.000	0.000	0.000	0.000	0.000	0.000
	Dolomite	0.000	0.000	0.000	0.190	0.118	0.116	0.312	0.152	0.241	0.000	0.000	0.278	0.000	0.000	0.000	0.000	0.000	0.000	0.000	0.000	0.000	0.018	0.000	0.020	0.010	0.000	0.000	0.000	0.000	0.000	0.000	0.000	0.000
	Others	0.000	0.000	0.000	0.000	0.000	0.000	0.004	0.000	0.022	0.000	0.000	0.000	0.000	0.000	0.001	0.000	0.000	0.000	0.000	0.000	0.000	0.005	0.000	0.002	0.000	0.000	0.002	0.000	0.082	0.001	0.000	0.000	0.000
	Subtotal	**88.580**	**87.733**	**87.640**	**63.980**	**65.152**	**61.654**	**84.918**	**85.368**	**85.374**	**57.920**	**51.491**	**58.293**	**67.570**	**68.313**	**67.620**	**45.550**	**41.594**	**43.211**	**46.790**	**39.440**	**45.119**	**44.551**	**46.725**	**45.115**	**47.750**	**45.399**	**43.263**	**44.830**	**43.228**	**44.516**	**59.434**	**60.752**	**60.261**
Silicate	Biotite	0.000	0.000	0.000	0.020	0.004	0.889	0.108	0.010	0.066	0.740	1.073	0.251	0.340	0.231	0.394	0.350	0.250	0.238	0.440	0.434	0.602	0.250	0.536	0.468	0.880	1.185	0.878	0.530	0.145	0.363	0.154	0.106	0.186
	Chlorite	0.000	0.000	0.000	0.030	0.009	0.028	0.009	0.043	0.022	0.010	0.005	0.381	0.130	0.064	0.071	0.360	0.117	0.073	0.100	0.329	0.154	0.109	0.172	0.308	0.030	0.004	0.020	0.070	0.117	0.224	0.049	0.095	0.020
	K_Feldspar	0.100	0.106	0.085	0.120	0.202	0.182	0.061	0.063	0.057	4.390	4.944	3.703	3.100	2.846	2.709	5.470	3.351	4.438	4.950	3.139	2.449	3.988	3.495	3.310	0.450	0.128	0.261	0.440	0.438	0.436	0.215	0.148	0.204
	Kaolinite	0.000	0.000	0.000	0.000	0.000	0.000	0.000	0.000	0.000	0.000	0.000	0.000	0.000	0.000	0.001	0.000	0.091	0.149	0.410	0.377	0.450	0.002	0.292	0.447	0.000	0.000	0.000	0.000	0.000	0.000	0.000	0.000	0.000
	Muscovite	0.000	0.000	0.000	0.000	0.000	0.000	0.000	0.000	0.000	0.000	0.000	0.001	0.040	0.073	0.092	0.020	0.004	0.005	0.000	0.112	0.000	0.054	0.044	0.075	0.000	0.000	0.000	0.170	0.000	0.000	0.000	0.000	0.000
	Plagioclase	0.560	0.518	0.584	0.860	0.570	1.957	0.299	0.443	0.463	8.050	9.784	10.375	6.260	6.896	6.548	15.240	15.737	13.905	14.610	22.298	19.108	11.157	12.775	11.032	2.520	3.095	2.311	2.430	1.542	1.852	0.479	0.825	0.466
	Pyroxene	3.320	3.321	3.711	13.680	11.455	12.076	5.153	4.687	4.362	10.300	6.533	5.848	5.850	5.984	5.400	7.860	8.552	8.894	8.200	7.073	8.526	7.422	7.305	7.420	7.110	7.928	9.942	9.370	9.722	9.152	14.415	12.686	14.007
	Quartz	0.590	0.704	0.706	0.000	0.000	0.001	0.044	0.004	0.043	0.400	1.242	1.249	0.920	1.099	0.896	1.000	1.350	1.312	0.790	0.952	1.324	1.127	1.735	1.693	1.660	1.299	1.478	0.990	1.946	2.065	1.237	1.093	1.157
	Talc	0.060	0.000	0.000	0.000	0.000	0.000	0.000	0.000	0.001	0.000	0.000	0.000	0.000	0.000	0.000	0.000	0.000	0.000	0.000	0.000	0.000	0.000	0.000	0.000	0.000	0.000	0.000	0.000	0.000	0.000	0.000	0.000	0.000
	Mica	0.050	0.059	0.081	0.690	0.266	0.286	0.159	0.373	0.151	4.370	3.906	3.814	3.560	4.622	4.577	3.830	3.481	2.588	2.980	2.306	1.965	3.140	3.512	3.441	0.500	0.450	0.588	0.530	0.543	0.506	0.256	0.094	0.172
	Titanite	0.100	0.026	0.278	0.060	0.008	0.010	0.092	0.162	0.064	1.180	0.010	1.129	0.470	1.283	1.492	0.680	0.544	0.949	0.400	1.195	0.892	0.555	1.641	1.171	0.110	0.179	0.180	0.140	0.020	0.595	0.072	0.015	0.020
	Others	6.340	7.273	6.648	18.870	19.095	19.322	6.077	5.866	6.247	9.540	12.099	4.871	6.500	3.774	4.521	15.070	14.965	14.034	11.880	11.501	9.769	10.888	8.100	9.373	28.320	29.063	30.344	31.060	31.111	29.812	15.485	16.218	15.739
	Subtotal	**11.120**	**12.007**	**12.093**	**34.330**	**31.610**	**34.750**	**12.003**	**11.650**	**11.476**	**38.980**	**39.598**	**31.623**	**27.170**	**26.871**	**26.700**	**49.880**	**48.443**	**46.584**	**44.760**	**49.716**	**45.239**	**38.692**	**39.606**	**38.739**	**41.580**	**43.330**	**46.004**	**45.730**	**45.586**	**45.006**	**32.363**	**31.280**	**31.970**
Phosphate	**Subtotal**	0.020	0.015	0.021	0.040	0.018	0.018	0.024	0.011	0.040	0.110	0.856	1.194	0.250	0.442	0.712	0.020	1.124	1.077	1.460	0.215	0.203	0.132	0.537	0.306	0.100	0.361	0.049	0.430	0.066	0.074	0.131	0.103	0.066
Oxide	FeOxyhydroxides	0.000	0.001	0.000	0.000	0.001	0.001	0.035	0.000	0.020	0.000	0.011	0.006	0.200	0.182	0.045	0.020	0.744	0.010	0.000	0.013	0.003	0.214	1.044	0.197	0.020	0.010	0.004	0.000	0.012	0.001	0.048	0.207	0.056
	Others	0.000	0.000	0.000	0.000	0.000	0.000	0.001	0.000	0.000	0.000	0.000	0.000	0.000	0.000	0.000	0.000	0.000	0.000	0.000	0.000	0.000	0.003	0.000	0.000	0.000	0.001	0.000	0.000	0.004	0.001	0.003	0.000	0.000
	Subtotal	**0.000**	**0.001**	**0.000**	**0.000**	**0.001**	**0.001**	**0.036**	**0.000**	**0.020**	**0.000**	**0.011**	**0.006**	**0.200**	**0.182**	**0.046**	**0.020**	**0.744**	**0.010**	**0.000**	**0.013**	**0.003**	**0.216**	**1.044**	**0.198**	**0.020**	**0.011**	**0.004**	**0.000**	**0.016**	**0.002**	**0.051**	**0.208**	**0.056**
Sulphate	FeSulphate	0.000	0.001	0.000	0.000	0.000	0.000	0.000	0.000	0.000	0.050	0.483	0.024	0.280	0.319	0.260	0.040	0.028	0.283	0.040	0.942	0.405	0.065	0.166	0.146	0.010	0.008	0.006	0.000	0.002	0.001	0.043	0.010	0.027
	Barite	0.000	0.000	0.000	0.000	0.000	0.000	0.000	0.000	0.000	0.000	0.000	0.000	0.000	0.000	0.000	0.000	0.000	0.000	0.000	0.000	0.000	0.000	0.000	0.000	0.000	0.000	0.000	0.000	0.000	0.000	0.000	0.000	0.000
	Gypsum	0.000	0.000	0.000	0.000	0.000	0.001	0.001	0.000	0.000	0.000	0.000	0.000	0.000	0.000	0.000	0.020	0.000	0.000	0.000	0.019	0.001	0.001	0.000	0.000	0.070	0.005	0.003	0.010	0.004	0.002	0.002	0.001	0.000
	Others	0.000	0.000	0.000	0.000	0.000	0.000	0.000	0.000	0.000	0.000	0.000	0.000	0.000	0.000	0.000	0.000	0.000	0.000	0.000	0.000	0.000	0.000	0.000	0.000	0.000	0.000	0.001	0.000	0.000	0.000	0.000	0.000	0.000
	Subtotal	**0.000**	**0.002**	**0.000**	**0.000**	**0.000**	**0.001**	**0.001**	**0.000**	**0.000**	**0.050**	**0.483**	**0.024**	**0.280**	**0.319**	**0.260**	**0.060**	**0.028**	**0.283**	**0.040**	**0.962**	**0.406**	**0.066**	**0.166**	**0.146**	**0.080**	**0.013**	**0.011**	**0.010**	**0.006**	**0.003**	**0.045**	**0.011**	**0.027**
Other	**Subtotal**	0.000	0.000	0.000	0.610	0.789	1.259	0.178	0.454	0.290	0.000	0.000	0.000	0.010	0.000	0.000	0.000	0.002	0.002	0.020	0.018	0.018	0.003	0.002	0.001	0.020	0.016	0.018	0.040	0.028	0.026	0.004	0.008	0.004
Total Mineralogy		**100.0**	**100.0**	**100.0**	**100.0**	**100.0**	**100.0**	**100.0**	**100.0**	**100.0**	**100.0**	**100.0**	**100.0**	**100.0**	**100.0**	**100.0**	**100.0**	**100.0**	**100.0**	**100.0**	**100.0**	**100.0**	**100.0**	**100.0**	**100.0**	**100.0**	**100.0**	**100.0**	**100.0**	**100.0**	**100.0**	**100.0**	**100.0**	**100.0**
# Particles Analyzed		2564	1968	1991	513	404	389	12579	3455	17702	295	301	295	4860	2001	5255	1110	879	868	819	951	917	7634	2423	7532	601	543	529	1222	1314	1288	7838	2667	12615
# Grains Analyzed		4299	3013	3151	8569	6512	7257	15110	3957	20256	5891	2010	2060	9565	3685	9658	6206	4049	4413	7087	4871	4726	17267	5361	16846	14754	9700	11439	8982	9645	9899	11463	3794	17523
# Frames Analyzed		72	54	54	60	63	63	112	30	165	64	64	64	96	36	96	72	72	72	63	72	72	108	36	108	70	70	70	63	72	72	105	28	140
Analysis Time (min)		32	23	23	43	39	40	49	13	68	36	33	32	41	14	45	36	35	34	31	32	38	54	17	53	54	54	54	34	38	40	46	19	63

APPENDIX 10 Effect of accelerating voltage

Modal Mineralogy (weight-%, normalized)

Mineral Group	Sample	A951 176m, Class B		A431 306m, Class A		A431 306m, Class A		A355 160.5m, Class C		A355 160.5m, Class C		A355 70.5m, Class B		A355 70.5m, Class B		A355 70.5m, Class B		A162 97.5m, Class A		A162 97.5m, Class A		A162 97.5m, Class A	
	Size Fraction	-300/+150 µm		-1190/+600 µm		-75/+53 µm		-1190/+600 µm		-150/+106 µm		-600/+300 µm		-600/+300 µm		-150/+106 µm		-1190/+600 µm		-600/+300 µm		-106/+75 µm	
	Accelerating Voltage (kV)	25	15	25	15	25	15	25	15	25	15	25	15	25	15	25	15	25	15	25	15	25	15
Sulphide	Bornite	0.000	0.000	0.020	0.007	0.051	0.065	0.000	0.000	0.000	0.000	0.000	0.000	0.000	0.000	0.000	0.000	0.500	0.513	0.360	0.331	0.916	0.756
	Galena	0.100	0.107	0.060	0.052	0.174	0.178	0.000	0.000	0.000	0.004	0.030	0.030	0.030	0.021	0.058	0.062	1.030	0.909	0.100	0.090	0.039	0.037
	Sphalerite	0.060	0.062	0.450	0.396	1.909	1.833	0.310	0.202	0.130	0.088	0.340	0.176	0.420	0.600	1.646	1.218	1.420	1.859	2.040	2.178	2.511	2.300
	Chalcopyrite	0.050	0.047	0.260	0.207	0.576	0.518	0.160	0.031	0.200	0.136	0.090	0.092	0.370	0.348	0.452	0.388	1.880	1.897	1.480	1.185	1.361	1.303
	Pyrrhotite	0.000	0.002	0.030	0.007	0.053	0.036	0.980	0.819	2.750	2.557	0.310	0.258	0.400	0.284	1.190	1.124	0.370	0.189	0.010	0.137	0.182	0.164
	Realgar-Orpiment	0.000	0.000	0.000	0.000	0.000	0.000	0.000	0.000	0.000	0.000	0.000	0.000	0.000	0.000	0.000	0.000	0.000	0.000	0.000	0.000	0.000	0.000
	Stibnite	0.000	0.000	0.000	0.000	0.000	0.000	0.000	0.000	0.000	0.000	0.000	0.000	0.000	0.000	0.000	0.000	0.020	0.029	0.000	0.028	0.001	0.005
	Watanabeite	0.000	0.000	0.000	0.000	0.000	0.000	0.000	0.000	0.000	0.000	0.000	0.000	0.000	0.000	0.000	0.000	3.730	1.197	2.930	1.602	2.041	1.373
	Pyrite	0.070	0.079	0.020	0.040	0.000	0.002	1.490	1.701	1.440	2.005	3.680	3.720	5.680	5.157	12.993	11.646	0.470	0.388	0.150	0.136	0.227	0.266
	Molybdenite	0.000	0.000	0.190	0.000	0.041	0.007	0.000	0.000	0.000	0.000	0.000	0.001	0.000	0.000	0.001	0.000	0.020	0.000	0.010	0.000	0.000	0.000
	Enargite	0.000	0.000	0.020	0.000	0.032	0.001	0.000	0.000	0.000	0.000	0.000	0.000	0.000	0.000	0.000	0.000	1.000	0.020	1.870	0.238	0.626	0.025
	Others	0.000	0.000	0.000	0.014	0.002	0.036	0.000	0.004	0.000	0.001	0.000	0.007	0.000	0.001	0.001	0.011	0.020	2.903	0.010	3.135	0.072	1.071
	Subtotal	**0.280**	**0.297**	**1.050**	**0.724**	**2.840**	**2.677**	**2.940**	**2.757**	**4.520**	**4.790**	**4.450**	**4.283**	**6.900**	**6.411**	**16.340**	**14.449**	**10.460**	**9.905**	**8.960**	**9.059**	**7.974**	**7.302**
Carbonate	Calcite	88.580	88.341	63.790	60.939	84.601	83.789	57.920	47.792	67.570	63.102	45.550	44.528	46.790	44.225	44.527	44.428	47.740	44.719	44.830	43.330	59.433	59.367
	Otavite	0.000	0.000	0.000	0.000	0.000	0.000	0.000	0.000	0.000	0.000	0.000	0.000	0.000	0.000	0.000	0.000	0.000	0.000	0.000	0.000	0.000	0.000
	Siderite	0.000	0.000	0.000	0.000	0.000	0.000	0.000	0.000	0.000	0.000	0.000	0.000	0.000	0.000	0.000	0.000	0.000	0.000	0.000	0.000	0.000	0.000
	Dolomite	0.000	0.041	0.190	0.082	0.312	0.056	0.000	0.000	0.000	0.299	0.000	0.859	0.000	0.513	0.018	0.303	0.010	0.003	0.000	0.007	0.000	0.017
	Others	0.000	0.000	0.000	0.001	0.004	0.005	0.000	0.000	0.000	0.004	0.000	0.000	0.000	0.000	0.005	0.013	0.000	0.000	0.000	0.000	0.000	0.000
	Subtotal	**88.580**	**88.382**	**63.980**	**61.022**	**84.918**	**83.850**	**57.920**	**47.793**	**67.570**	**63.406**	**45.550**	**45.387**	**46.790**	**44.738**	**44.551**	**44.745**	**47.750**	**44.722**	**44.830**	**43.337**	**59.434**	**59.384**
Silicate	Biotite	0.000	0.123	0.020	0.374	0.108	0.111	0.740	1.065	0.340	0.345	0.350	0.508	0.440	0.615	0.250	0.583	0.880	0.832	0.530	0.368	0.154	0.163
	Chlorite	0.000	0.000	0.030	0.000	0.009	0.000	0.010	0.008	0.130	0.048	0.360	0.026	0.100	0.303	0.109	0.192	0.030	0.068	0.070	0.002	0.049	0.014
	K_Feldspar	0.100	0.219	0.120	0.000	0.061	0.056	4.390	6.706	3.100	5.834	5.470	7.117	4.950	5.381	3.988	6.427	0.450	0.370	0.440	0.546	0.215	0.216
	Kaolinite	0.000	0.000	0.000	0.000	0.000	0.000	0.000	0.000	0.000	0.002	0.000	0.106	0.410	0.358	0.002	0.412	0.000	0.000	0.000	0.000	0.000	0.000
	Muscovite	0.000	0.022	0.000	0.077	0.000	0.007	0.000	0.119	0.040	0.195	0.020	0.639	0.000	0.598	0.054	0.775	0.000	0.020	0.170	0.000	0.000	0.026
	Plagioclase	0.560	0.353	0.860	1.674	0.299	1.126	8.050	11.527	6.260	7.271	15.240	13.349	14.610	13.658	11.157	9.354	2.520	1.709	2.430	1.889	0.479	0.944
	Pyroxene	3.320	3.526	13.680	16.556	5.153	4.838	10.300	13.917	5.850	10.624	7.860	15.813	8.200	15.745	7.422	12.787	7.110	7.892	9.370	11.379	14.415	13.799
	Quartz	0.590	0.751	0.000	2.095	0.044	0.801	0.400	1.069	0.920	1.268	1.000	1.473	0.790	1.570	1.127	1.852	1.660	2.145	0.990	3.037	1.237	1.375
	Talc	0.060	0.000	0.000	0.000	0.000	0.000	0.000	0.000	0.000	0.000	0.000	0.000	0.000	0.000	0.000	0.000	0.000	0.000	0.000	0.000	0.000	0.000
	Mica	0.050	0.000	0.690	0.558	0.159	0.355	4.370	0.742	3.560	0.965	3.830	1.679	2.980	1.467	3.140	1.523	0.500	0.469	0.530	0.305	0.256	0.161
	Titanite	0.100	0.013	0.060	0.034	0.092	0.108	1.180	2.279	0.470	0.166	0.680	0.794	0.400	0.423	0.555	0.416	0.110	0.058	0.140	0.251	0.072	0.015
	Others	6.340	6.298	18.870	16.081	6.077	5.847	9.540	11.600	6.500	4.817	15.070	8.393	11.880	8.392	10.888	5.672	28.320	31.679	31.060	29.626	15.485	16.416
	Subtotal	**11.120**	**11.304**	**34.330**	**37.448**	**12.003**	**13.248**	**38.980**	**49.032**	**27.170**	**31.535**	**49.880**	**49.896**	**44.760**	**48.511**	**38.692**	**39.993**	**41.580**	**45.241**	**45.730**	**47.404**	**32.363**	**33.130**
Phosphate	**Subtotal**	0.020	0.011	0.040	0.013	0.024	0.039	0.110	0.361	0.250	0.115	0.020	0.329	1.460	0.036	0.132	0.078	0.100	0.039	0.430	0.103	0.131	0.081
Oxide	FeOxyhydroxides	0.000	0.005	0.000	0.001	0.035	0.029	0.000	0.055	0.200	0.088	0.020	0.096	0.000	0.273	0.214	0.707	0.020	0.074	0.000	0.046	0.048	0.065
	Others	0.000	0.000	0.000	0.004	0.001	0.000	0.000	0.000	0.000	0.001	0.000	0.005	0.000	0.012	0.003	0.004	0.000	0.001	0.000	0.003	0.003	0.001
	Subtotal	**0.000**	**0.005**	**0.000**	**0.005**	**0.036**	**0.030**	**0.000**	**0.055**	**0.200**	**0.089**	**0.020**	**0.101**	**0.000**	**0.285**	**0.216**	**0.710**	**0.020**	**0.075**	**0.000**	**0.049**	**0.051**	**0.066**
Sulphate	FeSulphate	0.000	0.000	0.000	0.000	0.000	0.003	0.050	0.000	0.280	0.000	0.040	0.000	0.040	0.000	0.065	0.003	0.010	0.007	0.000	0.005	0.043	0.007
	Barite	0.000	0.000	0.000	0.000	0.000	0.000	0.000	0.000	0.000	0.000	0.000	0.000	0.000	0.000	0.000	0.000	0.000	0.000	0.000	0.000	0.000	0.000
	Gypsum	0.000	0.000	0.000	0.000	0.001	0.000	0.000	0.001	0.000	0.001	0.020	0.000	0.000	0.001	0.001	0.017	0.070	0.000	0.010	0.001	0.002	0.000
	Others	0.000	0.000	0.000	0.000	0.000	0.000	0.000	0.000	0.000	0.000	0.000	0.000	0.000	0.000	0.000	0.000	0.000	0.000	0.000	0.023	0.000	0.000
	Subtotal	**0.000**	**0.000**	**0.000**	**0.000**	**0.001**	**0.003**	**0.050**	**0.001**	**0.280**	**0.001**	**0.060**	**0.000**	**0.040**	**0.001**	**0.066**	**0.020**	**0.080**	**0.007**	**0.010**	**0.029**	**0.045**	**0.007**
Other	**Subtotal**	0.000	0.001	0.610	1.028	0.178	0.154	0.000	0.000	0.010	0.064	0.000	0.003	0.020	0.019	0.003	0.005	0.020	0.010	0.040	0.019	0.004	0.031
Total Mineralogy		**100.0**	**100.0**	**100.0**	**100.2**	**100.0**	**100.0**	**100.0**	**100.0**	**100.0**	**100.0**	**100.0**	**100.0**	**100.0**	**100.0**	**100.0**	**100.0**	**100.0**	**100.0**	**100.0**	**100.0**	**100.0**	**100.0**
# Particles Analyzed		2564	2328	513	377	12579	12638	295	308	4860	5320	1110	949	819	1020	7634	6663	601	526	1222	1278	7838	11059
# Grains Analyzed		4299	4253	8569	5826	15110	15859	5891	2884	9565	11811	6206	6489	7087	7239	17267	20372	14754	14328	8982	11789	11463	17856
# Frames Analyzed		72	63	60	63	112	120	64	64	96	88	72	64	63	64	108	96	70	63	63	64	105	117
Analysis Time (min)		32	34	43	54	49	63	36	46	41	49	36	40	31	40	54	67	54	64	34	46	46	76

APPENDIX 11 Effect of magnification (horizontal field width)

Modal Mineralogy (weight-%, normalized)

Mineral Group	Sample	A951 176m, Class B		A431 306m, Class A		A431 306m, Class A		A355 160.5m, Class C		A355 160.5m, Class		A355 70.5m, Class B		A355 70.5m, Class B		A355 70.5m, Class B		A162 97.5m, Class A		A162 97.5m, Class A		A162 97.5m, Class A	
	Size Fraction	-300/+150 µm		-1190/+600 µm		-75/+53 µm		-1190/+600 µm		-150/+106 µm		-600/+300 µm		-600/+300 µm		-150/+106 µm		-1190/+600 µm		-600/+300 µm		-106/+75 µm	
	Magnification	120	225	120	200	200	275	120	200	150	250	120	200	120	200	150	250	120	200	120	200	175	275
Sulphide	Bornite	0.000	0.000	0.020	0.021	0.051	0.066	0.000	0.000	0.000	0.000	0.000	0.000	0.000	0.000	0.000	0.000	0.500	0.612	0.360	0.559	0.916	0.795
	Galena	0.100	0.085	0.060	0.052	0.174	0.184	0.000	0.000	0.000	0.018	0.030	0.033	0.030	0.037	0.058	0.114	1.030	0.470	0.100	0.098	0.039	0.038
	Sphalerite	0.060	0.042	0.450	0.599	1.909	1.812	0.310	0.272	0.130	0.102	0.340	0.328	0.420	0.919	1.646	1.551	1.420	2.184	2.040	2.185	2.511	2.411
	Chalcopyrite	0.050	0.029	0.260	0.253	0.576	0.548	0.160	0.115	0.200	0.140	0.090	0.085	0.370	0.642	0.452	0.385	1.880	2.281	1.480	1.403	1.361	1.242
	Pyrrhotite	0.000	0.019	0.030	0.025	0.053	0.058	0.980	2.171	2.750	2.915	0.310	1.515	0.400	1.729	1.190	1.353	0.370	0.360	0.010	0.568	0.182	0.152
	Realgar-Orpiment	0.000	0.000	0.000	0.000	0.000	0.000	0.000	0.000	0.000	0.000	0.000	0.000	0.000	0.000	0.000	0.000	0.000	0.000	0.000	0.000	0.000	0.000
	Stibnite	0.000	0.000	0.000	0.000	0.000	0.000	0.000	0.000	0.000	0.000	0.000	0.000	0.000	0.000	0.000	0.000	0.020	0.002	0.000	0.003	0.001	0.007
	Watanabeite	0.000	0.000	0.000	0.001	0.000	0.000	0.000	0.000	0.000	0.000	0.000	0.000	0.000	0.000	0.000	0.000	3.730	1.764	2.930	3.295	2.041	1.896
	Pyrite	0.070	0.060	0.020	0.021	0.000	0.003	1.490	2.002	1.440	1.705	3.680	5.020	5.680	6.769	12.993	12.030	0.470	0.399	0.150	0.186	0.227	0.235
	Molybdenite	0.000	0.003	0.190	0.186	0.041	0.064	0.000	0.000	0.000	0.001	0.000	0.000	0.000	0.000	0.001	0.000	0.020	0.024	0.010	0.006	0.000	0.000
	Enargite	0.000	0.000	0.020	0.025	0.032	0.044	0.000	0.000	0.000	0.000	0.000	0.000	0.000	0.000	0.000	0.000	1.000	2.135	1.870	2.522	0.626	0.690
	Others	0.000	0.000	0.000	0.001	0.002	0.015	0.000	0.002	0.000	0.007	0.000	0.000	0.000	0.000	0.001	0.001	0.020	0.024	0.010	0.014	0.072	0.033
	Subtotal	**0.280**	**0.239**	**1.050**	**1.183**	**2.840**	**2.794**	**2.940**	**4.562**	**4.520**	**4.889**	**4.450**	**6.981**	**6.900**	**10.096**	**16.340**	**15.435**	**10.460**	**10.255**	**8.960**	**10.840**	**7.974**	**7.500**
Carbonate	Calcite	88.580	89.558	63.790	66.168	84.601	85.019	57.920	55.605	67.570	67.927	45.550	45.048	46.790	45.738	44.527	46.499	47.740	47.275	44.830	44.680	59.433	59.916
	Otavite	0.000	0.000	0.000	0.000	0.000	0.000	0.000	0.000	0.000	0.000	0.000	0.000	0.000	0.000	0.000	0.000	0.000	0.000	0.000	0.000	0.000	0.000
	Siderite	0.000	0.000	0.000	0.000	0.000	0.000	0.000	0.000	0.000	0.010	0.000	0.000	0.000	0.000	0.000	0.000	0.000	0.000	0.000	0.000	0.000	0.000
	Dolomite	0.000	0.000	0.190	0.136	0.312	0.121	0.000	0.000	0.000	0.000	0.000	0.000	0.000	0.000	0.018	0.019	0.010	0.000	0.000	0.001	0.000	0.000
	Others	0.000	0.002	0.000	0.001	0.004	0.010	0.000	0.000	0.000	0.002	0.000	0.000	0.000	0.000	0.005	0.004	0.000	0.001	0.000	0.000	0.000	0.000
	Subtotal	**88.580**	**89.560**	**63.980**	**66.306**	**84.918**	**85.150**	**57.920**	**55.605**	**67.570**	**67.939**	**45.550**	**45.048**	**46.790**	**45.739**	**44.551**	**46.522**	**47.750**	**47.276**	**44.830**	**44.682**	**59.434**	**59.916**
Silicate	Biotite	0.000	0.032	0.020	0.083	0.108	0.100	0.740	0.666	0.340	0.258	0.350	0.270	0.440	0.355	0.250	0.352	0.880	0.870	0.530	0.329	0.154	0.142
	Chlorite	0.000	0.000	0.030	0.015	0.009	0.022	0.010	0.013	0.130	0.058	0.360	0.396	0.100	0.375	0.109	0.291	0.030	0.018	0.070	0.033	0.049	0.049
	K_Feldspar	0.100	0.081	0.120	0.194	0.061	0.074	4.390	5.290	3.100	3.062	5.470	3.633	4.950	2.681	3.988	3.777	0.450	0.425	0.440	0.845	0.215	0.154
	Kaolinite	0.000	0.000	0.000	0.000	0.000	0.000	0.000	0.000	0.000	0.001	0.000	0.096	0.410	0.412	0.002	0.365	0.000	0.000	0.000	0.000	0.000	0.000
	Muscovite	0.000	0.000	0.000	0.000	0.000	0.000	0.000	0.001	0.040	0.004	0.020	0.026	0.000	0.014	0.054	0.063	0.000	0.000	0.170	0.001	0.000	0.006
	Plagioclase	0.560	0.191	0.860	0.305	0.299	0.355	8.050	8.903	6.260	5.545	15.240	12.699	14.610	12.828	11.157	10.444	2.520	2.269	2.430	0.494	0.479	0.405
	Pyroxene	3.320	2.856	13.680	9.750	5.153	4.489	10.300	7.340	5.850	5.096	7.860	10.596	8.200	8.678	7.422	7.718	7.110	6.741	9.370	10.137	14.415	14.319
	Quartz	0.590	0.587	0.000	0.003	0.044	0.063	0.400	0.500	0.920	0.923	1.000	1.479	0.790	1.195	1.127	1.710	1.660	1.571	0.990	2.077	1.237	1.182
	Talc	0.060	0.001	0.000	0.000	0.000	0.000	0.000	0.000	0.000	0.000	0.000	0.000	0.000	0.000	0.000	0.000	0.000	0.000	0.000	0.000	0.000	0.000
	Mica	0.050	0.098	0.690	0.244	0.159	0.202	4.370	6.951	3.560	4.798	3.830	3.492	2.980	3.970	3.140	3.990	0.500	0.497	0.530	0.398	0.256	0.313
	Titanite	0.100	0.090	0.060	0.030	0.092	0.083	1.180	1.888	0.470	2.157	0.680	3.626	0.400	2.113	0.555	1.769	0.110	0.092	0.140	0.049	0.072	0.064
	Others	6.340	6.217	18.870	20.160	6.077	6.296	9.540	5.802	6.500	4.359	15.070	10.773	11.880	10.641	10.888	6.633	28.320	28.636	31.060	29.955	15.485	15.751
	Subtotal	**11.120**	**10.153**	**34.330**	**30.785**	**12.003**	**11.685**	**38.980**	**37.355**	**27.170**	**26.262**	**49.880**	**47.084**	**44.760**	**43.261**	**38.692**	**37.114**	**41.580**	**41.119**	**45.730**	**44.317**	**32.363**	**32.386**
Phosphate	**Subtotal**	0.020	0.039	0.040	0.455	0.024	0.036	0.110	2.443	0.250	0.750	0.020	0.862	1.460	0.733	0.132	0.515	0.100	1.316	0.430	0.103	0.131	0.113
Oxide	FeOxyhydroxides	0.000	0.000	0.000	0.003	0.035	0.047	0.000	0.002	0.200	0.108	0.020	0.008	0.000	0.001	0.214	0.287	0.020	0.006	0.000	0.019	0.048	0.049
	Others	0.000	0.000	0.000	0.000	0.001	0.000	0.000	0.000	0.000	0.001	0.000	0.001	0.000	0.000	0.003	0.038	0.000	0.001	0.000	0.005	0.003	0.001
	Subtotal	**0.000**	**0.000**	**0.000**	**0.003**	**0.036**	**0.047**	**0.000**	**0.002**	**0.200**	**0.110**	**0.020**	**0.009**	**0.000**	**0.001**	**0.216**	**0.325**	**0.020**	**0.007**	**0.000**	**0.023**	**0.051**	**0.049**
Sulphate	FeSulphate	0.000	0.002	0.000	0.000	0.000	0.000	0.050	0.032	0.280	0.048	0.040	0.012	0.040	0.148	0.065	0.085	0.010	0.008	0.000	0.002	0.043	0.027
	Barite	0.000	0.000	0.000	0.000	0.000	0.000	0.000	0.000	0.000	0.000	0.000	0.000	0.000	0.000	0.000	0.000	0.000	0.000	0.000	0.000	0.000	0.000
	Gypsum	0.000	0.000	0.000	0.001	0.001	0.000	0.000	0.000	0.000	0.000	0.020	0.001	0.000	0.001	0.001	0.002	0.070	0.002	0.010	0.005	0.002	0.001
	Others	0.000	0.000	0.000	0.000	0.000	0.000	0.000	0.000	0.000	0.001	0.000	0.000	0.000	0.000	0.000	0.001	0.000	0.000	0.000	0.000	0.000	0.000
	Subtotal	**0.000**	**0.002**	**0.000**	**0.002**	**0.001**	**0.000**	**0.050**	**0.032**	**0.280**	**0.048**	**0.060**	**0.013**	**0.040**	**0.149**	**0.066**	**0.088**	**0.080**	**0.010**	**0.010**	**0.007**	**0.045**	**0.028**
Other	**Subtotal**	0.000	0.007	0.610	1.268	0.178	0.288	0.000	0.001	0.010	0.002	0.000	0.002	0.020	0.022	0.003	0.001	0.020	0.016	0.040	0.029	0.004	0.008
Total Mineralogy		**100.0**	**100.0**	**100.0**	**100.0**	**100.0**	**100.0**	**100.0**	**100.0**	**100.0**	**100.0**	**100.0**	**100.0**	**100.0**	**100.0**	**100.0**	**100.0**	**100.0**	**100.0**	**100.0**	**100.0**	**100.0**	**100.0**
# Particles Analyzed		2564	3263	513	892	12579	12355	295	469	4860	7464	1110	1374	819	1216	7634	8363	601	1081	1222	1755	7838	11206
# Grains Analyzed		4299	8282	8569	16551	15110	15353	5891	20491	9565	17456	6206	18178	7087	17087	17267	27357	14754	22610	8982	22363	11463	18567
# Frames Analyzed		72	208	60	153	112	190	64	180	96	306	72	180	63	169	108	270	70	168	63	169	105	260
Analysis Time (min)		32	86	43	120	49	74	36	129	41	126	36	100	31	91	54	124	54	133	34	105	46	106

APPENDIX 12 Effect of random sample mount surface analysis

Modal Mineralogy (weight-%, normalized)

Mineral Group	Sample	A951 176m, Class B		A431 306m, Class A		A431 306m, Class A		A355 160.5m, Class C		A355 160.5m, Class		A355 70.5m, Class B		A355 70.5m, Class B		A355 70.5m, Class B		A162 97.5m, Class A		A162 97.5m, Class A		A162 97.5m, Class A	
	Size Fraction	-300/+150 µm		-1190/+600 µm		-75/+53 µm		-1190/+600 µm		-150/+106 µm		-600/+300 µm		-600/+300 µm		-150/+106 µm		-1190/+600 µm		-600/+300 µm		-106/+75 µm	
	Random Position*	Base	Rotate	Base	Rotate	Base	Rotate	Base	Rotate	Base	Rotate	Base	Rotate	Base	Rotate	Base	Rotate	Base	Rotate	Base	Rotate	Base	Rotate
Sulphides	Bornite	0.000	0.000	0.020	0.019	0.051	0.066	0.000	0.000	0.000	0.000	0.000	0.000	0.000	0.000	0.000	0.000	0.500	0.936	0.360	0.299	0.916	0.936
	Galena	0.100	0.108	0.060	0.028	0.174	0.158	0.000	0.000	0.000	0.005	0.030	0.030	0.030	0.035	0.058	0.049	1.030	1.799	0.100	0.139	0.039	0.037
	Sphalerite	0.060	0.055	0.450	0.503	1.909	1.864	0.310	2.560	0.130	0.142	0.340	0.295	0.420	1.325	1.646	1.477	1.420	1.225	2.040	1.534	2.511	2.271
	Chalcopyrite	0.050	0.062	0.260	0.077	0.576	0.532	0.160	0.050	0.200	0.152	0.090	0.368	0.370	0.497	0.452	0.419	1.880	3.254	1.480	1.246	1.361	1.391
	Pyrrhotite	0.000	0.001	0.030	0.047	0.053	0.044	0.980	4.745	2.750	3.112	0.310	0.293	0.400	1.565	1.190	1.415	0.370	0.139	0.010	0.000	0.182	0.216
	Realgar-Orpiment	0.000	0.000	0.000	0.000	0.000	0.000	0.000	0.000	0.000	0.000	0.000	0.000	0.000	0.000	0.000	0.000	0.000	0.000	0.000	0.000	0.000	0.000
	Stibnite	0.000	0.000	0.000	0.000	0.000	0.000	0.000	0.000	0.000	0.000	0.000	0.000	0.000	0.000	0.000	0.000	0.020	0.005	0.000	0.000	0.001	0.000
	Watanabeite	0.000	0.000	0.000	0.000	0.000	0.000	0.000	0.000	0.000	0.000	0.000	0.000	0.000	0.000	0.000	0.000	3.730	5.524	2.930	2.631	2.041	1.734
	Pyrite	0.070	0.077	0.020	0.000	0.000	0.000	1.490	0.173	1.440	1.541	3.680	7.497	5.680	7.295	12.993	12.938	0.470	0.525	0.150	0.178	0.227	0.311
	Molybdenite	0.000	0.003	0.190	0.474	0.041	0.064	0.000	0.000	0.000	0.002	0.000	0.000	0.000	0.000	0.001	0.000	0.020	0.000	0.010	0.002	0.000	0.000
	Enargite	0.000	0.000	0.020	0.022	0.032	0.034	0.000	0.000	0.000	0.000	0.000	0.000	0.000	0.000	0.000	0.000	1.000	1.376	1.870	1.975	0.626	0.782
	Others	0.000	0.000	0.000	0.000	0.002	0.011	0.000	0.004	0.000	0.000	0.000	0.000	0.000	0.001	0.001	0.000	0.020	0.018	0.010	0.011	0.072	0.029
	Subtotal	**0.280**	**0.306**	**1.050**	**1.171**	**2.840**	**2.773**	**2.940**	**7.532**	**4.520**	**4.955**	**4.450**	**8.484**	**6.900**	**10.717**	**16.340**	**16.298**	**10.460**	**14.802**	**8.960**	**8.015**	**7.974**	**7.708**
Carbonates	Calcite	88.580	88.050	63.790	66.497	84.601	84.646	57.920	52.051	67.570	68.293	45.550	48.041	46.790	43.561	44.527	42.591	47.740	47.506	44.830	47.017	59.433	60.091
	Otavite	0.000	0.000	0.000	0.000	0.000	0.000	0.000	0.000	0.000	0.000	0.000	0.000	0.000	0.000	0.000	0.000	0.000	0.000	0.000	0.000	0.000	0.000
	Siderite	0.000	0.000	0.000	0.000	0.000	0.000	0.000	0.000	0.000	0.000	0.000	0.000	0.000	0.000	0.000	0.000	0.000	0.000	0.000	0.000	0.000	0.000
	Dolomite	0.000	0.000	0.190	0.079	0.312	0.223	0.000	0.000	0.000	0.000	0.000	0.000	0.000	0.000	0.018	0.021	0.010	0.000	0.000	0.001	0.000	0.008
	Others	0.000	0.000	0.000	0.000	0.004	0.018	0.000	0.000	0.000	0.013	0.000	0.000	0.000	0.000	0.005	0.004	0.000	0.000	0.000	0.000	0.000	0.010
	Subtotal	**88.580**	**88.050**	**63.980**	**66.576**	**84.918**	**84.887**	**57.920**	**52.051**	**67.570**	**68.307**	**45.550**	**48.041**	**46.790**	**43.561**	**44.551**	**42.615**	**47.750**	**47.507**	**44.830**	**47.018**	**59.434**	**60.109**
Silicates	Biotite	0.000	0.123	0.020	0.007	0.108	0.055	0.740	0.719	0.340	0.394	0.350	0.356	0.440	0.304	0.250	0.309	0.880	1.733	0.530	0.545	0.154	0.126
	Chlorite	0.000	0.000	0.030	0.022	0.009	0.020	0.010	0.001	0.130	0.075	0.360	0.135	0.100	0.281	0.109	0.259	0.030	0.015	0.070	0.011	0.049	0.032
	K_Feldspar	0.100	0.186	0.120	0.640	0.061	0.048	4.390	4.398	3.100	3.299	5.470	4.549	4.950	4.698	3.988	3.553	0.450	0.224	0.440	0.177	0.215	0.218
	Kaolinite	0.000	0.000	0.000	0.000	0.000	0.000	0.000	0.000	0.000	0.000	0.000	0.058	0.410	0.275	0.002	0.532	0.000	0.000	0.000	0.000	0.000	0.000
	Muscovite	0.000	0.000	0.000	0.000	0.000	0.000	0.000	0.002	0.040	0.001	0.020	0.034	0.000	0.000	0.054	0.062	0.000	0.000	0.170	0.051	0.000	0.000
	Plagioclase	0.560	0.755	0.860	0.559	0.299	0.480	8.050	13.569	6.260	6.843	15.240	12.083	14.610	15.201	11.157	13.196	2.520	0.568	2.430	1.445	0.479	0.660
	Pyroxene	3.320	3.607	13.680	12.139	5.153	4.805	10.300	5.083	5.850	5.245	7.860	9.150	8.200	9.905	7.422	6.898	7.110	7.749	9.370	10.849	14.415	13.871
	Quartz	0.590	0.485	0.000	0.000	0.044	0.048	0.400	2.964	0.920	1.004	1.000	0.703	0.790	0.915	1.127	1.737	1.660	0.858	0.990	1.271	1.237	1.086
	Talc	0.060	0.000	0.000	0.000	0.000	0.000	0.000	0.000	0.000	0.000	0.000	0.000	0.000	0.000	0.000	0.000	0.000	0.000	0.000	0.000	0.000	0.000
	Mica	0.050	0.112	0.690	0.452	0.159	0.258	4.370	9.008	3.560	3.716	3.830	2.802	2.980	3.416	3.140	3.195	0.500	1.070	0.530	1.120	0.256	0.210
	Titanite	0.100	0.045	0.060	0.018	0.092	0.070	1.180	0.664	0.470	1.078	0.680	1.825	0.400	0.344	0.555	0.921	0.110	0.353	0.140	0.102	0.072	0.031
	Others	6.340	6.317	18.870	17.259	6.077	6.220	9.540	3.843	6.500	4.325	15.070	11.161	11.880	9.151	10.888	9.787	28.320	25.035	31.060	29.142	15.485	15.795
	Subtotal	**11.120**	**11.630**	**34.330**	**31.096**	**12.003**	**12.004**	**38.980**	**40.251**	**27.170**	**25.981**	**49.880**	**42.857**	**44.760**	**44.489**	**38.692**	**40.448**	**41.580**	**37.606**	**45.730**	**44.713**	**32.363**	**32.030**
Phosphate	**Subtotal**	0.020	0.012	0.040	0.047	0.024	0.026	0.110	0.073	0.250	0.574	0.020	0.593	1.460	1.200	0.132	0.283	0.100	0.047	0.430	0.209	0.131	0.079
Oxides	FeOxyhydroxides	0.000	0.000	0.000	0.000	0.035	0.053	0.000	0.001	0.200	0.065	0.020	0.009	0.000	0.003	0.214	0.259	0.020	0.007	0.000	0.001	0.048	0.043
	Others	0.000	0.000	0.000	0.000	0.001	0.000	0.000	0.000	0.000	0.001	0.000	0.001	0.000	0.000	0.003	0.001	0.000	0.001	0.000	0.000	0.003	0.002
	Subtotal	**0.000**	**0.000**	**0.000**	**0.000**	**0.036**	**0.053**	**0.000**	**0.001**	**0.200**	**0.066**	**0.020**	**0.011**	**0.000**	**0.003**	**0.216**	**0.260**	**0.020**	**0.008**	**0.000**	**0.001**	**0.051**	**0.044**
Sulphates	FeSulphate	0.000	0.001	0.000	0.000	0.000	0.000	0.050	0.093	0.280	0.114	0.040	0.014	0.040	0.020	0.065	0.078	0.010	0.024	0.000	0.004	0.043	0.022
	Barite	0.000	0.000	0.000	0.000	0.000	0.000	0.000	0.000	0.000	0.000	0.000	0.000	0.000	0.000	0.000	0.000	0.000	0.000	0.000	0.000	0.000	0.000
	Gypsum	0.000	0.000	0.000	0.000	0.001	0.014	0.000	0.000	0.000	0.000	0.020	0.000	0.000	0.001	0.001	0.016	0.070	0.003	0.010	0.001	0.002	0.000
	Others	0.000	0.000	0.000	0.000	0.000	0.000	0.000	0.000	0.000	0.000	0.000	0.000	0.000	0.000	0.000	0.000	0.000	0.000	0.000	0.000	0.000	0.000
	Subtotal	**0.000**	**0.001**	**0.000**	**0.000**	**0.001**	**0.014**	**0.050**	**0.093**	**0.280**	**0.114**	**0.060**	**0.014**	**0.040**	**0.021**	**0.066**	**0.094**	**0.080**	**0.027**	**0.010**	**0.005**	**0.045**	**0.022**
Others	**Subtotal**	0.000	0.000	0.610	1.108	0.178	0.243	0.000	0.000	0.010	0.004	0.000	0.001	0.020	0.008	0.003	0.001	0.020	0.002	0.040	0.039	0.004	0.007
Total Mineralogy		**100.0**	**100.0**	**100.0**	**100.0**	**100.0**	**100.0**	**100.0**	**100.0**	**100.0**	**100.0**	**100.0**	**100.0**	**100.0**	**100.0**	**100.0**	**100.0**	**100.0**	**100.0**	**100.0**	**100.0**	**100.0**	**100.0**
# Particles Analyzed		2564	2472	513	328	12579	12201	295	177	4860	5773	1110	796	819	761	7634	6849	601	539	1222	1127	7838	11608
# Grains Analyzed		4299	3820	8569	3554	15110	13987	5891	1004	9565	10709	6206	4146	7087	3685	17267	20372	14754	5758	8982	6981	11463	15941
# Frames Analyzed		72	72	60	70	112	112	64	72	96	120	72	72	63	72	108	108	70	72	63	72	105	130
Analysis Time (min)		32	29	43	35	49	47	36	29	41	47	36	30	31	29	54	47	54	43	34	34	46	55

* Base position = initial analysis; Rotate = rotate sample mount 90° then re-analyze

MLA-calculated Assay (weight-%, normalized)

Sample	A951 176m, Class B		A431 306m, Class A		A431 306m, Class A		A355 160.5m, Class C		A355 160.5m, Class		A355 70.5m, Class B		A355 70.5m, Class B		A355 70.5m, Class B		A162 97.5m, Class A		A162 97.5m, Class A		A162 97.5m, Class A	
Size Fraction	-300/+150 µm		-1190/+600 µm		-75/+53 µm		-1190/+600 µm		-150/+106 µm		-600/+300 µm		-600/+300 µm		-150/+106 µm		-1190/+600 µm		-600/+300 µm		-106/+75 µm	
Random Position*	Base	Rotate	Base	Rotate	Base	Rotate	Base	Rotate	Base	Rotate	Base	Rotate	Base	Rotate	Base	Rotate	Base	Rotate	Base	Rotate	Base	Rotate
Ag	0	0	0	0	0.00111	0.00054	0	0	0	0	0	0	0.0001	0	0	0	0	0	0	0	0.00019	0
Al	1.12	1.15	2.66	2.47	0.86	0.92	4.35	4.44	3.00	2.76	6.08	4.73	5.89	5.55	2.97	4.87	4.59	3.81	4.64	4.56	2.33	2.42
As	0.00007	0.00008	0.00451	0.00438	0.00667	0.00939	0.00427	0.00787	0.02366	0.00973	0.00362	0.00118	0.0031	0.00167	0.00471	0.00767	0.64213	1.02692	0.76902	0.74316	0.40694	0.38965
Ba	0	0	0	0	0	0	0	0	0	0	0	0	0	0	0	0	0	0	0	0	0	0
Bi	0.00004	0.00002	0	0	0	0	0.00162	0.0033	0	0.00002	0.00035	0.00038	0.00045	0.0008	0	0.00004	0.001	0	0.00084	0.00103	0.00001	0.00011
C	10.63	10.57	7.68	7.99	10.19	10.19	6.95	6.25	8.11	8.20	5.47	5.76	5.62	5.23	7.40	5.11	5.34	5.70	5.38	5.64	7.13	7.21
Ca	36.2	36.0	28.5	29.1	35.1	35.1	26.9	23.2	29.3	29.7	22.2	23.0	22.6	21.3	27.7	20.2	22.2	22.9	23.2	23.7	27.6	27.7
Cd	0	0	0.00008	0	0.00017	0.00018	0	0	0	0	0	0	0	0	0.00003	0	0.0022	0.00302	0.00564	0.00316	0.00058	0.00111
Ce	0	0	0	0	0	0	0	0	0	0	0	0	0	0	0	0	0	0	0	0	0	0
Cl	0	0	0	0	0	0	0	0	0	0	0	0	0	0	0	0	0	0	0	0	0	0
Co	0	0	0	0	0	0	0	0	0	0	0	0	0	0	0	0	0	0	0.00154	0.00184	0	0
Cr	0	0	0	0	0	0	0	0	0	0	0	0	0	0	0	0	0	0	0	0	0	0
Cu	0.024	0.028	0.144	0.082	0.275	0.271	0.098	0.120	0.129	0.104	0.085	0.222	0.219	0.292	0.410	0.274	3.037	4.789	2.858	2.688	2.309	2.202
F	0.001	0.001	0.098	0.020	0.078	0.109	0.004	0.003	0.013	0.026	0.020	0.027	0.065	0.045	0.410	0.017	0.019	0.002	0.031	0.033	0.006	0.006
Fe	0.103	0.114	0.316	0.155	0.365	0.362	1.836	3.745	3.031	3.186	2.443	4.236	3.387	5.000	0.632	7.630	3.006	3.459	2.804	2.548	1.597	1.613
H	0.00047	0.00098	0.00259	0.00101	0.00182	0.00221	0.01699	0.03118	0.0164	0.01488	0.01916	0.01171	0.0184	0.01778	0.00622	0.02392	0.03439	0.03759	0.04262	0.03882	0.0145	0.01392
K	0.015	0.039	0.028	0.097	0.023	0.018	1.157	1.674	0.850	0.904	1.228	0.916	1.026	0.964	0.112	0.850	0.157	0.249	0.175	0.167	0.056	0.053
La	0	0	0	0	0	0	0	0	0	0	0	0	0	0	0	0	0	0	0	0	0	0
Mg	0.39	0.43	1.65	1.43	0.65	0.60	1.52	1.07	0.95	0.88	1.37	1.34	1.26	1.45	1.46	1.11	0.99	1.09	1.15	1.37	1.67	1.60
Mn	1.58	1.63	5.51	5.13	1.69	1.73	0.61	0.92	0.78	0.38	2.31	2.15	1.70	1.45	5.62	1.76	4.57	2.73	3.31	2.98	2.38	2.47
Mo	0.000	0.002	0.115	0.284	0.025	0.038	0.001	0.002	0.005	0.003	0.001	0.000	0.001	0.001	0.105	0.001	0.015	0.001	0.004	0.001	0.000	0.000
Na	0.024	0.033	0.037	0.024	0.014	0.022	0.530	0.651	0.380	0.382	0.890	0.621	0.752	0.733	0.084	0.678	0.108	0.055	0.145	0.067	0.028	0.034
Nd	0	0	0	0	0	0	0	0	0	0	0	0	0	0	0	0	0	0	0	0	0	0
Ni	0	0	0	0	0	0	0	0	0	0	0	0	0	0	0	0	0	0	0.0008	0.00096	0	0
O	47.3	47.2	45.1	45.2	45.8	45.8	45.4	43.4	44.9	44.7	44.2	42.2	43.3	41.5	44.3	38.9	40.3	39.0	41.4	42.1	42.7	42.8
P	0.0035	0.0023	0.0069	0.0087	0.0045	0.0047	0.0204	0.0134	0.0462	0.1056	0.0043	0.1090	0.2687	0.2209	0.0032	0.0521	0.0196	0.0087	0.0800	0.0385	0.0241	0.0146
Pb	0.086	0.091	0.073	0.027	0.159	0.144	0.076	0.044	0.040	0.083	0.069	0.151	0.084	0.073	0.427	0.125	0.882	1.494	0.131	0.152	0.060	0.081
S	0.08	0.09	0.35	0.41	0.89	0.88	1.31	2.64	1.92	2.07	2.23	4.34	3.45	5.06	0.67	8.06	3.24	4.19	2.71	2.45	2.47	2.43
Sb	0.00003	0.00001	0.00022	0.00001	0.00015	0.00001	0	0	0	0.00002	0.00003	0	0.00009	0	0.00003	0	0.43985	0.69948	0.3699	0.33185	0.25784	0.21876
Se	0.0036	0.0040	0.0022	0.0011	0.0066	0.0059	0.0000	0.0000	0.0000	0.0002	0.0011	0.0011	0.0011	0.0013	0.0195	0.0018	0.0393	0.0666	0.0037	0.0051	0.0014	0.0014
Si	2.40	2.50	7.13	6.49	2.54	2.52	8.80	9.94	6.28	6.09	10.98	9.43	9.98	10.11	7.13	9.16	8.77	7.53	9.18	9.18	7.24	7.10
Sn	0	0	0	0	0	0	0	0	0.00011	0	0	0	0	0	0	0	0	0	0	0	0	0
Sr	0	0	0	0.00003	0	0	0	0	0	0	0	0	0	0	0	0	0	0	0	0	0	0
Th	0	0	0	0	0	0	0	0	0	0	0	0	0	0	0	0	0	0	0	0	0	0
Ti	0.021	0.009	0.011	0.004	0.020	0.015	0.279	0.223	0.130	0.254	0.171	0.387	0.104	0.093	0.002	0.212	0.032	0.076	0.036	0.026	0.016	0.008
W	0.000	0.000	0.264	0.684	0.011	0.011	0.000	0.000	0.000	0.000	0.001	0.001	0.014	0.002	0.267	0.000	0.000	0.000	0.000	0.000	0.000	0.000
Zn	0.039	0.039	0.302	0.335	1.258	1.239	0.200	1.639	0.092	0.100	0.224	0.211	0.291	0.875	0.308	0.959	1.550	1.053	1.535	1.175	1.733	1.582
Zr	0.00043	0.0003	0.00076	0.00039	0.00248	0.00189	0.00108	0.00194	0.00028	0.00045	0.00131	0.14517	0.00081	0.00059	0.00044	0.00065	0.00013	0	0.00016	0	0	0.00005
Total	100.00	100.00	100.00	100.00	100.00	100.00	100.00	100.00	100.00	100.00	100.00	100.00	100.00	100.00	100.00	100.00	100.00	100.00	100.00	100.00	100.00	100.00

* Base position = initial analysis; Rotate = rotate sample mount 90° then re-analyze

Metal Distribution by Mineral (weight-%, normalized)

Element of Concern ANTIMONY, Sb

Sample	A951 176m, Class B		A431 306m, Class A		A431 306m, Class A		A355 160.5m, Class C		A355 160.5m, Class		A355 70.5m, Class B		A355 70.5m, Class B		A355 70.5m, Class B		A162 97.5m, Class A		A162 97.5m, Class A		A162 97.5m, Class A	
Size Fraction	-300/+150 µm		-1190/+600 µm		-75/+53 µm		-1190/+600 µm		-150/+106 µm		-600/+300 µm		-600/+300 µm		-150/+106 µm		-1190/+600 µm		-600/+300 µm		-106/+75 µm	
Random Position*	Base	Rotate	Base	Rotate	Base	Rotate	Base	Rotate	Base	Rotate	Base	Rotate	Base	Rotate	Base	Rotate	Base	Rotate	Base	Rotate	Base	Rotate
Stibnite	0.0000	0.0000	0.0001	0.0000	0.0002	0.0000	0.0000	0.0000	0.0000	0.0000	0.0000	0.0000	0.0000	0.0000	0.0000	0.0000	0.0061	0.0004	0.0019	0.0005	0.0010	0.0004
WatanabeiteZn	0.0000	0.0000	0.0017	0.0001	0.0001	0.0001	0.0000	0.0000	0.0000	0.0000	0.0000	0.0000	0.0000	0.0330	0.0000	0.0000	1.8574	1.7341	2.9251	2.6311	2.0406	1.7341
Bismutostibiconite	0.0001	0.0000	0.0002	0.0000	0.0000	0.0000	0.0000	0.0000	0.0000	0.0001	0.0001	0.0000	0.0003	0.0004	0.0002	0.0000	0.0000	0.0000	0.0000	0.0000	0.0000	0.0000
Subtotal	**0.0001**	**0.0000**	**0.0021**	**0.0001**	**0.0003**	**0.0001**	**0.0000**	**0.0000**	**0.0000**	**0.0001**	**0.0001**	**0.0000**	**0.0003**	**0.0335**	**0.0002**	**0.0000**	**1.8635**	**1.7345**	**2.9270**	**2.6316**	**2.0417**	**1.7345**
Sulphide	0.28	0.31	1.71	1.17	2.84	2.77	2.35	7.53	4.52	4.95	4.46	8.48	6.91	12.30	16.34	16.30	7.14	5.97	6.03	5.38	5.93	5.97
Carbonate	88.58	88.05	64.52	66.58	84.92	84.89	55.43	52.05	67.57	68.31	45.55	48.04	46.80	49.85	44.55	42.62	48.33	60.11	44.83	47.02	59.43	60.11
Silicate	11.12	11.63	33.01	31.10	12.00	12.00	41.97	40.25	27.16	25.98	49.88	42.86	44.77	37.42	38.69	40.45	42.51	32.03	45.72	44.71	32.36	32.03
Phosphate	0.019	0.012	0.059	0.047	0.024	0.026	0.135	0.073	0.251	0.574	0.023	0.593	1.460	0.120	0.132	0.283	0.111	0.079	0.435	0.209	0.131	0.079
Oxide	0.000	0.000	0.004	0.000	0.036	0.053	0.001	0.001	0.206	0.066	0.023	0.011	0.005	0.241	0.216	0.260	0.004	0.044	0.009	0.001	0.051	0.044
Sulphate	0.002	0.001	0.012	0.000	0.002	0.014	0.109	0.093	0.283	0.114	0.067	0.014	0.040	0.026	0.066	0.094	0.029	0.022	0.008	0.005	0.045	0.022
Other	0.00	0.00	0.68	1.11	0.18	0.24	0.00	0.00	0.01	0.00	0.00	0.00	0.02	0.01	0.00	0.00	0.02	0.01	0.04	0.04	0.00	0.01
Subtotal	**100.000**	**100.000**	**99.998**	**100.000**	**100.000**	**100.000**	**100.000**	**100.000**	**100.000**	**100.000**	**100.000**	**100.000**	**100.000**	**99.967**	**100.000**	**100.000**	**98.137**	**98.266**	**97.073**	**97.368**	**97.958**	**98.266**
Total	100.0	100.0	100.0	100.0	100.0	100.0	100.0	100.0	100.0	100.0	100.0	100.0	100.0	100.0	100.0	100.0	100.0	100.0	100.0	100.0	100.0	100.0

* Base position = initial analysis; Rotate = rotate sample mount 90° then re-analyze

Element of Concern ARSENIC, As

Sample	A951 176m, Class B		A431 306m, Class A		A431 306m, Class A		A355 160.5m, Class C		A355 160.5m, Class		A355 70.5m, Class B		A355 70.5m, Class B		A355 70.5m, Class B		A162 97.5m, Class A		A162 97.5m, Class A		A162 97.5m, Class A	
Size Fraction	-300/+150 µm		-1190/+600 µm		-75/+53 µm		-1190/+600 µm		-150/+106 µm		-600/+300 µm		-600/+300 µm		-150/+106 µm		-1190/+600 µm		-600/+300 µm		-106/+75 µm	
Random Position*	Base	Rotate	Base	Rotate	Base	Rotate	Base	Rotate	Base	Rotate	Base	Rotate	Base	Rotate	Base	Rotate	Base	Rotate	Base	Rotate	Base	Rotate
Arsenopyrite	0.0000	0.0000	0.0000	0.0000	0.0000	0.0000	0.0000	0.0000	0.0000	0.0000	0.0000	0.0000	0.0000	0.0000	0.0000	0.0000	0.0000	0.0000	0.0000	0.0000	0.0000	0.0000
RealgarOrpiment	0.0000	0.0000	0.0000	0.0000	0.0000	0.0000	0.0000	0.0000	0.0000	0.0000	0.0000	0.0000	0.0000	0.0000	0.0000	0.0000	0.0000	0.0000	0.0000	0.0000	0.0000	0.0000
Enargite	0.0000	0.0000	0.0075	0.0225	0.0026	0.0040	0.0000	0.0000	0.0000	0.0000	0.0000	0.0000	0.0000	0.0001	0.0000	0.0000	0.4820	0.5962	0.9288	1.4479	0.5283	0.5962
EnargiteZn	0.0000	0.0000	0.0135	0.0000	0.0292	0.0303	0.0000	0.0000	0.0006	0.0000	0.0000	0.0000	0.0000	0.0000	0.0000	0.0000	0.3660	0.1855	0.9392	0.5270	0.0975	0.1855
TennantiteZnFe	0.0000	0.0000	0.0011	0.0003	0.0001	0.0107	0.0000	0.0000	0.0000	0.0000	0.0000	0.0000	0.0000	0.0000	0.0000	0.0000	0.0139	0.0082	0.0042	0.0046	0.0414	0.0082
WatanabeiteZn	0.0000	0.0000	0.0004	0.0001	0.0001	0.0001	0.0000	0.0000	0.0000	0.0000	0.0000	0.0000	0.0000	0.0330	0.0000	0.0000	3.4656	1.7341	2.9251	2.6311	2.0406	1.7341
FeOxideSulphateCuPbZnAs	0.0000	0.0000	0.0031	0.0003	0.0348	0.0530	0.0010	0.0005	0.1328	0.0060	0.0190	0.0064	0.0046	0.2355	0.2137	0.2584	0.0008	0.0419	0.0044	0.0006	0.0472	0.0419
SideriteMnAsZnCrCu	0.0000	0.0000	0.0000	0.0004	0.0000	0.0000	0.0000	0.0000	0.0000	0.0000	0.0000	0.0000	0.0000	0.0055	0.0003	0.0000	0.0000	0.0000	0.0000	0.0000	0.0000	0.0000
FeSulphateLimoniteCuAsMoZ	0.0008	0.0010	0.0001	0.0002	0.0000	0.0000	0.0503	0.0926	0.2707	0.1142	0.0416	0.0136	0.0363	0.0237	0.0633	0.0781	0.0103	0.0038	0.0017	0.0044	0.0022	0.0038
FornaciteConichalcite	0.0000	0.0000	0.0000	0.0000	0.0000	0.0000	0.0000	0.0000	0.0000	0.0000	0.0000	0.0000	0.0000	0.0000	0.0000	0.0000	0.0000	0.0000	0.0000	0.0000	0.0000	0.0000
TyrolitePb	0.0000	0.0000	0.0000	0.0000	0.0000	0.0000	0.0000	0.0000	0.0000	0.0000	0.0000	0.0000	0.0000	0.0000	0.0000	0.0000	0.0000	0.0000	0.0000	0.0000	0.0000	0.0000
Subtotal	**0.0008**	**0.0010**	**0.0257**	**0.0238**	**0.0668**	**0.0979**	**0.0512**	**0.0931**	**0.4041**	**0.1201**	**0.0606**	**0.0201**	**0.0409**	**0.2978**	**0.2773**	**0.3365**	**4.3386**	**2.5697**	**4.8034**	**4.6156**	**2.7573**	**2.5697**
Sulphide	0.28	0.31	1.03	1.15	2.81	2.73	2.93	7.53	4.52	4.95	4.46	8.48	6.91	12.30	16.34	16.30	6.70	5.18	4.16	3.40	5.27	5.18
Carbonate	88.58	88.05	63.97	66.58	84.92	84.89	57.92	52.05	67.62	68.31	45.55	48.04	46.80	49.85	44.55	42.62	44.52	60.11	44.83	47.02	59.43	60.11
Silicate	11.12	11.63	34.32	31.10	12.00	12.00	38.98	40.25	27.16	25.98	49.88	42.86	44.77	37.42	38.69	40.45	44.36	32.03	45.72	44.71	32.36	32.03
Phosphate	0.019	0.012	0.037	0.047	0.024	0.026	0.111	0.073	0.251	0.574	0.023	0.593	1.460	0.120	0.132	0.283	0.107	0.079	0.435	0.209	0.131	0.079
Oxide	0.000	0.000	0.000	0.000	0.002	0.000	0.000	0.000	0.073	0.060	0.004	0.004	0.000	0.006	0.003	0.002	0.004	0.003	0.005	0.000	0.004	0.003
Sulphate	0.001	0.000	0.005	0.000	0.001	0.014	0.000	0.000	0.013	0.000	0.025	0.000	0.004	0.002	0.003	0.016	0.015	0.018	0.006	0.001	0.042	0.018
Other	0.00	0.00	0.61	1.11	0.18	0.24	0.00	0.00	0.01	0.00	0.00	0.00	0.02	0.01	0.00	0.00	0.01	0.01	0.04	0.04	0.00	0.01
Subtotal	**100.0**	**100.0**	**100.0**	**100.0**	**99.9**	**99.9**	**99.9**	**99.9**	**99.6**	**99.9**	**99.9**	**100.0**	**100.0**	**99.7**	**99.7**	**99.7**	**95.7**	**97.4**	**95.2**	**95.4**	**97.2**	**97.4**
Total	100.0	100.0	100.0	100.0	100.0	100.0	100.0	100.0	100.0	100.0	100.0	100.0	100.0	100.0	100.0	100.0	100.1	100.0	100.0	100.0	100.0	100.0

* Base position = initial analysis; Rotate = rotate sample mount 90° then re-analyze

Element of Concern COPPER, Cu

Sample	A951 176m, Class B		A431 306m, Class A		A431 306m, Class A		A355 160.5m, Class C		A355 160.5m, Class		A355 70.5m, Class B		A355 70.5m, Class B		A355 70.5m, Class B		A162 97.5m, Class A		A162 97.5m, Class A		A162 97.5m, Class A	
Size Fraction	-300/+150 µm		-1190/+600 µm		-75/+53 µm		-1190/+600 µm		-150/+106 µm		-600/+300 µm		-600/+300 µm		-150/+106 µm		-1190/+600 µm		-600/+300 µm		-106/+75 µm	
Random Position*	Base	Rotate	Base	Rotate	Base	Rotate	Base	Rotate	Base	Rotate	Base	Rotate	Base	Rotate	Base	Rotate	Base	Rotate	Base	Rotate	Base	Rotate
TrampMetal	0.0000	0.0000	0.0002	0.0002	0.0027	0.0029	0.0006	0.0000	0.0079	0.0040	0.0011	0.0001	0.0013	0.0020	0.0011	0.0003	0.0004	0.0018	0.0048	0.0001	0.0010	0.0018
PyriteCu	0.0003	0.0010	0.0000	0.0000	0.0000	0.0000	0.0005	0.0037	0.0333	0.0040	0.0774	0.0050	0.1906	0.0756	0.2044	0.3330	0.0193	0.0292	0.0211	0.0077	0.0170	0.0292
Chalcocite	0.0000	0.0000	0.0013	0.0000	0.0000	0.0000	0.0000	0.0000	0.0000	0.0000	0.0000	0.0000	0.0000	0.0001	0.0000	0.0000	0.0094	0.0206	0.0017	0.0000	0.0302	0.0206
Bornite	0.0000	0.0000	0.0212	0.0192	0.0514	0.0657	0.0000	0.0000	0.0000	0.0000	0.0000	0.0000	0.0000	0.0003	0.0001	0.0001	0.7221	0.9361	0.3591	0.2986	0.9158	0.9361
Chalcopyrite	0.0453	0.0464	0.0349	0.0558	0.3665	0.3794	0.1181	0.0272	0.1830	0.1312	0.0590	0.2614	0.3076	0.4264	0.3159	0.2266	1.7339	0.8157	0.9783	0.8577	1.0027	0.8157
ChalcopyritePb	0.0024	0.0138	0.2089	0.0212	0.1055	0.1009	0.0300	0.0197	0.0126	0.0209	0.0255	0.0502	0.0628	0.0688	0.1051	0.1424	0.1372	0.4732	0.3391	0.3061	0.1992	0.4732
ChalcopyriteZn	0.0000	0.0015	0.0134	0.0001	0.1041	0.0516	0.0074	0.0034	0.0044	0.0000	0.0018	0.0561	0.0017	0.0307	0.0310	0.0499	0.0939	0.1020	0.1660	0.0823	0.1588	0.1020
Enargite	0.0000	0.0000	0.0075	0.0225	0.0026	0.0040	0.0000	0.0000	0.0000	0.0000	0.0000	0.0000	0.0000	0.0001	0.0000	0.0000	0.4820	0.5962	0.9288	1.4479	0.5283	0.5962
EnargiteZn	0.0000	0.0000	0.0135	0.0000	0.0292	0.0303	0.0000	0.0000	0.0006	0.0000	0.0000	0.0000	0.0000	0.0000	0.0000	0.0000	0.3660	0.1855	0.9392	0.5270	0.0975	0.1855
TennantiteZnFe	0.0000	0.0000	0.0011	0.0003	0.0001	0.0107	0.0000	0.0000	0.0000	0.0000	0.0000	0.0000	0.0000	0.0000	0.0000	0.0000	0.0139	0.0082	0.0042	0.0046	0.0414	0.0082
WatanabeiteZn	0.0000	0.0000	0.0004	0.0001	0.0001	0.0001	0.0000	0.0000	0.0000	0.0000	0.0000	0.0000	0.0000	0.0330	0.0000	0.0000	3.4656	1.7341	2.9251	2.6311	2.0406	1.7341
SphaleriteCu	0.0582	0.0011	0.3301	0.2626	0.9172	0.6262	0.3007	2.5580	0.1281	0.0713	0.3252	0.1084	0.3717	1.0913	1.5631	1.3804	0.4316	0.8803	0.8745	0.2109	1.4360	0.8803
SiegeniteCuFe	0.0000	0.0000	0.0000	0.0000	0.0000	0.0000	0.0000	0.0000	0.0000	0.0000	0.0000	0.0000	0.0000	0.0000	0.0000	0.0000	0.0000	0.0000	0.0044	0.0053	0.0000	0.0000
SiegeniteCuZn	0.0000	0.0000	0.0000	0.0000	0.0000	0.0000	0.0000	0.0000	0.0000	0.0000	0.0000	0.0000	0.0000	0.0000	0.0000	0.0000	0.0000	0.0000	0.0000	0.0000	0.0000	0.0000
FeOxideSulphateCuPbZnAs	0.0000	0.0000	0.0031	0.0003	0.0348	0.0530	0.0010	0.0005	0.1328	0.0060	0.0190	0.0064	0.0046	0.2355	0.2137	0.2584	0.0008	0.0419	0.0044	0.0006	0.0472	0.0419
Cuprite	0.0000	0.0000	0.0000	0.0000	0.0000	0.0000	0.0000	0.0000	0.0016	0.0000	0.0000	0.0000	0.0000	0.0000	0.0011	0.0000	0.0002	0.0013	0.0000	0.0000	0.0032	0.0013
ParamelaconiteZn	0.0000	0.0000	0.0000	0.0000	0.0000	0.0000	0.0000	0.0000	0.0000	0.0000	0.0000	0.0000	0.0000	0.0001	0.0000	0.0000	0.0000	0.0000	0.0000	0.0000	0.0000	0.0000
PbMoOxide	0.0000	0.0000	0.0000	0.0000	0.0014	0.0000	0.0000	0.0001	0.0000	0.0000	0.0001	0.0000	0.0000	0.0000	0.0000	0.0000	0.0001	0.0000	0.0000	0.0000	0.0000	0.0000
SideriteMnAsZnCrCu	0.0000	0.0000	0.0000	0.0004	0.0000	0.0000	0.0000	0.0000	0.0000	0.0000	0.0000	0.0000	0.0000	0.0055	0.0003	0.0000	0.0000	0.0000	0.0000	0.0000	0.0000	0.0000
Smithsonite_trans	0.0000	0.0000	0.0000	0.0000	0.0000	0.0000	0.0000	0.0000	0.0000	0.0000	0.0000	0.0000	0.0000	0.0000	0.0000	0.0000	0.0000	0.0000	0.0000	0.0000	0.0000	0.0000
GruneritePbCuZn	0.0054	0.0000	0.0001	0.0000	0.0001	0.0001	0.0002	0.0001	0.0000	0.0040	0.0000	0.0000	0.0000	0.0001	0.0000	0.0000	0.0014	0.0007	0.0000	0.0000	0.0000	0.0007
Malachite	0.0000	0.0000	0.0000	0.0000	0.0000	0.0000	0.0000	0.0000	0.0000	0.0000	0.0000	0.0000	0.0000	0.0000	0.0000	0.0000	0.0000	0.0000	0.0000	0.0000	0.0000	0.0000
OtaviteZnCu	0.0000	0.0000	0.0000	0.0000	0.0000	0.0000	0.0000	0.0000	0.0000	0.0000	0.0000	0.0000	0.0000	0.0000	0.0000	0.0000	0.0000	0.0000	0.0000	0.0000	0.0000	0.0000
FeSulphateLimoniteCuAsMoZ	0.0008	0.0010	0.0001	0.0002	0.0000	0.0000	0.0503	0.0926	0.2707	0.1142	0.0416	0.0136	0.0363	0.0237	0.0633	0.0781	0.0103	0.0038	0.0017	0.0044	0.0022	0.0038
JarositeCu	0.0000	0.0000	0.0000	0.0000	0.0000	0.0000	0.0000	0.0000	0.0001	0.0000	0.0000	0.0000	0.0002	0.0001	0.0001	0.0000	0.0000	0.0000	0.0000	0.0001	0.0000	0.0000
MoCaSulphateMnCuFeZn	0.0000	0.0000	0.0000	0.0000	0.0000	0.0000	0.0000	0.0000	0.0000	0.0000	0.0002	0.0000	0.0001	0.0001	0.0000	0.0000	0.0030	0.0000	0.0000	0.0000	0.0000	0.0000
MolybdofornaciteZnCu	0.0000	0.0000	0.0002	0.0000	0.0001	0.0000	0.0000	0.0002	0.0000	0.0000	0.0002	0.0000	0.0005	0.0004	0.0011	0.0000	0.0020	0.0019	0.0014	0.0009	0.0010	0.0019
Powellite_trans	0.0000	0.0000	0.0000	0.0000	0.0000	0.0000	0.0000	0.0000	0.0000	0.0000	0.0000	0.0000	0.0000	0.0000	0.0000	0.0000	0.0000	0.0000	0.0000	0.0000	0.0000	0.0000
Wulfenite_trans	0.0000	0.0000	0.0000	0.0000	0.0001	0.0000	0.0000	0.0000	0.0000	0.0000	0.0001	0.0000	0.0002	0.0003	0.0004	0.0000	0.0001	0.0000	0.0000	0.0000	0.0000	0.0000
ApatiteCuPbZn	0.0189	0.0110	0.0374	0.0448	0.0201	0.0255	0.1106	0.0689	0.2512	0.5352	0.0231	0.5924	1.4603	0.1158	0.1304	0.2819	0.1060	0.0788	0.4341	0.2092	0.1306	0.0788
FornaciteConichalcite	0.0000	0.0000	0.0000	0.0000	0.0000	0.0000	0.0000	0.0000	0.0000	0.0000	0.0000	0.0000	0.0000	0.0000	0.0000	0.0000	0.0000	0.0000	0.0000	0.0000	0.0000	0.0000
TyrolitePb	0.0000	0.0000	0.0000	0.0000	0.0000	0.0000	0.0000	0.0000	0.0000	0.0000	0.0000	0.0000	0.0000	0.0000	0.0000	0.0000	0.0000	0.0000	0.0000	0.0000	0.0000	0.0000
MicaAlteredCuZn	0.0473	0.1122	0.6831	0.4457	0.1397	0.2287	0.0925	0.0143	0.1918	0.1440	0.3653	0.8013	0.6163	0.4327	0.2332	0.5029	0.0645	0.1454	0.1113	0.5342	0.1821	0.1454
FeOxideCu	0.0000	0.0000	0.0004	0.0000	0.0008	0.0002	0.0000	0.0000	0.0003	0.0010	0.0011	0.0000	0.0000	0.0082	0.0013	0.0323	0.0000	0.0000	0.0000	0.0000	0.0000	0.0000
MoSulphatePowelliteClay	0.0000	0.0000	0.0000	0.0000	0.0000	0.0000	0.0000	0.0000	0.0000	0.0000	0.0000	0.0000	0.0000	0.0001	0.0003	0.0000	0.0000	0.0000	0.0000	0.0000	0.0000	0.0000
TitaniteMixPbCu	0.1048	0.0452	0.0552	0.0182	0.0916	0.0698	1.1764	0.6645	0.4652	1.0785	0.6770	1.8251	0.3969	0.6906	0.5551	0.9213	0.1557	0.0312	0.1449	0.1017	0.0721	0.0312
Subtotal	**0.2835**	**0.2332**	**1.4121**	**0.8915**	**1.8681**	**1.6488**	**1.8882**	**3.4532**	**1.6835**	**2.1142**	**1.6176**	**3.7201**	**3.4510**	**3.2413**	**3.4209**	**4.2076**	**7.8193**	**6.0880**	**8.2440**	**7.2304**	**6.9068**	**6.0880**
Sulphide	0.17	0.24	0.42	0.79	1.26	1.50	2.48	4.92	4.16	4.73	3.97	8.00	5.97	10.60	14.12	14.17	3.55	1.93	1.41	1.64	1.51	1.93
Carbonate	88.58	88.05	63.97	66.58	84.92	84.89	57.92	52.05	67.57	68.31	45.55	48.04	46.80	49.85	44.55	42.62	44.46	60.11	44.83	47.02	59.43	60.11
Silicate	10.96	11.47	33.58	30.63	11.77	11.71	37.71	39.57	26.50	24.75	48.83	40.23	43.76	36.29	37.90	38.99	44.14	31.85	45.47	44.08	32.11	31.85
Phosphate	0.000	0.001	0.000	0.003	0.004	0.000	0.000	0.004	0.000	0.039	0.000	0.000	0.000	0.004	0.001	0.001	0.001	0.001	0.001	0.000	0.000	0.001
Oxide	0.000	0.000	0.000	0.000	0.000	0.000	0.000	0.000	0.071	0.060	0.004	0.004	0.000	0.006	0.002	0.002	0.004	0.001	0.005	0.000	0.001	0.001
Sulphate	0.001	0.000	0.005	0.000	0.001	0.014	0.000	0.000	0.013	0.000	0.025	0.000	0.004	0.002	0.003	0.016	0.012	0.018	0.006	0.001	0.042	0.018
Other	0.00	0.00	0.61	1.11	0.17	0.24	0.00	0.00	0.00	0.00	0.00	0.00	0.02	0.01	0.00	0.00	0.01	0.00	0.03	0.04	0.00	0.00
Subtotal	**99.717**	**99.767**	**98.588**	**99.109**	**98.132**	**98.351**	**98.112**	**96.547**	**98.317**	**97.886**	**98.382**	**96.280**	**96.549**	**96.759**	**96.579**	**95.792**	**92.181**	**93.912**	**91.756**	**92.770**	**93.093**	**93.912**
Total	100.0	100.0	100.0	100.0	100.0	100.0	100.0	100.0	100.0	100.0	100.0	100.0	100.0	100.0	100.0	100.0	100.0	100.0	100.0	100.0	100.0	100.0

* Base position = initial analysis; Rotate = rotate sample mount 90° then re-analyze

Element of Concern MOLYBDENUM, Mo

Sample	A951 176m, Class B		A431 306m, Class A		A431 306m, Class A		A355 160.5m, Class C		A355 160.5m, Class		A355 70.5m, Class B		A355 70.5m, Class B		A355 70.5m, Class B		A162 97.5m, Class A		A162 97.5m, Class A		A162 97.5m, Class A	
Size Fraction	-300/+150 µm		-1190/+600 µm		-75/+53 µm		-1190/+600 µm		-150/+106 µm		-600/+300 µm		-600/+300 µm		-150/+106 µm		-1190/+600 µm		-600/+300 µm		-106/+75 µm	
Random Position*	Base	Rotate	Base	Rotate	Base	Rotate	Base	Rotate	Base	Rotate	Base	Rotate	Base	Rotate	Base	Rotate	Base	Rotate	Base	Rotate	Base	Rotate
Molybdenite	0.0004	0.0032	0.1919	0.4739	0.0412	0.0636	0.0000	0.0000	0.0000	0.0022	0.0002	0.0000	0.0003	0.0004	0.0006	0.0000	0.0221	0.0000	0.0061	0.0017	0.0000	0.0000
PbMoOxide	0.0000	0.0000	0.0000	0.0000	0.0014	0.0000	0.0000	0.0001	0.0000	0.0000	0.0001	0.0000	0.0000	0.0000	0.0000	0.0000	0.0001	0.0000	0.0000	0.0000	0.0000	0.0000
PbCaOxideMoZnW	0.0000	0.0000	0.0000	0.0000	0.0000	0.0000	0.0000	0.0000	0.0000	0.0000	0.0000	0.0000	0.0000	0.0000	0.0000	0.0000	0.0000	0.0000	0.0000	0.0000	0.0000	0.0000
FeSulphateLimoniteCuAsMoZ	0.0008	0.0010	0.0001	0.0002	0.0000	0.0000	0.0503	0.0926	0.2707	0.1142	0.0416	0.0136	0.0363	0.0237	0.0633	0.0781	0.0103	0.0038	0.0017	0.0044	0.0022	0.0038
MoCaSulphateMnCuFeZn	0.0000	0.0000	0.0000	0.0000	0.0000	0.0000	0.0000	0.0000	0.0000	0.0000	0.0002	0.0000	0.0001	0.0001	0.0000	0.0000	0.0030	0.0000	0.0000	0.0000	0.0000	0.0000
MolybdofornaciteZnCu	0.0000	0.0000	0.0002	0.0000	0.0001	0.0000	0.0000	0.0002	0.0000	0.0000	0.0002	0.0000	0.0005	0.0004	0.0011	0.0000	0.0020	0.0019	0.0014	0.0009	0.0010	0.0019
Powellite_trans	0.0000	0.0000	0.0000	0.0000	0.0000	0.0000	0.0000	0.0000	0.0000	0.0000	0.0000	0.0000	0.0000	0.0000	0.0000	0.0000	0.0000	0.0000	0.0000	0.0000	0.0000	0.0000
Wulfenite_trans	0.0000	0.0000	0.0000	0.0000	0.0001	0.0000	0.0000	0.0000	0.0000	0.0000	0.0001	0.0000	0.0002	0.0003	0.0004	0.0000	0.0001	0.0000	0.0000	0.0000	0.0000	0.0000
CaMoSilicate	0.0000	0.0000	0.0000	0.0000	0.0000	0.0000	0.0000	0.0002	0.0000	0.0000	0.0000	0.0000	0.0000	0.0000	0.0000	0.0000	0.0000	0.0000	0.0000	0.0000	0.0000	0.0000
MoSulphatePowelliteClay	0.0000	0.0000	0.0000	0.0000	0.0000	0.0000	0.0000	0.0000	0.0000	0.0000	0.0000	0.0000	0.0000	0.0001	0.0003	0.0000	0.0000	0.0000	0.0000	0.0000	0.0000	0.0000
Subtotal	**0.0011**	**0.0042**	**0.1922**	**0.4741**	**0.0428**	**0.0636**	**0.0503**	**0.0930**	**0.2708**	**0.1164**	**0.0424**	**0.0136**	**0.0375**	**0.0249**	**0.0657**	**0.0781**	**0.0376**	**0.0057**	**0.0092**	**0.0069**	**0.0033**	**0.0057**
Sulphide	0.28	0.30	0.86	0.70	2.80	2.71	2.93	7.53	4.52	4.95	4.46	8.48	6.91	12.33	16.34	16.30	11.00	7.71	8.95	8.01	7.97	7.71
Carbonate	88.58	88.05	63.98	66.58	84.92	84.89	57.92	52.05	67.57	68.31	45.55	48.04	46.80	49.85	44.55	42.62	44.46	60.11	44.83	47.02	59.43	60.11
Silicate	11.12	11.63	34.32	31.10	12.00	12.00	38.98	40.25	27.16	25.98	49.88	42.86	44.77	37.42	38.69	40.45	44.36	32.03	45.72	44.71	32.36	32.03
Phosphate	0.019	0.012	0.037	0.047	0.024	0.026	0.111	0.073	0.251	0.574	0.023	0.593	1.460	0.120	0.132	0.283	0.107	0.079	0.435	0.209	0.131	0.079
Oxide	0.000	0.000	0.003	0.000	0.035	0.053	0.001	0.001	0.206	0.066	0.023	0.011	0.005	0.241	0.216	0.260	0.005	0.044	0.009	0.001	0.051	0.044
Sulphate	0.001	0.000	0.005	0.000	0.001	0.014	0.000	0.000	0.013	0.000	0.025	0.000	0.004	0.002	0.003	0.016	0.012	0.018	0.006	0.001	0.042	0.018
Other	0.00	0.00	0.61	1.11	0.18	0.24	0.00	0.00	0.01	0.00	0.00	0.00	0.02	0.01	0.00	0.00	0.01	0.01	0.04	0.04	0.00	0.01
Subtotal	**100.0**	**100.0**	**99.8**	**99.5**	**100.0**	**99.9**	**99.9**	**99.9**	**99.7**	**99.9**	**100.0**	**100.0**	**100.0**	**100.0**	**99.9**	**99.9**	**100.0**	**100.0**	**100.0**	**100.0**	**100.0**	**100.0**
Total	100.0	100.0	100.0	100.0	100.0	100.0	100.0	100.0	100.0	100.0	100.0	100.0	100.0	100.0	100.0	100.0	100.0	100.0	100.0	100.0	100.0	100.0

* Base position = initial analysis; Rotate = rotate sample mount 90° then re-analyze

Element of Concern LEAD, Pb

Sample	A951 176m, Class B		A431 306m, Class A		A431 306m, Class A		A355 160.5m, Class C		A355 160.5m, Class		A355 70.5m, Class B		A355 70.5m, Class B		A355 70.5m, Class B		A162 97.5m, Class A		A162 97.5m, Class A		A162 97.5m, Class A	
Size Fraction	-300/+150 µm		-1190/+600 µm		-75/+53 µm		-1190/+600 µm		-150/+106 µm		-600/+300 µm		-600/+300 µm		-150/+106 µm		-1190/+600 µm		-600/+300 µm		-106/+75 µm	
Random Position*	Base	Rotate	Base	Rotate	Base	Rotate	Base	Rotate	Base	Rotate	Base	Rotate	Base	Rotate	Base	Rotate	Base	Rotate	Base	Rotate	Base	Rotate
ChalcopyritePb	0.0024	0.0138	0.1485	0.0212	0.1055	0.1009	0.0300	0.0197	0.0126	0.0209	0.0255	0.0502	0.0628	0.0688	0.1051	0.1424	0.1372	0.4732	0.3391	0.3061	0.1992	0.4732
GalenaSe	0.0972	0.1082	0.1548	0.0284	0.1745	0.1576	0.0002	0.0004	0.0007	0.0051	0.0304	0.0300	0.0288	0.0323	0.0576	0.0493	1.0617	0.0373	0.0991	0.1387	0.0385	0.0373
Galenobismutite	0.0000	0.0000	0.0000	0.0000	0.0000	0.0000	0.0000	0.0000	0.0000	0.0000	0.0000	0.0000	0.0000	0.0000	0.0000	0.0000	0.0000	0.0000	0.0000	0.0000	0.0000	0.0000
FeOxideSulphateCuPbZnAs	0.0000	0.0000	0.0035	0.0003	0.0348	0.0530	0.0010	0.0005	0.1328	0.0060	0.0190	0.0064	0.0046	0.2355	0.2137	0.2584	0.0008	0.0419	0.0044	0.0006	0.0472	0.0419
PbMoOxide	0.0000	0.0000	0.0001	0.0000	0.0014	0.0000	0.0000	0.0001	0.0000	0.0000	0.0001	0.0000	0.0000	0.0000	0.0000	0.0000	0.0001	0.0000	0.0000	0.0000	0.0000	0.0000
PbCaOxideMoZnW	0.0000	0.0000	0.0000	0.0000	0.0000	0.0000	0.0000	0.0000	0.0000	0.0000	0.0000	0.0000	0.0000	0.0000	0.0000	0.0000	0.0000	0.0000	0.0000	0.0000	0.0000	0.0000
GruneritePbCuZn	0.0054	0.0000	0.0011	0.0000	0.0001	0.0001	0.0002	0.0001	0.0000	0.0040	0.0000	0.0000	0.0000	0.0001	0.0000	0.0000	0.0014	0.0007	0.0000	0.0000	0.0000	0.0007
MolybdofornaciteZnCu	0.0000	0.0000	0.0007	0.0000	0.0001	0.0000	0.0000	0.0002	0.0000	0.0000	0.0002	0.0000	0.0005	0.0004	0.0011	0.0000	0.0020	0.0019	0.0014	0.0009	0.0010	0.0019
Powellite_trans	0.0000	0.0000	0.0000	0.0000	0.0000	0.0000	0.0000	0.0000	0.0000	0.0000	0.0000	0.0000	0.0000	0.0000	0.0000	0.0000	0.0000	0.0000	0.0000	0.0000	0.0000	0.0000
Wulfenite_trans	0.0000	0.0000	0.0008	0.0000	0.0001	0.0000	0.0000	0.0000	0.0000	0.0000	0.0001	0.0000	0.0002	0.0003	0.0004	0.0000	0.0001	0.0000	0.0000	0.0000	0.0000	0.0000
ApatiteCuPbZn	0.0189	0.0110	0.0589	0.0448	0.0201	0.0255	0.1106	0.0689	0.2512	0.5352	0.0231	0.5924	1.4603	0.1158	0.1304	0.2819	0.1060	0.0788	0.4341	0.2092	0.1306	0.0788
FornaciteConichalcite	0.0000	0.0000	0.0000	0.0000	0.0000	0.0000	0.0000	0.0000	0.0000	0.0000	0.0000	0.0000	0.0000	0.0000	0.0000	0.0000	0.0000	0.0000	0.0000	0.0000	0.0000	0.0000
TyrolitePb	0.0000	0.0000	0.0000	0.0000	0.0000	0.0000	0.0000	0.0000	0.0000	0.0000	0.0000	0.0000	0.0000	0.0000	0.0000	0.0000	0.0000	0.0000	0.0000	0.0000	0.0000	0.0000
MoSulphatePowelliteClay	0.0000	0.0000	0.0000	0.0000	0.0000	0.0000	0.0000	0.0000	0.0000	0.0000	0.0000	0.0000	0.0000	0.0001	0.0003	0.0000	0.0000	0.0000	0.0000	0.0000	0.0000	0.0000
TitaniteMixPbCu	0.1048	0.0452	0.0705	0.0182	0.0916	0.0698	1.1764	0.6645	0.4652	1.0785	0.6770	1.8251	0.3969	0.6906	0.5551	0.9213	0.1557	0.0312	0.1449	0.1017	0.0721	0.0312
Subtotal	**0.2287**	**0.1781**	**0.4387**	**0.1128**	**0.4281**	**0.4069**	**1.3184**	**0.7543**	**0.8625**	**1.6496**	**0.7752**	**2.5042**	**1.9540**	**1.1437**	**1.0637**	**1.6532**	**1.4650**	**0.6650**	**1.0230**	**0.7573**	**0.4887**	**0.6650**
Sulphides	0.18	0.18	1.41	1.12	2.56	2.51	2.90	7.51	4.51	4.93	4.40	8.40	6.81	12.23	16.18	16.11	9.82	7.20	8.52	7.57	7.74	7.20
Carbonates	88.58	88.05	64.52	66.58	84.92	84.89	57.92	52.05	67.57	68.31	45.55	48.04	46.80	49.85	44.55	42.62	44.46	60.11	44.83	47.02	59.43	60.11
Silicates	11.01	11.58	32.93	31.08	11.91	11.93	37.81	39.59	26.69	24.90	49.20	41.03	44.37	36.73	38.14	39.53	44.21	32.00	45.58	44.61	32.29	32.00
Phosphates	0.000	0.001	0.000	0.003	0.004	0.000	0.000	0.004	0.000	0.039	0.000	0.000	0.000	0.004	0.001	0.001	0.001	0.001	0.001	0.000	0.000	0.001
Oxides	0.000	0.000	0.001	0.000	0.000	0.000	0.000	0.000	0.073	0.060	0.004	0.004	0.000	0.006	0.003	0.002	0.004	0.003	0.005	0.000	0.004	0.003
Sulphates	0.002	0.001	0.012	0.000	0.002	0.014	0.051	0.093	0.283	0.114	0.067	0.014	0.040	0.026	0.066	0.094	0.025	0.022	0.008	0.005	0.045	0.022
Other	0.00	0.00	0.68	1.11	0.18	0.24	0.00	0.00	0.01	0.00	0.00	0.00	0.02	0.01	0.00	0.00	0.01	0.01	0.04	0.04	0.00	0.01
Subtotal	**99.77**	**99.82**	**99.56**	**99.89**	**99.57**	**99.59**	**98.68**	**99.25**	**99.14**	**98.35**	**99.22**	**97.50**	**98.05**	**98.86**	**98.94**	**98.35**	**98.54**	**99.34**	**98.98**	**99.24**	**99.51**	**99.34**
Total	100.0	100.0	100.0	100.0	100.0	100.0	100.0	100.0	100.0	100.0	100.0	100.0	100.0	100.0	100.0	100.0	100.0	100.0	100.0	100.0	100.0	100.0

* Base position = initial analysis; Rotate = rotate sample mount 90° then re-analyze

Element of Concern ZINC,Zn

Sample	A951 176m, Class B		A431 306m, Class A		A431 306m, Class A		A355 160.5m, Class C		A355 160.5m, Class		A355 70.5m, Class B		A355 70.5m, Class B		A355 70.5m, Class B		A162 97.5m, Class A		A162 97.5m, Class A		A162 97.5m, Class A	
Size Fraction	-300/+150 µm		-1190/+600 µm		-75/+53 µm		-1190/+600 µm		-150/+106 µm		-600/+300 µm		-600/+300 µm		-150/+106 µm		-1190/+600 µm		-600/+300 µm		-106/+75 µm	
Random Position*	Base	Rotate	Base	Rotate	Base	Rotate	Base	Rotate	Base	Rotate	Base	Rotate	Base	Rotate	Base	Rotate	Base	Rotate	Base	Rotate	Base	Rotate
TrampMetal	0.0000	0.0000	0.0002	0.0002	0.0017	0.0029	0.0006	0.0000	0.0079	0.0040	0.0011	0.0001	0.0013	0.0020	0.0011	0.0003	0.0004	0.0018	0.0048	0.0001	0.0010	0.0018
AgSulphosalt	0.0000	0.0000	0.0000	0.0000	0.1041	0.0008	0.0000	0.0000	0.0000	0.0000	0.0000	0.0000	0.0002	0.0000	0.0000	0.0000	0.0000	0.0000	0.0000	0.0000	0.0003	0.0000
ChalcopyriteZn	0.0000	0.0015	0.0134	0.0001	0.0292	0.0516	0.0074	0.0034	0.0044	0.0000	0.0018	0.0561	0.0017	0.0307	0.0310	0.0499	0.0939	0.1020	0.1660	0.0823	0.1588	0.1020
EnargiteZn	0.0000	0.0000	0.0135	0.0000	0.0001	0.0303	0.0000	0.0000	0.0006	0.0000	0.0000	0.0000	0.0000	0.0000	0.0000	0.0000	0.3660	0.1855	0.9392	0.5270	0.0975	0.1855
TennantiteZnFe	0.0000	0.0000	0.0011	0.0003	0.0001	0.0107	0.0000	0.0000	0.0000	0.0000	0.0000	0.0000	0.0000	0.0000	0.0000	0.0000	0.0139	0.0082	0.0042	0.0046	0.0414	0.0082
WatanabeiteZn	0.0000	0.0000	0.0004	0.0001	0.9920	0.0001	0.0000	0.0000	0.0000	0.0000	0.0000	0.0000	0.0000	0.0330	0.0000	0.0000	3.4656	1.7341	2.9251	2.6311	2.0406	1.7341
Sphalerite	0.0009	0.0541	0.1191	0.2401	0.9172	1.2381	0.0068	0.0015	0.0057	0.0707	0.0156	0.1869	0.0468	0.1221	0.0828	0.0967	1.6521	1.3910	1.1637	1.3234	1.0749	1.3910
SphaleriteCu	0.0582	0.0011	0.3301	0.2626	0.0000	0.6262	0.3007	2.5580	0.1281	0.0713	0.3252	0.1084	0.3717	1.0913	1.5631	1.3804	0.4316	0.8803	0.8745	0.2109	1.4360	0.8803
SiegeniteCuZn	0.0000	0.0000	0.0000	0.0000	0.0348	0.0000	0.0000	0.0000	0.0000	0.0000	0.0000	0.0000	0.0000	0.0000	0.0000	0.0000	0.0000	0.0000	0.0000	0.0000	0.0000	0.0000
FeOxideSulphateCuPbZnAs	0.0000	0.0000	0.0031	0.0003	0.0000	0.0530	0.0010	0.0005	0.1328	0.0060	0.0190	0.0064	0.0046	0.2355	0.2137	0.2584	0.0008	0.0419	0.0044	0.0006	0.0472	0.0419
ParamelaconiteZn	0.0000	0.0000	0.0000	0.0000	0.0000	0.0000	0.0000	0.0000	0.0000	0.0000	0.0000	0.0000	0.0000	0.0001	0.0000	0.0000	0.0000	0.0000	0.0000	0.0000	0.0000	0.0000
Wulfingite	0.0000	0.0000	0.0000	0.0000	0.0000	0.0000	0.0000	0.0000	0.0000	0.0000	0.0000	0.0000	0.0000	0.0000	0.0000	0.0000	0.0000	0.0000	0.0000	0.0000	0.0000	0.0000
PbCaOxideMoZnW	0.0000	0.0000	0.0000	0.0000	0.0000	0.0000	0.0000	0.0000	0.0000	0.0000	0.0000	0.0000	0.0000	0.0000	0.0000	0.0000	0.0000	0.0000	0.0000	0.0000	0.0000	0.0000
SideriteMnAsZnCrCu	0.0000	0.0000	0.0000	0.0004	0.0000	0.0000	0.0000	0.0000	0.0000	0.0000	0.0000	0.0000	0.0000	0.0055	0.0003	0.0000	0.0000	0.0000	0.0000	0.0000	0.0000	0.0000
Smithsonite_trans	0.0000	0.0000	0.0000	0.0000	0.0001	0.0000	0.0000	0.0000	0.0000	0.0000	0.0000	0.0000	0.0000	0.0000	0.0000	0.0000	0.0000	0.0000	0.0000	0.0000	0.0000	0.0000
GruneritePbCuZn	0.0054	0.0000	0.0001	0.0000	0.0000	0.0001	0.0002	0.0001	0.0000	0.0040	0.0000	0.0000	0.0000	0.0001	0.0000	0.0000	0.0014	0.0007	0.0000	0.0000	0.0000	0.0007
OtaviteZnCu	0.0000	0.0000	0.0000	0.0000	0.0001	0.0000	0.0000	0.0000	0.0000	0.0000	0.0000	0.0000	0.0000	0.0000	0.0000	0.0000	0.0000	0.0000	0.0000	0.0000	0.0000	0.0000
Goslarite	0.0000	0.0000	0.0003	0.0000	0.0000	0.0000	0.0001	0.0000	0.0000	0.0000	0.0002	0.0000	0.0000	0.0000	0.0001	0.0003	0.0010	0.0000	0.0001	0.0000	0.0000	0.0000
FeSulphateLimoniteCuAsMoZ	0.0008	0.0010	0.0001	0.0002	0.0000	0.0000	0.0503	0.0926	0.2707	0.1142	0.0416	0.0136	0.0363	0.0237	0.0633	0.0781	0.0103	0.0038	0.0017	0.0044	0.0022	0.0038
MoCaSulphateMnCuFeZn	0.0000	0.0000	0.0000	0.0000	0.0001	0.0000	0.0000	0.0000	0.0000	0.0000	0.0002	0.0000	0.0001	0.0001	0.0000	0.0000	0.0030	0.0000	0.0000	0.0000	0.0000	0.0000
MolybdofornaciteZnCu	0.0000	0.0000	0.0002	0.0000	0.0000	0.0000	0.0000	0.0002	0.0000	0.0000	0.0002	0.0000	0.0005	0.0004	0.0011	0.0000	0.0020	0.0019	0.0014	0.0009	0.0010	0.0019
Powellite_trans	0.0000	0.0000	0.0000	0.0000	0.0001	0.0000	0.0000	0.0000	0.0000	0.0000	0.0000	0.0000	0.0000	0.0000	0.0000	0.0000	0.0000	0.0000	0.0000	0.0000	0.0000	0.0000
Wulfenite_trans	0.0000	0.0000	0.0000	0.0000	0.0201	0.0000	0.0000	0.0000	0.0000	0.0000	0.0001	0.0000	0.0002	0.0003	0.0004	0.0000	0.0001	0.0000	0.0000	0.0000	0.0000	0.0000
ApatiteCuPbZn	0.0189	0.0110	0.0374	0.0448	0.0000	0.0255	0.1106	0.0689	0.2512	0.5352	0.0231	0.5924	1.4603	0.1158	0.1304	0.2819	0.1060	0.0788	0.4341	0.2092	0.1306	0.0788
TyrolitePb	0.0000	0.0000	0.0000	0.0000	0.1397	0.0000	0.0000	0.0000	0.0000	0.0000	0.0000	0.0000	0.0000	0.0000	0.0000	0.0000	0.0000	0.0000	0.0000	0.0000	0.0000	0.0000
MicaAlteredCuZn	0.0473	0.1122	0.6831	0.4457	0.0000	0.2287	0.0925	0.0143	0.1918	0.1440	0.3653	0.8013	0.6163	0.4327	0.2332	0.5029	0.0645	0.1454	0.1113	0.5342	0.1821	0.1454
Willemite	0.0000	0.0000	0.0000	0.0000	0.7954	0.0000	0.0000	0.0000	0.0000	0.0000	0.0000	0.0000	0.0000	0.0000	0.0000	0.0000	0.0000	0.0000	0.0000	0.0000	0.0000	0.0000
Subtotal	**0.1315**	**0.1808**	**1.2021**	**0.9948**	**3.0347**	**2.2678**	**0.5701**	**2.7395**	**0.9932**	**0.9493**	**0.7933**	**1.7652**	**2.5399**	**2.0932**	**2.3205**	**2.6489**	**6.2125**	**4.5754**	**6.6304**	**5.5289**	**5.2136**	**4.5754**
Sulphides	0.22	0.25	0.57	0.67	0.85	0.82	2.62	4.97	4.38	4.81	4.11	8.13	6.49	11.05	14.66	14.77	5.00	3.41	2.88	3.24	3.12	3.41
Carbonates	88.58	88.05	63.97	66.58	84.92	84.89	57.92	52.05	67.57	68.31	45.55	48.04	46.80	49.85	44.55	42.62	44.46	60.11	44.83	47.02	59.43	60.11
Silicates	11.07	11.52	33.63	30.65	11.86	11.78	38.89	40.24	26.96	25.83	49.51	42.06	44.15	36.98	38.46	39.95	44.30	31.88	45.61	44.18	32.18	31.88
Phosphates	0.000	0.001	0.000	0.003	0.00	0.000	0.000	0.004	0.000	0.039	0.000	0.000	0.000	0.004	0.001	0.001	0.001	0.001	0.001	0.000	0.000	0.001
Oxides	0.000	0.000	0.000	0.000	0.00	0.000	0.000	0.000	0.073	0.060	0.004	0.004	0.000	0.006	0.003	0.002	0.004	0.003	0.005	0.000	0.004	0.003
Sulphates	0.001	0.000	0.004	0.000	0.00	0.014	0.000	0.000	0.013	0.000	0.025	0.000	0.004	0.002	0.003	0.016	0.011	0.018	0.006	0.001	0.042	0.018
Other	0.00	0.00	0.61	1.11	0.17	0.24	0.00	0.00	0.00	0.00	0.00	0.00	0.02	0.01	0.00	0.00	0.01	0.00	0.03	0.04	0.00	0.00
Subtotal	**99.868**	**99.819**	**98.798**	**99.005**	**97.76**	**97.732**	**99.430**	**97.260**	**99.007**	**99.051**	**99.207**	**98.235**	**97.460**	**97.907**	**97.680**	**97.351**	**93.787**	**95.425**	**93.370**	**94.471**	**94.786**	**95.425**
Total	100.0	100.0	100.0	100.0	100.000	100.0	100.0	100.0	100.0	100.0	100.0	100.0	100.0	100.0	100.0	100.0	100.0	100.0	100.0	100.0	100.0	100.0

* Base position = initial analysis; Rotate = rotate sample mount 90° then re-analyze

APPENDIX 13 Effect of duplicate and replicate included in analysis

Modal Mineralogy (weight-%, normalized)

Sample	A1018 17.25m, Class C				A1018 17.25m, Class C				A951 176m, Class B				A431 306m, Class A				A355 160.5m, Class C				A355 70.5m, Class C				A162A 97.5m, Class A			
Size Fraction	-1190/+600 µm				-106/+75 µm				-150/+106 µm				-300/+150 µm				-1190/+600 µm				-1190/+600 µm				-1190/+600 µm			
Type	Append	S1	S2	S1_Dup	Append	S1	S2	S2_Dup	Append	S1	S2	S2_Dup	Append	S1	S2	S1_Dup	Append	S1	S2	S2_Dup	Append	S1	S2	S2_Dup	Append	S1	S2	S2_Dup
Bornite	0.00043	0.00002	0.00086	0	0.00166	0.00149	0.00184	0	0	0	0	0	0.00925	0.01277	0.00604	0.05139	0	0	0	0	0.00002	0	0.00004	0	0.48748	0.26995	0.72211	0.49926
Galena	0.10794	0.20962	0.00138	0.14661	0.02059	0.02423	0.01689	0.02132	0.00066	0.00066	0.00105	0	0.05817	0.05274	0.06313	0.17446	0.00036	0.00018	0.00056	0.00069	0.01625	0.01012	0.02293	0.02554	0.57265	0.1192	1.06171	1.02523
Sphalerite	0.08165	0.13752	0.02311	0.14105	0.25751	0.19449	0.32184	0.34487	0.05555	0.05555	0.0951	0.1024	0.96368	1.00262	0.92811	1.90928	0.16057	0.30753	0.0001	0.00697	0.28871	0.10356	0.49052	0.49699	2.73109	3.33131	2.08371	1.42167
Chalcopyrite	0.07603	0.1401	0.00889	0.0938	0.10017	0.08641	0.1142	0.0571	0.15826	0.15826	0.06332	0.07679	0.09835	0.14333	0.05727	0.57613	0.10735	0.15554	0.05473	0.04971	0.06147	0.05334	0.07032	0.06213	1.47751	1.0256	1.96492	1.87569
Pyrrhotite	0.61419	0.54607	0.68557	0.59864	0.57251	0.51365	0.63259	0.48371	0.05778	0.05778	0.03384	0.06379	0.06577	0.12291	0.01358	0.05347	0.92697	0.98195	0.86693	0.91885	0.31225	0.30108	0.32442	0.34135	0.17472	0.01642	0.34546	0.37344
RealgarOrpiment	0	0	0	0	0	0	0	0	0	0	0	0	0	0	0	0	0	0	0	0	0	0	0	0	0	0	0	0
Stibnite	0	0	0	0	0.00001	0	0.00001	0	0.00003	0.00003	0.00007	0.00012	0.0002	0	0.00038	0.0002	0	0	0	0	0	0	0	0	0.00605	0.00757	0.00441	0.01517
Watanabeite	0	0	0	0	0	0	0	0	0.00066	0.00066	0.00143	0.00029	0.00003	0	0.00005	0.0001	0	0	0	0	0	0	0	0	1.85739	0.36634	3.46558	3.73395
Pyrite	0.0399	0.07444	0.0037	0.07973	0.16407	0.19341	0.13412	0.19897	0.01261	0.01261	0.00432	0	0.00566	0	0.01083	0	1.15547	1.48635	0.79416	0.78602	2.07532	2.62107	1.48048	1.49703	0.36467	0.2575	0.48027	0.46866
Molybdenite	0	0	0	0	0.0001	0.00014	0.00006	0	0.01227	0.01227	0.02197	0	0.01324	0.00136	0.02409	0.04118	0	0	0	0	0.00012	0.00023	0	0.00008	0.01068	0.00011	0.02209	0.02351
Enargite	0	0	0	0.0001	0.00001	0	0.00003	0	0.00213	0.00213	0	0.00005	0.00269	0.00481	0.00075	0.03177	0	0	0	0	0	0	0	0	1.27241	1.66589	0.84803	0.99859
OtherSulphide	0.00001	0.00002	0	0.00007	0	0	0	0	0.00024	0.00024	0	0	0.00005	0	0.00009	0.00172	0.00104	0.002	0	0.00002	0.00061	0.0001	0.00117	0.00006	0.04461	0.0633	0.02445	0.02407
Sub-Total	**0.92015**	**1.10779**	**0.72351**	**1.06**	**1.11663**	**1.01382**	**1.22158**	**1.10597**	**0.30019**	**0.30019**	**0.2211**	**0.24344**	**1.21709**	**1.34054**	**1.10432**	**2.8397**	**2.35176**	**2.93355**	**1.71648**	**1.76226**	**2.75475**	**3.0895**	**2.38988**	**2.42318**	**8.99926**	**7.12319**	**11.02274**	**10.45924**
Calcite	50.73091	52.51092	48.86564	47.13237	66.60421	66.46484	66.74646	67.0239	87.7394	87.7394	87.58092	87.0925	91.69716	91.03343	92.30336	84.60148	55.42981	57.92074	52.70993	50.22925	44.091	43.44131	44.79916	47.6619	48.32963	51.91439	44.46328	47.74148
Otavite	0	0	0	0	0	0	0	0	0	0	0	0	0	0	0	0	0	0	0	0	0	0	0	0	0	0	0	0
Siderite	0	0	0	0	0.00008	0.00017	0	0.00006	0	0	0	0	0	0	0	0.00001	0	0	0	0	0	0	0	0	0	0	0	0
Dolomite	0.00011	0.00018	0.00003	0.00074	0.00073	0.00085	0.0006	0.00095	0.00011	0.00011	0.00022	0.00036	0.11479	0.10716	0.12175	0.3124	0.00018	0.00014	0.00023	0.00021	0.00006	0.00005	0.00008	0.00016	0.00022	0.00002	0.00044	0.00563
OtherCarbonate	0.00033	0.00038	0.00027	0.00404	0.00623	0.00856	0.00386	0.00838	0.00019	0.00019	0.00002	0.00011	0.00071	0.00018	0.00119	0.00382	0.00012	0.00011	0.00012	0.00032	0.00061	0.00077	0.00045	0.00046	0.00096	0.00072	0.00122	0.00086
Sub-Total	**50.73135**	**52.51148**	**48.86594**	**47.13715**	**66.61125**	**66.47442**	**66.75092**	**67.03329**	**87.7397**	**87.7397**	**87.58116**	**87.09297**	**91.81266**	**91.14077**	**92.4263**	**84.91771**	**55.43011**	**57.92099**	**52.71028**	**50.22978**	**44.09167**	**43.44213**	**44.79969**	**47.66252**	**48.33081**	**51.91513**	**44.46494**	**47.74797**
Biotite	3.41923	3.45288	3.38397	3.31416	1.68459	1.83784	1.52816	1.49325	0.01569	0.01569	0.03357	0.00041	0.05358	0.02519	0.07952	0.10822	0.39801	0.741	0.02349	2.55006	0.13169	0.03195	0.2404	0.25039	0.47534	0.39497	0.56201	0.87878
Chlorite	0.0029	0.0017	0.00417	0.36072	0.03202	0.03667	0.02729	0.00999	0.00195	0.00195	0	0.00158	0.00625	0.00397	0.00834	0.0094	0.00703	0.01032	0.00344	0.00323	0.16104	0.22683	0.08933	0.19217	0.02849	0.03858	0.01762	0.0276
K_Feldspar	0.09446	0.16165	0.02406	0.11811	1.71476	1.82071	1.60661	1.49143	0.20397	0.20397	0.14398	0.16025	0.05987	0.04652	0.07206	0.06098	5.96786	4.39497	7.68532	5.48765	4.43781	5.36558	3.42655	3.25477	0.47713	0.39316	0.56768	0.45052
Kaolinite	0	0.00001	0	0	0.00326	0.00644	0	0	0	0	0	0	0	0	0	0	0.00005	0	0.00011	0	0.00076	0.00145	0	0.13424	0	0	0	0
Muscovite	0	0.00001	0	0	0.01821	0.02453	0.01176	0.08481	0	0	0	0	0	0	0	0	0.00063	0.00058	0.00068	0.00029	0.00061	0.00073	0.00047	0.00039	0.00168	0.00297	0.00028	0.00006
Plagioclase	7.66084	6.47951	8.89876	8.67614	3.37131	3.25933	3.4856	2.81032	0.43897	0.43897	0.47763	0.40796	0.34857	0.55434	0.16063	0.29911	10.89231	8.05473	13.99071	15.78273	18.37619	21.49887	14.97251	19.82248	1.05714	0.39834	1.76768	2.51516
Pyroxene	17.42667	15.30436	19.65063	17.25201	13.51523	13.54896	13.48081	13.91364	3.21619	3.21619	2.88104	3.03625	3.34241	3.16738	3.50227	5.15258	9.40514	10.29755	8.4307	7.37445	9.03478	6.07845	12.25713	7.20573	7.29999	6.80025	7.83899	7.10633
Quartz	0.17104	0.05997	0.28743	0.11546	0.68503	0.73133	0.63777	0.65256	0.6598	0.6598	0.74781	0.61854	0.01059	0.00272	0.01777	0.04439	0.34311	0.40188	0.27895	0.24657	0.87599	0.84904	0.90538	0.89252	1.08638	1.16643	1.00004	1.66337
Talc	0	0	0	0	0	0	0	0	0	0	0	0	0	0	0	0	0	0	0	0	0	0	0	0	0	0	0	0
Mica	0.82003	1.32096	0.29512	0.52338	1.31684	1.40773	1.22406	1.3941	0.0428	0.0428	0.00324	0.0086	0.10027	0.07738	0.12118	0.15946	5.36569	4.36736	6.45578	6.14275	2.58428	3.51748	1.5671	0.96273	0.46558	0.81574	0.08792	0.49686
Titanite	0.01503	0.0115	0.01872	0.10844	0.15574	0.14884	0.16278	0.13775	0.1212	0.1212	0.17101	0.23418	0.03361	0.04016	0.02762	0.09157	0.72041	1.17637	0.22253	0.25162	0.39214	0.02922	0.78772	0.67193	0.11404	0.07543	0.15568	0.1075
OtherSilicate	18.1536	18.89265	17.37916	20.93035	9.48361	9.39143	9.5777	9.55775	7.19253	7.19253	7.67983	8.15331	2.89132	3.4979	2.33732	6.07682	8.87153	9.53733	8.14454	9.9252	17.01356	15.65901	18.49	16.42186	31.50109	30.69923	32.36593	28.3223
Sub-Total	**47.7638**	**45.6852**	**49.94202**	**51.39877**	**31.9806**	**32.21381**	**31.74254**	**31.5456**	**11.8931**	**11.8931**	**12.13811**	**12.62108**	**6.84647**	**7.41556**	**6.32671**	**12.00253**	**41.97177**	**38.98209**	**45.23625**	**47.76455**	**53.00885**	**53.25861**	**52.73659**	**49.80921**	**42.50686**	**40.7851**	**44.36383**	**41.56848**
Phosphate	0.5288	0.65345	0.39819	0.32637	0.21058	0.24972	0.17062	0.18756	0.03376	0.03376	0.02689	0.0375	0.03139	0.03408	0.02894	0.02438	0.13507	0.11078	0.16159	0.17487	0.08588	0.15075	0.01517	0.0537	0.11069	0.1145	0.10659	0.09538
FeOxyhydroxide	0.00589	0.00018	0.01187	0.0002	0.02682	0.01317	0.04076	0.04868	0.01668	0.01668	0.00001	0	0.0402	0.00004	0.07687	0.03498	0.00074	0.00095	0.00051	0.00053	0.01087	0.01205	0.00959	0.00256	0.00268	0.00183	0.0036	0.02308
OtherOxides	0.00029	0.00056	0	0.00054	0.00078	0.00042	0.00114	0.00097	0.00045	0.00045	0.00094	0.00039	0.00331	0.00045	0.00592	0.00143	0.00026	0.00035	0.00016	0.0002	0.00076	0.00115	0.00033	0.00014	0.00132	0.00157	0.00106	0.00164
Sub-Total	**0.00618**	**0.00074**	**0.01187**	**0.00074**	**0.0276**	**0.01359**	**0.0419**	**0.04965**	**0.01713**	**0.01713**	**0.00095**	**0.00039**	**0.04351**	**0.00049**	**0.08279**	**0.03641**	**0.001**	**0.0013**	**0.00067**	**0.00073**	**0.01163**	**0.0132**	**0.00992**	**0.0027**	**0.004**	**0.0034**	**0.00466**	**0.02472**
FeSulphate	0.04721	0.04021	0.05454	0.07367	0.05249	0.03368	0.07169	0.06648	0.01504	0.01504	0.03134	0.00039	0.00038	0.00065	0.00013	0.00002	0.10876	0.05041	0.17247	0.06647	0.04441	0.04221	0.04681	0.04669	0.0118	0.01315	0.01035	0.01407
Barite	0	0	0	0	0	0	0	0	0	0	0	0	0	0	0	0	0	0	0	0	0	0	0	0	0	0	0	0
Gypsum	0.00032	0.00033	0.00031	0.00096	0.00049	0.0004	0.00059	0.00062	0.00053	0.00053	0.00039	0.00301	0.00009	0.00007	0.00011	0.00138	0.00066	0.00014	0.00123	0.00078	0.00149	0.00258	0.00031	0.00025	0.01458	0.01802	0.01087	0.06906
OtherSulphate	0.00002	0.00003	0	0.00001	0.00005	0.00011	0	0.00001	0	0	0	0	0.00001	0.00002	0.00001	0.00009	0.00006	0.00011	0	0.00001	0.00017	0.00004	0.0003	0.00028	0.00254	0.00121	0.00398	0.00044
Sub-Total	**0.04755**	**0.04057**	**0.05485**	**0.07464**	**0.05303**	**0.03419**	**0.07228**	**0.06711**	**0.01557**	**0.01557**	**0.03173**	**0.0034**	**0.00048**	**0.00074**	**0.00025**	**0.00149**	**0.10948**	**0.05066**	**0.1737**	**0.06726**	**0.04607**	**0.04483**	**0.04742**	**0.04722**	**0.02892**	**0.03238**	**0.0252**	**0.08357**
Other	0.00217	0.00079	0.00362	0.00231	0.00031	0.00046	0.00015	0.01085	0.00053	0.00053	0.00005	0.00121	0.04843	0.06781	0.03072	0.17776	0.00081	0.00061	0.00102	0.00054	0.00116	0.001	0.00134	0.00144	0.01945	0.02631	0.01205	0.02066
Total	100	100	100	100	100	100	100	100	100	100	100	100	100	100	100	100	100	100	100	100	100	100	100	100	100	100	100	100

NOTE: S1 = sample 1; S2 = second cut of sample 1; Sn_Dup = similar to Sn; Append = merging data from S1 and S2

Modal Mineralogy (weight-%, normalized)

Sample	A355 160.5m, Class C		A355 70.5m, Class C		A162A 97.5m, Class A	
Size Fraction	-106/+75 µm		-106/+75 µm		-75/+53 µm	
Type	S1	S1_Rep	S1	S1_Rep	S1	S1_Rep
Bornite	0	0	0.00004	0.00009	0.84135	0.83378
Galena	0.00075	0.00043	0.06654	0.08761	0.02363	0.0285
Sphalerite	0.16481	0.16117	1.71267	1.69637	2.66927	2.65593
Chalcopyrite	0.15017	0.11818	0.66616	0.56593	1.74998	1.72408
Pyrrhotite	2.83663	2.8615	1.40726	1.3721	0.10744	0.12712
RealgarOrpiment	0	0	0	0	0	0
Stibnite	0	0.00016	0	0	0.00317	0.00216
Watanabeite	0.00003	0	0	0	1.96183	2.05855
Pyrite	1.38276	1.23649	11.7875	11.1588	0.25753	0.21834
Molybdenite	0	0.00022	0.00015	0.00004	0.03013	0.0301
Enargite	0	0.00001	0	0	0.62174	0.54221
OtherSulphide	0.00193	0.00262	0.00009	0.00036	0.0167	0.0228
Sub-Total	**4.53708**	**4.38078**	**15.64041**	**14.8813**	**8.28277**	**8.24357**
Calcite	67.34622	66.61893	49.25962	48.1939	51.73814	51.73792
Otavite	0	0	0	0	0	0
Siderite	0.00001	0	0	0	0	0
Dolomite	0.0221	0.01248	0.01419	0.00254	0.00067	0.00006
OtherCarbonate	0.01404	0.0165	0.00037	0.00033	0.00015	0.00012
Sub-Total	**67.38237**	**66.64791**	**49.27418**	**48.19677**	**51.73896**	**51.7381**
Biotite	0.26128	0.34486	0.56027	0.6595	0.23184	0.21505
Chlorite	0.07041	0.07673	0.08996	0.28665	0.09035	0.1077
K_Feldspar	4.12829	4.16375	4.59676	4.68917	0.26913	0.21388
Kaolinite	0.00021	0.00238	0	0.58287	0	0
Muscovite	0.01848	0.02137	0.07258	0.05592	0	0.00132
Plagioclase	5.5333	6.33404	9.13777	8.75002	0.70128	0.76124
Pyroxene	5.61098	5.89103	6.77512	6.52807	19.53314	19.58829
Quartz	1.16793	1.11229	1.25099	2.04199	0.87255	0.88013
Talc	0	0	0	0	0	0
Mica	4.99018	4.41236	3.37176	3.82472	0.18581	0.23047
Titanite	0.38819	0.5454	0.38348	0.68975	0.06029	0.09654
OtherSilicate	5.51689	5.58421	8.28385	8.38412	17.87625	17.71906
Sub-Total	**27.68614**	**28.48842**	**34.52254**	**36.49278**	**39.82064**	**39.81368**
Phosphate	0.09321	0.12875	0.10766	0.10553	0.11411	0.12
FeOxyhydroxide	0.15342	0.19825	0.30304	0.25233	0.00237	0.04065
OtherOxides	0.00149	0.00183	0.02174	0.00051	0.00002	0.00141
Sub-Total	**0.15491**	**0.20008**	**0.32478**	**0.25284**	**0.00239**	**0.04206**
FeSulphate	0.1338	0.13784	0.12027	0.05898	0.02678	0.02909
Barite	0	0	0	0	0.00009	0.00006
Gypsum	0.00072	0.01393	0.00234	0.00829	0.00818	0.00902
OtherSulphate	0.00006	0.00003	0.00048	0.00011	0.00001	0.00002
Sub-Total	**0.13458**	**0.1518**	**0.12309**	**0.06738**	**0.03506**	**0.03819**
Other	0.01174	0.00226	0.00735	0.00339	0.00608	0.00439
Total	100	100	100	100	100	100

NOTE: S1 = sample 1; S2 = second cut of sample 1; Sn_Rep = original sample Sn analyzed on different day on different MLA

= Nugget effect

APPENDIX 14 MLA application: bulk modal mineralogy

Grouped Modal Mineralogy (see Table 3.2.3)

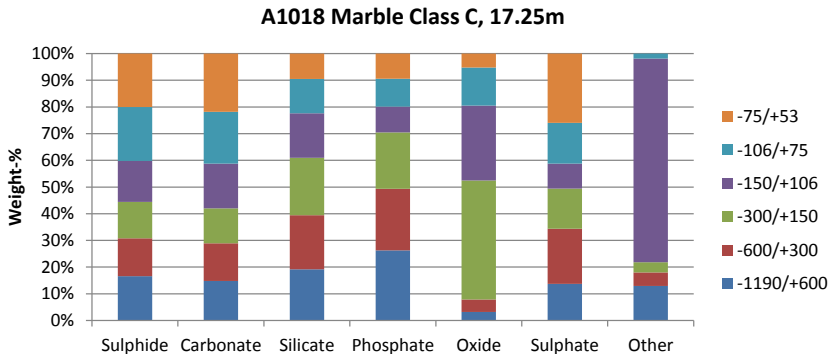

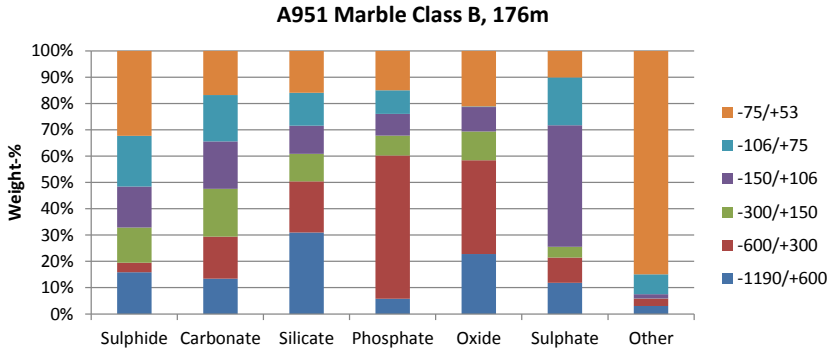

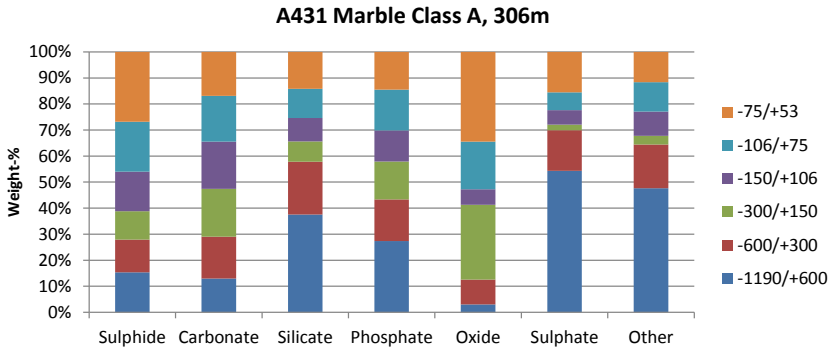

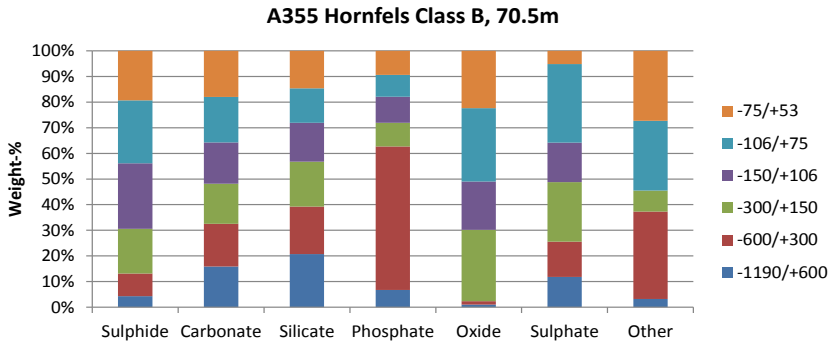

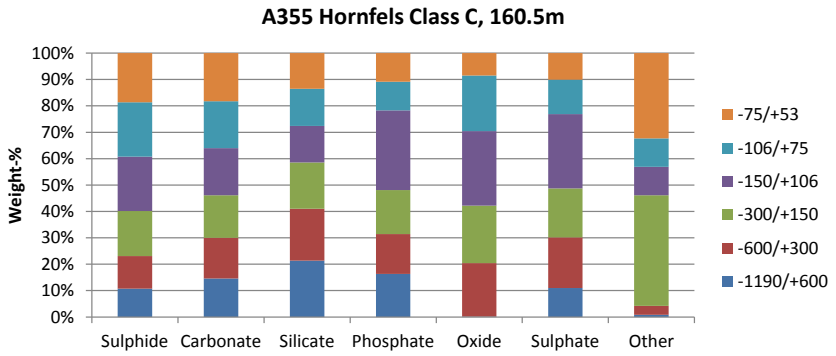

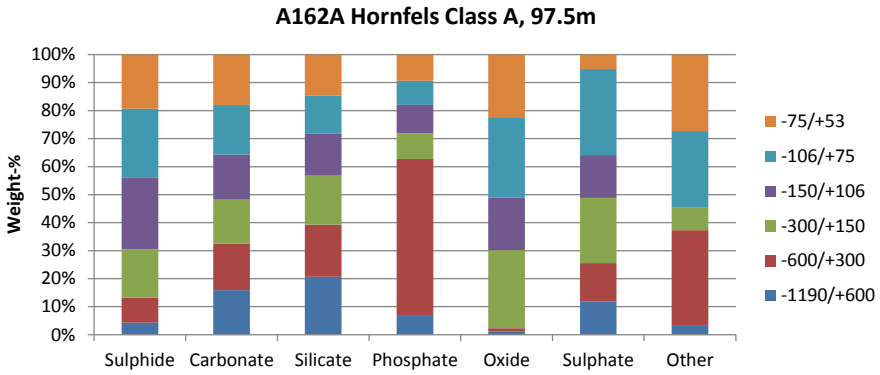

Note: legend refers to size fractions (microns).

Grouped Modal Mineralogy (see Table 3.2.1)

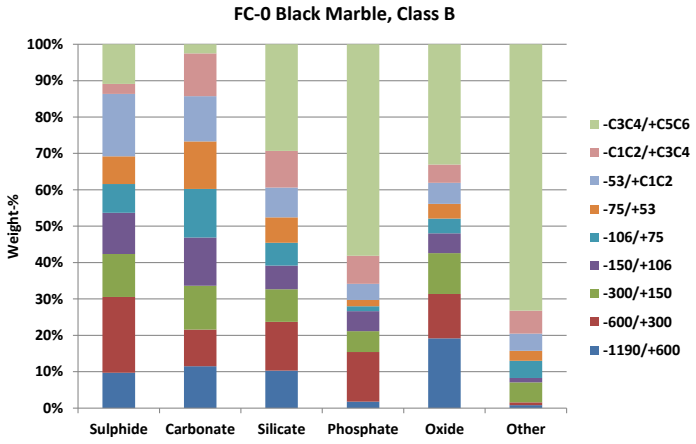

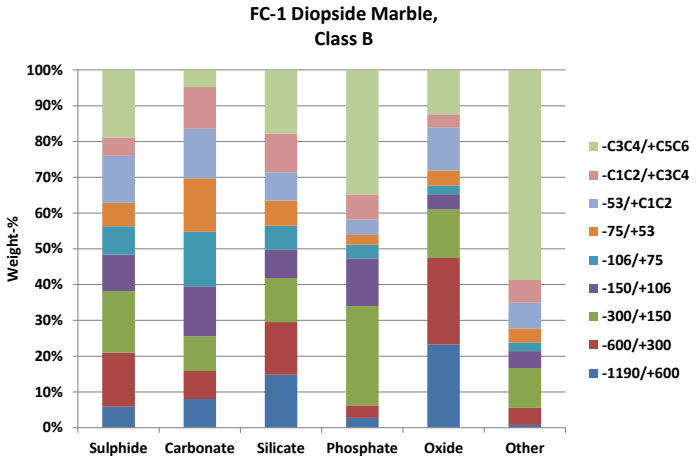

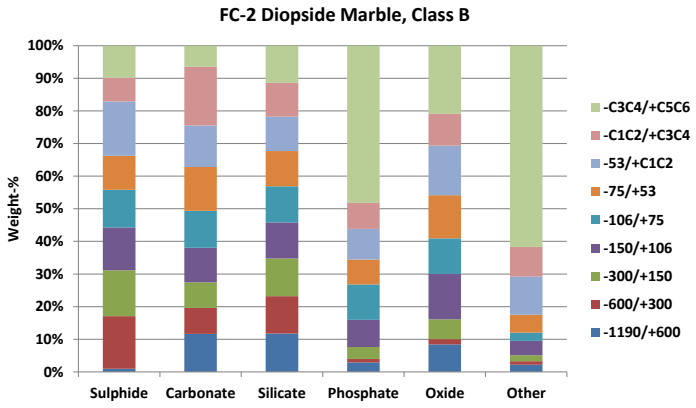

Note: legend refers to size fractions (microns).

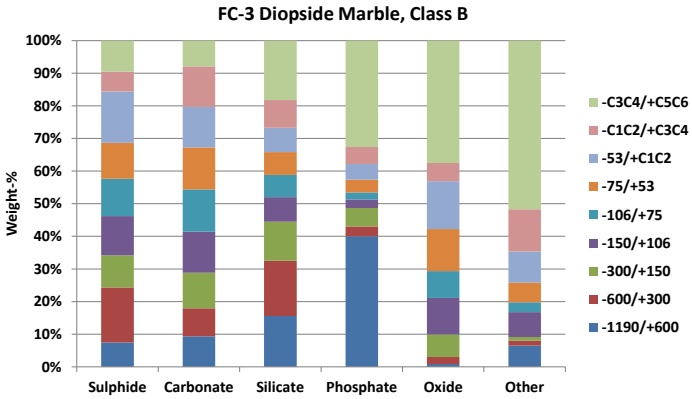

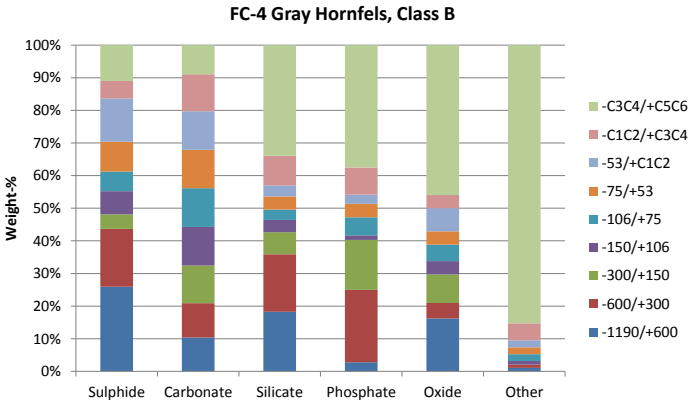

Note: legend refers to size fractions (microns).

APPENDIX 15 Mineral Liberation Analyzer application: modal mineralogy based on availability (or locking)

Note: All plots derived from data collected from Table 3.2.1, 3.2.3 and 3.2.4.

Liberated (>90% exposed), Partial (30-90% exposed), Locked (<30% exposed).

Horizontal axis = size fraction (microns); Vertical axis = weight-% (normalized).

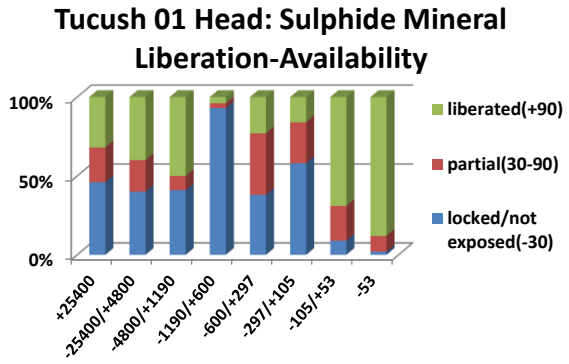

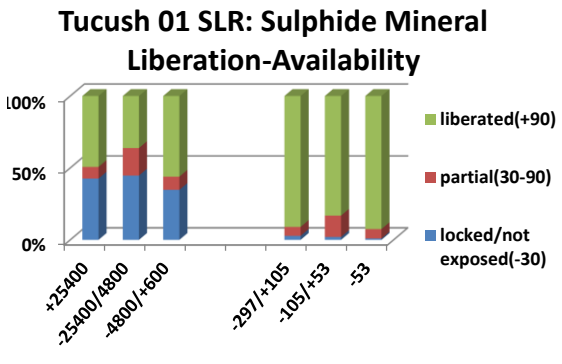

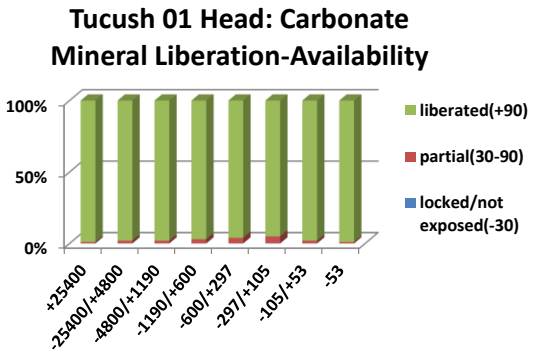

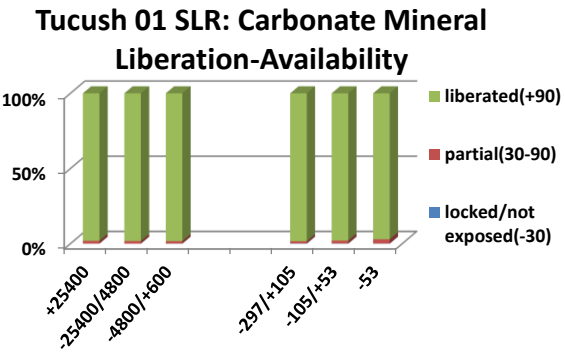

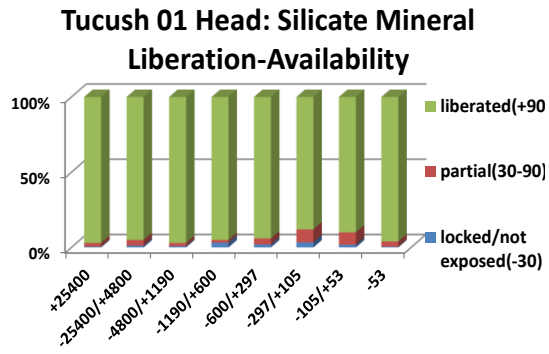

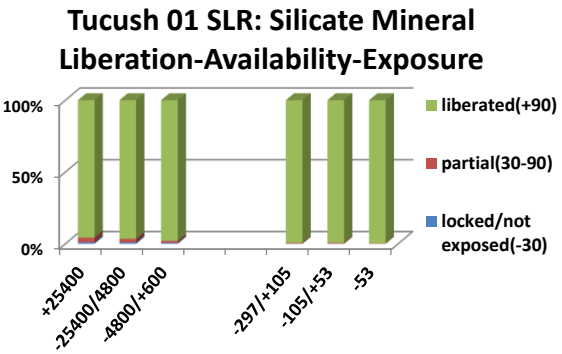

Tucush 01 Head: Sb-Mineral Liberation-Availability

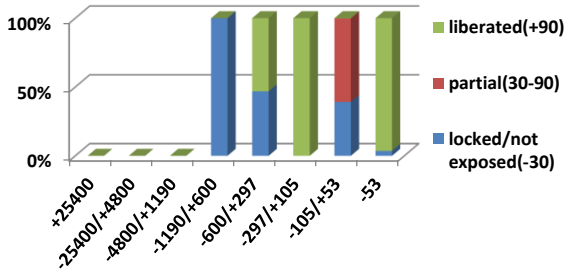

Tucush 01 SLR: Sb-Mineral Liberation-Availability

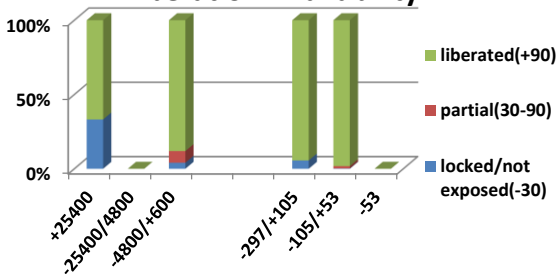

Tucush 01 Head: As-Mineral Liberation-Availability

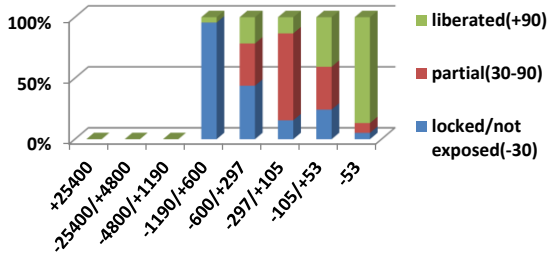

Tucush 01 SLR: As-Mineral Liberation-Availability

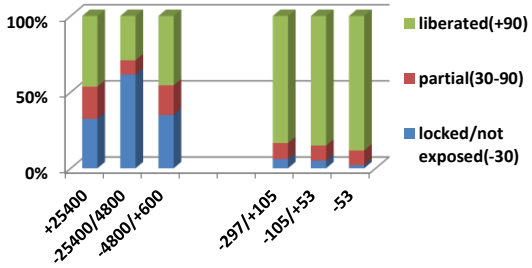

Tucush 01 Head: Cu-Mineral Liberation-Availability

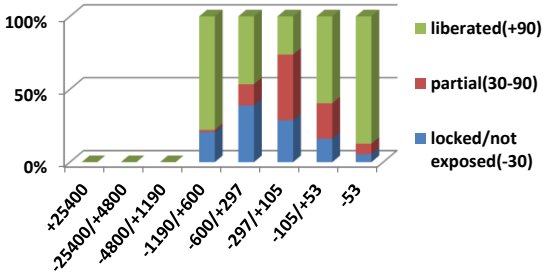

Tucush 01 SLR: Cu-Mineral Liberation-Availability

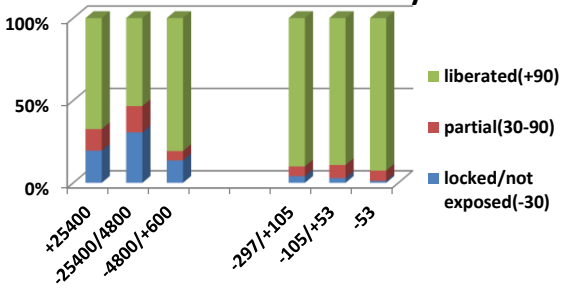

Tucush 01 Head: Mo-Mineral Liberation-Availability

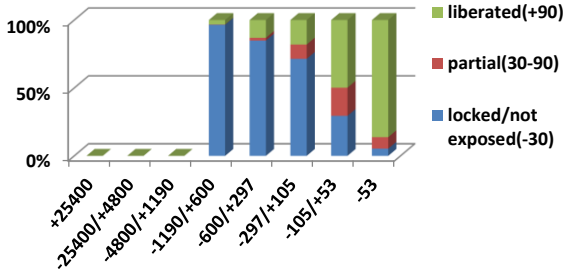

Tucush 01 SLR: Mo-Mineral Liberation-Availability

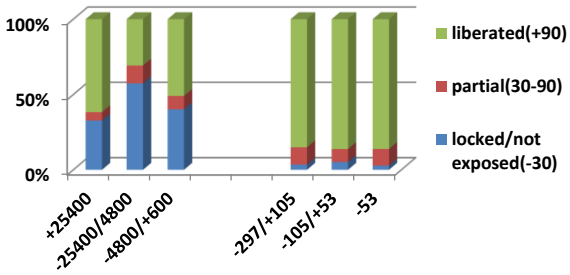

Tucush 01 Head: Pb-Mineral Liberation-Availability

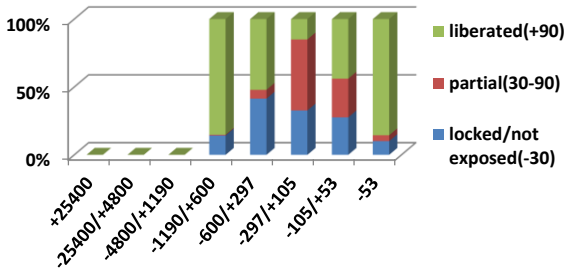

Tucush 01 SLR: Pb-Mineral Liberation-Availability

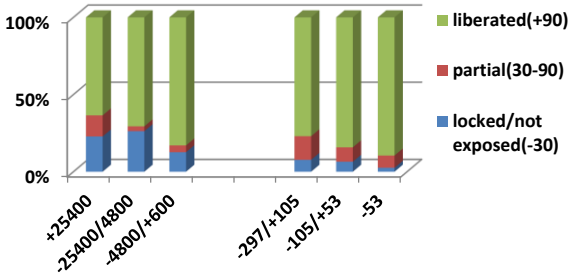

Tucush 01 Head: Zn-Mineral Liberation-Availability

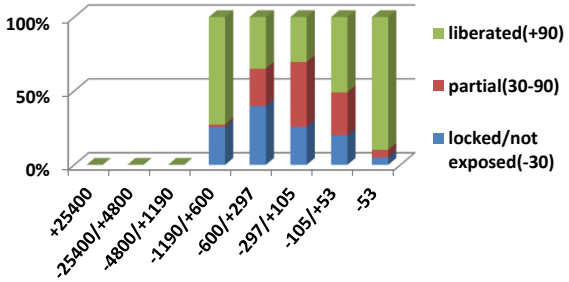

Tucush 01 SLR: Zn-Mineral Liberation-Availability

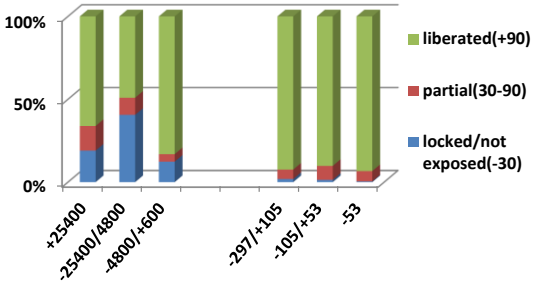

Tucush 03 Head: Sulphide Mineral Liberation-Availability

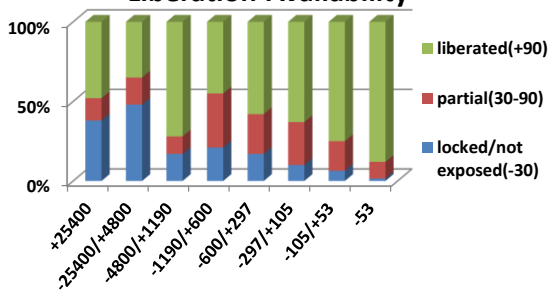

Tucush 03 SLR: Sulphide Mineral Liberation-Availability

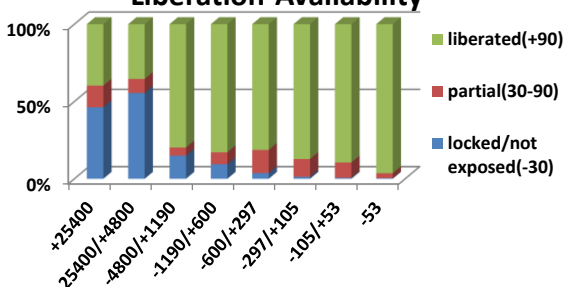

Tucush 03 Head: Carbonate Mineral Liberation-Availability

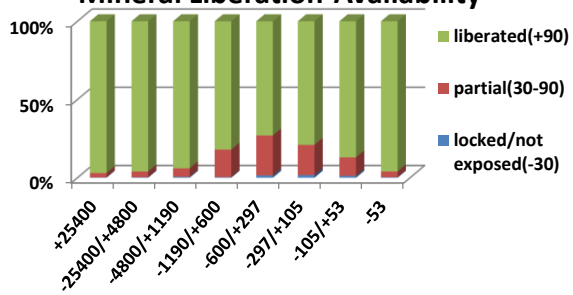

Tucush 03 SLR: Carbonate Mineral Liberation-Availability

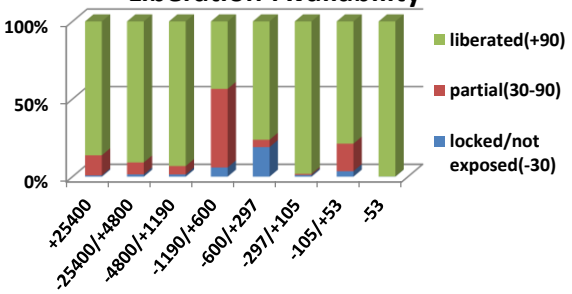

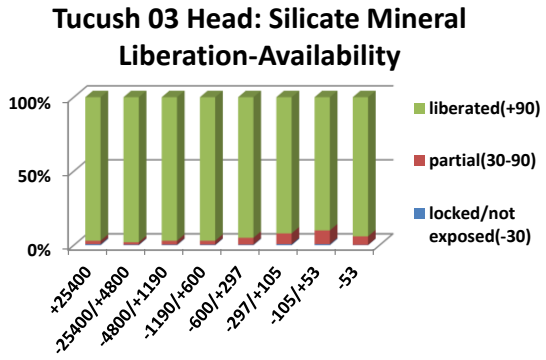
Tucush 03 Head: Silicate Mineral Liberation-Availability
100%
50%
0%
liberated(+90)
partial(30-90)
locked/not exposed(-30)
+25400
-25400/+4800
-4800/+1190
-1190/+600
-600/+297
-297/+105
-105/+53
-53

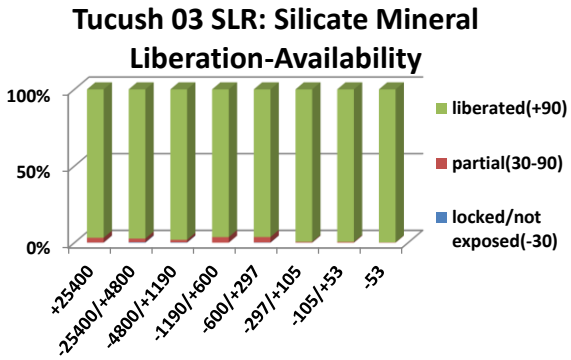
Tucush 03 SLR: Silicate Mineral Liberation-Availability
100%
50%
0%
liberated(+90)
partial(30-90)
locked/not exposed(-30)
+25400
-25400/+4800
-4800/+1190
-1190/+600
-600/+297
-297/+105
-105/+53
-53

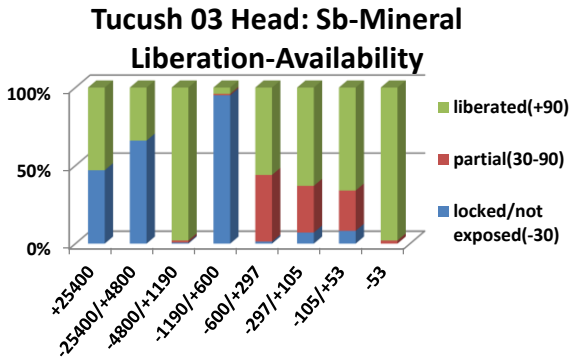
Tucush 03 Head: Sb-Mineral Liberation-Availability
100%
50%
0%
liberated(+90)
partial(30-90)
locked/not exposed(-30)
+25400
-25400/+4800
-4800/+1190
-1190/+600
-600/+297
-297/+105
-105/+53
-53

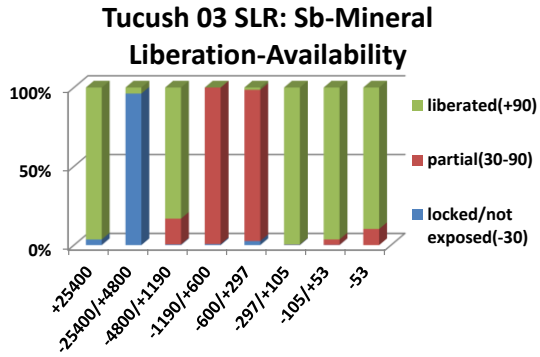
Tucush 03 SLR: Sb-Mineral Liberation-Availability
100%
50%
0%
liberated(+90)
partial(30-90)
locked/not exposed(-30)
+25400
-25400/+4800
-4800/+1190
-1190/+600
-600/+297
-297/+105
-105/+53
-53

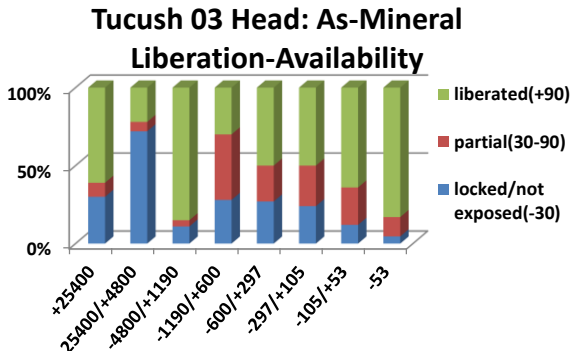
Tucush 03 Head: As-Mineral Liberation-Availability
100%
50%
0%
liberated(+90)
partial(30-90)
locked/not exposed(-30)
+25400
-25400/+4800
-4800/+1190
-1190/+600
-600/+297
-297/+105
-105/+53
-53

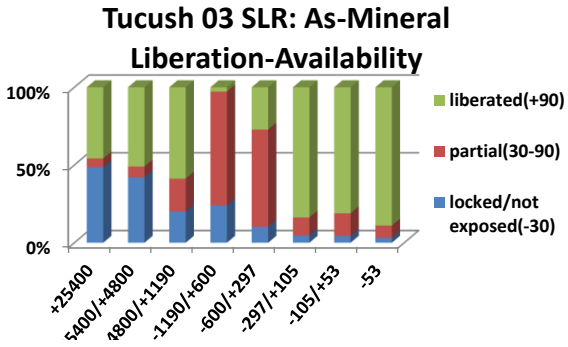
Tucush 03 SLR: As-Mineral Liberation-Availability
100%
50%
0%
liberated(+90)
partial(30-90)
locked/not exposed(-30)
+25400
-25400/+4800
-4800/+1190
-1190/+600
-600/+297
-297/+105
-105/+53
-53

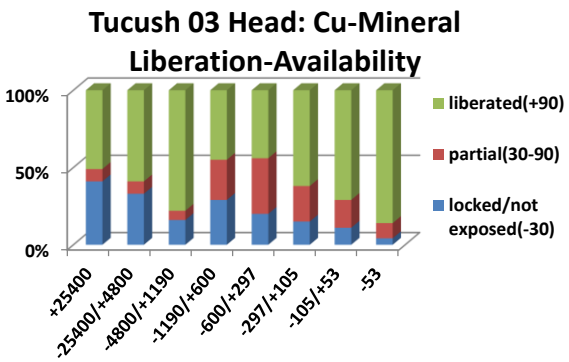
Tucush 03 Head: Cu-Mineral Liberation-Availability
100%
50%
0%
liberated(+90)
partial(30-90)
locked/not exposed(-30)
+25400
-25400/+4800
-4800/+1190
-1190/+600
-600/+297
-297/+105
-105/+53
-53

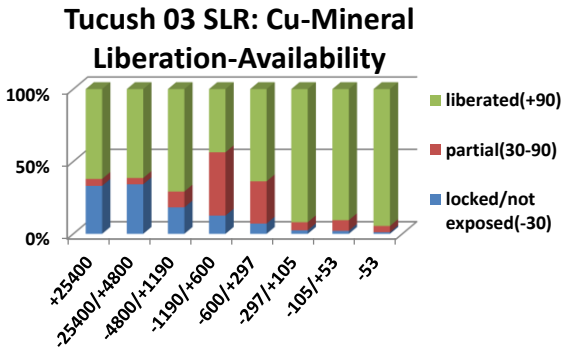
Tucush 03 SLR: Cu-Mineral Liberation-Availability
100%
50%
0%
liberated(+90)
partial(30-90)
locked/not exposed(-30)
+25400
-25400/+4800
-4800/+1190
-1190/+600
-600/+297
-297/+105
-105/+53
-53

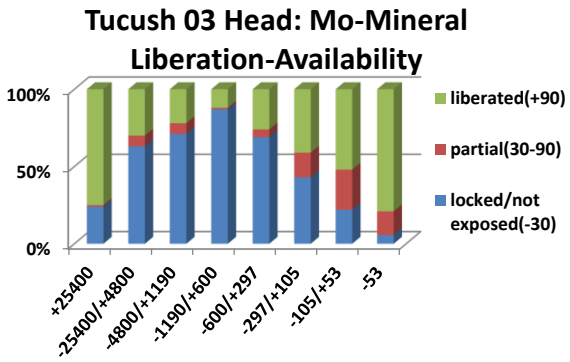
Tucush 03 Head: Mo-Mineral Liberation-Availability
100%
50%
0%
liberated(+90)
partial(30-90)
locked/not exposed(-30)
+25400
-25400/+4800
-4800/+1190
-1190/+600
-600/+297
-297/+105
-105/+53
-53

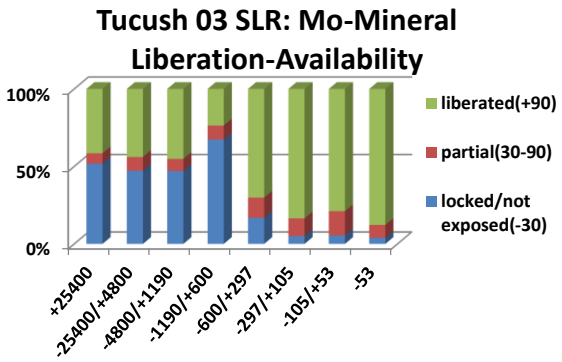
Tucush 03 SLR: Mo-Mineral Liberation-Availability
100%
50%
0%
liberated(+90)
partial(30-90)
locked/not exposed(-30)
+25400
-25400/+4800
-4800/+1190
-1190/+600
-600/+297
-297/+105
-105/+53
-53

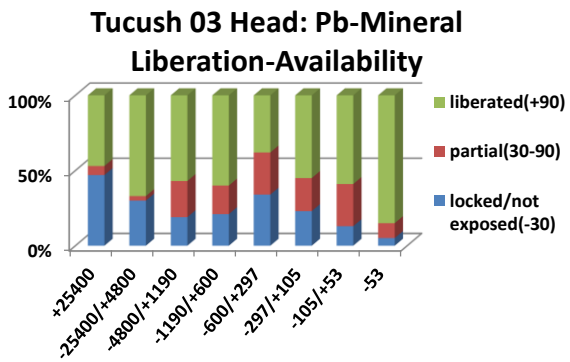
Tucush 03 Head: Pb-Mineral Liberation-Availability
100%
50%
0%
liberated(+90)
partial(30-90)
locked/not exposed(-30)
+25400
-25400/+4800
-4800/+1190
-1190/+600
-600/+297
-297/+105
-105/+53
-53

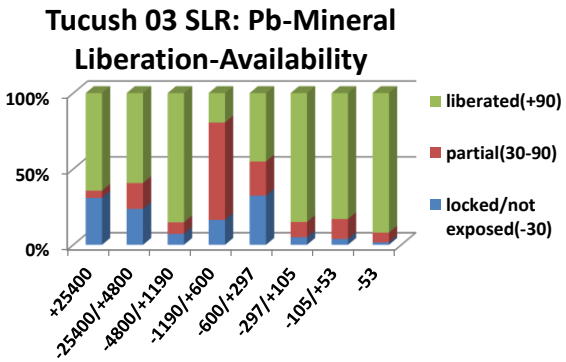
Tucush 03 SLR: Pb-Mineral Liberation-Availability
100%
50%
0%
liberated(+90)
partial(30-90)
locked/not exposed(-30)
+25400
-25400/+4800
-4800/+1190
-1190/+600
-600/+297
-297/+105
-105/+53
-53

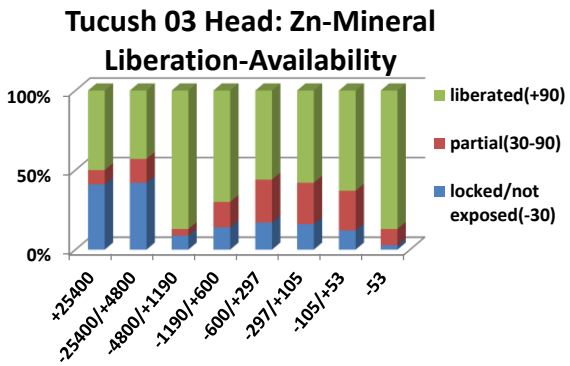
Tucush 03 Head: Zn-Mineral Liberation-Availability
100%
50%
0%
liberated(+90)
partial(30-90)
locked/not exposed(-30)
+25400
-25400/+4800
-4800/+1190
-1190/+600
-600/+297
-297/+105
-105/+53
-53

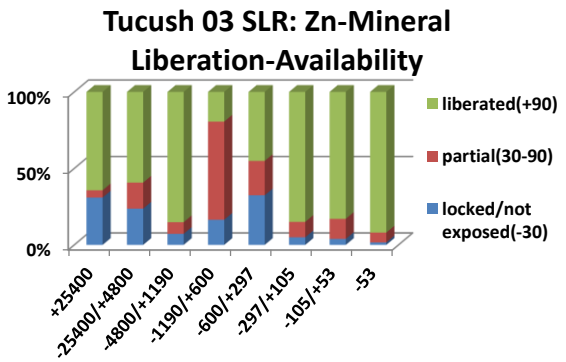
Tucush 03 SLR: Zn-Mineral Liberation-Availability
100%
50%
0%
liberated(+90)
partial(30-90)
locked/not exposed(-30)
+25400
-25400/+4800
-4800/+1190
-1190/+600
-600/+297
-297/+105
-105/+53
-53

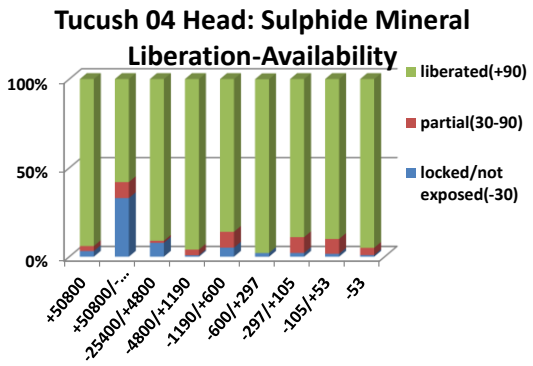
Tucush 04 Head: Sulphide Mineral Liberation-Availability
100%
50%
0%
liberated(+90)
partial(30-90)
locked/not exposed(-30)
+50800
+50800/-...
-25400/+4800
-4800/+1190
-1190/+600
-600/+297
-297/+105
-105/+53
-53

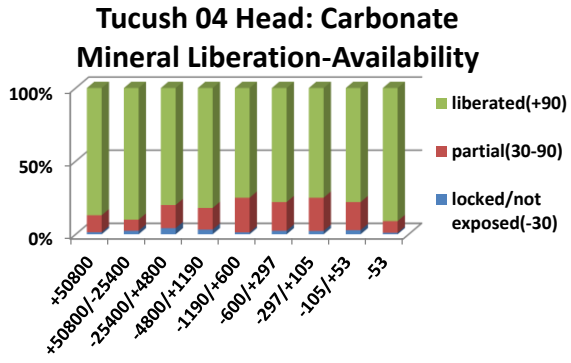
Tucush 04 Head: Carbonate Mineral Liberation-Availability
100%
50%
0%
liberated(+90)
partial(30-90)
locked/not exposed(-30)
+50800
+50800/-25400
-25400/+4800
-4800/+1190
-1190/+600
-600/+297
-297/+105
-105/+53
-53

Tucush 04 Head: Silicate Mineral Liberation-Availability

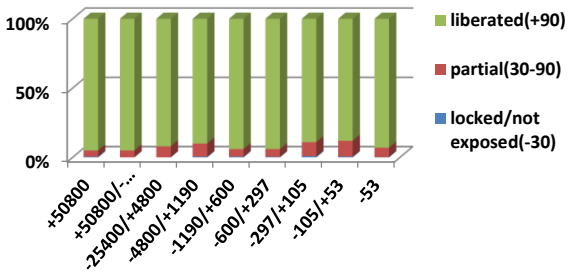

Tucush 04 Head: Sb-Mineral Liberation-Availability

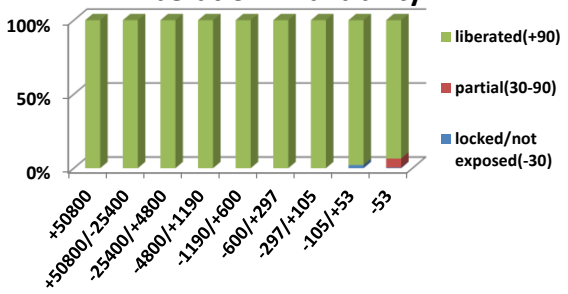

Tucush 04 Head: As-Mineral Liberation-Availability

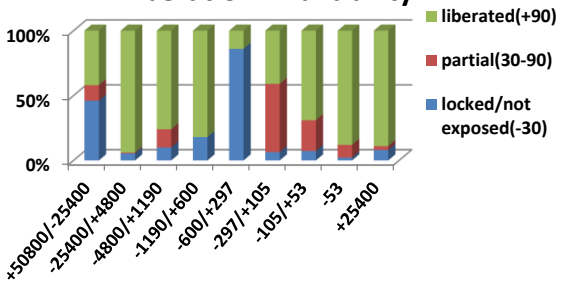

Tucush 04 Head: Cu-Mineral Liberation-Availability

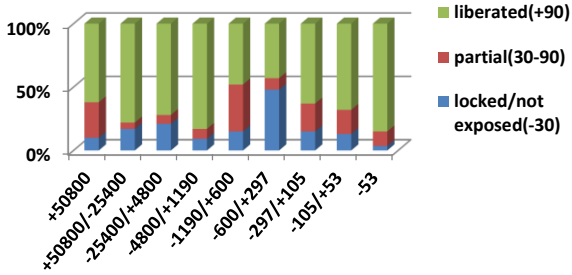

Tucush 04 Head: Mo-Mineral Liberation-Availability

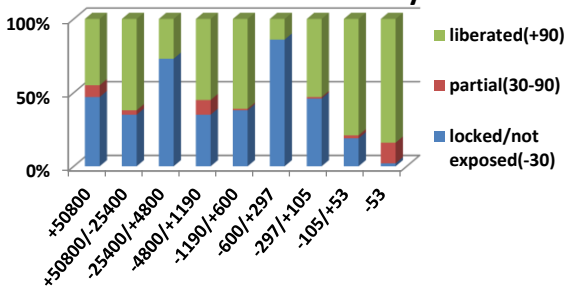

Tucush 04 Head: Pb-Mineral Liberation-Availability

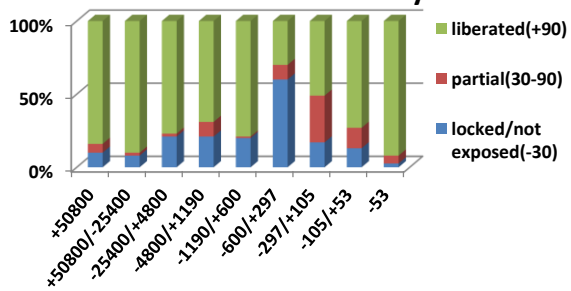

Tucush 04 Head: Zn-Mineral Liberation-Availability

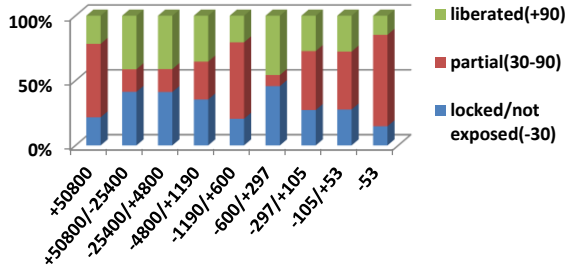

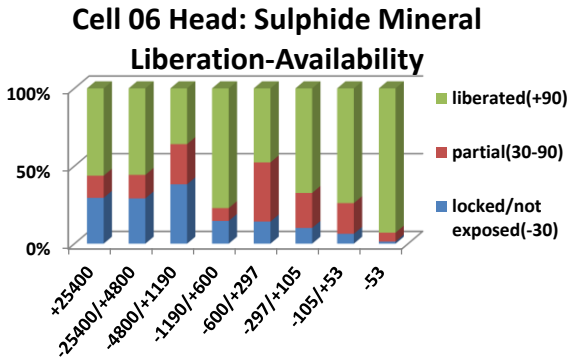
Cell 06 Head: Sulphide Mineral Liberation-Availability
100%
50%
0%
liberated(+90)
partial(30-90)
locked/not exposed(-30)
+25400
-25400/+4800
-4800/+1190
-1190/+600
-600/+297
-297/+105
-105/+53
-53

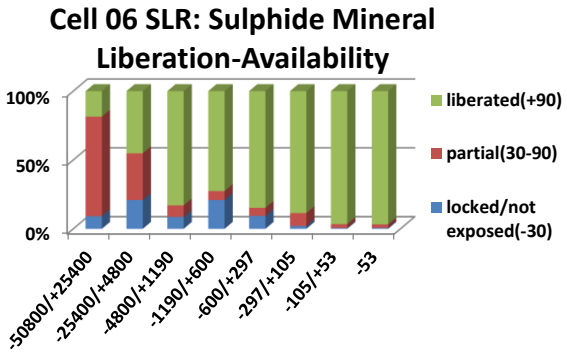
Cell 06 SLR: Sulphide Mineral Liberation-Availability
100%
50%
0%
liberated(+90)
partial(30-90)
locked/not exposed(-30)
-50800/+25400
-25400/+4800
-4800/+1190
-1190/+600
-600/+297
-297/+105
-105/+53
-53

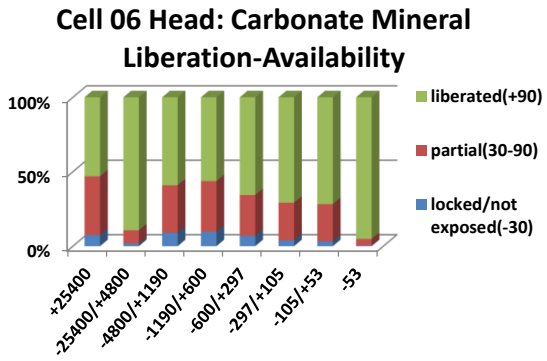
Cell 06 Head: Carbonate Mineral Liberation-Availability
100%
50%
0%
liberated(+90)
partial(30-90)
locked/not exposed(-30)
+25400
-25400/+4800
-4800/+1190
-1190/+600
-600/+297
-297/+105
-105/+53
-53

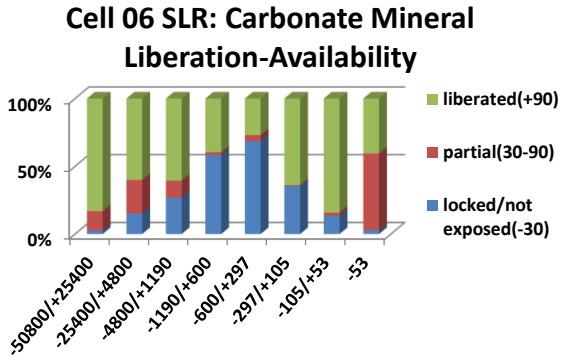
Cell 06 SLR: Carbonate Mineral Liberation-Availability
100%
50%
0%
liberated(+90)
partial(30-90)
locked/not exposed(-30)
-50800/+25400
-25400/+4800
-4800/+1190
-1190/+600
-600/+297
-297/+105
-105/+53
-53

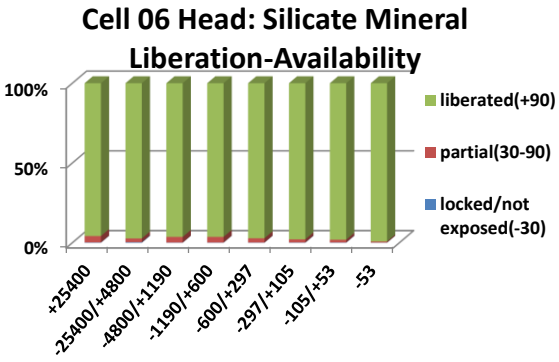
Cell 06 Head: Silicate Mineral Liberation-Availability
100%
50%
0%
liberated(+90)
partial(30-90)
locked/not exposed(-30)
+25400
-25400/+4800
-4800/+1190
-1190/+600
-600/+297
-297/+105
-105/+53
-53

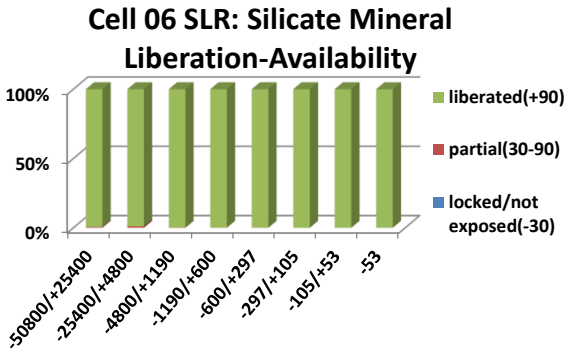
Cell 06 SLR: Silicate Mineral Liberation-Availability
100%
50%
0%
liberated(+90)
partial(30-90)
locked/not exposed(-30)
-50800/+25400
-25400/+4800
-4800/+1190
-1190/+600
-600/+297
-297/+105
-105/+53
-53

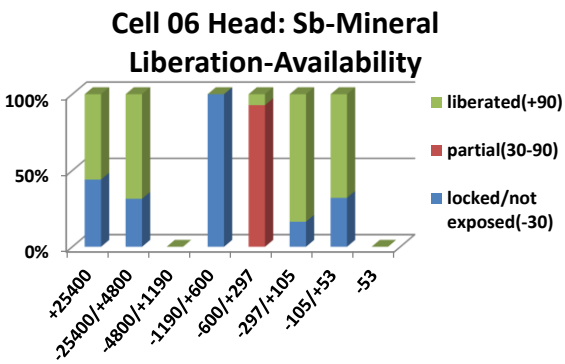
Cell 06 Head: Sb-Mineral Liberation-Availability
100%
50%
0%
liberated(+90)
partial(30-90)
locked/not exposed(-30)
+25400
-25400/+4800
-4800/+1190
-1190/+600
-600/+297
-297/+105
-105/+53
-53

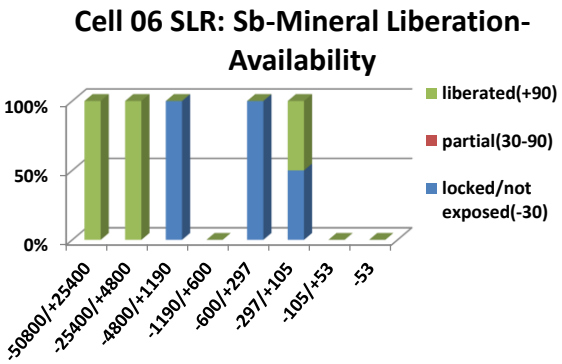
Cell 06 SLR: Sb-Mineral Liberation-Availability
100%
50%
0%
liberated(+90)
partial(30-90)
locked/not exposed(-30)
-50800/+25400
-25400/+4800
-4800/+1190
-1190/+600
-600/+297
-297/+105
-105/+53
-53

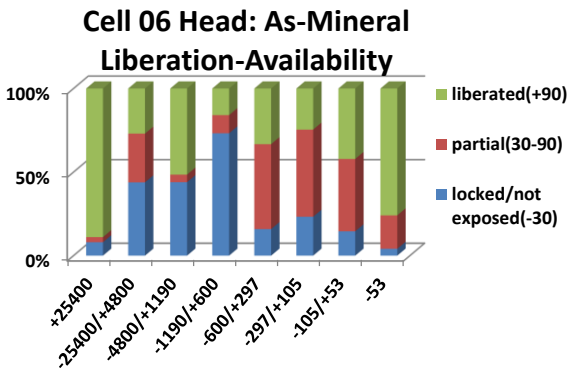
Cell 06 Head: As-Mineral Liberation-Availability
100%
50%
0%
liberated(+90)
partial(30-90)
locked/not exposed(-30)
+25400
-25400/+4800
-4800/+1190
-1190/+600
-600/+297
-297/+105
-105/+53
-53

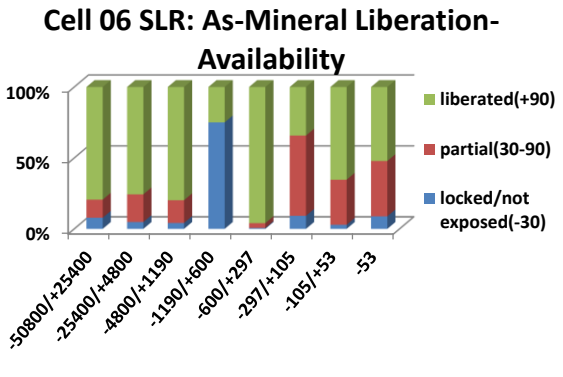
Cell 06 SLR: As-Mineral Liberation-Availability
100%
50%
0%
liberated(+90)
partial(30-90)
locked/not exposed(-30)
-50800/+25400
-25400/+4800
-4800/+1190
-1190/+600
-600/+297
-297/+105
-105/+53
-53

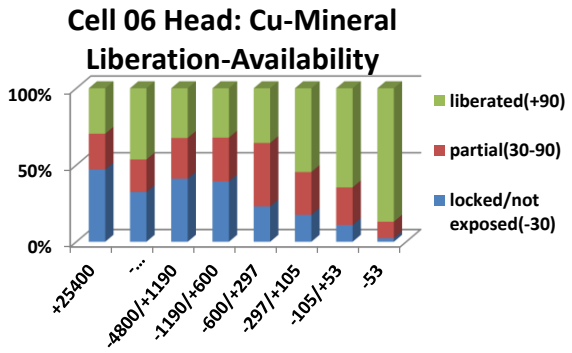
Cell 06 Head: Cu-Mineral Liberation-Availability
100%
50%
0%
liberated(+90)
partial(30-90)
locked/not exposed(-30)
+25400
-4800/+1190
-1190/+600
-600/+297
-297/+105
-105/+53
-53

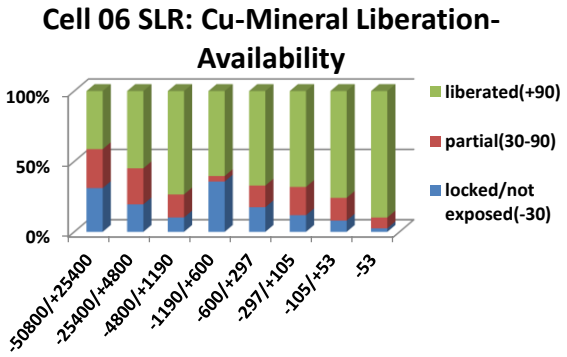
Cell 06 SLR: Cu-Mineral Liberation-Availability
100%
50%
0%
liberated(+90)
partial(30-90)
locked/not exposed(-30)
-50800/+25400
-25400/+4800
-4800/+1190
-1190/+600
-600/+297
-297/+105
-105/+53
-53

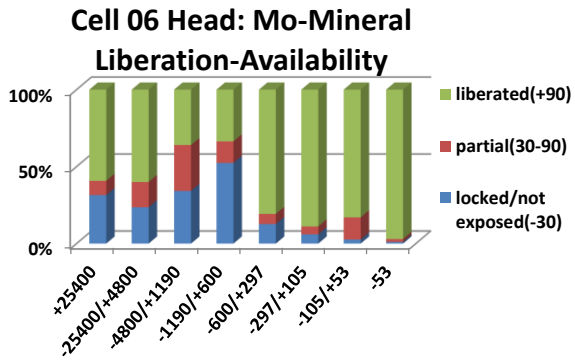
Cell 06 Head: Mo-Mineral Liberation-Availability
100%
50%
0%
liberated(+90)
partial(30-90)
locked/not exposed(-30)
+25400
-25400/+4800
-4800/+1190
-1190/+600
-600/+297
-297/+105
-105/+53
-53

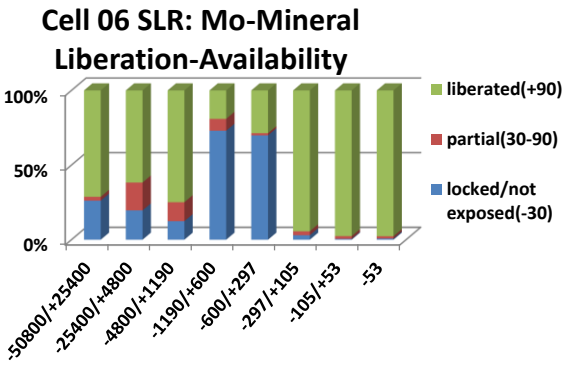
Cell 06 SLR: Mo-Mineral Liberation-Availability
100%
50%
0%
liberated(+90)
partial(30-90)
locked/not exposed(-30)
-50800/+25400
-25400/+4800
-4800/+1190
-1190/+600
-600/+297
-297/+105
-105/+53
-53

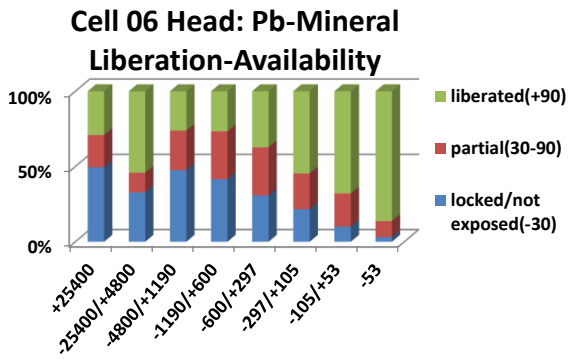
Cell 06 Head: Pb-Mineral Liberation-Availability
100%
50%
0%
liberated(+90)
partial(30-90)
locked/not exposed(-30)
+25400
-25400/+4800
-4800/+1190
-1190/+600
-600/+297
-297/+105
-105/+53
-53

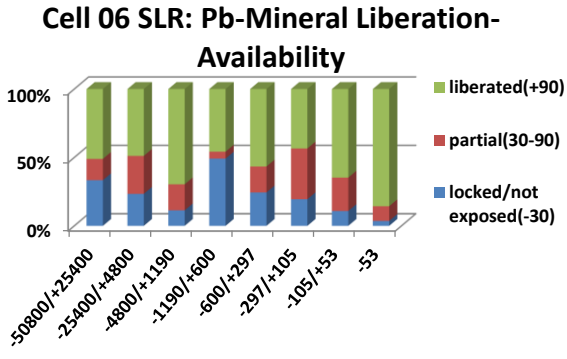
Cell 06 SLR: Pb-Mineral Liberation-Availability
100%
50%
0%
liberated(+90)
partial(30-90)
locked/not exposed(-30)
-50800/+25400
-25400/+4800
-4800/+1190
-1190/+600
-600/+297
-297/+105
-105/+53
-53

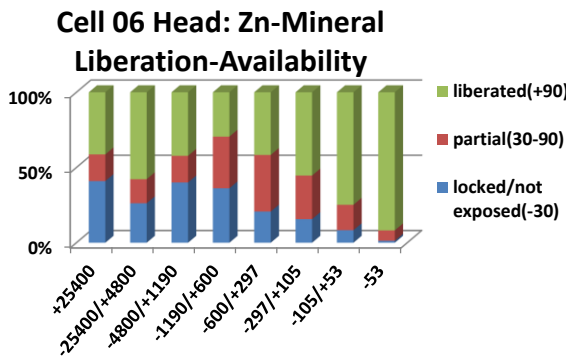
Cell 06 Head: Zn-Mineral Liberation-Availability
100%
50%
0%
+25400
-25400/+4800
-4800/+1190
-1190/+600
-600/+297
-297/+105
-105/+53
-53
liberated(+90)
partial(30-90)
locked/not exposed(-30)

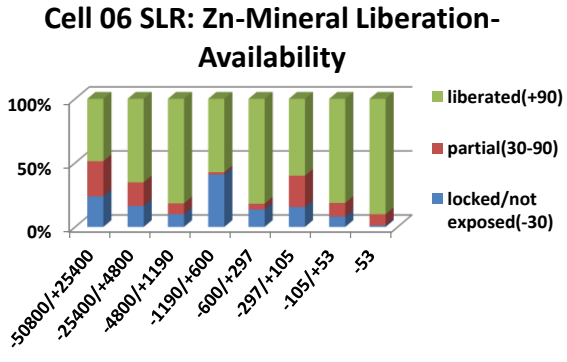
Cell 06 SLR: Zn-Mineral Liberation-Availability
100%
50%
0%
-50800/+25400
-25400/+4800
-4800/+1190
-1190/+600
-600/+297
-297/+105
-105/+53
-53
liberated(+90)
partial(30-90)
locked/not exposed(-30)

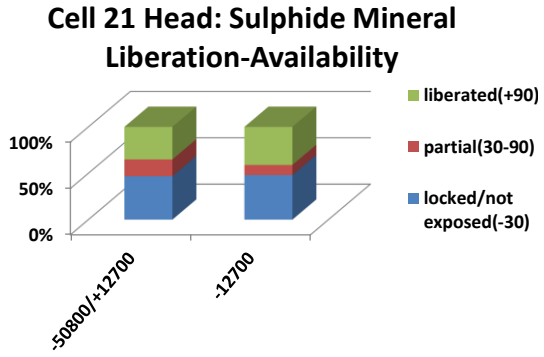
Cell 21 Head: Sulphide Mineral Liberation-Availability
100%
50%
0%
-50800/+12700
-12700
liberated(+90)
partial(30-90)
locked/not exposed(-30)

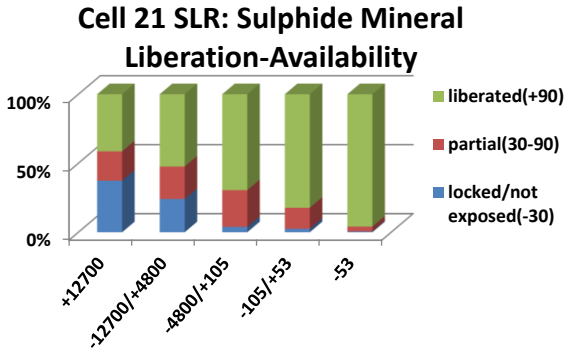
Cell 21 SLR: Sulphide Mineral Liberation-Availability
100%
50%
0%
+12700
-12700/+4800
-4800/+105
-105/+53
-53
liberated(+90)
partial(30-90)
locked/not exposed(-30)

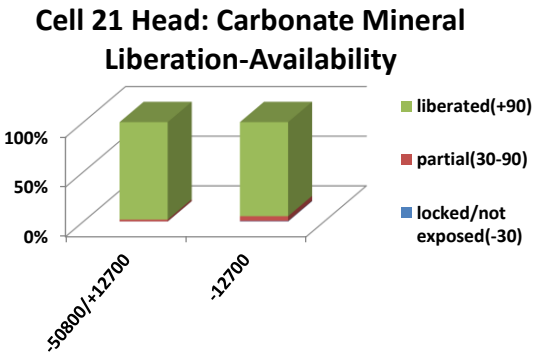
Cell 21 Head: Carbonate Mineral Liberation-Availability
100%
50%
0%
-50800/+12700
-12700
liberated(+90)
partial(30-90)
locked/not exposed(-30)

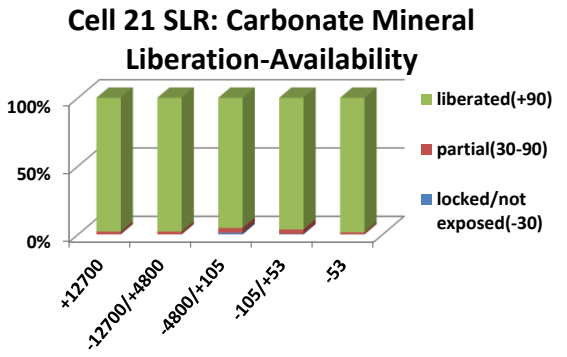
Cell 21 SLR: Carbonate Mineral Liberation-Availability
100%
50%
0%
+12700
-12700/+4800
-4800/+105
-105/+53
-53
liberated(+90)
partial(30-90)
locked/not exposed(-30)

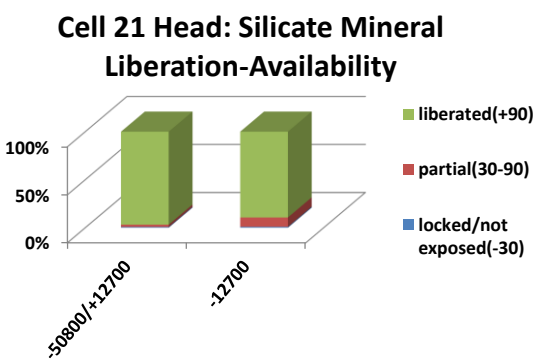
Cell 21 Head: Silicate Mineral Liberation-Availability
100%
50%
0%
-50800/+12700
-12700
liberated(+90)
partial(30-90)
locked/not exposed(-30)

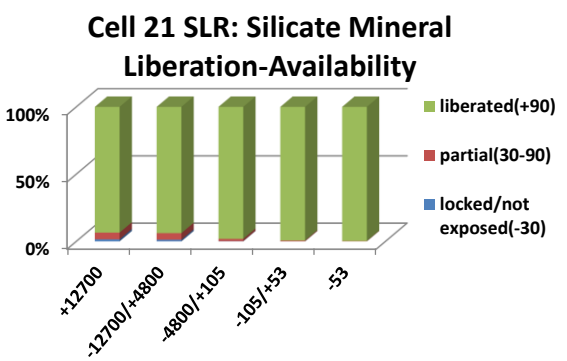
Cell 21 SLR: Silicate Mineral Liberation-Availability
100%
50%
0%
+12700
-12700/+4800
-4800/+105
-105/+53
-53
liberated(+90)
partial(30-90)
locked/not exposed(-30)

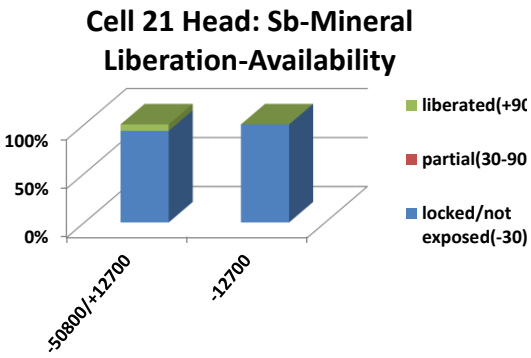
Cell 21 Head: Sb-Mineral Liberation-Availability
100%
50%
0%
-50800/+12700
-12700
liberated(+90
partial(30-90
locked/not exposed(-30)

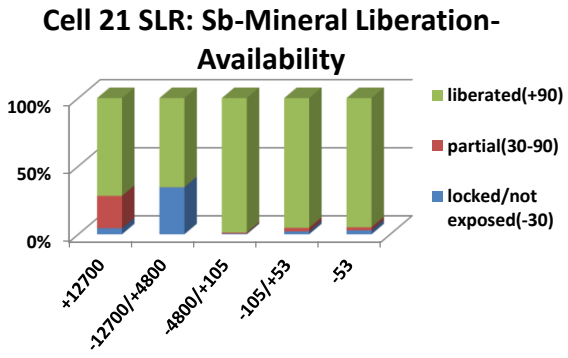
Cell 21 SLR: Sb-Mineral Liberation-Availability
100%
50%
0%
+12700
-12700/+4800
-4800/+105
-105/+53
-53
liberated(+90)
partial(30-90)
locked/not exposed(-30)

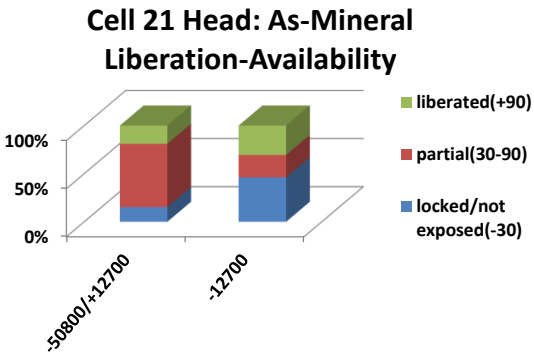
Cell 21 Head: As-Mineral Liberation-Availability
100%
50%
0%
-50800/+12700
-12700
liberated(+90)
partial(30-90)
locked/not exposed(-30)

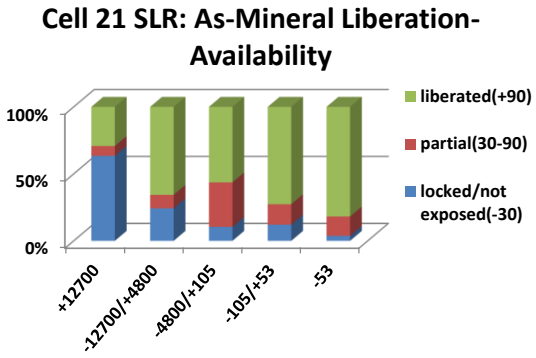
Cell 21 SLR: As-Mineral Liberation-Availability
100%
50%
0%
+12700
-12700/+4800
-4800/+105
-105/+53
-53
liberated(+90)
partial(30-90)
locked/not exposed(-30)

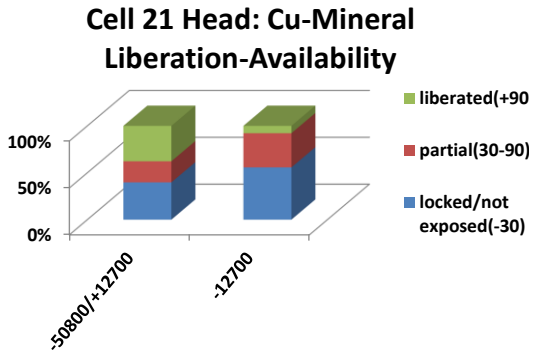
Cell 21 Head: Cu-Mineral Liberation-Availability
100%
50%
0%
-50800/+12700
-12700
liberated(+90
partial(30-90)
locked/not exposed(-30)

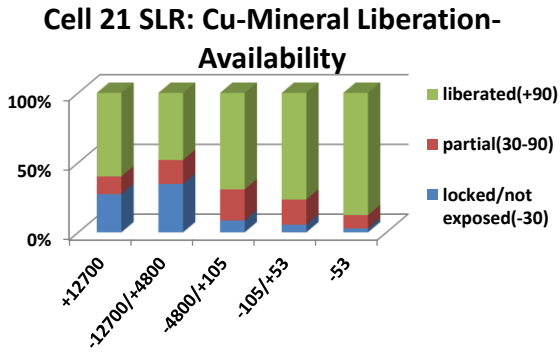
Cell 21 SLR: Cu-Mineral Liberation-Availability
100%
50%
0%
+12700
-12700/+4800
-4800/+105
-105/+53
-53
liberated(+90)
partial(30-90)
locked/not exposed(-30)

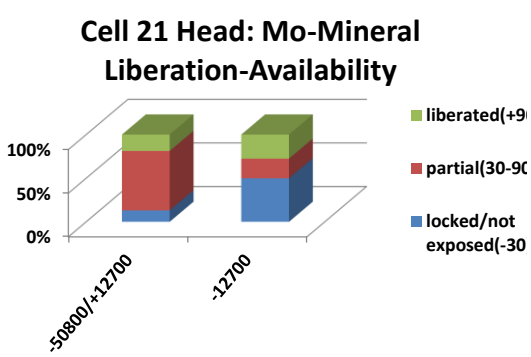
Cell 21 Head: Mo-Mineral Liberation-Availability
100%
50%
0%
-50800/+12700
-12700
liberated(+9
partial(30-9(
locked/not exposed(-30

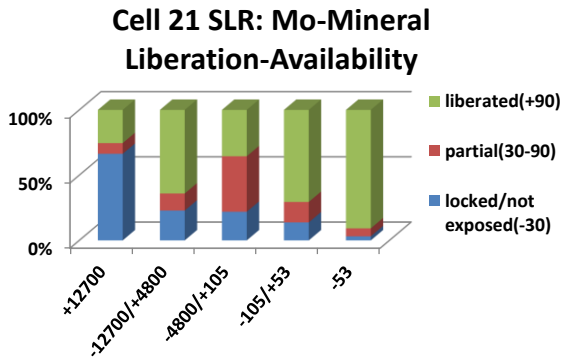
Cell 21 SLR: Mo-Mineral Liberation-Availability
100%
50%
0%
+12700
-12700/+4800
-4800/+105
-105/+53
-53
liberated(+90)
partial(30-90)
locked/not exposed(-30)

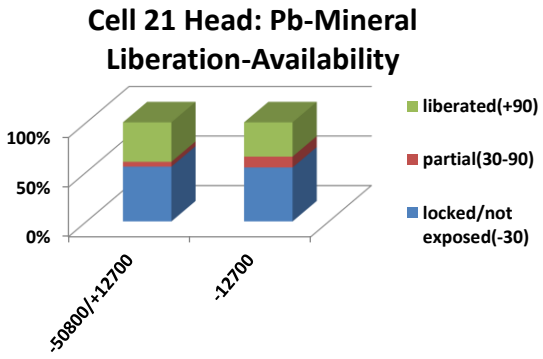
Cell 21 Head: Pb-Mineral Liberation-Availability
100%
50%
0%
-50800/+12700
-12700
liberated(+90)
partial(30-90)
locked/not exposed(-30)

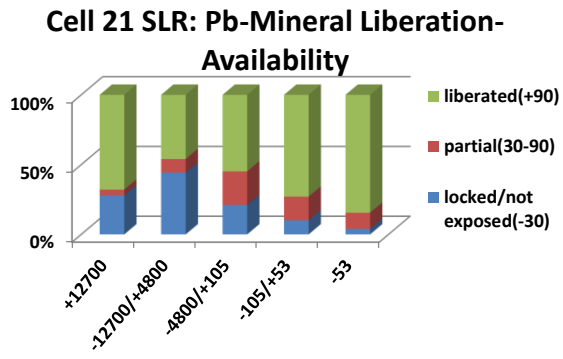
Cell 21 SLR: Pb-Mineral Liberation-Availability
100%
50%
0%
+12700
-12700/+4800
-4800/+105
-105/+53
-53
liberated(+90)
partial(30-90)
locked/not exposed(-30)

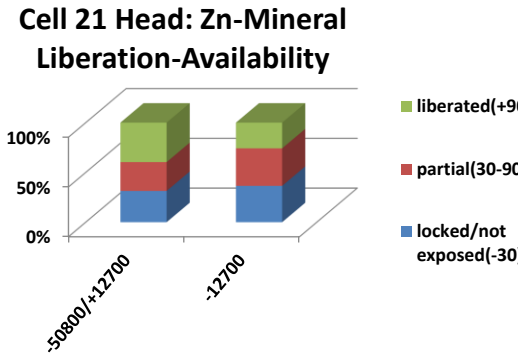
Cell 21 Head: Zn-Mineral Liberation-Availability
100%
50%
0%
-50800/+12700
-12700
liberated(+9
partial(30-9
locked/not exposed(-30

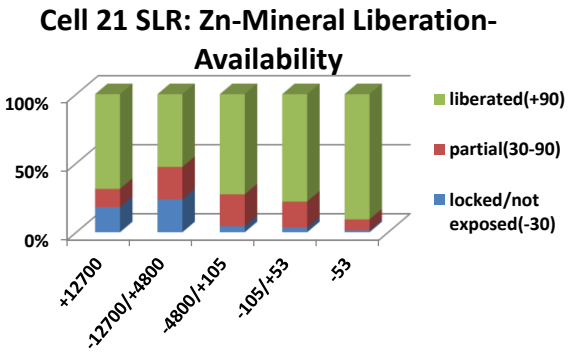
Cell 21 SLR: Zn-Mineral Liberation-Availability
100%
50%
0%
+12700
-12700/+4800
-4800/+105
-105/+53
-53
liberated(+90)
partial(30-90)
locked/not exposed(-30)

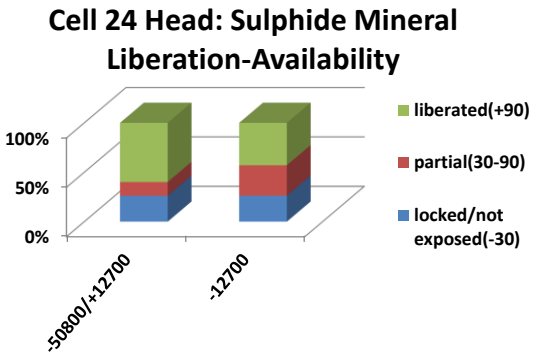
Cell 24 Head: Sulphide Mineral Liberation-Availability
100%
50%
0%
-50800/+12700
-12700
liberated(+90)
partial(30-90)
locked/not exposed(-30)

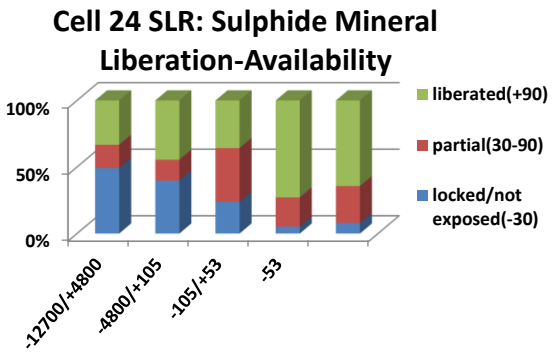
Cell 24 SLR: Sulphide Mineral Liberation-Availability
100%
50%
0%
-12700/+4800
-4800/+105
-105/+53
-53
liberated(+90)
partial(30-90)
locked/not exposed(-30)

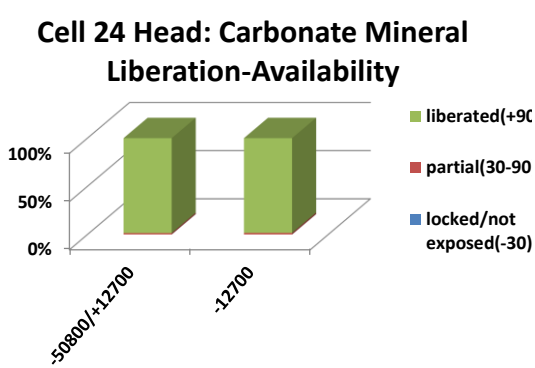
Cell 24 Head: Carbonate Mineral Liberation-Availability
100%
50%
0%
-50800/+12700
-12700
liberated(+90
partial(30-90
locked/not exposed(-30)

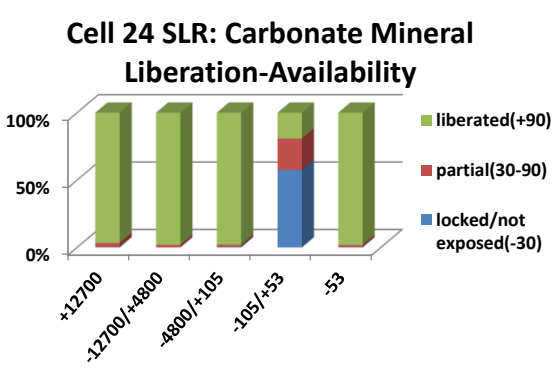
Cell 24 SLR: Carbonate Mineral Liberation-Availability
100%
50%
0%
+12700
-12700/+4800
-4800/+105
-105/+53
-53
liberated(+90)
partial(30-90)
locked/not exposed(-30)

Cell 24 Head: Silicate Mineral Liberation-Availability

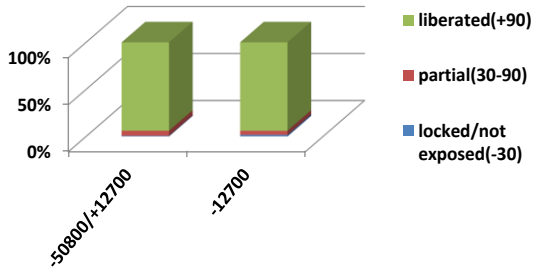

Cell 24 SLR: Silicate Mineral Liberation-Availability

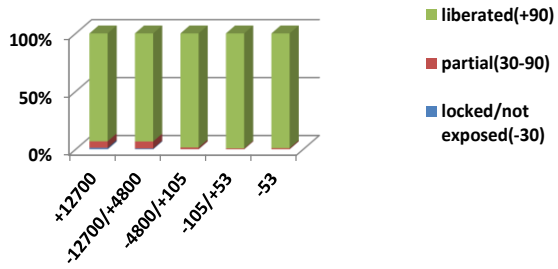

Cell 24 Head: Sb-Mineral Liberation-Availability

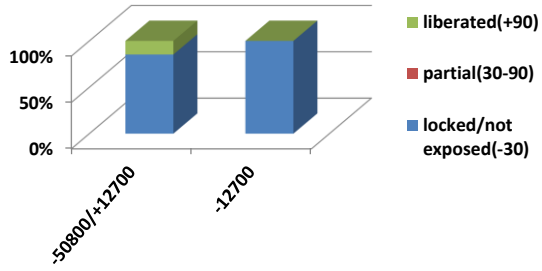

Cell 24 SLR: Sb-Mineral Liberation-Availability

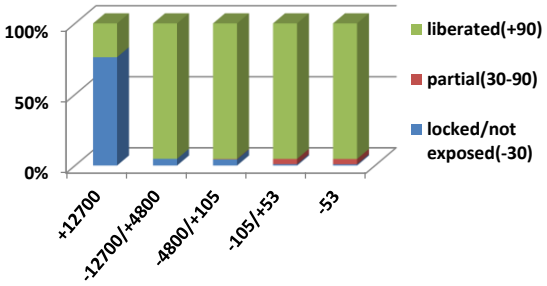

Cell 24 Head: As-Mineral Liberation-Availability

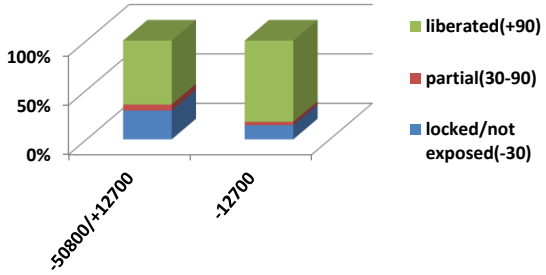

Cell 24 SLR: As-Mineral Liberation-Availability

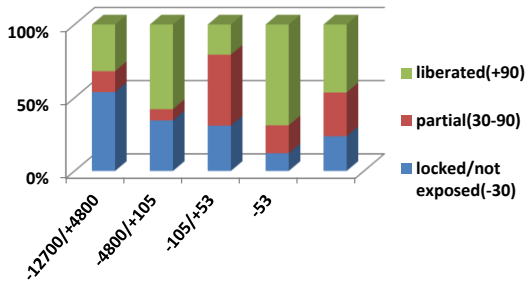

Cell 24 Head: Cu-Mineral Liberation-Availability

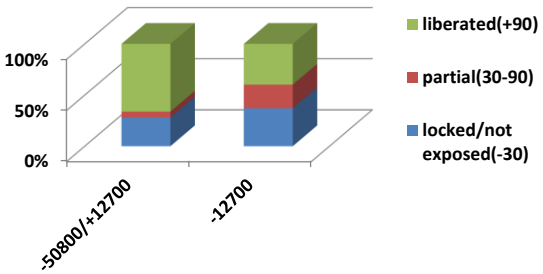

Cell 24 SLR: Cu-Mineral Liberation-Availability

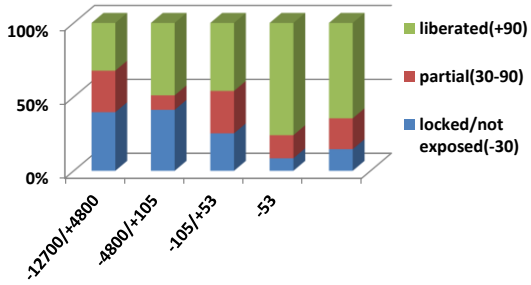

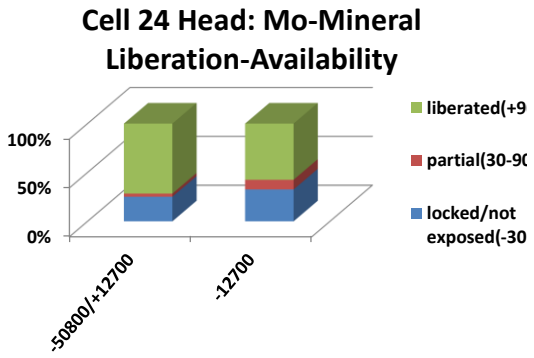
Cell 24 Head: Mo-Mineral Liberation-Availability
100%
50%
0%
-50800/+12700
-12700
liberated(+9
partial(30-9(
locked/not exposed(-30

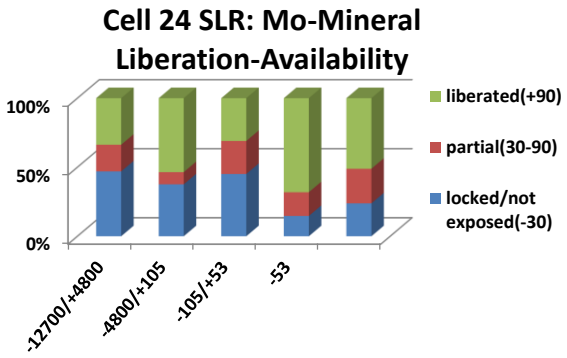
Cell 24 SLR: Mo-Mineral Liberation-Availability
100%
50%
0%
-12700/+4800
-4800/+105
-105/+53
-53
liberated(+90)
partial(30-90)
locked/not exposed(-30)

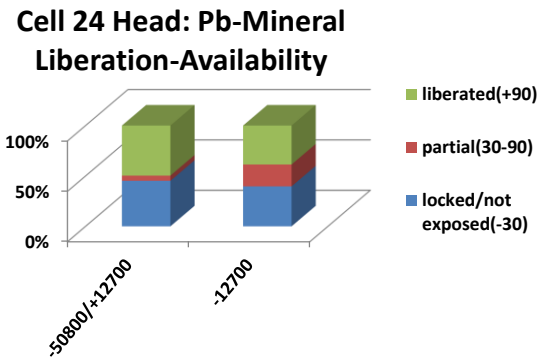
Cell 24 Head: Pb-Mineral Liberation-Availability
100%
50%
0%
-50800/+12700
-12700
liberated(+90)
partial(30-90)
locked/not exposed(-30)

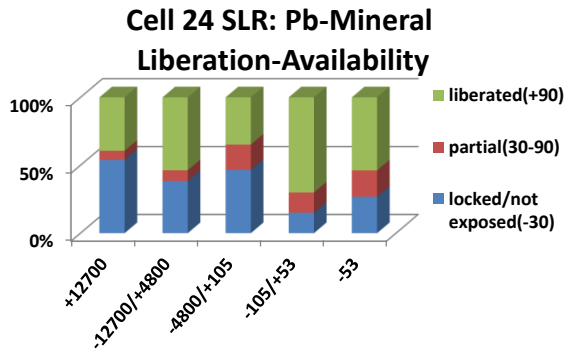
Cell 24 SLR: Pb-Mineral Liberation-Availability
100%
50%
0%
+12700
-12700/+4800
-4800/+105
-105/+53
-53
liberated(+90)
partial(30-90)
locked/not exposed(-30)

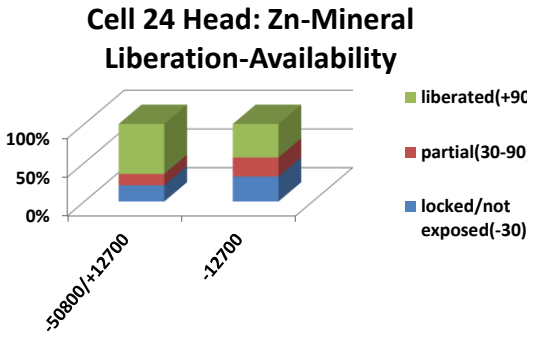
Cell 24 Head: Zn-Mineral Liberation-Availability
100%
50%
0%
-50800/+12700
-12700
liberated(+90
partial(30-90
locked/not exposed(-30)

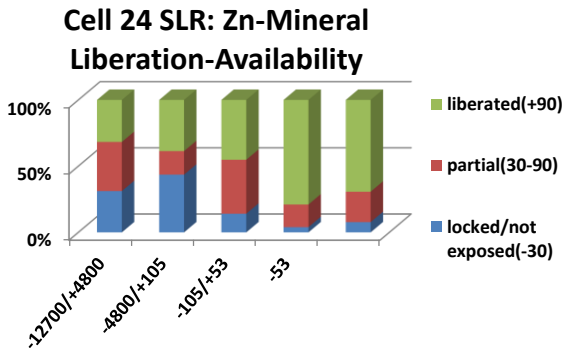
Cell 24 SLR: Zn-Mineral Liberation-Availability
100%
50%
0%
-12700/+4800
-4800/+105
-105/+53
-53
liberated(+90)
partial(30-90)
locked/not exposed(-30)

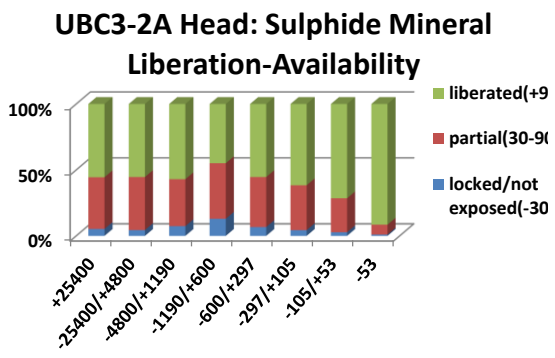
UBC3-2A Head: Sulphide Mineral Liberation-Availability
100%
50%
0%
+25400
-25400/+4800
-4800/+1190
-1190/+600
-600/+297
-297/+105
-105/+53
-53
liberated(+9
partial(30-9(
locked/not exposed(-30

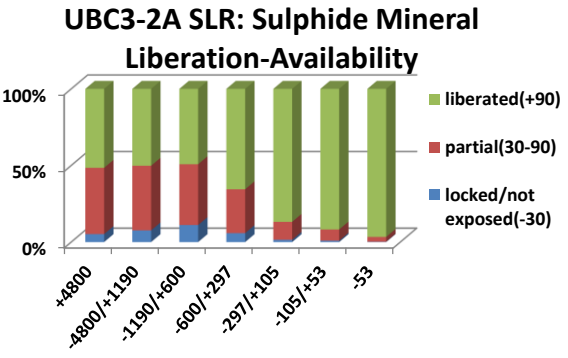
UBC3-2A SLR: Sulphide Mineral Liberation-Availability
100%
50%
0%
+4800
-4800/+1190
-1190/+600
-600/+297
-297/+105
-105/+53
-53
liberated(+90)
partial(30-90)
locked/not exposed(-30)

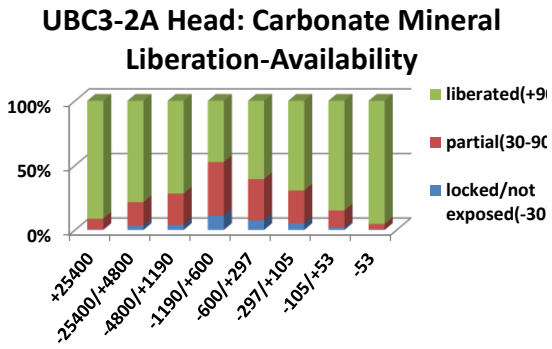
UBC3-2A Head: Carbonate Mineral Liberation-Availability
100%
50%
0%
+25400
-25400/+4800
-4800/+1190
-1190/+600
-600/+297
-297/+105
-105/+53
-53
liberated(+9
partial(30-9
locked/not exposed(-30

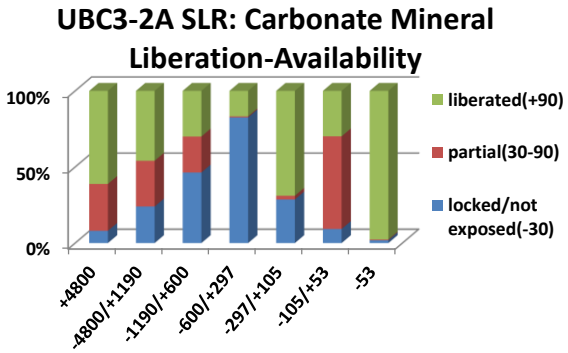
UBC3-2A SLR: Carbonate Mineral Liberation-Availability
100%
50%
0%
+4800
-4800/+1190
-1190/+600
-600/+297
-297/+105
-105/+53
-53
liberated(+90)
partial(30-90)
locked/not exposed(-30)

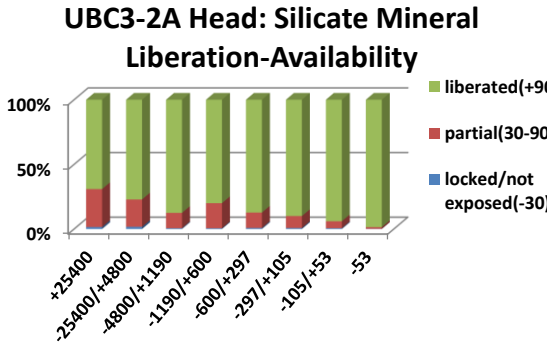
UBC3-2A Head: Silicate Mineral Liberation-Availability
100%
50%
0%
+25400
-25400/+4800
-4800/+1190
-1190/+600
-600/+297
-297/+105
-105/+53
-53
liberated(+9
partial(30-90
locked/not exposed(-30)

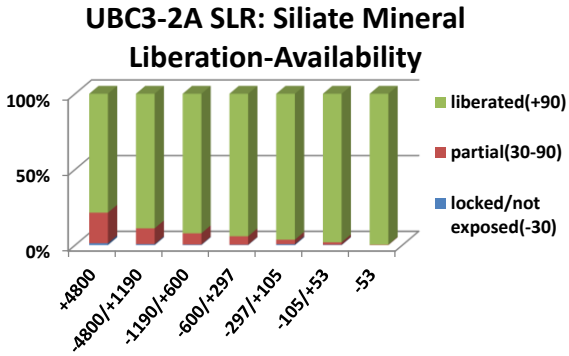
UBC3-2A SLR: Siliate Mineral Liberation-Availability
100%
50%
0%
+4800
-4800/+1190
-1190/+600
-600/+297
-297/+105
-105/+53
-53
liberated(+90)
partial(30-90)
locked/not exposed(-30)

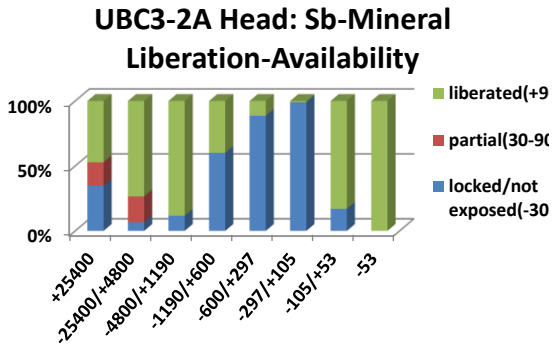
UBC3-2A Head: Sb-Mineral Liberation-Availability
100%
50%
0%
+25400
-25400/+4800
-4800/+1190
-1190/+600
-600/+297
-297/+105
-105/+53
-53
liberated(+9
partial(30-9
locked/not exposed(-30

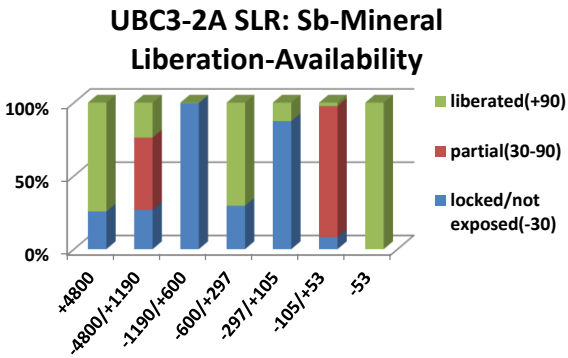
UBC3-2A SLR: Sb-Mineral Liberation-Availability
100%
50%
0%
+4800
-4800/+1190
-1190/+600
-600/+297
-297/+105
-105/+53
-53
liberated(+90)
partial(30-90)
locked/not exposed(-30)

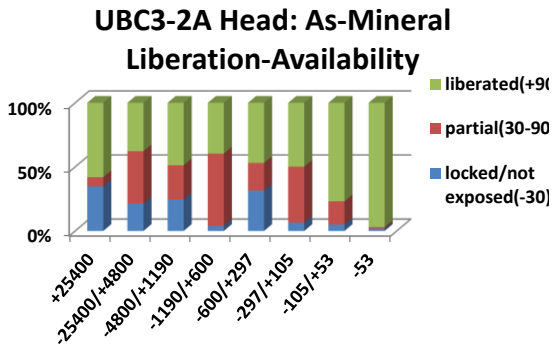
UBC3-2A Head: As-Mineral Liberation-Availability
100%
50%
0%
+25400
-25400/+4800
-4800/+1190
-1190/+600
-600/+297
-297/+105
-105/+53
-53
liberated(+9
partial(30-90
locked/not exposed(-30)

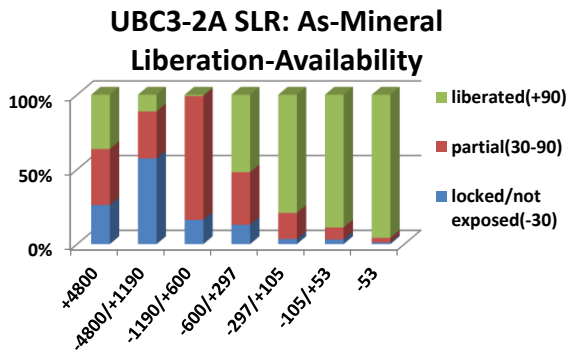
UBC3-2A SLR: As-Mineral Liberation-Availability
100%
50%
0%
+4800
-4800/+1190
-1190/+600
-600/+297
-297/+105
-105/+53
-53
liberated(+90)
partial(30-90)
locked/not exposed(-30)

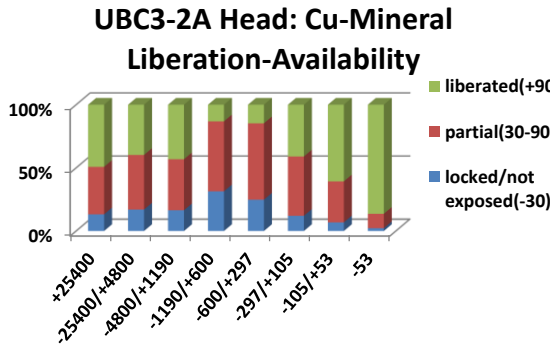
UBC3-2A Head: Cu-Mineral Liberation-Availability
100%
50%
0%
+25400
-25400/+4800
-4800/+1190
-1190/+600
-600/+297
-297/+105
-105/+53
-53
liberated(+9(
partial(30-90
locked/not exposed(-30)

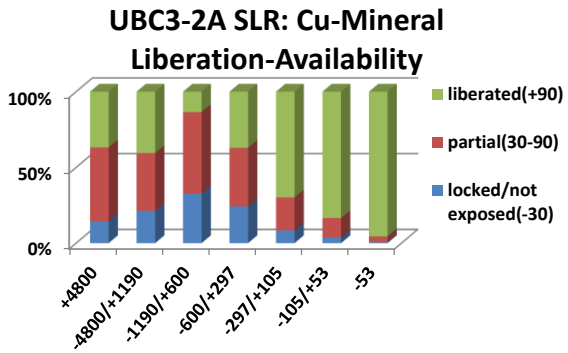
UBC3-2A SLR: Cu-Mineral Liberation-Availability
100%
50%
0%
+4800
-4800/+1190
-1190/+600
-600/+297
-297/+105
-105/+53
-53
liberated(+90)
partial(30-90)
locked/not exposed(-30)

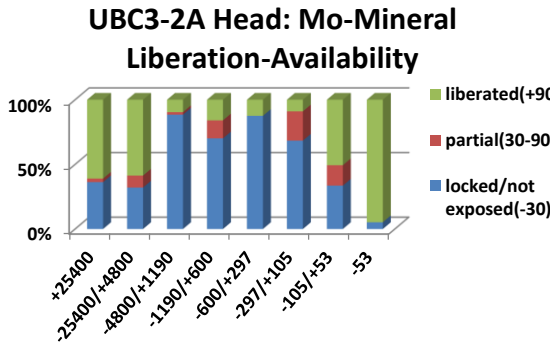
UBC3-2A Head: Mo-Mineral Liberation-Availability
100%
50%
0%
+25400
-25400/+4800
-4800/+1190
-1190/+600
-600/+297
-297/+105
-105/+53
-53
liberated(+9(
partial(30-90
locked/not exposed(-30)

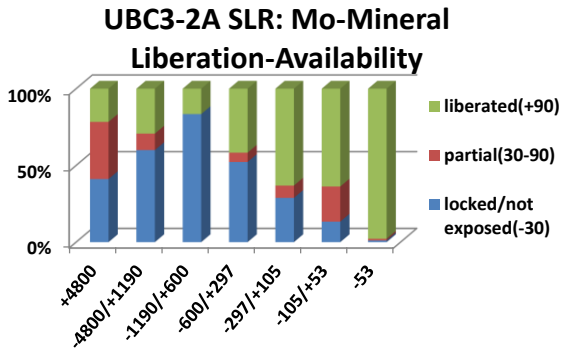
UBC3-2A SLR: Mo-Mineral Liberation-Availability
100%
50%
0%
+4800
-4800/+1190
-1190/+600
-600/+297
-297/+105
-105/+53
-53
liberated(+90)
partial(30-90)
locked/not exposed(-30)

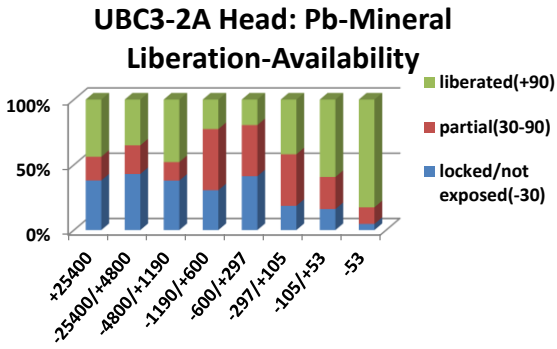
UBC3-2A Head: Pb-Mineral Liberation-Availability
100%
50%
0%
+25400
-25400/+4800
-4800/+1190
-1190/+600
-600/+297
-297/+105
-105/+53
-53
liberated(+90)
partial(30-90)
locked/not exposed(-30)

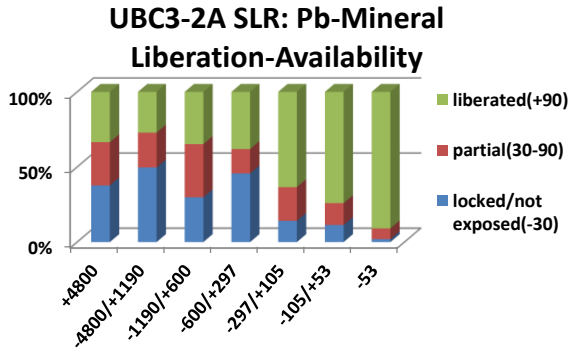
UBC3-2A SLR: Pb-Mineral Liberation-Availability
100%
50%
0%
+4800
-4800/+1190
-1190/+600
-600/+297
-297/+105
-105/+53
-53
liberated(+90)
partial(30-90)
locked/not exposed(-30)

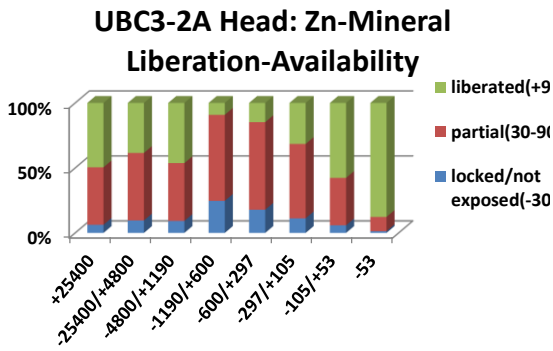
UBC3-2A Head: Zn-Mineral Liberation-Availability
100%
50%
0%
+25400
-25400/+4800
-4800/+1190
-1190/+600
-600/+297
-297/+105
-105/+53
-53
liberated(+9
partial(30-9(
locked/not exposed(-30

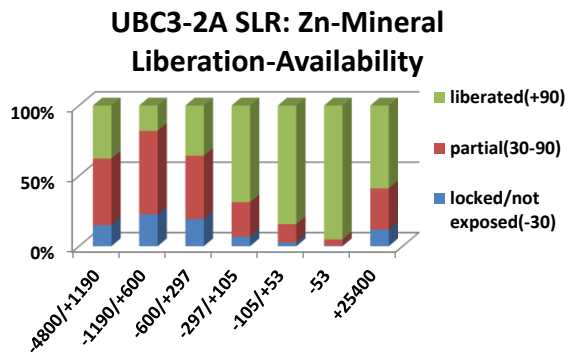
UBC3-2A SLR: Zn-Mineral Liberation-Availability
100%
50%
0%
-4800/+1190
-1190/+600
-600/+297
-297/+105
-105/+53
-53
+25400
liberated(+90)
partial(30-90)
locked/not exposed(-30)

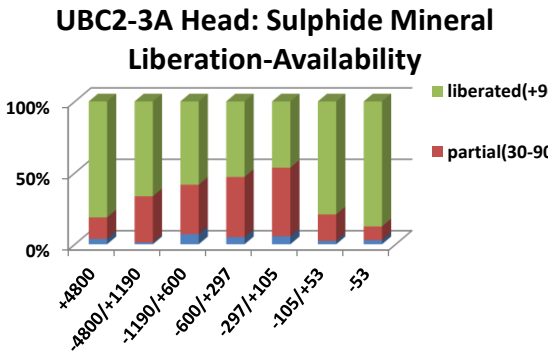
UBC2-3A Head: Sulphide Mineral Liberation-Availability
100%
50%
0%
liberated(+9
partial(30-9(
+4800
-4800/+1190
-1190/+600
-600/+297
-297/+105
-105/+53
-53

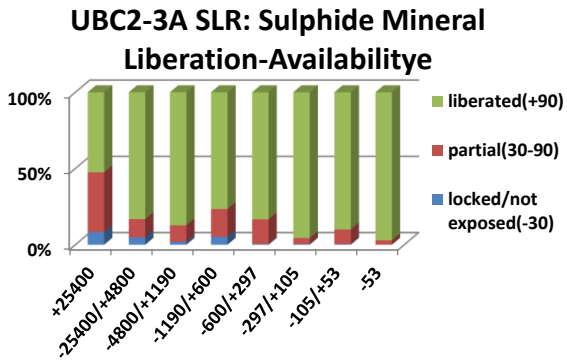
UBC2-3A SLR: Sulphide Mineral Liberation-Availabilitye
100%
50%
0%
liberated(+90)
partial(30-90)
locked/not exposed(-30)
+25400
-25400/+4800
-4800/+1190
-1190/+600
-600/+297
-297/+105
-105/+53
-53

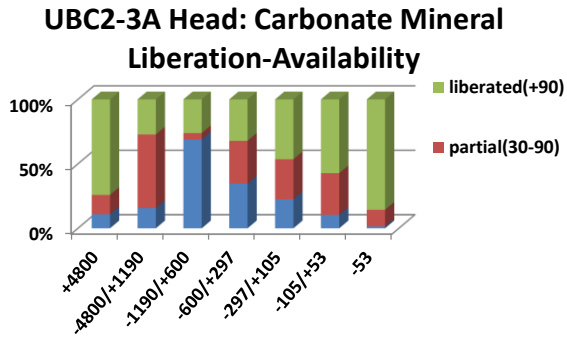
UBC2-3A Head: Carbonate Mineral Liberation-Availability
100%
50%
0%
liberated(+90)
partial(30-90)
+4800
-4800/+1190
-1190/+600
-600/+297
-297/+105
-105/+53
-53

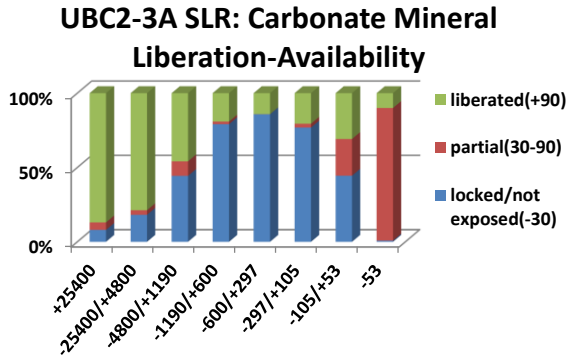
UBC2-3A SLR: Carbonate Mineral Liberation-Availability
100%
50%
0%
liberated(+90)
partial(30-90)
locked/not exposed(-30)
+25400
-25400/+4800
-4800/+1190
-1190/+600
-600/+297
-297/+105
-105/+53
-53

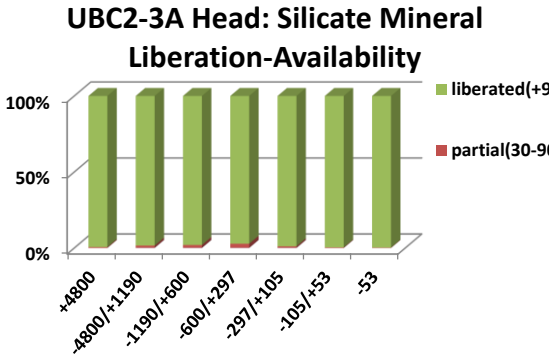
UBC2-3A Head: Silicate Mineral Liberation-Availability
100%
50%
0%
liberated(+9
partial(30-9(
+4800
-4800/+1190
-1190/+600
-600/+297
-297/+105
-105/+53
-53

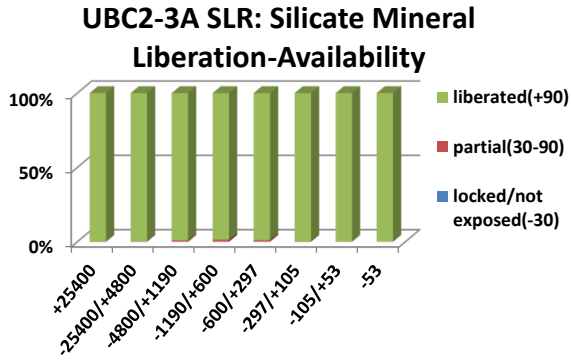
UBC2-3A SLR: Silicate Mineral Liberation-Availability
100%
50%
0%
liberated(+90)
partial(30-90)
locked/not exposed(-30)
+25400
-25400/+4800
-4800/+1190
-1190/+600
-600/+297
-297/+105
-105/+53
-53

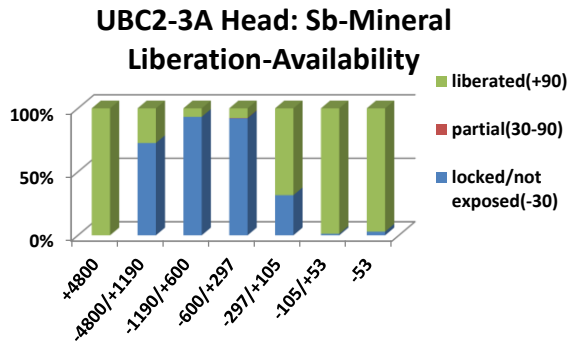
UBC2-3A Head: Sb-Mineral Liberation-Availability
100%
50%
0%
liberated(+90)
partial(30-90)
locked/not exposed(-30)
+4800
-4800/+1190
-1190/+600
-600/+297
-297/+105
-105/+53
-53

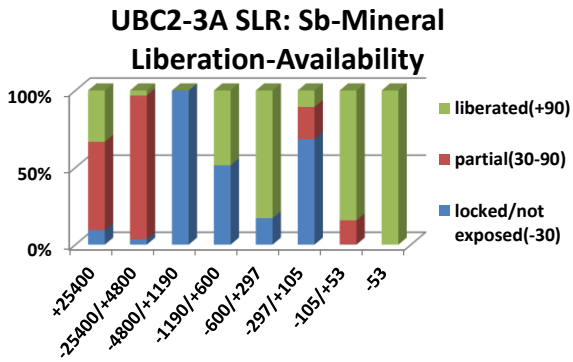
UBC2-3A SLR: Sb-Mineral Liberation-Availability
100%
50%
0%
liberated(+90)
partial(30-90)
locked/not exposed(-30)
+25400
-25400/+4800
-4800/+1190
-1190/+600
-600/+297
-297/+105
-105/+53
-53

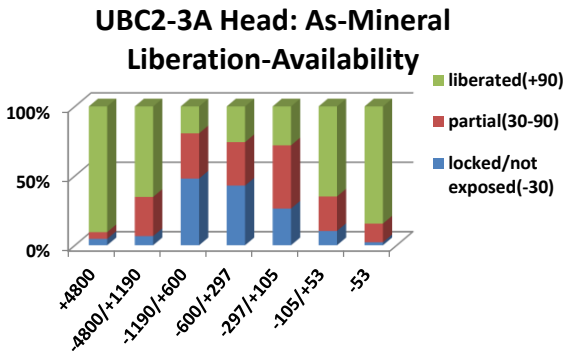
UBC2-3A Head: As-Mineral
Liberation-Availability
liberated(+90)
partial(30-90)
locked/not exposed(-30)
100%
50%
0%
+4800
-4800/+1190
-1190/+600
-600/+297
-297/+105
-105/+53
-53

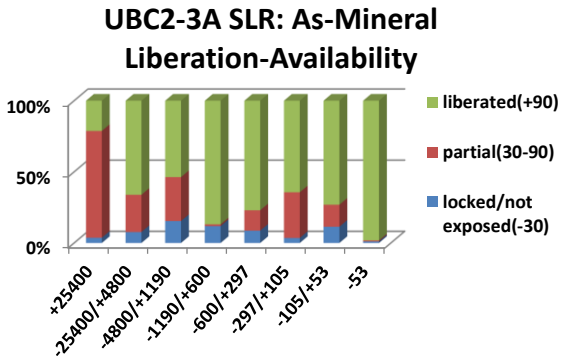
UBC2-3A SLR: As-Mineral
Liberation-Availability
liberated(+90)
partial(30-90)
locked/not exposed(-30)
100%
50%
0%
+25400
-25400/+4800
-4800/+1190
-1190/+600
-600/+297
-297/+105
-105/+53
-53

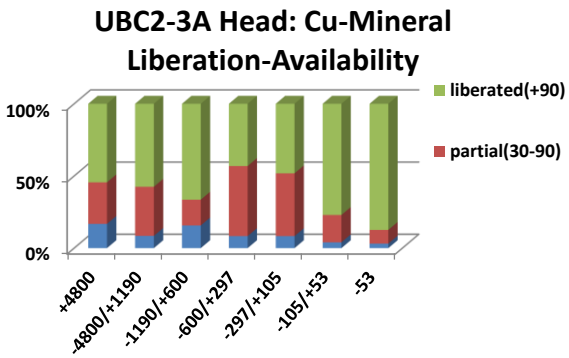
UBC2-3A Head: Cu-Mineral
Liberation-Availability
liberated(+90)
partial(30-90)
100%
50%
0%
+4800
-4800/+1190
-1190/+600
-600/+297
-297/+105
-105/+53
-53

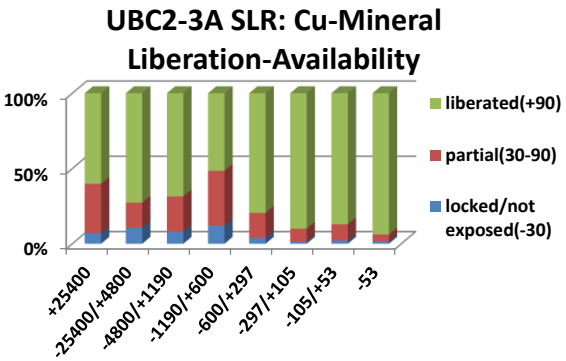
UBC2-3A SLR: Cu-Mineral
Liberation-Availability
liberated(+90)
partial(30-90)
locked/not exposed(-30)
100%
50%
0%
+25400
-25400/+4800
-4800/+1190
-1190/+600
-600/+297
-297/+105
-105/+53
-53

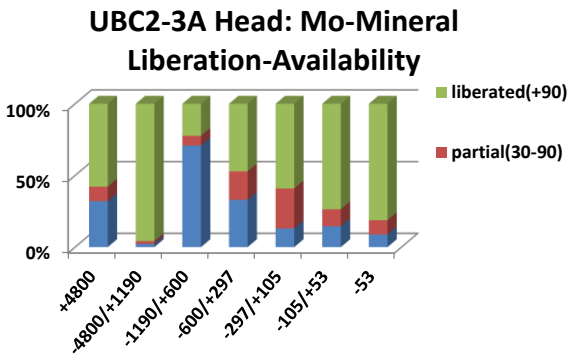
UBC2-3A Head: Mo-Mineral
Liberation-Availability
liberated(+90)
partial(30-90)
100%
50%
0%
+4800
-4800/+1190
-1190/+600
-600/+297
-297/+105
-105/+53
-53

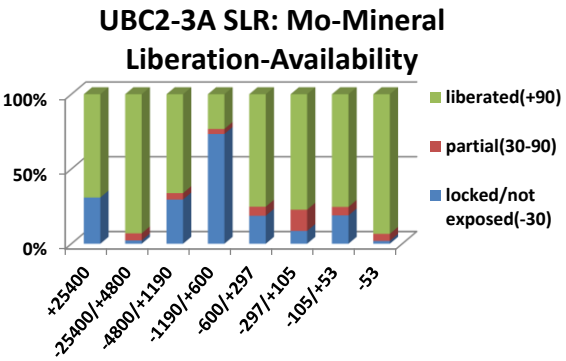
UBC2-3A SLR: Mo-Mineral
Liberation-Availability
liberated(+90)
partial(30-90)
locked/not exposed(-30)
100%
50%
0%
+25400
-25400/+4800
-4800/+1190
-1190/+600
-600/+297
-297/+105
-105/+53
-53

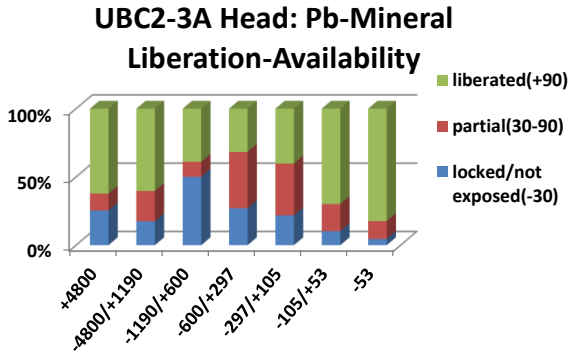
UBC2-3A Head: Pb-Mineral
Liberation-Availability
liberated(+90)
partial(30-90)
locked/not exposed(-30)
100%
50%
0%
+4800
-4800/+1190
-1190/+600
-600/+297
-297/+105
-105/+53
-53

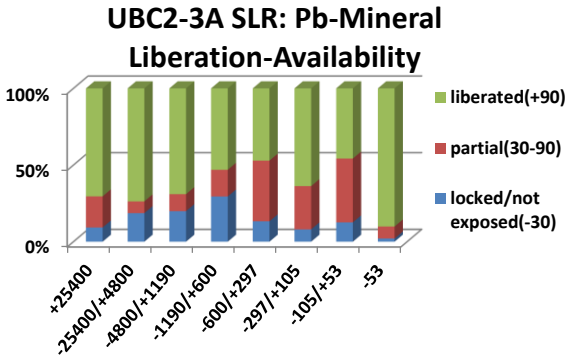
UBC2-3A SLR: Pb-Mineral
Liberation-Availability
liberated(+90)
partial(30-90)
locked/not exposed(-30)
100%
50%
0%
+25400
-25400/+4800
-4800/+1190
-1190/+600
-600/+297
-297/+105
-105/+53
-53

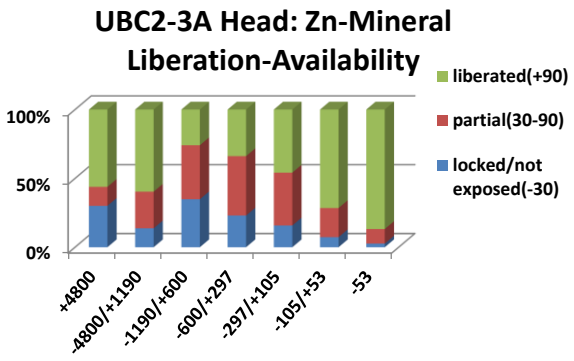
UBC2-3A Head: Zn-Mineral Liberation-Availability
100%
50%
0%
+4800
-4800/+1190
-1190/+600
-600/+297
-297/+105
-105/+53
-53
liberated(+90)
partial(30-90)
locked/not exposed(-30)

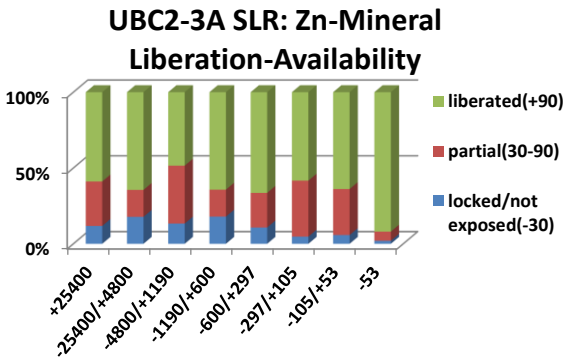
UBC2-3A SLR: Zn-Mineral Liberation-Availability
100%
50%
0%
+25400
-25400/+4800
-4800/+1190
-1190/+600
-600/+297
-297/+105
-105/+53
-53
liberated(+90)
partial(30-90)
locked/not exposed(-30)

APPENDIX 16 Mineral Liberation Analyzer application: modal mineralogy based on metal association

Note: All plots derived from data collected from Table 3.2.1, 3.2.3 and 3.2.4.

Liberated (>90% exposed), Partial (30-90% exposed), Locked (<30% exposed).

Horizontal axis = size fraction (microns); Vertical axis = weight-% (normalized).

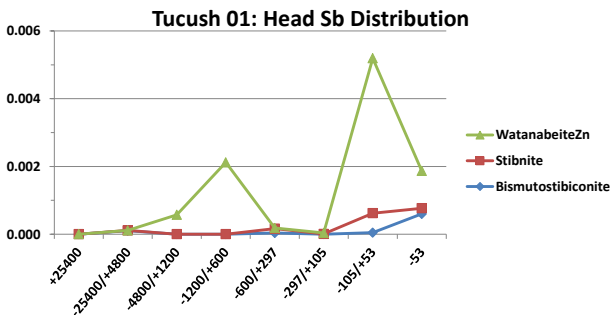

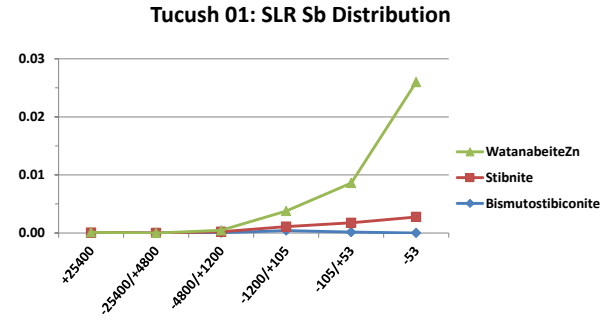

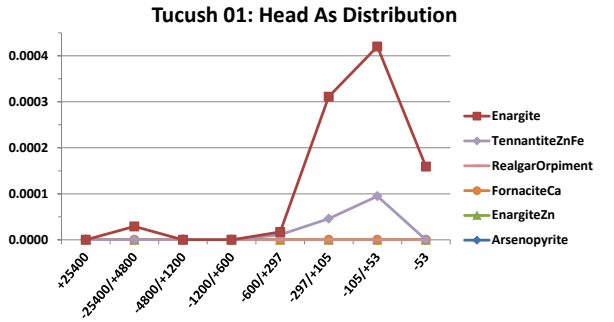

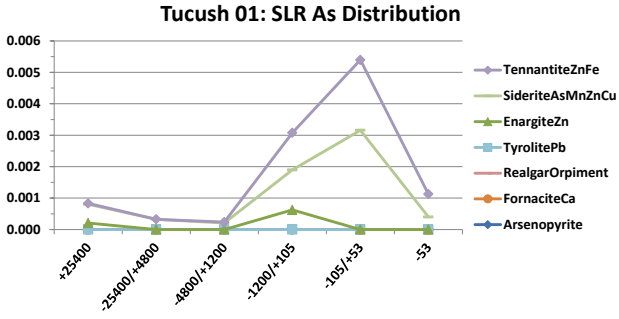

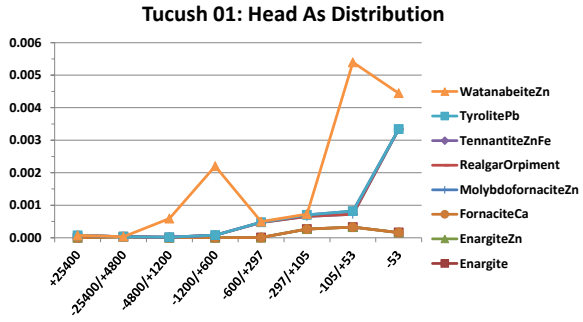

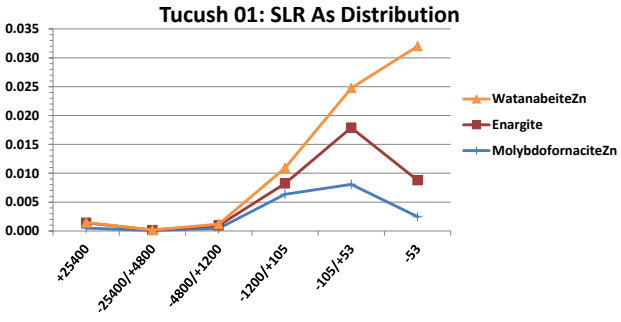

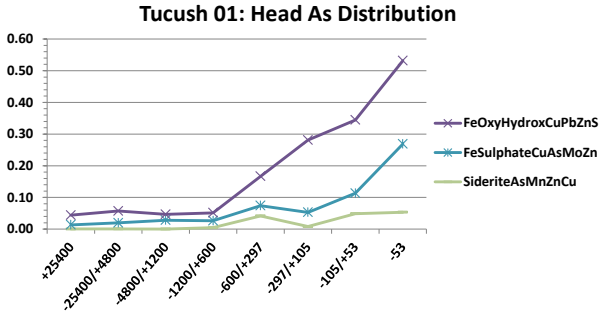

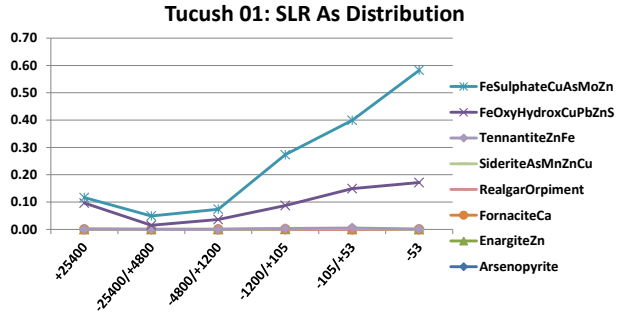

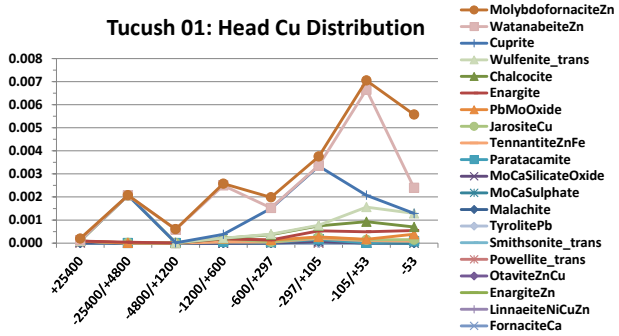
Tucush 01: Head Cu Distribution
0.008
0.007
0.006
0.005
0.004
0.003
0.002
0.001
0.000
+25400
-25400/+4800
-4800/+1200
-1200/+600
-600/+297
-297/+105
-105/+53
-53
MolybdofornaciteZn
WatanabeiteZn
Cuprite
Wulfenite_trans
Chalcocite
Enargite
PbMoOxide
JarositeCu
TennantiteZnFe
Paratacamite
MoCaSilicateOxide
MoCaSulphate
Malachite
TyrolitePb
Smithsonite_trans
Powellite_trans
OtaviteZnCu
EnargiteZn
LinnaeiteNiCuZn
FornaciteCa

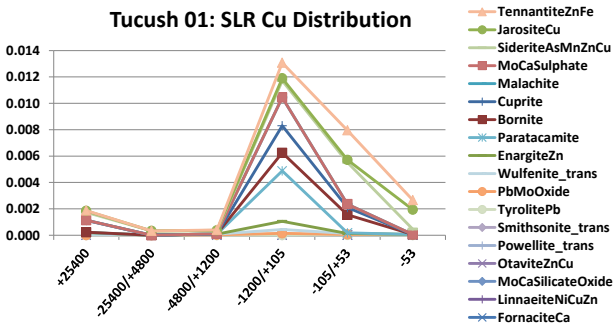
Tucush 01: SLR Cu Distribution
0.014
0.012
0.010
0.008
0.006
0.004
0.002
0.000
+25400
-25400/+4800
-4800/+1200
-1200/+105
-105/+53
-53
TennantiteZnFe
JarositeCu
SideriteAsMnZnCu
MoCaSulphate
Malachite
Cuprite
Bornite
Paratacamite
EnargiteZn
Wulfenite_trans
PbMoOxide
TyrolitePb
Smithsonite_trans
Powellite_trans
OtaviteZnCu
MoCaSilicateOxide
LinnaeiteNiCuZn
FornaciteCa

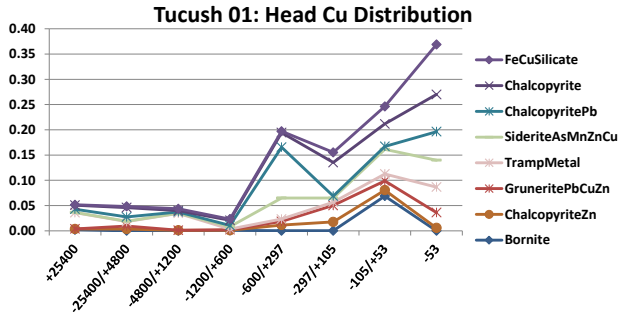
Tucush 01: Head Cu Distribution
0.40
0.35
0.30
0.25
0.20
0.15
0.10
0.05
0.00
+25400
-25400/+4800
-4800/+1200
-1200/+600
-600/+297
-297/+105
-105/+53
-53
FeCuSilicate
Chalcopyrite
ChalcopyritePb
SideriteAsMnZnCu
TrampMetal
GruneritePbCuZn
ChalcopyriteZn
Bornite

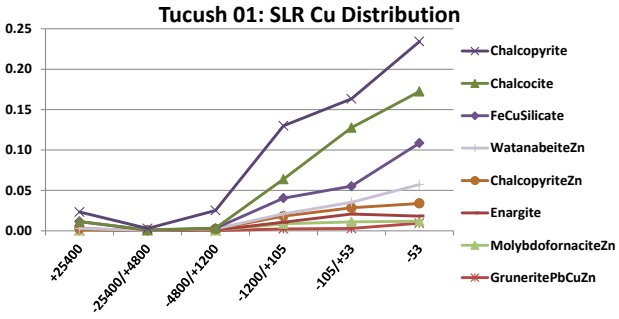
Tucush 01: SLR Cu Distribution
0.25
0.20
0.15
0.10
0.05
0.00
+25400
-25400/+4800
-4800/+1200
-1200/+105
-105/+53
-53
Chalcopyrite
Chalcocite
FeCuSilicate
WatanabeiteZn
ChalcopyriteZn
Enargite
MolybdofornaciteZn
GruneritePbCuZn

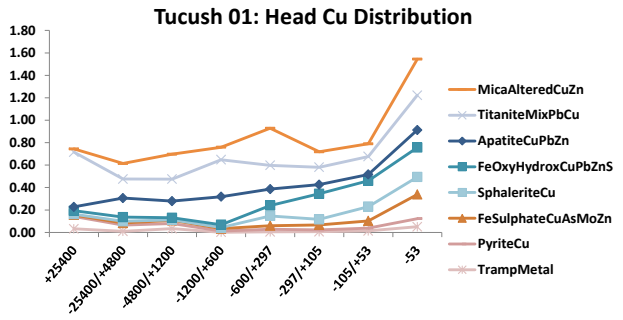
Tucush 01: Head Cu Distribution
1.80
1.60
1.40
1.20
1.00
0.80
0.60
0.40
0.20
0.00
+25400
-25400/+4800
-4800/+1200
-1200/+600
-600/+297
-297/+105
-105/+53
-53
MicaAlteredCuZn
TitaniteMixPbCu
ApatiteCuPbZn
FeOxyHydroxCuPbZnS
SphaleriteCu
FeSulphateCuAsMoZn
PyriteCu
TrampMetal

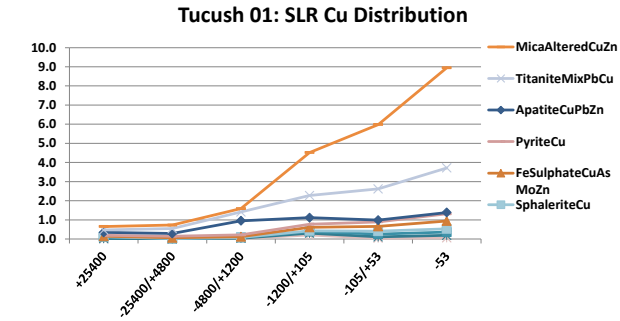
Tucush 01: SLR Cu Distribution
10.0
9.0
8.0
7.0
6.0
5.0
4.0
3.0
2.0
1.0
0.0
+25400
-25400/+4800
-4800/+1200
-1200/+105
-105/+53
-53
MicaAlteredCuZn
TitaniteMixPbCu
ApatiteCuPbZn
PyriteCu
FeSulphateCuAsMoZn
SphaleriteCu

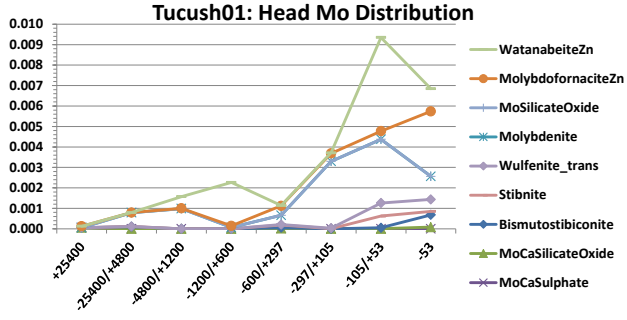
Tucush01: Head Mo Distribution
0.010
0.009
0.008
0.007
0.006
0.005
0.004
0.003
0.002
0.001
0.000
+25400
-25400/+4800
-4800/+1200
-1200/+600
-600/+297
-297/+105
-105/+53
-53
WatanabeiteZn
MolybdofornaciteZn
MoSilicateOxide
Molybdenite
Wulfenite_trans
Stibnite
Bismutostibiconite
MoCaSilicateOxide
MoCaSulphate

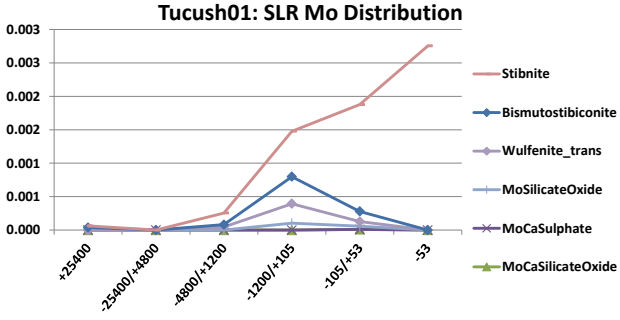
Tucush01: SLR Mo Distribution
0.003
0.003
0.002
0.002
0.001
0.001
0.000
+25400
-25400/+4800
-4800/+1200
-1200/+105
-105/+53
-53
Stibnite
Bismutostibiconite
Wulfenite_trans
MoSilicateOxide
MoCaSulphate
MoCaSilicateOxide

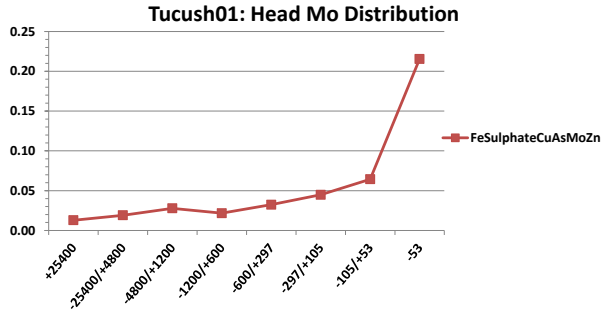
Tucush01: Head Mo Distribution
0.25
0.20
0.15
0.10
0.05
0.00
+25400
-25400/+4800
-4800/+1200
-1200/+600
-600/+297
-297/+105
-105/+53
-53
FeSulphateCuAsMoZn

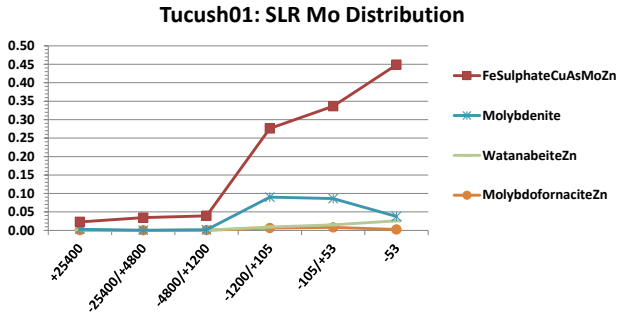
Tucush01: SLR Mo Distribution
0.50
0.45
0.40
0.35
0.30
0.25
0.20
0.15
0.10
0.05
0.00
+25400
-25400/+4800
-4800/+1200
-1200/+105
-105/+53
-53
FeSulphateCuAsMoZn
Molybdenite
WatanabeiteZn
MolybdofornaciteZn

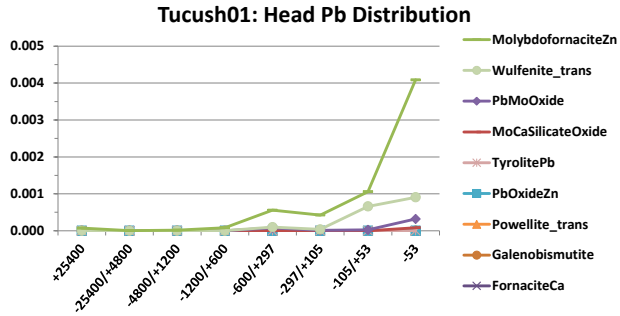
Tucush01: Head Pb Distribution
0.005
0.004
0.003
0.002
0.001
0.000
+25400
-25400/+4800
-4800/+1200
-1200/+600
-600/+297
-297/+105
-105/+53
-53
MolybdofornaciteZn
Wulfenite_trans
PbMoOxide
MoCaSilicateOxide
TyrolitePb
PbOxideZn
Powellite_trans
Galenobismutite
FornaciteCa

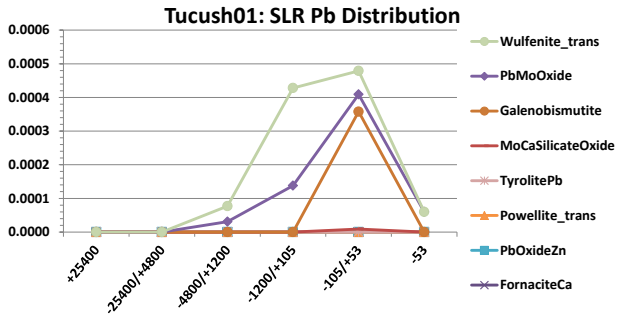
Tucush01: SLR Pb Distribution
0.0006
0.0005
0.0004
0.0003
0.0002
0.0001
0.0000
+25400
-25400/+4800
-4800/+1200
-1200/+105
-105/+53
-53
Wulfenite_trans
PbMoOxide
Galenobismutite
MoCaSilicateOxide
TyrolitePb
Powellite_trans
PbOxideZn
FornaciteCa

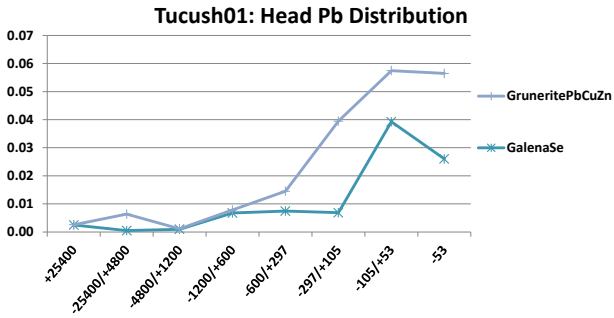
Tucush01: Head Pb Distribution
0.07
0.06
0.05
0.04
0.03
0.02
0.01
0.00
+25400
-25400/+4800
-4800/+1200
-1200/+600
-600/+297
-297/+105
-105/+53
-53
GruneritePbCuZn
GalenaSe

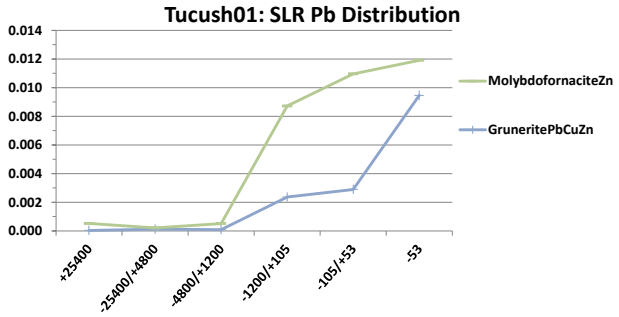
Tucush01: SLR Pb Distribution
0.014
0.012
0.010
0.008
0.006
0.004
0.002
0.000
+25400
-25400/+4800
-4800/+1200
-1200/+105
-105/+53
-53
MolybdofornaciteZn
GruneritePbCuZn

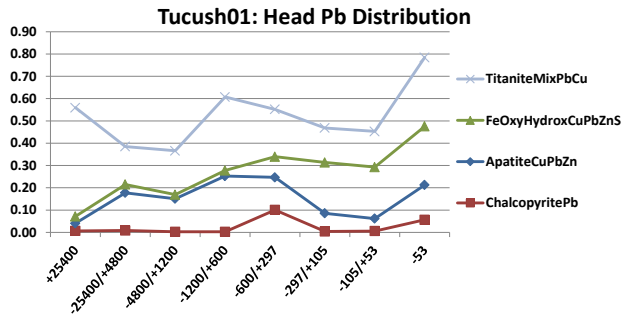
Tucush01: Head Pb Distribution
0.90
0.80
0.70
0.60
0.50
0.40
0.30
0.20
0.10
0.00
+25400
-25400/+4800
-4800/+1200
-1200/+600
-600/+297
-297/+105
-105/+53
-53
TitaniteMixPbCu
FeOxyHydroxCuPbZnS
ApatiteCuPbZn
ChalcopyritePb

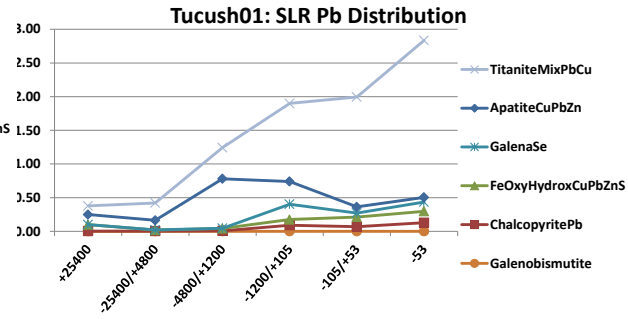
Tucush01: SLR Pb Distribution
3.00
2.50
2.00
1.50
1.00
0.50
0.00
+25400
-25400/+4800
-4800/+1200
-1200/+105
-105/+53
-53
TitaniteMixPbCu
ApatiteCuPbZn
GalenaSe
FeOxyHydroxCuPbZnS
ChalcopyritePb
Galenobismutite

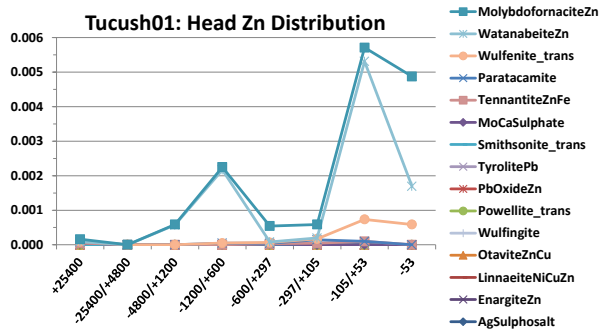
Tucush01: Head Zn Distribution
0.006
0.005
0.004
0.003
0.002
0.001
0.000
+25400
-25400/+4800
-4800/+1200
-1200/+600
-600/+297
-297/+105
-105/+53
-53
MolybdofornaciteZn
WatanabeiteZn
Wulfenite_trans
Paratacamite
TennantiteZnFe
MoCaSulphate
Smithsonite_trans
TyrolitePb
PbOxideZn
Powellite_trans
Wulfingite
OtaviteZnCu
LinnaeiteNiCuZn
EnargiteZn
AgSulphosalt

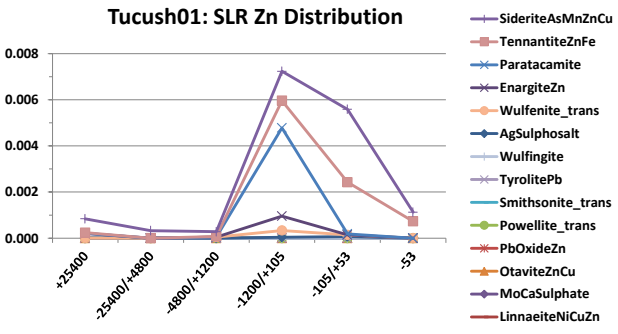
Tucush01: SLR Zn Distribution
0.008
0.006
0.004
0.002
0.000
+25400
-25400/+4800
-4800/+1200
-1200/+105
-105/+53
-53
SideriteAsMnZnCu
TennantiteZnFe
Paratacamite
EnargiteZn
Wulfenite_trans
AgSulphosalt
Wulfingite
TyrolitePb
Smithsonite_trans
Powellite_trans
PbOxideZn
OtaviteZnCu
MoCaSulphate
LinnaeiteNiCuZn

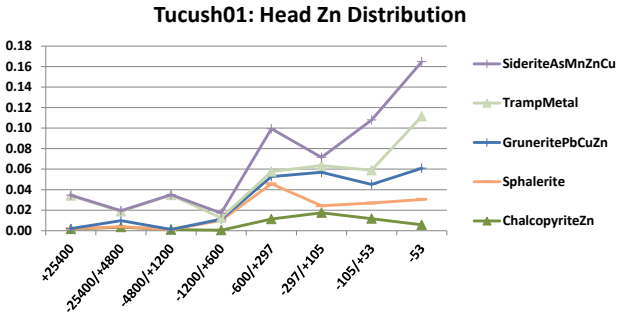
Tucush01: Head Zn Distribution
0.18
0.16
0.14
0.12
0.10
0.08
0.06
0.04
0.02
0.00
+25400
-25400/+4800
-4800/+1200
-1200/+600
-600/+297
-297/+105
-105/+53
-53
SideriteAsMnZnCu
TrampMetal
GruneritePbCuZn
Sphalerite
ChalcopyriteZn

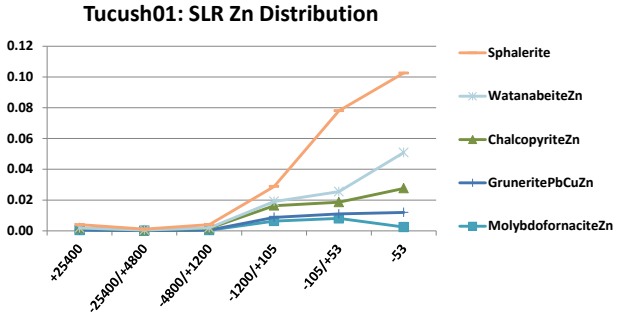
Tucush01: SLR Zn Distribution
0.12
0.10
0.08
0.06
0.04
0.02
0.00
+25400
-25400/+4800
-4800/+1200
-1200/+105
-105/+53
-53
Sphalerite
WatanabeiteZn
ChalcopyriteZn
GruneritePbCuZn
MolybdofornaciteZn

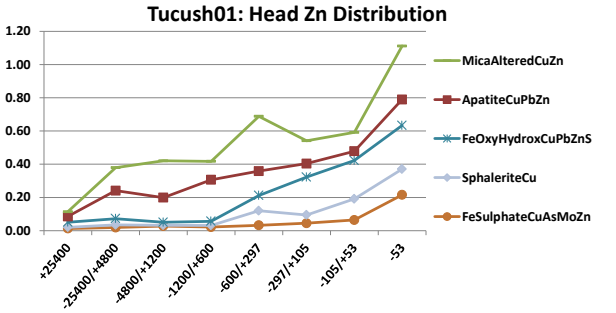
Tucush01: Head Zn Distribution
1.20
1.00
0.80
0.60
0.40
0.20
0.00
+25400
-25400/+4800
-4800/+1200
-1200/+600
-600/+297
-297/+105
-105/+53
-53
MicaAlteredCuZn
ApatiteCuPbZn
FeOxyHydroxCuPbZnS
SphaleriteCu
FeSulphateCuAsMoZn

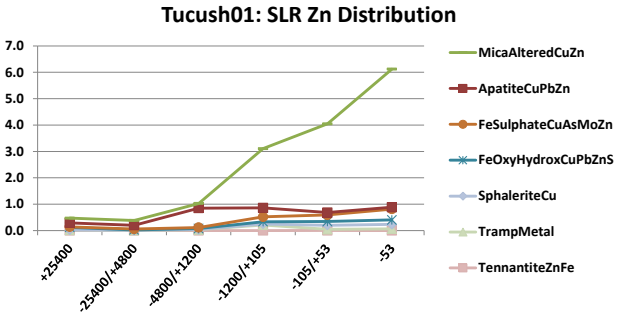
Tucush01: SLR Zn Distribution
7.0
6.0
5.0
4.0
3.0
2.0
1.0
0.0
+25400
-25400/+4800
-4800/+1200
-1200/+105
-105/+53
-53
MicaAlteredCuZn
ApatiteCuPbZn
FeSulphateCuAsMoZn
FeOxyHydroxCuPbZnS
SphaleriteCu
TrampMetal
TennantiteZnFe

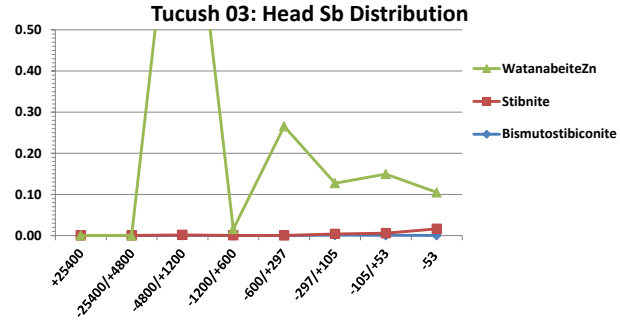
Tucush 03: Head Sb Distribution
0.50
0.40
0.30
0.20
0.10
0.00
+25400
-25400/+4800
-4800/+1200
-1200/+600
-600/+297
-297/+105
-105/+53
-53
WatanabeiteZn
Stibnite
Bismutostibiconite

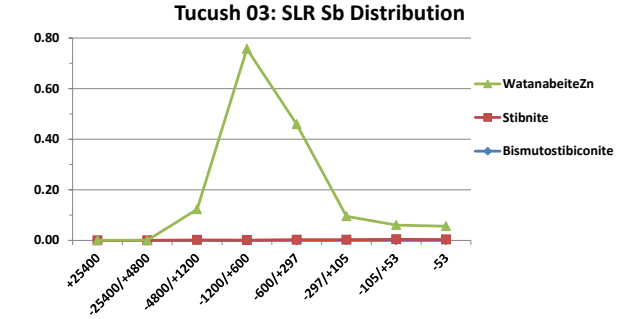
Tucush 03: SLR Sb Distribution
0.80
0.60
0.40
0.20
0.00
+25400
-25400/+4800
-4800/+1200
-1200/+600
-600/+297
-297/+105
-105/+53
-53
WatanabeiteZn
Stibnite
Bismutostibiconite

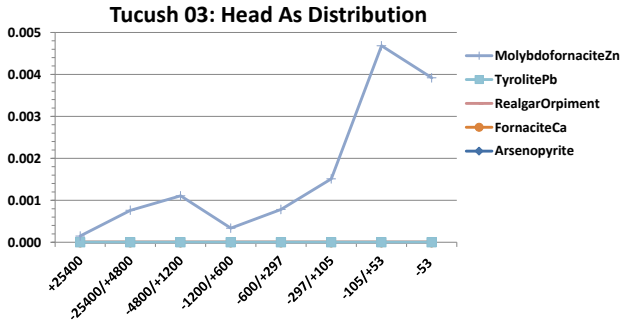
Tucush 03: Head As Distribution
0.005
0.004
0.003
0.002
0.001
0.000
+25400
-25400/+4800
-4800/+1200
-1200/+600
-600/+297
-297/+105
-105/+53
-53
MolybdofornaciteZn
TyrolitePb
RealgarOrpiment
FornaciteCa
Arsenopyrite

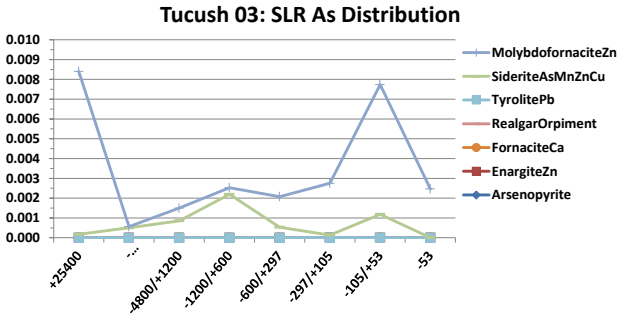
Tucush 03: SLR As Distribution
0.010
0.009
0.008
0.007
0.006
0.005
0.004
0.003
0.002
0.001
0.000
+25400
-4800/+1200
-1200/+600
-600/+297
-297/+105
-105/+53
-53
MolybdofornaciteZn
SideriteAsMnZnCu
TyrolitePb
RealgarOrpiment
FornaciteCa
EnargiteZn
Arsenopyrite

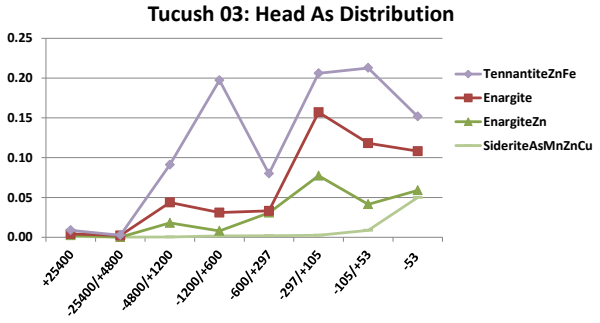
Tucush 03: Head As Distribution
0.25
0.20
0.15
0.10
0.05
0.00
+25400
-25400/+4800
-4800/+1200
-1200/+600
-600/+297
-297/+105
-105/+53
-53
TennantiteZnFe
Enargite
EnargiteZn
SideriteAsMnZnCu

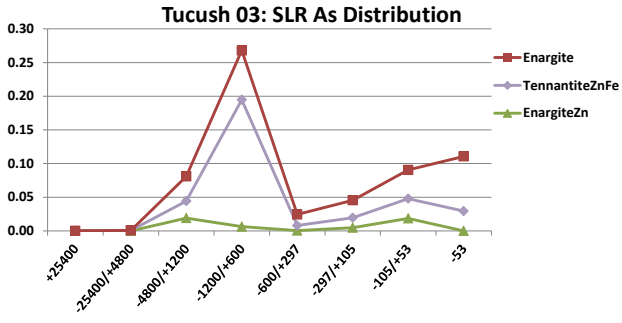
Tucush 03: SLR As Distribution
0.30
0.25
0.20
0.15
0.10
0.05
0.00
+25400
-25400/+4800
-4800/+1200
-1200/+600
-600/+297
-297/+105
-105/+53
-53
Enargite
TennantiteZnFe
EnargiteZn

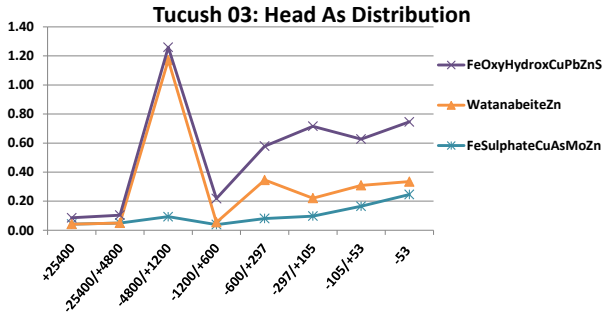
Tucush 03: Head As Distribution
1.40
1.20
1.00
0.80
0.60
0.40
0.20
0.00
+25400
-25400/+4800
-4800/+1200
-1200/+600
-600/+297
-297/+105
-105/+53
-53
FeOxyHydroxCuPbZnS
WatanabeiteZn
FeSulphateCuAsMoZn

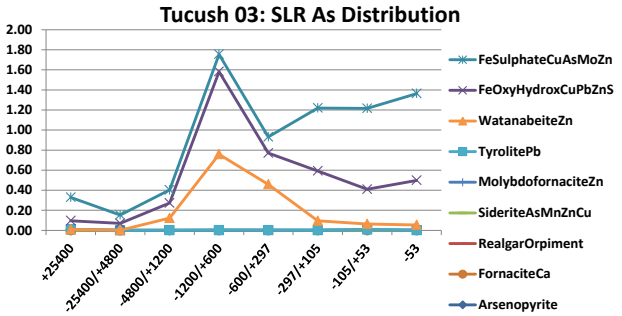
Tucush 03: SLR As Distribution
2.00
1.80
1.60
1.40
1.20
1.00
0.80
0.60
0.40
0.20
0.00
+25400
-25400/+4800
-4800/+1200
-1200/+600
-600/+297
-297/+105
-105/+53
-53
FeSulphateCuAsMoZn
FeOxyHydroxCuPbZnS
WatanabeiteZn
TyrolitePb
MolybdofornaciteZn
SideriteAsMnZnCu
RealgarOrpiment
FornaciteCa
Arsenopyrite

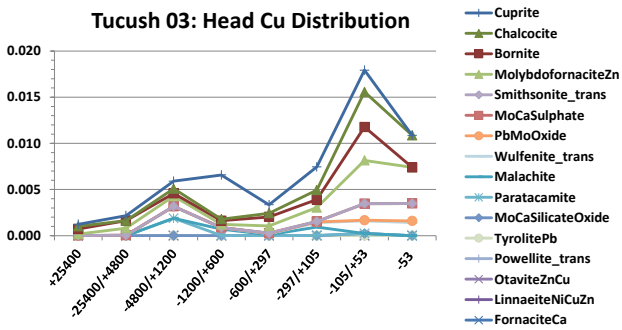
Tucush 03: Head Cu Distribution
0.020
0.015
0.010
0.005
0.000
+25400
-25400/+4800
-4800/+1200
-1200/+600
-600/+297
-297/+105
-105/+53
-53
Cuprite
Chalcocite
Bornite
MolybdofornaciteZn
Smithsonite_trans
MoCaSulphate
PbMoOxide
Wulfenite_trans
Malachite
Paratacamite
MoCaSilicateOxide
TyrolitePb
Powellite_trans
OtaviteZnCu
LinnaeiteNiCuZn
FornaciteCa

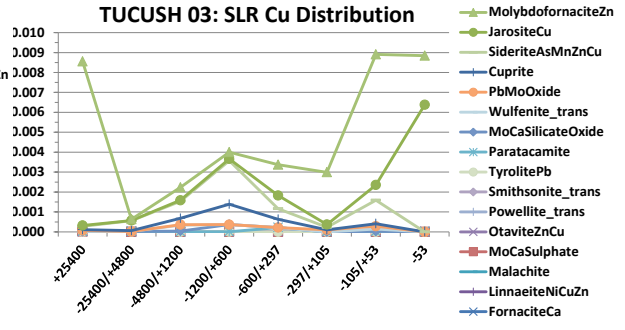
TUCUSH 03: SLR Cu Distribution
0.010
0.009
0.008
0.007
0.006
0.005
0.004
0.003
0.002
0.001
0.000
+25400
-25400/+4800
-4800/+1200
-1200/+600
-600/+297
-297/+105
-105/+53
-53
MolybdofornaciteZn
JarositeCu
SideriteAsMnZnCu
Cuprite
PbMoOxide
Wulfenite_trans
MoCaSilicateOxide
Paratacamite
TyrolitePb
Smithsonite_trans
Powellite_trans
OtaviteZnCu
MoCaSulphate
Malachite
LinnaeiteNiCuZn
FornaciteCa

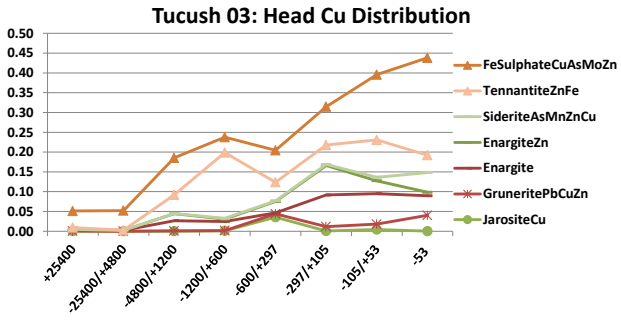
Tucush 03: Head Cu Distribution
0.50
0.45
0.40
0.35
0.30
0.25
0.20
0.15
0.10
0.05
0.00
+25400
-25400/+4800
-4800/+1200
-1200/+600
-600/+297
-297/+105
-105/+53
-53
FeSulphateCuAsMoZn
TennantiteZnFe
SideriteAsMnZnCu
EnargiteZn
Enargite
GruneritePbCuZn
JarositeCu

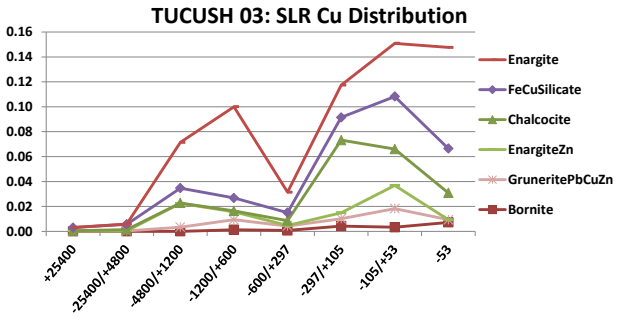
TUCUSH 03: SLR Cu Distribution
0.16
0.14
0.12
0.10
0.08
0.06
0.04
0.02
0.00
+25400
-25400/+4800
-4800/+1200
-1200/+600
-600/+297
-297/+105
-105/+53
-53
Enargite
FeCuSilicate
Chalcocite
EnargiteZn
GruneritePbCuZn
Bornite

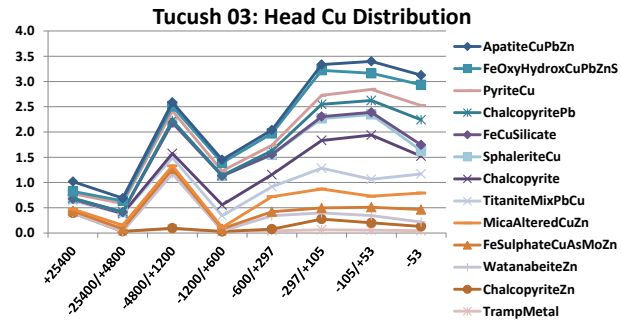
Tucush 03: Head Cu Distribution
4.0
3.5
3.0
2.5
2.0
1.5
1.0
0.5
0.0
+25400
-25400/+4800
-4800/+1200
-1200/+600
-600/+297
-297/+105
-105/+53
-53
ApatiteCuPbZn
FeOxyHydroxCuPbZnS
PyriteCu
ChalcopyritePb
FeCuSilicate
SphaleriteCu
Chalcopyrite
TitaniteMixPbCu
MicaAlteredCuZn
FeSulphateCuAsMoZn
WatanabeiteZn
ChalcopyriteZn
TrampMetal

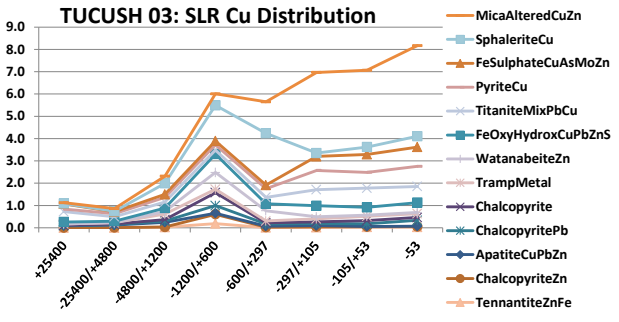
TUCUSH 03: SLR Cu Distribution
9.0
8.0
7.0
6.0
5.0
4.0
3.0
2.0
1.0
0.0
+25400
-25400/+4800
-4800/+1200
-1200/+600
-600/+297
-297/+105
-105/+53
-53
MicaAlteredCuZn
SphaleriteCu
FeSulphateCuAsMoZn
PyriteCu
TitaniteMixPbCu
FeOxyHydroxCuPbZnS
WatanabeiteZn
TrampMetal
Chalcopyrite
ChalcopyritePb
ApatiteCuPbZn
ChalcopyriteZn
TennantiteZnFe

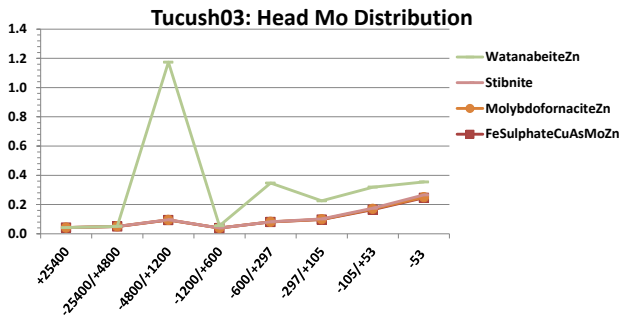
Tucush03: Head Mo Distribution
1.4
1.2
1.0
0.8
0.6
0.4
0.2
0.0
+25400
-25400/+4800
-4800/+1200
-1200/+600
-600/+297
-297/+105
-105/+53
-53
WatanabeiteZn
Stibnite
MolybdofornaciteZn
FeSulphateCuAsMoZn

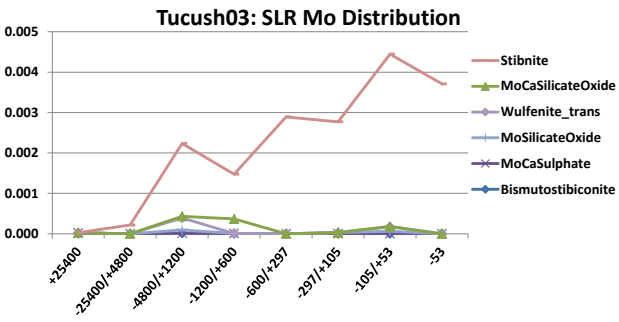
Tucush03: SLR Mo Distribution
0.005
0.004
0.003
0.002
0.001
0.000
+25400
-25400/+4800
-4800/+1200
-1200/+600
-600/+297
-297/+105
-105/+53
-53
Stibnite
MoCaSilicateOxide
Wulfenite_trans
MoSilicateOxide
MoCaSulphate
Bismutostibiconite

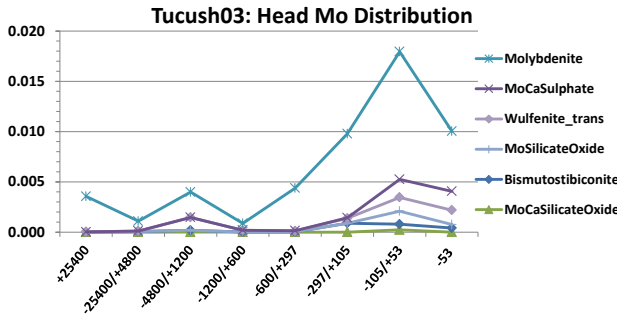
Tucush03: Head Mo Distribution
0.020
0.015
0.010
0.005
0.000
+25400
-25400/+4800
-4800/+1200
-1200/+600
-600/+297
-297/+105
-105/+53
-53
Molybdenite
MoCaSulphate
Wulfenite_trans
MoSilicateOxide
Bismutostibiconite
MoCaSilicateOxide

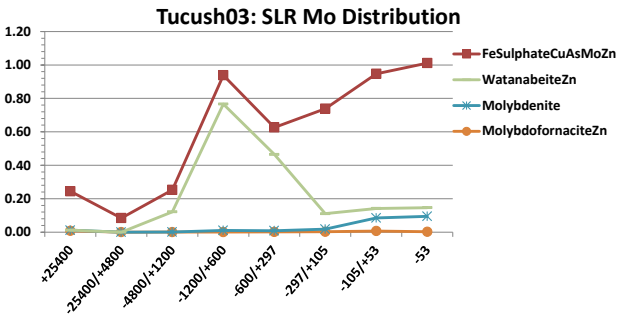
Tucush03: SLR Mo Distribution
1.20
1.00
0.80
0.60
0.40
0.20
0.00
+25400
-25400/+4800
-4800/+1200
-1200/+600
-600/+297
-297/+105
-105/+53
-53
FeSulphateCuAsMoZn
WatanabeiteZn
Molybdenite
MolybdofornaciteZn

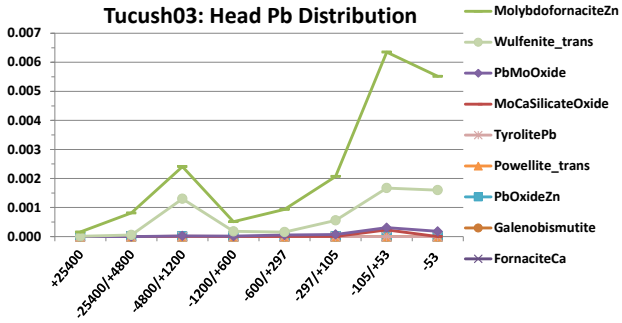
Tucush03: Head Pb Distribution
0.007
0.006
0.005
0.004
0.003
0.002
0.001
0.000
+25400
-25400/+4800
-4800/+1200
-1200/+600
-600/+297
-297/+105
-105/+53
-53
MolybdofornaciteZn
Wulfenite_trans
PbMoOxide
MoCaSilicateOxide
TyrolitePb
Powellite_trans
PbOxideZn
Galenobismutite
FornaciteCa

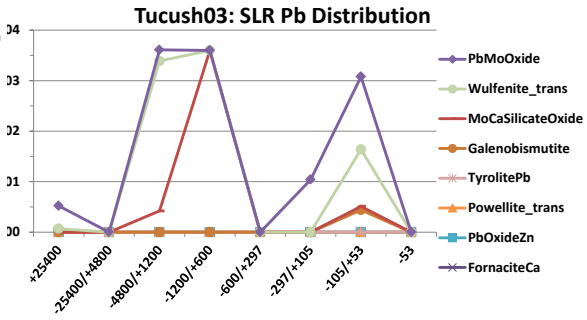
Tucush03: SLR Pb Distribution
PbMoOxide
Wulfenite_trans
MoCaSilicateOxide
Galenobismutite
TyrolitePb
Powellite_trans
PbOxideZn
FornaciteCa

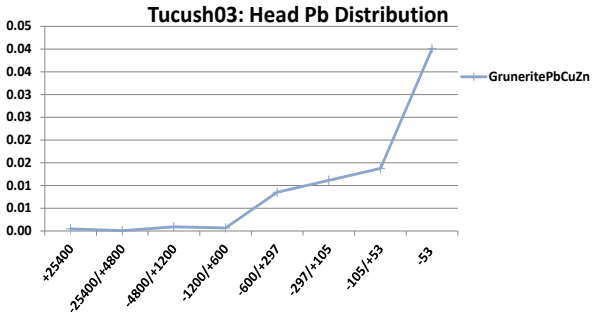
Tucush03: Head Pb Distribution
0.05
0.04
0.04
0.03
0.03
0.02
0.02
0.01
0.01
0.00
+25400
-25400/+4800
-4800/+1200
-1200/+600
-600/+297
-297/+105
-105/+53
-53
GruneritePbCuZn

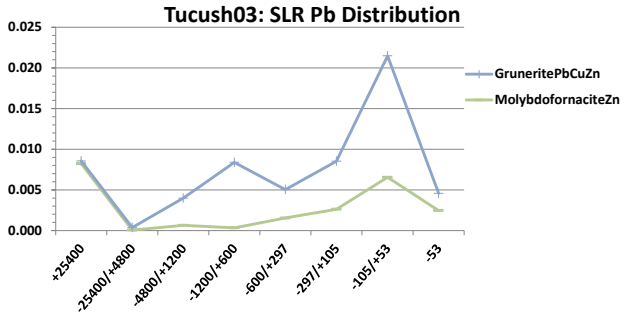
Tucush03: SLR Pb Distribution
0.025
0.020
0.015
0.010
0.005
0.000
+25400
-25400/+4800
-4800/+1200
-1200/+600
-600/+297
-297/+105
-105/+53
-53
GruneritePbCuZn
MolybdofornaciteZn

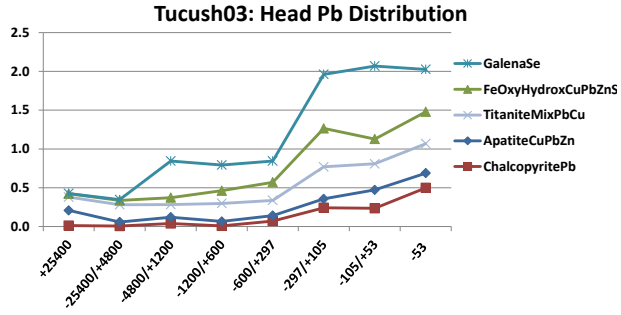
Tucush03: Head Pb Distribution
2.5
2.0
1.5
1.0
0.5
0.0
+25400
-25400/+4800
-4800/+1200
-1200/+600
-600/+297
-297/+105
-105/+53
-53
GalenaSe
FeOxyHydroxCuPbZnS
TitaniteMixPbCu
ApatiteCuPbZn
ChalcopyritePb

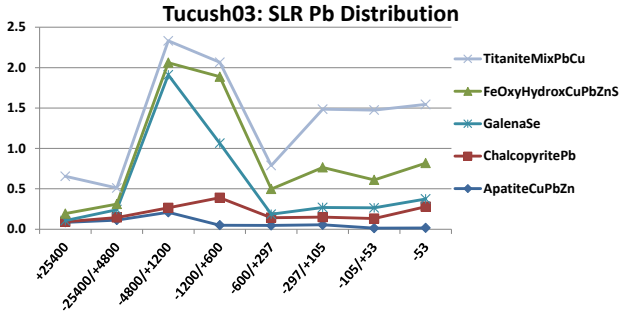
Tucush03: SLR Pb Distribution
2.5
2.0
1.5
1.0
0.5
0.0
+25400
-25400/+4800
-4800/+1200
-1200/+600
-600/+297
-297/+105
-105/+53
-53
TitaniteMixPbCu
FeOxyHydroxCuPbZnS
GalenaSe
ChalcopyritePb
ApatiteCuPbZn

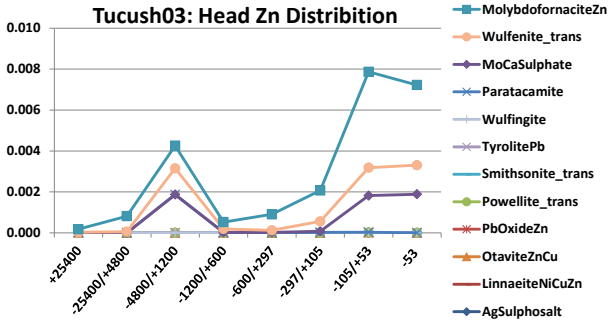
Tucush03: Head Zn Distribition
0.010
0.008
0.006
0.004
0.002
0.000
+25400
-25400/+4800
-4800/+1200
-1200/+600
-600/+297
-297/+105
-105/+53
-53
MolybdofornaciteZn
Wulfenite_trans
MoCaSulphate
Paratacamite
Wulfingite
TyrolitePb
Smithsonite_trans
Powellite_trans
PbOxideZn
OtaviteZnCu
LinnaeiteNiCuZn
AgSulphosalt

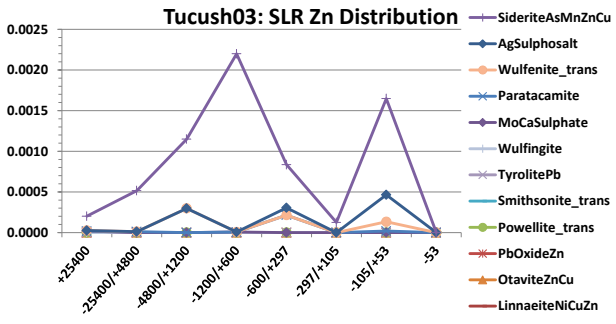
Tucush03: SLR Zn Distribution
0.0025
0.0020
0.0015
0.0010
0.0005
0.0000
+25400
-25400/+4800
-4800/+1200
-1200/+600
-600/+297
-297/+105
-105/+53
-53
SideriteAsMnZnCu
AgSulphosalt
Wulfenite_trans
Paratacamite
MoCaSulphate
Wulfingite
TyrolitePb
Smithsonite_trans
Powellite_trans
PbOxideZn
OtaviteZnCu
LinnaeiteNiCuZn

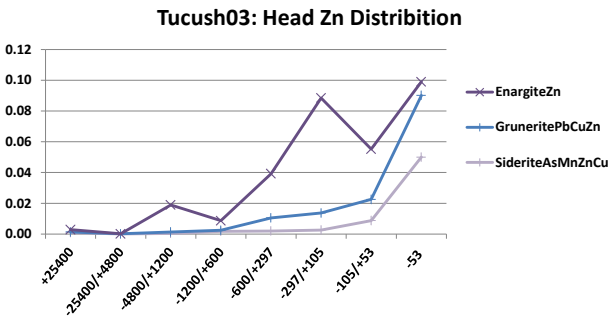
Tucush03: Head Zn Distribition
0.12
0.10
0.08
0.06
0.04
0.02
0.00
+25400
-25400/+4800
-4800/+1200
-1200/+600
-600/+297
-297/+105
-105/+53
-53
EnargiteZn
GruneritePbCuZn
SideriteAsMnZnCu

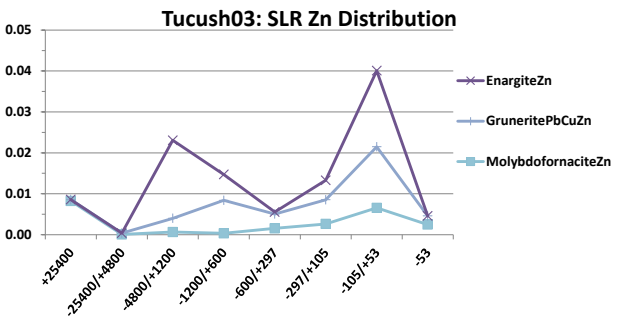
Tucush03: SLR Zn Distribution
0.05
0.04
0.03
0.02
0.01
0.00
+25400
-25400/+4800
-4800/+1200
-1200/+600
-600/+297
-297/+105
-105/+53
-53
EnargiteZn
GruneritePbCuZn
MolybdofornaciteZn

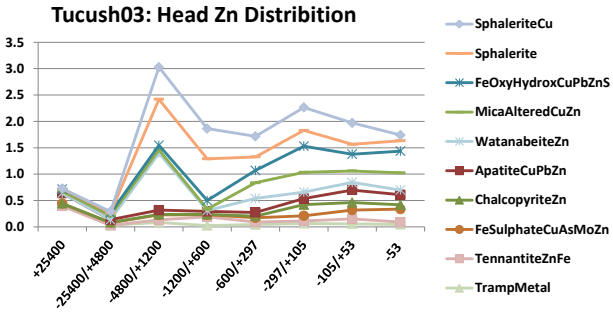
Tucush03: Head Zn Distribition
3.5
3.0
2.5
2.0
1.5
1.0
0.5
0.0
+25400
-25400/+4800
-4800/+1200
-1200/+600
-600/+297
-297/+105
-105/+53
-53
SphaleriteCu
Sphalerite
FeOxyHydroxCuPbZnS
MicaAlteredCuZn
WatanabeiteZn
ApatiteCuPbZn
ChalcopyriteZn
FeSulphateCuAsMoZn
TennantiteZnFe
TrampMetal

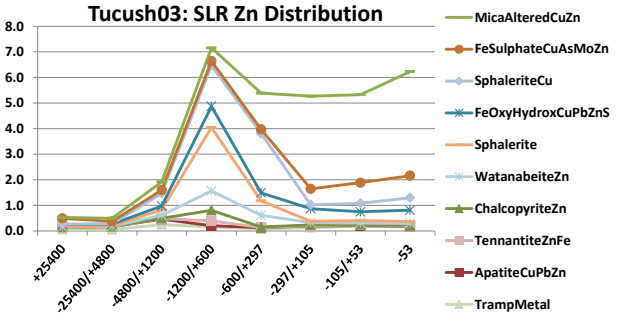
Tucush03: SLR Zn Distribution
8.0
7.0
6.0
5.0
4.0
3.0
2.0
1.0
0.0
+25400
-25400/+4800
-4800/+1200
-1200/+600
-600/+297
-297/+105
-105/+53
-53
MicaAlteredCuZn
FeSulphateCuAsMoZn
SphaleriteCu
FeOxyHydroxCuPbZnS
Sphalerite
WatanabeiteZn
ChalcopyriteZn
TennantiteZnFe
ApatiteCuPbZn
TrampMetal

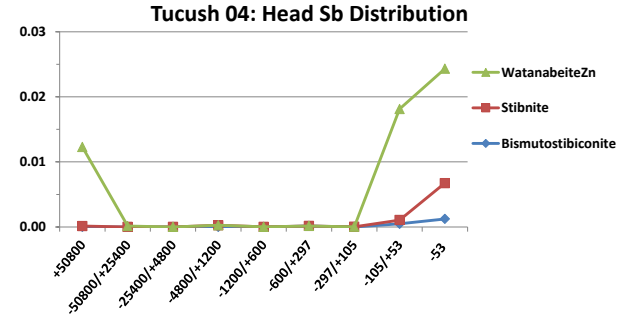
Tucush 04: Head Sb Distribution
0.03
0.02
0.01
0.00
+50800
-50800/+25400
-25400/+4800
-4800/+1200
-1200/+600
-600/+297
-297/+105
-105/+53
-53
WatanabeiteZn
Stibnite
Bismutostibiconite

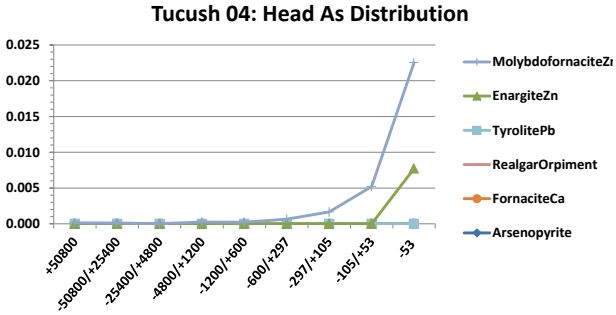
Tucush 04: Head As Distribution
0.025
0.020
0.015
0.010
0.005
0.000
+50800
-50800/+25400
-25400/+4800
-4800/+1200
-1200/+600
-600/+297
-297/+105
-105/+53
-53
MolybdofornaciteZ
EnargiteZn
TyrolitePb
RealgarOrpiment
FornaciteCa
Arsenopyrite

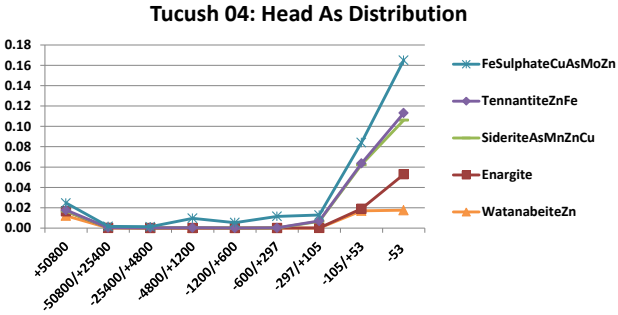
Tucush 04: Head As Distribution
0.18
0.16
0.14
0.12
0.10
0.08
0.06
0.04
0.02
0.00
+50800
-50800/+25400
-25400/+4800
-4800/+1200
-1200/+600
-600/+297
-297/+105
-105/+53
-53
FeSulphateCuAsMoZn
TennantiteZnFe
SideriteAsMnZnCu
Enargite
WatanabeiteZn

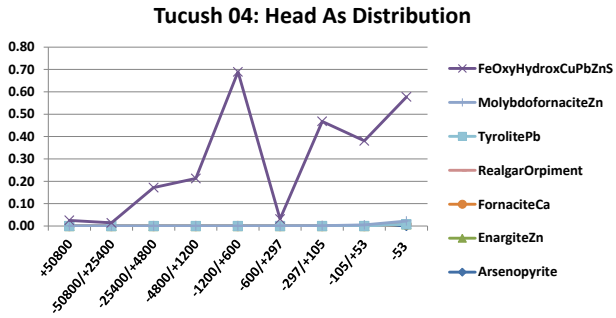
Tucush 04: Head As Distribution
0.80
0.70
0.60
0.50
0.40
0.30
0.20
0.10
0.00
+50800
-50800/+25400
-25400/+4800
-4800/+1200
-1200/+600
-600/+297
-297/+105
-105/+53
-53
FeOxyHydroxCuPbZnS
MolybdofornaciteZn
TyrolitePb
RealgarOrpiment
FornaciteCa
EnargiteZn
Arsenopyrite

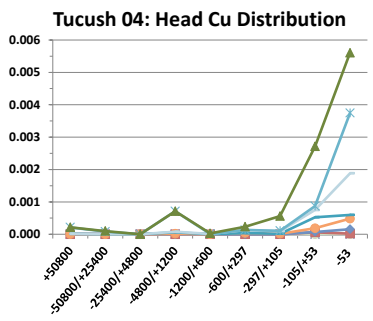
Tucush 04: Head Cu Distribution
0.006
0.005
0.004
0.003
0.002
0.001
0.000
+50800
-50800/+25400
-25400/+4800
-4800/+1200
-1200/+600
-600/+297
-297/+105
-105/+53
-53
Chalcocite
Paratacamite
Wulfenite_trans
Malachite
PbMoOxide
MoCaSilicateOxide
MoCaSulphate
TyrolitePb
Smithsonite_trans
Powellite_trans
OtaviteZnCu
LinnaeiteNiCuZn
FornaciteCa

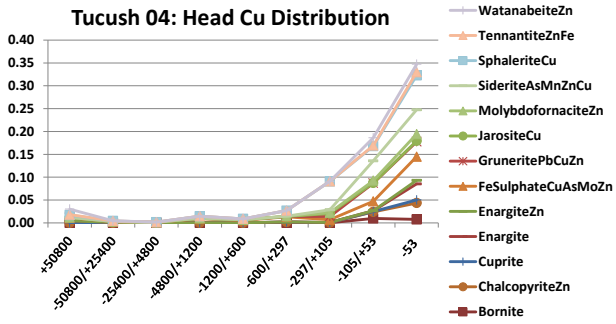
Tucush 04: Head Cu Distribution
0.40
0.35
0.30
0.25
0.20
0.15
0.10
0.05
0.00
+50800
-50800/+25400
-25400/+4800
-4800/+1200
-1200/+600
-600/+297
-297/+105
-105/+53
-53
WatanabeiteZn
TennantiteZnFe
SphaleriteCu
SideriteAsMnZnCu
MolybdofornaciteZn
JarositeCu
GruneritePbCuZn
FeSulphateCuAsMoZn
EnargiteZn
Enargite
Cuprite
ChalcopyriteZn
Bornite

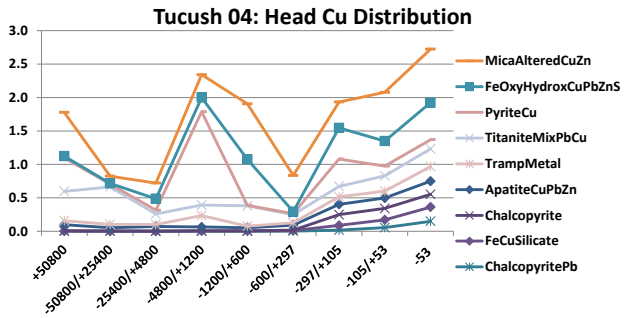
Tucush 04: Head Cu Distribution
3.0
2.5
2.0
1.5
1.0
0.5
0.0
+50800
-50800/+25400
-25400/+4800
-4800/+1200
-1200/+600
-600/+297
-297/+105
-105/+53
-53
MicaAlteredCuZn
FeOxyHydroxCuPbZnS
PyriteCu
TitaniteMixPbCu
TrampMetal
ApatiteCuPbZn
Chalcopyrite
FeCuSilicate
ChalcopyritePb

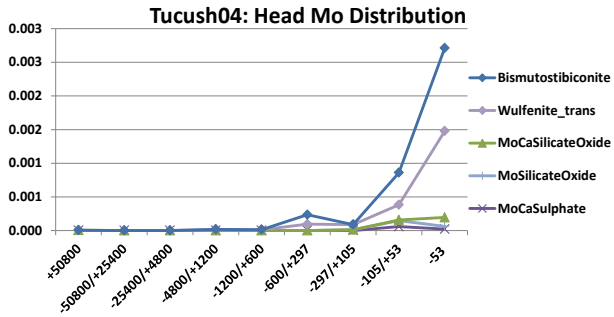
Tucush04: Head Mo Distribution
0.003
0.003
0.002
0.002
0.001
0.001
0.000
+50800
-50800/+25400
-25400/+4800
-4800/+1200
-1200/+600
-600/+297
-297/+105
-105/+53
-53
Bismutostibiconite
Wulfenite_trans
MoCaSilicateOxide
MoSilicateOxide
MoCaSulphate

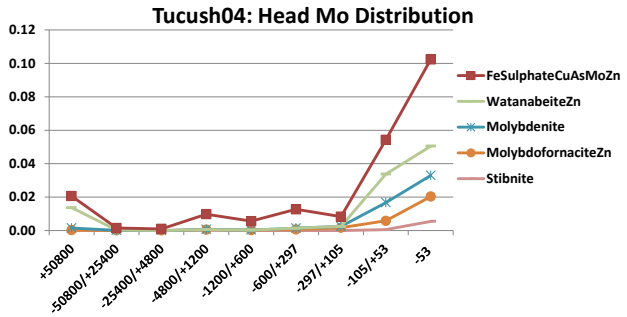
Tucush04: Head Mo Distribution
0.12
0.10
0.08
0.06
0.04
0.02
0.00
+50800
-50800/+25400
-25400/+4800
-4800/+1200
-1200/+600
-600/+297
-297/+105
-105/+53
-53
FeSulphateCuAsMoZn
WatanabeiteZn
Molybdenite
MolybdofornaciteZn
Stibnite

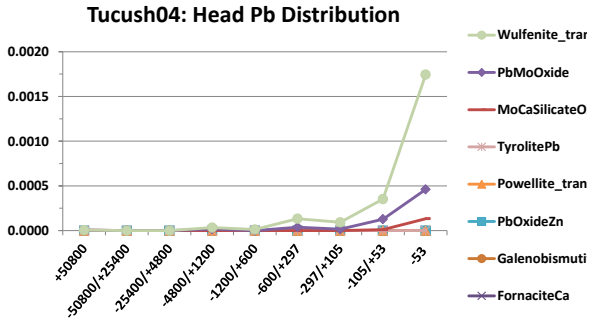
Tucush04: Head Pb Distribution
0.0020
0.0015
0.0010
0.0005
0.0000
+50800
-50800/+25400
-25400/+4800
-4800/+1200
-1200/+600
-600/+297
-297/+105
-105/+53
-53
Wulfenite_trar
PbMoOxide
MoCaSilicateO
TyrolitePb
Powellite_tran
PbOxideZn
Galenobismuti
FornaciteCa

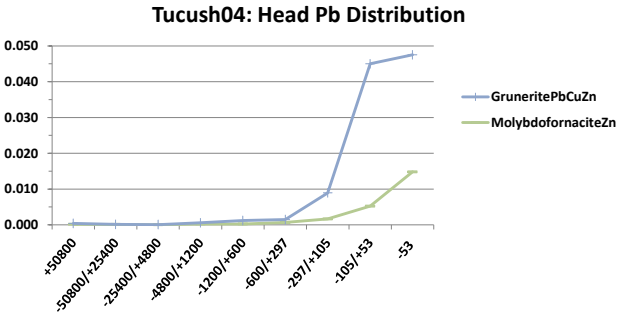
Tucush04: Head Pb Distribution
0.050
0.040
0.030
0.020
0.010
0.000
+50800
-50800/+25400
-25400/+4800
-4800/+1200
-1200/+600
-600/+297
-297/+105
-105/+53
-53
GruneritePbCuZn
MolybdofornaciteZn

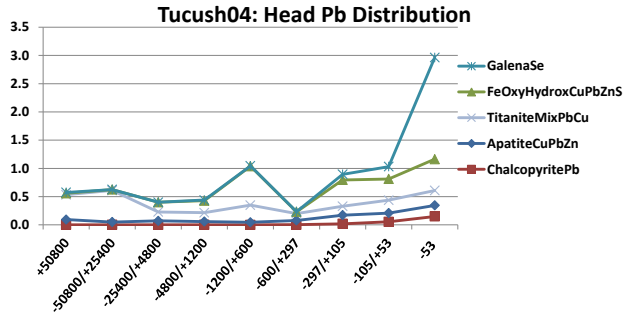
Tucush04: Head Pb Distribution
3.5
3.0
2.5
2.0
1.5
1.0
0.5
0.0
+50800
-50800/+25400
-25400/+4800
-4800/+1200
-1200/+600
-600/+297
-297/+105
-105/+53
-53
GalenaSe
FeOxyHydroxCuPbZnS
TitaniteMixPbCu
ApatiteCuPbZn
ChalcopyritePb

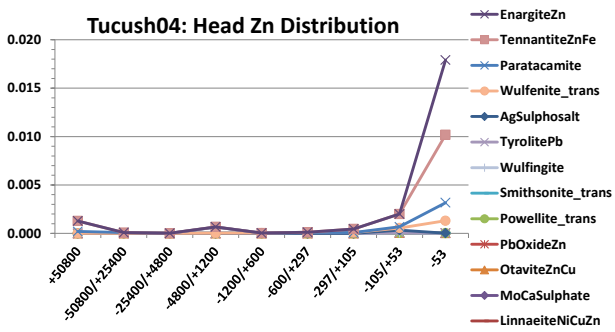
Tucush04: Head Zn Distribution
0.020
0.015
0.010
0.005
0.000
+50800
-50800/+25400
-25400/+4800
-4800/+1200
-1200/+600
-600/+297
-297/+105
-105/+53
-53
EnargiteZn
TennantiteZnFe
Paratacamite
Wulfenite_trans
AgSulphosalt
TyrolitePb
Wulfingite
Smithsonite_trans
Powellite_trans
PbOxideZn
OtaviteZnCu
MoCaSulphate
LinnaeiteNiCuZn

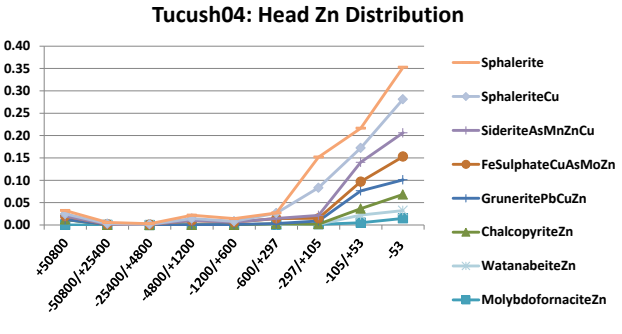
Tucush04: Head Zn Distribution
0.40
0.35
0.30
0.25
0.20
0.15
0.10
0.05
0.00
+50800
-50800/+25400
-25400/+4800
-4800/+1200
-1200/+600
-600/+297
-297/+105
-105/+53
-53
Sphalerite
SphaleriteCu
SideriteAsMnZnCu
FeSulphateCuAsMoZn
GruneritePbCuZn
ChalcopyriteZn
WatanabeiteZn
MolybdofornaciteZn

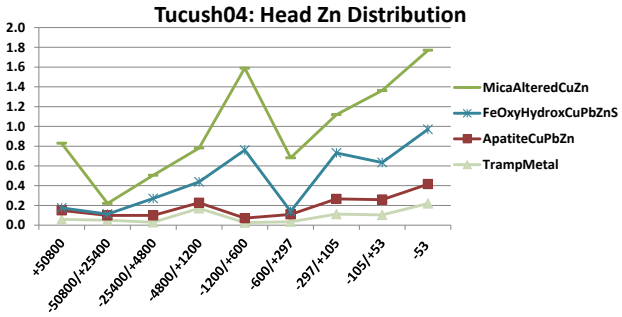
Tucush04: Head Zn Distribution
2.0
1.8
1.6
1.4
1.2
1.0
0.8
0.6
0.4
0.2
0.0
+50800
-50800/+25400
-25400/+4800
-4800/+1200
-1200/+600
-600/+297
-297/+105
-105/+53
-53
MicaAlteredCuZn
FeOxyHydroxCuPbZnS
ApatiteCuPbZn
TrampMetal

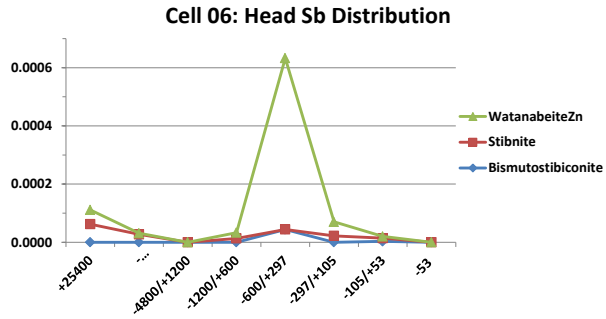
Cell 06: Head Sb Distribution
0.0006
0.0004
0.0002
0.0000
+25400
-4800/+1200
-1200/+600
-600/+297
-297/+105
-105/+53
-53
WatanabeiteZn
Stibnite
Bismutostibiconite

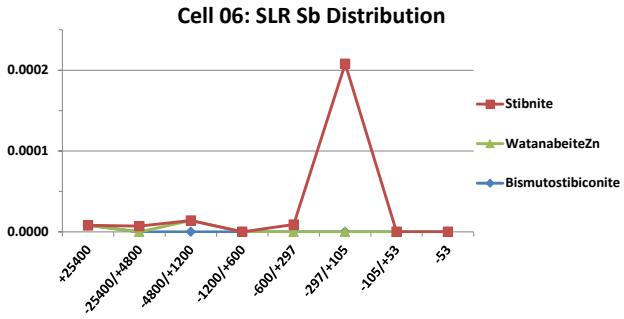
Cell 06: SLR Sb Distribution
0.0002
0.0001
0.0000
+25400
-25400/+4800
-4800/+1200
-1200/+600
-600/+297
-297/+105
-105/+53
-53
Stibnite
WatanabeiteZn
Bismutostibiconite

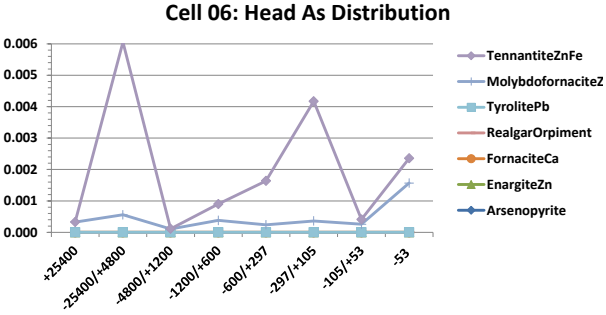
Cell 06: Head As Distribution
0.006
0.005
0.004
0.003
0.002
0.001
0.000
+25400
-25400/+4800
-4800/+1200
-1200/+600
-600/+297
-297/+105
-105/+53
-53
TennantiteZnFe
MolybdofornaciteZ
TyrolitePb
RealgarOrpiment
FornaciteCa
EnargiteZn
Arsenopyrite

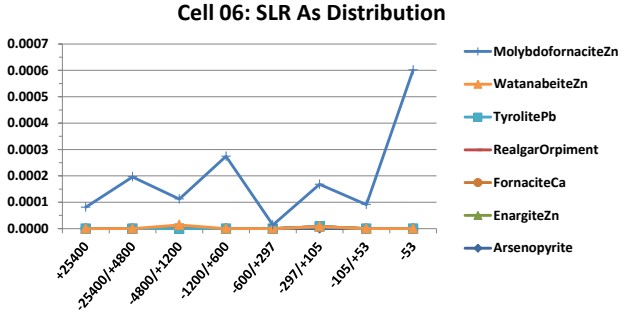
Cell 06: SLR As Distribution
0.0007
0.0006
0.0005
0.0004
0.0003
0.0002
0.0001
0.0000
+25400
-25400/+4800
-4800/+1200
-1200/+600
-600/+297
-297/+105
-105/+53
-53
MolybdofornaciteZn
WatanabeiteZn
TyrolitePb
RealgarOrpiment
FornaciteCa
EnargiteZn
Arsenopyrite

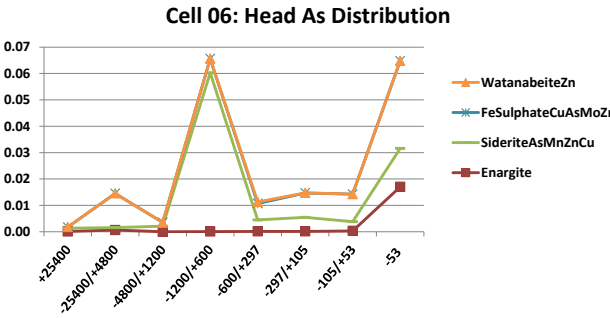
Cell 06: Head As Distribution
0.07
0.06
0.05
0.04
0.03
0.02
0.01
0.00
+25400
-25400/+4800
-4800/+1200
-1200/+600
-600/+297
-297/+105
-105/+53
-53
WatanabeiteZn
FeSulphateCuAsMoZ
SideriteAsMnZnCu
Enargite

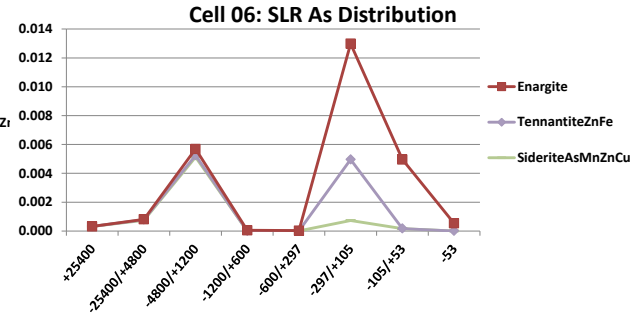
Cell 06: SLR As Distribution
0.014
0.012
0.010
0.008
0.006
0.004
0.002
0.000
+25400
-25400/+4800
-4800/+1200
-1200/+600
-600/+297
-297/+105
-105/+53
-53
Enargite
TennantiteZnFe
SideriteAsMnZnCu

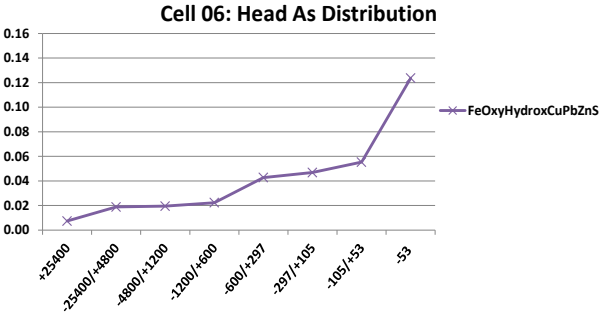
Cell 06: Head As Distribution
0.16
0.14
0.12
0.10
0.08
0.06
0.04
0.02
0.00
+25400
-25400/+4800
-4800/+1200
-1200/+600
-600/+297
-297/+105
-105/+53
-53
FeOxyHydroxCuPbZnS

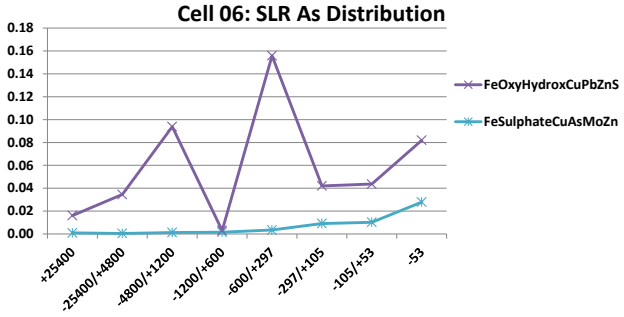
Cell 06: SLR As Distribution
0.18
0.16
0.14
0.12
0.10
0.08
0.06
0.04
0.02
0.00
+25400
-25400/+4800
-4800/+1200
-1200/+600
-600/+297
-297/+105
-105/+53
-53
FeOxyHydroxCuPbZnS
FeSulphateCuAsMoZn

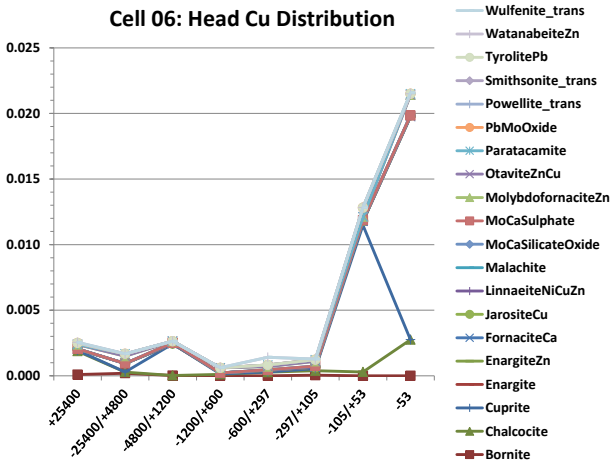
Cell 06: Head Cu Distribution
0.025
0.020
0.015
0.010
0.005
0.000
+25400
-25400/+4800
-4800/+1200
-1200/+600
-600/+297
-297/+105
-105/+53
-53
Wulfenite_trans
WatanabeiteZn
TyrolitePb
Smithsonite_trans
Powellite_trans
PbMoOxide
Paratacamite
OtaviteZnCu
MolybdofornaciteZn
MoCaSulphate
MoCaSilicateOxide
Malachite
LinnaeiteNiCuZn
JarositeCu
FornaciteCa
EnargiteZn
Enargite
Cuprite
Chalcocite
Bornite

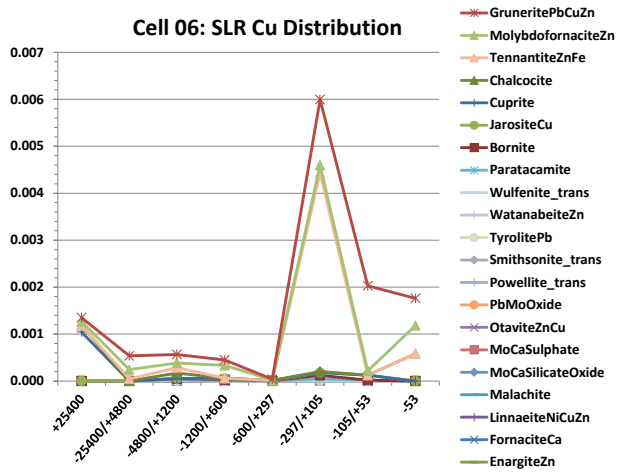
Cell 06: SLR Cu Distribution
0.007
0.006
0.005
0.004
0.003
0.002
0.001
0.000
+25400
-25400/+4800
-4800/+1200
-1200/+600
-600/+297
-297/+105
-105/+53
-53
GruneritePbCuZn
MolybdofornaciteZn
TennantiteZnFe
Chalcocite
Cuprite
JarositeCu
Bornite
Paratacamite
Wulfenite_trans
WatanabeiteZn
TyrolitePb
Smithsonite_trans
Powellite_trans
PbMoOxide
OtaviteZnCu
MoCaSulphate
MoCaSilicateOxide
Malachite
LinnaeiteNiCuZn
FornaciteCa
EnargiteZn

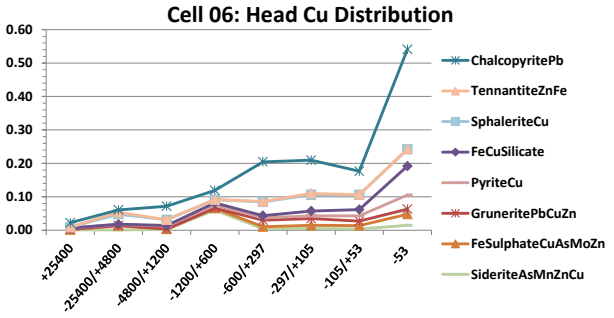
Cell 06: Head Cu Distribution
0.60
0.50
0.40
0.30
0.20
0.10
0.00
+25400
-25400/+4800
-4800/+1200
-1200/+600
-600/+297
-297/+105
-105/+53
-53
ChalcopyritePb
TennantiteZnFe
SphaleriteCu
FeCuSilicate
PyriteCu
GruneritePbCuZn
FeSulphateCuAsMoZn
SideriteAsMnZnCu

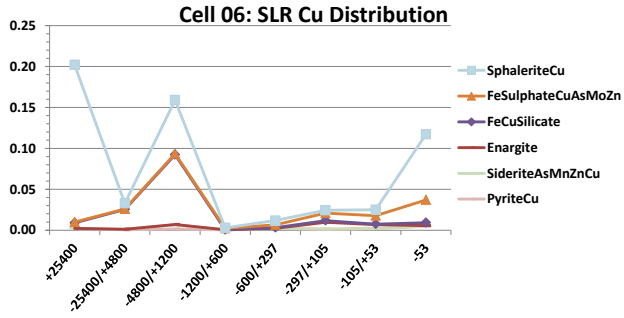
Cell 06: SLR Cu Distribution
0.25
0.20
0.15
0.10
0.05
0.00
+25400
-25400/+4800
-4800/+1200
-1200/+600
-600/+297
-297/+105
-105/+53
-53
SphaleriteCu
FeSulphateCuAsMoZn
FeCuSilicate
Enargite
SideriteAsMnZnCu
PyriteCu

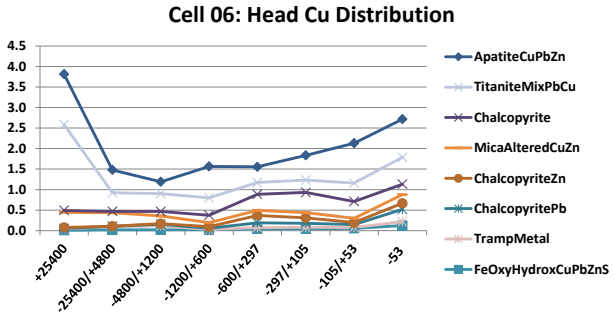
Cell 06: Head Cu Distribution
4.5
4.0
3.5
3.0
2.5
2.0
1.5
1.0
0.5
0.0
+25400
-25400/+4800
-4800/+1200
-1200/+600
-600/+297
-297/+105
-105/+53
-53
ApatiteCuPbZn
TitaniteMixPbCu
Chalcopyrite
MicaAlteredCuZn
ChalcopyriteZn
ChalcopyritePb
TrampMetal
FeOxyHydroxCuPbZnS

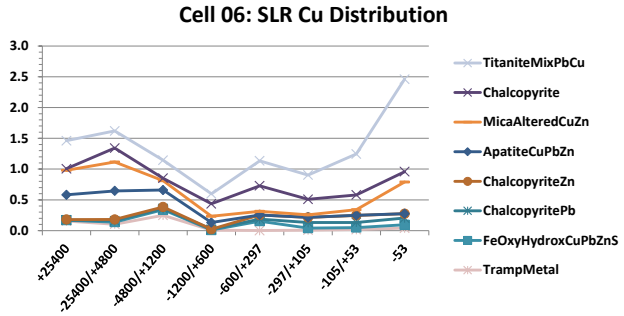
Cell 06: SLR Cu Distribution
3.0
2.5
2.0
1.5
1.0
0.5
0.0
+25400
-25400/+4800
-4800/+1200
-1200/+600
-600/+297
-297/+105
-105/+53
-53
TitaniteMixPbCu
Chalcopyrite
MicaAlteredCuZn
ApatiteCuPbZn
ChalcopyriteZn
ChalcopyritePb
FeOxyHydroxCuPbZnS
TrampMetal

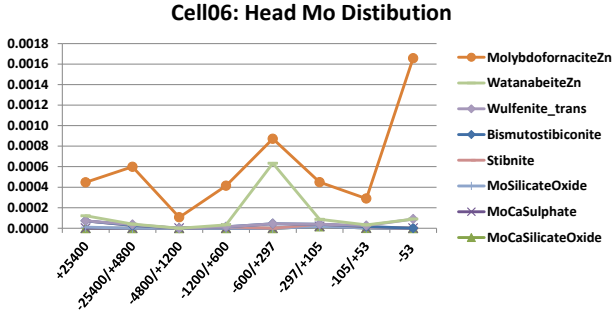
Cell06: Head Mo Distibution
0.0018
0.0016
0.0014
0.0012
0.0010
0.0008
0.0006
0.0004
0.0002
0.0000
+25400
-25400/+4800
-4800/+1200
-1200/+600
-600/+297
-297/+105
-105/+53
-53
MolybdofornaciteZn
WatanabeiteZn
Wulfenite_trans
Bismutostibiconite
Stibnite
MoSilicateOxide
MoCaSulphate
MoCaSilicateOxide

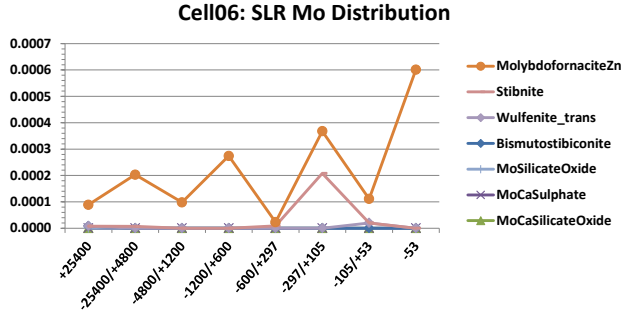
Cell06: SLR Mo Distribution
0.0007
0.0006
0.0005
0.0004
0.0003
0.0002
0.0001
0.0000
+25400
-25400/+4800
-4800/+1200
-1200/+600
-600/+297
-297/+105
-105/+53
-53
MolybdofornaciteZn
Stibnite
Wulfenite_trans
Bismutostibiconite
MoSilicateOxide
MoCaSulphate
MoCaSilicateOxide

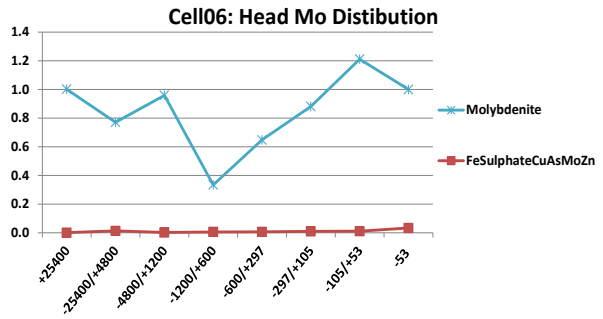
Cell06: Head Mo Distibution
1.4
1.2
1.0
0.8
0.6
0.4
0.2
0.0
+25400
-25400/+4800
-4800/+1200
-1200/+600
-600/+297
-297/+105
-105/+53
-53
Molybdenite
FeSulphateCuAsMoZn

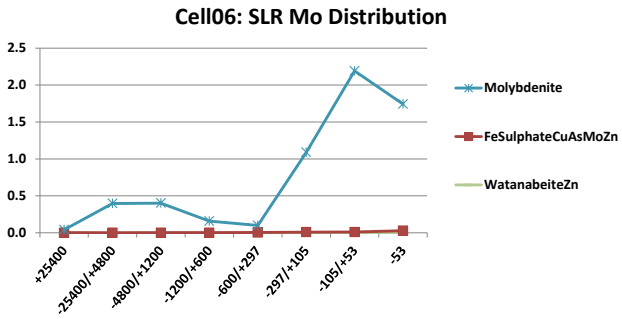
Cell06: SLR Mo Distribution
2.5
2.0
1.5
1.0
0.5
0.0
+25400
-25400/+4800
-4800/+1200
-1200/+600
-600/+297
-297/+105
-105/+53
-53
Molybdenite
FeSulphateCuAsMoZn
WatanabeiteZn

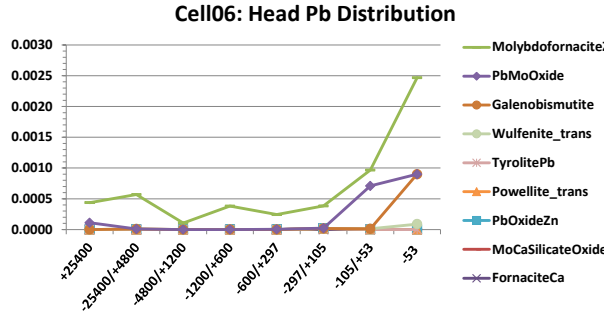
Cell06: Head Pb Distribution
0.0030
0.0025
0.0020
0.0015
0.0010
0.0005
0.0000
+25400
-25400/+4800
-4800/+1200
-1200/+600
-600/+297
-297/+105
-105/+53
-53
Molybdofornacite
PbMoOxide
Galenobismutite
Wulfenite_trans
TyrolitePb
Powellite_trans
PbOxideZn
MoCaSilicateOxide
FornaciteCa

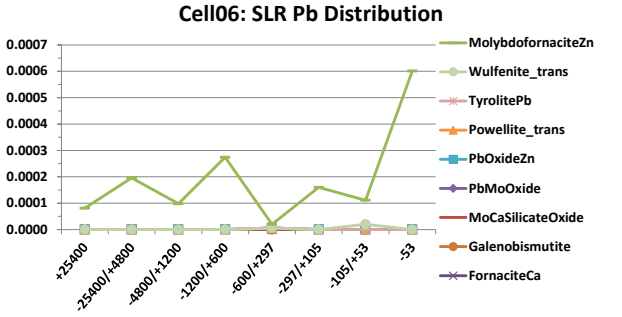
Cell06: SLR Pb Distribution
0.0007
0.0006
0.0005
0.0004
0.0003
0.0002
0.0001
0.0000
+25400
-25400/+4800
-4800/+1200
-1200/+600
-600/+297
-297/+105
-105/+53
-53
MolybdofornaciteZn
Wulfenite_trans
TyrolitePb
Powellite_trans
PbOxideZn
PbMoOxide
MoCaSilicateOxide
Galenobismutite
FornaciteCa

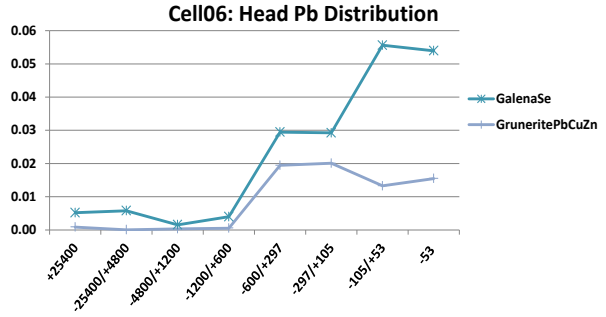
Cell06: Head Pb Distribution
0.06
0.05
0.04
0.03
0.02
0.01
0.00
+25400
-25400/+4800
-4800/+1200
-1200/+600
-600/+297
-297/+105
-105/+53
-53
GalenaSe
GruneritePbCuZn

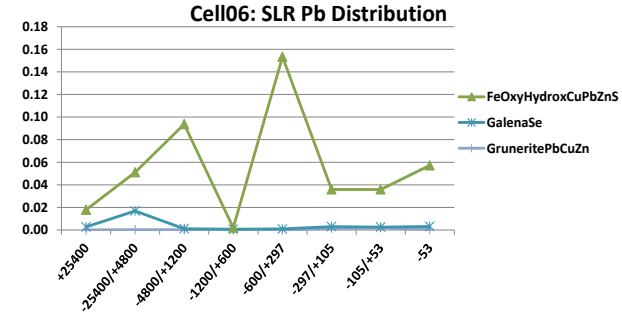
Cell06: SLR Pb Distribution
0.18
0.16
0.14
0.12
0.10
0.08
0.06
0.04
0.02
0.00
+25400
-25400/+4800
-4800/+1200
-1200/+600
-600/+297
-297/+105
-105/+53
-53
FeOxyHydroxCuPbZnS
GalenaSe
GruneritePbCuZn

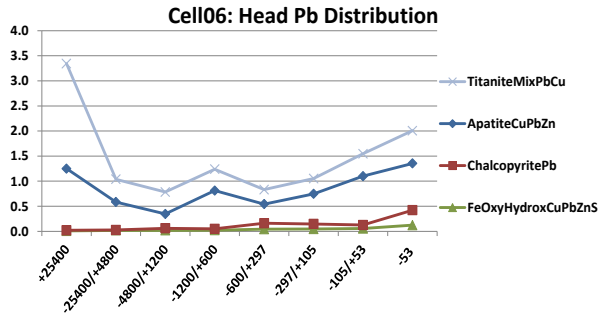
Cell06: Head Pb Distribution
4.0
3.5
3.0
2.5
2.0
1.5
1.0
0.5
0.0
+25400
-25400/+4800
-4800/+1200
-1200/+600
-600/+297
-297/+105
-105/+53
-53
TitaniteMixPbCu
ApatiteCuPbZn
ChalcopyritePb
FeOxyHydroxCuPbZnS

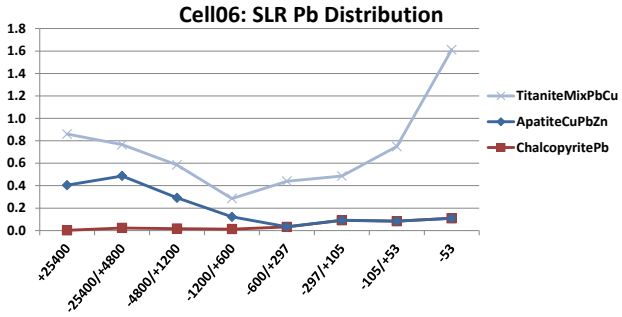
Cell06: SLR Pb Distribution
1.8
1.6
1.4
1.2
1.0
0.8
0.6
0.4
0.2
0.0
+25400
-25400/+4800
-4800/+1200
-1200/+600
-600/+297
-297/+105
-105/+53
-53
TitaniteMixPbCu
ApatiteCuPbZn
ChalcopyritePb

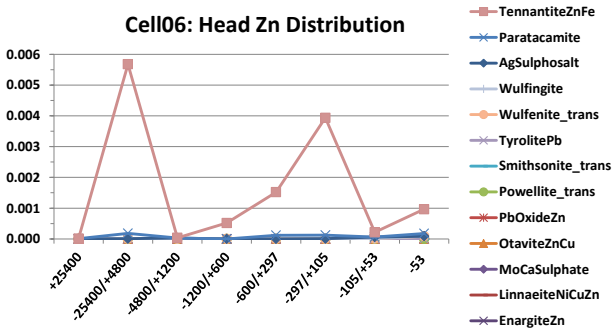
Cell06: Head Zn Distribution
0.006
0.005
0.004
0.003
0.002
0.001
0.000
+25400
-25400/+4800
-4800/+1200
-1200/+600
-600/+297
-297/+105
-105/+53
-53
TennantiteZnFe
Paratacamite
AgSulphosalt
Wulfingite
Wulfenite_trans
TyrolitePb
Smithsonite_trans
Powellite_trans
PbOxideZn
OtaviteZnCu
MoCaSulphate
LinnaeiteNiCuZn
EnargiteZn

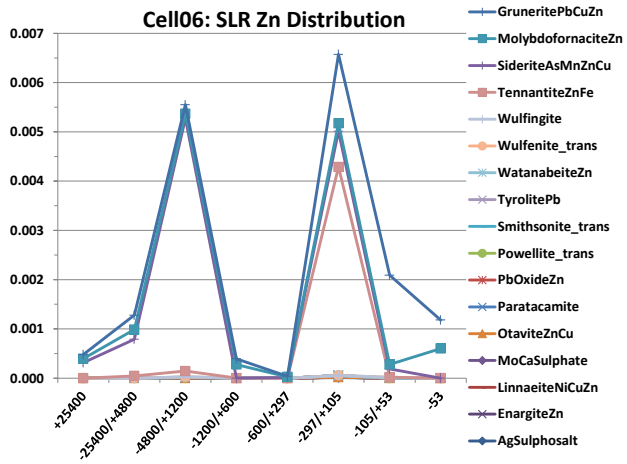
Cell06: SLR Zn Distribution
0.007
0.006
0.005
0.004
0.003
0.002
0.001
0.000
+25400
-25400/+4800
-4800/+1200
-1200/+600
-600/+297
-297/+105
-105/+53
-53
GruneritePbCuZn
MolybdofornaciteZn
SideriteAsMnZnCu
TennantiteZnFe
Wulfingite
Wulfenite_trans
WatanabeiteZn
TyrolitePb
Smithsonite_trans
Powellite_trans
PbOxideZn
Paratacamite
OtaviteZnCu
MoCaSulphate
LinnaeiteNiCuZn
EnargiteZn
AgSulphosalt

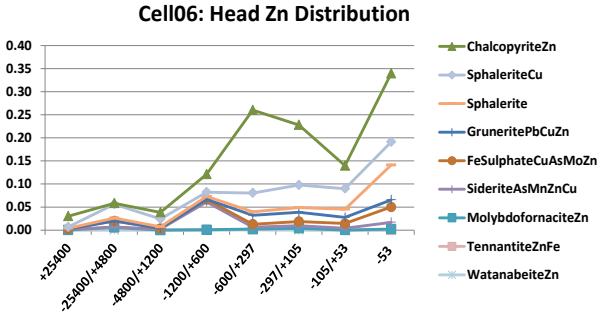
Cell06: Head Zn Distribution
0.40
0.35
0.30
0.25
0.20
0.15
0.10
0.05
0.00
+25400
-25400/+4800
-4800/+1200
-1200/+600
-600/+297
-297/+105
-105/+53
-53
ChalcopyriteZn
SphaleriteCu
Sphalerite
GruneritePbCuZn
FeSulphateCuAsMoZn
SideriteAsMnZnCu
MolybdofornaciteZn
TennantiteZnFe
WatanabeiteZn

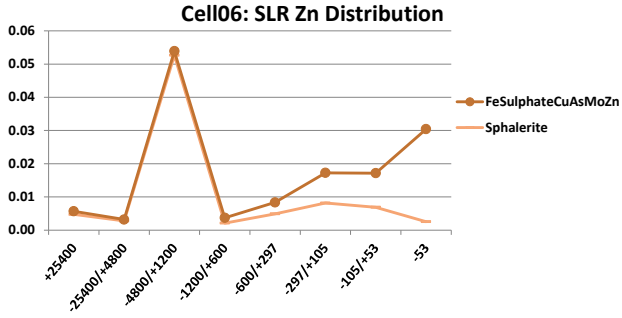
Cell06: SLR Zn Distribution
0.06
0.05
0.04
0.03
0.02
0.01
0.00
+25400
-25400/+4800
-4800/+1200
-1200/+600
-600/+297
-297/+105
-105/+53
-53
FeSulphateCuAsMoZn
Sphalerite

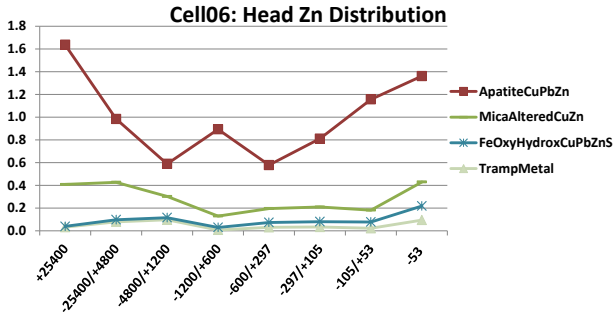
Cell06: Head Zn Distribution
1.8
1.6
1.4
1.2
1.0
0.8
0.6
0.4
0.2
0.0
+25400
-25400/+4800
-4800/+1200
-1200/+600
-600/+297
-297/+105
-105/+53
-53
ApatiteCuPbZn
MicaAlteredCuZn
FeOxyHydroxCuPbZnS
TrampMetal

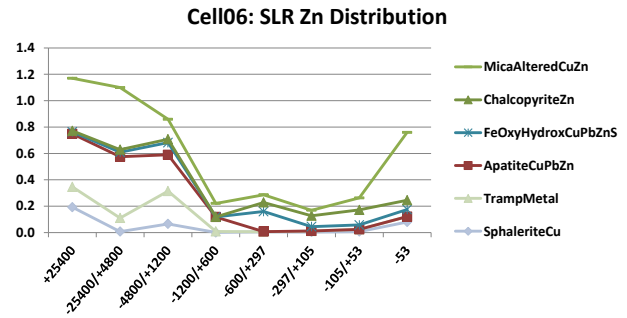
Cell06: SLR Zn Distribution
1.4
1.2
1.0
0.8
0.6
0.4
0.2
0.0
+25400
-25400/+4800
-4800/+1200
-1200/+600
-600/+297
-297/+105
-105/+53
-53
MicaAlteredCuZn
ChalcopyriteZn
FeOxyHydroxCuPbZnS
ApatiteCuPbZn
TrampMetal
SphaleriteCu

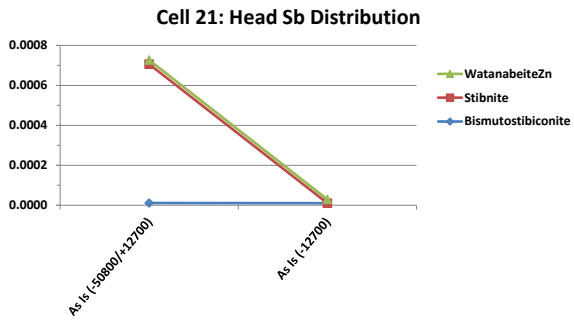
Cell 21: Head Sb Distribution
0.0008
0.0006
0.0004
0.0002
0.0000
As Is (-50800/+12700)
As Is (-12700)
WatanabeiteZn
Stibnite
Bismutostibiconite

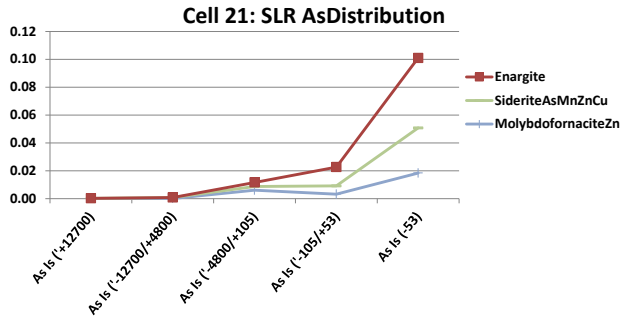
Cell 21: SLR AsDistribution
0.12
0.10
0.08
0.06
0.04
0.02
0.00
As Is (+12700)
As Is (-12700/+4800)
As Is (-4800/+105)
As Is (-105/+53)
As Is (-53)
Enargite
SideriteAsMnZnCu
MolybdofornaciteZn

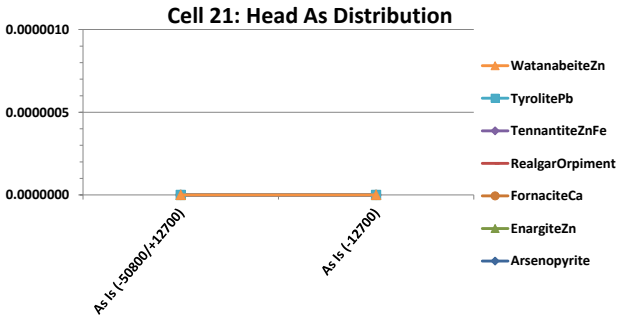
Cell 21: Head As Distribution
0.0000010
0.0000005
0.0000000
As Is (-50800/+12700)
As Is (-12700)
WatanabeiteZn
TyrolitePb
TennantiteZnFe
RealgarOrpiment
FornaciteCa
EnargiteZn
Arsenopyrite

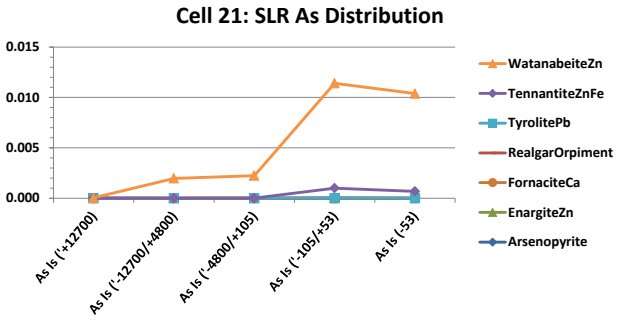
Cell 21: SLR As Distribution
0.015
0.010
0.005
0.000
As Is (+12700)
As Is (-12700/+4800)
As Is (-4800/+105)
As Is (-105/+53)
As Is (-53)
WatanabeiteZn
TennantiteZnFe
TyrolitePb
RealgarOrpiment
FornaciteCa
EnargiteZn
Arsenopyrite

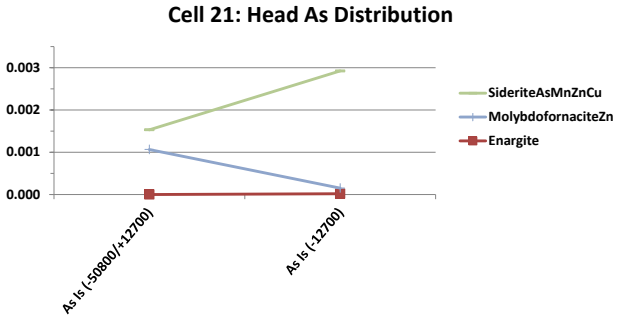
Cell 21: Head As Distribution
0.003
0.002
0.001
0.000
As Is (-50800/+12700)
As Is (-12700)
SideriteAsMnZnCu
MolybdofornaciteZn
Enargite

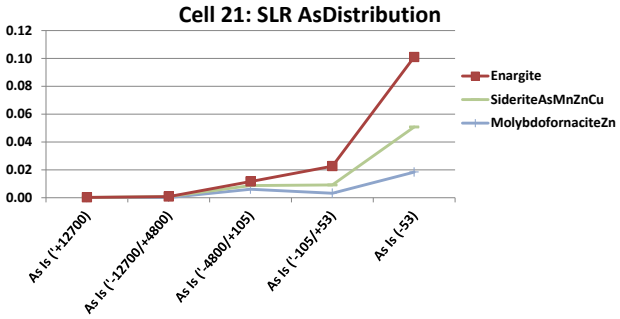
Cell 21: SLR AsDistribution
0.12
0.10
0.08
0.06
0.04
0.02
0.00
As Is (+12700)
As Is (-12700/+4800)
As Is (-4800/+105)
As Is (-105/+53)
As Is (-53)
Enargite
SideriteAsMnZnCu
MolybdofornaciteZn

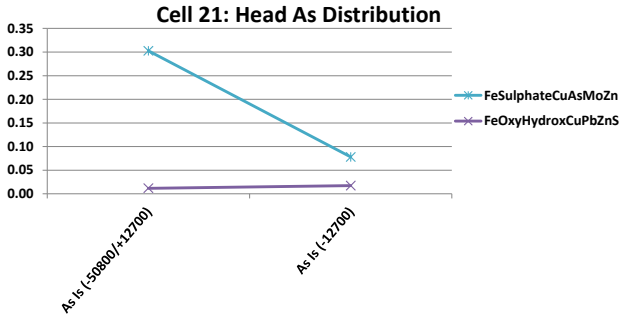
Cell 21: Head As Distribution
0.35
0.30
0.25
0.20
0.15
0.10
0.05
0.00
As Is (-50800/+12700)
As Is (-12700)
FeSulphateCuAsMoZn
FeOxyHydroxCuPbZnS

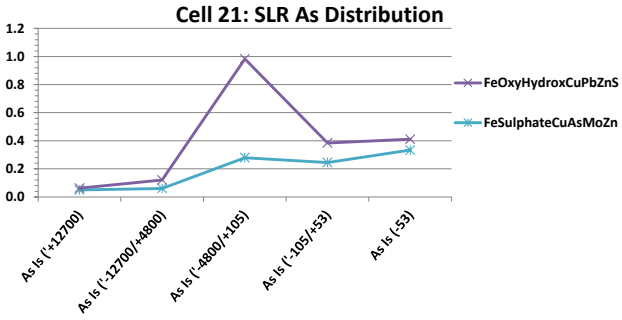
Cell 21: SLR As Distribution
1.2
1.0
0.8
0.6
0.4
0.2
0.0
As Is (+12700)
As Is (-12700/+4800)
As Is (-4800/+105)
As Is (-105/+53)
As Is (-53)
FeOxyHydroxCuPbZnS
FeSulphateCuAsMoZn

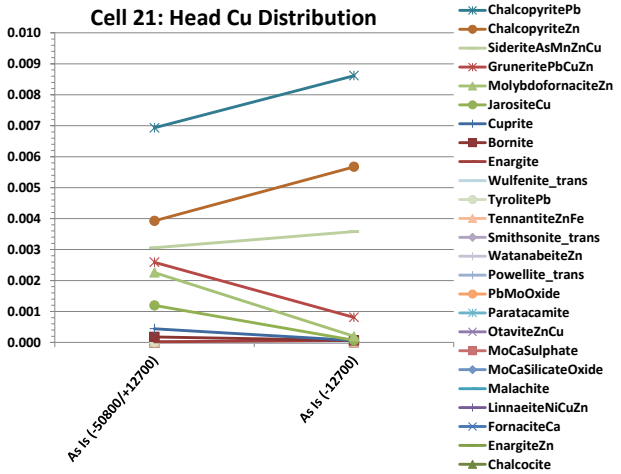
Cell 21: Head Cu Distribution
0.010
0.009
0.008
0.007
0.006
0.005
0.004
0.003
0.002
0.001
0.000
As Is (-50800/+12700)
As Is (-12700)
ChalcopyritePb
ChalcopyriteZn
SideriteAsMnZnCu
GruneritePbCuZn
MolybdofornaciteZn
JarositeCu
Cuprite
Bornite
Enargite
Wulfenite_trans
TyrolitePb
TennantiteZnFe
Smithsonite_trans
WatanabeiteZn
Powellite_trans
PbMoOxide
Paratacamite
OtaviteZnCu
MoCaSulphate
MoCaSilicateOxide
Malachite
LinnaeiteNiCuZn
FornaciteCa
EnargiteZn
Chalcocite

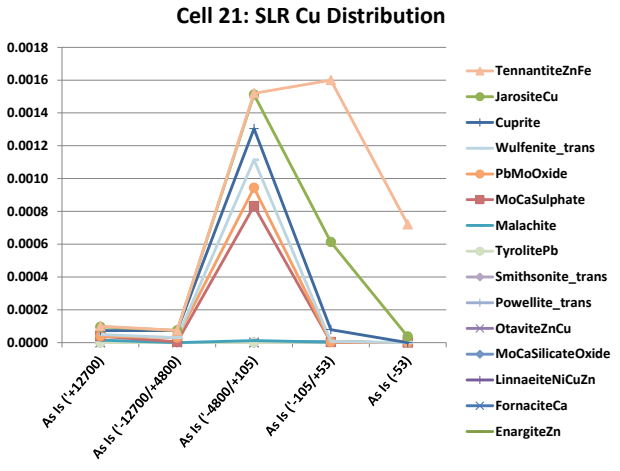
Cell 21: SLR Cu Distribution
0.0018
0.0016
0.0014
0.0012
0.0010
0.0008
0.0006
0.0004
0.0002
0.0000
As Is (+12700)
As Is (-12700/+4800)
As Is (-4800/+105)
As Is (-105/+53)
As Is (-53)
TennantiteZnFe
JarositeCu
Cuprite
Wulfenite_trans
PbMoOxide
MoCaSulphate
Malachite
TyrolitePb
Smithsonite_trans
Powellite_trans
OtaviteZnCu
MoCaSilicateOxide
LinnaeiteNiCuZn
FornaciteCa
EnargiteZn

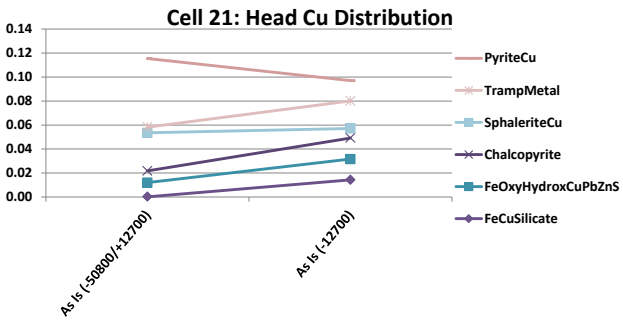
Cell 21: Head Cu Distribution
0.14
0.12
0.10
0.08
0.06
0.04
0.02
0.00
As Is (-50800/+12700)
As Is (-12700)
PyriteCu
TrampMetal
SphaleriteCu
Chalcopyrite
FeOxyHydroxCuPbZnS
FeCuSilicate

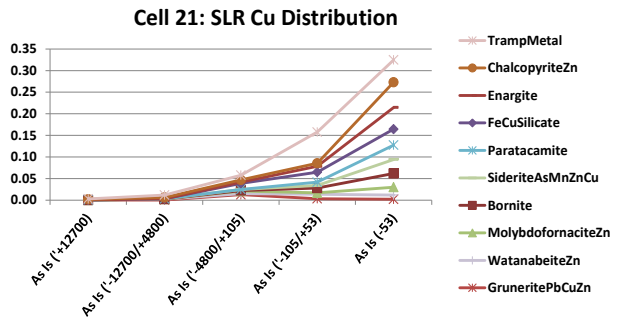
Cell 21: SLR Cu Distribution
0.35
0.30
0.25
0.20
0.15
0.10
0.05
0.00
As Is (+12700)
As Is (-12700/+4800)
As Is (-4800/+105)
As Is (-105/+53)
As Is (-53)
TrampMetal
ChalcopyriteZn
Enargite
FeCuSilicate
Paratacamite
SideriteAsMnZnCu
Bornite
MolybdofornaciteZn
WatanabeiteZn
GruneritePbCuZn

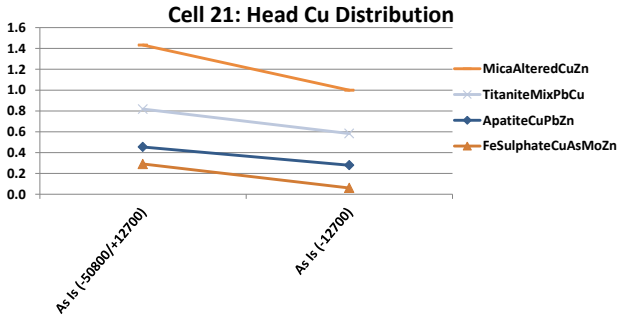
Cell 21: Head Cu Distribution
1.6
1.4
1.2
1.0
0.8
0.6
0.4
0.2
0.0
As Is (-50800/+12700)
As Is (-12700)
MicaAlteredCuZn
TitaniteMixPbCu
ApatiteCuPbZn
FeSulphateCuAsMoZn

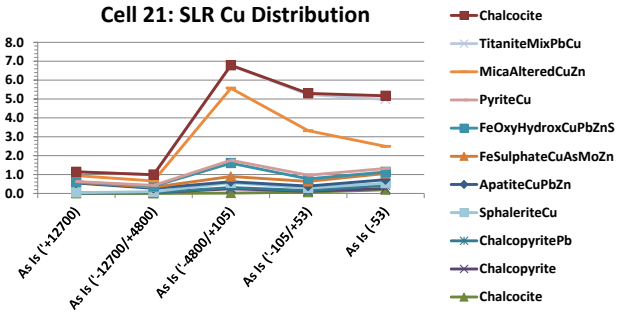
Cell 21: SLR Cu Distribution
8.0
7.0
6.0
5.0
4.0
3.0
2.0
1.0
0.0
As Is (+12700)
As Is (-12700/+4800)
As Is (-4800/+105)
As Is (-105/+53)
As Is (-53)
Chalcocite
TitaniteMixPbCu
MicaAlteredCuZn
PyriteCu
FeOxyHydroxCuPbZnS
FeSulphateCuAsMoZn
ApatiteCuPbZn
SphaleriteCu
ChalcopyritePb
Chalcopyrite
Chalcocite

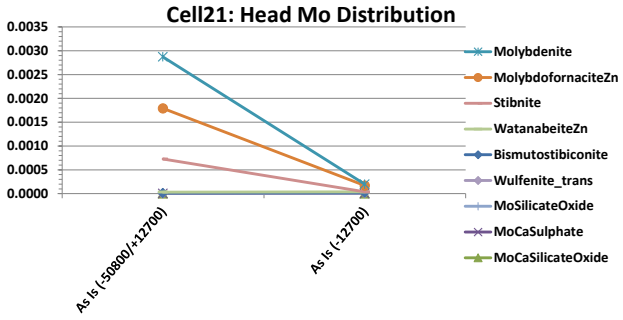
Cell21: Head Mo Distribution
0.0035
0.0030
0.0025
0.0020
0.0015
0.0010
0.0005
0.0000
As Is (-50800/+12700)
As Is (-12700)
Molybdenite
MolybdofornaciteZn
Stibnite
WatanabeiteZn
Bismutostibiconite
Wulfenite_trans
MoSilicateOxide
MoCaSulphate
MoCaSilicateOxide

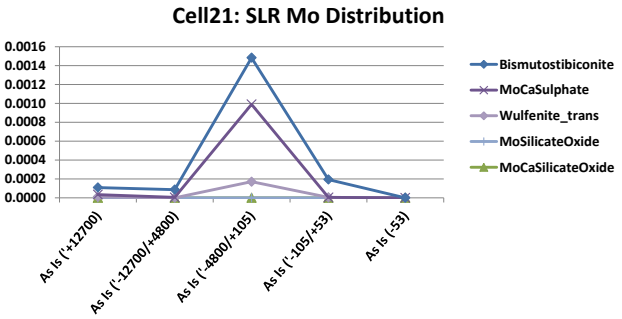
Cell21: SLR Mo Distribution
0.0016
0.0014
0.0012
0.0010
0.0008
0.0006
0.0004
0.0002
0.0000
As Is (+12700)
As Is (-12700/+4800)
As Is (-4800/+105)
As Is (-105/+53)
As Is (-53)
Bismutostibiconite
MoCaSulphate
Wulfenite_trans
MoSilicateOxide
MoCaSilicateOxide

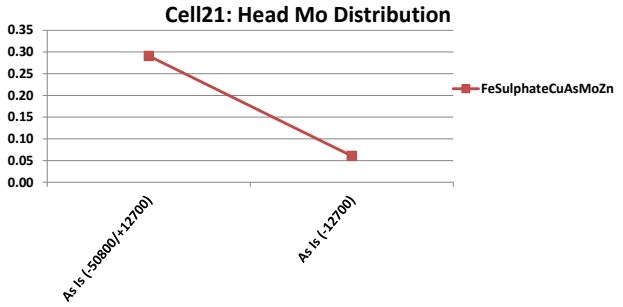
Cell21: Head Mo Distribution
0.35
0.30
0.25
0.20
0.15
0.10
0.05
0.00
As Is (-50800/+12700)
As Is (-12700)
FeSulphateCuAsMoZn

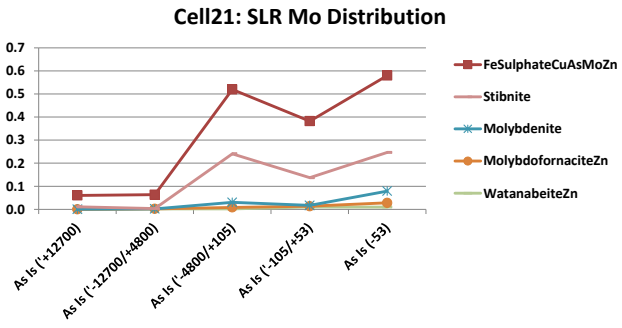
Cell21: SLR Mo Distribution
0.7
0.6
0.5
0.4
0.3
0.2
0.1
0.0
As Is (+12700)
As Is (-12700/+4800)
As Is (-4800/+105)
As Is (-105/+53)
As Is (-53)
FeSulphateCuAsMoZn
Stibnite
Molybdenite
MolybdofornaciteZn
WatanabeiteZn

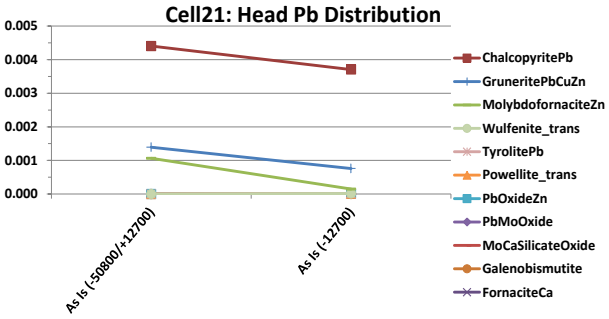
Cell21: Head Pb Distribution
0.005
0.004
0.003
0.002
0.001
0.000
As Is (-50800/+12700)
As Is (-12700)
ChalcopyritePb
GruneritePbCuZn
MolybdofornaciteZn
Wulfenite_trans
TyrolitePb
Powellite_trans
PbOxideZn
PbMoOxide
MoCaSilicateOxide
Galenobismutite
FornaciteCa

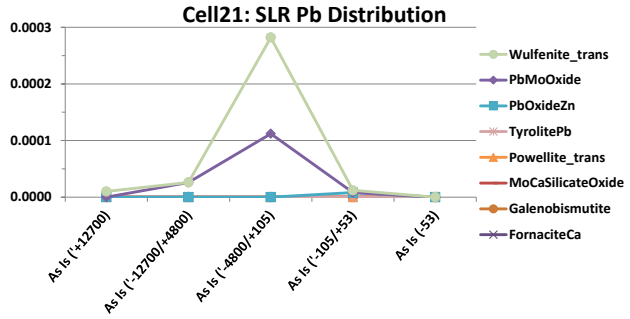
Cell21: SLR Pb Distribution
0.0003
0.0002
0.0001
0.0000
As Is (+12700)
As Is (-12700/+4800)
As Is (-4800/+105)
As Is (-105/+53)
As Is (-53)
Wulfenite_trans
PbMoOxide
PbOxideZn
TyrolitePb
Powellite_trans
MoCaSilicateOxide
Galenobismutite
FornaciteCa

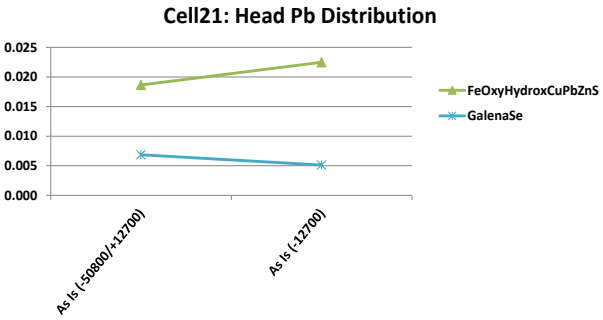
Cell21: Head Pb Distribution
0.025
0.020
0.015
0.010
0.005
0.000
As Is (-50800/+12700)
As Is (-12700)
FeOxyHydroxCuPbZnS
GalenaSe

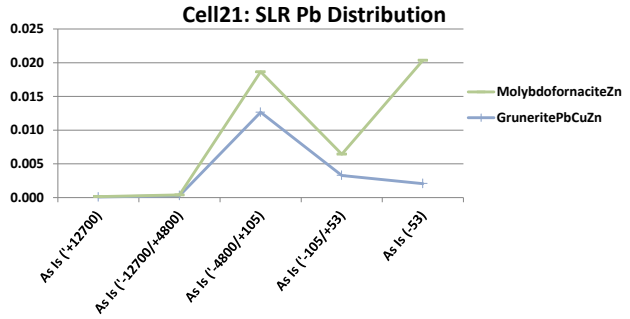
Cell21: SLR Pb Distribution
0.025
0.020
0.015
0.010
0.005
0.000
As Is (+12700)
As Is (-12700/+4800)
As Is (-4800/+105)
As Is (-105/+53)
As Is (-53)
MolybdofornaciteZn
GruneritePbCuZn

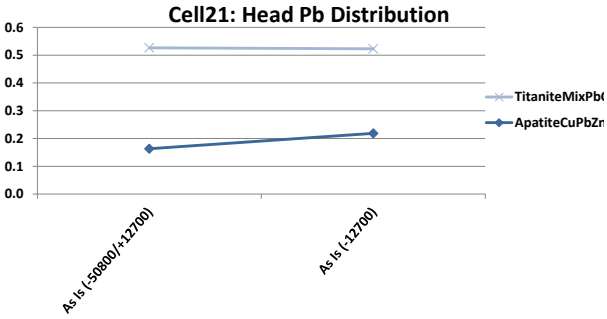
Cell21: Head Pb Distribution
0.6
0.5
0.4
0.3
0.2
0.1
0.0
As Is (-50800/+12700)
As Is (-12700)
TitaniteMixPbC
ApatiteCuPbZn

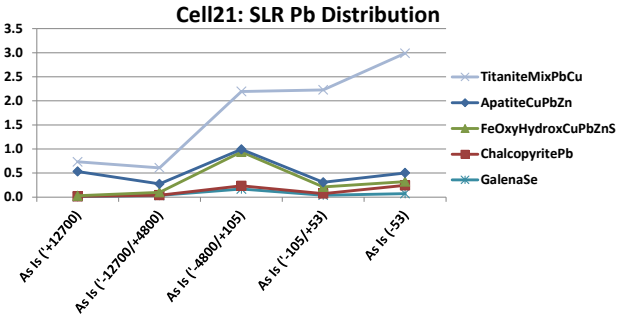
Cell21: SLR Pb Distribution
3.5
3.0
2.5
2.0
1.5
1.0
0.5
0.0
As Is (+12700)
As Is (-12700/+4800)
As Is (-4800/+105)
As Is (-105/+53)
As Is (-53)
TitaniteMixPbCu
ApatiteCuPbZn
FeOxyHydroxCuPbZnS
ChalcopyritePb
GalenaSe

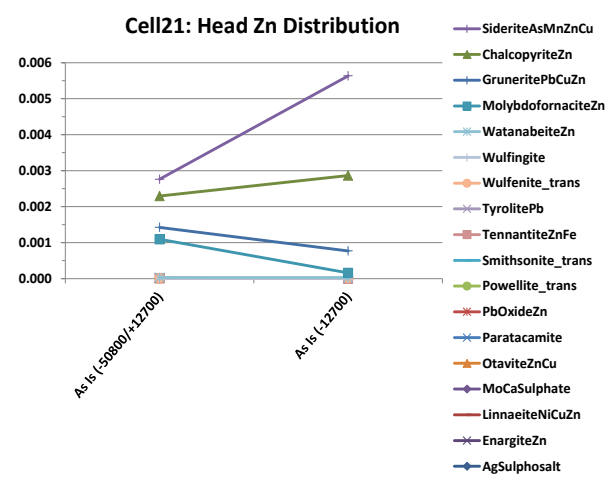
Cell21: Head Zn Distribution
0.006
0.005
0.004
0.003
0.002
0.001
0.000
As Is (-50800/+12700)
As Is (-12700)
SideriteAsMnZnCu
ChalcopyriteZn
GruneritePbCuZn
MolybdofornaciteZn
WatanabeiteZn
Wulfingite
Wulfenite_trans
TyrolitePb
TennantiteZnFe
Smithsonite_trans
Powellite_trans
PbOxideZn
Paratacamite
OtaviteZnCu
MoCaSulphate
LinnaeiteNiCuZn
EnargiteZn
AgSulphosalt

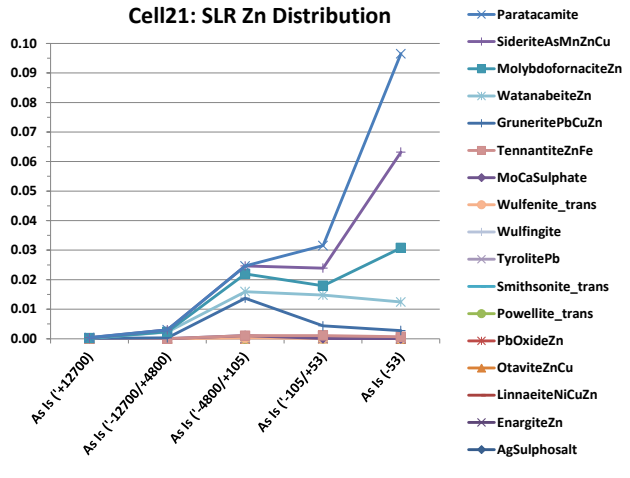
Cell21: SLR Zn Distribution
0.10
0.09
0.08
0.07
0.06
0.05
0.04
0.03
0.02
0.01
0.00
As Is (+12700)
As Is (-12700/+4800)
As Is (-4800/+105)
As Is (-105/+53)
As Is (-53)
Paratacamite
SideriteAsMnZnCu
MolybdofornaciteZn
WatanabeiteZn
GruneritePbCuZn
TennantiteZnFe
MoCaSulphate
Wulfenite_trans
Wulfingite
TyrolitePb
Smithsonite_trans
Powellite_trans
PbOxideZn
OtaviteZnCu
LinnaeiteNiCuZn
EnargiteZn
AgSulphosalt

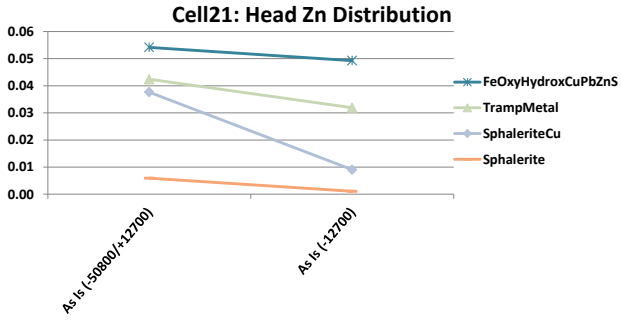
Cell21: Head Zn Distribution
0.06
0.05
0.04
0.03
0.02
0.01
0.00
As Is (-50800/+12700)
As Is (-12700)
FeOxyHydroxCuPbZnS
TrampMetal
SphaleriteCu
Sphalerite

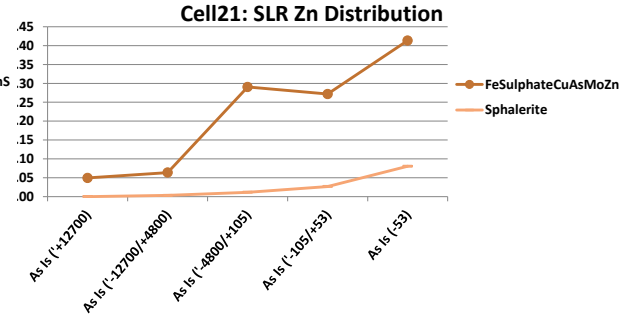
Cell21: SLR Zn Distribution
.45
.40
.35
.30
.25
.20
.15
.10
.05
.00
As Is (+12700)
As Is (-12700/+4800)
As Is (-4800/+105)
As Is (-105/+53)
As Is (-53)
FeSulphateCuAsMoZn
Sphalerite

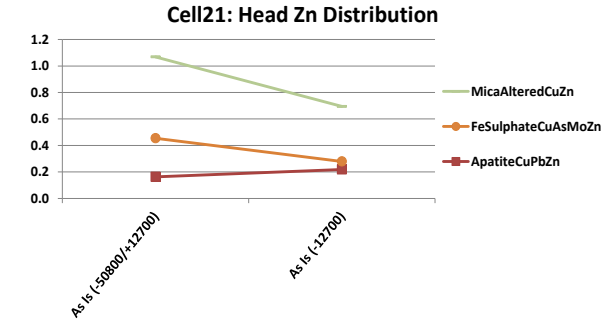
Cell21: Head Zn Distribution
1.2
1.0
0.8
0.6
0.4
0.2
0.0
As Is (-50800/+12700)
As Is (-12700)
MicaAlteredCuZn
FeSulphateCuAsMoZn
ApatiteCuPbZn

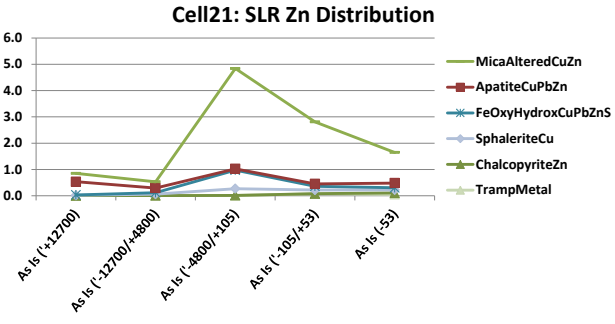
Cell21: SLR Zn Distribution
6.0
5.0
4.0
3.0
2.0
1.0
0.0
As Is (+12700)
As Is (-12700/+4800)
As Is (-4800/+105)
As Is (-105/+53)
As Is (-53)
MicaAlteredCuZn
ApatiteCuPbZn
FeOxyHydroxCuPbZnS
SphaleriteCu
ChalcopyriteZn
TrampMetal

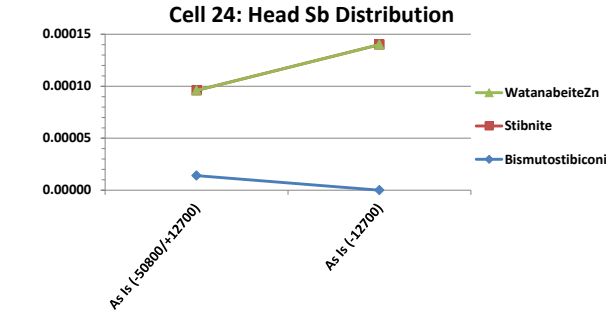
Cell 24: Head Sb Distribution
0.00015
0.00010
0.00005
0.00000
As Is (-50800/+12700)
As Is (-12700)
WatanabeiteZn
Stibnite
Bismutostibiconi

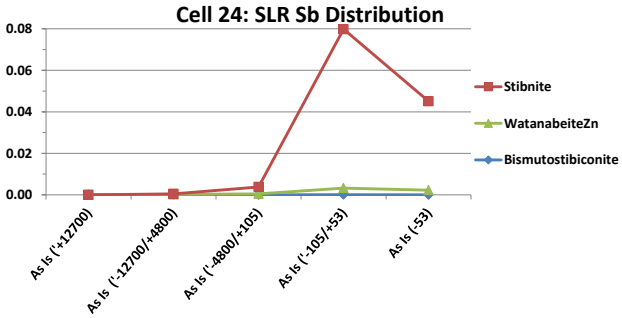
Cell 24: SLR Sb Distribution
0.08
0.06
0.04
0.02
0.00
As Is (+12700)
As Is (-12700/+4800)
As Is (-4800/+105)
As Is (-105/+53)
As Is (-53)
Stibnite
WatanabeiteZn
Bismutostibiconite

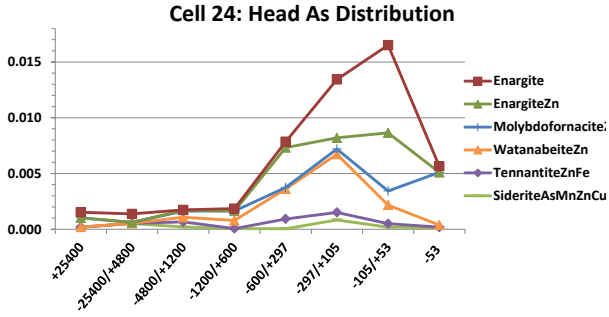
Cell 24: Head As Distribution
0.015
0.010
0.005
0.000
+25400
-25400/+4800
-4800/+1200
-1200/+600
-600/+297
-297/+105
-105/+53
-53
Enargite
EnargiteZn
Molybdofornacite
WatanabeiteZn
TennantiteZnFe
SideriteAsMnZnCu

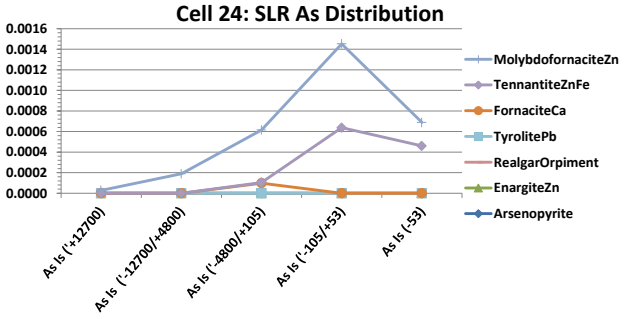
Cell 24: SLR As Distribution
0.0016
0.0014
0.0012
0.0010
0.0008
0.0006
0.0004
0.0002
0.0000
As Is (+12700)
As Is (-12700/+4800)
As Is (-4800/+105)
As Is (-105/+53)
As Is (-53)
MolybdofornaciteZn
TennantiteZnFe
FornaciteCa
TyrolitePb
RealgarOrpiment
EnargiteZn
Arsenopyrite

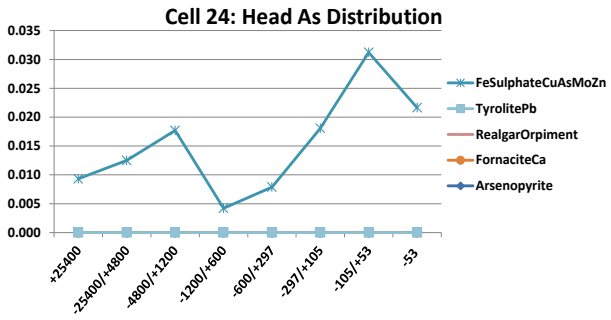
Cell 24: Head As Distribution
0.035
0.030
0.025
0.020
0.015
0.010
0.005
0.000
+25400
-25400/+4800
-4800/+1200
-1200/+600
-600/+297
-297/+105
-105/+53
-53
FeSulphateCuAsMoZn
TyrolitePb
RealgarOrpiment
FornaciteCa
Arsenopyrite

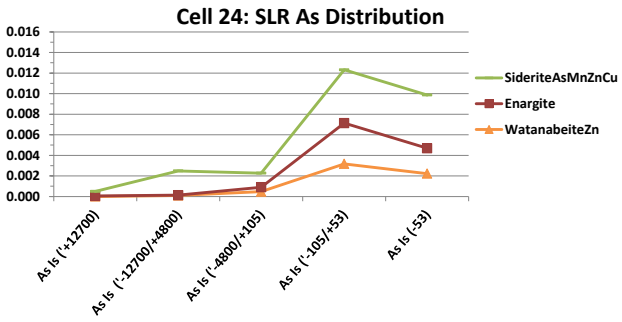
Cell 24: SLR As Distribution
0.016
0.014
0.012
0.010
0.008
0.006
0.004
0.002
0.000
As Is (+12700)
As Is (-12700/+4800)
As Is (-4800/+105)
As Is (-105/+53)
As Is (-53)
SideriteAsMnZnCu
Enargite
WatanabeiteZn

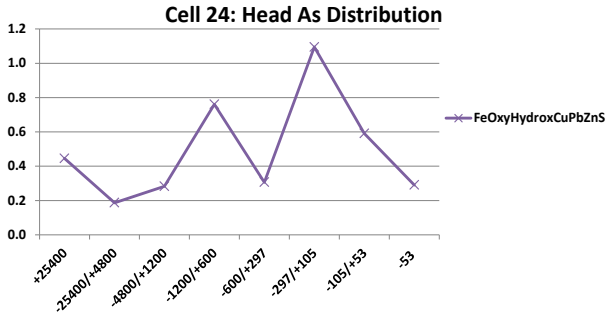
Cell 24: Head As Distribution
1.2
1.0
0.8
0.6
0.4
0.2
0.0
+25400
-25400/+4800
-4800/+1200
-1200/+600
-600/+297
-297/+105
-105/+53
-53
FeOxyHydroxCuPbZnS

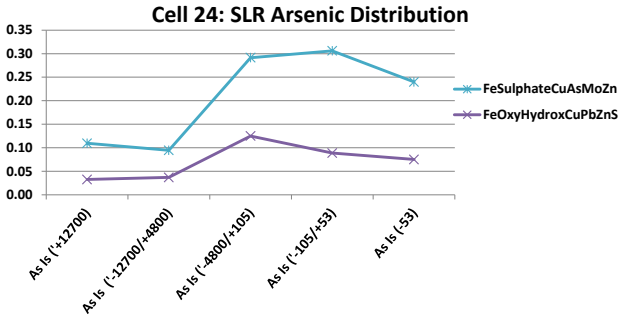
Cell 24: SLR Arsenic Distribution
0.35
0.30
0.25
0.20
0.15
0.10
0.05
0.00
As Is (+12700)
As Is (-12700/+4800)
As Is (-4800/+105)
As Is (-105/+53)
As Is (-53)
FeSulphateCuAsMoZn
FeOxyHydroxCuPbZnS

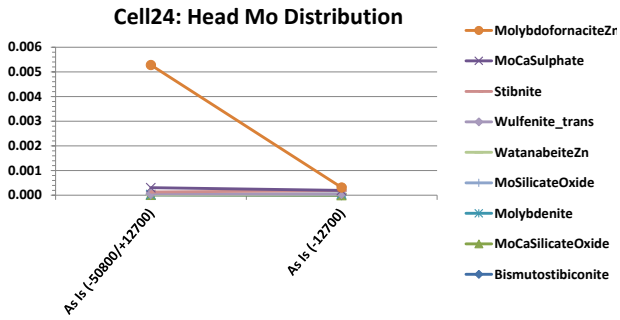
Cell24: Head Mo Distribution
0.006
0.005
0.004
0.003
0.002
0.001
0.000
As Is (-50800/+12700)
As Is (-12700)
MolybdofornaciteZr
MoCaSulphate
Stibnite
Wulfenite_trans
WatanabeiteZn
MoSilicateOxide
Molybdenite
MoCaSilicateOxide
Bismutostibiconite

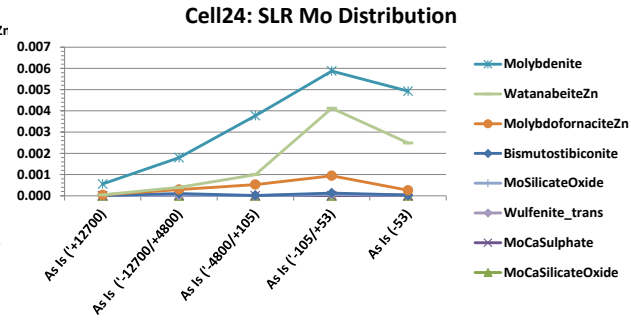
Cell24: SLR Mo Distribution
0.007
0.006
0.005
0.004
0.003
0.002
0.001
0.000
As Is (+12700)
As Is (-12700/+4800)
As Is (-4800/+105)
As Is (-105/+53)
As Is (-53)
Molybdenite
WatanabeiteZn
MolybdofornaciteZn
Bismutostibiconite
MoSilicateOxide
Wulfenite_trans
MoCaSulphate
MoCaSilicateOxide

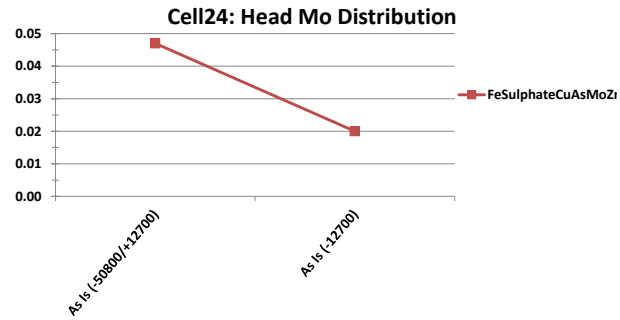
Cell24: Head Mo Distribution
0.05
0.04
0.03
0.02
0.01
0.00
As Is (-50800/+12700)
As Is (-12700)
FeSulphateCuAsMoZn

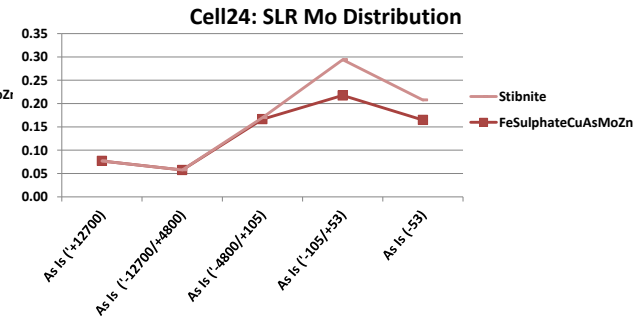
Cell24: SLR Mo Distribution
0.35
0.30
0.25
0.20
0.15
0.10
0.05
0.00
As Is (+12700)
As Is (-12700/+4800)
As Is (-4800/+105)
As Is (-105/+53)
As Is (-53)
Stibnite
FeSulphateCuAsMoZn

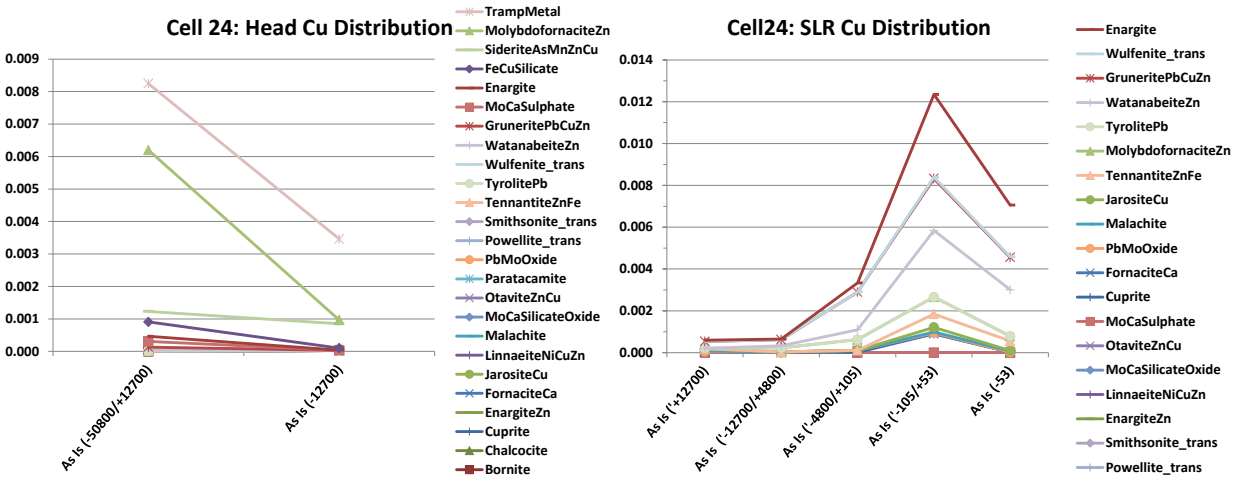
Cell 24: Head Cu Distribution
TrampMetal
MolybdofornaciteZn
SideriteAsMnZnCu
FeCuSilicate
Enargite
MoCaSulphate
GruneritePbCuZn
WatanabeiteZn
Wulfenite_trans
TyrolitePb
TennantiteZnFe
Smithsonite_trans
Powellite_trans
PbMoOxide
Paratacamite
OtaviteZnCu
MoCaSilicateOxide
Malachite
LinnaeiteNiCuZn
JarositeCu
FornaciteCa
EnargiteZn
Cuprite
Chalcocite
Bornite
As Is (-50800/+12700)
As Is (-12700)
Cell24: SLR Cu Distribution
Enargite
Wulfenite_trans
GruneritePbCuZn
WatanabeiteZn
TyrolitePb
MolybdofornaciteZn
TennantiteZnFe
JarositeCu
Malachite
PbMoOxide
FornaciteCa
Cuprite
MoCaSulphate
OtaviteZnCu
MoCaSilicateOxide
LinnaeiteNiCuZn
EnargiteZn
Smithsonite_trans
Powellite_trans
As Is (+12700)
As Is (-12700/+4800)
As Is (-4800/+105)
As Is (-105/+53)
As Is (-53)

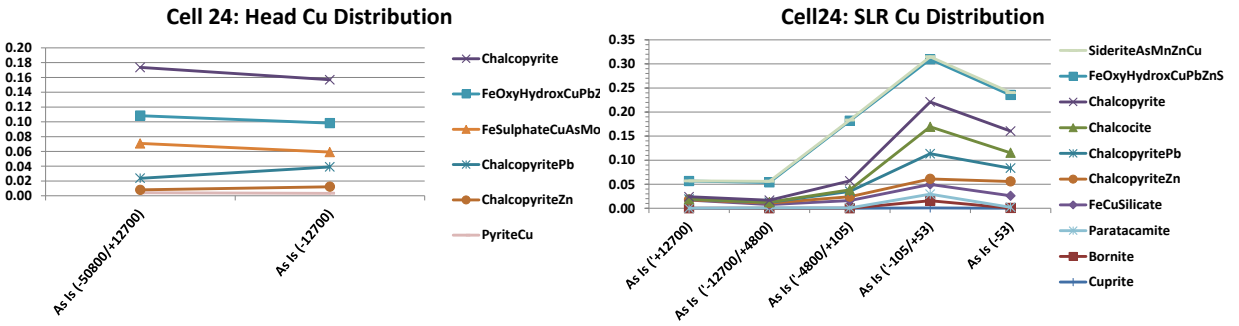
Cell 24: Head Cu Distribution
Chalcopyrite
FeOxyHydroxCuPbZ
FeSulphateCuAsMo
ChalcopyritePb
ChalcopyriteZn
PyriteCu
As Is (-50800/+12700)
As Is (-12700)
Cell24: SLR Cu Distribution
SideriteAsMnZnCu
FeOxyHydroxCuPbZnS
Chalcopyrite
Chalcocite
ChalcopyritePb
ChalcopyriteZn
FeCuSilicate
Paratacamite
Bornite
Cuprite
As Is (+12700)
As Is (-12700/+4800)
As Is (-4800/+105)
As Is (-105/+53)
As Is (-53)

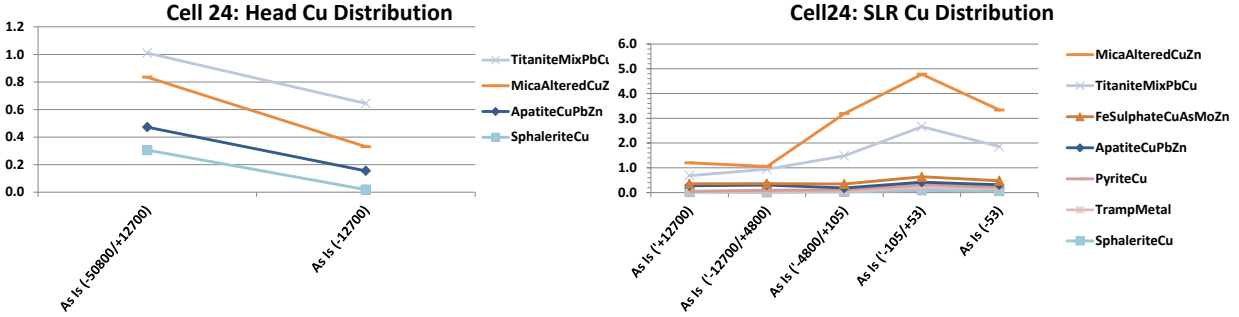
Cell 24: Head Cu Distribution
TitaniteMixPbCu
MicaAlteredCuZ
ApatiteCuPbZn
SphaleriteCu
As Is (-50800/+12700)
As Is (-12700)
Cell24: SLR Cu Distribution
MicaAlteredCuZn
TitaniteMixPbCu
FeSulphateCuAsMoZn
ApatiteCuPbZn
PyriteCu
TrampMetal
SphaleriteCu
As Is (+12700)
As Is (-12700/+4800)
As Is (-4800/+105)
As Is (-105/+53)
As Is (-53)

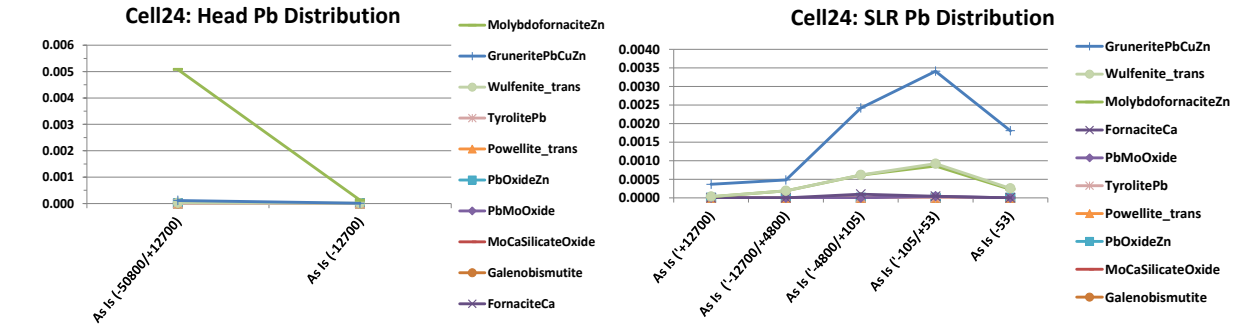
Cell24: Head Pb Distribution
MolybdofornaciteZn
GruneritePbCuZn
Wulfenite_trans
TyrolitePb
Powellite_trans
PbOxideZn
PbMoOxide
MoCaSilicateOxide
Galenobismutite
FornaciteCa
As Is (-50800/+12700)
As Is (-12700)
Cell24: SLR Pb Distribution
GruneritePbCuZn
Wulfenite_trans
MolybdofornaciteZn
FornaciteCa
PbMoOxide
TyrolitePb
Powellite_trans
PbOxideZn
MoCaSilicateOxide
Galenobismutite
As Is (+12700)
As Is (-12700/+4800)
As Is (-4800/+105)
As Is (-105/+53)
As Is (-53)

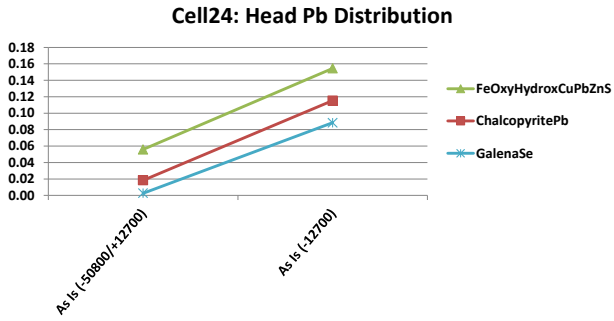
Cell24: Head Pb Distribution
0.18
0.16
0.14
0.12
0.10
0.08
0.06
0.04
0.02
0.00
As Is (-50800/+12700)
As Is (-12700)
FeOxyHydroxCuPbZnS
ChalcopyritePb
GalenaSe

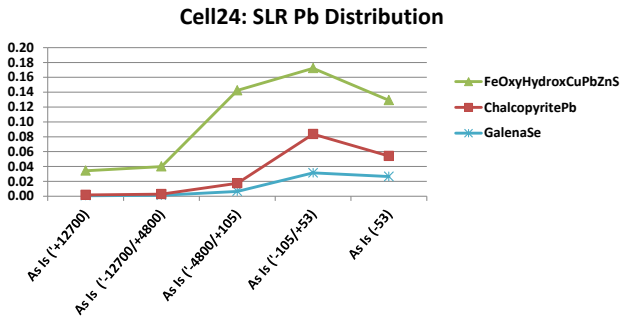
Cell24: SLR Pb Distribution
0.20
0.18
0.16
0.14
0.12
0.10
0.08
0.06
0.04
0.02
0.00
As Is ('+12700)
As Is ('-12700/+4800)
As Is ('-4800/+105)
As Is ('-105/+53)
As Is (-53)
FeOxyHydroxCuPbZnS
ChalcopyritePb
GalenaSe

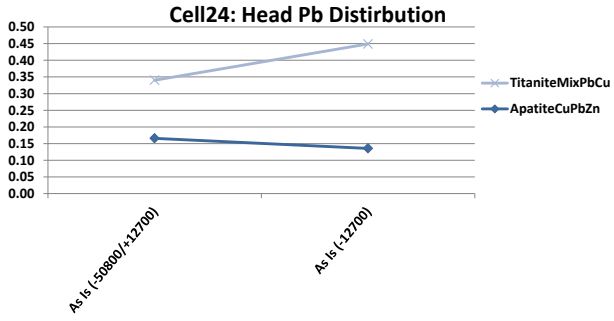
Cell24: Head Pb Distirbution
0.50
0.45
0.40
0.35
0.30
0.25
0.20
0.15
0.10
0.05
0.00
As Is (-50800/+12700)
As Is (-12700)
TitaniteMixPbCu
ApatiteCuPbZn

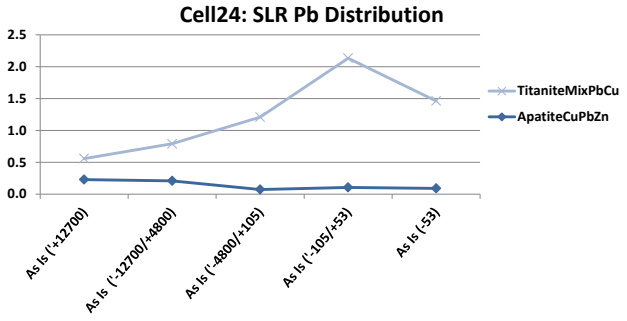
Cell24: SLR Pb Distribution
2.5
2.0
1.5
1.0
0.5
0.0
As Is ('+12700)
As Is ('-12700/+4800)
As Is ('-4800/+105)
As Is ('-105/+53)
As Is (-53)
TitaniteMixPbCu
ApatiteCuPbZn

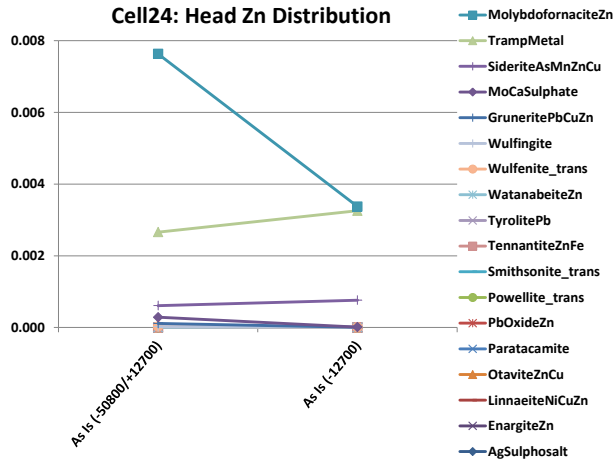
Cell24: Head Zn Distribution
0.008
0.006
0.004
0.002
0.000
As Is (-50800/+12700)
As Is (-12700)
MolybdofornaciteZn
TrampMetal
SideriteAsMnZnCu
MoCaSulphate
GruneritePbCuZn
Wulfingite
Wulfenite_trans
WatanabeiteZn
TyrolitePb
TennantiteZnFe
Smithsonite_trans
Powellite_trans
PbOxideZn
Paratacamite
OtaviteZnCu
LinnaeiteNiCuZn
EnargiteZn
AgSulphosalt

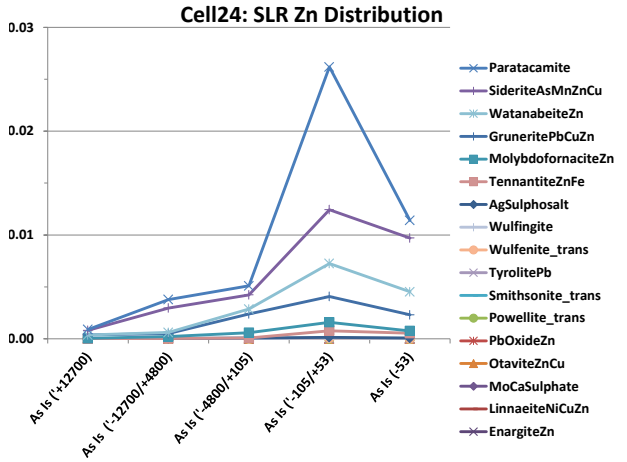
Cell24: SLR Zn Distribution
0.03
0.02
0.01
0.00
As Is ('+12700)
As Is ('-12700/+4800)
As Is ('-4800/+105)
As Is ('-105/+53)
As Is (-53)
Paratacamite
SideriteAsMnZnCu
WatanabeiteZn
GruneritePbCuZn
MolybdofornaciteZn
TennantiteZnFe
AgSulphosalt
Wulfingite
Wulfenite_trans
TyrolitePb
Smithsonite_trans
Powellite_trans
PbOxideZn
OtaviteZnCu
MoCaSulphate
LinnaeiteNiCuZn
EnargiteZn

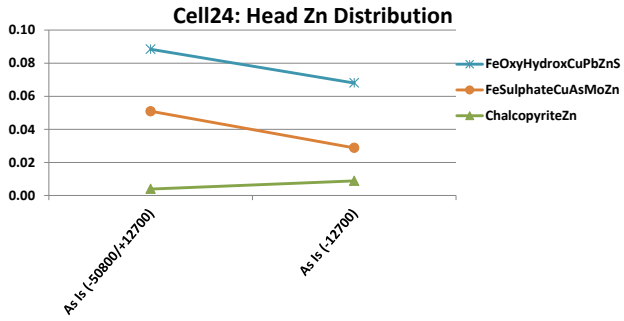
Cell24: Head Zn Distribution
0.10
0.08
0.06
0.04
0.02
0.00
As Is (-50800/+12700)
As Is (-12700)
FeOxyHydroxCuPbZnS
FeSulphateCuAsMoZn
ChalcopyriteZn

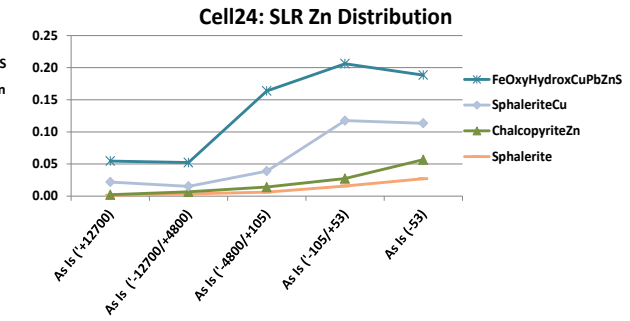
Cell24: SLR Zn Distribution
0.25
0.20
0.15
0.10
0.05
0.00
As Is ('+12700)
As Is ('-12700/+4800)
As Is ('-4800/+105)
As Is ('-105/+53)
As Is (-53)
FeOxyHydroxCuPbZnS
SphaleriteCu
ChalcopyriteZn
Sphalerite

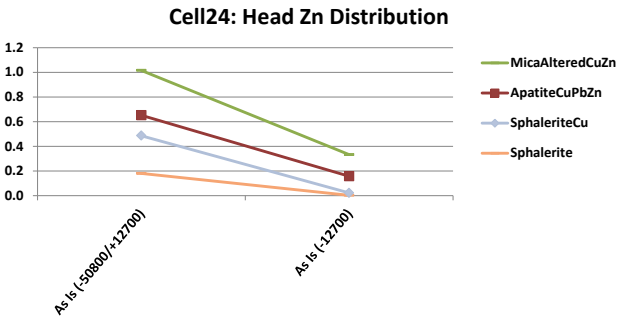
Cell24: Head Zn Distribution
1.2
1.0
0.8
0.6
0.4
0.2
0.0
As Is (-50800/+12700)
As Is (-12700)
MicaAlteredCuZn
ApatiteCuPbZn
SphaleriteCu
Sphalerite

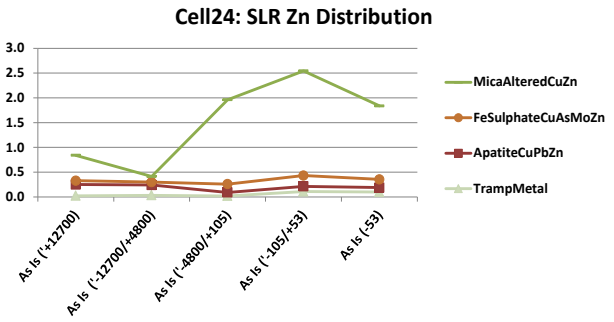
Cell24: SLR Zn Distribution
3.0
2.5
2.0
1.5
1.0
0.5
0.0
As Is (+12700)
As Is (-12700/+4800)
As Is (-4800/+105)
As Is (-105/+53)
As Is (-53)
MicaAlteredCuZn
FeSulphateCuAsMoZn
ApatiteCuPbZn
TrampMetal

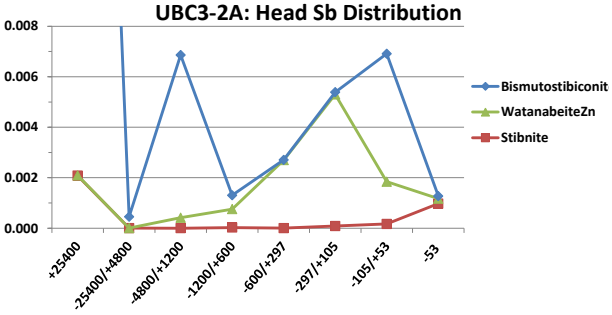
UBC3-2A: Head Sb Distribution
0.008
0.006
0.004
0.002
0.000
+25400
-25400/+4800
-4800/+1200
-1200/+600
-600/+297
-297/+105
-105/+53
-53
Bismutostibiconit
WatanabeiteZn
Stibnite

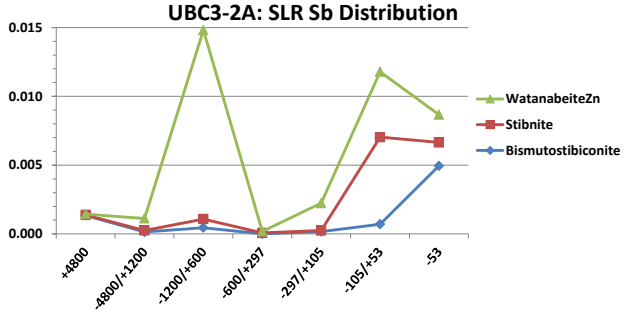
UBC3-2A: SLR Sb Distribution
0.015
0.010
0.005
0.000
+4800
-4800/+1200
-1200/+600
-600/+297
-297/+105
-105/+53
-53
WatanabeiteZn
Stibnite
Bismutostibiconite

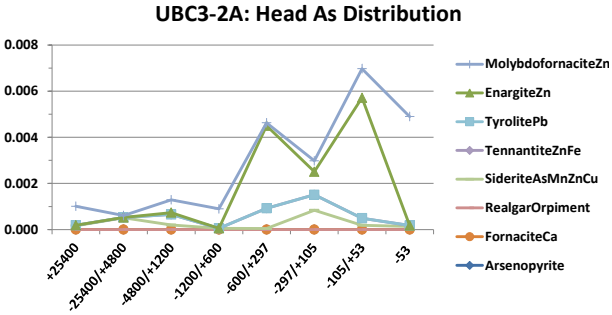
UBC3-2A: Head As Distribution
0.008
0.006
0.004
0.002
0.000
+25400
-25400/+4800
-4800/+1200
-1200/+600
-600/+297
-297/+105
-105/+53
-53
MolybdofornaciteZn
EnargiteZn
TyrolitePb
TennantiteZnFe
SideriteAsMnZnCu
RealgarOrpiment
FornaciteCa
Arsenopyrite

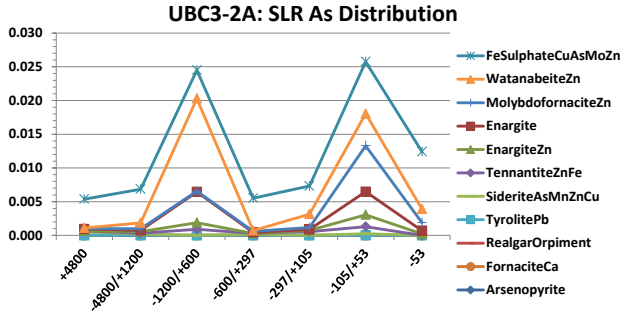
UBC3-2A: SLR As Distribution
0.030
0.025
0.020
0.015
0.010
0.005
0.000
+4800
-4800/+1200
-1200/+600
-600/+297
-297/+105
-105/+53
-53
FeSulphateCuAsMoZn
WatanabeiteZn
MolybdofornaciteZn
Enargite
EnargiteZn
TennantiteZnFe
SideriteAsMnZnCu
TyrolitePb
RealgarOrpiment
FornaciteCa
Arsenopyrite

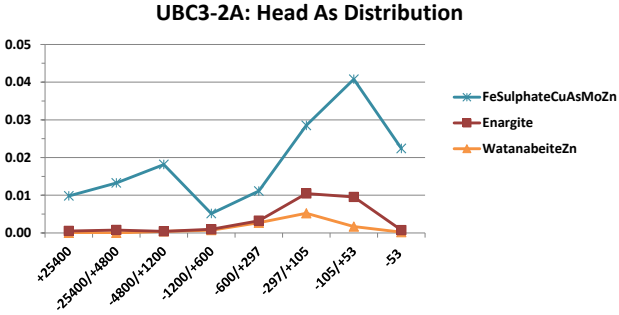
UBC3-2A: Head As Distribution
0.05
0.04
0.03
0.02
0.01
0.00
+25400
-25400/+4800
-4800/+1200
-1200/+600
-600/+297
-297/+105
-105/+53
-53
FeSulphateCuAsMoZn
Enargite
WatanabeiteZn

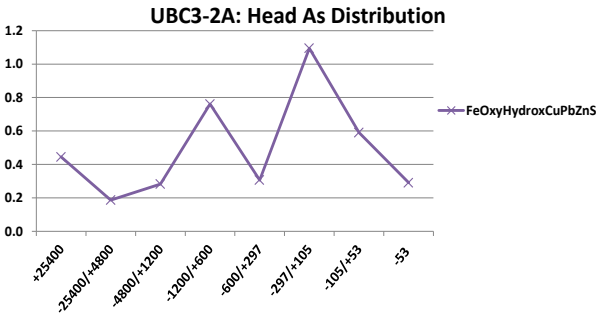
UBC3-2A: Head As Distribution
1.2
1.0
0.8
0.6
0.4
0.2
0.0
+25400
-25400/+4800
-4800/+1200
-1200/+600
-600/+297
-297/+105
-105/+53
-53
FeOxyHydroxCuPbZnS

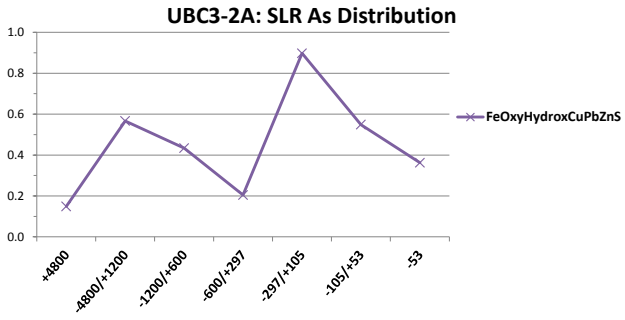
UBC3-2A: SLR As Distribution
1.0
0.8
0.6
0.4
0.2
0.0
+4800
-4800/+1200
-1200/+600
-600/+297
-297/+105
-105/+53
-53
FeOxyHydroxCuPbZnS

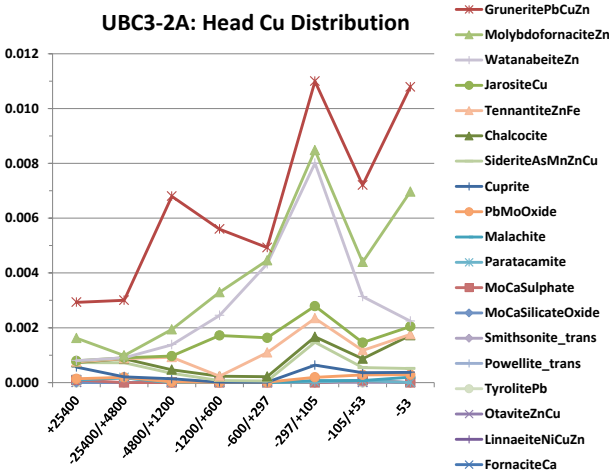
UBC3-2A: Head Cu Distribution
0.012
0.010
0.008
0.006
0.004
0.002
0.000
+25400
-25400/+4800
-4800/+1200
-1200/+600
-600/+297
-297/+105
-105/+53
-53
GruneritePbCuZn
MolybdofornaciteZn
WatanabeiteZn
JarositeCu
TennantiteZnFe
Chalcocite
SideriteAsMnZnCu
Cuprite
PbMoOxide
Malachite
Paratacamite
MoCaSulphate
MoCaSilicateOxide
Smithsonite_trans
Powellite_trans
TyrolitePb
OtaviteZnCu
LinnaeiteNiCuZn
FornaciteCa

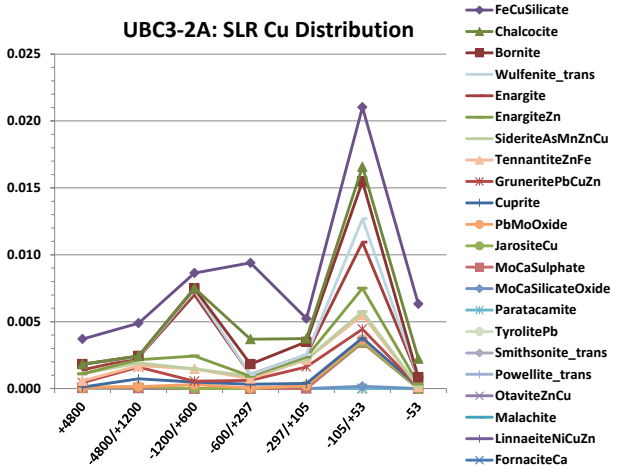
UBC3-2A: SLR Cu Distribution
0.025
0.020
0.015
0.010
0.005
0.000
+4800
-4800/+1200
-1200/+600
-600/+297
-297/+105
-105/+53
-53
FeCuSilicate
Chalcocite
Bornite
Wulfenite_trans
Enargite
EnargiteZn
SideriteAsMnZnCu
TennantiteZnFe
GruneritePbCuZn
Cuprite
PbMoOxide
JarositeCu
MoCaSulphate
MoCaSilicateOxide
Paratacamite
TyrolitePb
Smithsonite_trans
Powellite_trans
OtaviteZnCu
Malachite
LinnaeiteNiCuZn
FornaciteCa

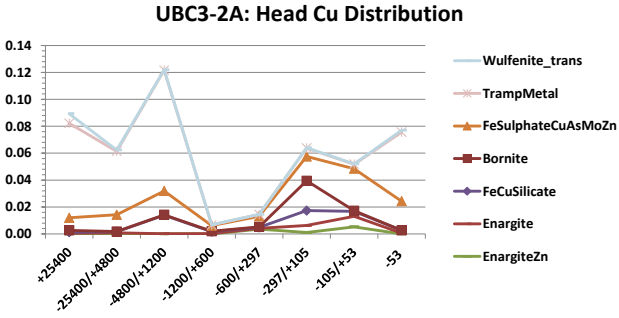
UBC3-2A: Head Cu Distribution
0.14
0.12
0.10
0.08
0.06
0.04
0.02
0.00
+25400
-25400/+4800
-4800/+1200
-1200/+600
-600/+297
-297/+105
-105/+53
-53
Wulfenite_trans
TrampMetal
FeSulphateCuAsMoZn
Bornite
FeCuSilicate
Enargite
EnargiteZn

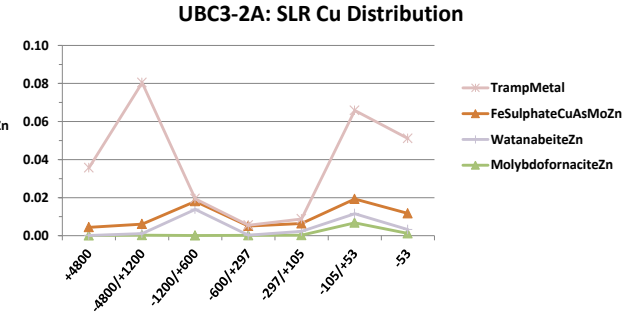
UBC3-2A: SLR Cu Distribution
0.10
0.08
0.06
0.04
0.02
0.00
+4800
-4800/+1200
-1200/+600
-600/+297
-297/+105
-105/+53
-53
TrampMetal
FeSulphateCuAsMoZn
WatanabeiteZn
MolybdofornaciteZn

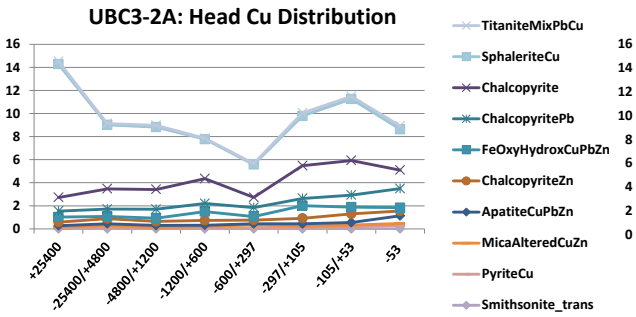
UBC3-2A: Head Cu Distribution
16
14
12
10
8
6
4
2
0
+25400
-25400/+4800
-4800/+1200
-1200/+600
-600/+297
-297/+105
-105/+53
-53
TitaniteMixPbCu
SphaleriteCu
Chalcopyrite
ChalcopyritePb
FeOxyHydroxCuPbZn
ChalcopyriteZn
ApatiteCuPbZn
MicaAlteredCuZn
PyriteCu
Smithsonite_trans

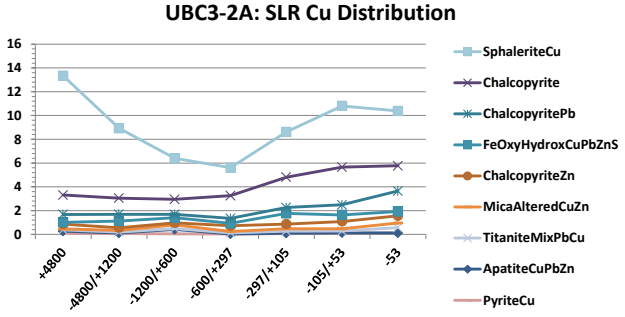
UBC3-2A: SLR Cu Distribution
16
14
12
10
8
6
4
2
0
+4800
-4800/+1200
-1200/+600
-600/+297
-297/+105
-105/+53
-53
SphaleriteCu
Chalcopyrite
ChalcopyritePb
FeOxyHydroxCuPbZnS
ChalcopyriteZn
MicaAlteredCuZn
TitaniteMixPbCu
ApatiteCuPbZn
PyriteCu

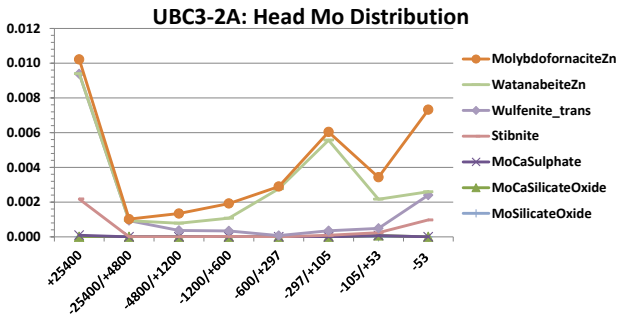
UBC3-2A: Head Mo Distribution
0.012
0.010
0.008
0.006
0.004
0.002
0.000
+25400
-25400/+4800
-4800/+1200
-1200/+600
-600/+297
-297/+105
-105/+53
-53
MolybdofornaciteZn
WatanabeiteZn
Wulfenite_trans
Stibnite
MoCaSulphate
MoCaSilicateOxide
MoSilicateOxide

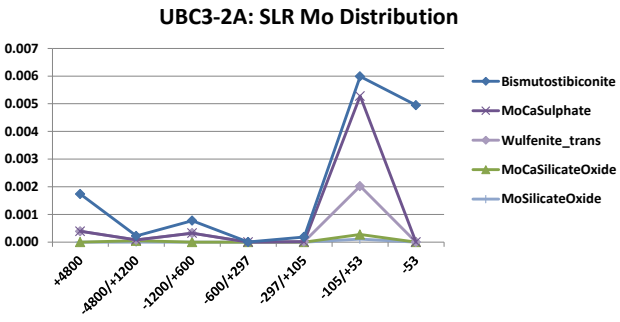
UBC3-2A: SLR Mo Distribution
0.007
0.006
0.005
0.004
0.003
0.002
0.001
0.000
+4800
-4800/+1200
-1200/+600
-600/+297
-297/+105
-105/+53
-53
Bismutostibiconite
MoCaSulphate
Wulfenite_trans
MoCaSilicateOxide
MoSilicateOxide

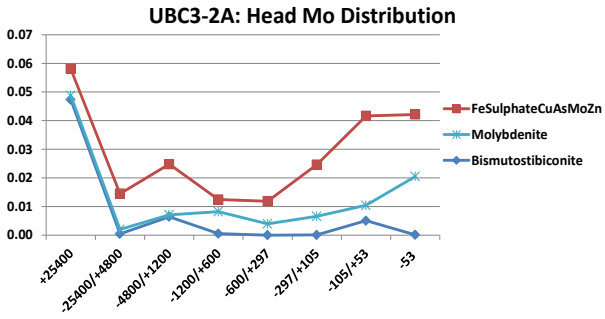
UBC3-2A: Head Mo Distribution
0.07
0.06
0.05
0.04
0.03
0.02
0.01
0.00
+25400
-25400/+4800
-4800/+1200
-1200/+600
-600/+297
-297/+105
-105/+53
-53
FeSulphateCuAsMoZn
Molybdenite
Bismutostibiconite

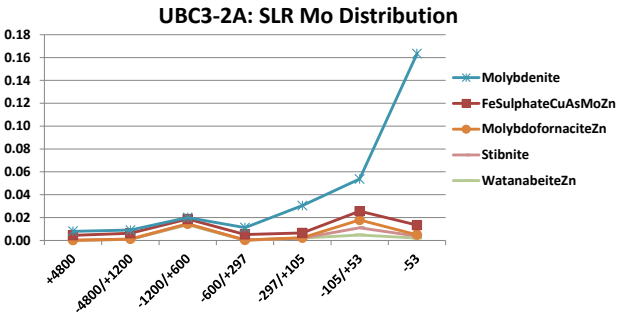
UBC3-2A: SLR Mo Distribution
0.18
0.16
0.14
0.12
0.10
0.08
0.06
0.04
0.02
0.00
+4800
-4800/+1200
-1200/+600
-600/+297
-297/+105
-105/+53
-53
Molybdenite
FeSulphateCuAsMoZn
MolybdofornaciteZn
Stibnite
WatanabeiteZn

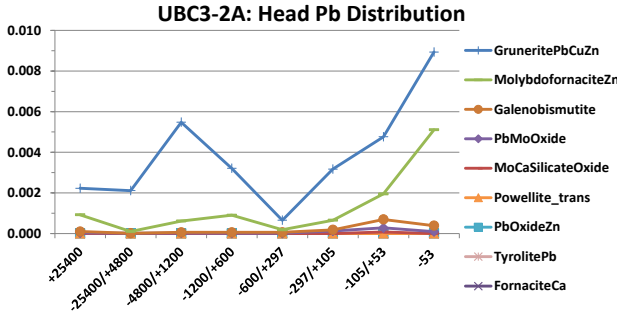
UBC3-2A: Head Pb Distribution
0.010
0.008
0.006
0.004
0.002
0.000
+25400
-25400/+4800
-4800/+1200
-1200/+600
-600/+297
-297/+105
-105/+53
-53
GruneritePbCuZn
MolybdofornaciteZn
Galenobismutite
PbMoOxide
MoCaSilicateOxide
Powellite_trans
PbOxideZn
TyrolitePb
FornaciteCa

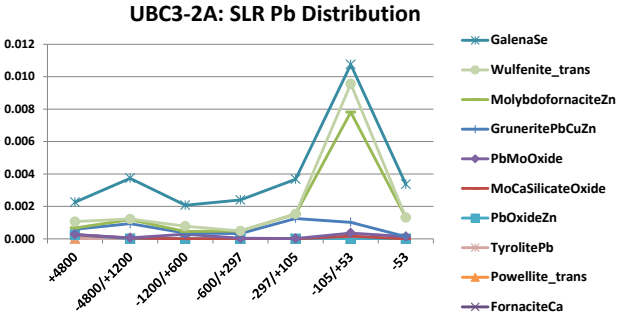
UBC3-2A: SLR Pb Distribution
0.012
0.010
0.008
0.006
0.004
0.002
0.000
+4800
-4800/+1200
-1200/+600
-600/+297
-297/+105
-105/+53
-53
GalenaSe
Wulfenite_trans
MolybdofornaciteZn
GruneritePbCuZn
PbMoOxide
MoCaSilicateOxide
PbOxideZn
TyrolitePb
Powellite_trans
FornaciteCa

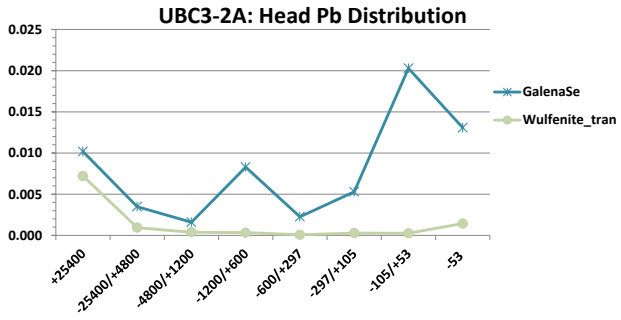
UBC3-2A: Head Pb Distribution
0.025
0.020
0.015
0.010
0.005
0.000
+25400
-25400/+4800
-4800/+1200
-1200/+600
-600/+297
-297/+105
-105/+53
-53
GalenaSe
Wulfenite_tran

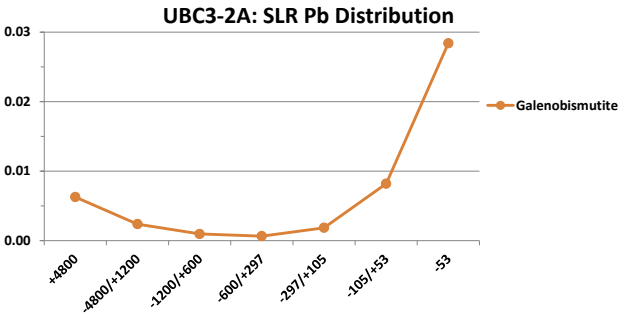
UBC3-2A: SLR Pb Distribution
0.03
0.02
0.01
0.00
+4800
-4800/+1200
-1200/+600
-600/+297
-297/+105
-105/+53
-53
Galenobismutite

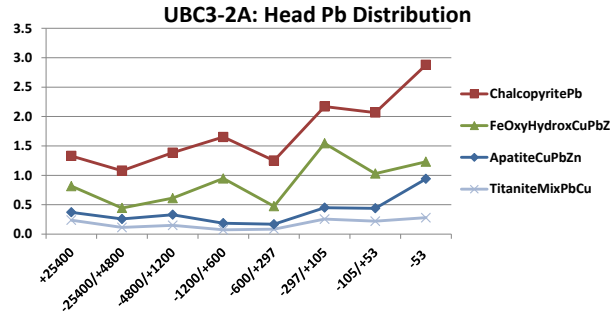
UBC3-2A: Head Pb Distribution
3.5
3.0
2.5
2.0
1.5
1.0
0.5
0.0
+25400
-25400/+4800
-4800/+1200
-1200/+600
-600/+297
-297/+105
-105/+53
-53
ChalcopyritePb
FeOxyHydroxCuPbZ
ApatiteCuPbZn
TitaniteMixPbCu

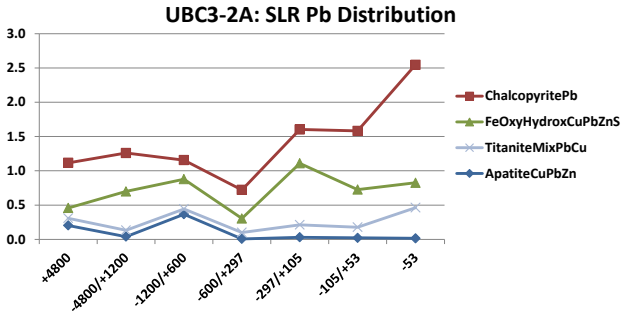
UBC3-2A: SLR Pb Distribution
3.0
2.5
2.0
1.5
1.0
0.5
0.0
+4800
-4800/+1200
-1200/+600
-600/+297
-297/+105
-105/+53
-53
ChalcopyritePb
FeOxyHydroxCuPbZnS
TitaniteMixPbCu
ApatiteCuPbZn

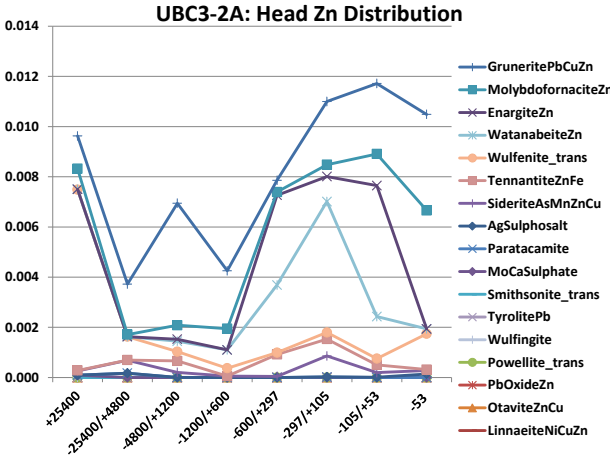
UBC3-2A: Head Zn Distribution
0.014
0.012
0.010
0.008
0.006
0.004
0.002
0.000
+25400
-25400/+4800
-4800/+1200
-1200/+600
-600/+297
-297/+105
-105/+53
-53
GruneritePbCuZn
MolybdofornaciteZr
EnargiteZn
WatanabeiteZn
Wulfenite_trans
TennantiteZnFe
SideriteAsMnZnCu
AgSulphosalt
Paratacamite
MoCaSulphate
Smithsonite_trans
TyrolitePb
Wulfingite
Powellite_trans
PbOxideZn
OtaviteZnCu
LinnaeiteNiCuZn

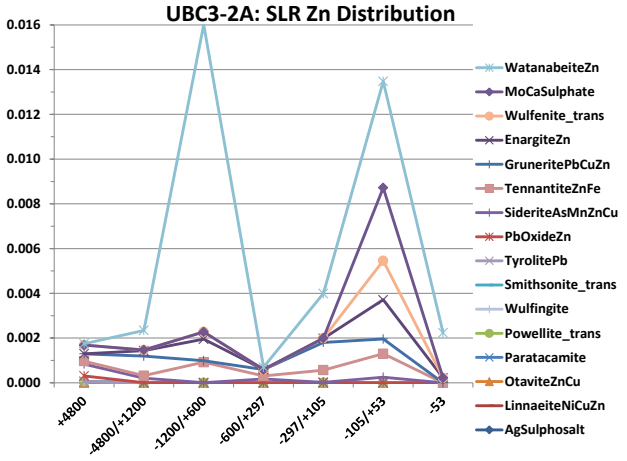
UBC3-2A: SLR Zn Distribution
0.016
0.014
0.012
0.010
0.008
0.006
0.004
0.002
0.000
+4800
-4800/+1200
-1200/+600
-600/+297
-297/+105
-105/+53
-53
WatanabeiteZn
MoCaSulphate
Wulfenite_trans
EnargiteZn
GruneritePbCuZn
TennantiteZnFe
SideriteAsMnZnCu
PbOxideZn
TyrolitePb
Smithsonite_trans
Wulfingite
Powellite_trans
Paratacamite
OtaviteZnCu
LinnaeiteNiCuZn
AgSulphosalt

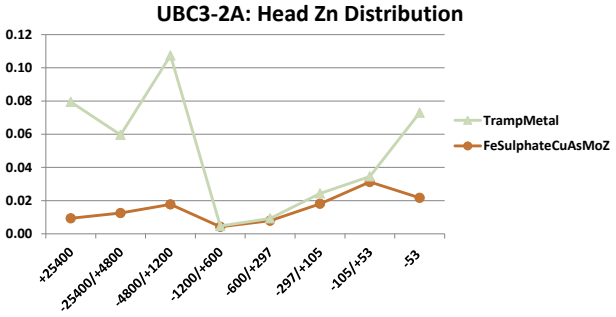
UBC3-2A: Head Zn Distribution
0.12
0.10
0.08
0.06
0.04
0.02
0.00
+25400
-25400/+4800
-4800/+1200
-1200/+600
-600/+297
-297/+105
-105/+53
-53
TrampMetal
FeSulphateCuAsMoZ

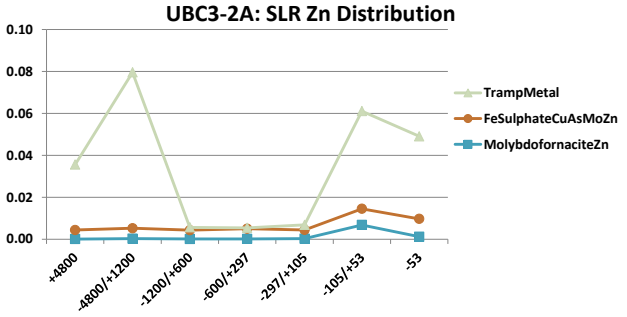
UBC3-2A: SLR Zn Distribution
0.10
0.08
0.06
0.04
0.02
0.00
+4800
-4800/+1200
-1200/+600
-600/+297
-297/+105
-105/+53
-53
TrampMetal
FeSulphateCuAsMoZn
MolybdofornaciteZn

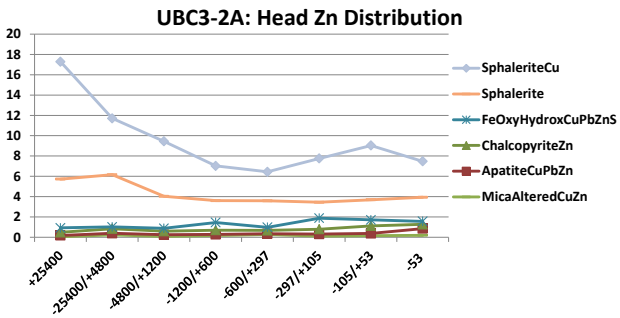
UBC3-2A: Head Zn Distribution
20
18
16
14
12
10
8
6
4
2
0
+25400
-25400/+4800
-4800/+1200
-1200/+600
-600/+297
-297/+105
-105/+53
-53
SphaleriteCu
Sphalerite
FeOxyHydroxCuPbZnS
ChalcopyriteZn
ApatiteCuPbZn
MicaAlteredCuZn

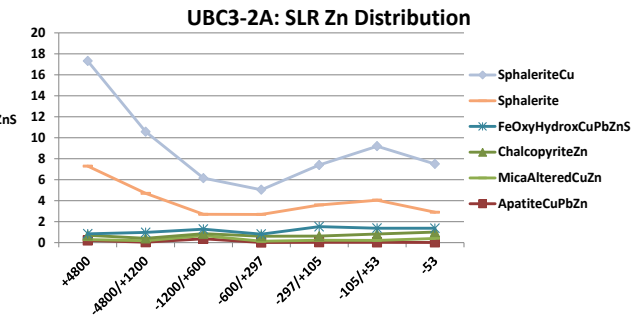
UBC3-2A: SLR Zn Distribution
20
18
16
14
12
10
8
6
4
2
0
+4800
-4800/+1200
-1200/+600
-600/+297
-297/+105
-105/+53
-53
SphaleriteCu
Sphalerite
FeOxyHydroxCuPbZnS
ChalcopyriteZn
MicaAlteredCuZn
ApatiteCuPbZn

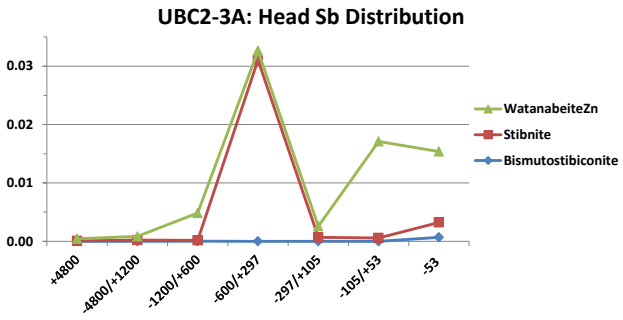
UBC2-3A: Head Sb Distribution
0.03
0.02
0.01
0.00
+4800
-4800/+1200
-1200/+600
-600/+297
-297/+105
-105/+53
-53
WatanabeiteZn
Stibnite
Bismutostibiconite

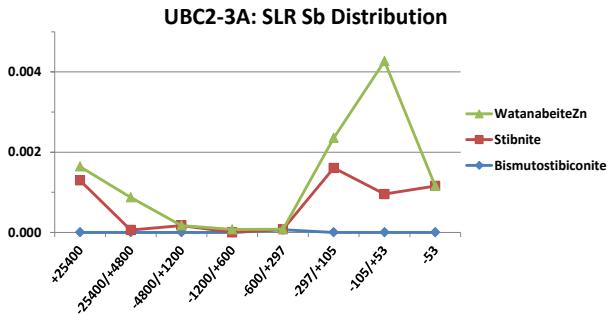
UBC2-3A: SLR Sb Distribution
0.004
0.002
0.000
+25400
-25400/+4800
-4800/+1200
-1200/+600
-600/+297
-297/+105
-105/+53
-53
WatanabeiteZn
Stibnite
Bismutostibiconite

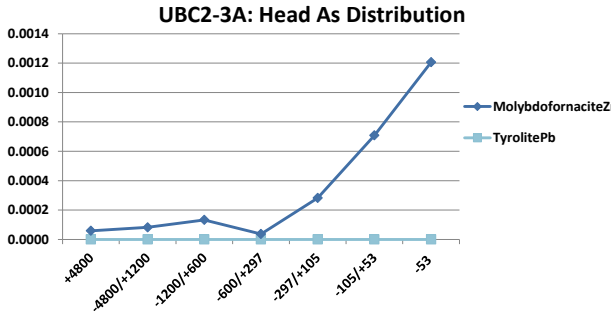
UBC2-3A: Head As Distribution
0.0014
0.0012
0.0010
0.0008
0.0006
0.0004
0.0002
0.0000
+4800
-4800/+1200
-1200/+600
-600/+297
-297/+105
-105/+53
-53
MolybdofornaciteZ
TyrolitePb

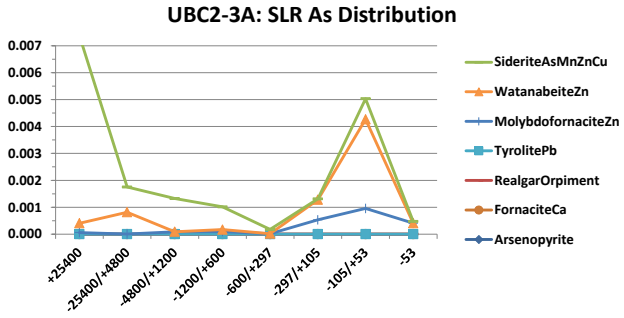
UBC2-3A: SLR As Distribution
0.007
0.006
0.005
0.004
0.003
0.002
0.001
0.000
+25400
-25400/+4800
-4800/+1200
-1200/+600
-600/+297
-297/+105
-105/+53
-53
SideriteAsMnZnCu
WatanabeiteZn
MolybdofornaciteZn
TyrolitePb
RealgarOrpiment
FornaciteCa
Arsenopyrite

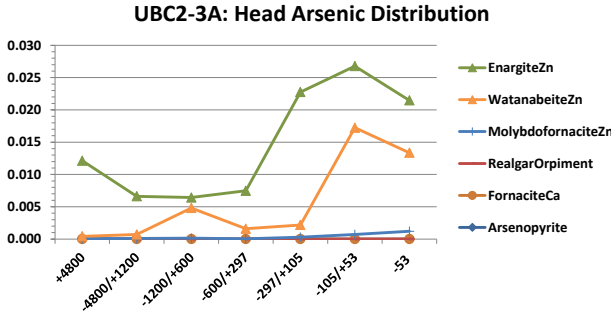
UBC2-3A: Head Arsenic Distribution
0.030
0.025
0.020
0.015
0.010
0.005
0.000
+4800
-4800/+1200
-1200/+600
-600/+297
-297/+105
-105/+53
-53
EnargiteZn
WatanabeiteZn
MolybdofornaciteZn
RealgarOrpiment
FornaciteCa
Arsenopyrite

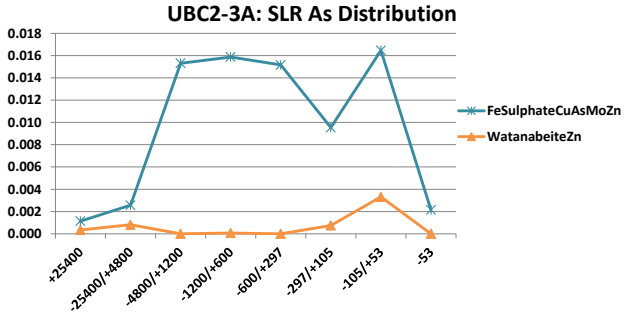
UBC2-3A: SLR As Distribution
0.018
0.016
0.014
0.012
0.010
0.008
0.006
0.004
0.002
0.000
+25400
-25400/+4800
-4800/+1200
-1200/+600
-600/+297
-297/+105
-105/+53
-53
FeSulphateCuAsMoZn
WatanabeiteZn

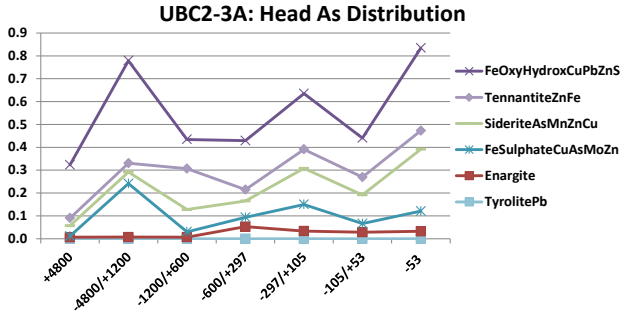
UBC2-3A: Head As Distribution
0.9
0.8
0.7
0.6
0.5
0.4
0.3
0.2
0.1
0.0
+4800
-4800/+1200
-1200/+600
-600/+297
-297/+105
-105/+53
-53
FeOxyHydroxCuPbZnS
TennantiteZnFe
SideriteAsMnZnCu
FeSulphateCuAsMoZn
Enargite
TyrolitePb

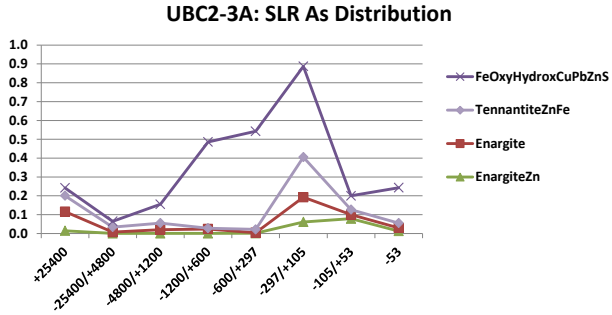
UBC2-3A: SLR As Distribution
1.0
0.9
0.8
0.7
0.6
0.5
0.4
0.3
0.2
0.1
0.0
+25400
-25400/+4800
-4800/+1200
-1200/+600
-600/+297
-297/+105
-105/+53
-53
FeOxyHydroxCuPbZnS
TennantiteZnFe
Enargite
EnargiteZn

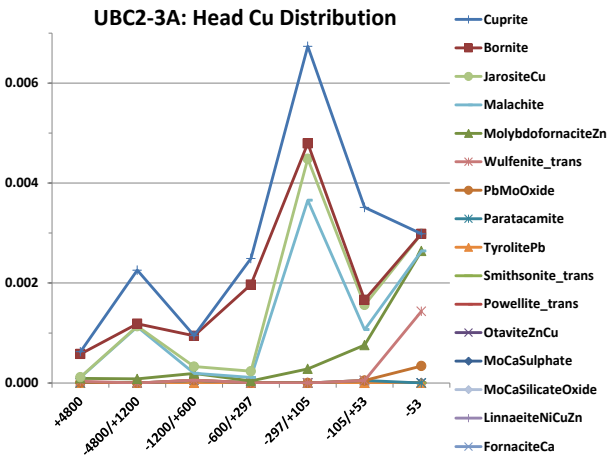
UBC2-3A: Head Cu Distribution
0.006
0.004
0.002
0.000
+4800
-4800/+1200
-1200/+600
-600/+297
-297/+105
-105/+53
-53
Cuprite
Bornite
JarositeCu
Malachite
MolybdofornaciteZn
Wulfenite_trans
PbMoOxide
Paratacamite
TyrolitePb
Smithsonite_trans
Powellite_trans
OtaviteZnCu
MoCaSulphate
MoCaSilicateOxide
LinnaeiteNiCuZn
FornaciteCa

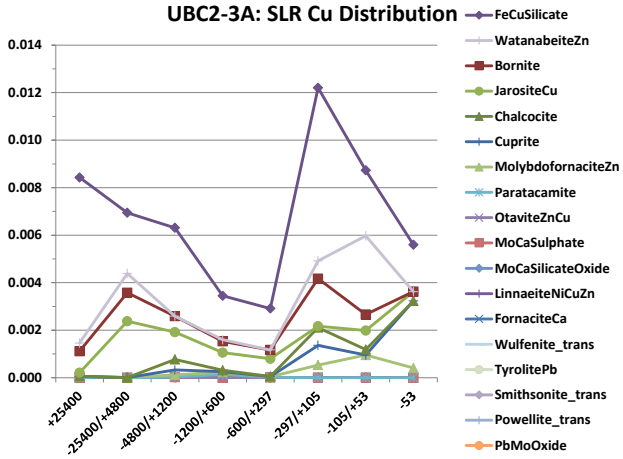
UBC2-3A: SLR Cu Distribution
0.014
0.012
0.010
0.008
0.006
0.004
0.002
0.000
+25400
-25400/+4800
-4800/+1200
-1200/+600
-600/+297
-297/+105
-105/+53
-53
FeCuSilicate
WatanabeiteZn
Bornite
JarositeCu
Chalcocite
Cuprite
MolybdofornaciteZn
Paratacamite
OtaviteZnCu
MoCaSulphate
MoCaSilicateOxide
LinnaeiteNiCuZn
FornaciteCa
Wulfenite_trans
TyrolitePb
Smithsonite_trans
Powellite_trans
PbMoOxide

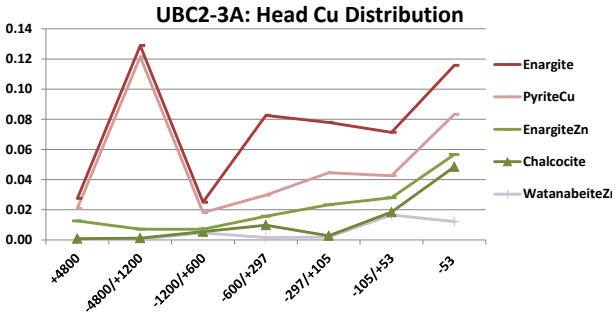
UBC2-3A: Head Cu Distribution
0.14
0.12
0.10
0.08
0.06
0.04
0.02
0.00
+4800
-4800/+1200
-1200/+600
-600/+297
-297/+105
-105/+53
-53
Enargite
PyriteCu
EnargiteZn
Chalcocite
WatanabeiteZ

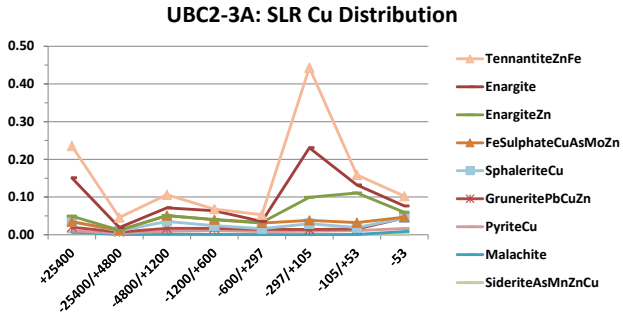
UBC2-3A: SLR Cu Distribution
0.50
0.40
0.30
0.20
0.10
0.00
+25400
-25400/+4800
-4800/+1200
-1200/+600
-600/+297
-297/+105
-105/+53
-53
TennantiteZnFe
Enargite
EnargiteZn
FeSulphateCuAsMoZn
SphaleriteCu
GruneritePbCuZn
PyriteCu
Malachite
SideriteAsMnZnCu

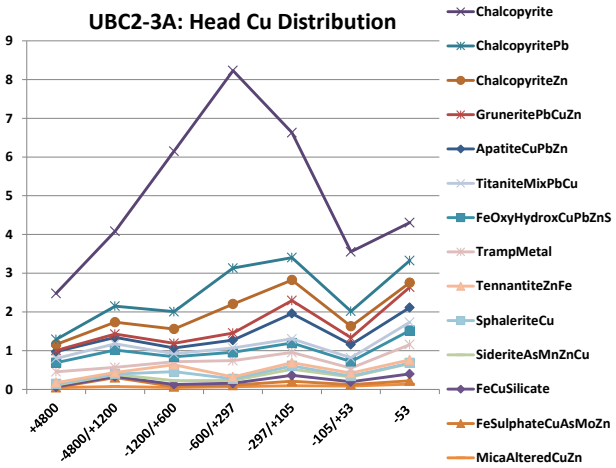
UBC2-3A: Head Cu Distribution
9
8
7
6
5
4
3
2
1
0
+4800
-4800/+1200
-1200/+600
-600/+297
-297/+105
-105/+53
-53
Chalcopyrite
ChalcopyritePb
ChalcopyriteZn
GruneritePbCuZn
ApatiteCuPbZn
TitaniteMixPbCu
FeOxyHydroxCuPbZnS
TrampMetal
TennantiteZnFe
SphaleriteCu
SideriteAsMnZnCu
FeCuSilicate
FeSulphateCuAsMoZn
MicaAlteredCuZn

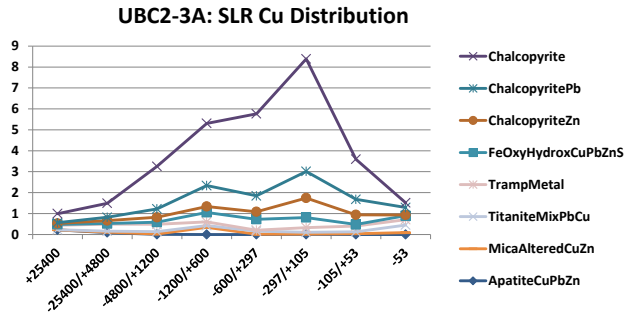
UBC2-3A: SLR Cu Distribution
9
8
7
6
5
4
3
2
1
0
+25400
-25400/+4800
-4800/+1200
-1200/+600
-600/+297
-297/+105
-105/+53
-53
Chalcopyrite
ChalcopyritePb
ChalcopyriteZn
FeOxyHydroxCuPbZnS
TrampMetal
TitaniteMixPbCu
MicaAlteredCuZn
ApatiteCuPbZn

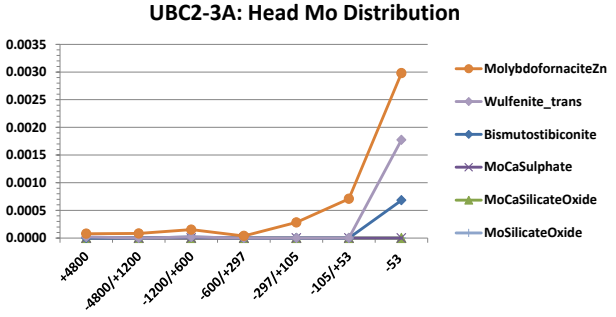
UBC2-3A: Head Mo Distribution
0.0035
0.0030
0.0025
0.0020
0.0015
0.0010
0.0005
0.0000
+4800
-4800/+1200
-1200/+600
-600/+297
-297/+105
-105/+53
-53
MolybdofornaciteZn
Wulfenite_trans
Bismutostibiconite
MoCaSulphate
MoCaSilicateOxide
MoSilicateOxide

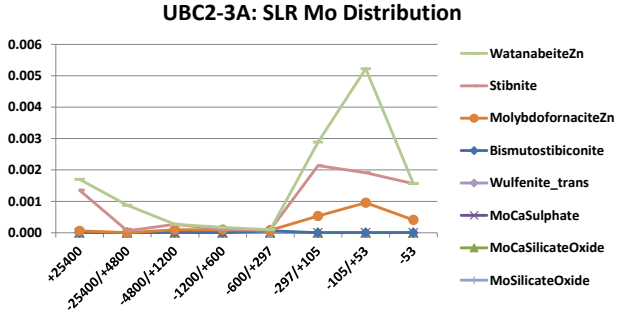
UBC2-3A: SLR Mo Distribution
0.006
0.005
0.004
0.003
0.002
0.001
0.000
+25400
-25400/+4800
-4800/+1200
-1200/+600
-600/+297
-297/+105
-105/+53
-53
WatanabeiteZn
Stibnite
MolybdofornaciteZn
Bismutostibiconite
Wulfenite_trans
MoCaSulphate
MoCaSilicateOxide
MoSilicateOxide

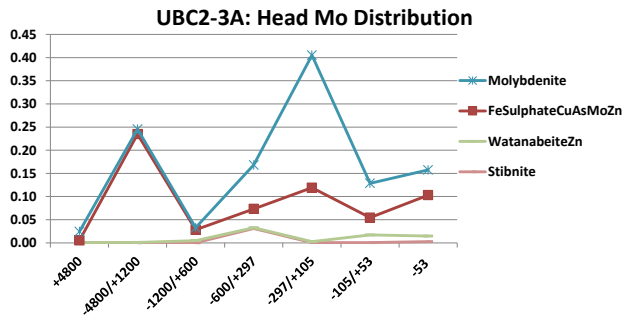
UBC2-3A: Head Mo Distribution
0.45
0.40
0.35
0.30
0.25
0.20
0.15
0.10
0.05
0.00
+4800
-4800/+1200
-1200/+600
-600/+297
-297/+105
-105/+53
-53
Molybdenite
FeSulphateCuAsMoZn
WatanabeiteZn
Stibnite

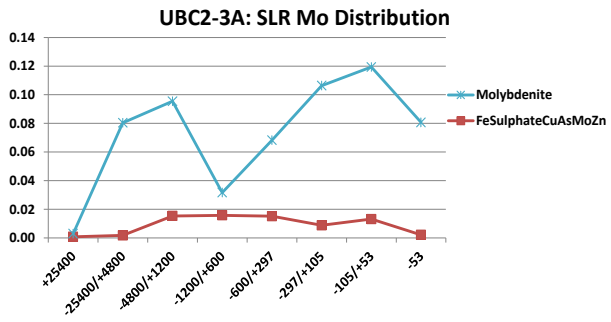
UBC2-3A: SLR Mo Distribution
0.14
0.12
0.10
0.08
0.06
0.04
0.02
0.00
+25400
-25400/+4800
-4800/+1200
-1200/+600
-600/+297
-297/+105
-105/+53
-53
Molybdenite
FeSulphateCuAsMoZn

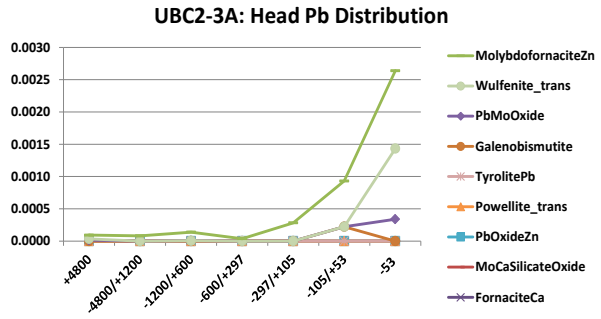
UBC2-3A: Head Pb Distribution
0.0030
0.0025
0.0020
0.0015
0.0010
0.0005
0.0000
+4800
-4800/+1200
-1200/+600
-600/+297
-297/+105
-105/+53
-53
MolybdofornaciteZn
Wulfenite_trans
PbMoOxide
Galenobismutite
TyrolitePb
Powellite_trans
PbOxideZn
MoCaSilicateOxide
FornaciteCa

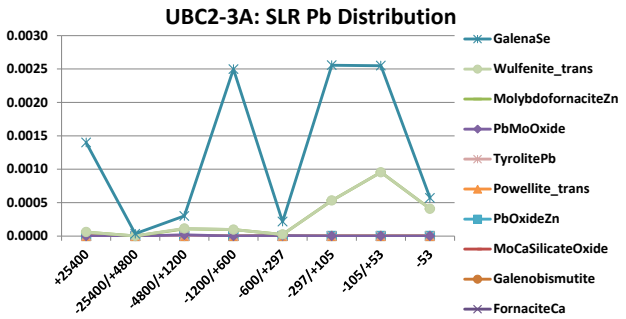
UBC2-3A: SLR Pb Distribution
0.0030
0.0025
0.0020
0.0015
0.0010
0.0005
0.0000
+25400
-25400/+4800
-4800/+1200
-1200/+600
-600/+297
-297/+105
-105/+53
-53
GalenaSe
Wulfenite_trans
MolybdofornaciteZn
PbMoOxide
TyrolitePb
Powellite_trans
PbOxideZn
MoCaSilicateOxide
Galenobismutite
FornaciteCa

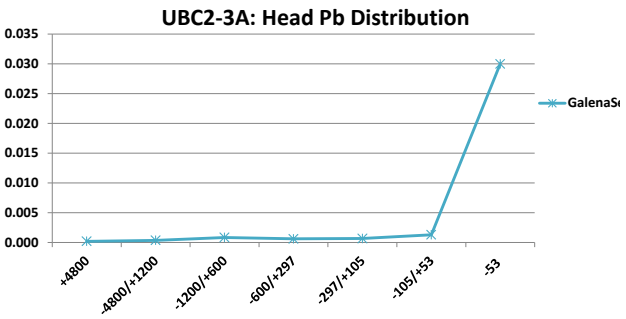
UBC2-3A: Head Pb Distribution
0.035
0.030
0.025
0.020
0.015
0.010
0.005
0.000
+4800
-4800/+1200
-1200/+600
-600/+297
-297/+105
-105/+53
-53
GalenaSe

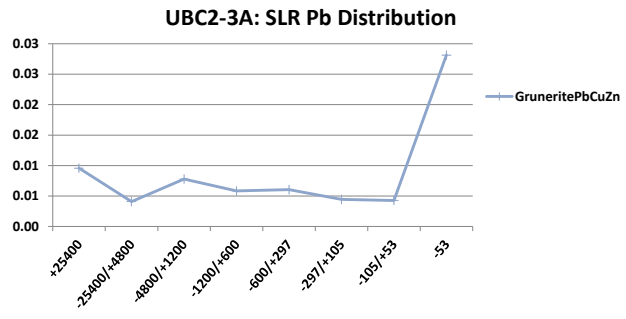
UBC2-3A: SLR Pb Distribution
0.03
0.03
0.02
0.02
0.01
0.01
0.00
+25400
-25400/+4800
-4800/+1200
-1200/+600
-600/+297
-297/+105
-105/+53
-53
GruneritePbCuZn

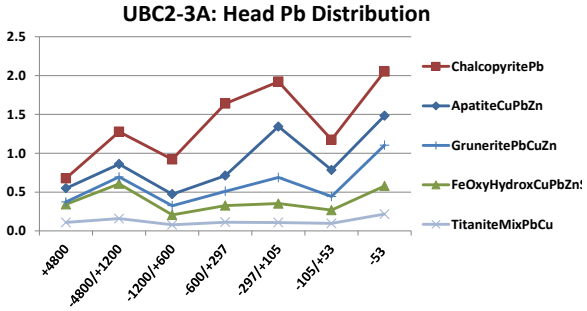
UBC2-3A: Head Pb Distribution
2.5
2.0
1.5
1.0
0.5
0.0
+4800
-4800/+1200
-1200/+600
-600/+297
-297/+105
-105/+53
-53
ChalcopyritePb
ApatiteCuPbZn
GruneritePbCuZn
FeOxyHydroxCuPbZnS
TitaniteMixPbCu

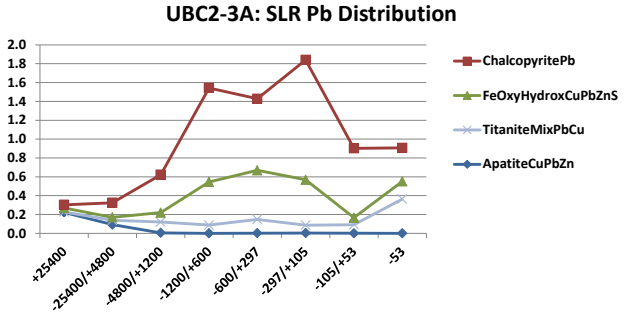
UBC2-3A: SLR Pb Distribution
2.0
1.8
1.6
1.4
1.2
1.0
0.8
0.6
0.4
0.2
0.0
+25400
-25400/+4800
-4800/+1200
-1200/+600
-600/+297
-297/+105
-105/+53
-53
ChalcopyritePb
FeOxyHydroxCuPbZnS
TitaniteMixPbCu
ApatiteCuPbZn

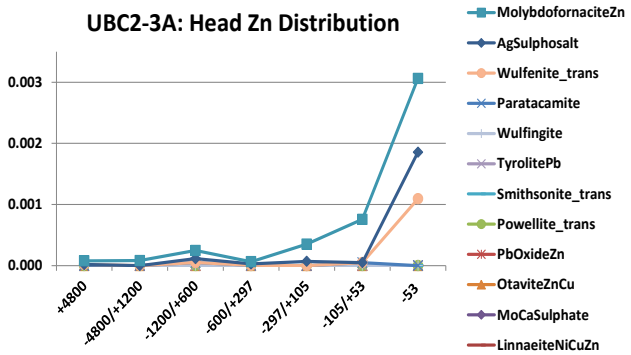
UBC2-3A: Head Zn Distribution
0.003
0.002
0.001
0.000
+4800
-4800/+1200
-1200/+600
-600/+297
-297/+105
-105/+53
-53
MolybdofornaciteZn
AgSulphosalt
Wulfenite_trans
Paratacamite
Wulfingite
TyrolitePb
Smithsonite_trans
Powellite_trans
PbOxideZn
OtaviteZnCu
MoCaSulphate
LinnaeiteNiCuZn

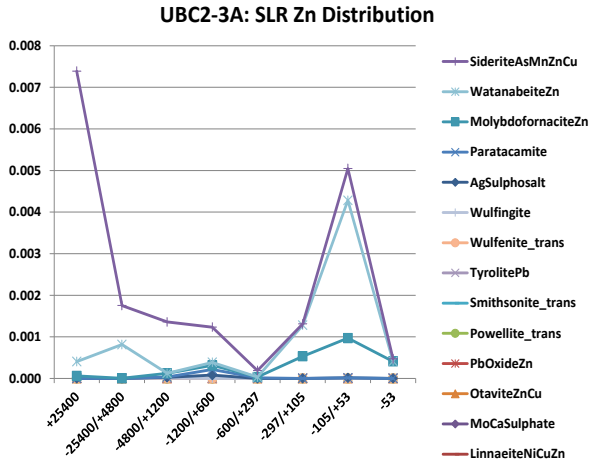
UBC2-3A: SLR Zn Distribution
0.008
0.007
0.006
0.005
0.004
0.003
0.002
0.001
0.000
+25400
-25400/+4800
-4800/+1200
-1200/+600
-600/+297
-297/+105
-105/+53
-53
SideriteAsMnZnCu
WatanabeiteZn
MolybdofornaciteZn
Paratacamite
AgSulphosalt
Wulfingite
Wulfenite_trans
TyrolitePb
Smithsonite_trans
Powellite_trans
PbOxideZn
OtaviteZnCu
MoCaSulphate
LinnaeiteNiCuZn

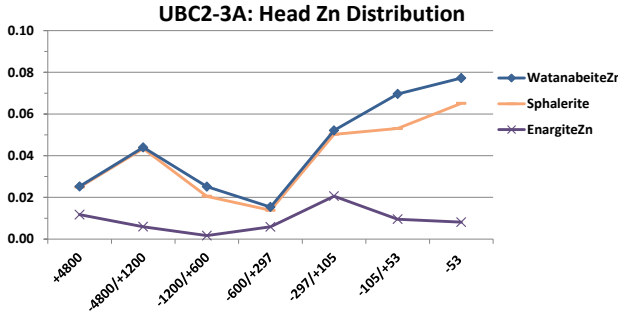
UBC2-3A: Head Zn Distribution
0.10
0.08
0.06
0.04
0.02
0.00
+4800
-4800/+1200
-1200/+600
-600/+297
-297/+105
-105/+53
-53
WatanabeiteZr
Sphalerite
EnargiteZn

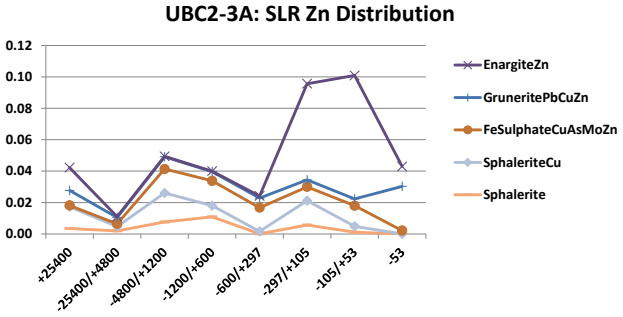
UBC2-3A: SLR Zn Distribution
0.12
0.10
0.08
0.06
0.04
0.02
0.00
+25400
-25400/+4800
-4800/+1200
-1200/+600
-600/+297
-297/+105
-105/+53
-53
EnargiteZn
GruneritePbCuZn
FeSulphateCuAsMoZn
SphaleriteCu
Sphalerite

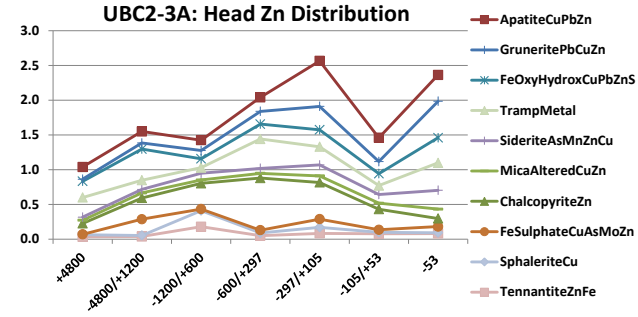
UBC2-3A: Head Zn Distribution
3.0
2.5
2.0
1.5
1.0
0.5
0.0
+4800
-4800/+1200
-1200/+600
-600/+297
-297/+105
-105/+53
-53
ApatiteCuPbZn
GruneritePbCuZn
FeOxyHydroxCuPbZnS
TrampMetal
SideriteAsMnZnCu
MicaAlteredCuZn
ChalcopyriteZn
FeSulphateCuAsMoZn
SphaleriteCu
TennantiteZnFe

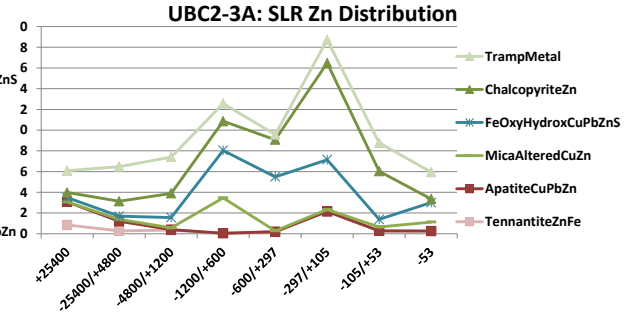
UBC2-3A: SLR Zn Distribution
0
8
6
4
2
0
8
6
4
2
0
+25400
-25400/+4800
-4800/+1200
-1200/+600
-600/+297
-297/+105
-105/+53
-53
TrampMetal
ChalcopyriteZn
FeOxyHydroxCuPbZnS
MicaAlteredCuZn
ApatiteCuPbZn
TennantiteZnFe

APPENDIX 17 Mineral Liberation Analyzer application: modal mineralogy based on grain size

Note: All plots derived from data collected from Table 3.2.4.

Particle size groupings within each submitted size fraction for each sample.

Legend refers to particle size grouping (millimeter).

Horizontal axis = size fraction (microns); Vertical axis = weight-% (normalized).

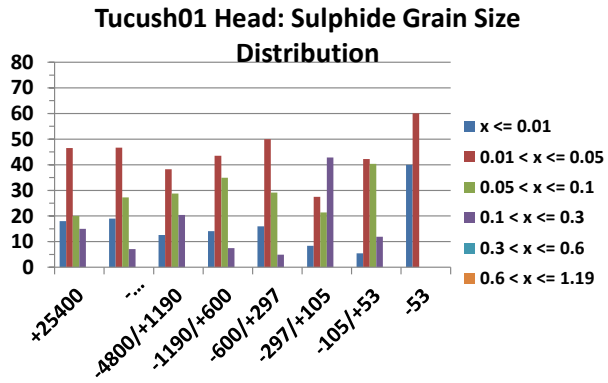

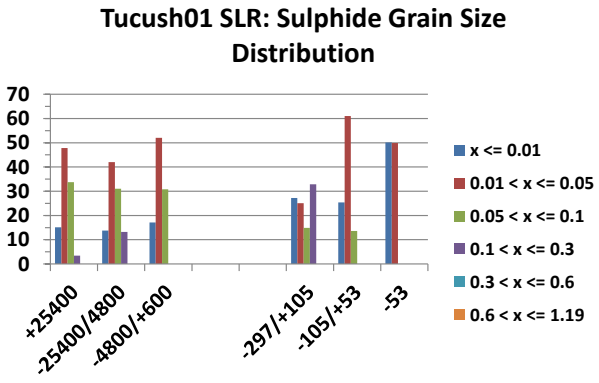

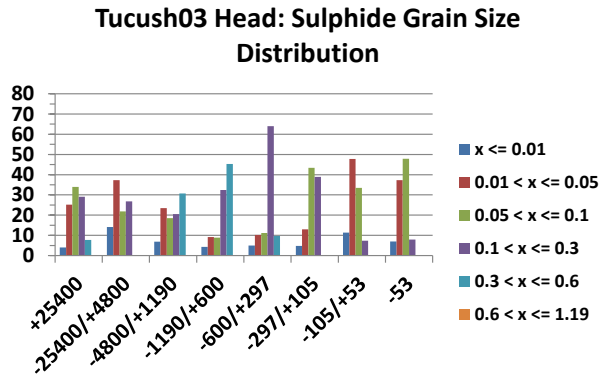

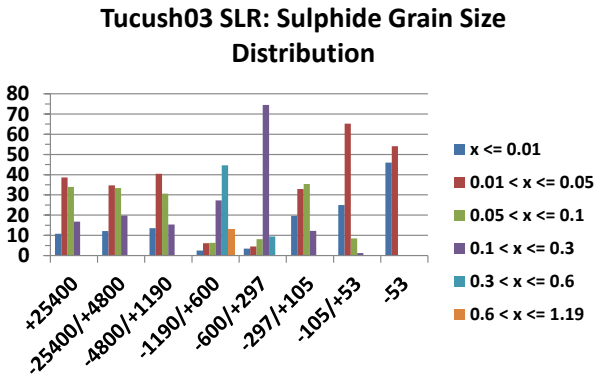

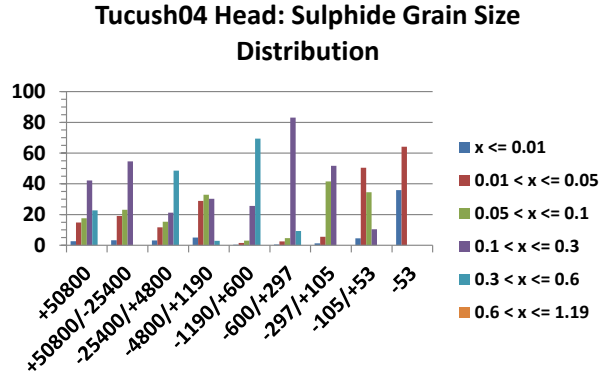

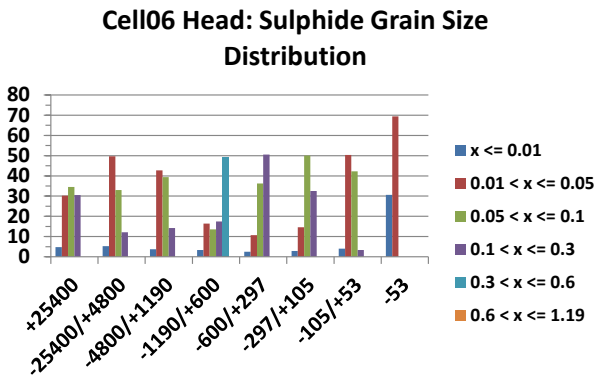
Cell06 Head: Sulphide Grain Size Distribution
80
70
60
50
40
30
20
10
0
+25400
-25400/+4800
-4800/+1190
-1190/+600
-600/+297
-297/+105
-105/+53
-53
x <= 0.01
0.01 < x <= 0.05
0.05 < x <= 0.1
0.1 < x <= 0.3
0.3 < x <= 0.6
0.6 < x <= 1.19

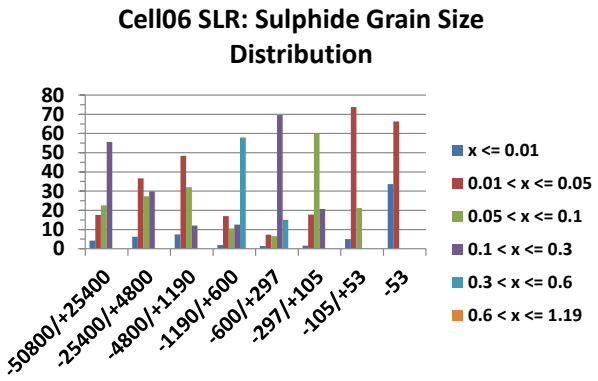
Cell06 SLR: Sulphide Grain Size Distribution
80
70
60
50
40
30
20
10
0
-50800/+25400
-25400/+4800
-4800/+1190
-1190/+600
-600/+297
-297/+105
-105/+53
-53
x <= 0.01
0.01 < x <= 0.05
0.05 < x <= 0.1
0.1 < x <= 0.3
0.3 < x <= 0.6
0.6 < x <= 1.19

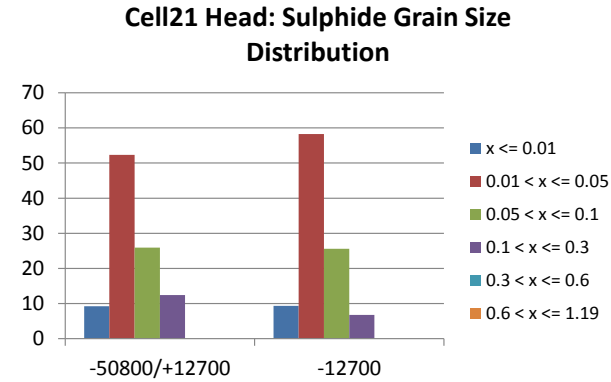
Cell21 Head: Sulphide Grain Size Distribution
70
60
50
40
30
20
10
0
-50800/+12700
-12700
x <= 0.01
0.01 < x <= 0.05
0.05 < x <= 0.1
0.1 < x <= 0.3
0.3 < x <= 0.6
0.6 < x <= 1.19

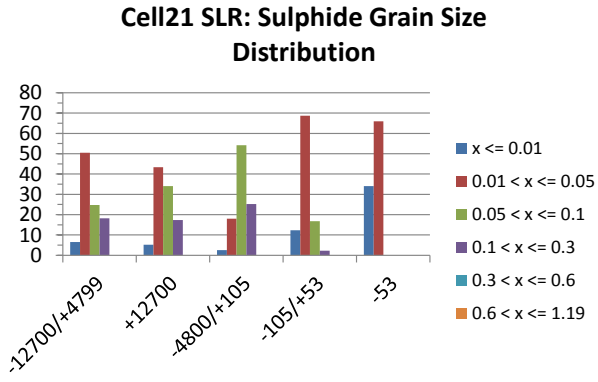
Cell21 SLR: Sulphide Grain Size Distribution
80
70
60
50
40
30
20
10
0
-12700/+4799
+12700
-4800/+105
-105/+53
-53
x <= 0.01
0.01 < x <= 0.05
0.05 < x <= 0.1
0.1 < x <= 0.3
0.3 < x <= 0.6
0.6 < x <= 1.19

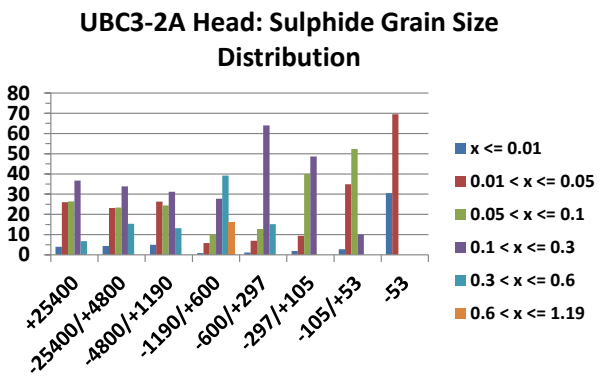
UBC3-2A Head: Sulphide Grain Size Distribution
80
70
60
50
40
30
20
10
0
+25400
-25400/+4800
-4800/+1190
-1190/+600
-600/+297
-297/+105
-105/+53
-53
x <= 0.01
0.01 < x <= 0.05
0.05 < x <= 0.1
0.1 < x <= 0.3
0.3 < x <= 0.6
0.6 < x <= 1.19

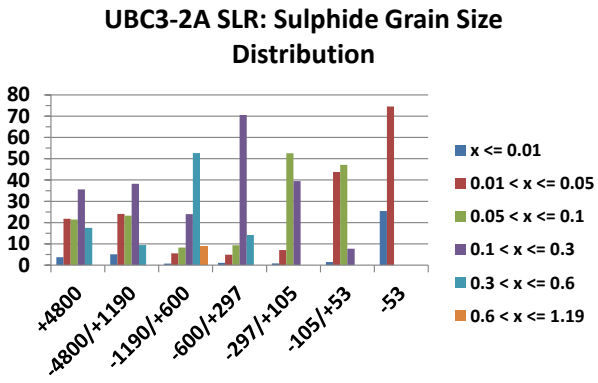
UBC3-2A SLR: Sulphide Grain Size Distribution
80
70
60
50
40
30
20
10
0
+4800
-4800/+1190
-1190/+600
-600/+297
-297/+105
-105/+53
-53
x <= 0.01
0.01 < x <= 0.05
0.05 < x <= 0.1
0.1 < x <= 0.3
0.3 < x <= 0.6
0.6 < x <= 1.19

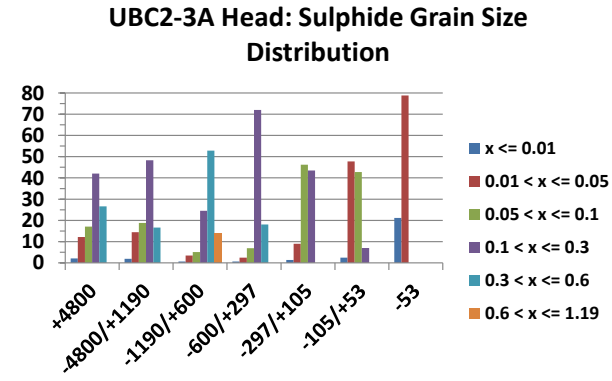
UBC2-3A Head: Sulphide Grain Size Distribution
80
70
60
50
40
30
20
10
0
+4800
-4800/+1190
-1190/+600
-600/+297
-297/+105
-105/+53
-53
x <= 0.01
0.01 < x <= 0.05
0.05 < x <= 0.1
0.1 < x <= 0.3
0.3 < x <= 0.6
0.6 < x <= 1.19

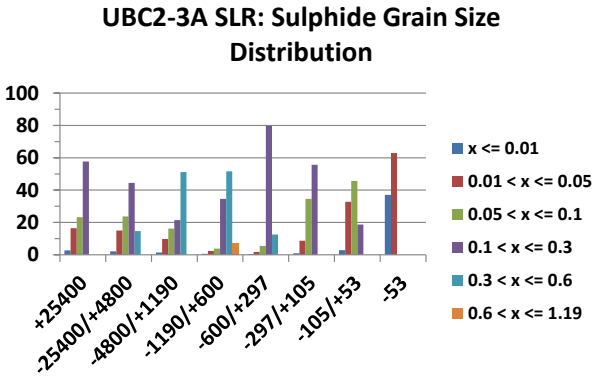
UBC2-3A SLR: Sulphide Grain Size Distribution
100
80
60
40
20
0
+25400
-25400/+4800
-4800/+1190
-1190/+600
-600/+297
-297/+105
-105/+53
-53
x <= 0.01
0.01 < x <= 0.05
0.05 < x <= 0.1
0.1 < x <= 0.3
0.3 < x <= 0.6
0.6 < x <= 1.19

Tucush01 Head: Carbonate Grain Size Distribution

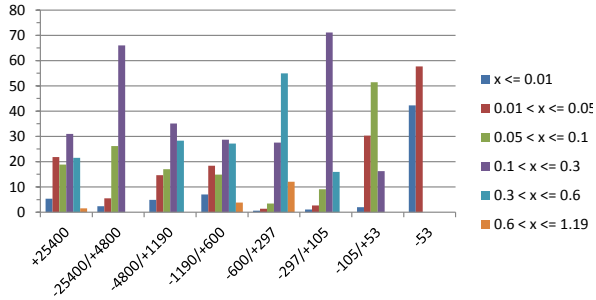

Tucush01 SLR: Carbonate Grain Size Distribution

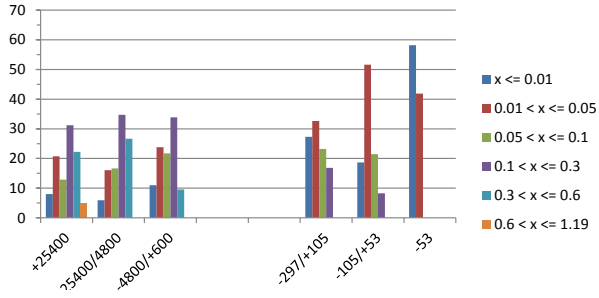

Tucush03 Head: Carbonate Grain Size Distribution

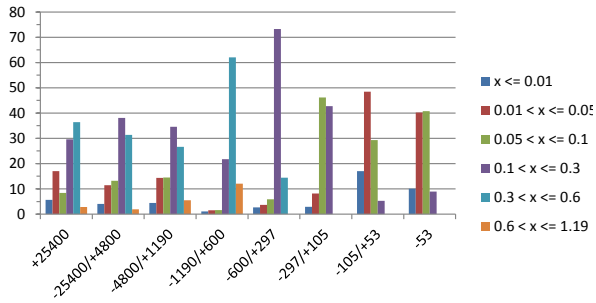

Tucush03 SLR: Carbonate Grain Size Distribution

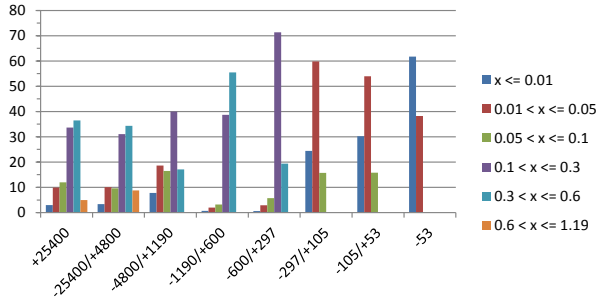

Tucush04 Head: Carbonate Grain Size Distribution

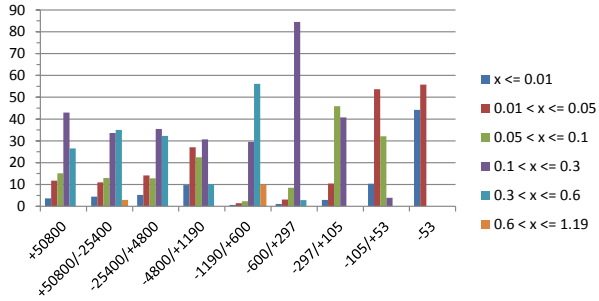

Cell06 Head: Carbonate Grain Size Distribution

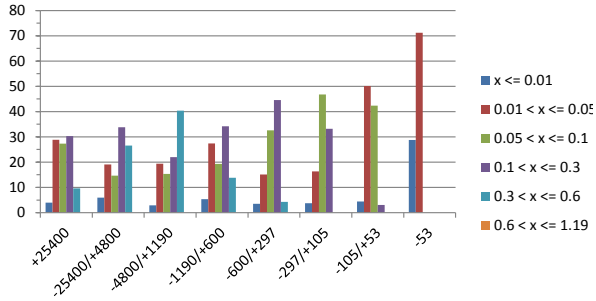

Cell06 SLR: Carbonate Grain Size Distribution

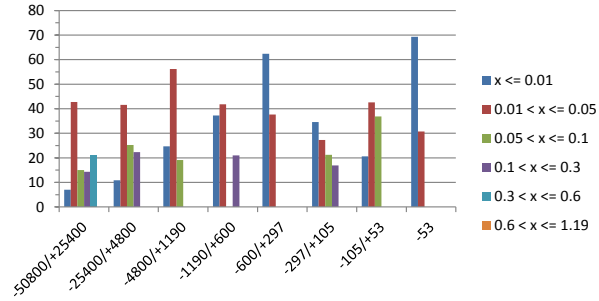

Cell21 Head: Carbonate Grain Size Distribution

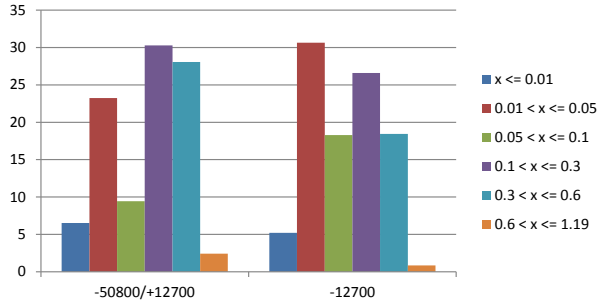

Cell21 SLR: Carbonate Grain Size Distribution

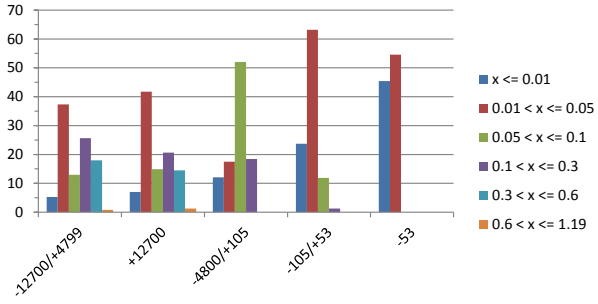

Cell24 Head: Carbonate Grain Size Distribution

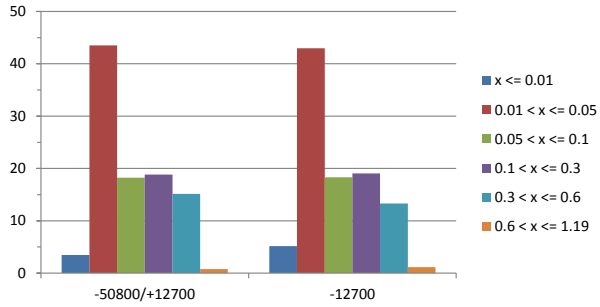

Cell24 SLR: Carbonate Grain Size Distribution

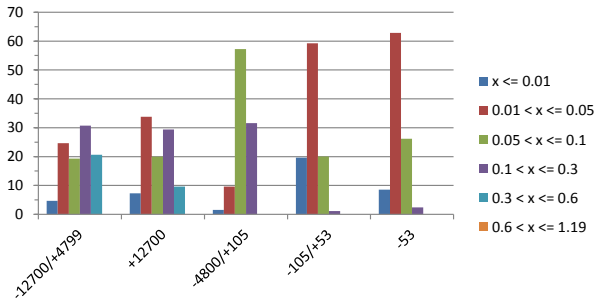

UBC3-2A Head: Carbonate Grain Size Distribution

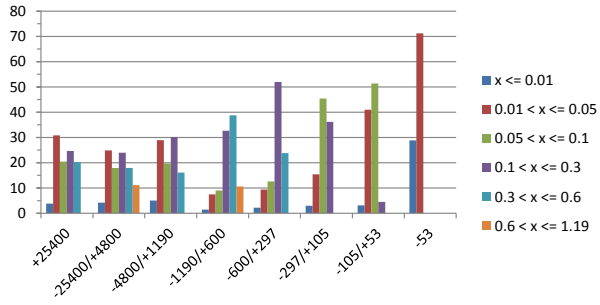

UBC3-2A SLR: Carbonate Grain Size Distribution

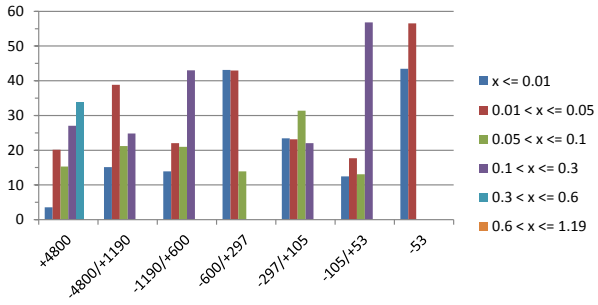

UBC2-3A Head: Carbonate Grain Size Distribution

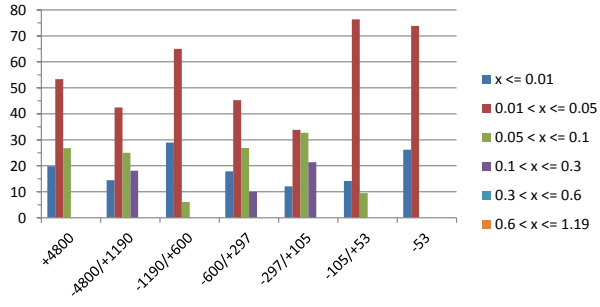

UBC2-3A SLR: Carbonate Grain Size Distribution

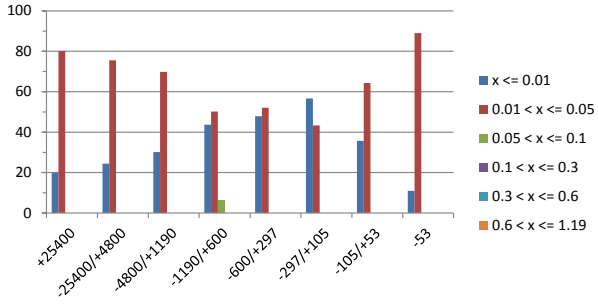

Tucush01 Head: Silicate Grain Size Distribution

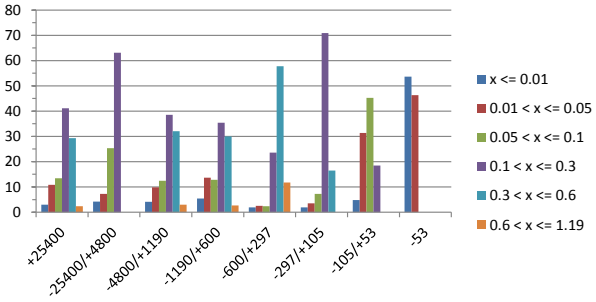

Tucush01 SLR: Silicate Grain Size Distribution

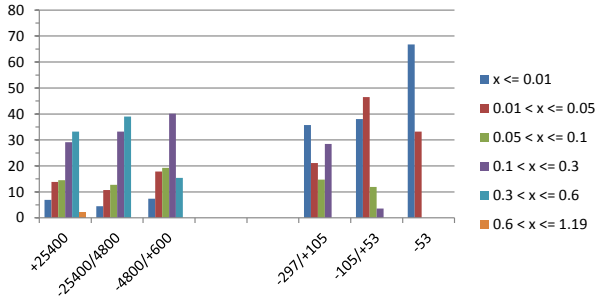

Tucush03 Head: Silicate Grain Size Distribution

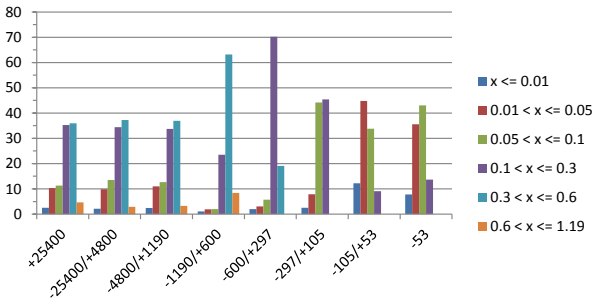

Tucush03 SLR: Silicate Grain Size Distribution

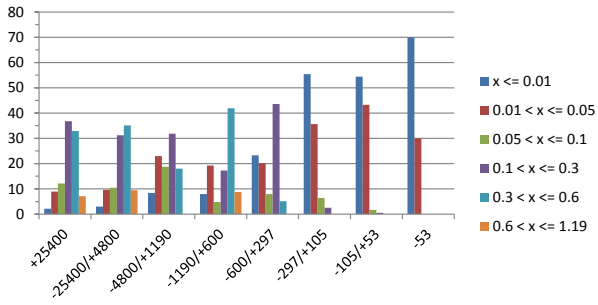

Tucush04 Head: Silicate Grain Size Distribution

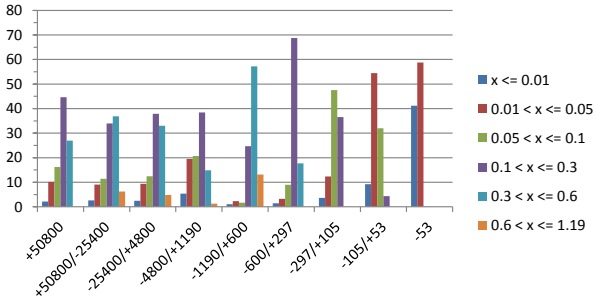

Cell06 Head:Silicate Grain Size Distribution

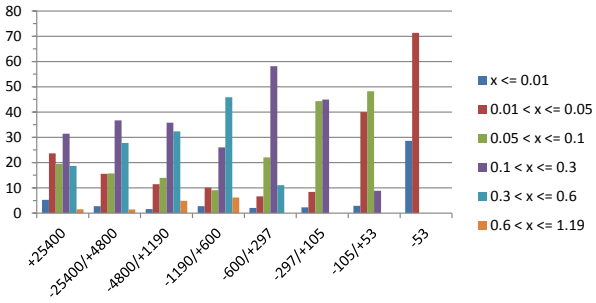

Cell06 SLR: Silicate Grain Size Distribution

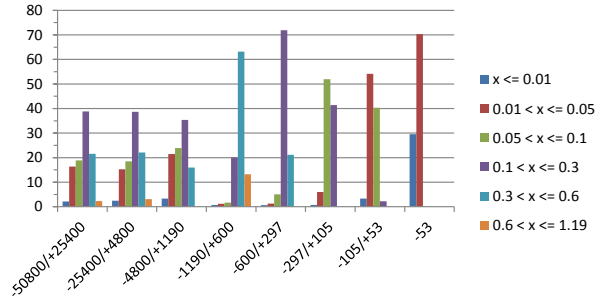

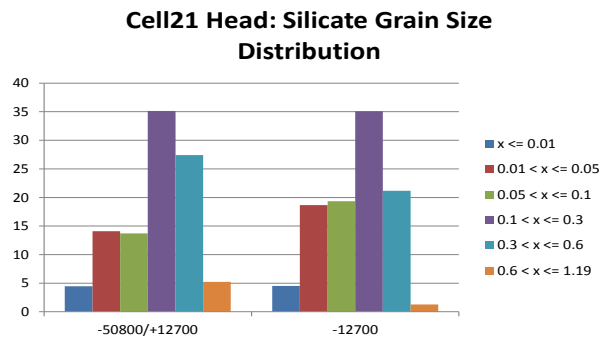
Cell21 Head: Silicate Grain Size Distribution
40
35
30
25
20
15
10
5
0
-50800/+12700
-12700
x <= 0.01
0.01 < x <= 0.05
0.05 < x <= 0.1
0.1 < x <= 0.3
0.3 < x <= 0.6
0.6 < x <= 1.19

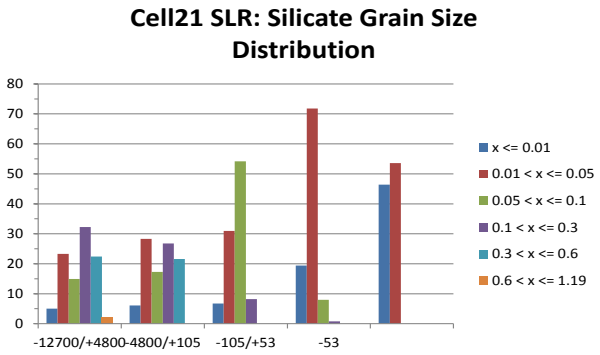
Cell21 SLR: Silicate Grain Size Distribution
80
70
60
50
40
30
20
10
0
-12700/+4800
-4800/+105
-105/+53
-53
x <= 0.01
0.01 < x <= 0.05
0.05 < x <= 0.1
0.1 < x <= 0.3
0.3 < x <= 0.6
0.6 < x <= 1.19

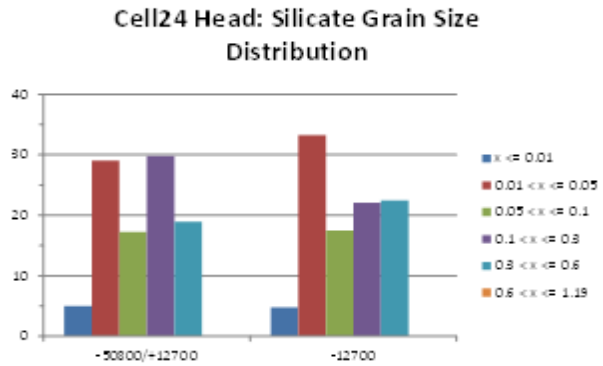
Cell24 Head: Silicate Grain Size Distribution
40
30
20
10
0
-50800/+12700
-12700

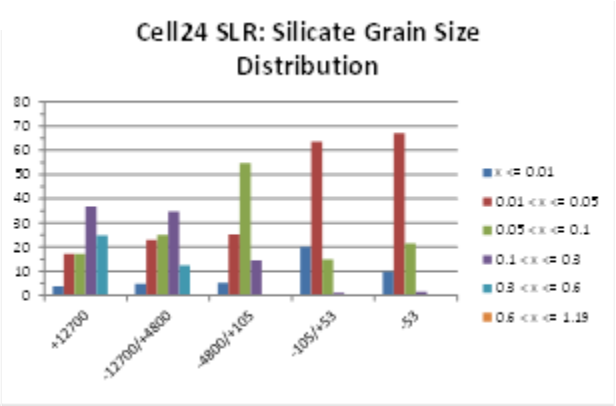
Cell24 SLR: Silicate Grain Size Distribution
80
70
60
50
40
30
20
10
0
+12700
-12700/+4800
-4800/+105
-105/+53
-53

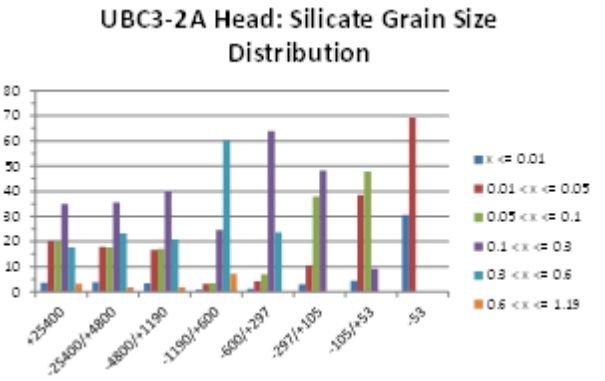
UBC3-2A Head: Silicate Grain Size Distribution
80
70
60
50
40
30
20
10
0
+25400
-25400/+4800
-4800/+1190
-1190/+600
-600/+297
-297/+105
-105/+53
-53

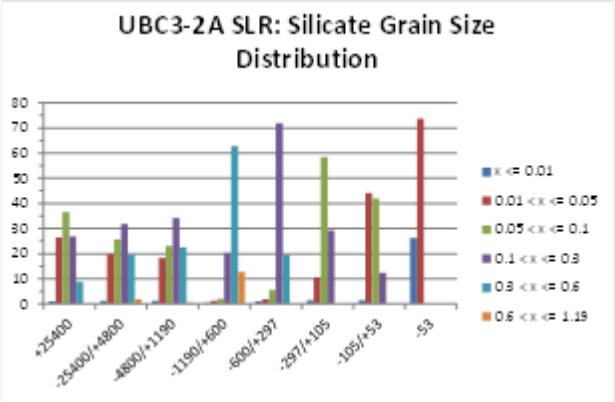
UBC3-2A SLR: Silicate Grain Size Distribution
80
70
60
50
40
30
20
10
0
+25400
-25400/+4800
-4800/+1190
-1190/+600
-600/+297
-297/+105
-105/+53
-53

UBC2-3A Head: Silicate Grain Size Distribution

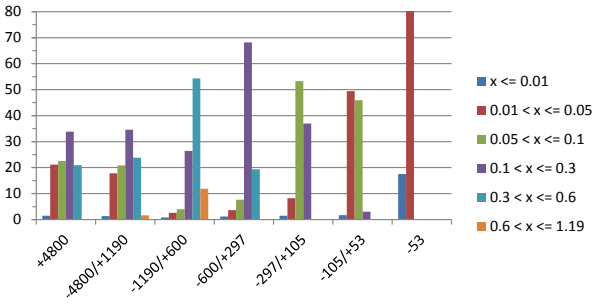

UBC2-3A SLR: Silicate Grain Size Distribution

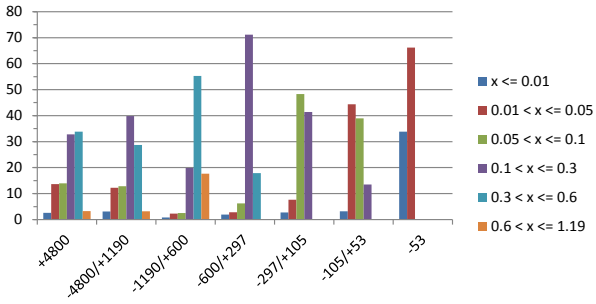

Tucush01 Head: Sb-bearing MOI Grain Size Distribution

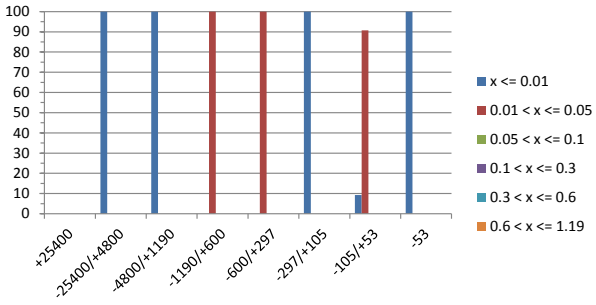

Tucush01 SLR: Sb-bearing MOI Grain Size Distribution

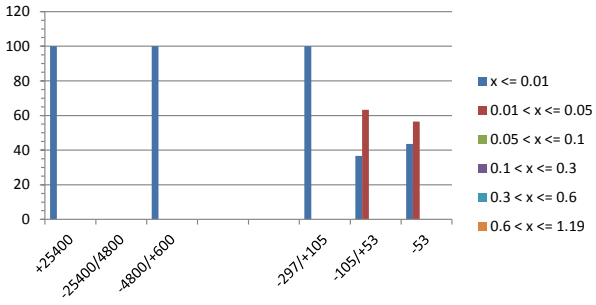

Tucush03 Head: Sb-bearing MOI Grain Size Distribution

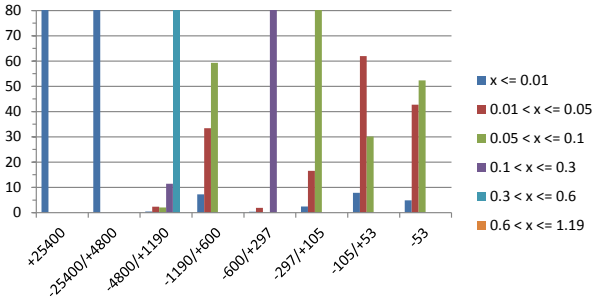

Tucush03 SLR: Sb-bearing MOI Grain Size Distribution

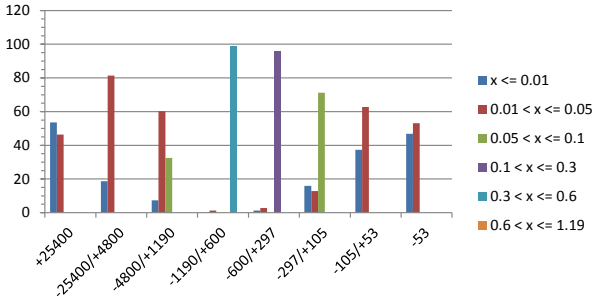

Tucush04 Head: Sb-bearing MOI Grain Size Distribution

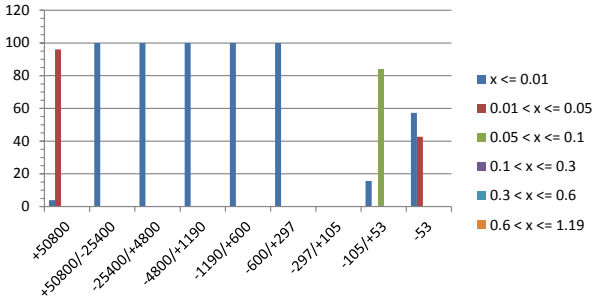

Cell06 Head:Sb-bearing MOI Grain Size Distribution

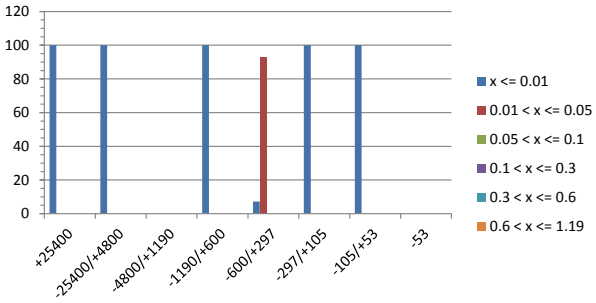

Cell06 SLR: Sb-bearing MOI Grain Size Distribution

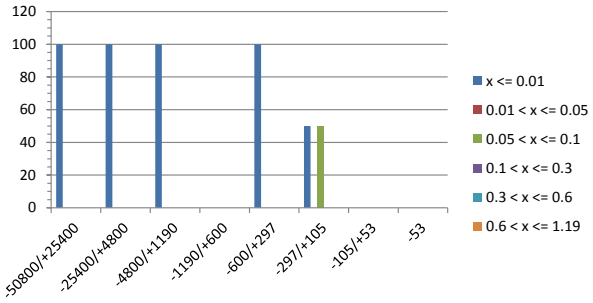

Cell21 Head: Sb-bearing MOIGrain Size Distribution

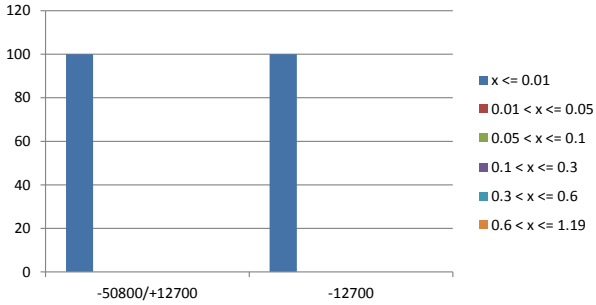

Cell24 Head: Sb-bearing MOI Grain Size Distribution

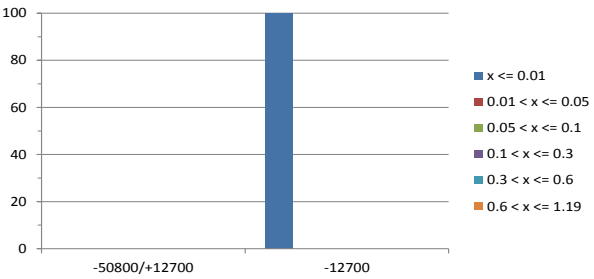

Cell21 SLR: Sb-bearing MOI Grain Size Distribution

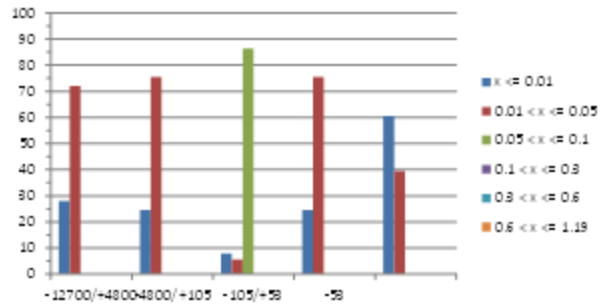

Cell24 SLR: Sb-bearing MOI Grain Size Distribution

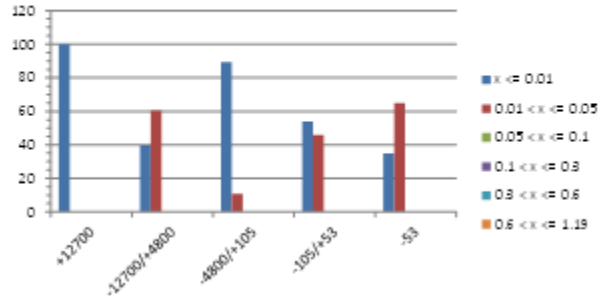

UBC3-2A Head: Sb-bearing MOI Grain Size Distribution

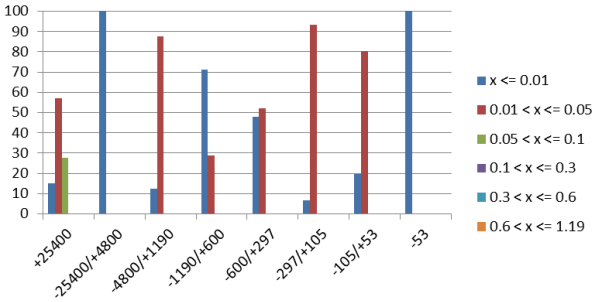

UBC3-2A SLR: Sb-bearing MOI Grain Size Distribution

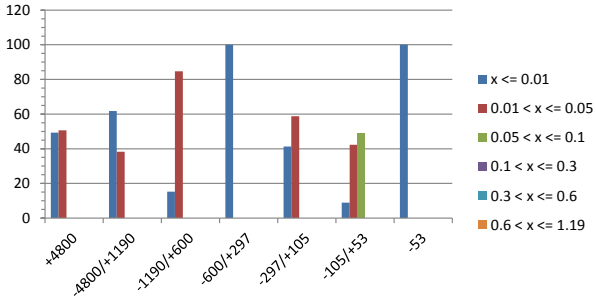

UBC2-3A Head: Sb-bearing MOI Grain Size Distribution

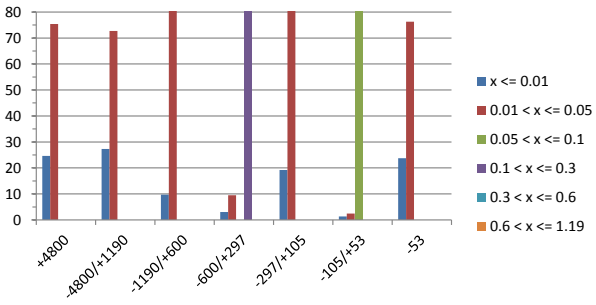

UBC2-3A SLR: Sb-bearing MOI Grain Size Distribution

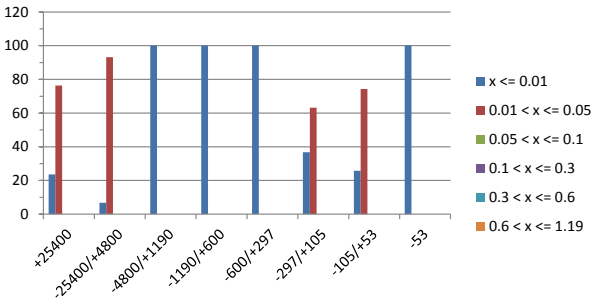

Tucush01 Head: As-bearing MOI Grain Size Distribution

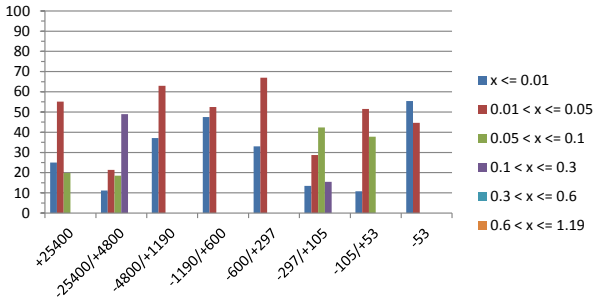

Tucush01 SLR: As-bearing MOI Grain Size Distribution

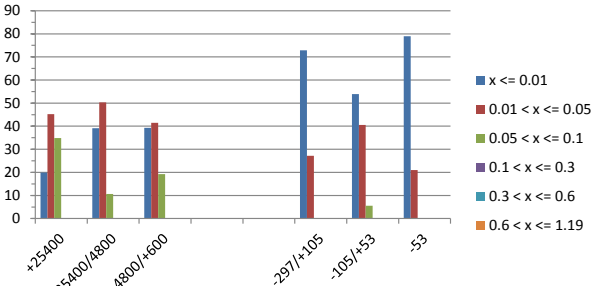

Tucush03 Head: As-bearing MOI Grain Size Distribution

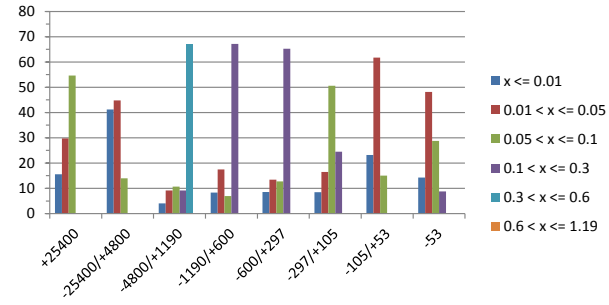

Tucush03 SLR: As-bearing MOI Grain Size Distribution

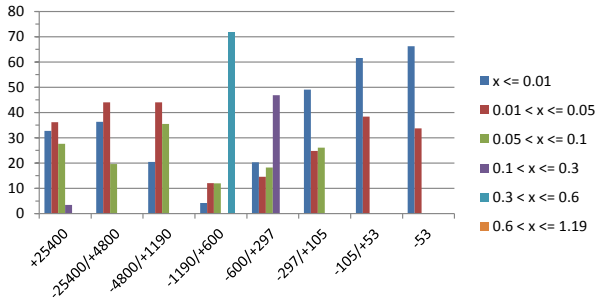

Tucush04 Head: As-bearing MOI Grain Size Distribution

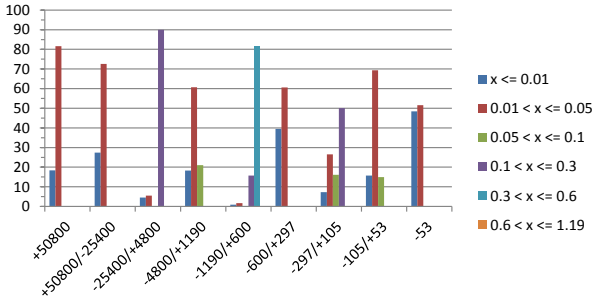

Cell06 Head:As-bearing MOI Grain Size Distribution

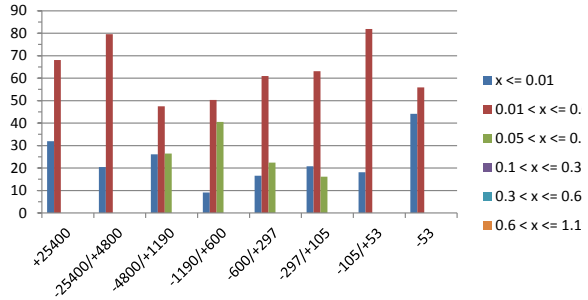

Cell06 SLR: As-bearing MOI Grain Size Distribution

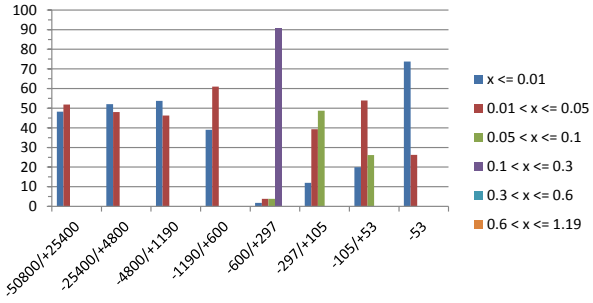

Cell21 Head: As-bearing MOIGrain Size Distribution

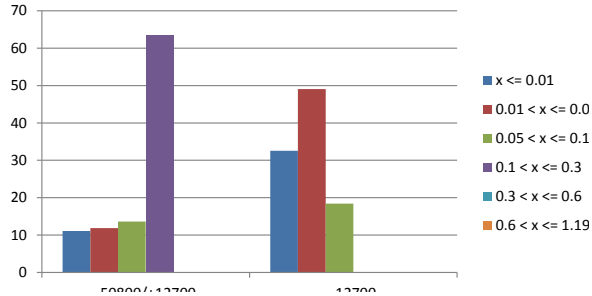

Cell21 SLR: As-bearing MOI Grain Size Distribution

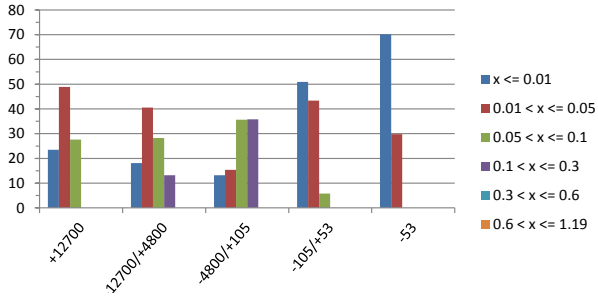

Cell24 Head: As-bearing MOI Grain Size Distribution

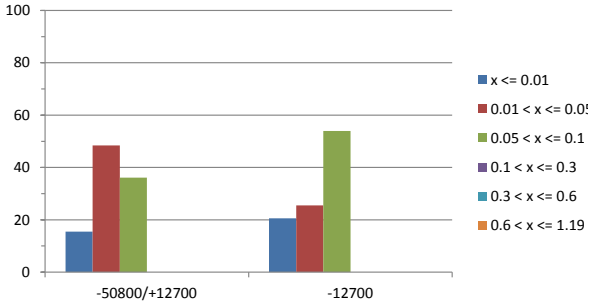

Cell24 SLR: As-bearing MOI Grain Size Distribution

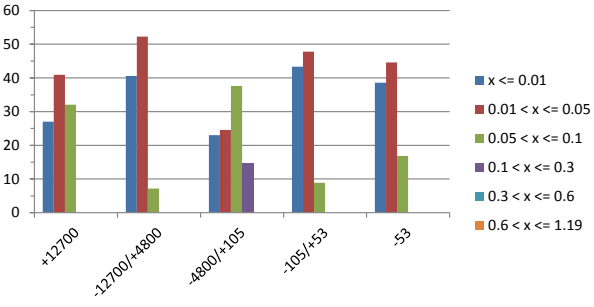

UBC3-2A Head: As-bearing MOI Grain Size Distribution

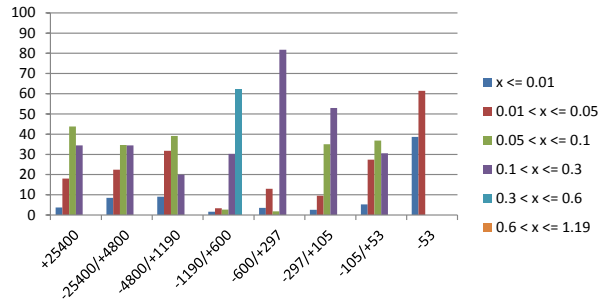

UBC3-2A SLR: As-bearing MOI Grain Size Distribution

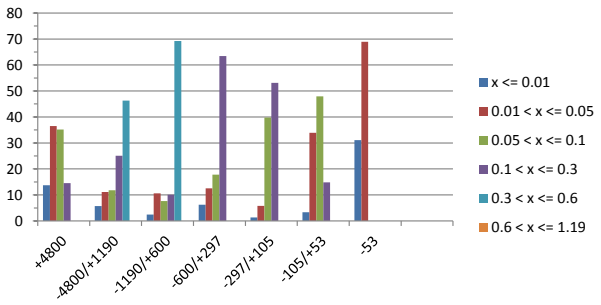

UBC2-3A Head: As-bearing MOI Grain Size Distribution

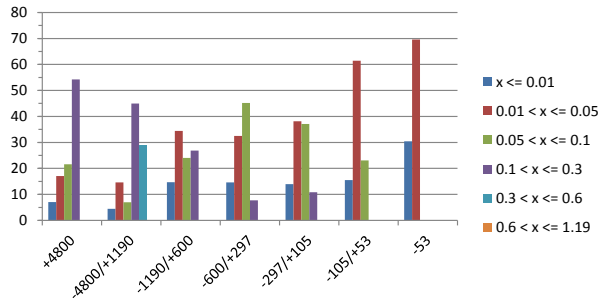

UBC2-3A SLR: As-bearing MOI Grain Size Distribution

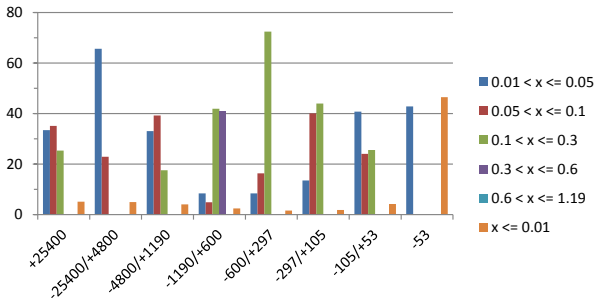

Tucush01 Head: Cu-bearing MOI Grain Size Distribution

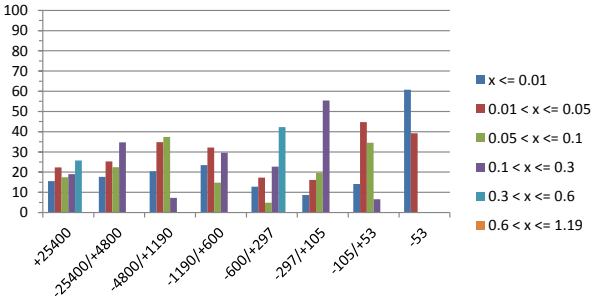

Tucush01 SLR: Cu-bearing MOI Grain Size Distribution

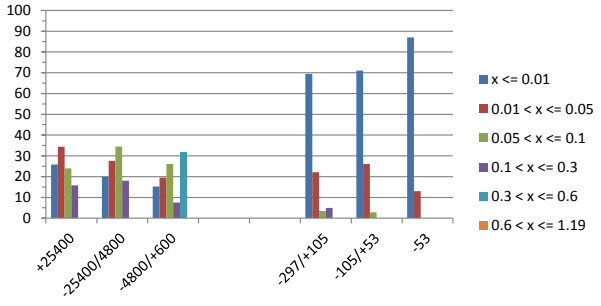

Tucush03 Head: Cu-bearing MOI Grain Size Distribution

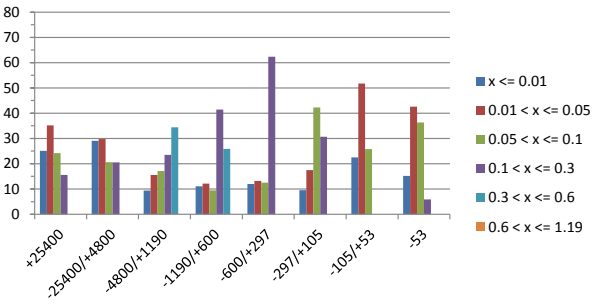

Tucush03 SLR: Cu-bearing MOI Grain Size Distribution

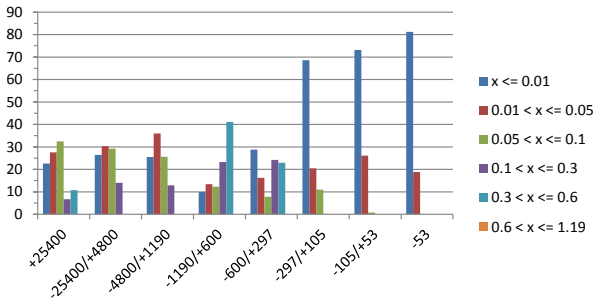

Tucush04 Head: Cu-bearing MOI Grain Size Distribution

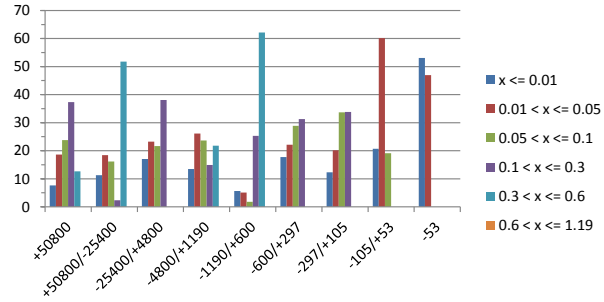

Cell06 Head:Cu-bearing MOI Grain Size Distribution

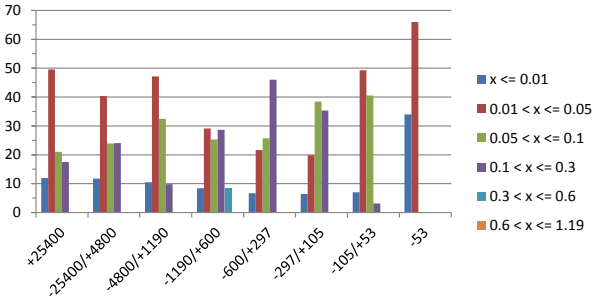

Cell06 SLR: Cu-bearing MOI Grain Size Distribution

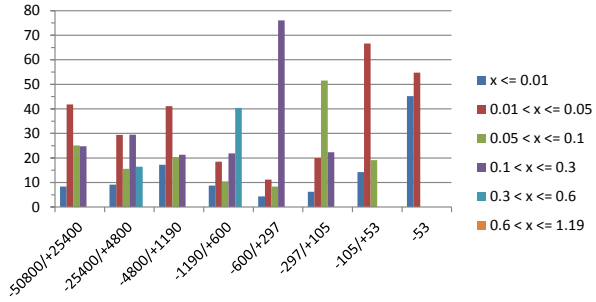

Cell21 Head: Cu-bearing MOI Grain Size Distribution

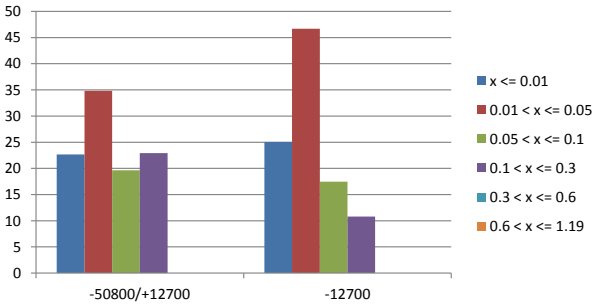

Cell21 SLR: Cu-bearing MOI Grain Size Distribution

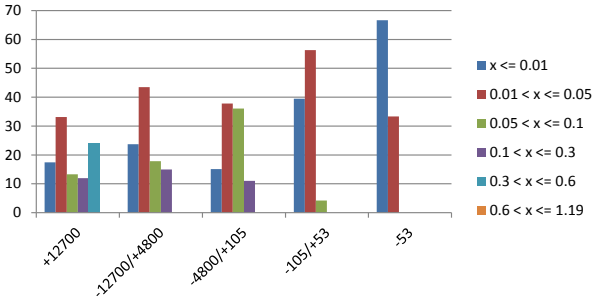

Cell24 Head: Cu-bearing MOI Grain Size Distribution

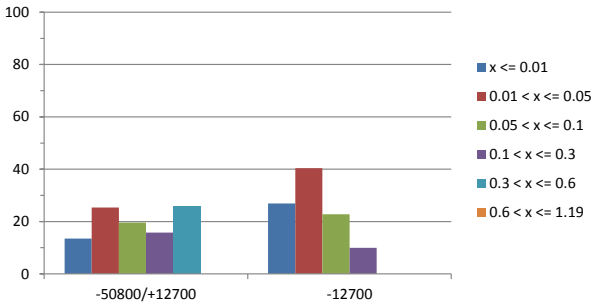

Cell24 SLR: Cu-bearing MOI Grain Size Distribution

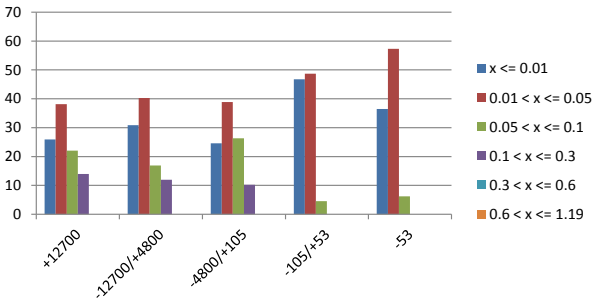

UBC3-2A Head: Cu-bearing MOI Grain Size Distribution

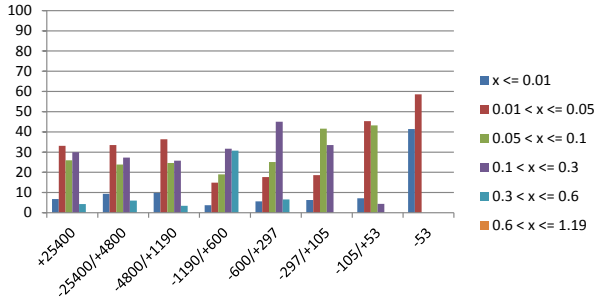

UBC3-2A SLR: Cu-bearing MOI Grain Distribution

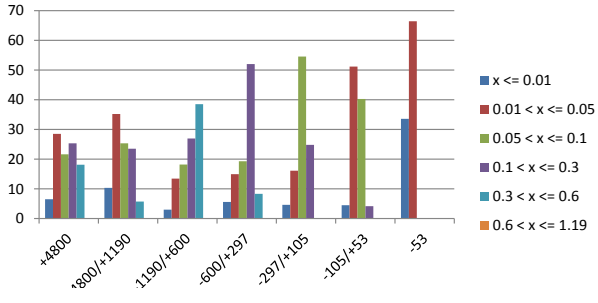

UBC2-3A Head: Cu-bearing MOI Grain Size Distribution

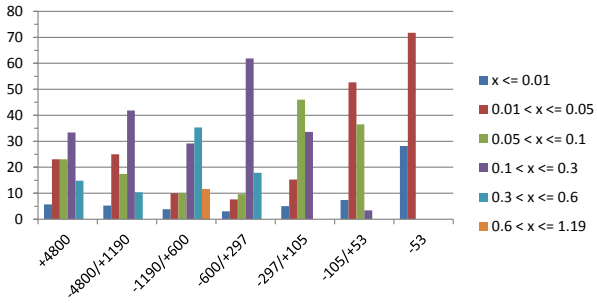

UBC2-3A SLR: Cu-bearing MOI Grain Size Distribution

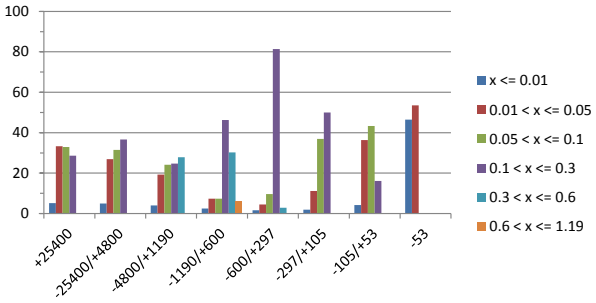

Tucush01 Head: Mo-bearing MOI Grain Size Distribution

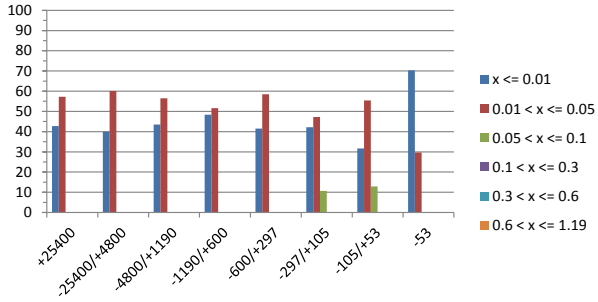

Tucush01 SLR: Mo-bearing MOI Grain Size Distribution

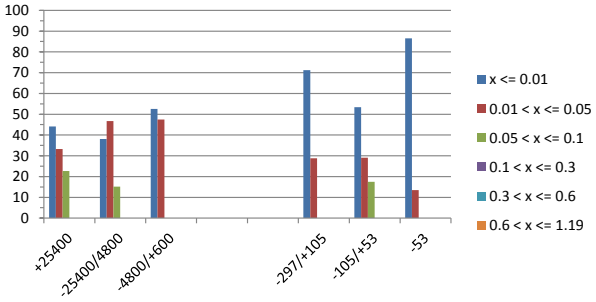

Tucush03 Head: Mo-bearing MOI Grain Size Distribution

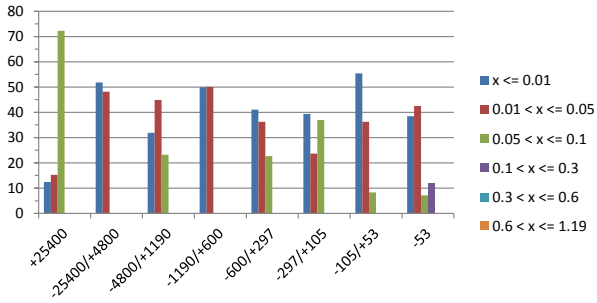

Tucush03 SLR: Mo-bearing MOI Grain Size Distribution

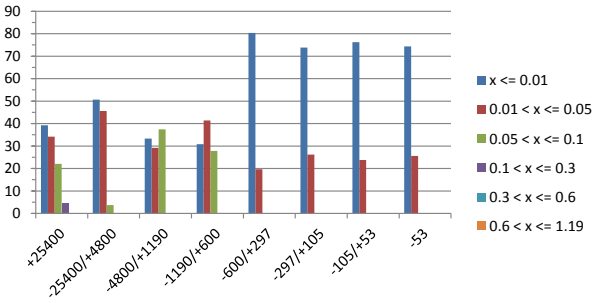

Tucush04 Head: Mo-bearing MOI Grain Size Distribution

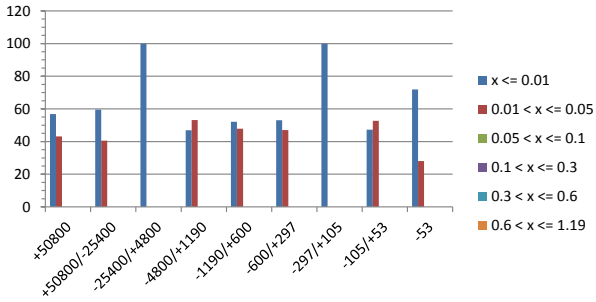

Cell06 Head:Mo-bearing MOI Grain Size Distribution

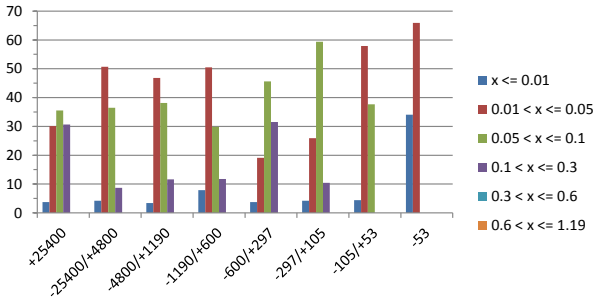

Cell06 SLR: Mo-bearing MOI Grain Size Distribution

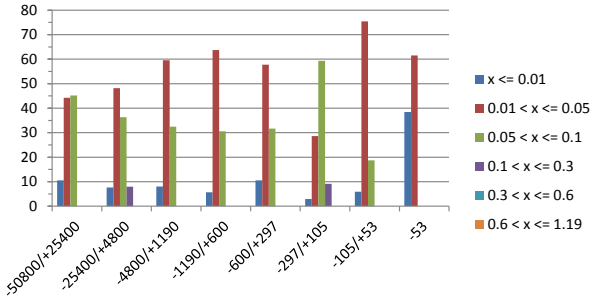

Cell21 SLR: Mo-bearing MOI Grain Distribution

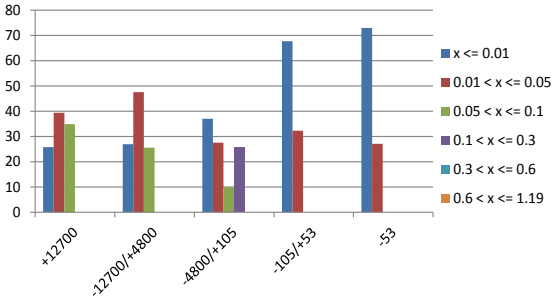

Cell21 Head: Mo-bearing MOIGrain Size Distribution

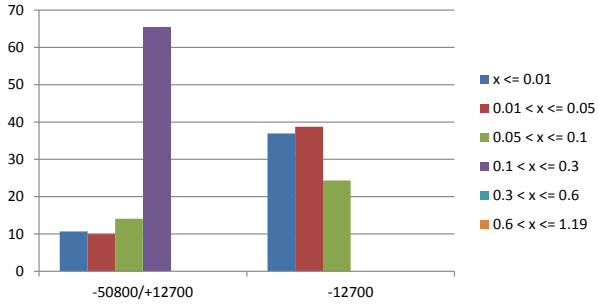

Cell24 Head: Mo-bearing MOI Grain Size Distribution

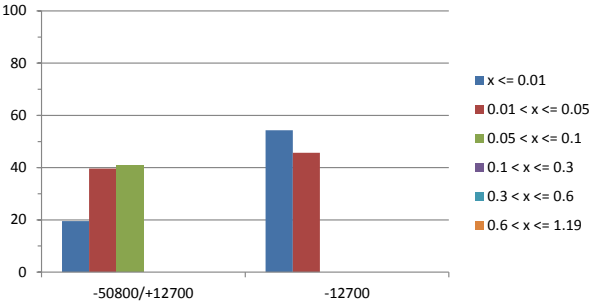

Cell24 SLR: Mo-bearing MOI Grain Distribution

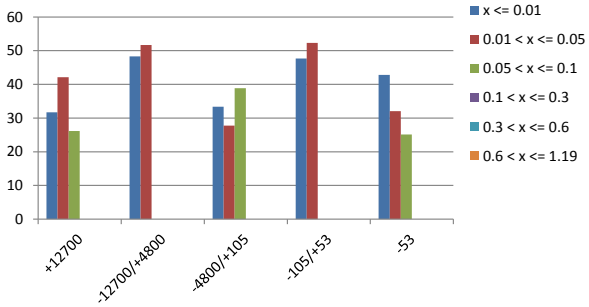

UBC3-2A Head: Mo-bearing MOI Grain Size Distribution

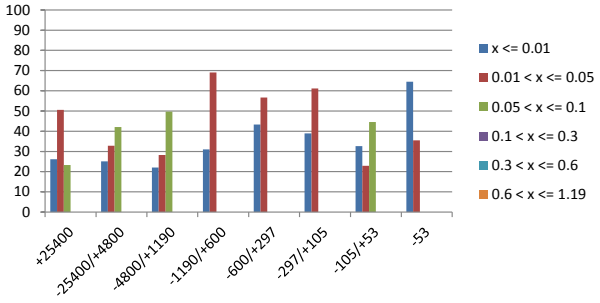

UBC3-2A SLR: Mo-bearing MOI Grain Distribution

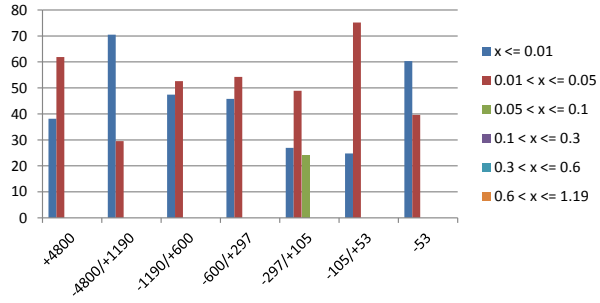

UBC2-3A Head: Mo-bearing MOI Grain Size Distribution

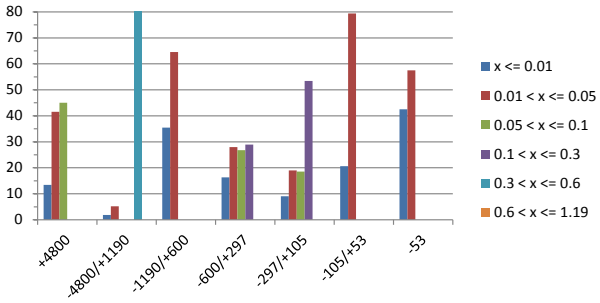

UBC2-3A SLR: Mo-bearing MOI Grain Size Distribution

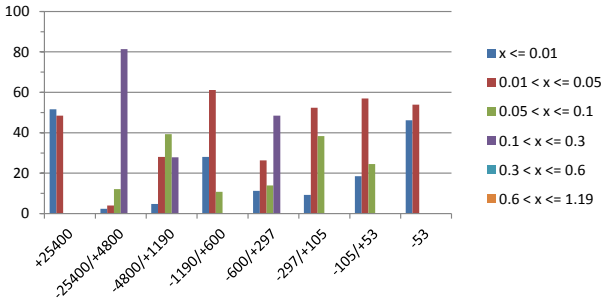

Tucush01 Head: Pb-bearing MOI Grain Size Distribution

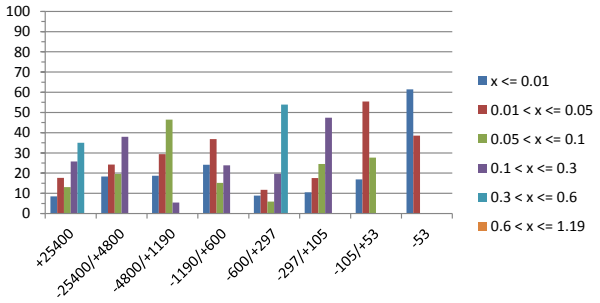

Tucush01 SLR: Pb-bearing MOI Grain Size Distribution

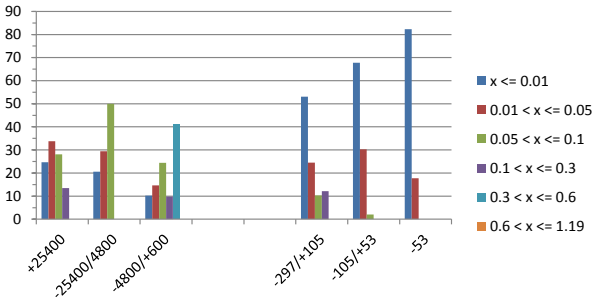

Tucush03 Head: Pb-bearing MOI Grain Size Distribution

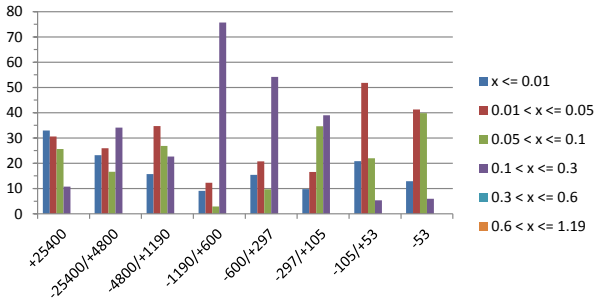

Tucush03 SLR: Pb-bearing MOI Grain Size Distribution

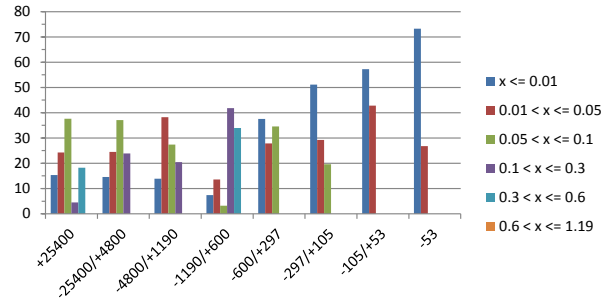

Tucush04 Head: Pb-bearing MOI Grain Size Distribution

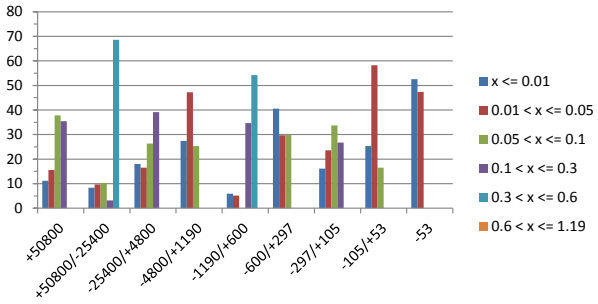

Cell06 Head:Pb-bearing MOI Grain Size Distribution

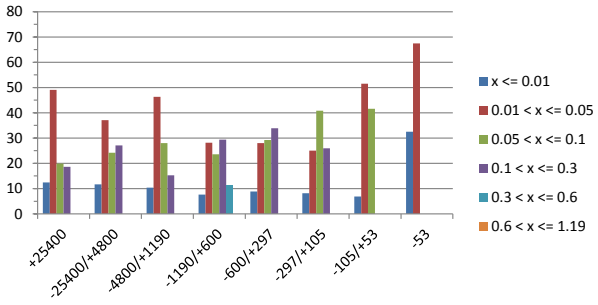

Cell06 SLR: Pb-bearing MOI Grain Size Distribution

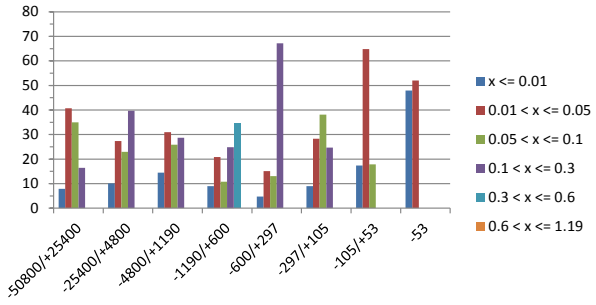

Cell21 Head: Pb-bearing MOI Grain Size Distribution

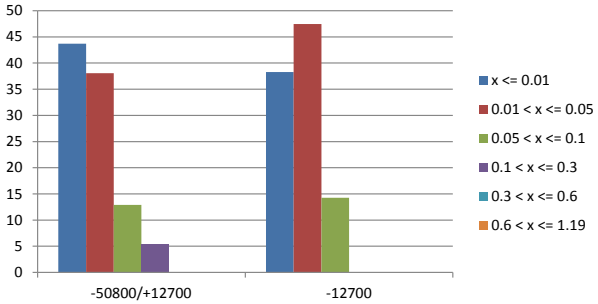

Cell21 SLR: Pb-bearing MOI Grain Distribution

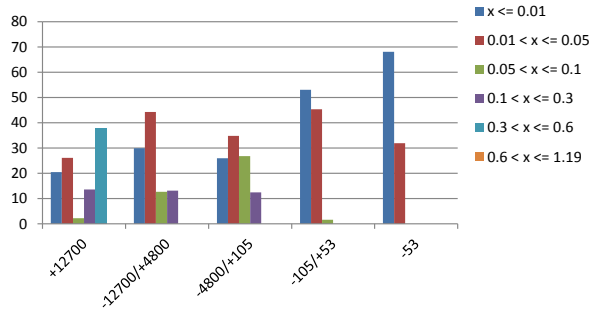

Cell24 Head: Pb-bearing MOI Grain Size Distribution

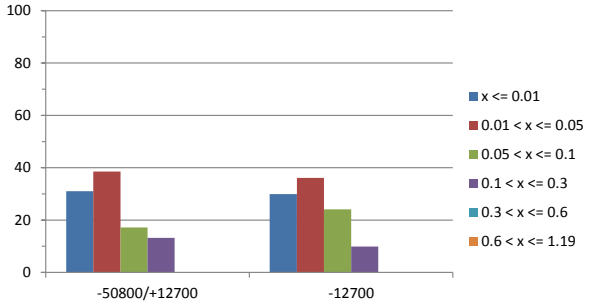

Cell24 SLR: Pb-bearing MOI Grain Size Distribution

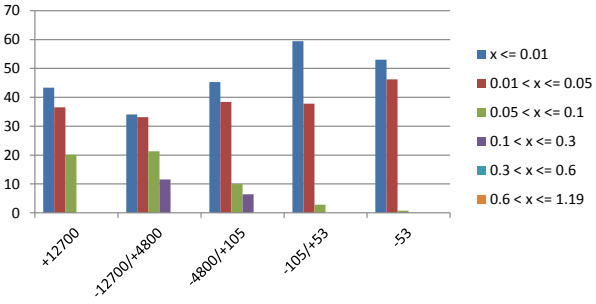

UBC3-2A Head: Pb-bearing MOI Grain Size Distribution

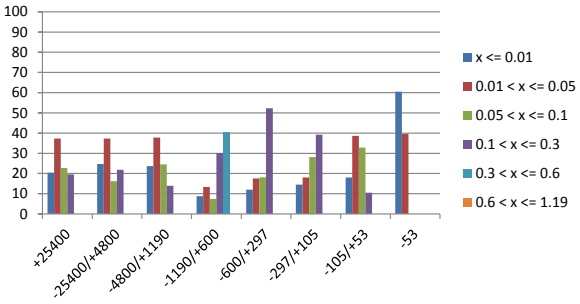

UBC3-2A SLR: Pb-bearing MOI Grain Size Distribution

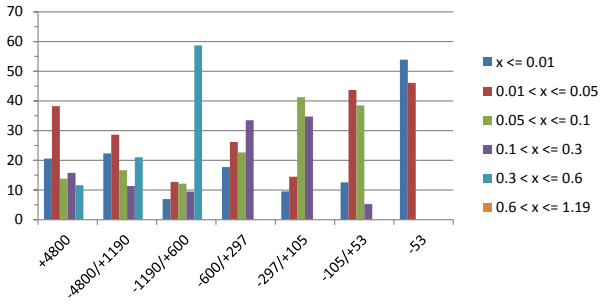

UBC2-3A Head: Pb-bearing MOI Grain Size Distribution

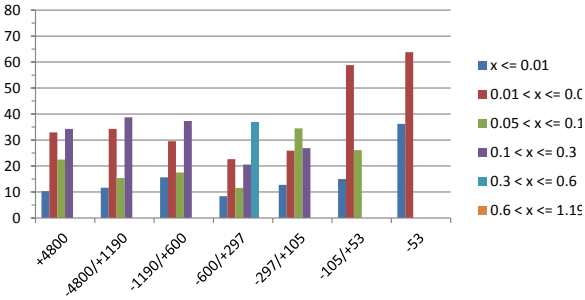

UBC2-3A SLR: Pb-bearing MOI Grain Size Distribution

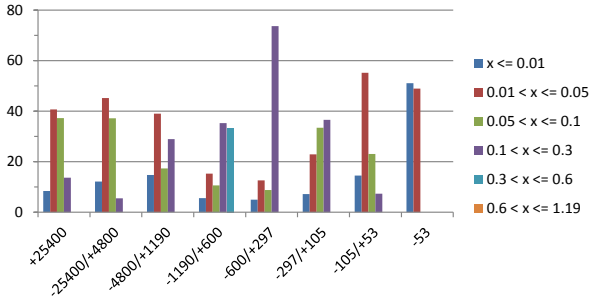

Tucush01 Head: Zn-bearing MOI Grain Size Distribution

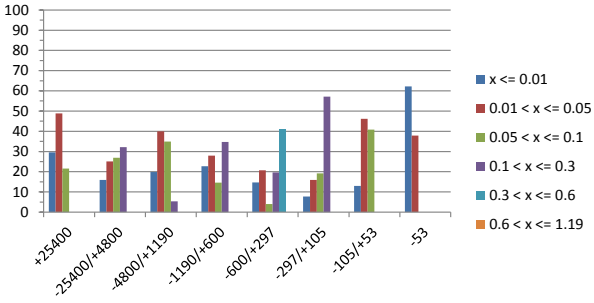

Tucush01 SLR: Zn-bearing MOI Grain Size Distribution

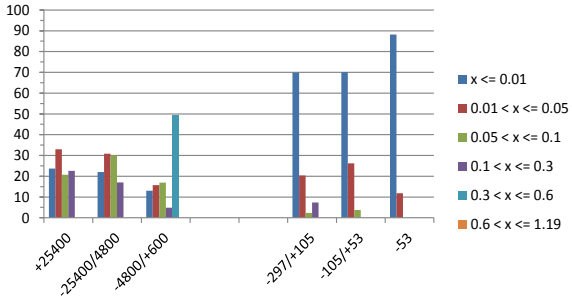

Tucush03 Head: Zn-bearing MOI Grain Size Distribution

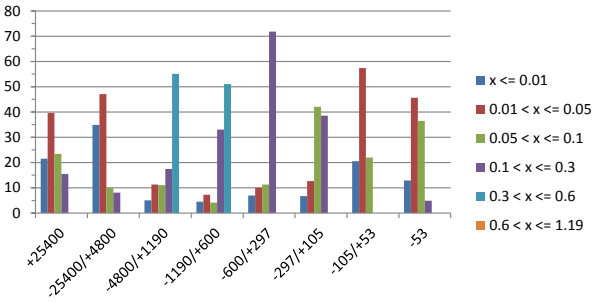

Tucush03 SLR: Zn-bearing MOI Grain Size Distribution

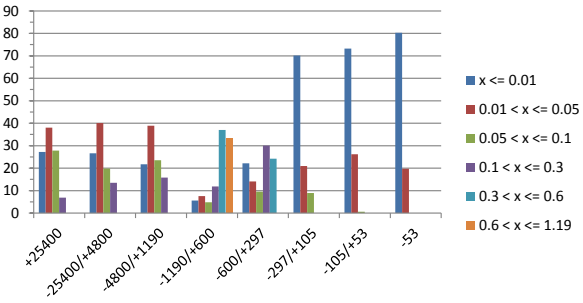

Tucush04 Head: Zn-bearing MOI Grain Size Distribution

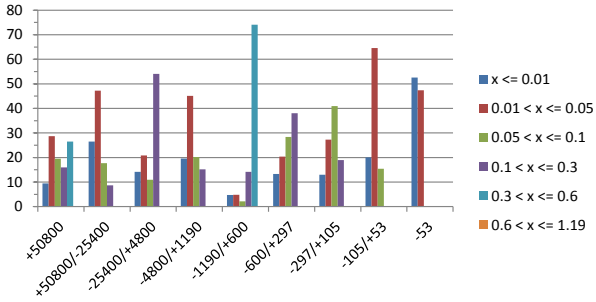

Cell06 Head:Zn-bearing MOI Grain Size Distribution

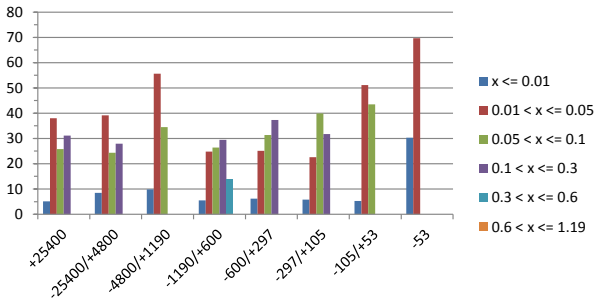

Cell06 SLR: Zn-bearing MOI Grain Size Distribution

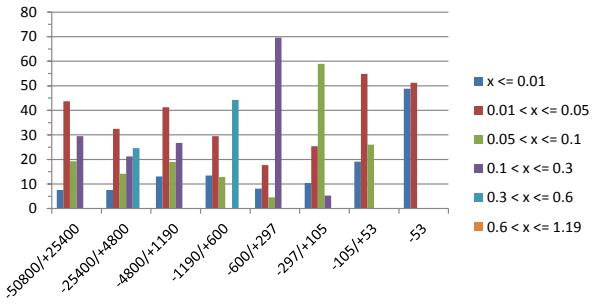

Cell21 Head: Zn-bearing MOIGrain Size Distribution

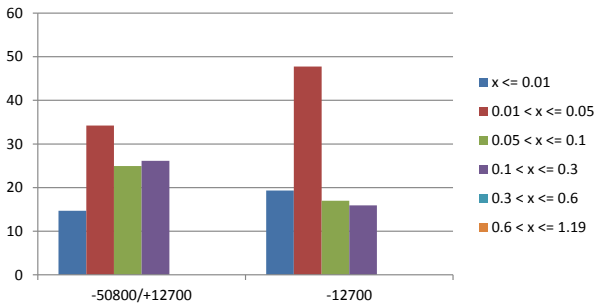

Cell21 SLR: Zn-bearing MOI Grain Size Distribution

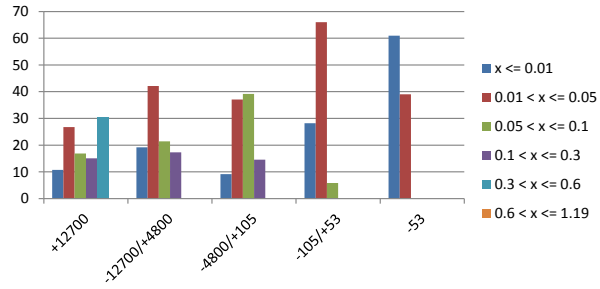

Cell24 Head: Zn-bearing MOI Grain Size Distribution

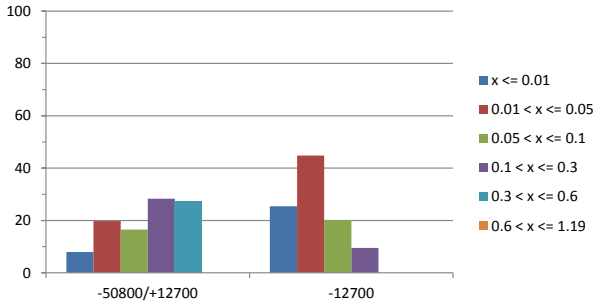

Cell24 SLR: Zn-bearing MOI Grain Size Distribution

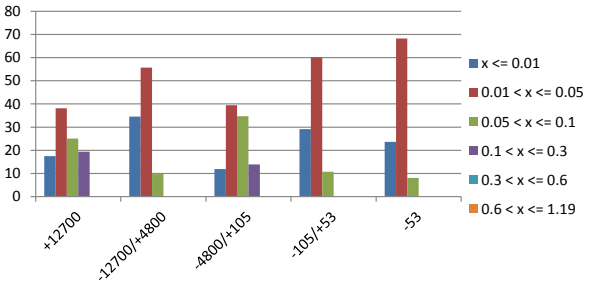

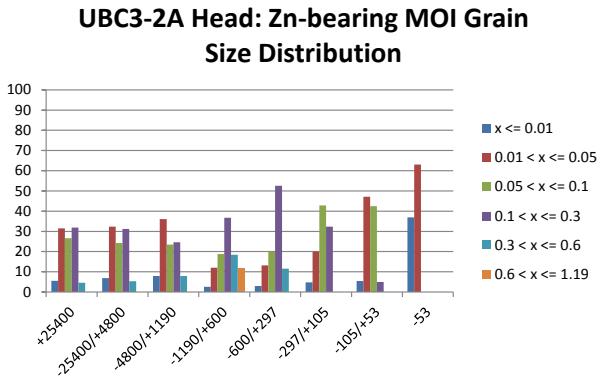
UBC3-2A Head: Zn-bearing MOI Grain Size Distribution
100
90
80
70
60
50
40
30
20
10
0
+25400
-25400/+4800
-4800/+1190
-1190/+600
-600/+297
-297/+105
-105/+53
-53
x <= 0.01
0.01 < x <= 0.05
0.05 < x <= 0.1
0.1 < x <= 0.3
0.3 < x <= 0.6
0.6 < x <= 1.19

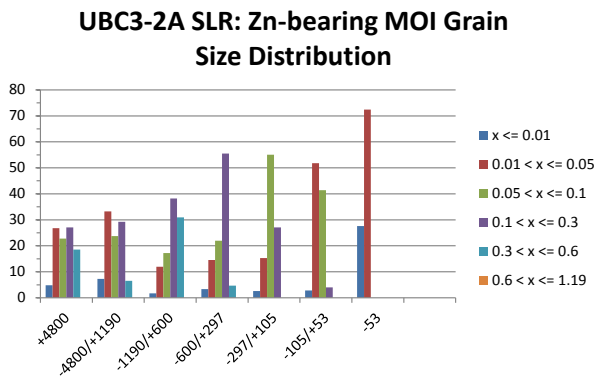
UBC3-2A SLR: Zn-bearing MOI Grain Size Distribution
80
70
60
50
40
30
20
10
0
+4800
-4800/+1190
-1190/+600
-600/+297
-297/+105
-105/+53
-53
x <= 0.01
0.01 < x <= 0.05
0.05 < x <= 0.1
0.1 < x <= 0.3
0.3 < x <= 0.6
0.6 < x <= 1.19

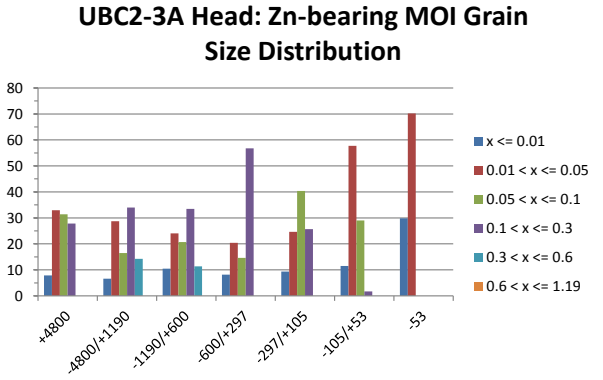
UBC2-3A Head: Zn-bearing MOI Grain Size Distribution
80
70
60
50
40
30
20
10
0
+4800
-4800/+1190
-1190/+600
-600/+297
-297/+105
-105/+53
-53
x <= 0.01
0.01 < x <= 0.05
0.05 < x <= 0.1
0.1 < x <= 0.3
0.3 < x <= 0.6
0.6 < x <= 1.19

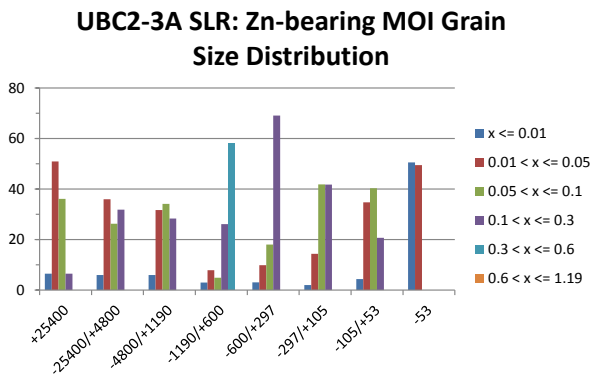
UBC2-3A SLR: Zn-bearing MOI Grain Size Distribution
80
60
40
20
0
+25400
-25400/+4800
-4800/+1190
-1190/+600
-600/+297
-297/+105
-105/+53
-53
x <= 0.01
0.01 < x <= 0.05
0.05 < x <= 0.1
0.1 < x <= 0.3
0.3 < x <= 0.6
0.6 < x <= 1.19

APPENDIX 18 Mineral Liberation Analyzer application: modal mineralogy based on metal association

Note: All plots derived from data collected from Table 3.2.4.

Legend refers to simple grouping of MOIs: Sulphide (binary); Carbonate (binary); Silicate (binary); Other (binary); Liberated (pure MOI); and, Ternary+ (at least three MOIs in contact with each other).

Horizontal axis = size fraction (microns); Vertical axis = weight-% (normalized).

Tucush01 Head, Summary of Locking: Sulphide MOI

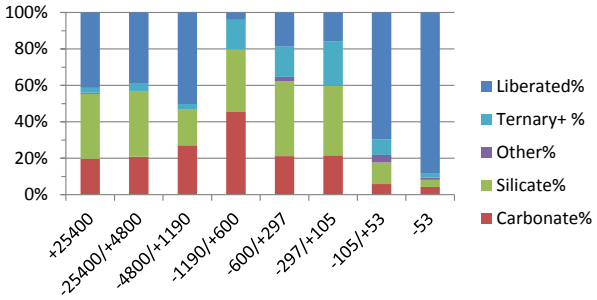

Tucush01 SLR, Summary of Locking: Sulphide MOI

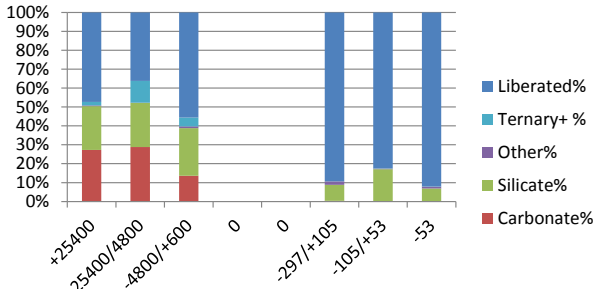

Tucush03 Head, Summary of Contact Association: Sulphide MOI

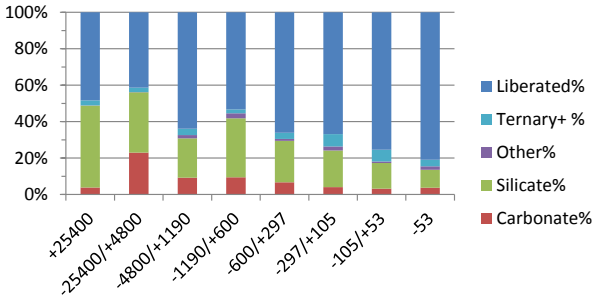

Tucush03 SLR, Summary of Contact Association: Sulphide MOI

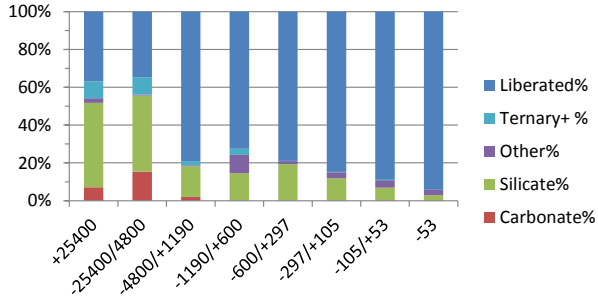

Tucush04 Head, Summary of Locking: Sulphide MOI

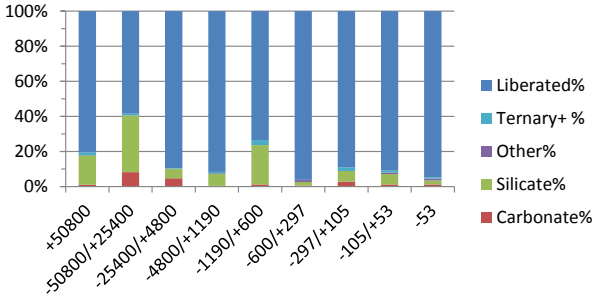

Cell06 Head, Summary of Locking: Sulphide MOI

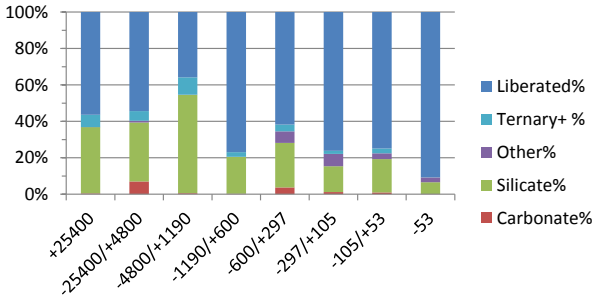

Cell06 SLR, Summary of Locking: Sulphide MOI

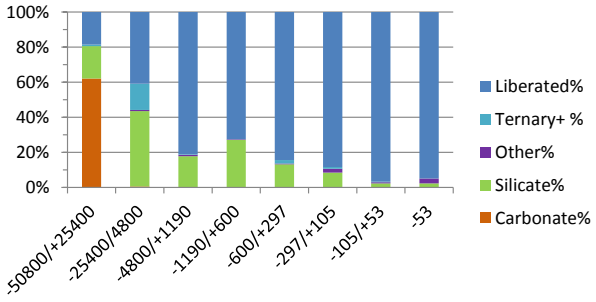

Cell21 Head, Summary of Locking: Sulphide MOI

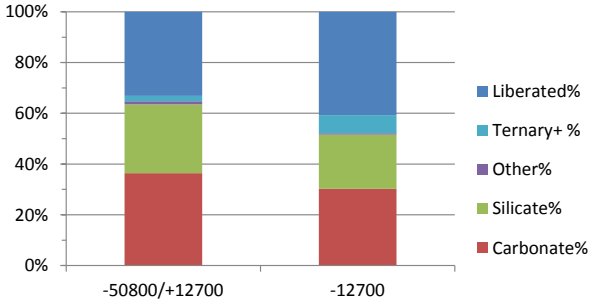

Cell21 SLR, Summary of Locking: Sulphide MOI

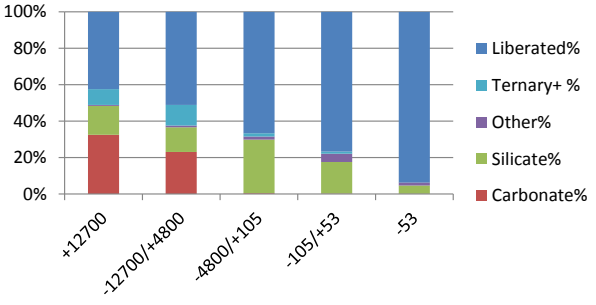

Cell24 Head, Summary of Locking: Sulphide MOI

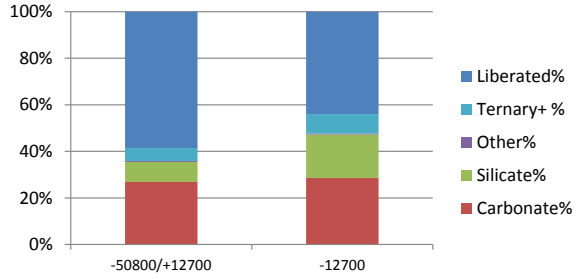

Cell24 SLR, Summary of Locking: Sulphide MOI

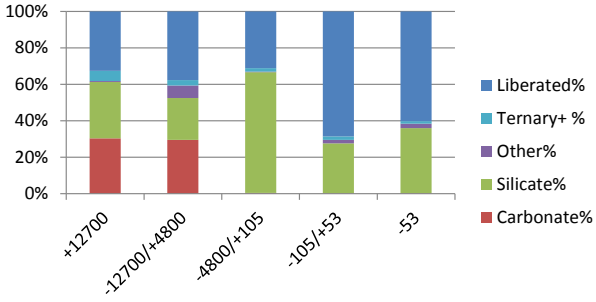

UBC3-2A Head, Summery of Locking: Sulphide MOI

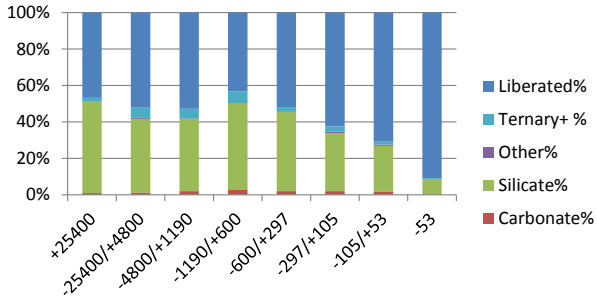

UBC3-2A SLR, Summary of Locking: Sulphide MOI

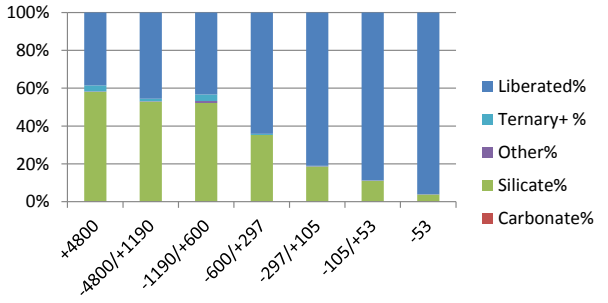

UBC2-3A Head, Summary of Locking: Sulphide MOI

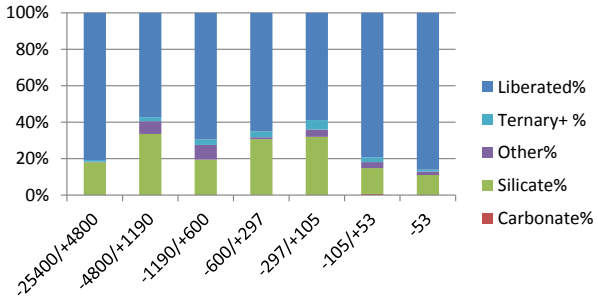

UBC2-3A SLR, Summary of Locking: Sulphide MOI

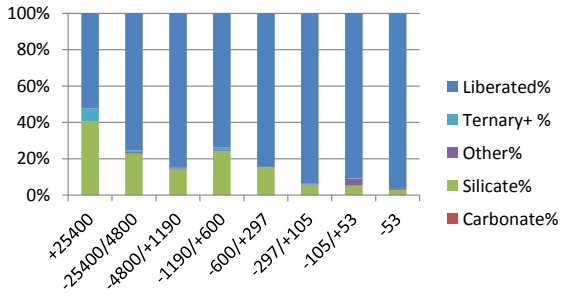

Tucush01 Head, Summary of Locking: Carbonate MOI

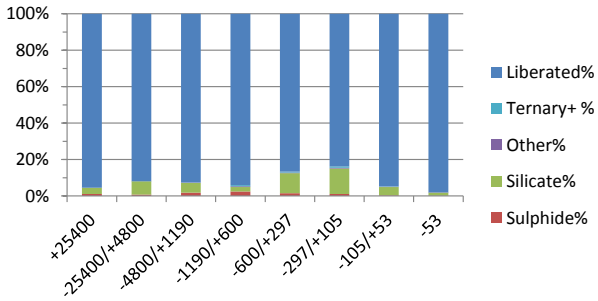

Tucush01 SLR, Summary of locking: Carbonate MOI

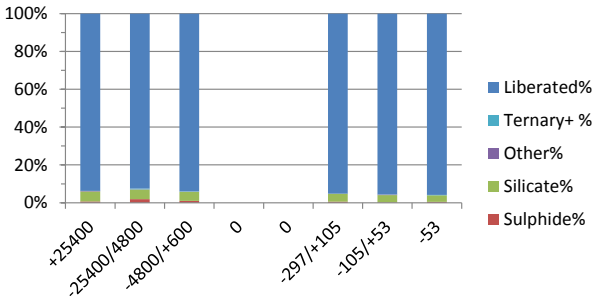

Tucush03 Head, Summary of Contact Association: Carbonate MOI

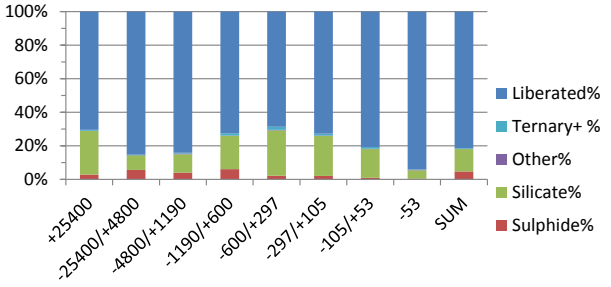

Tucush03 SLR. Summary of Locking: Carbonate MOI

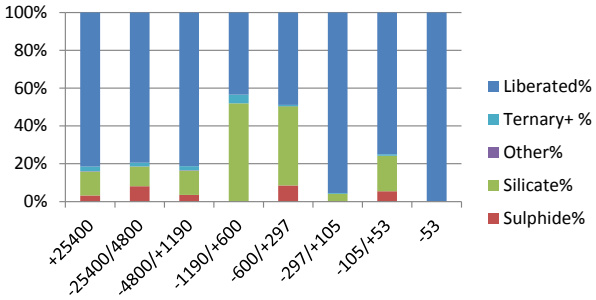

Tucush04 Head, Summery of Locking: Carbonate MOI

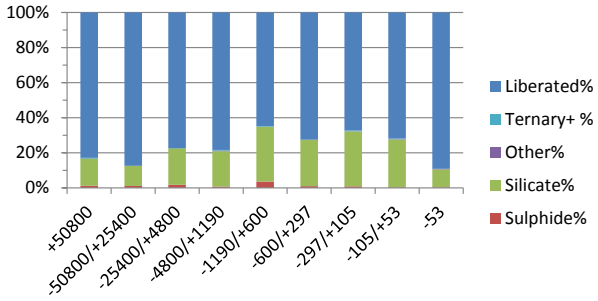

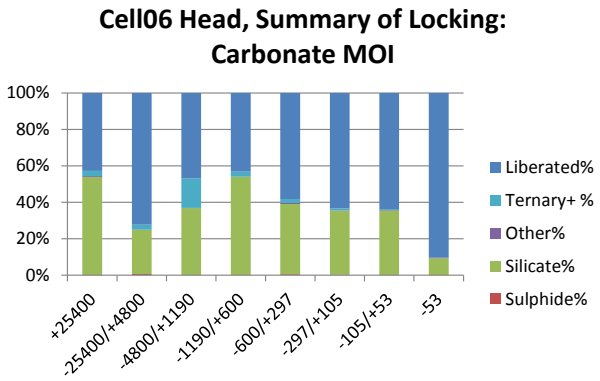
Cell06 Head, Summary of Locking: Carbonate MOI
100%
80%
60%
40%
20%
0%
+25400
-25400/+4800
-4800/+1190
-1190/+600
-600/+297
-297/+105
-105/+53
-53
Liberated%
Ternary+ %
Other%
Silicate%
Sulphide%

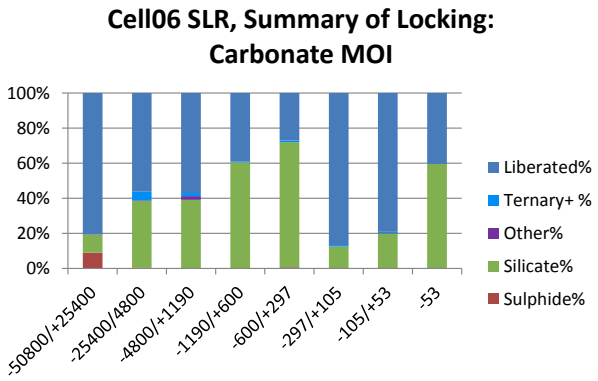
Cell06 SLR, Summary of Locking: Carbonate MOI
100%
80%
60%
40%
20%
0%
-50800/+25400
-25400/4800
-4800/+1190
-1190/+600
-600/+297
-297/+105
-105/+53
-53
Liberated%
Ternary+ %
Other%
Silicate%
Sulphide%

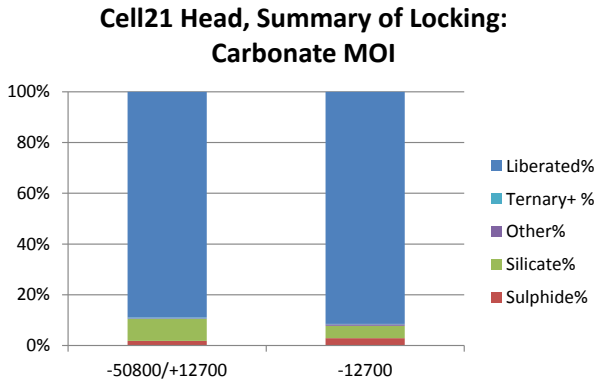
Cell21 Head, Summary of Locking: Carbonate MOI
100%
80%
60%
40%
20%
0%
-50800/+12700
-12700
Liberated%
Ternary+ %
Other%
Silicate%
Sulphide%

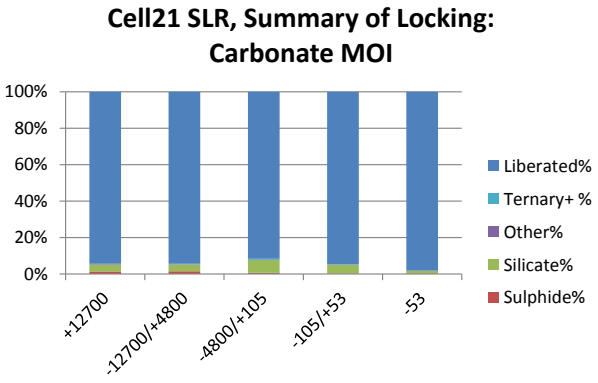
Cell21 SLR, Summary of Locking: Carbonate MOI
100%
80%
60%
40%
20%
0%
+12700
-12700/+4800
-4800/+105
-105/+53
-53
Liberated%
Ternary+ %
Other%
Silicate%
Sulphide%

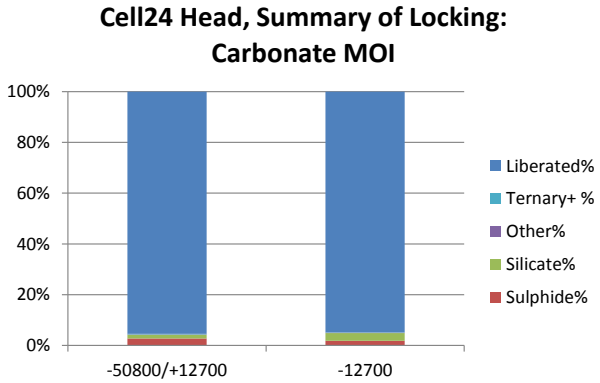
Cell24 Head, Summary of Locking: Carbonate MOI
100%
80%
60%
40%
20%
0%
-50800/+12700
-12700
Liberated%
Ternary+ %
Other%
Silicate%
Sulphide%

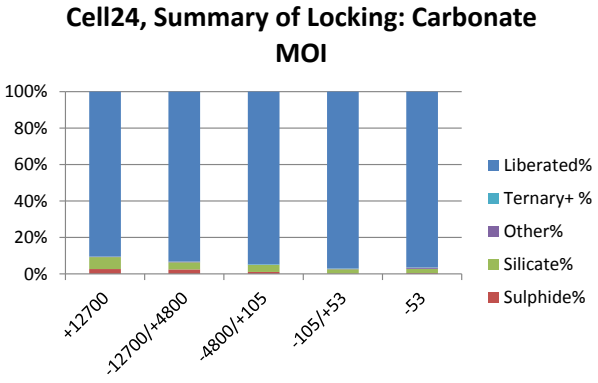
Cell24, Summary of Locking: Carbonate MOI
100%
80%
60%
40%
20%
0%
+12700
-12700/+4800
-4800/+105
-105/+53
-53
Liberated%
Ternary+ %
Other%
Silicate%
Sulphide%

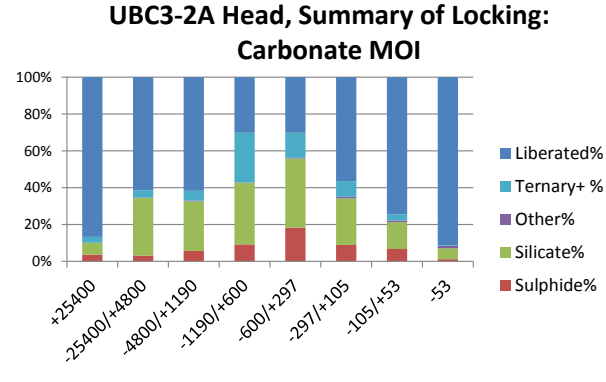
UBC3-2A Head, Summary of Locking: Carbonate MOI
100%
80%
60%
40%
20%
0%
+25400
-25400/+4800
-4800/+1190
-1190/+600
-600/+297
-297/+105
-105/+53
-53
Liberated%
Ternary+ %
Other%
Silicate%
Sulphide%

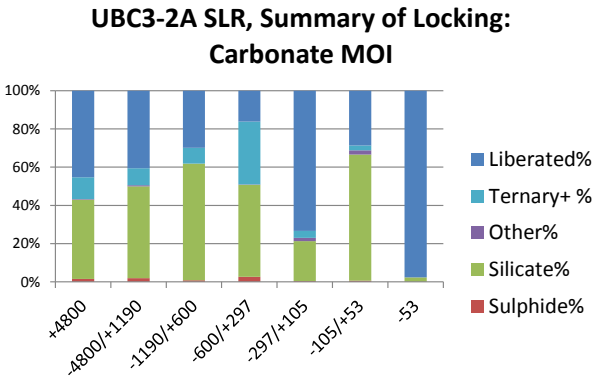
UBC3-2A SLR, Summary of Locking: Carbonate MOI
100%
80%
60%
40%
20%
0%
+4800
-4800/+1190
-1190/+600
-600/+297
-297/+105
-105/+53
-53
Liberated%
Ternary+ %
Other%
Silicate%
Sulphide%

UBC2-3A Head, Summary of Locking: Carbonate MOI

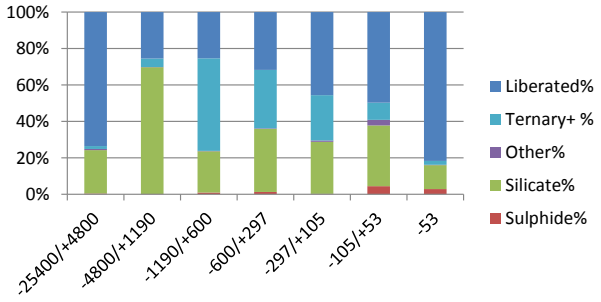

UBC2-3A SLR, Summary of Locking: Carbonate MOI

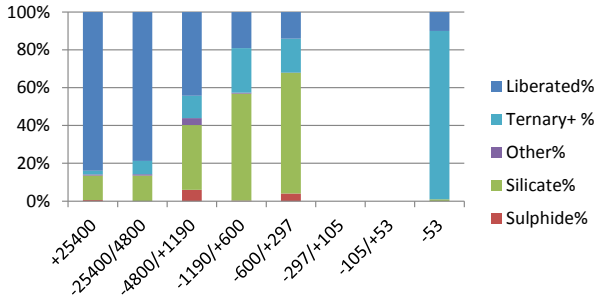

Tucush01 Head, Summary of Locking: Silicate MOI

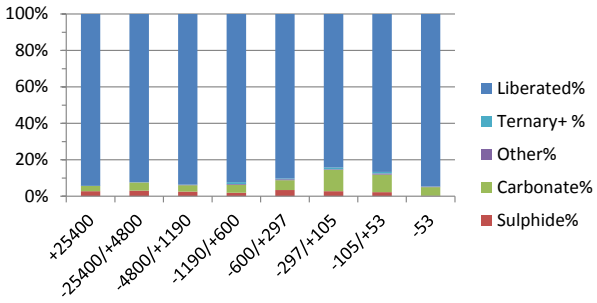

Tucush01 SLR, Summary of Locking: Silicate MOI

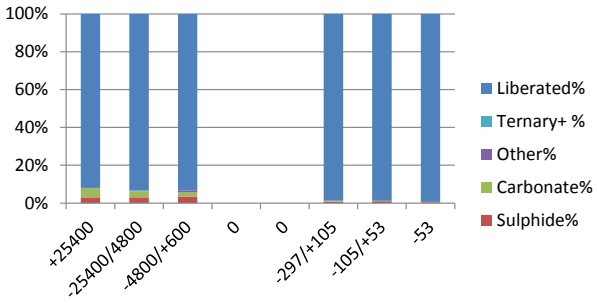

Tucush03 Head, Summary of Locking: Silicate MOI

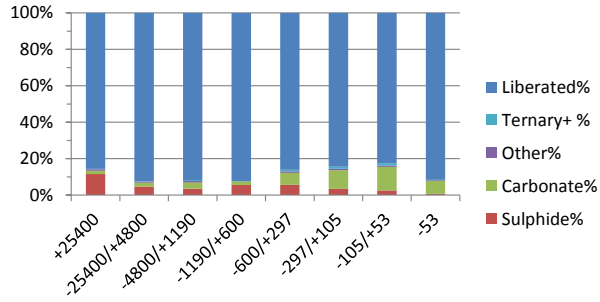

Tucush03 SLR, Summary of Locking: Silicate MOI

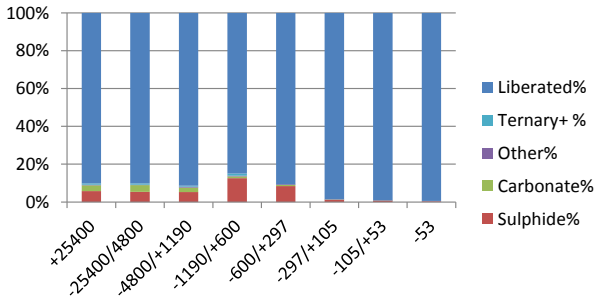

Tucush04 Head, Summary of Locking: Silicate MOI

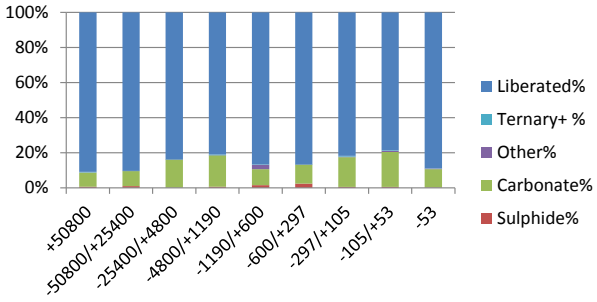

Cell06 Head, Summary of Locking: Silicate MOI

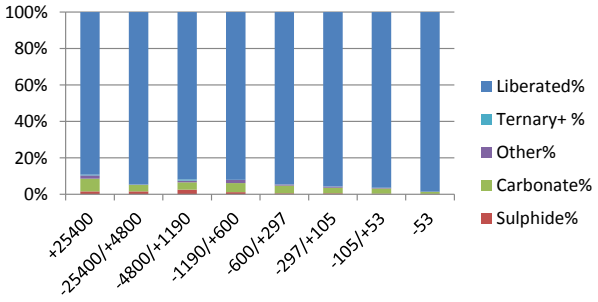

Cell06 SLR, Summary of Locking: Silicate MOI

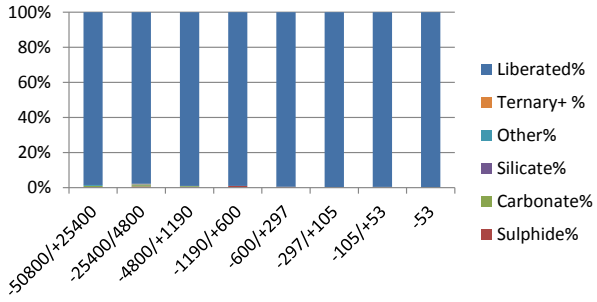

Cell21 Head, Summary of Locking: Silicate MOI

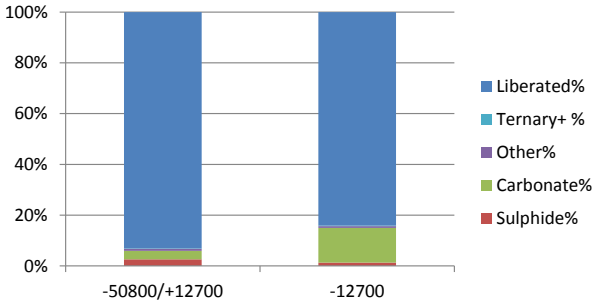

Cell21 SLR, Summary of Locing: Silicate MOI

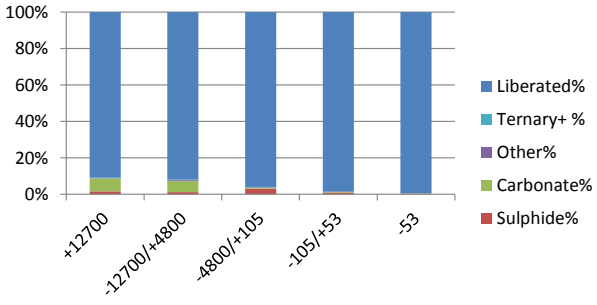

Cell24 Head, Summary of Locking: Silicate MOI

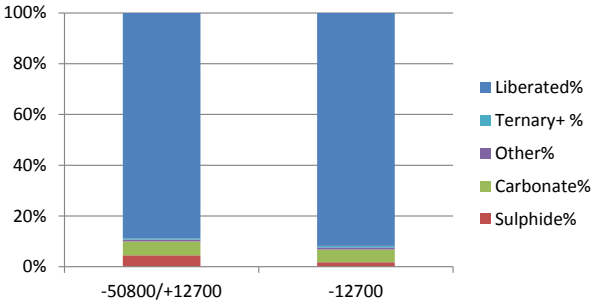

Cell24 SLR, Summary of Locking: Silicate MOI

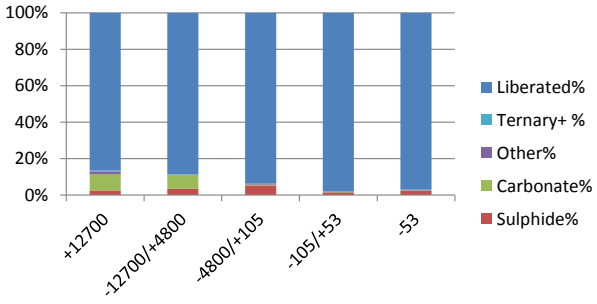

UBC3-2A Head, Summary of Locking: Silicate MOI

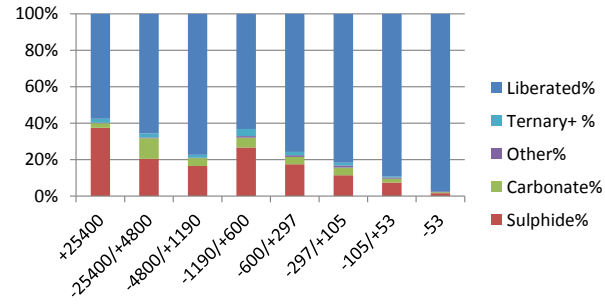

UBC3-2A SLR, Summary of Locking: Silicate MOI

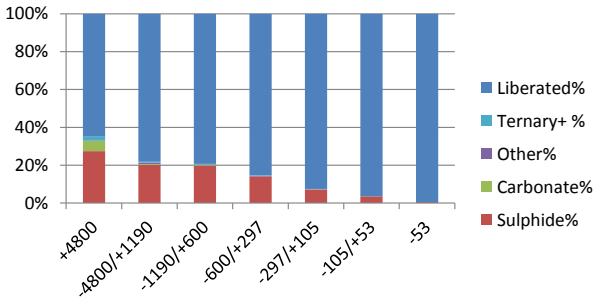

UBC2-3A Head, Summary of Locking: Silicate MOI

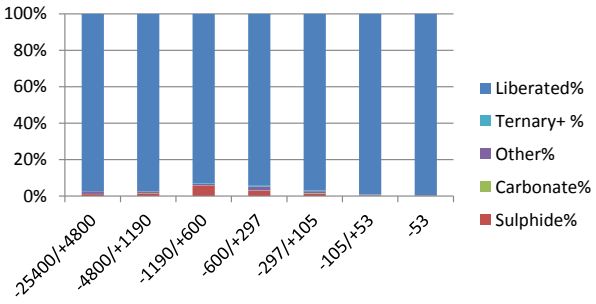

UBC2-3A SLR, Summary of Locking: Silicate MOI

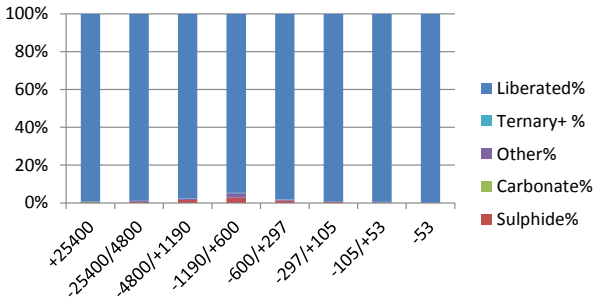

Tucush01 Head, Summary of Locking: Sb-bearing MOI

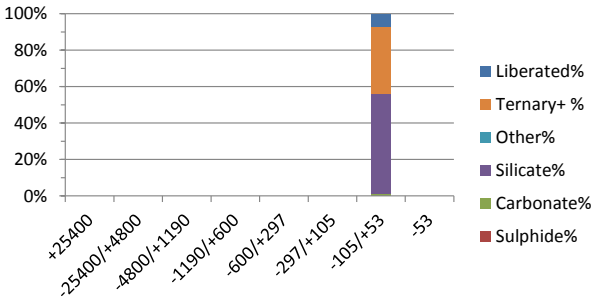

Tucush01 SLR, Summary of Locking Sb-bearing MOI

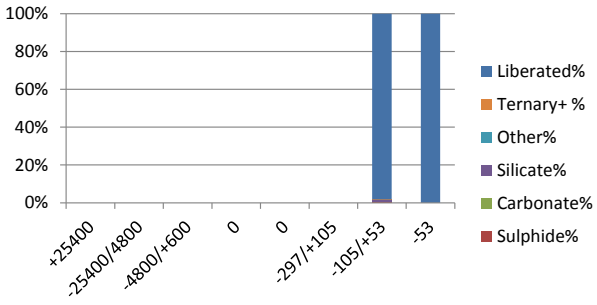

Tucush03 Head, Summary of Contact Association: Sb-bearing MOI

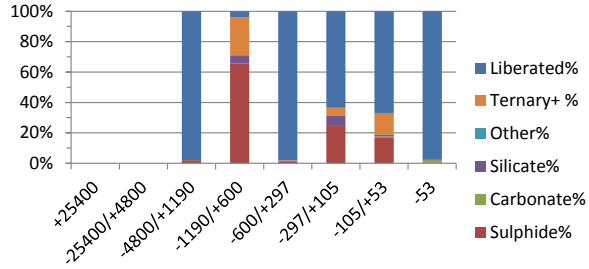

Tucush03 SLR, Summary of Contact Association: Sb-bearing MOI

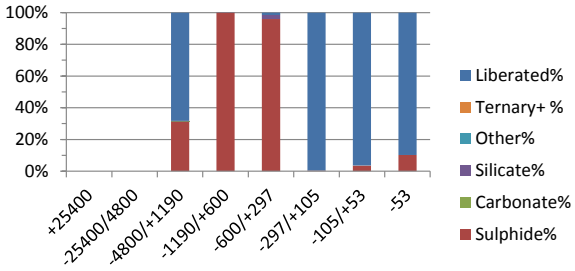

Tucush04 Head, Summary of Locking: Sb-bearing MOI

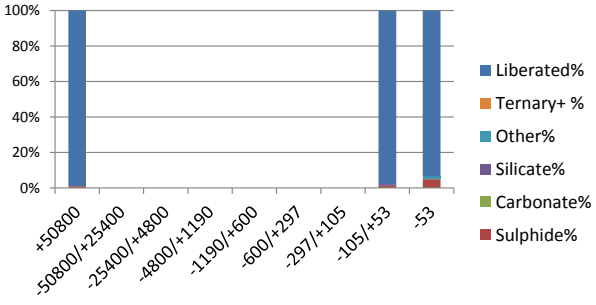

Cell06 Head, Summery of Locking: Sb-bearing MOI

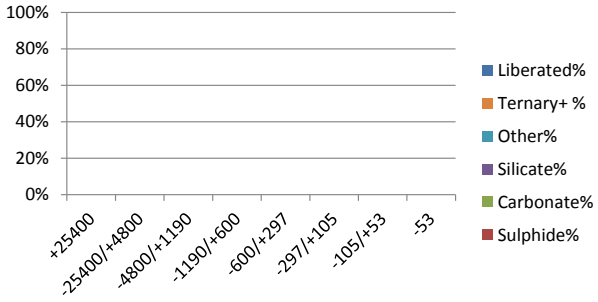

Cell06 SLR, Summary of Locking: Sb-bearing MOI

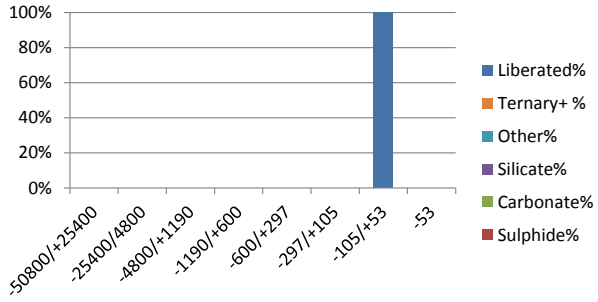

Cell21 Head, Summary of Locking: Sb-bearing MOI

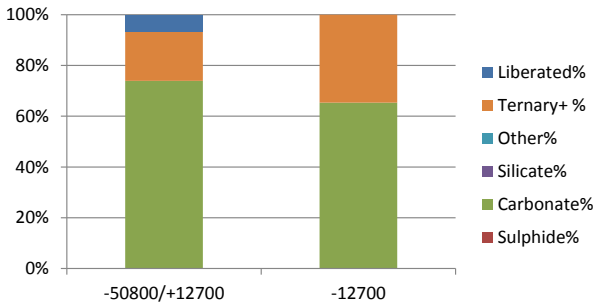

Cell21 SLR, Summary of Locking: Sb-bearing MOI

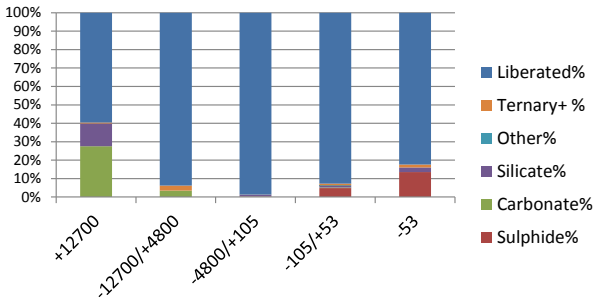

Cell24 Head, Summary of Locking: Sb-bearing MOI

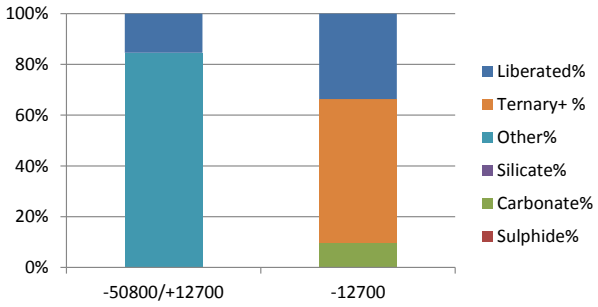

Cell24 SLR, Summary of locking: Sb-bearing MOI

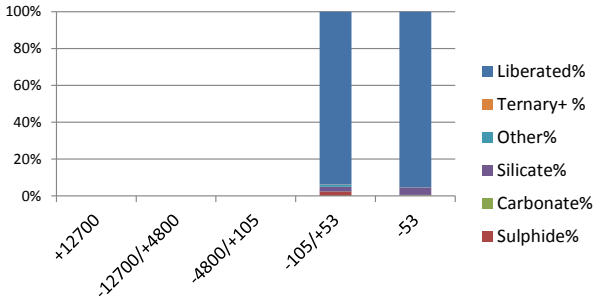

UBC3-2A Head, Summary of Locking: Sb-bearing MOI

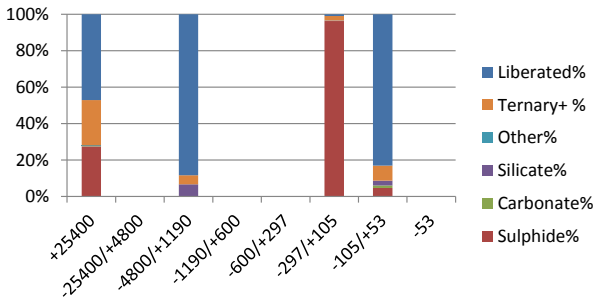

UBC3-2A SLR, Summary of Locking: Sb-bearing MOI

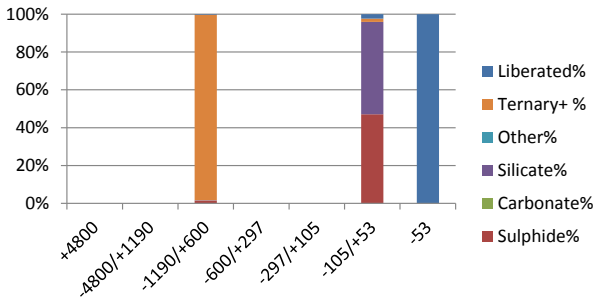

UBC2-3A Head, Summary of Locking: Sb-bearing MOI

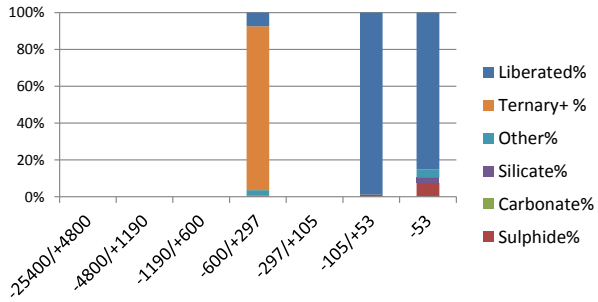

UBC2-3A SLR, Summary of Locking: Sb-bearing MOI

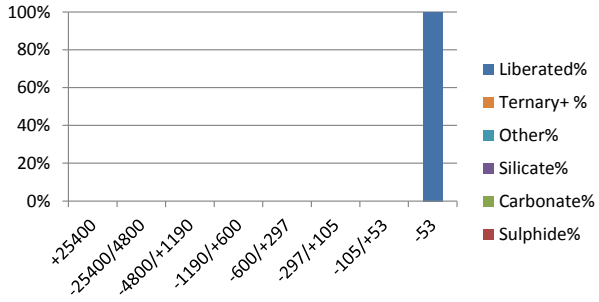

Tucush01 Head, Summary of Locking: As-bearing MOI

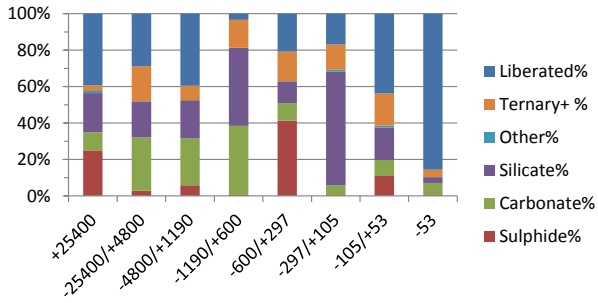

Tucush01 SLR, Summary of Locking: As-bearing MOI

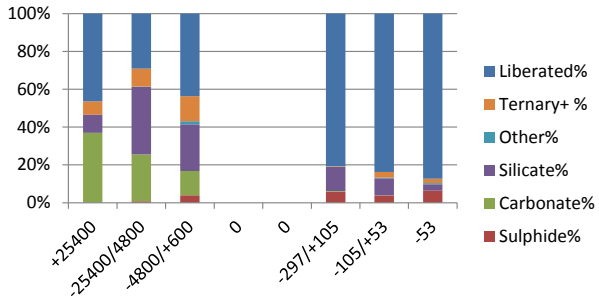

Tucush03 Head, Summary of Locking: As-bearing MOI

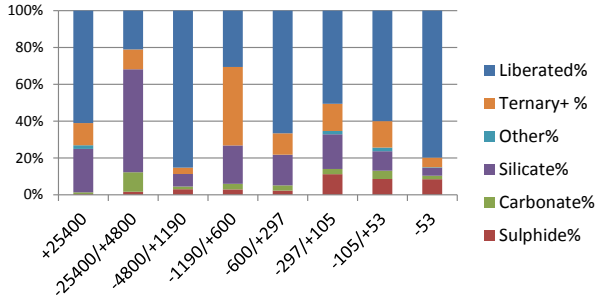

Tucush03 SLR, Summary of Locking: As-bearing MOI

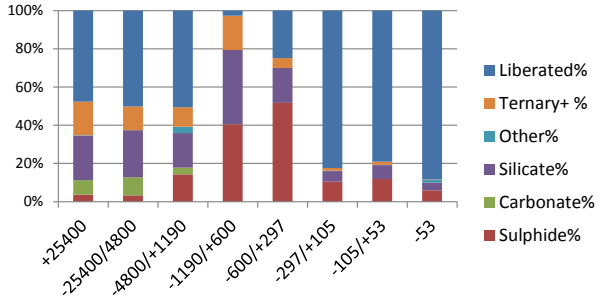

Tucush04 Head, Summary og Locking: As-bearing MOI

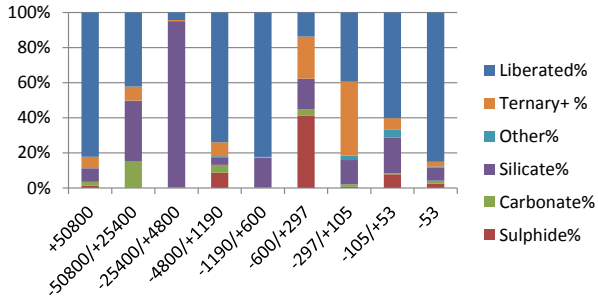

Cell06 Head, Summery of Locking: As-bearing MOI

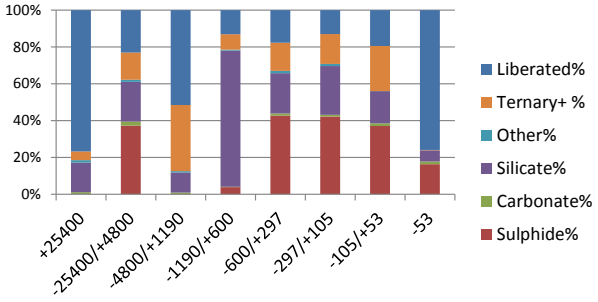

Cell06 SLR, Summary of Locking: As-bearing MOI

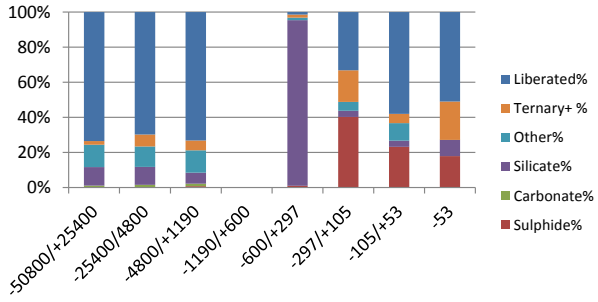

Cell21 Head, Summary of Locing: As-bearing MOI

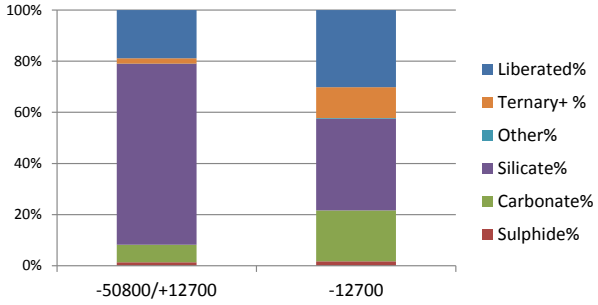

Cell21 SLR, Summary of Locking: As-bearing MOI

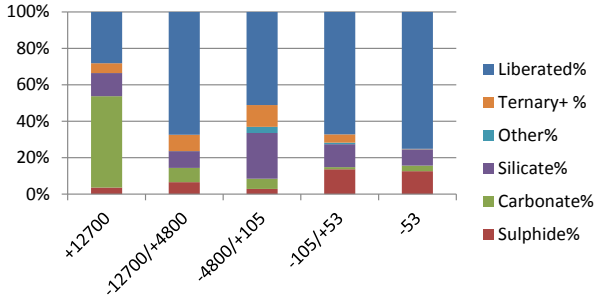

Cell24 Head, Summary of Locking: As-bearing MOI

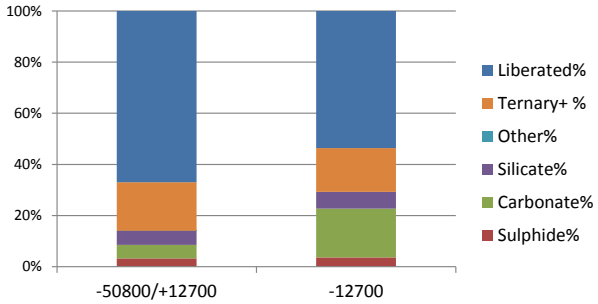

Cell24 SLR, Summary of Locking: As-bearing MOI

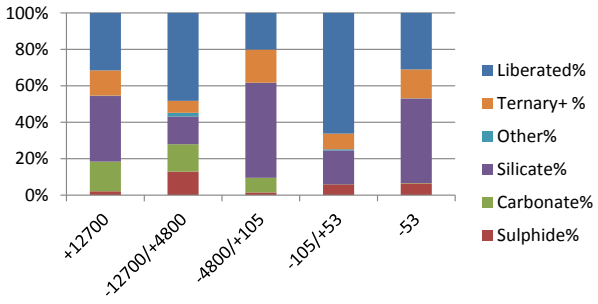

UBC3-2A Head, Summary of Locking: As-bearing MOI

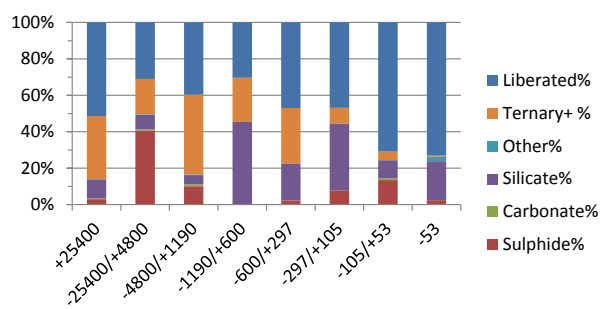

UBC3-2A SLR, Summary of Contact Association: As-bearing MOI

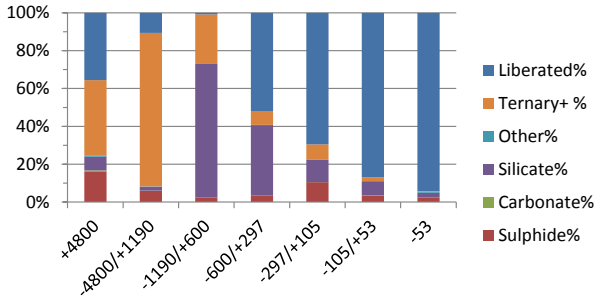

UBC2-3A Head, Summary of Contact Association: As-bearing MOI

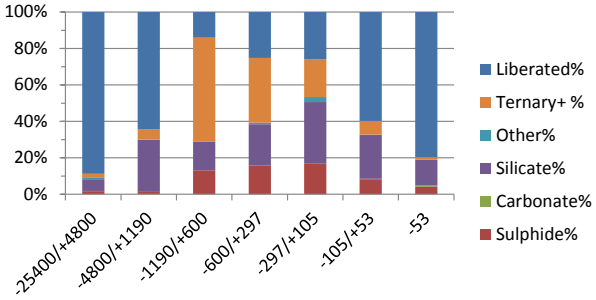

UBC2-3A SLR, Summary of Locking: As-bearing MOI

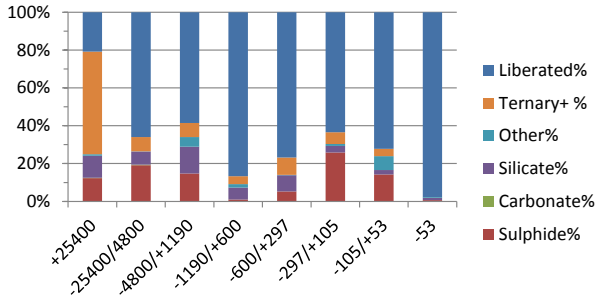

Tucush01 Head, Summary of Locking: Cu-bearing MOI

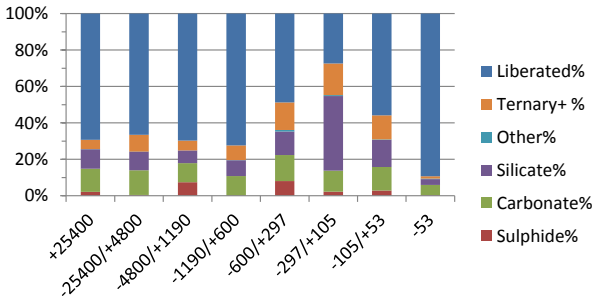

Tucush01 SLR, Summary of Locking: Cu-bearing MOI

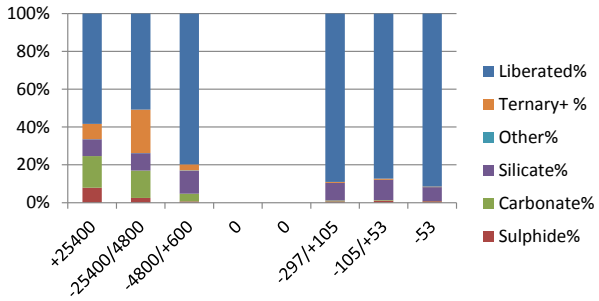

Tucush03 Head, Summary of Locking: Cu-bearing MOI

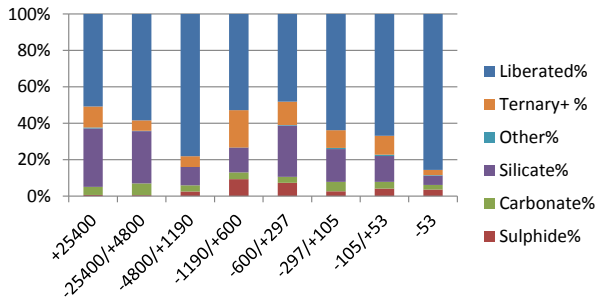

Tucush03 SLR, Summary of Locking: Cu-bearing MOI

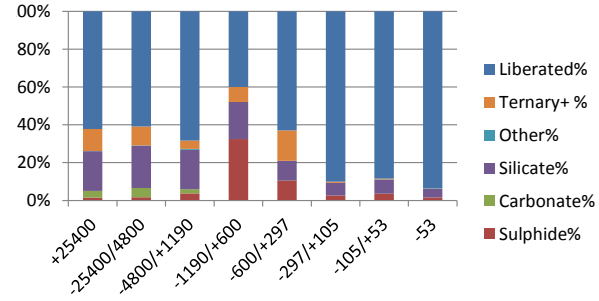

Tucush04 Head, Summery of Locking: Cu-bearing MOI

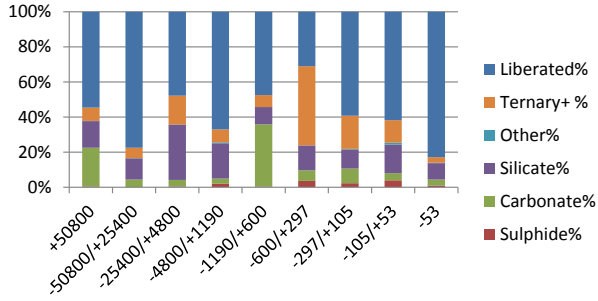

Cell06 Head, Summary of Locking: Cu-bearing MOI

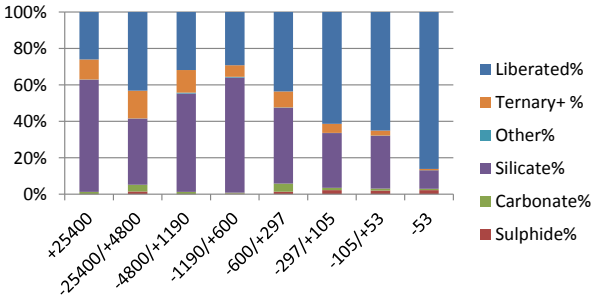

Cell06 SLR, Summary of Locking: Cu-bearing MOI

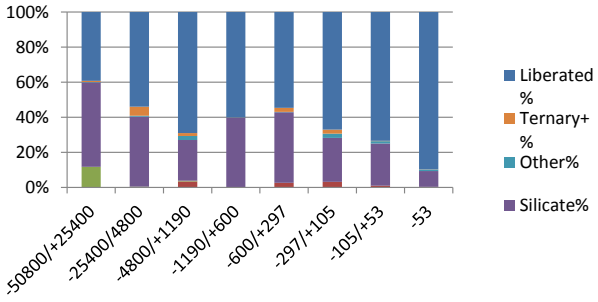

Cell21 Head, Summary of Locking: Cu-bearing MOI

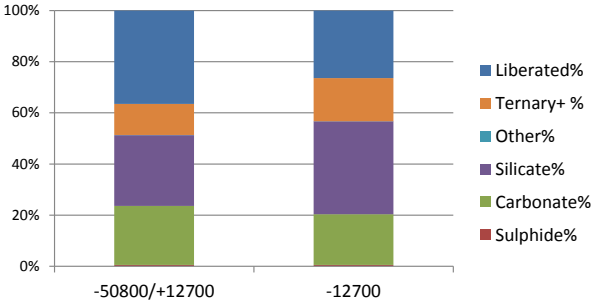

Cell21 SLR, Summary of Locking: Cu-bearing MOI

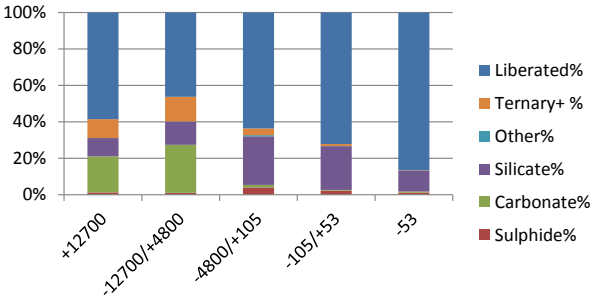

Cell24 Head, Summary of Locking: Cu-bearing MOI

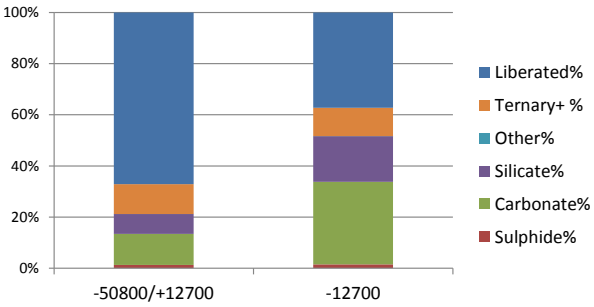

Cell24 SLR, Summary of Locking: Cu-bearing MOI

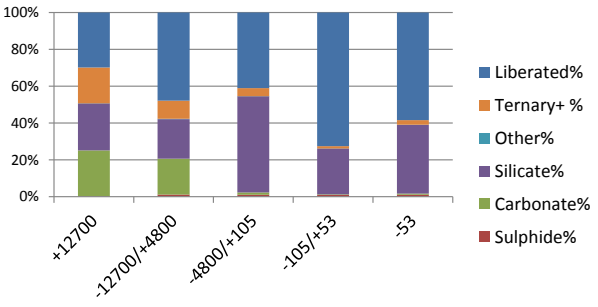

UBC3-2A Head, Summary of Locking: Cu-bearing MOI

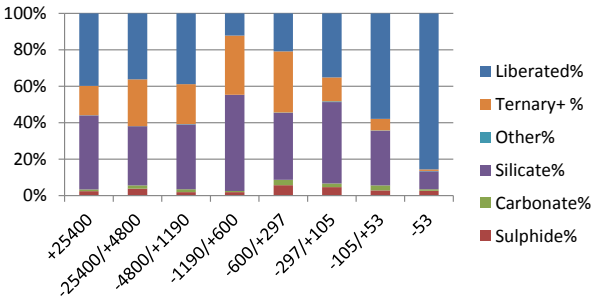

UBC3-2A SLR, Summary of Locking: Cu-bearing MOI

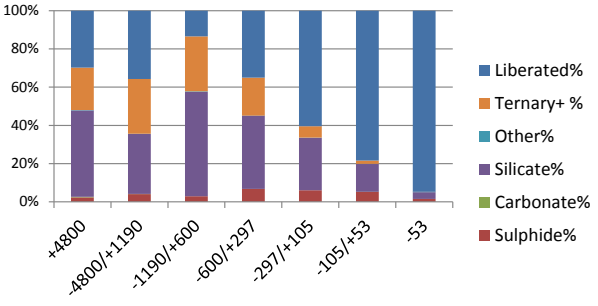

UBC2-3A Head, Summary of Locking: Cu-bearing MOI

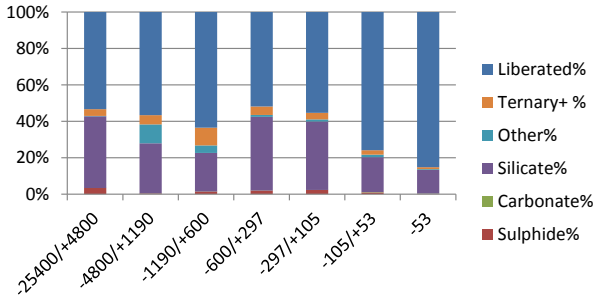

UBC2-3A SLR, Summary of Locking: Cu-bearing MOI

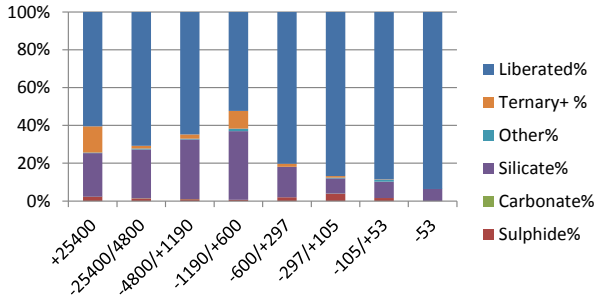

Tucush01 Head, Summary of locking: Mo-bearing MOI

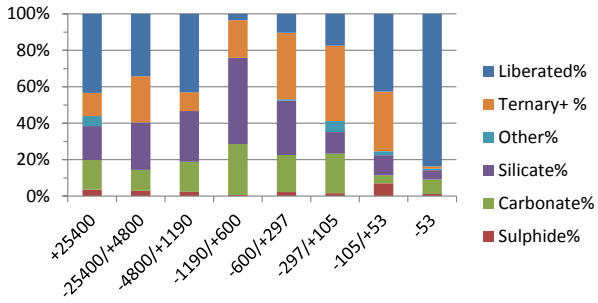

Tucush01 SLR, Summary of Locking: Mo-bearing MOI

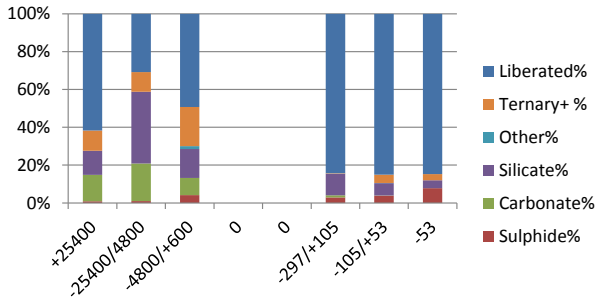

Tucush03 Head, Summary of Locking: Mo-bearing MOI

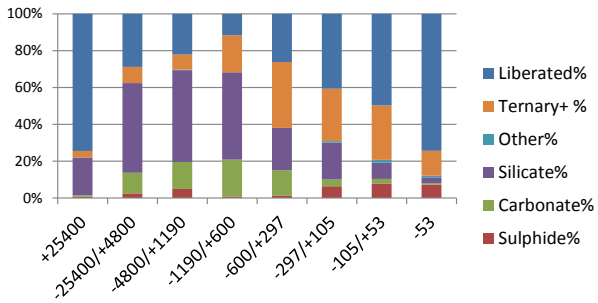

Tucush03 SLR, Summary of Locking: Mo-bearing MOI

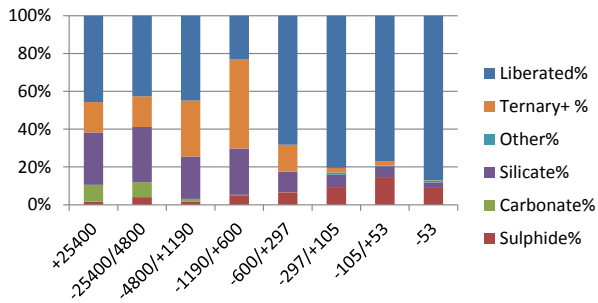

Tucush04 Head, Summery of Locking: Mo-bearing MOI

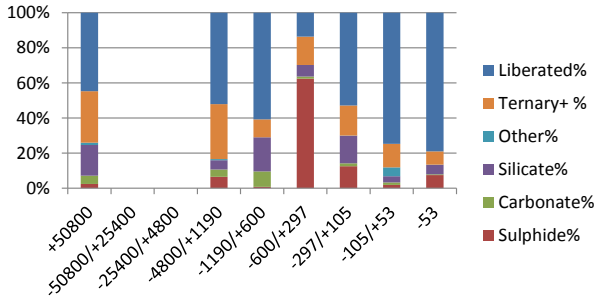

Cell06 Head, Summary of Contact Association: Mo-bearing MOI

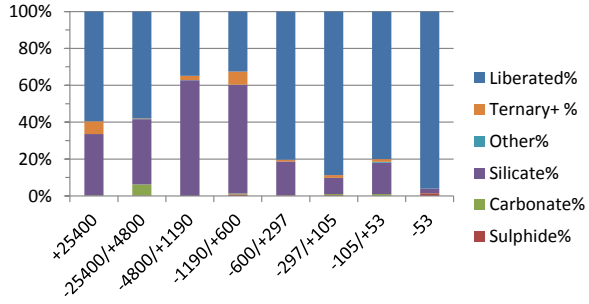

Cell06 SLR, Summary of Contact Association: Mo-bearing MOI

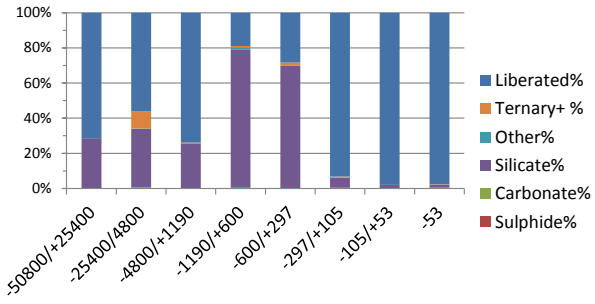

Cell21 Head, Summary of Locking: Mo-bearing MOI

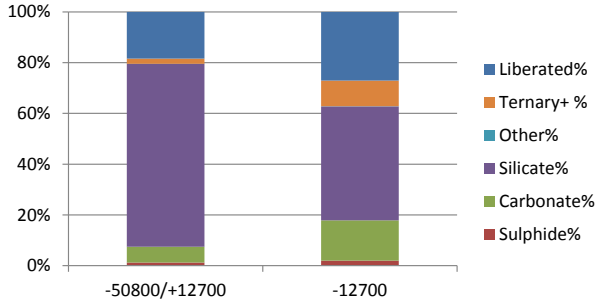

Cell21 SLR, Summary of Locking: Mo-bearing MOI

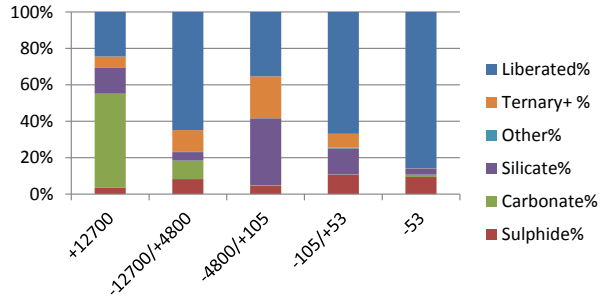

Cell24 Head, Summary of Locking: Mo-bearing MOI

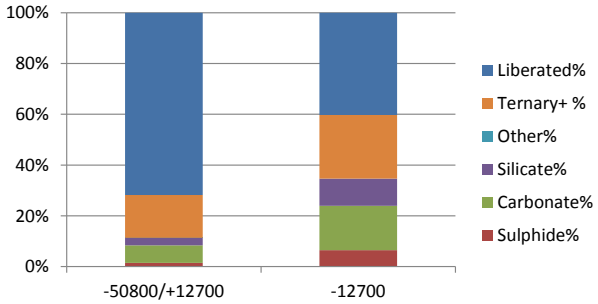

Cell24 SLR, Summary of Locking: Mo-bearing MOI

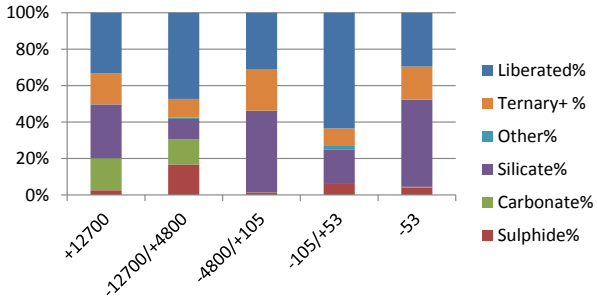

UBC3-2A Head, Summary of Locking: Mo-bearing

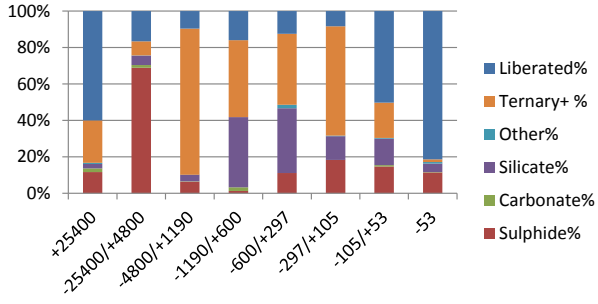

UBC3-2A SLR, Summary of Locking: Mo-bearing MOI

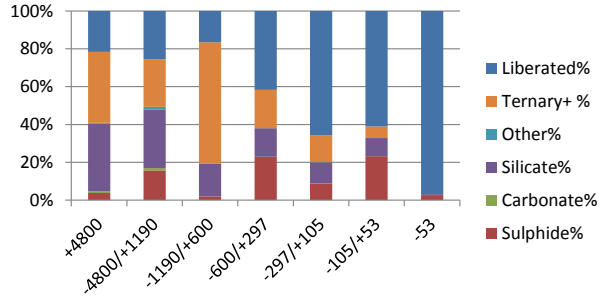

UBC2-3A Head, Summary of Locking: Mo-bearing MOI

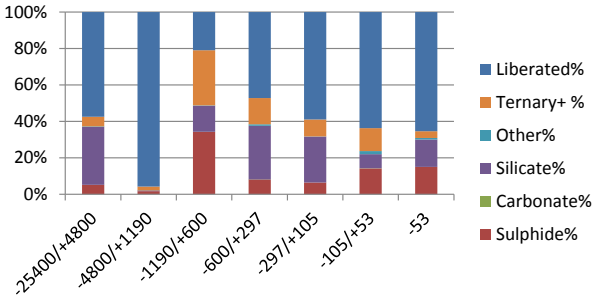

UBC2-3A SLR, Summary of Locking: Mo-bearing MOI

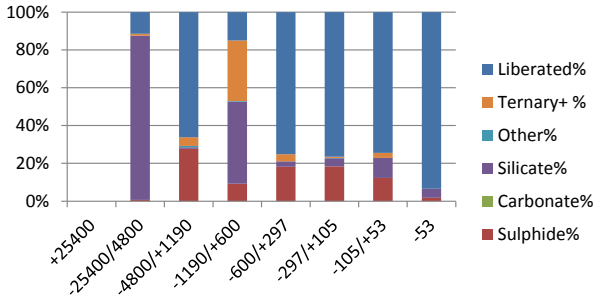

Tucush01 Head, Summary of Locking: Pb-bearing MOI

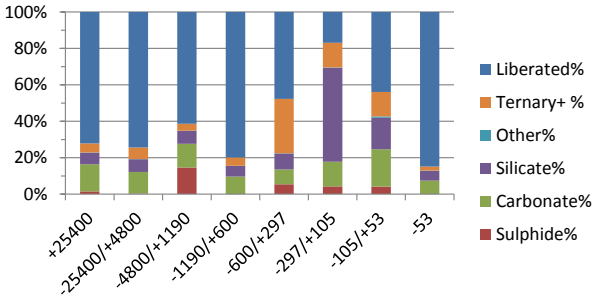

Tucush01 SLR, Summary of Locking: Pb-bearing MOI

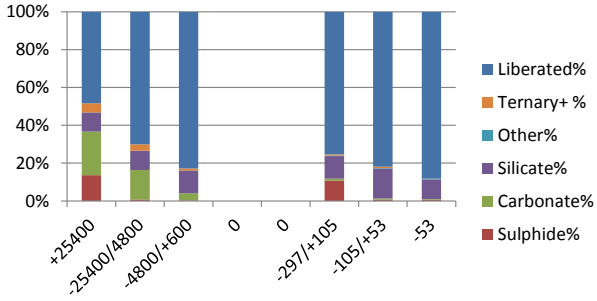

Tucush03 Head, Summary of Locking: Pb-bearing MOI

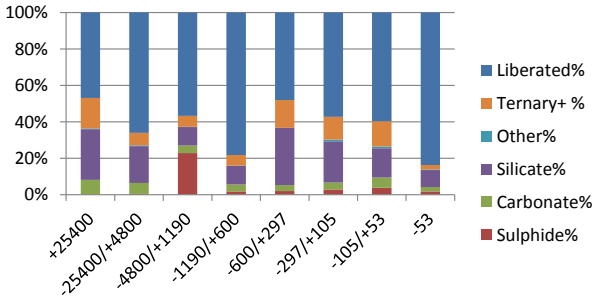

Tucush03 SLR, Summary of Locking: Pb-bearing MOI

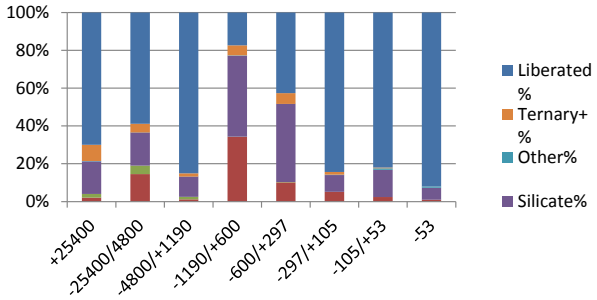

Tucush04 Head, Summary of Locking: Pb-bearing MOI

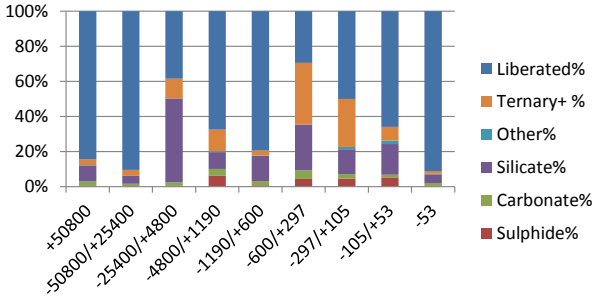

Cell06 Head, Summary of Locking: Pb-bearing MOI

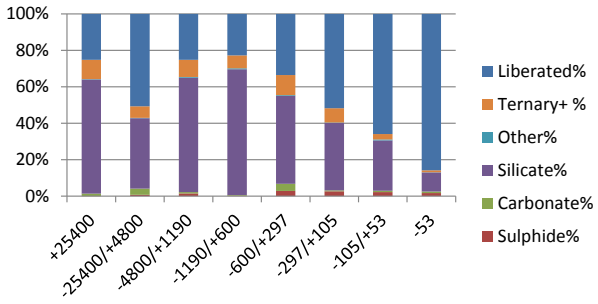

Cell06 SLR, Summary of Locking: Pb-bearing MOI

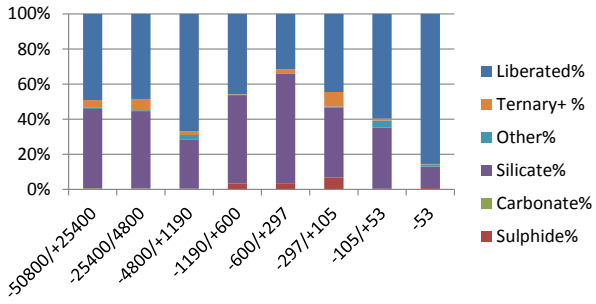

Cell21 Head, Summary of Locking: Pb-bearing MOI

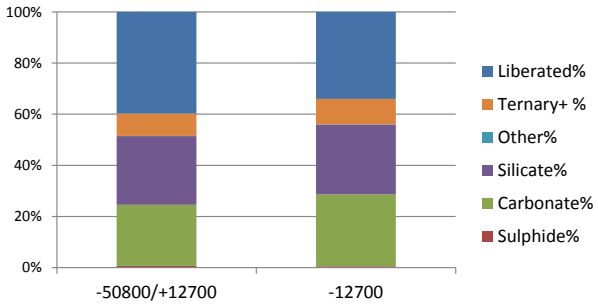

Cell21 SLR, Summary of Locking: Pb-bearing MOI

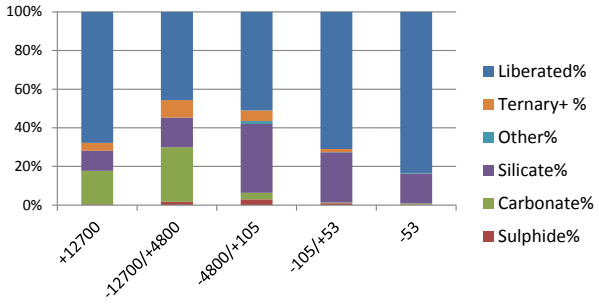

Cell24 Head, Summary of Locking: Pb-bearing MOI

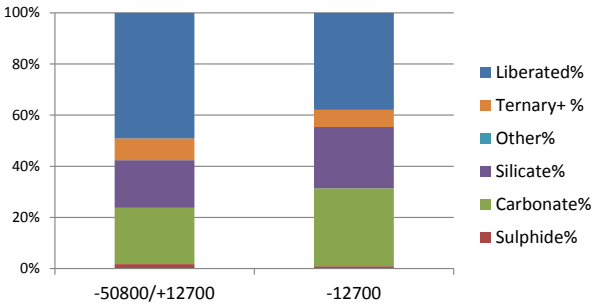

Cell24 SLR, Summary of Locking: Pb-bearing MOI

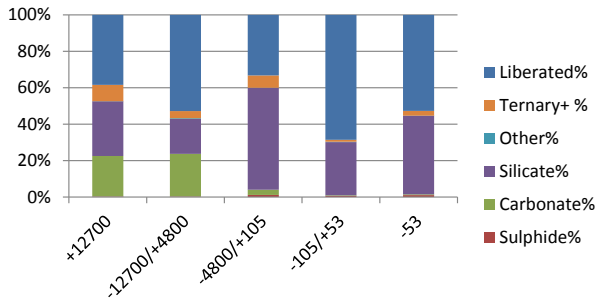

UBC3-2A, Summary of Locking: Pb-bearing MOI

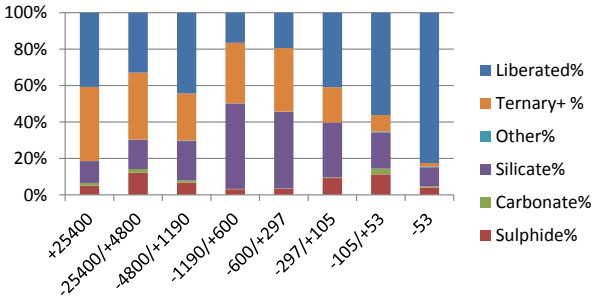

UBC3-2A SLR, Summary of Contact Association: Pb-bearing MOI

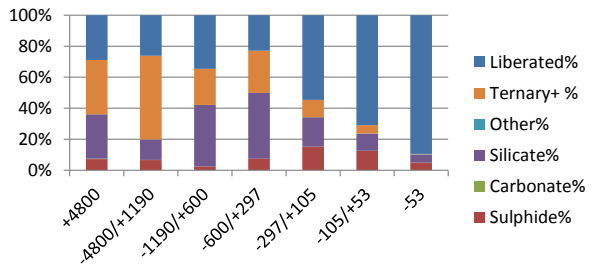

UBC2-3A Head, Summary of Contact Association: Pb-bearing MOI

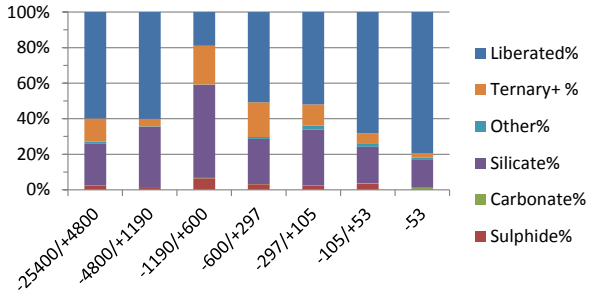

UBC2-3A SLR, Summary of Locking: Pb-bearing MOI

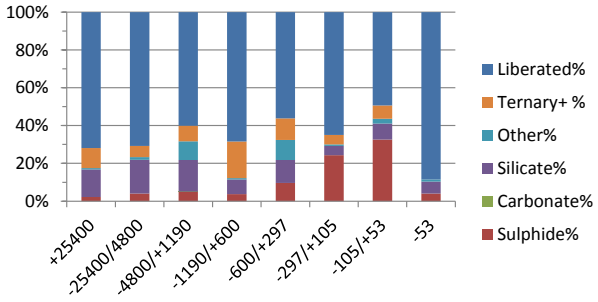

Tucush01 Head, Summary of locking: Zn-bearing MOI

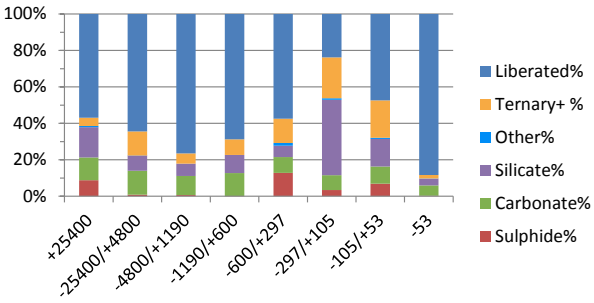

Tucush01 SLR, Summary of Locking: Zn-bearing

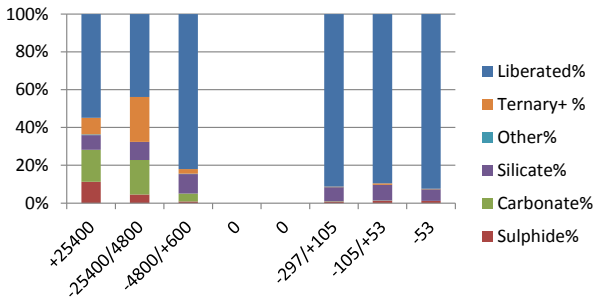

Tucush03 Head, Summary of Locking: Zn-bearing MOI

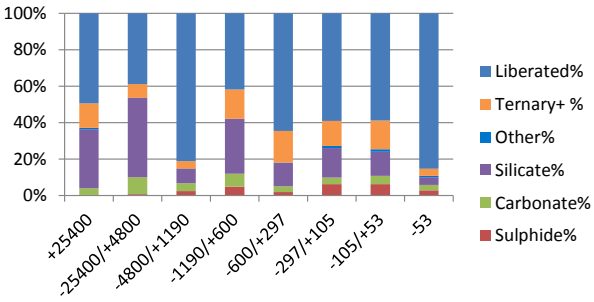

Tucush03 SLR, Summary of Locking: Zn-bearing

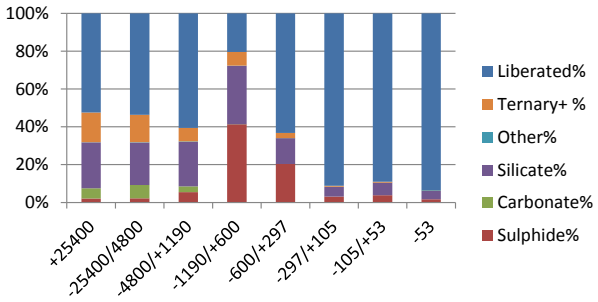

Tucush04 Head, Summery of Locking: Zn-bearing

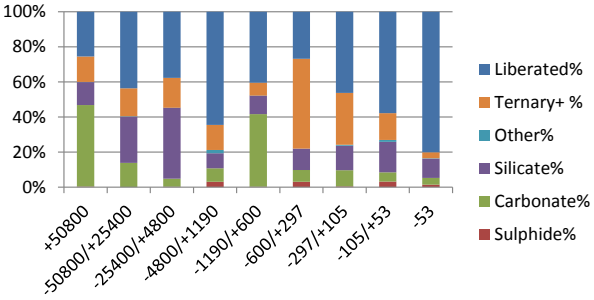

Cell06 Head, Summery of Locking: Zn-bearing MOI

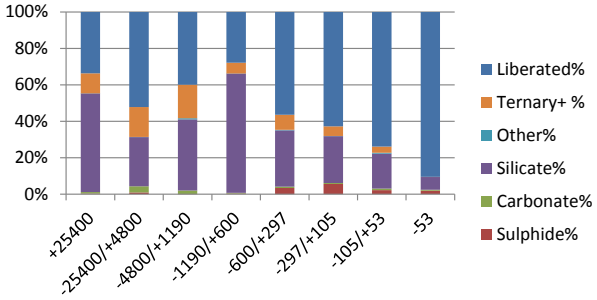

Cell06 SLR, Summary of Locking: Zn-bearing MOI

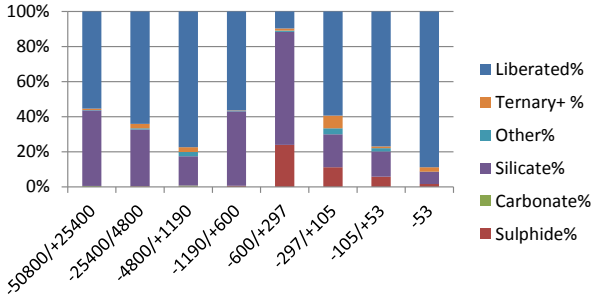

Cell21 Head, Summary of Locking: Zn-bearing MOI

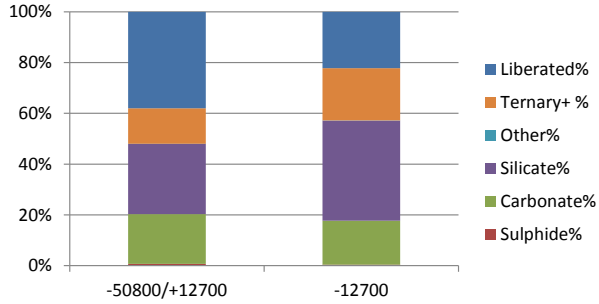

Cell21 SLR, Summary of Locking: Zn-bearing MOI

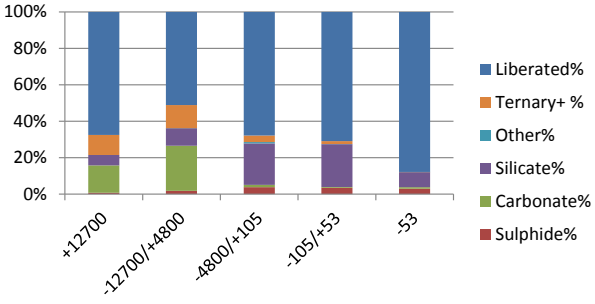

Cell24 Head, Summary of Locking: Zn-bearing MOI

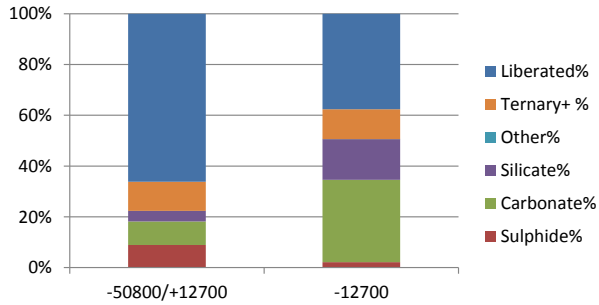

Cell24 SLR, Summary of Locking: Zn-bearing MOI

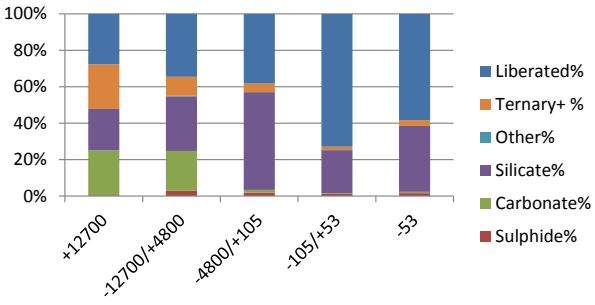

UBC3-2A Head, Summary of Locking: Zn-bearing MOI

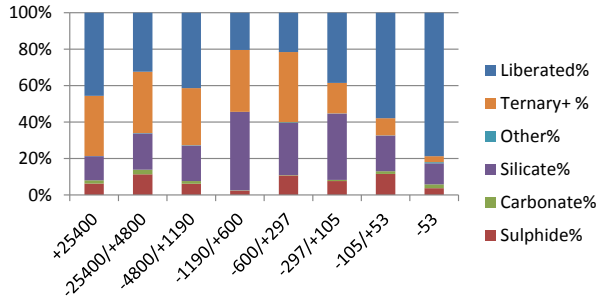

UBC3-2A SLR, Summary of Locking: Zn-bearing MOI

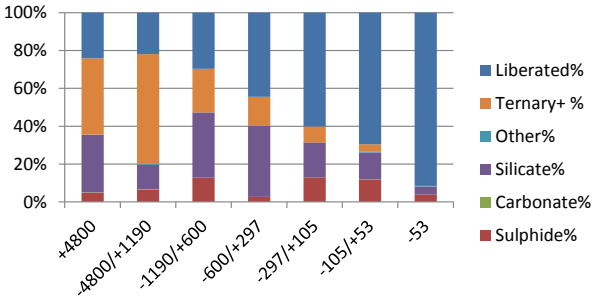

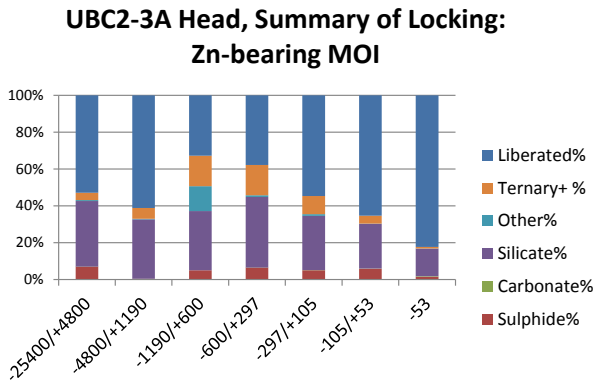
UBC2-3A Head, Summary of Locking: Zn-bearing MOI
100%
80%
60%
40%
20%
0%
-25400/+4800
-4800/+1190
-1190/+600
-600/+297
-297/+105
-105/+53
-53
Liberated%
Ternary+ %
Other%
Silicate%
Carbonate%
Sulphide%

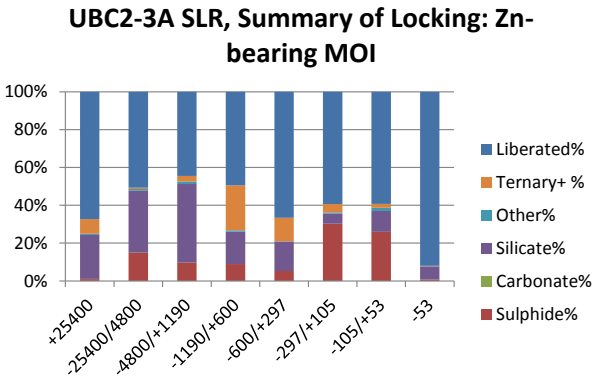
UBC2-3A SLR, Summary of Locking: Zn-bearing MOI
100%
80%
60%
40%
20%
0%
+25400
-25400/4800
-4800/+1190
-1190/+600
-600/+297
-297/+105
-105/+53
-53
Liberated%
Ternary+ %
Other%
Silicate%
Carbonate%
Sulphide%